IFMBE Proceedings

Dössel • Schlegel (Eds.)

Volume 25/13

World Congress on Medical Physics and Biomedical Engineering

7–12 September 2009
Munich, Germany

Special Topics and Workshops

Springer

IFMBE Proceedings Volume 25/XIII

Series Editor: R. Magjarevic

11th International
Congress of the IUPESM

MEDICAL PHYSICS AND BIOMEDICAL ENGINEERING

WORLD CONGRESS 2009

For the benefit
of the Patient.

Sept 7–12, 2009
Munich, Germany

IUPESM
IOMP IFMBE

International Organization for Medical Physics
IOMP

The International Federation for Medical and Biological Engineering, IFMBE, is a federation of national and transnational organizations representing internationally the interests of medical and biological engineering and sciences. The IFMBE is a non-profit organization fostering the creation, dissemination and application of medical and biological engineering knowledge and the management of technology for improved health and quality of life. Its activities include participation in the formulation of public policy and the dissemination of information through publications and forums. Within the field of medical, clinical, and biological engineering, IFMBE's aims are to encourage research and the application of knowledge, and to disseminate information and promote collaboration. The objectives of the IFMBE are scientific, technological, literary, and educational.

The IFMBE is a WHO accredited NGO covering the full range of biomedical and clinical engineering, healthcare, healthcare technology and management. It is representing through its 58 member societies some 120.000 professionals involved in the various issues of improved health and health care delivery.

Previous Editions:

IFMBE Proceedings WC 2009, "World Congress on Medical Physics and Biomedical Engineering",
Vol. 25, 2009, Munich, Germany, CD

IFMBE Proceedings SBEC 2009, "25th Southern Biomedical Engineering Conference 2009",
Vol. 24, 2009, Miami, FL, USA, CD

IFMBE Proceedings ICBME 2008, "13th International Conference on Biomedical Engineering"
Vol. 23, 2008, Singapore, CD

IFMBE Proceedings ECIFMBE 2008 "4th European Conference of the International Federation for Medical and Biological Engineering", Vol. 22, 2008, Antwerp, Belgium, CD

IFMBE Proceedings BIOMED 2008 "4th Kuala Lumpur International Conference on Biomedical Engineering",
Vol. 21, 2008, Kuala Lumpur, Malaysia, CD

IFMBE Proceedings NBC 2008 "14th Nordic-Baltic Conference on Biomedical Engineering and Medical Physics",
Vol. 20, 2008, Riga, Latvia, CD

IFMBE Proceedings APCMBE 2008 "7th Asian-Pacific Conference on Medical and Biological Engineering",
Vol. 19, 2008, Beijing, China, CD

IFMBE Proceedings CLAIB 2007 "IV Latin American Congress on Biomedical Engineering 2007, Bioengineering Solution for Latin America Health", Vol. 18, 2007, Margarita Island, Venezuela, CD

IFMBE Proceedings ICEBI 2007 "13th International Conference on Electrical Bioimpedance and the 8th Conference on Electrical Impedance Tomography", Vol. 17, 2007, Graz, Austria, CD

IFMBE Proceedings MEDICON 2007 "11th Mediterranean Conference on Medical and Biological Engineering and Computing 2007", Vol. 16, 2007, Ljubljana, Slovenia, CD

IFMBE Proceedings BIOMED 2006 "Kuala Lumpur International Conference on Biomedical Engineering",
Vol. 15, 2004, Kuala Lumpur, Malaysia, CD

IFMBE Proceedings WC 2006 "World Congress on Medical Physics and Biomedical Engineering",
Vol. 14, 2006, Seoul, Korea, DVD

IFMBE Proceedings BSN 2007 "4th International Workshop on Wearable and Implantable Body Sensor Networks",
Vol. 13, 2006, Aachen, Germany

IFMBE Proceedings ICBMEC 2005 "The 12th International Conference on Biomedical Engineering",
Vol. 12, 2005, Singapore, CD

IFMBE Proceedings EMBEC'05 "3rd European Medical & Biological Engineering Conference, IFMBE European Conference on Biomedical Engineering", Vol. 11, 2005, Prague, Czech Republic, CD

IFMBE Proceedings ICCE 2005 "The 7th International Conference on Cellular Engineering",
Vol. 10, 2005, Seoul, Korea, CD

IFMBE Proceedings NBC 2005 "13th Nordic Baltic Conference on Biomedical Engineering and Medical Physics",
Vol. 9, 2005, Umeå, Sweden

IFMBE Proceedings Vol. 25/XIII
Olaf Dössel · Wolfgang C. Schlegel (Eds.)

World Congress on Medical Physics and Biomedical Engineering 7–12 September, 2009 Munich, Germany

Special Topics and Workshops

Springer

Editors

Prof. Dr. Olaf Dössel
Univ. Karlsruhe
Inst. Biomedizinische Technik
Kaiserstr. 12
76128 Karlsruhe
Germany
E-mail: olaf.doessel@ibt.uni-karlsruhe.de

Prof. Dr. Wolfgang C. Schlegel
Deutsche Krebsforschungszentrum (DKFZ)
Abt. Medizinische Physik in der
Strahlentherapie
Im Neuenheimer Feld 280
69120 Heidelberg
Germany
E-mail: w.schlegel@dkfz-heidelberg.de

ISSN 1680-0737
ISBN 978-3-642-03894-5 e-ISBN 978-3-642-03895-2

Also available as set Vol. I–XIII ISBN 978-3-642-03897-6

DOI 10.1007/978-3-642-03895-2

Library of Congress Control Number: 2009934297

The IFMBE Proceedings is an Offical Publication of the International Federation for Medical and Biological Engineering (IFMBE)

Typesetting: Data supplied by the authors
Production & Cover design: Scientific Publishing Services Pvt. Ltd., Chennai, India.

Printed on acid-free paper

9 8 7 6 5 4 3 2 1

springer.com

Preface

Present Your Research to the World!

The World Congress 2009 on Medical Physics and Biomedical Engineering – the triennial scientific meeting of the IUPESM - is the world's leading forum for presenting the results of current scientific work in health-related physics and technologies to an international audience. With more than 2,800 presentations it will be the biggest conference in the fields of Medical Physics and Biomedical Engineering in 2009!

Medical physics, biomedical engineering and bioengineering have been driving forces of innovation and progress in medicine and healthcare over the past two decades. As new key technologies arise with significant potential to open new options in diagnostics and therapeutics, it is a multidisciplinary task to evaluate their benefit for medicine and healthcare with respect to the quality of performance and therapeutic output.

Covering key aspects such as information and communication technologies, micro- and nanosystems, optics and biotechnology, the congress will serve as an inter- and multidisciplinary platform that brings together people from basic research, R&D, industry and medical application to discuss these issues.

As a major event for science, medicine and technology the congress provides a comprehensive overview and in–depth, first-hand information on new developments, advanced technologies and current and future applications.

With this Final Program we would like to give you an overview of the dimension of the congress and invite you to join us in Munich!

Olaf Dössel
Congress President

Wolfgang C. Schlegel
Congress President

Preface

Welcome to World Congress 2009!

Since the first World Congress on Medical Physics and Biomedical Engineering convened in 1982, medically and biologically oriented engineers and physicists from all continents have gathered every three years to discuss how physics and engineering can advance medicine, health and health care and to assess the clinical, scientific, technical and professional progress in their fields. In the tradition and the mission of our professions, which are the only ones involved in the whole loop of health and health care from basic research to the development, assessment, production, management and application of medical technologies, the theme of WC 2009 is "For the Benefit of the Patient". Thus, in addition to scientific aspects, the Congress will focus on all aspects of safe and efficient health technology in both industrialized and developing countries, including economic issues, the perspectives that advanced technologies and innovations in medicine and healthcare offer for the patients and the development of societies, the progress of MBE and MP, including health policy and educational issues as well as the need for the regulation and classification as health professionals of those biomedical/clinical engineers and medical physicists who are working in the health care systems.

The World Congress as the most important meeting of our professions, bringing together physicists, engineers and physicians from all over the world, including the delegates of the 138 constituent organizations of the IUPESM representing some 140,000 individual members, is the best place to discuss these issues, thereby contributing to the advancement of the physical and engineering sciences, our professions and thus to global health.

It gives me great pleasure to welcome you to this important event. I wish you a rewarding and enjoyable congress and a most pleasant time in Munich, the ‘metropolis with heart’ that has so much to offer.

Joachim H. Nagel
President of the IUPESM

Preface

Let's talk!
Is our level of communication between Medical Physics, Biomedical Engineering, Clinical Engineering, Medical Informatics, Tissue Engineering, etc. and Medicine good enough? We would like to answer: yes, we are quite good, but not good enough! There is a lot of room for improvement. Let' start right on the spot - on the World Congress on Medical Physics and Biomedical Engineering 2009. And please remember: communication is 50% talking and 50% listening.

Let's work together!
Do we have a perfect level of collaboration in our field? OK, we are quite good, but we can do better. Just to give an example: there should be no funded project in Medical Physics or Biomedical Engineering where there is no medical partner. And vice versa: medical doctors should join their forces with physicists and engineers if they are aiming at improvements on medical devices or healthcare systems. Let's start right here in Munich, September 2009, with innovative projects and innovative ways of cooperation.

Let's get to know each other!
It's known for more than thousand years: people who know each other personally and from face to face can talk with better mutual understanding, collaborate with less friction losses, are much more successful ..... and have much more fun. Plenty of chances to make new friends and to refresh old relations on World Congress on Medical Physics and Biomedical Engineering 2009!

And here are the numbers:
More than 3000 scientists working in the field of Medical Physics and Biomedical Engineering meet in September 2009 in Munich. They come from more than 100 nations. They submitted about 2800 contributions. 10 plenary talks and 46 keynote lectures bring us to the top level of science in our field. 75 companies show their latest achievements in the industrial exhibition. It's definitely the largest market place of ideas and innovations in Medical Physics and Biomedical Engineering of the year 2009.

August 2009 Olaf Dössel

Table of Contents

Education and Training of the Medical Physicist in Europe

S. Christofides[1], W.Schlegel[2], R. Padovani[3], P. F. Sharp[4], A. Torresin[5], M. Wasilewska-Radwanska[6], Wil van der Putten[7], E. Guibelalde[8] and K. U. Kasch[9]

[1] Medical Physics Department, Nicosia General Hospital, Nicosia, Cyprus
[2] DKFZ, Abteilung Medizinische Physik in der Strahlentherapie, Heidelberg, Germany
[3] SO di Fisica Sanitaria, Ospedale S. Maria della Misericordia, Udine, Italy
[4] Bio-Medical Physics & Bio-Engineering, University of Aberdeen & Grampian Hospitals NHS Trust, Aberdeen, United Kingdom
[5] Medical Physics Dept, Azienda Ospedale Niguarda, Milano, Italy
[6] AGH University of Science and Technology, Faculty of Physics and Applied Computer Science, Krakow, Poland
[7] HSE West, University Hospital Galway, Galway, Ireland
[8] Medical Physics Department, Facultad de Medicina, Universidad Complutense, Madrid, Spain
[9] University of Applied Sciences (TFH) Berlin, Germany

Abstract— **One of the main aims of the European Federation of Organisations for Medical Physics is to propose guidelines for education, training and accreditation programmes. This is achieved through the publication of Policy Statements and the organisation of education and training courses, seminars and conferences. It represents a long-term work-programme aimed at harmonising the education and training of the Medical Physicist across Europe. This paper presents these efforts together with the challenges EFOMP needs to overcome in order to achieve these aims.**

Keywords— **EFOMP, Education, Training, Policy Statement, Continuous Professional Development.**

I. Introduction

The European Federation for Organisations of Medical Physics - EFOMP was set up in 1980 in London [1]. Among its aims and objectives is the production of guidelines for education, training and accreditation programmes.

EFOMP's Policy Statement No. 12 [2] describes the present status of Medical Physics education and training in Europe. This Policy Statement takes into consideration the European Union Directives relevant to education and training.

The European School of Medical Physics – ESMP, is a long standing EFOMP activity, in partnership with the European Scientific Institute – ESI (Archamps, France), in providing a forum for the Education and Training of young Medical Physicists [3]

An essential component of professionalism is Continuous Professional Development - CPD. EFOMP has been, and continues to be, very active in this area by publishing policy statements for CPD schemes and establishing National Accreditation systems for Medical Physicists [4, 5 and 6]. Also, EFOMP has recently established the European Network of Medical Physics Schools – ENMPS [7]. The aim of this Network is to assist in the harmonisation of CPD courses across Europe.

The exchange of information is a very important component of CPD and for the education and training of any professional. Therefore the support, sponsorship and organisation of educational as well as scientific meetings, is another essential component of the work that EFOMP is carrying out to advance the professionalism of the Medical Physicist in Europe [8, 9, 10 and 11].

A number of recent European initiatives in lifelong learning [12, 13 and 14] have an impact on the education and training of all professionals including Medical Physicists. In this area EFOMP has to compare its relevant policy statement with these recommendations so that any gaps can be identified and taken care of.

Also, the European Directive on the recognition of professional qualifications [15 and 16], has an impact on the recognition of Medical Physics as a recognised profession. The recognition of Medical Physics as a profession by the European Union will allow the free movement of the Medical Physicist in all the European Union Member States.

II. discussion

The discussion that follows analyses the efforts of EFOMP and challenges than need to be met in each of the areas identified in the introduction in relation with the conclusions of Policy Statement No.12.

Policy Statement No. 12

This policy statement is based on the replies from a survey that was carried out between the EFOMP National Member Organisations (NMOs) in 2005 [17]. Twenty five out of the thirty four NMOs have participated in the survey.

O. Dössel and W.C. Schlegel (Eds.): WC 2009, IFMBE Proceedings 25/XIII, pp. 1–4, 2009.
www.springerlink.com

The most relevant conclusions can be summarised as follows:

- *Basic education:*
  - In all countries, the basic requirement to enter Medical Physics is a university degree. Master's degree 36%, BSc 28% and the remainder refer to a diploma, a license, first degree, etc.
  - The length of the basic university education ranges from 1½ to 5 years.
- *Post-graduate education in Medical Physics:*
  - Unfortunately, Medical Physics education is not yet regulated in some countries.
  - A nationally approved educational programme is in operation in 64% of the countries. The university gives approval in 16% of them, whereas in 40% the ministry of health is also involved in the approval. National Societies for Medical Physics having played an important role in setting-up the educational programmes in most countries.
  - There are basically 3 different approaches to post-graduate education:
    a) University studies only, leading to a Master's Degree or PhD in Medical Physics (12% of the overall countries).
    b) Hospital only: on-the-job training (12% of the overall countries).
    c) Combining University and Hospital (68%). In this approach the time spent in the hospital ranges from 1 month to 3 years.
  - The total length of Medical Physics education and training (basic university and post-graduate training) ranges from 2½ years to 9 years.
  - Completion of the educational programme leads to a diploma/license named very differently in each country.
- *Diploma or license to work as a Medical Physicist:*
  - In 56% of the countries, it is mandatory to hold a diploma or license to work as a Medical Physicist. In 4 countries this is only mandatory for 1 physicist per centre, or only to act as responsible Medical Physicist.
  - This diploma or licence is ''official'' in the sense that it is delivered by a governmental body in 48% of the countries.
  - Holding this diploma/license is the only way to be eligible for the job in 56% of the countries. Other possibilities such as: ''hold a Master's degree'' or ''3 years' work experience'', are also possible for the remaining countries.
  - It allows one to work as a Medical Physics Expert (MPE) in 52% of the countries.
  - It is equivalent to Qualified Medical Physicist (QMP), EFOMP definition, in 24% of the countries.
  - It is equivalent to Specialist Medical Physicist (SMP), EFOMP definition, in 28% of the countries.
  - It allows one to work in all areas of competence in 56% of the countries, whereas in 4 countries (16%) it depends on the areas selected by the Medical Physicist in their education and training programme (only one or two areas per training programme are possible).
- *Register of professionals:*
  - 68% of the countries have a register for Medical Physicists.
  - In 59% of them, an official body manages the register, whereas in 41% the Board of their own National Society for Medical Physics exclusively does so.
  - The register is compulsory in 35% of the cases and voluntary based in 53%. For the remainder it can be considered ''automatic''.
  - A renewal mechanism is in operation in 65% of the registers.
- *Continuous Professional Development (CPD):*
  - A formal CPD programme is in operation in 52% of the countries, fully or partially complying with the EFOMP recommendations.
  - CPD is used as a renewal mechanism in the Register in all of them.
  - The CPD cycle time, credit-point based ranges from 5 to 6 years.

It is evident from the above conclusions that the education and training in Medical Physics across Europe is far from being harmonised.

Also Continuous Professional Development programmes and Accreditation schemes are not established in all the survey participating National Member Organisations.

The European School of Medical Physics

This is an annual event in collaboration with the European Scientific Institute - ESI and takes place in Archamps, France. It consists of six weeks of intensive training in Medical Physics [3]. One week is spend on covering each of Medical Imaging with Non-ionising Radiation, Medical Imaging with Ionising Radiation, Medical Computing, Physics of Modern Radiotherapy, Brachytherapy, and Radiation Protection.

The first school was held in 1998.

European Network of Medical Physics Schools

This is a new initiative that is currently under development [7]. Moving a step further from just publishing policy statements the EFOMP Officer's have recently had discussions with interested parties on the establishment of a process for coordinating across Europe Continuous Professional Development Courses for Medical Physicists. This would ensure that these are harmonised and offer the same level of education irrespective of the institution delivering them.

Once the network is established details will be available on EFOMP's website.

EFOMP Sponsoring Programmes

The sponsorship of meetings and congresses is instrumental in disseminating and encouraging the adaptation of the policy statements. EFOMP organise, co-organise, support and recognise meetings, congresses and courses with its NMOs. Guidelines that explain the above terms and the requirements for interested NMOs to collaborate in such events can be found on EFOMP's website [8 and 9].

The purpose of these Guidelines is to help NMOs to obtain EFOMP sponsorship for their events by setting out the steps that they need to take and the conditions that must be fulfilled.

The biggest event is the biennial European Congress on Medical Physics. Note that there are detailed guidelines on the requirements for this event.

The encouragement of young scientists to pursue the profession of Medical Physics is of enormous importance to EFOMP. For this reason EFOMP gives awards to young scientists at the EFOMP Congress and provides bursaries to young scientists to attend the European School of Medical Physics [10 and 11].

Lifelong Learning

On the 23rd of April 2008, the European Parliament and the Council has issued recommendations on the establishment of the European Qualifications Framework (EQF) for lifelong learning [12]. With these recommendations the European Union is encouraging its Member States to compare and align their education and training qualifications with the eight (8) levels of learning outcomes described in these recommendations.

The purpose of this active EFOMP project is to position the various stages of the Education, Training and CPD of the Medical Physicist in Europe, as stated in the various EFOMP Policy Statements, within the eight levels of the EQF) for lifelong learning and identify any gaps that need to be addressed.

Figure 1 shows the preliminary results of the various stages of the education and training of the Medical Physicist in Europe according to EFOMP Policy Statement No.12 using the eight levels of the EQF for lifelong learning.

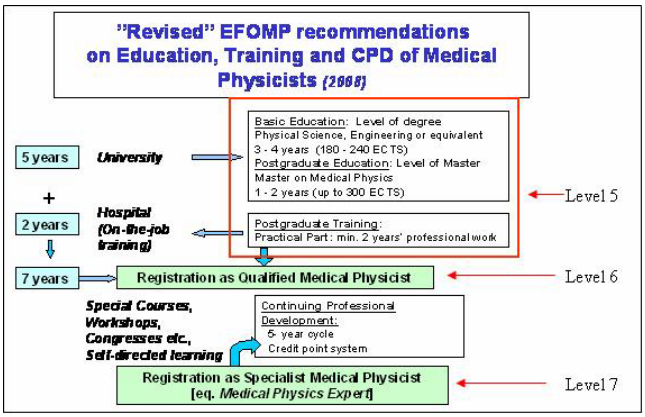

Fig. 1 The various stages of Education and Training of the Medical Physicist in Europe according to EFOMP Policy Statement No.12 using the 8 levels of the EQF for lifelong learning.

The level of graduation (Master's level) of the Medical Physicist corresponds to level 5 of the EQF for lifelong learning and the level of the QMP correspond to level 6. The level of the MPE corresponds to level 7.

Level 8 of the EQF for lifelong learning goes beyond the EFOMP Policy Statement No.12 and it corresponds to the Medical Physicist holding a Doctoral Degree (PhD) or higher, working in a research environment (University or Research institution).

EFOMP needs to develop a Policy Statement to bridge the gap between level 7 and level 8 of the EQF.

Medical Physics as a Profession

In due consideration of the following facts, EFOMP believes that Medical Physics should be recognised by the European Union as a regulated Health Profession in accordance with the EU Directive on the recognition of professional qualifications [15]:

a) Medical Physicists have a formal education and training in Anatomy, Physiology and Radiation Protection as applied to medical activities.
b) Medical Physicists have the necessary skills to manage the quality of the performance of the equipment used in hospitals.
c) Medical Physicists have a relatively long practical training in Hospitals.

d) Clinical professionals regard medical physicists as invaluable specialists who facilitate the safe use of radiation in hospitals.
e) Quality Assurance and Quality Control in Radiotherapy, Nuclear Medicine and X-Ray diagnosis is, normally, done by medical physicists. The results of these activities have clear implications on patient diagnosis, treatment and safety.
f) In most European Countries Medical Physics is a regulated profession by law.

There is more than enough evidence to prove all the above statements apart from two very important issues:

a) The education and training of the medical physicist is not harmonised across Europe according to the EFOMP Policy Statement No. 12.
b) The Medical Physics Profession is not regulated in all European Member States.

These two issues can only be resolved by the individual Member States by applying the EFOMP recommendations.

III. CONCLUSIONS

The above brief discussion describes the activities of EFOMP in the area of Education, Training and Professional Development of the European Medical Physicist.

These activities can only materialise through the collaboration of all the Medical Physicists of EFOMP's NMOs. The NMOs must actively adopt and implement the guidelines of the policy statements as well as participate in the various events organised by EFOMP in collaboration with its NMOs.

The contributions of all interested parties are more than welcome in order to further develop the harmonisation of the education, training and professional status of the Medical Physicist in Europe.

ACKNOWLEDGMENT

EFOMP acknowledges all those that have contributed to the development of its policy statements as well as all those involved in the organisation of educational and training events under its auspices.

EFOMP also would like to express its sincere thanks to all those that through the years have contributed actively in promoting the Profession of Medical Physics.

REFERENCES

1. Constitution of the European Federation of Organisations for Medical Physics, www.efomp.org/federation.html
2. EFOMP *Policy Statement 12:* The Present Status of Medical Physics Education and Training in Europe. New perspectives and EFOMP Recommendations. www.efomp.org
3. EFOMP European Schools of Medical Physics, www.efomp.org/federation.html
4. EFOMP *Policy Statement 6:* "Recommended guidelines of National Registration Schemes for Medical Physicists", www.efomp.org and Physica Medica XI(4), 1995, 157-159
5. EFOMP *Policy Statement 8:* "Continuing Professional Development for the Medical Physicist", www.efomp.org and Physica Medica XIV, 1998, 81-83
6. EFOMP *Policy Statement 10:* "Recommended Guidelines on National Schemes for Continuing Professional Development of Medical Physicists", www.efomp.org and Physica Medica XVII, 2001, 97-101
7. European Network of Medical Physics Schools,
8. EFOMP support of meetings, congresses and courses: Guidelines for National Member Organisations, www.efomp.org/federation.html
9. EFOMP Congresses: Policy and General Requirements, www.efomp.org /federation.html
10. EFOMP Congress awards for young physicists, www.efomp.org/federation.html
11. EFOMP ESMP bursaries for young physicists, www.efomp.org/federation.html
12. Recommendation of the European Parliament and of the Council of 23 April 2008 on the establishment of the European Qualifications Framework for lifelong learning, (2008/C 111/01), OJ C111, p. 1-7
13. Resolution of the Council and of the Representatives of the Governments of the Member States, meeting within the Council of 21 November 2008 on better integrating lifelong guidance into lifelong learning strategies, (2008/C 319/02), OJ C319, p. 4-7
14. Decision no 1357/2008/EC of the European Parliament and of the Council of 16 December 2008 amending Decision No 1720/2006/EC establishing an action programme in the field of lifelong learning, OJ L350, p. 56-57
15. Directive 2005/36/EC of the European Parliament and of the Council of 7 September 2005 on the recognition of professional qualifications, OJ L255, p. 22-142
16. Corrigendum to Directive 2005/36/EC of the European Parliament and of the Council of 7 September 2005 on the recognition of professional qualifications, OJ L271, p. 18-19
17. T. Eudaldo and K. Olsen, "The present status of Medical Physics in Europe: An EFOMP Survey", Physica Medica (2008), 24, p. 3-20.

Author: S. Christofides
Institute: Medical Physics Department, Nicosia General Hospital
Street: 215 Old Nicosia Limassol Road
City: Nicosia 2029
Country: Cyprus
Email: cstelios@cytanet,com,cy

Concerns of Editors and Publishers: Plagiarism, Rights of Authors, Open Access, etc.

C. G. Orton, Ph.D.

Wayne State University, Detroit, Michigan, USA

Abstract— **This presentation addresses concerns of Editors and publishers of journals including ethical problems, such as duplicate publication, fabrication and falsification of data, piracy and plagiarism, and mechanisms for journals to deal with these ethical issues. Also covered will be rights of authors and copyright issues, various forms of open access, the benefits of open access to society and potential problems it will cause for journals, authors, readers, and medical physicists in general.**

Keywords—**publication ethics, plagiarism, open access, journals, data falsification, data fabrication**

I. Introduction

Anything that concerns Editors and publishers is also of concern to authors and readers. These include ethical problems, such as duplicate publication, falsification and fabrication of data, piracy and plagiarism. Also of importance are the rights of authors, usually specified in a Copyright Agreement and, of vital importance for the viable future of journal publication in its current form, open (or "free") access.

II. Ethical problems

A. Duplicate publication

The Instructions for Authors for most journals specifically warn authors against simultaneous submission of identical, or near-identical, papers to different journals. Nevertheless, some authors still do this in order to increase the chances that their papers will be accepted for publication. Occasionally such an article makes its way through the reviewing process for two journals without detection of duel submission, and the paper gets published in both journals. Fortunately, such duplication is sometimes caught well before acceptance such as when a Referee is asked to review the same article by two journals and notifies the Editors. More commonly, however, duplicate publications are not uncovered until a reader realizes that two papers are identical and notifies the Editors.

B. Falsification and fabrication

In a recent study [1], it was demonstrated that publication of falsified and fabricated data was far more prevalent than commonly realized. The authors of this study contacted over 4000 scientists asking them to respond to questions related to ethical misconduct. A total of 2212 scientists (a 51% response rate) completed the questionnaire and, of these, 192 (8.7%) reported that they had observed significant breaches of research integrity by their fellow scientists. A total of 265 incidents were indicated. About 60% of these related to falsification or fabrication of data, and about 36% plagiarism. The academic ranks of culprits was fairly evenly distributed, with about 22% Professors or Senior Scientists, 14% Associate Professors or Scientists, 17% Assistant Professors or Scientists, 25% Postdoctoral fellows, and 14% graduate students.

One of the most highly publicized cases of research fraud involved the research paper of Dr. Hwang Woo Suk published in the journal *Science*, where he claimed that he had obtained stem cells from cloned human embryos, a stupendous achievement, of Nobel Prize proportions. Unfortunately, a University panel investigating claims of fraud discovered that he had fabricated much of his data and he subsequently resigned from his university post and lost the support for his research.

C. Piracy and plagiarism

The Council of Scientific Editors White Paper on Promoting Integrity in Scientific Journal Publications [2], defines piracy as *"the appropriation of ideas, data, or methods from others without adequate permission or acknowledgment",* and states: *"Deceit plays a central role in this form of misconduct. The intent is the untruthful portrayal of the ideas or methods as one's own"*. One of the most common forms of such piracy is plagiarism, defined as "*the use of text or other items (figures, images, tables) without permission or acknowledgment of the source of these materials*" and, most importantly, passing it off as if it were the author's own work. Common forms of plagiarism include reproducing, word-for-word, sentences of others, and often complete paragraphs, in papers, book chapters, or even complete books submitted for publication, and reproducing figures and illustrations without indicating the source.

O. Dössel and W.C. Schlegel (Eds.): WC 2009, IFMBE Proceedings 25/XIII, pp. 5–7, 2009.
www.springerlink.com

A blatant example: A physicist, in the process of reviewing a medical physics book, found that the author had reproduced entire paragraphs and figures from papers published in medical physics journals such as *PMB* and *Medical Physics*, without indicating their origins. He notified the Editors of these journals who, upon investigation, found that about 50% of the book had been plagiarized. The publisher was informed and subsequently withdrew this and a previous book by the same author that had been similarly plagiarized from sale and further printing.

Another example: A manuscript was submitted for publication to a medical physics journal and, during the review process, one of the Referees was astounded to realize that this was an exact reproduction of a paper he himself had published some years before in a different journal. He neither knew any of the authors of the submitted paper nor had given them permission to republish his work. The paper was, of course, rejected, and the author's institution was informed of this breach of ethics.

D. *Courses of action*

Most publishers and journals have established procedures to handle ethical misconduct. Elsevier, publishers of *Physica Medica*, for example, have published an Ethics Resource Kit that is available for all its journals [3]. Furthermore, Elsevier lists all its journals with the Committee on Publication Ethics (COPE) which, among other things, assists Editors of journals when dealing with potential cases of publication misconduct [http://publicationethics.org/]. Elsevier, as are most other publishers of scientific journals, is also involved in the use of plagiarism identification software and has a pilot study using CrossCheck, for example [http://www.crossref.org/crosscheck.html]. *Medical Physics* has a specific policy on plagiarism [4], and the Editor, Bill Hendee has written "An editorial on plagiarism" which was 1st published by the IOMP in the June 2008 issue of *Medical Physics World* [5] and subsequently reproduced in slightly modified form in both *Medical Physics* and *PMB*. *PMB* is covered by the Institute of Physics ethical policy for journals [6].

III. Rights of authors

All journals require authors to consent to a Copyright Agreement which usually transfers the copyright to the journal or publisher. Some authors are exempt from this, however, such as when the work described in the paper has been sponsored by certain granting agencies or the authors are government employees. These copyright agreements do, however, give authors and their employers certain rights of reproduction of their papers. Such rights typically include permission to post the final, formatted version of the paper on their own or their employer's website, and the right to post the author's version (not the formatted published version) on an e-Print server such as arXiv.org, provided a link to the online Abstract at the journal's website is provided.

A. *Reproduction of published material*

Any author wishing to reproduce any part of a copyright-protected article is required to first obtain permission of the author and the publisher. This includes short extracts, tables, figures, and diagrams. Publishers usually provide a "permission request" form for this purpose.

IV. Open access

Open (or free) access means that an article is made available to read online at no cost to the reader. Open access has many obvious benefits. Firstly, granting agencies claim that they (and often taxpayers) have already paid for the research, so why should they also pay for the publication? Secondly, libraries are constantly being required to reduce their expenditures and this would help their budgets considerably. Finally, with free access, authors' works would gain wider dissemination.

A. *Forms of open access*

Open access can take several forms. A journal might choose to make a few articles available online; some journals have agreed to make the entire contents available free online to scientists from developing countries; some online-only journals might make access to all articles free to all readers; some e-Print servers might make formatted published versions of some articles free and/or non-formatted published or otherwise unpublished articles free.

A few articles open access: journals might provide free access to certain articles for a variety of reasons. For example, authors may be given the option of paying a fee to have their papers placed free-access online (sometimes called "open choice"), or the journal thinks that certain articles are so important that they need to be widely disseminated, or when a granting agency is going to publish the article free online on an e-Print server anyway, why not make it free on the journal website?

Open access for developing countries: medical physics journals such as *PMB*, *Medical Physics*, and *Physica Medica*, provide free access to all their content to readers from developing countries via the eJournals Delivery Service of the ICTP [http://www.ejds.org]. In order to avoid abuse,

there is, however, a quota on article downloads per user: 3/day, 12/month, and 100/year.

Totally open access journals: several journals that publish medical physics articles are available entirely free to readers. These include the *Journal of Applied Clinical Medical Physics* of the American College of Medical Physics [http://www.jacmp.org/index.php/jacmp/index)], *BioMed Central Medical Physics* (a BioMed Central journal) [http://www.biomedcentral.com/bmcmedphys], *BioMed Central Medical Imaging* (also a BioMed Central journal) [http://www.biomedcentral.com/bmcmedimaging], and *Radiation Oncology* [http://www.ro-journal.com], again a BioMed Central journal. All BioMed Central journals are supported by article-processing charges. Current (2009) processing charges for *BioMed Central Medical Physics*, for example, are £1025/US$1465/€1140 per article. Since most authors are not used to paying page or article charges for publication in medical physics journals, it is not surprising that this journal has only been averaging about five articles published/year. Of interest with BioMed Central journals, is that the pre-publication history is published along with the article, including the names of the Referees and their reviews. Readers' comments are published also.

E-Print servers: two of the most important e-Print servers are PubMed Central and arXiv.org. PubMed Central, operated by the US National Institutes of Health (NIH), is a free digital archive of biomedical and life sciences articles which have been supported by funding from certain agencies, especially the NIH. Since these are published articles, they have already been peer-reviewed prior to posting in PubMed Central. In contrast, arXiv.org publishes articles that have not been published elsewhere and have not been peer-reviewed.

V. Why should editors and others be concerned about open access?

Clearly, open access has many benefits for potential readers, but there are serious issues to be considered by Editors and publishers, authors and readers.

A. Concerns of Editors and publishers

Journals need subscription funds to support the editorial process and the infrastructure needed to handle manuscripts such as reviewing, editing, formatting, and copyediting. All these will suffer if subscriptions are reduced or eliminated. Also, the open-access movement will drive journals to become online-only, thus eliminating the paper product which, for journals that publish advertisements, will decrease advertizing revenue considerably.

B. Concerns of authors and readers

If journals become open access, authors will need to bear the brunt of publication costs in the form of article or page charges. Authors might be more inclined to submit their papers to e-Print servers such as arXiv.org where there is no charge for publication but little or no peer-review. Clearly, quality will suffer.

C. Concerns of medical physicists

Medical physicists need to be concerned because journals often provide considerable financial support for their societies and this enables these organizations to, in turn, provide other valuable services to their members. These additional services will be reduced if journal profits decline, and/or annual membership subscriptions will need to be increased.

VI. Summary and conclusions

Publishing ethics is an increasing problem for Editors and publishers, especially plagiarism, which is difficult to detect but for which detection software is beginning to be employed. Copyright agreements strip authors of the rights of ownership of their material, but certain rights for posting their papers online are preserved. The open access movement is very active and this has many benefits for readers, especially those in developing countries. Editors, publishers, authors, readers, and medical physicists in general, need to be concerned, however, for a variety of reasons.

References

1. Titus, S., Wells, J., Rhoades, J. (2008) Repairing research integrity. Nature 453:980–982
2. Scott-Lichter, D. et al. The Council of Scientific Editors white paper on promoting integrity in scientific journal publications (2006) [http://www.councilscienceeditors.org/index.cfm]
3. Elsevier Publishing Ethics Resource Kit (PERK) (2008) [http://www.elsevier.com/wps/find/editorshome.editors/Introduction]
4. AAPM (2005) Policy on plagiarism in *Medical Physics* [http://www.aapm.org/org/policies/details.asp?id=206&type=PP&current=true]
5. Hendee, W. (2008) An editorial on plagiarism. Med. Phys. World 24:9,17 [http://www.iomp.org/mpweditions.htm]
6. Institute of Physics. Ethical policy for journals [http://authors.iop.org/atom/help.nsf/0/F18C019D6808524380256F630037B3C2?OpenDocument]

Electroporation of Bone Tissue: Implications for Use in the Treatment of Bone Metastasis with Electrochemotherapy

R. Cadossi[1], M. Fini[2], M. Ronchetti[1], F. De Terlizzi[1], and F. Cavani[3]

[1] IGEA – Clinical Biophysics, Carpi, Italy
[2] Laboratory of Preclinical Surgical Studies, Istituto Ortopedico Rizzoli, Bologna, Italy
[3] Department of Anatomy University of Modena and Reggio Emilia, Italy

Abstract – **Electrical pulses were applied to the distal femur of rabbits by inserting four electrodes in order to evaluate if and to what extent cell electroporation could be achieved in such a non-homogenous tissue. Dose response effect of number of pulses delivered was observed. 120 pulses at 1750V/cm successfully removed all osteogenetic activity among the electrodes, as evidenced by tetracyclin staining. These preclinical results lay the foundation for use of electroporation in the treatment of bone metastases.**

Key words – **Bone metastasis, electroporation, tumour ablation, tetracycline, electrochemotherapy.**

I. Introduction

Large electric fields, when applied across a cell, have the ability to permeabilize the cell membrane: this process is named "electroporation" and results in an increase in membrane permeability associated with the formation of nanoscale pores in the cell membrane [1]. Electroporation does not cause thermal damage, protein or collagen denaturation, this characteristic may be exploited when treating lesions proximal to critical anatomical features such as major blood vessels and nerves.

Electrochemotherapy (ECT) designates the combination of electroporation and cytotoxic agents, such as bleomycin or cisplatin, with the aim of creating transient direct access to the tumor cell cytosol for the drug and increase its cytotoxic activity [2,3]. In ECT clinical practice 8 pulses are used [4]. Increasing the number of pulses applied does not allow cell membrane repair resulting in cell death due to loss of homeostatic mechanisms, possibly as a consequence of uncontrolled Ca2+ influx into the cytosol.

Malignant bone disease is a devastating condition that is prevalent in patients with advanced cancers. The most common complications of bone metastasis are: pain, pathological fractures, medullar compression, hypercalcemia, reduction of movement and performance status. Effective treatments of bone metastasis are not yet available. In bone tumour and bone metastasis tumour cells at the margins of the lesion are interspersed within healthy bone trabeculae, thus posing a relatively high risk of local recurrence.

The use of ECT to eradicate tumour cells may play an important role as the presence of bone trabeculae may have a limited impact on the electric field. To the best of the authors' knowledge, the possibility of safely and effectively electroporate bone tissue in vivo has never been investigated. In this study, we examined the possibility of effectively electroporating osteoblasts and osteocytes as well as cell interspersed among bone trabeculae.

II. Methods

According to a protocol approved by the Institutional Review Board and strictly following Italian Laws on animal experiments eight male adult rabbits were used. The distal femur condyles were exposed and 4 stainless steel electrode with a 0.7 mm diameter were inserted in a square configuration at a distance of 4 mm in both legs, electrodes were cut and left within the bone until sacrifice to allow easier sample identification.

A custom tissue electroporation device derived from the Cliniporator™ (IGEA, Carpi, Italy) was employed. Electric pulses were delivered between two electrodes at a time in the six possible combinations: four sides and two diagonals. Approximated square wave 100 microseconds pulses at 4 Hz were applied. Potential between electrodes was 700 V over 4 mm and 1000 V over 5.7 mm (square diagonal): this yielded a nominal electric field of 1750 V/cm. Increasing number of pulse were tested: 50, 80 or 120 pulses. The animals well tolerated the treatment and returned to normal activity after the procedure. Animals were sacrificed seven days after electroporation.

To evidence the area residual osteoblastic viability in the electroporated tissue tetracyclin was administered i.m. 1 and 2 days after the procedure. At sacrifice, femur condyles were recovered and sectioned. Half of each sample was embedded in polymethlymethacrylate, microradiographed and evaluated under fluorescent light; the other half was

O. Dössel and W.C. Schlegel (Eds.): WC 2009, IFMBE Proceedings 25/XIII, pp. 8–9, 2009.
www.springerlink.com

decalcified and stained with Haematoxylin and Eosin for histological analysis.

III. Results

Microradiographic analysis of undecalcified sections showed no alteration of the mineral component of the bone tissue as a consequence of electroporation (figure 1).

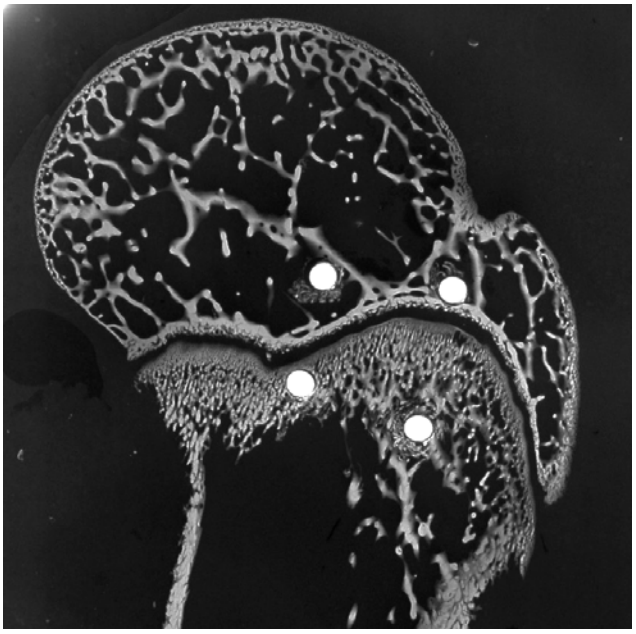

Fig. 1 Microradiographic image of the distal femur of a rabbit and the inserted electrodes.

Tetracycline staining showed lack of bone apposition (osteogenic activity) within the square delimited by the electrodes. The maximum ablated area was achieved with 120 pulses.

Toluidine Blue and Fast Green staining showed complete ablation of osteoblasts lining the trabeculae as well as osteocytes in the volume enclosed by the electrodes when 120 pulses were applied. Haematoxylin and Eosin staining of decalcified sections showed ablation of the cells interspersed within the trabeculae and the presence of inflammation and fibrin deposition in the electroporated area consistent with induced cell death.

IV. Discussion

The results of this preclinical study demonstrate the feasibility of electroporation for bone tissues ablation. The heterogeneous structure of bone did not prevent the complete electroporation of the cells within the electrodes and the extent of the ablated area around the electrodes depended on the number of pulses applied; at the same time the structural integrity of the bone and of the extracellular matrix was maintained. Altogether the findings lay the foundation for the development for the treatment of bone metastasis by electroporation.

References

1. Neumann E, Schaefer-Ridder M, et al. (1982) Gene transfer into mouse lyoma cells by electroporation in high electrical fields. The EMBO Journal 1, 841-845
2. Mir LM, Belehdradek M, Domenge C et al. (1991) Electrochemotherapy, a new antitumor treatment: first clinical trial. Comptes Rendus de l'Academie des Sciences Serie III Sciences de la Vie 313, 613-618
3. Orlowski S, Behradek Jr J amd Paoletti C (1988) Transient electropermeabilization of cells in culture. Increase in the cyttoxicity of anticancer drugs. Biochem Pharmacol 37, 4724-4733
4. Marty M, Sersa G, Garbay J R and (2006) Electrochemotherapy – An easy, highly effective and safe treatment of cutaneous and subcutaneous metastases: Results of ESOPE (European Standard Operating Procedures of Electrochemotherapy) study. EJC Supp 4, 3-13.

Ruggero Cadossi MD
Clinical Biophysics
IGEA
Via Parmenide 10/A
41012 Carpi (MO)
Italy
E mail: r.cadossi@igea.it

Education, clinical training and professional recognition of medical physicists

Ahmed Meghzifene

International Atomic Energy Agency, Vienna, Austria

Abstract— **the medical physicist fulfils an essential role in the safe and effective use of radiation in medicine, most commonly in cancer treatment or diagnostic imaging. Cancer rates are rising worldwide. This rate of increase is significantly higher in developing counties, thus requiring additional medical physics support. In recent years, the increasing complexity of both treatment and diagnostic radiation equipment, coupled with the raising of the expectations of good health care standards, as well as the implementation of more stringent radiation safety standards and accreditation requirements, has exacerbated the already critical shortage of fully qualified medical physicists in the developing world.**

The qualifications of an entry level medical physicist should consist of an appropriate academic degree at the postgraduate level followed by clinical training and professional accreditation, recognition or registration. While there are examples of countries with functioning academic, clinical and accreditation processes in place, many countries, in Africa and Asia for example, have limited or no programmes at all. The IAEA has a long history of involvement in medical physics education and training. As part of its technology transfer scheme in the field of human health, the IAEA provides support for education, on the job training and for attendance of specialized courses. Currently, the IAEA supports the training of around 200 medical physicists per year through short courses. The long-term strategy of the IAEA is to contribute to the establishment and harmonization of educational programmes in medical physics, including clinical training and professional accreditation/registration, in Member States. It is however recognized that this can only be achieved and sustained in countries where there is a critical mass of applications in radiation medicine (treatment and imaging) providing a foundation for structured practice. For countries where there is only a limited number of medical applications, the concept of consolidating medical physics education within larger regions is applied. The IAEA works in close collaboration with professional bodies and other international organizations to further strengthen medical physics education and professional recognition. As of 2009, the IAEA has launched a new initiative to strengthen medical physics in radiation medicine through an interregional technical cooperation project.

Keywords— **Medical physics, education, training, recognition**

I. Introduction

The medical physicist working in a hospital is a member of a health care team responsible for the diagnosis and treatment of patients. The qualified clinical medical physicist has an essential role in the overall diagnosis and treatment process, as well as in developing and implementing Quality Assurance (QA) programmes necessary to ensure the safe and effective care of patients. The specific duties required of the medical physicist will vary depending on the size of the institution. In smaller hospitals, the medical physicist may be responsible for the support of all areas including therapy, diagnostic radiology, nuclear medicine and radiation safety. In larger hospitals, the medical physicist may only be responsible for the support of one of these areas. In many cases, teaching and research is also included in the medical physics tasks.

In radiation oncology, medical physicists play a key role in accurately delivering radiation treatment to patients. They are also expected to provide support for updating equipment and implementing it safely within regulatory standards [1]. In the field of imaging, the primary responsibility of the medical physicist is development and supervision of implementation of a quantitative quality control program.

Proper training is a vital requisite for the medical physicist to properly fulfil their roles and responsibilities. The adequate training of a medical physicist should include academic training at the postgraduate level, as well as structured clinical training. Participation in a professional continuing education programme is also necessary to ensure the knowledge of the medical physicist is informed and current.

With proper training, the medical physicist can play a central role in modern clinics. The International Basic Safety Standards [2], published by the IAEA, has called for the involvement and support of a qualified medical physicists in radiation medicine. Subsequently the Directives of the European Union concerning basic safety standards and medical exposures [3, 4] have asserted a statutory requirement for physicists to be involved in the medical uses of ionizing radiation.

O. Dössel and W.C. Schlegel (Eds.): WC 2009, IFMBE Proceedings 25/XIII, pp. 10–12, 2009.
www.springerlink.com

II. THE ROLE OF THE IAEA AND ITS ACTIVITIES

A. The role of the IAEA

One of the statutory objectives of the IAEA is to promote the safe use of nuclear techniques in health. This is realized by transferring relevant technologies, including those used in medicine, to its Member States and emphasizing the need for QA for the safe and effective use of these technologies. In radiation medicine, it is especially important that procedures be supported with rigorous QA processes, and take into account the clinical, physical, technical, and safety aspects involved. Since the competency of the health care professionals is vital in treating and diagnosing patents, their education and training are considered paramount by the IAEA. Thus, the assistance provided by the Agency in the transfer of technology includes a large human resource component that deals with training. This is evidenced for example, by the fact that during 2006-2007 30 national and regional training courses were conducted in medical radiation physics (Fig. 1), which complimented technology transfers or facility upgrades. Follow-up communication with the course participants is now underway, and is being compiled in an effort to asses the impact such courses have had. In addition to this training component the IAEA has also engaged in the development of syllabi and Handbooks for teachers and students to assist Member States in setting-up indigenous education programmes in medical physics. The first such handbook was dedicated to radiotherapy physics and was published in 2005 [5]. To support the implementation of the Handbook for the training of medical physicists, relevant educational material has been made available in PowerPoint presentation format and, along with the handbook, is available for free download at the IAEA website [6]. Spurred by the success of this project, two similar Handbooks on medical physics in diagnostic radiology and nuclear medicine physics are in preparation.

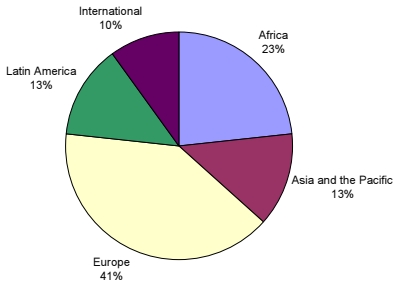

Figure 1. *Regional distribution of training courses and workshops in medical physics during 2006-2007*

B. IAEA approach to education and training requirements

An adequate education for a medical physicist should consist of an appropriate academic qualifications at the postgraduate level followed by a structured clinical training (residency programme) performed at a recognized or accredited hospital. A professional accreditation or registration with a competent body should be in place to ensure fulfillment of compliance. At present however, these comprehensive requirements are far from being carried out world wide. While there are examples of countries that do have adequate academic, clinical and accreditation processes in place, there are other countries in Asia, Europe, Latin America and Africa, that do not have clinical or accreditation/registration programs, and even some that do not have any functioning educational programs at all. In an effort to address world wide standards on the issue of clinical education, the IAEA is supporting regional Technical Cooperation (TC) projects in the field of medical physics, currently running in Asia, Africa and Latin America. These projects include the development and trialing of clinical training programs. However, a harmonization of clinical training requirements will be required at the international level. As part of these efforts, relevant professional societies are encouraged to assist with the harmonization process, and in the development of mechanisms of accreditation or registration.

C. IAEA's new initiative

The shortage of properly qualified clinical medical physicists, insufficient training (especially clinical training) and lack of professional recognition were identified as the main problems to be addressed by the IAEA. During the past few years, significant progress has been achieved in many countries through IAEA assistance. However, IAEA support has been targeted to the specific countries or regions that have requested assistance through the IAEA's TC programme.

To aid in the above mentioned issues, a new Interregional TC project "Strengthening Medical Physics in Radiation Medicine" (INT/6/054) has recently been approved and will be implemented during 2009-2012. This project will offer a unique opportunity to respond to the growing need for an internationally accepted definition of the role of a clinical medical physicist, initiate activities that support the harmonization of educational and clinical training material, and also promote the recognition of medical physics as a profession worldwide. This new IAEA initiative is supported by the professional societies.

III. CONCLUSIONS

In collaboration with international organizations and professional societies, the IAEA is in the unique situation of being able to assist in strengthening the professional structure of medical physics and ensuring the safe and effective use of radiation in medicine. Through its activities, it has established itself as a global tool for bettering the field, both in its capacity to collect international expertise and to respond to the needs of Member States. Inherent in this effort is the need to appropriately define what a clinical medical physicist is, to design activities that support the harmonization of educational material, and to promote the recognition of medical physics as a profession worldwide. These are goals which are actively being pursued by the IAEA.

ACKNOWLEDGMENT

The author would like to acknowledge the comments and input received from his colleagues Adam Kesner and Don Mc Lean.

REFERENCES

1. International Atomic Energy Agency, Setting up a Radiotherapy Programme: Clinical, Medical Physics, radiation Protection and safety Aspects, IAEA, Vienna, 2008
2. International Atomic Energy Agency, International Basic Safety Standards for Protection against Ionizing Radiation and for the Safety of Radiation Sources, Safety Series No. 115, IAEA, Vienna, 1996
3. European Commission. Council Directive 96/29/
4. European Commission. Council Directive 97/43/Eurotom
5. Radiation Oncology Physics: A Handbook for Teachers and Students, IAEA, Vienna, 2005
6. Slides Radiation Oncology Physics handbook, http://www-naweb.iaea.org/nahu/dmrp/slides.shtm)

Quantification of the experimental limitations of a semiconductor PET camera

D.C. Oxley[1*], A.J. Boston[1], H.C. Boston[1], J.R. Cresswell[1], A.N. Grint[1], L. J. Harkness[1], D. S. Judson[1], P.J. Nolan[1], I.H. Lazarus[2]

[1] University of Liverpool, Department of Physics, Liverpool, UK
[2] STFC Daresbury Laboratory, Warrington, UK

Abstract— **An investigation of the applicability of semiconductors to small animal positron emission tomography has been conducted. The SmartPET collaboration has been responsible for successful experimental work demonstrating how these detectors could enhance small animal imaging devices. Highly encouraging experimental results present an improvement in image resolution to ~2mm (full width at half maximum). In order to understand current experimental limitations and overcome these in future systems, we have carried out a Monte Carlo study to systematically quantify experimental image distortions in terms of the image resolution of a point source. With a full understanding of experimental sources of error, the full potential of the existing SmartPET system can be understood. This ground work will allow the imaging of more complex phantom geometries to assist a transition into preclinical trials. This work also permits an optimized system to be designed in future.**

Keywords— **high-purity germanium, PET, system modeling, semiconductor**

I. Introduction

The developments of non-invasive, structural and functional imaging techniques have permitted great advancements in medicine. Positron Emission Tomography (PET) is a functional imaging modality which relies on the annihilation of a positron (e^+) with an electron to create two back-to-back 511keV γ-rays. Their coincident detection defines a line of response (LOR) from which the annihilation point is reconstructed. By radiochemically tagging a specific component of the bloodstream with an e^+ emitter, the oxygen consumption of an organ can be assessed, from which its behavior and health can be inferred. Such scans are conducted on small animals to provide an essential pre-clinical testing platform for pharmaceutical drugs. In addition, they can enhance symptom identification for diagnostic purposes and are a large data source for psychological studies.

In recent years, segmented semiconductors have been proposed as an alternative detector type to the currently favored scintillators in small animal imaging. Scintillators are chosen for their high stopping power, efficiency and low cost. However the position-dependent charge collection of a semiconductor is a means to improve spatial resolution down to the mm^3 level. This level of spatial precision is challenging to obtain using scintillators due to restrictions in the size of the photomultiplier tube. Current scintillator systems also struggle to accurately determine the depth of interaction (DOI) without introducing additional detector layers at further cost. The three dimensional sensitivity of semiconductor detectors enables higher position resolution in this dimension. The lower Z of a semiconductor reduces the number of single full-energy absorptions; however their spectroscopic ability allows the γ-ray's path within the crystal to be tracked regaining a large fraction of events. The aim of this work is to understand the experimentally achieved results using a prototype small animal imaging system (SmartPET) based on high-purity germanium (HPGe). GEANT4 [1] simulations have been conducted of SmartPET to systematically quantify the various contributions to image distortion. This prototype system has also found applications in electronically collimated single photon emission computed tomography (SPECT) [2].

II. The SmartPET System

A. The experimental system

The SmartPET system is a dual-headed PET camera utilizing two HPGe planar detectors. The SmartPET detectors were manufactured by ORTEC to the specifications of the University of Liverpool. Each of the detectors has a crystal size of 74mm x 74mm x 20mm, with an active volume of 60mm x 60mm x 20mm. The outermost 7mm of each of the lateral (x-z) dimensions form the guard ring of the detector. The crystal is cooled to 77K and assembled in a vacuum cryostat. The charge generated by an interaction is collected on contacts of 50μm or 0.3μm thickness (depending on the detector face). Both charge collection contacts are electronically segmented, orthogonally, into two sets of 12 strips. This segmentation allows a position resolution of 5mm x 5mm x 20mm by cross-referencing which strips recorded charge. The application of pulse shape analysis [3] enables the position resolution to be enhanced beyond the dimen-

O. Dössel and W.C. Schlegel (Eds.): WC 2009, IFMBE Proceedings 25/XIII, pp. 13–16, 2009.
www.springerlink.com

sions of the raw pixels into 1mm x 1mm x 2mm voxels. An example of the experimental capabilities is given in Figure 1. The figure depicts a reconstruction of a glass rod with an inner diameter d_{in}=2.5mm filled a liquid e^+ emitter (^{22}Na). The reconstructed width of the glass rod is 2.7mm. A more detailed description can be found in reference [4].

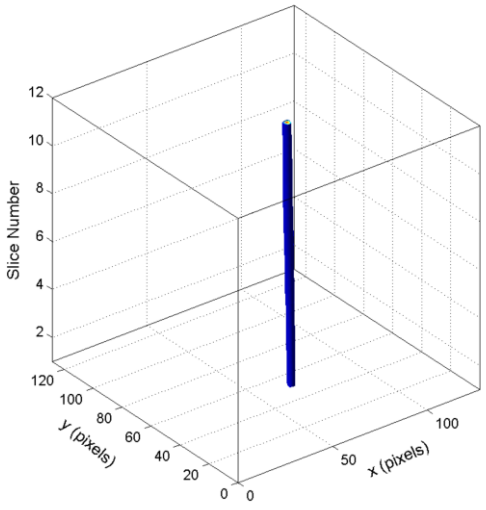

Figure 1: A reconstruction of experimentally acquired data from a glass rod filled with ^{22}Na. The full width at half maximum of the rod is 2.7mm.

B. The SmartPET model

The previously described SmartPET scanner was modeled using GEANT4 [1], a very flexible and versatile Monte-Carlo simulation package developed to reliably reproduce the interactions of radiation with matter. In all simulations it is important to compare the results with experimental measurements to ensure confidence in the theoretical data. This validation was performed for the SmartPET model by comparing absolute efficiencies at various energies ranging from 60keV – 1400keV. A close agreement between experiment and simulation is obtained. A more detailed discussion of the experimental validation is found in [5].

C. Data Acquisition

Data were simulated by rotating the two planar detectors in increments of 10˚ over a range of 0˚ - 180˚. In the simulations, as in the experiment, the detectors were separated by a distance d =13cm. An event was stored if a coincidence was detected between the two 511keV photons created by the positron-electron annihilation. No energy gates were applied. Images were produced using a 2.5D imaging algorithm [6], which reconstructs the volume of the field of view (FOV) as multiple 2-dimensional planar slices. Therefore, to reduce the amount of data and the simulation running time, a further restriction was placed on the coincidence being in the same x-dimensional slice. As these are the only events processed by the imaging algorithm, no data is lost by applying this restraint. The effect of this condition on image resolution was investigated and shown to be insignificant [7].

A point source was positioned at the (0.25, 0.0, 0.0) cm coordinate. The offset in x-dimension places the source centrally within a reconstruction slice. 50 million e^+ emissions were simulated per angular position.

III. Quantifying Experimental Uncertainties

In order to understand the impact which semiconductor technology could have on the small animal imaging field, the effect of the individual sources of image distortion must be quantified. Although some of these uncertainties have a physical nature, many can be improved by using an optimized semiconductor system. Empirical work on understanding resolution degradation for scintillator PET exists in [8]. This study takes a quantitative approach for semiconductor PET and focuses on the lateral position resolution of the detector, the depth of interaction (DOI), the positron range and the clustering of events within a pixel. All these parameters may be fully manipulated through the simulation software.

A. The "Perfect" Reconstruction

The first stage of this process is to define a perfect image. In this image, there shall be no kinetic energy assigned to the positron, reducing the range to zero. The precise interaction positions shall be reconstructed directly without any additional pixelization or blurring. The lateral (Δx, Δz) and depth (Δy) position resolution of the interactions are set to 0.25mm, as this corresponds to the maximum number of positions processable by the reconstruction algorithm. For PET reconstruction, it is important to identify the first interaction in order to define a correct LOR. This shall also be done accurately for every event.[1] A point source was reconstructed using a filtered backprojection (FBP) [6] algorithm under these conditions. The full width at half maximum (FWHM) was found to be 0.4mm.

[1] The effects of a first hit misidentification shall not be studied here.

B. The Positron Range

In β^+-decay the Q-value (Q_V) of the reaction is shared between the two light reaction products, a positron (e^+) and a neutrino (ν). The continuous β^+ energy spectrum for the positron has been reproduced using (1), where[2] α =2, β=5 and P(E,α,β) is the probability of an emitted energy E.

$$P(E,\alpha,\beta) = E^{\alpha-1}(1-E)^{\beta-1} \quad (1)$$

The probability distribution is then normalized to ensure the total probability is unity. A kinetic energy E_{kin} = P(E,α,β)*Q_V was assigned to the positron in order to understand the image distortion caused solely by its distance traveled before annihilation (positron range). This multiplication scales the energy correctly to match the distribution expected from a β-decay product. In our experiments [4] ^{22}Na sources (Q_V = 545keV) were imaged. This Q-value corresponds closely to the Q-value of ^{18}F (Q_V =634keV) allowing these results to be transferred to a clinical environment. The final FWHM of the image including the positron range is 1.17mm.

C. The Effect of Lateral Spatial Resolution

The spatial resolution of the simulation was degraded in order for it to match the achievable spatial resolution of the detector. The lateral spatial resolution was distorted in isolation from the depth resolution for two reasons. Firstly, in a semiconductor the methods [3] by which the spatial resolution is enhanced differs for the x-z plane and the y dimension. Secondly in a clinical context, using scintillator PET, the DOI is much harder to determine than the lateral interaction position. It is therefore profitable to separate these parameters.

The SmartPET system is currently capable of 1mm lateral spatial resolution. For this case, the image resolution degrades to 1.4mm. The relationship between image resolution and lateral spatial resolution is illustrated in Figure 2. The x-axis values are negative to allow increase in resolution to flow from left to right.

D. The Effect of Depth Resolution

For geometric reasons the impact of the depth sensitivity (Δy) on the reconstructed image will always depend on the separation between the detectors (d). In these results, d was a constant value of 13cm. For this setup with a point source reconstructed with a 1mm lateral position resolution the depth was shown to have minimal effect on image quality. Specifically using Δy = 20mm for no position enhancement the FWHM of the reconstructed image is 2.1mm. If Δy decreases, the image resolution improves only at first. This is believed to be because an offset in depth of a few mm has low impact on a LOR defined across 13cm separation. A geometrical calculation verifies the worst-case angular parallax error on a LOR introduced by Δy is >2° for Δy=20mm but < 0.2° for Δy=2mm.

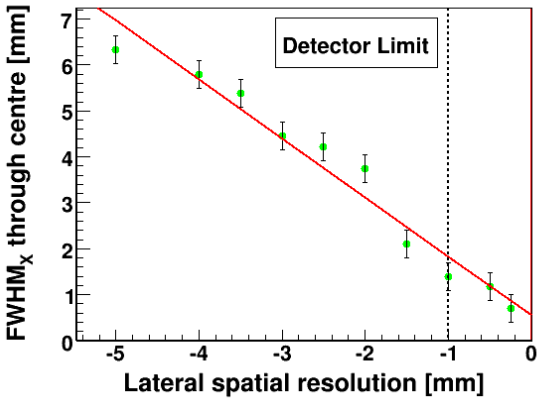

Figure 2: The effect of adding lateral spatial resolution on image resolution. The vertical line indicates the currently achievable detector limit.

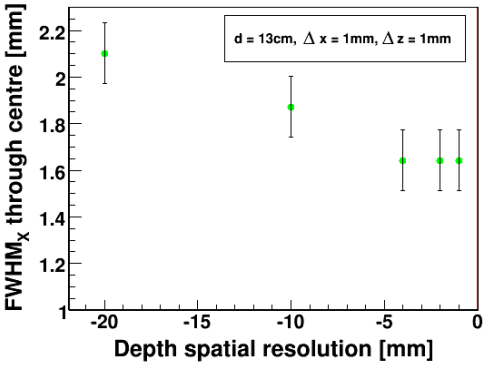

Figure 3: The FWHM of the reconstructed image as a function of the depth resolution (Δy).

E. Clustering of Interactions

In an HPGe detector the probability of multiple interactions is higher than in a scintillation counter due to the lower Z. Simulations have shown that the average number of interactions within one SmartPET detector at 511keV is ~2. Simulations indicate ~32% of the γ-ray interactions are confined to one 5mm x 5mm x 20mm voxel in both SmartPET detectors. Yet within this subset there is also a significant (64%) probability of multiple interactions occurring

[2] These values were selected for the continuous distribution of counts vs. energy to closely match a β particle energy spectrum.

within this voxel. Currently, the implemented algorithms are unable to distinguish these interactions and the summed interaction is processed. Such algorithms are being developed in [7]. To account for the image blurring caused by this eventuality, two images were reconstructed. Both were produced using only events where, in each detector, the energy deposits were confined to one voxel, including data with multiple interactions in one voxel. For one image, the first hit within the voxel was correctly identified and utilized in the image reconstruction. In the second image, multiple interactions (if present), were combined using a weighted average algorithm based on (2), where x_s,y_s,z_s are the summed x, y, z coordinates of N interactions with energies E_1, E_2…E_N.

$$\begin{pmatrix} x_S \\ y_S \\ z_S \end{pmatrix} = \frac{E_1 * \begin{pmatrix} x_1 \\ y_1 \\ z_1 \end{pmatrix} + E_2 * \begin{pmatrix} x_2 \\ y_2 \\ z_2 \end{pmatrix} + \ldots + E_N * \begin{pmatrix} x_N \\ y_N \\ z_N \end{pmatrix}}{E_1 + E_2 + \ldots + E_N} \quad (2)$$

The distortion caused by the offset in the first interaction due to the presence of N other interactions was investigated. The FWHM of the point source was 1.64mm (2.11mm) before (after) the algorithm was applied. Both data sets have a 1mm lateral spatial resolution and a depth resolution of 4mm.

The final stage of this analysis is to include all experimental image distortions simultaneously. A reconstruction of this data set is displayed in Figure 5. The FWHM of this image is slightly less than the FWHM of existing experimental point sources (2.98mm) acquired using the SmartPET system [4, 6]. This is believed to be due to higher statistics in the simulation and the impact of random events. A systematic documentation of the effect of each individual distortion parameter on image quality is found Table 1. Unless otherwise stated, "lateral" refers to a resolution of 1mm in x and z-dimensions and "depth" to resolution of 4mm in the y-dimension.

IV. Conclusions

By using simulated data, the impacts of various sources of image distortion have been quantified. This step is very important in both the expansion of semiconductor techniques and the design of new systems. The two parameters which introduce the largest distortion in a reconstructed image are the positron range and the clustering of interactions within pixels. This work has lead to the development of a technique to deconvolve multiple interactions within a voxel to regain image resolution [7].

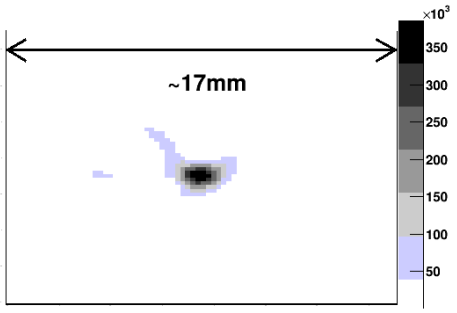

Figure 4: A summation of all experimental distortions investigated in the same image. The FWHM is 2.34mm

Image Type	FWHM[mm]	Error
"Perfect"	0.4	0.17
"Perfect" + e^+	1.17	0.17
"Perfect"+lateral	1.40	0.17
"Perfect"+lateral+depth(20mm)	1.87	0.17
"Perfect"+lateral+depth	1.64	0.17
"Perfect"+lateral+depth+e^+	1.64	0.17
"Perfect"+lateral+depth+cluster	2.11	0.17
"Perfect"+lateral+depth+cluster+e^+	2.34	0.17
Experiment[4]	2.98	0.17

Table 1: The effects of the individual sources of image distortion in various combinations are documented.

Acknowledgment

The authors would like to thank the EPSRC for their financial support.

References

1. Agostinelli, S. et al. Nucl. Instr. and Meth. A 506 (2003) 250-303
2. Harkness L. et al. Nucl. Inst. And Meth. A. *In Press*
3. Vetter, K et al.., (2000) Nucl. Instr. and Meth. A 452: 223 -228
4. Cooper, R.J. et al. (2009) Nucl. Instr. and Meth. A *submitted*
5. Oxley, D.C., et al. Nucl. Instr. and Meth. A (2009) *In Press*
6. Mather, A.R., PhD Thesis, University of Liverpool (2006)
7. Oxley, D. C. et al. PhD Thesis, University of Liverpool, *in preparation*
8. Moses, W. W. et al. J. Nucl. Med., vol. 34 (1993) pp. 101P.

Author: D Oxley
Institute: Department of Physics, University of Liverpool
Street: Oxford Street
City: Liverpool
Country: UK
Email: dco@ns.ph.liv.ac.uk

Nanosecond-Duration Electric Pulses Open Nanometer-Size Pores in Cell Plasma Membrane

A.G. Pakhomov[1], B.L. Ibey[2], A.M. Bowman[1], F.M. Andre[1], and O.N. Pakhomova[3]

[1] Old Dominion University, Frank Reidy Research Centre for Bioelectrics, Norfolk, VA, USA
[2] Radio Frequency Radiation Branch, Human Effectiveness Directorate, Air Force Research Laboratory, Brooks City Base, TX, USA
[3] University of Texas Health Science Center, Department of Biochemistry, San Antonio, TX, USA

Abstract— **We found that ultra-short electric pulses (60 or 600 ns duration) applied to mammalian cells cause profound, dose-dependent increase of plasma membrane electrical conductance. This effect is detectable even minutes after the exposure and is explained by formation of long-lived, voltage-sensitive, inward-rectifying pores of nanometer diameter ("nanopores"). The phenomenon of nanoelectroporation and the extended lifetime of nanopores can also be demonstrated by a surge of Tl^+ uptake in the presence of K^+ channel blockers, as well as in CHO cells that express no endogenous voltage-gated K^+ channels. Due to their long lifetime, nanopores can have significant impact on cell physiology.**

Keywords— **electroporation, cell membrane, lipidic pores**

I. Introduction

Commonly known effects of electric pulses are electrostimulation and cell membrane electroporation. The study expands conventional electrophysiology into a new area of bioeffects of ultrashort, high-voltage electric pulses (USEP). USEP were found to be able to induce some unique bioeffects, probably because of (1) producing very fast, large transmembrane voltage gradients, and (2) electric field penetration through plasma membrane to intracellular structures. Our previous studies established that USEP cause long-lasting (minutes) increase of plasma membrane electrical conductance [1, 2]. Exposure to multiple pulses caused cell swelling and blebbing due to osmotic misbalance. At the same time, the plasma membrane remained mostly impermeable to larger (1.2-1.5 nm) ions that are commonly employed to test the membrane integrity, such as propidium$^+$. Hence, one can conclude that a USEP treatment opens conduction pores (CPs) that allow for passage of small ions and thereby increase transmembrane electrical conductance, but do not allow for passage of larger ion species. The present study was intended to analyze the conductive properties, permeability, and lifetime of USEP-opened CPs.

II. Methods

Cell cultures. We used GH3 (a murine pituitary) and CHO-K1 (Chinese hamster ovary) cell lines. These cell lines have distinctly different morphology and physiology, which could potentially affect their sensitivity to USEP. Pituitary cells, including GH3, may express numerous plasma membrane channels, including tetrodotoxin-sensitive Na^+ channels, voltage-sensitive Ca^{2+} channels, transient and delayed rectifying K^+ channels and multiple Ca^{2+}-sensitive K^+ channel subtypes. In contrast, CHO cells express few endogenous channels and typically display no voltage-sensitive currents at all. Hence, comparison of USEP effects in GH3 and CHO cells could help understanding of how various ion channels contribute to the change in plasma membrane properties after USEP exposure.

Both cell lines, cell growth media and supplements were obtained from American Type Culture Collection (ATCC, Manassas, VA). Cells were grown in 75-cm^2 flasks at 37°C with 5% CO_2 in air. GH3 cells were cultured in Ham's F12K medium supplemented with 2.5% fetal bovine serum (FBS) and 15% horse serum. CHO cells were propagated in Ham's F12K medium supplemented with 10% FBS. The growth media also contained 1% penicillin/streptomycin. Immediately preceding the experiments, cells were transferred onto glass cover slips pre-treated with poly-L-lysine (Sigma-Aldrich, St. Louis, MO) to improve cell adherence.

Chemicals and solutions. A standard extracellular buffer contained (mM): 135 NaCl, 0 or 5 KCl, 2 $MgCl_2$, 10 HEPES, and 10 glucose. Pipette solution typically contained 150 KCl, 2 or 4 $MgCl_2$, and 5 HEPES. Depending on the needs of a particular experiment, the solutions could be modified by (a) replacing Na^+ and/or K^+ with other monovalent cations, (b) replacing most of Cl^- with other monovalent anions, (c) adding 5 mM EGTA for chelating any free C^{2+} ions, and (d) removing glucose from the extracellular buffer, and using such extracellular buffers also for pipette filling ("symmetrical" conditions).

O. Dössel and W.C. Schlegel (Eds.): WC 2009, IFMBE Proceedings 25/XIII, pp. 17–20, 2009.
www.springerlink.com

The pH level of the buffers was adjusted to 7.2 (pipette) or 7.4 (bath) by titration with the base of the principal cation. The osmolality of all solutions was between 290 and 310 mOsm, as measured with a freezing point microosmometer (Advanced Instruments, Inc., Norwood, MA, USA). All chemicals were purchased from Sigma-Aldrich.

Patch clamp recording. Cells on a cover slip were transferred into a glass-bottomed chamber (Warner Instruments, Hamden, CT) mounted on a motorized stage (Prior Scientific Inc., Rockland, MA) of an IX71 inverted microscope (Olympus America Inc., Center Valley, PA), configured with an Olympus FluoView TM 300 confocal laser scanning microscope. Pipettes for patch-clamp recording were manufactured from borosilicate glass (1B150F-4, World Precision Instruments, Sarasota, FL, or BF150-86-10, Sutter Instrument, Novato, CA). They were pulled to a tip resistance of 1.5-3 MOhm using a Flaming/Brown P-97 Micropipette puller (Sutter). Electrophysiology data were acquired using a Multiclamp 700B amplifier, Digidata 1322A A-D converter, and pCLAMP 10 software (Molecular Devices, Foster City, CA). The analog signal was low-pass filtered at 2 or 5 kHz, and digitized at "oversampling" rates of 10 to 50 kHz. The series resistance was not compensated. Typical values of the seal and access resistance were 2-8 GOhm and 4-10 MOhm, respectively.

All transmembrane voltage values reported below were corrected for respective junction potentials.

Exposure to USEP and local E-field modeling. Nearly rectangular 600-ns pulses were generated in a transmission line-type circuit, by closing a MOSFET switch upon delivery of a TTL trigger pulse from pCLAMP via a Digidata output. USEP were delivered to the selected cell by a pair of tungsten rod electrodes (0.1 mm electrode diameter, 0.14-0.2 mm gap). With a help of a micromanipulator, the electrodes were positioned touching the surface of the cover slip on the sides of the selected cell (Fig. 1). Alternatively, the electrodes could be placed precisely 50 um above the cover slip surface (to avoid any mechanical shift of the cover slip with cells, which could destroy the patch-clamp recording configuration).

The E-field between the electrodes was determined by a 3D simulation with the finite element Maxwell equations solver Amaze-3D (Field Precision, Albuquerque, NM). The E-field at the location of the cell was practically uniform, yielding about 60 kV/cm per 1 kV amplitude of the applied pulse (or about 40 kV/cm per 1 kV when the electrodes were 50 um above the cover slip).

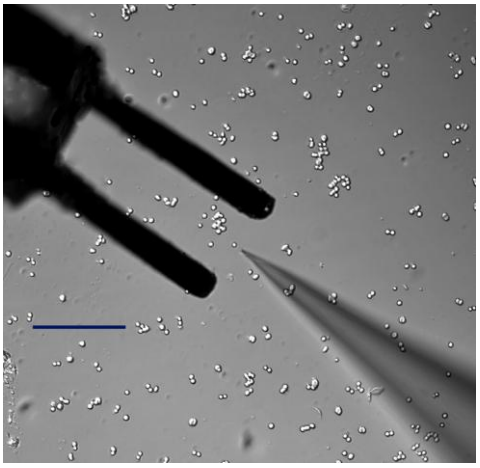

Fig. 1 Relative positions of stimulation electrodes for USEP delivery and a patch-clamp recording pipette. The cell that will be exposed to USEP in this experiment is in the front of the pipette tip. Calibration bar: 200 μm.

In isolated experiments, we also used 60-ns pulses, which were delivered to cells in a similar manner. More detail about the 60-ns pulse exposure can be found in earlier papers [1, 2]

III. Results

Dose-response studies. As a first step, we explored how the effect of USEP on cell plasma membrane depends on physical parameters of USEP. Specifically, we compared the effects of 60- and 600-ns pulses at E-field intensities from 1 to 22 kV/cm, in GH3 and CHO cell lines [3].

The resting membrane resistance (Rm) was measured in voltage clamp mode, 100-140 sec after the pulse, by applying a 10- or 15-mV positive voltage steps from the holding level of -80 mV. We found that both 60- and 600-ns pulses decreased Rm, with the threshold at less than 6 kV/cm for 60-ns pulses, and at less than 1 kV/cm for 600-ns pulses. Further analysis established that USEP at both tested pulse durations produced equal bioeffects when the absorbed dose (AD) was the same (Fig. 2). In other words, it was AD rather than any other single parameter of exposure (E-field; pulse width; specific absorption rate; exact pulse shape or rise time) that determined biological effectiveness of USEP. The threshold AD to produce plasma membrane effects was at or below 10 mJ/g both in GH3 and CHO cells. Despite being determined by the dose, the USEP effect clearly was not thermal, as the maximum heating at the threshold dose was less than 0.01 ^{o}C.

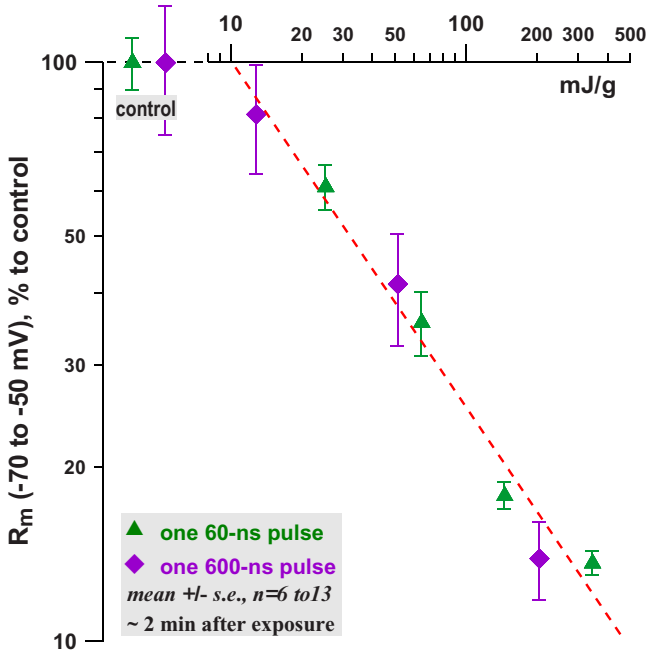

Fig. 2 The effect of 60- and 600-ns pulses on membrane resistance in CHO cells plotted against the absorbed dose.

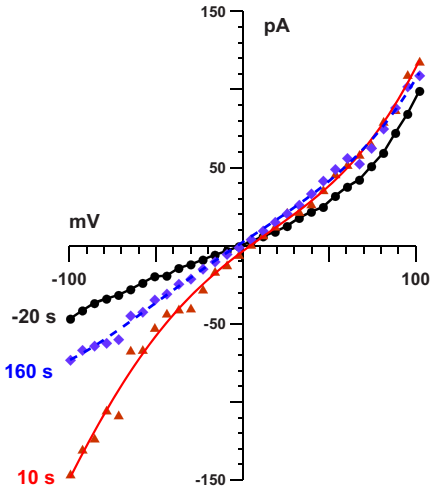

Fig. 3. Typical effect of a single USEP on transmembrane conductance. The current-voltage (I-V) curves were recorded in a whole-cell configuration 20 s before a 600-ns, 1.6 kV/cm pulse (●), and 10 sec (▲) and 160 sec (◆) after it. Measurements were performed in symmetrical solutions containing (mmol) K-Acetate, 150; $MgCl_2$, 1; HEPES, 5. Note profound increase of the inward current (at negative voltages) after USEP exposure, but little or no effect at positive voltages ("inward rectification"). Note also partial recovery by 160 sec after the treatment.

Inward rectification. Perhaps the most characteristic feature of cell permeabilization by USEP was inward rectification of the current through the plasma membrane. Inward rectification was not simply a result of different ionic composition of the bath and pipette solutions, because making these solutions identical did not eliminate rectification As shown in Fig. 3, USEP drastically increased the inward current, but had no effect on the outward one. The recovery the initial level of membrane conductance typically took several minutes.

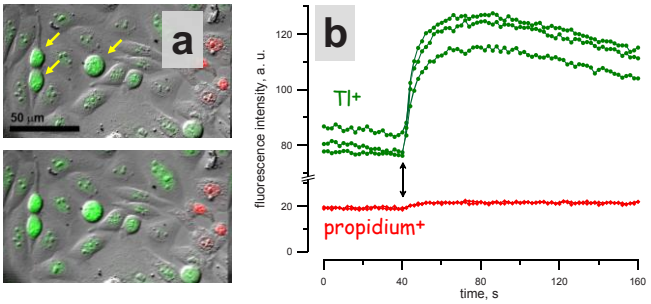

Fig. 4. USEP exposure triggers Tl^+ uptake, but cells remain impermeable to propidium$^+$. CHO cells were pre-loaded with a Tl^+-sensitive fluorophore FluxOR™ and placed in a buffer that contained Tl^+ cations, a cocktail of K^+ channel blockers, and 30 μg/ml of propidium iodide. (**a**) Overlaid Tl^+-dependent emission (green) and propidium emission (red) and DIC images before (top) and 10 sec after one 600-ns pulse at 8.8 kV/cm (bottom). A group of cells that were "dead' (displayed red fluorescence) prior to USEP exposure served as a positive control for propidium uptake. Note increase in Tl^+-dependent fluorescence, but no propidium uptake by nsEP-exposed cells. (**b**) Quantitation of USEP-induced emission changes in three cells identified by arrows in panel (a). USEP was applied at 40 sec into the experiment. Note that an apparent increase in propidium emission (red trace) actually is an artefact due to incomplete separation of Tl^+ and propidium emissions. This increase disappeared if Tl^+ was omitted from the bath buffer.

Non-electrophysiological detection of USEP-opened CPs. While patch clamp is arguably the most informative approach to explore nanopores' currents, the membrane permeabilization effect can be verified independently by non-electrophysiological methods. We employed a FluxOR™ Thallium Detection Kit (Invitrogen, Eugene, OR) to visualize nsEP-triggered Tl^+ entry into GH3 and CHO cells (Fig 4). Since Tl^+ can potentially enter the cell via voltage-gated K^+ channels (if they are somehow activated by nsEP), the bath buffer contained a cocktail of potent K^+ channel blockers. USEP caused a distinct surge in Tl^+-dependent fluorescence in GH3 cells and even greater response in CHO cells (which do not even express voltage-gated K^+ channels). Notably, USEP intensities sufficient for sustained Tl^+ entry were far below the threshold for propidium uptake. When both propidium and Tl^+ where present in the bath buffer throughout the experiment, nsEP-treated cells displayed profound increase in Tl^+-dependent fluorescence, but no change in propidium fluorescence

(except for a minor bump due to a "cross-talk" of the two detector channels). The removal of Tl^+ from the bath medium and its replacement with Cs^+ fully eliminated the "bump" in propidium emission (data not shown).

To probe the lifetime of USEP-opened pores, Tl^+ was removed from the medium prior to USEP treatment, and replaced with an equimolar amount of Cs^+. Addition of the Tl^+-containing buffer at various time intervals after USEP caused a profound surge in fluorescence if the cells were still permeable to Tl^+. As can be seen from Fig. 5, resealing of USEP-opened pores can take several minutes. This finding is fully consistent with our earlier observation using patch-clamp that restoration of membrane electrical resistance after USEP can take as long as 10-15 min [1].

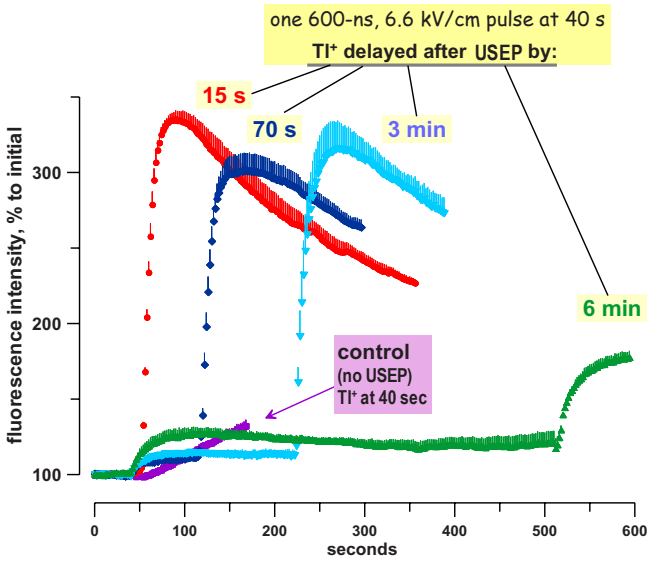

Fig. 5. Probing the lifetime of USEP-opened pores by delayed Tl^+ uptake. CHO cells loaded with FluxOR dye were placed in a solution that contained a cocktail of K^+ channel blockers, but no Tl^+. Cells were stimulated by one 600-ns, 6.6 kV/cm pulse at 40 sec into the experiment. Tl^+-containing buffer was added at different time intervals after USEP, causing an immediate surge in emission if the cells were still permeable to Tl^+ (i.e., if the USEP-opened pores have not resealed yet). On the contrary, addition of the Tl^+-containing buffer to cells that were not treated by USEP caused just a slow, gradual increase of emission due to Tl^+ endocytosis (negative control). Shown are mean values +/- s.e. for 3 to 6 cells per group; error bars are shown in direction only for clarity.

IV. Summary and Discussion

The experiments described above established that USEP produced long lasting permeabilization of plasma membrane in mammalian cells. Contrary to pores opened by conventional electroporation, USEP-opened pores were inward-rectifying, voltage-sensitive, and impermeable to propidium cation. Based on propidium ion crystal structure box dimensions (13.8 x 11.5 x 5.4 A), the maximum diameter of USEP-opened electropores can be estimated at about 1 nm (hence the name "nanopores"). When nanopores were first introduced in literature [4], their lifetime was expected to be on the order on nanoseconds, or microseconds at most. However, we have clearly showed it by both patch-clamp [1] and by the fluorescent imaging (Fig.5) that nanopores are anomalously stable and have the lifetime on the order of minutes. We suggest that it could be the continuity of the water column within the nanopore that prevents it from collapse; however, this conjecture needs to be experimentally verified.

Thanks to their extended lifetime, nanopores can have profound impact on the transmembrane ion balance, membrane potential, and cell physiology. The effects observed thus far, but not discussed in this presentation include inhibition of voltage-gated Na^+ and Ca^+ channels; both inhibitory and stimulatory effects on voltage-gated K^+ channels; cell swelling and blebbing and cytoplasm granulation. Analysis of these effects opens new avenues for selective manipulation of different cell functions, with potential applications in biomedical research and clinical practice.

Acknowledgment

The work was supported in part by R01CA125482 from the National Cancer Institute, by Air Force Research Laboratory Fellows funding from Michael R. Murphy, by funding from the Office of Naval Research (USA), and by HQAF SGRS Clinical Investigation Program (Neurological Impacts of Nanosecond Electric Pulse Exposure).

References

1. Pakhomov AG, Kolb J, White J et al. (2007) Long-lasting plasma membrane permeabilization in mammalian cells by nanosecond pulsed electric field. Bioelectromagnetics 28:655-663.
2. Pakhomov AG, Shevin R, White J et al. (2007) Membrane permeabilization and cell damage by ultrashort electric field shocks. Archives of Biochemistry and Biophysics 465:109-118.
3. Ibey BL, Xiao S, Schoenbach KS et al. (2009) Plasma membrane permeabilization by 60- and 600-ns electric pulses is determined by the absorbed dose. Bioelectromagnetics 30:92-99.
4. Vernier PT, Sun Y, Marcu L et al. (2004) Nanoelectropulse-induced phosphatidylserine translocation. Biophys J 86: 4040-4048.

Author: Andrei G. Pakhomov
Institute: Frank Reidy Research Centre for Bioelectrics, Old Dominion University
Street: 830 Southampton Ave., Suite 5100
City: Norfolk, VA
Country: USA
Email: andrei@pakhomov.net

Thermosensitive Mn^{2+}- Liposomes for MR-Guided Hyperthermia – Solvent-Dependent Mn^{2+}- Release.

H.M. Reinl[1], M. Hossann[2], L.H. Lindner[3] and M. Reiser[1]

[1] Department of Clinical Radiology, University of Munich, Klinikum Grosshadern, Germany
[2] Max Planck Innovation GmbH, Munich, Germany
[3] Department of Internal Medicine III, University Hospital, Ludwig-Maximilians University, Munich, Germany and CCG-Hyperthermia, Helmholtz Zentrum München, German Research Center for Environmental Health, Munich, Germany

Abstract— **Newly designed phosphatidylglyceroglycerol-based liposomes are shown to be a temperature sensitive contrast agent for MRI when MR-active manganese(II)ions are trapped inside. At the therapeutic temperature of hyperthermia of 42 - 43°C the encapsulated Mn^{2+} can be detected by T_1 changes in a MRI-Hyperthermia hybrid-system. The physical properties of the liposomes are characterized by lipid composition, size, morphology and not least solvent composition. Dependent on the solvent two mechanisms for the T_1 changes can be found, enhanced water exchange through the lipid membrane or release of Mn^{2+}.**

Our results indicate that our new liposomal system has the potentiality to improve temperature monitoring of hyperthermia and thus the therapeutic outcome. Moreover, the liposomes may also be used for specific release of chemotherapeutics by moderate hyperthermia.

Keywords— **Hyperthermia, MRI, thermosensitive liposome, Phosphatidylglyceroglycerol, contrast agent.**

I. Introduction

Hyperthermia has proven to be an effective treatment concept for locally advanced deep-seated tumors in combination with chemo- and radiotherapy (1,2). Reaching the therapeutic temperature slightly above 40°C is a crucial factor for the outcome of the hyperthermic tumor treatment (3). Nevertheless, adequate online temperature control in heated tumours is only possible with invasive temperature sensors, which are feasible for one-dimensional temperature measurement. Unfortunately, the use of catheters is often accompanied by side effects like infections and bleeding. MRI could provide non-invasive temperature control of local hyperthermia (4.5), but only supply information on temperature changes. It has been shown that paramagnetic liposomes may support MR thermometry by a pronounced contrast change due to a change in the longitudinal T_1 - relaxation time at the phase transition temperature T_m of the liposomal membrane (6,7). We demonstrated the feasibility of MR thermometry with novel thermosensitive liposomes (TSL) with the encapsulated paramagnetic contrast agent gadodiamide (8,9,10). Other possible contrast agent are manganese(II)salts, moreover, this type of liposomes could be used for active loading of doxorubicin (DOX), a potent chemotherapeutic agent (7,11).

Our TSL composed of the phospholipids 1,2-dipalmitoyl-*sn*-glycero-3-phosphoglyceroglycerol (DPPGOG), 1,2-dipalmitoyl-*sn*-glycero-3-phosphocholine (DPPC) and 1,2-distearoyl-*sn*-glycero-3-phosphocholine (DSPC) showed markedly enhanced circulation time *in vivo* in rats ($t_{1/2}$ = 5h) or hamsters ($t_{1/2}$ = 9.6h) (12). The synthetic lipid DPPGOG not only increases the *in vivo* half life, it further increases the content release of DOX around the main phase transition temperature T_m at 42-43°C (13).

The purpose of this study was to investigate the influence of the solvent composition on T_1 – change of Mn-TSL.

II. Material and methods

A. Liposomes

The phospholipids DPPC and DSPC were purchased from Genzyme Pharmaceuticals (Liestal, Switzerland). The synthetic lipid DPPGOG was synthesized as described previously (14). Fetal calf serum (FCS) was from Invitrogen (Carlsbad, USA), Triton X-100 was purchased from Sigma-Aldrich Chemie GmbH (Munich, Germany). All other chemicals were from Carl Roth GmbH (Karlsruhe, Germany).

Mn-TSL were prepared by the lipid film hydration and extrusion method. The molar ratio of the phospholipids was DPPC:DSPC:DPPGOG 50:20:30. The dry lipid film was hydrated with 300mM $MnSO_4$ pH 4.0 to passively encapsulate paramagnetic manganese(II)ions in the TSL. Large unilamellar vesicles (LUV) were obtained by extrusion through two polycarbonate nanopore filters of 200nm pore size using a thermobarrel extruder at 60°C. Free Mn^{2+} was removed from the liposome suspension by dialysis against physiological sodium chloride solution (6,10). TSL concentration was measured with a phosphate assay (13). The size and ζ-potential was determined by photon correlation spec-

O. Dössel and W.C. Schlegel (Eds.): WC 2009, IFMBE Proceedings 25/XIII, pp. 21–24, 2009.
www.springerlink.com

troscopy and lipid composition was analyzed with thin layer chromatography (TLC) (13).

B. MR Measurements

The relaxation time T_1 measurements were performed at 0.47 Tesla with a Minispec 120 (Bruker, Germany) by the inversion recovery method.

The TSL were first heated from 35 to 50°C, measurements were performed every 1°C. For the second set of measurements the sample was cooled down from 50 to 35°C. The third set of measurements was performed with 10% triton in the buffer to ensure that all Mn^{2+} was set free. These three sets of measurements were done with two samples using different solvents. Sample 1 was prepared with HEPES buffered saline (HN-buffer), sample 2 with FCS:HN-buffer 1:1 (v/v), both at pH 7.4.

The time interval between the measurements was 10 minutes, the temperatures were corrected due to a calibration function.

For analysis the relaxation rate R_1 (= $1/T_1$) normalised to the manganese concentration was derived. The manganese concentration was calculated from T_1 at 45°C, slightly above the phase transition temperature, due to a calibration function.

III. RESULTS AND DISCUSSION

For the study, three independent charges of Mn-TSL were prepared. Photon correlation spectroscopy revealed a size of 165±14nm (mean ± SD) with a polydispersity index of 0.06±0.05, indicating a narrow size distribution. Surface charge measured in isotonic sodium solution was -24.6±10.7mV, though no Mn^{2+} ions were bound to the negatively charged DPPGOG on the TSL surface. Final phospholipid concentration was 39.5±4.5 mM. TLC of freshly prepared TSL showed no signs of decomposition, e.g. hydrolysis of phospholipids as consequence of the acidic buffer inside the liposome. DPPGOG content was 31.3± 3.7%. While Gd-TSL (10) and TSL with encapsulated DOX (data not shown) of the same lipid composition and particle size showed particles with one single lipid bilayer in freeze fracture electron microscopy, unilamellarity was also assumed for the Mn-TSL used in this study.

Figure 1 shows the change of the relaxation rate R_1 of sample 1, HN-buffer used, in a sigmoid course between 2.1 and 6.9 $(mM\ s)^{-1}$ with a center temperature at 43.5±0.2°C during heating. The cooling of the sample also yields a sigmoid course with R_1 in the same range but a 1°C lower center temperature. The triton measurements show the known temperature dependence of R_1 for free Mn^{2+} rising to lower temperatures (see also Fig.1).

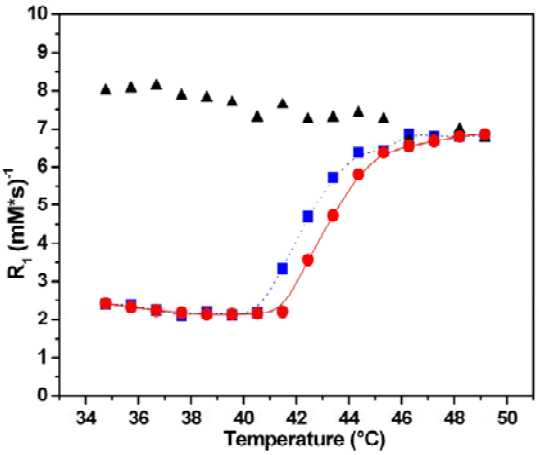

Fig.1: Change of the relaxation rate R_1 with temperature of Mn-TSL in HN-buffer (sample 1).
The sigmoidal heating scan (●) indicates an enhanced water exchange through the lipid membrane. The cooling scan (■) shows a complete reversibility of that process at lower temperature. Incubation with Triton (▲): free Mn^{2+} shows an increase of R_1 to lower temperature.
The lines are drawn to guide the eye.

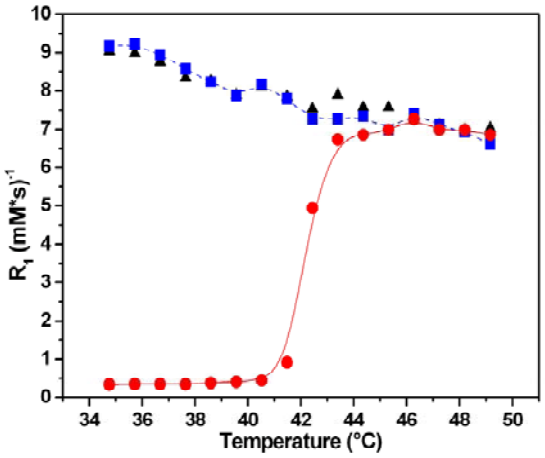

Fig.2: Change of the relaxation rate R_1 with temperature of Mn-TSL in FCS-containing buffer (sample 2).
The sigmoidal heating scan (●) shows the enhanced water exchange and the release of encapsulated Mn^{2+}. The cooling scan (■) shows that Mn^{2+} was set free and R_1 behaves like the Triton measurement (▲).
The lines are drawn to guide the eye.

The change of R_1 with temperature of sample 2, FCS-buffer used, is shown in Figure 2. Here also a sigmoid course is found for the heating scan with values of R_1 between 0.3 and 7.3 $(mM\ s)^{-1}$ and a center temperature at 42.5±0.2°C. The phase transition width is clearly smaller (41.5 – 43.5°C) than for sample 1. Cooling the sample, R_1 follows the course of the triton measurements also shown in Figure 2.

At the main phase transition T_m of the liposomes the lipid membrane converts from a more rigid gel-phase to a liquid-crystalline phase with increasing temperature. The liquid-crystalline phase is affected by increased dynamics, so that the fast exchange of water molecules between exterior (bulk) and interior water increases, resulting in a pronounced dipolar relaxation due to the Mn^{2+} inside the liposomes, R_1 is increased. This process is reversible as long as the Mn^{2+} stays encapsulated in the liposomes, like we found in sample 1 for the liposomes in HN-buffer. We tested that reversibility with repeated heating and cooling (Data not shown).

Under certain circumstances, like phase separation in the membrane caused by lipid–protein interaction or lipid exchange with other membranes the liposomes can be disrupted and the contents is released. Free Mn^{2+} increases R_1 in an irreversible process, like we found for liposomes dispersed in FCS containing HN-buffer (sample 2). It can be shown that for a second heating the values of R_1 stay at the course of free Mn^{2+} (Data not shown).

Lately it was shown that Gd release from Gd-TSL is also strongly dependent on the solvent. Gd release is accelerated when Gd-TSL are dispersed in FCS containing samples (9). This finding supports our results.

For FCS was used to mimic *in vivo* conditions and regarding the presented results, the use of the Mn-TSL as "off-on-switch" can not be considered because the process is not reversible. Our results show that such a reversible process may only be derived in FCS-free solvent.

But the characterization of Mn^{2+}-TSL in FCS-buffer shows that the system has potential for MR thermometry in hyperthermia, especially when the chemotherapeutic agent DOX is involved. Active loading of liposomes with DOX can be facilitated with Mn^{2+}, which leads to a complex formation inside the liposome. DOX will be released in the heated tumor from the TSL, therapeutic temperature and doxorubicin concentration are monitored by the simultaneously released manganese(II)ions (7,11).

IV. CONCLUSIONS

In the present *in vitro* study Mn-TSL were shown to be useful as possible contrast agent to monitor temperature during hyperthermia treatment. Detection of temperature dependent Mn^{2+} -release demonstrates the technical feasibility of temperature measurement using Mn-TSL. The prominent role of FCS for content release from TSL was clearly shown. Finally Mn^{2+}/DOX loaded liposomes could be used for *in vivo* monitoring of liposome concentration distribution and drug release using MRI. However, the use of the Mn-TSL requires further investigations to evaluate the potentials as tumor agent.

ACKNOWLEDGMENT

The authors thank Prof. Hansjörg Eibl for the synthesis of DPPGOG, Anja Zengerle for excellent technical assistance and Prof. Ernst Wagner for use of facilities. This work was financially supported by Helmholtz-Gemeinschaft (VH-VI-140, Clinical Hyperthermia and Related Technology) and grant SFB 455.

REFERENCES

1. Issels R. (2008) Hyperthermia adds to chemotherapy. Eur. J. Cancer 44:2546
2. Falk M. et al (2001) Hyperthermia in oncology. Int. J. of Hyperthermia 17(1):1
3. Wendtner C.M. et al (2002) Response to neoadjuvant chemotherapy combined with regional hyperthermia predicts long-term survival for adult patients with retroperitoneal and visceral high-risk soft tissue sarcomas. J. Clin. Oncol. 2(14):3156
4. Peller M. et al (1999) MRI-controlled regional hyperthermia. Radiologe 39(9):756
5. Peller M. et al (2002) T1 relaxation time at 0.2 Tesla for monitoring regional hyperthermia: Feasibility study in muscle and adipose tissue. Magn. Reson. Med. 47:1194
6. Fossheim S.L. et al (2000) Thermosensitive paramagnetic liposomes for temperature control during MR imaging-guided hyperthermia: in vitro feasibility studies. Acad. Radiol 7(12):1107
7. Viglianti B.L. et al (2004) In vivo monitoring of tissue pharmacokinetics of liposome/drug using MRI: illustration of targeted delivery. Magn. Reson. Med. 51:1153
8. Reinl H.M. et al (2003) New thermosensitive liposomes for MR-guided hyperthermia. Proc.Intl.Soc.Mag.Reson.Med. 11:1209
9. Peller M. et al (2008) MR characterization of mild hyperthermia-induced gadodiamide release from thermosensitive liposomes in solid tumors. Invest. Radiol. 43(12):877
10. Wang T. et al (2008) In vitro characterization of phosphatidylglyceroglycerol-based thermosensitive liposomes with encapsulated 1H MR T1-shortening gadodiamide. Contrast Media Mol Imaging 3(1):19
11. Viglianti B.L. et al (2006) Chemodosimetry of in vivo tumor liposomal drug concentration using MRI. Magn. Reson. Med. 56:1011
12. Lindner, L.H. et al (2004) Novel temperature-sensitive liposomes with prolonged circulation time. Clin.Cancer Res.,10:2168
13. Hossann M. et al. (2007) In vitro stability and content release properties of phosphatidylglyceroglycerol containing thermosensitive liposomes. Biochim. Biophys. Acta, 1768: 2491-9.
14. Eibl H. Synthesis of glycerophospholipids. *Chem Phys Lipids*. 1980;26:405

Author: Herbert M. Reinl
Institute: Department of Clinical Radiology, University Hospitals
Street: Marchioninistr. 15
City: 81377 Munich
Country: Germany
Email: hreinl@med.lmu.de

Status of Education and Training in Africa: Focus on South Africa

W.I.D. Rae[1]

[1] Department of Medical Physics, University of the Free State, Bloemfontein, South Africa

Abstract— **Medical Physics training and education in Africa continues to be limited in many ways. Information gathering is difficult in the region due to limited communication channels and relatively few formal contact people within the field. It appears only five countries in Africa have formal courses offered toward recognized Medical Physics qualifications. Much of the training is achieved via International Atomic Energy Agency (IAEA) sponsored training courses. These focus on specific training needs and are presented around the continent in member countries. Many qualified individuals currently in Africa obtained their qualifications in other countries.**

Formal recognition of the profession is well established in South Africa (SA) where professional registration with the Health Professions Council of SA is required after formal, structured and approved training. An active education and training program has been in place there since the 1960s. The regulations are kept current by national regulatory authorities to ensure that areas within health care where Medical Physicists are employed are adequately serviced by properly educated professionals. Functional academic and practical training programs are available at six accredited SA universities and most offer postgraduate training programs up to PhD level. Postgraduate students from at least seven other African states are currently studying at SA institutions.

Active efforts have been made since the 2006 IOMP World Congress in Seoul to form a regional federation of African Medical Physics organizations in order to attempt to address some of the urgent needs in the field. This process is well supported by the IAEA and the IOMP, and is aimed at comprehensive support of the profession on the continent.

Many challenges exist in providing Medical Physics services within Africa. To overcome these coordinated education and training is vital.

Keywords— **Education, Training, Africa, Medical Physics, IAEA.**

I. Introduction

The training and education of Medical Physicists in Africa is very limited and is available in only a few countries. It is very difficult to get accurate information on the status of the profession within Africa, as there is limited communications technology and there are many countries where the profession is not officially recognized in any way. This makes it difficult to define how many people in Africa are doing the work of a Medical Physicist. Not all countries in Africa have current technology for the diagnosis and treatment of many of the common diseases which afflict the people of the region. Some countries do have access to the technology, but do not have the support services to properly utilize the technology within the constraints on their finances. The services of Medical Physicists are generally more limited than in the rest of the World. Usually they are only available in Radiotherapy Departments. The limited immediate need and lack of recognition mean that the training of people to carry out the tasks of Medical Physicists within Africa is often sporadic and not comprehensive, nor is it strongly supported by governments with apparently more pressing priorities. Often that training does not give them a qualification, or the ability to register as a Medical Physicist within either the country where the training was given, or in their home country. In many countries even those adequately educated and trained abroad do not get properly recognized as Medical Physicists. The support for all aspects of their function is limited, from recruitment and training to professional recognition and remuneration.

If the situation is to improve, good quality coordinated support for comprehensive appropriate training of Medical Physicists must be provided within the countries where it is needed.

II. Current status

From the information that is available it seems only five countries on the continent (of 61 territories within Africa) provide formal education and training courses toward a recognized Medical Physics qualification. Many of the territories in Africa are small and rely on neighbors for health care services that require the expertise of a Medical Physicist. The education and training that does take place is due largely to the inputs of the International Atomic Energy Agency (IAEA) which funds and organizes about 5 or 6 training workshops relevant to the field of Medical Physics each year through one of their African Regional Cooperation Agreement (AFRA) projects (Table 1) [1].

These projects have specific goals and aims and often provide training within the narrow goals set for the projects. The courses are usually presented by experts in the various fields and these experts

O. Dössel and W.C. Schlegel (Eds.): WC 2009, IFMBE Proceedings 25/XIII, pp. 25–27, 2009.
www.springerlink.com

are often from countries outside Africa. The projects through which these training programs are funded often also have a component which includes expert visits in order to support Medical Physicists, amongst other professionals, in the region.

Table 1 IAEA AFRA Projects

Project Number	Title
RAF/6/024	Management of the Most Common Cancers in Africa (AFRA II-4)
RAF/6/027	Strengthening Regional Capability in Medical Physics (AFRA II-5)
RAF/6/030	Diagnosing Diseases using Clinical Nuclear Medicine
RAF/6/031	Medical Physics in the Support of Cancer Management (AFRA II-8)
RAF/6/032	Promoting Regional and National Quality Assurance Programmes for Medical Physics in Nuclear Medicine (AFRA II-7)
RAF/6/035	Enhancing Accessibility and Quality in the Care of Cancer Patients (AFRA II-10)

The IAEA also provides Fellowships to many to study at various institutions in various countries around the World. Unfortunately there are still many who perform profession specific tasks (carried out on other continents by specifically trained and qualified people) who do not have formal recognized profession specific qualifications. Currently many qualified individuals working in the field obtained their qualifications in other countries. These qualifications are often not entirely appropriate and offer only limited registration possibilities upon completion.

Formal regulatory recognition of the profession is well established in South Africa (SA) where national registration following formal, structured and approved training is required for individuals to practice in the profession. This registration requirement has been in place since the 1950s when the then Atomic Energy Board was formed. Since then various bodies have regulated the profession which is currently controlled by the Health Professions Council of South Africa. An active education and training program has been in place since the 1960s. Most of the Founder Members of the South African Association of Physicists in Medicine and Biology (SAAPMB) were trained overseas, but they soon set up formal education programs in SA. The national regulatory authorities have ensured that current needs within the fields where Medical Physicists are employed are adequately serviced by properly educated professionals. The curriculum is well defined. Educational institutions and training hospitals are properly accredited by peer review. Functional academic and practical training programs are available at six accredited universities in SA and some of these offer active undergraduate and postgraduate training programs up to PhD level [2].

The active education and training program in SA has had some effect in other countries to the North. Over the past several years many SA experts have been used by the IAEA on missions into other countries. Many foreign students have studied for various degrees in SA. Postgraduates from at least seven African states are currently studying in South African institutions.

III. Education for the future

Various efforts are underway at different levels around the continent to improve the situation.

The IAEA has several projects currently running which have as part of their stated objectives the improvement of academic and clinical training. This focused effort will hopefully improve not only the training and education of Medical Physicists, but also ameliorate the shortage and enhance recognition by national registration authorities, all with the ultimate goal of improving the therapeutic and diagnostic services offered to people in Africa.

The Education and Training Committee (ETC) of the IOMP has been functional for many years and has several very relevant stated goals within its charge. It is stated in the ETC charge [3] that:

"1 The charge to the IOMP Education and Training Committee (ETC) is to improve medical physics worldwide by disseminating systemized knowledge through education and training of medical physicists especially in developing countries.

"2 The mission of the IOMP ETC is to advance the practice of physics in medicine by fostering the education, training and professional development of medical physicists, and by promoting highest quality medical services for patients worldwide."

The charge continues and covers all of the major requirements for education and training within African institutions, including the provision of support and education materials. It endorses cooperation with the IAEA in an attempt to ensure that appropriate education and training is done in all countries, even to the extent of setting up training centers.

"8 The ETC will stimulate the foundation of regional centers for education and training in collaboration with IAEA, WHO and other agencies."

This commitment by the IOMP should make a significant difference to the current situation, especially when considered along with the efforts of the IAEA.

On a more regional scale the formation of a Federation of the existing Medical Physics Organizations within Africa could also be used as a forum for support of education and lobbying for accepting the status of Medical Physics. Efforts have been made since the 2006 World Congress in Seoul to form a regional Federation of African Medical Physics Organizations (FAMPO) in order to at-

tempt to address some of the urgent needs in the field. This process is well supported by the IAEA and the IOMP, and is aimed at supporting the profession in all ways on the continent. It has also led to a greater interest within national groupings and many of these are making an effort to become more structured and functional. This should be of significant benefit when attempting to coordinate efforts in the region.

IV. Conclusions

After considering the needs and the current condition of Medical Physics education and training within Africa, it is felt that coordinated efforts on the part of international (IOMP and IAEA) and regional organizations (National and Regional representative bodies) will be required to adequately address the needs. There is much available capacity to achieve good quality education. This will be required before meaningful formal registration of Medical Physicists in all countries will be possible as we aim to ensure that the people of the continent get the best quality of care available.

References

1. IAEA-TC Projects by Cooperative Agreement: AFRA - African Regional Cooperative Agreement for Research, Development and Training at http://www-tc.iaea.org/tcweb/projectinfo/default.asp
2. University of the Free State Faculty of Health, B.Med.Sc. (Radiation Sciences) at http://www.ufs.ac.za/apps/yearbooks/index.php?id=96&sid=2848
3. Bylaws of the International Organization for Medical Physics approved 27 August 2003 in Sydney at http://www.iomp.org/bylaws.htm

Author: Dr William I.D. Rae
Institute: Department of Medical Physics (G68)
Faculty of Health Sciences
University of the Free State
Street: Nelson Mandela Drive
City: Bloemfontein
Country: South Africa
Email: raewid.MD@ufs.ac.za

Treatment Planning Methods for Efficient Dose Delivery in Radiation Therapy Using Laser Accelerated Particle Beams

S. Schell and J.J. Wilkens

Department of Radiation Oncology, Technische Universität München, Klinikum rechts der Isar, München, Germany

Abstract— **With laser acceleration it might be possible to reduce the overall costs of radiation therapy with ions. However, the produced particles have some distinct properties that make them different compared to conventionally accelerated ones. Two of these properties are a broader energy spectrum and dose quantization. Therefore conventional spot scanning seems not feasible. Instead, a reduction of the total number of dose spots is necessary. This work presents a method to accomplish this by building clusters of dose points in lateral and depth direction with the use of a multi leaf collimator and broad energy spectra respectively. Preliminary results on lateral clustering show that this can be achieved without sacrificing the treatment plan quality.**

Keywords— **laser accelerated ion therapy, dose delivery, MLC, broad energy spectrum.**

I. Introduction

Laser based ion acceleration systems are a promising new technology of accelerating charged particles to energies that are high enough for therapeutic use in radiation therapy [1]. Nowadays large and expensive cyclotrons or even synchrotrons have to be used for this task. The mechanism of laser acceleration might potentially reduce the overall costs of ion therapy in cancer treatment with ionizing radiation. The long term goal of current research is to build a laser based treatment machine that is not much bigger than a conventional photon linac. This would enable the widespread use of the superior properties of protons or heavier ions compared to conventional x-ray radiation.

However, much research needs to be done until a commercial laser accelerated treatment device can be build. Currently the most obvious problem is that there is no laser available that can produce energies that are high enough for the treatment of patients, but there is hope that this can be achieved soon.

Another problem is the energy spectrum of the ion beam. Cyclotrons or synchrotrons that are used conventionally produce a sharp energy with only little spread therein which gives rise to the sharp Bragg peak in the depth dose curve. Laser accelerated ions on the other hand will probably not be monoenergetic. Much work is being done to produce sharper energy spectra but it is highly probable that they will never be as sharp as for conventional acceleration methods. Therefore energy selection systems have been proposed [2]. With the help of high magnetic fields the different energies of the broad energy spectrum can be separated in space allowing the selection of only parts of the spectrum by blocking the unwanted particles. Afterwards, with further magnetic fields, the desired particles can be remerged to one beam. This can in principle restore monoenergetic beams; however, the blocked particles have to deposit their energy somewhere else. Secondary radiation will be generated, with neutrons as the biggest problem because they cannot be shielded easily [3]. Therefore, it is highly recommended to use as many of the accelerated particles as possible. The total particle efficiency of the system is not only a matter of costs and time, it is necessary to reduce unwanted photon and neutron radiation.

Due to the time structure of the laser beam, laser acceleration does not produce a continuous beam but a series of very short (possibly on a nanosecond scale) and dense particle bunches - one for each laser shot. It will be impossible to scan the beam magnetically across the target within one bunch, or to deliver only a fraction of the particles contained in one bunch. Hence, the dose will be quantized. How much dose is actually delivered within one laser shot and how many shots are feasible in total is still not clear and greatly depends on the final design of the laser setup.

These two properties of laser accelerated particles, the energy spread and the quantization of the dose, need to be included when considering potential dose delivery systems for treatment devices. Trying to produce a beam that is as close to the conventional beam as possible is one way to deal with these properties. In this paper we present an approach that uses these properties instead of trying to minimize them. First, tumors usually have a larger extend in beam direction than the width of one sharp Bragg peak. In conventional ion accelerators the energy spectrum is broadened artificially by the use of either simple spread out Bragg peaks (SOBP) or in general by energy modulation of multiple dose spots. This allows delivering dose to the whole depth of the tumor. For laser based acceleration an efficient algorithm should be able to utilize as much of a given energy spectrum as possible. Second, to have more control over the area where the dose of one shot is spread, a broadened beam (using a scattering

O. Dössel and W.C. Schlegel (Eds.): WC 2009, IFMBE Proceedings 25/XIII, pp. 28–31, 2009.
www.springerlink.com

system or preferably magnetic beam optics) and lateral beam shaping devices like a multi leaf collimator (MLC) should be considered. Combining these two possibilities makes the quantization less important and simultaneously increases the particle efficiency. In the following we describe a method to optimize dose delivery for laser accelerated ion therapy.

II. Methods

A. Current dose delivery methods

The most advanced technique of dose delivery for conventionally accelerated ions is spot scanning. The beam's energy is varied to position the spots in depth. Since the energy spectrum of conventionally produced ions is very sharp, the Bragg peak is very thin in longitudinal direction and therefore the dose can be localized in a small area around the spot position. To place the spots laterally two magnetic dipoles are used. Since the beam is continuous and the monitoring system can switch off the beam very fast as soon as the desired number of particles is reached, every spot can be irradiated independently with the desired dose.

B. The depth dose curve

As mentioned above, the energy spectrum of laser accelerated ions is broader than the one of conventionally accelerated ions. Figure 1 shows an exemplary energy spectrum and the corresponding depth dose curve for conventionally and laser accelerated protons as calculated with an analytical depth dose curve approximation by Bortfeld [4]. It is clear that smaller spectra are the better choice. However, if broader spectra are applied to inner tumor voxels, where steep gradients are not necessary, they still have a clearly definable localization of the dose maximum and are therefore advantageous over photons. Hence, using a very sharp spectrum is not always necessary, and at least for some parts of the treatment volume laser accelerated particle acceleration can be made more efficient by using a higher percentage of the produced particles.

C. Dose quantization

Regarding dose quantization we assume that the laser system is able to produce particle numbers in discrete steps. If the number of usable protons per shot is too small, the limited repetition rate of the laser will be a problem. Currently 10 Hz seems to be a realistic midterm limit [5]. To finish the treatment in a reasonable time the number of shots should be below about 10,000 (corresponding to about 17 min without gantry rotation and MLC movement). Because every beam spot will need several shots to reach the desired

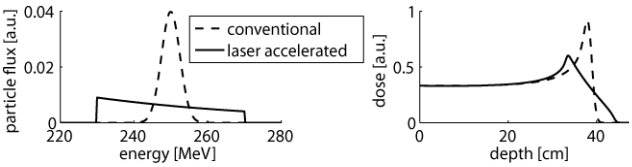

Fig. 1 Energy spectrum and depth dose curve of protons for conventional and laser acceleration. Both plots are scaled to the same particle number.

dose the total number of beam spots has to be significantly lower than 10,000. Having too many particles per shot is also problematic since it decreases the ability to safely deliver a precise number of particles to small subvolumes as required for intensity modulation techniques. Because we do not want to waste particles (limited number of shots and secondary radiation) there must be a way to spread the dose over a well defined but bigger area without losing the flexibility of general intensity modulation.

D. Spot clustering

To get around the broad produced energy spectrum and the quantization of the dose the following method can be applied. The broadness of the used energy spectrum has to be variable and the lateral spread of the dose has to be controlled with a MLC. With the assumption of this flexibility, figure 2 depicts different possibilities to deliver dose with laser accelerated particles. First, the treatment volume is partitioned into a three-dimensional rectangular grid of dose delivery points. In conventional therapy with spot scanning one would deliver dose to each of these points independently. But if two points are close to each other there is a high probability that they will need an equal amount of dose. Therefore, one can cluster points together. If done in the right way the flexibility of the intensity modulation remains but the number of independent dose spots is reduced significantly. The spot size denoted with (A) is the smallest possible volume that can receive the same dose. Its size is given by the smallest MLC and energy selection

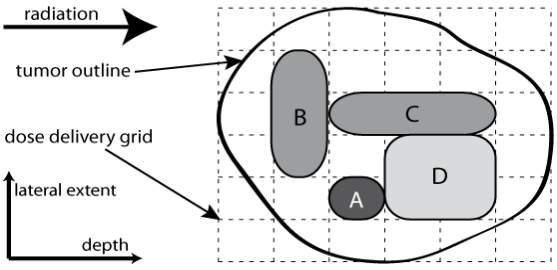

Fig. 2 Efficient dose delivery for laser accelerated particles. (A) Small spot shape with very low particle efficiency. (B) Lateral clustering. (C) Axial clustering. (D) Lateral and axial clustering with high particle efficiency.

setting. Spot shape (B) shows the application of lateral clustering. The dose is spread over two dose delivery points with the help of a MLC. The third possibility (C) is the use of a broader energy spectrum to extend the dose in depth. Finally, spot shape (D) uses both, lateral and axial clustering. It is the most efficient possibility but it comes with a reduced flexibility in intensity modulation. It is up to a good algorithm to decide where to place which kind of spot shape to find a tradeoff between efficiency and flexibility.

E. Lateral spot clustering

A possible method of performing lateral clustering is depicted in figure 3 which shows the beam's eye view of one arbitrarily selected energy layer of a beam. The tumor is partitioned into equally sized spots that can be irradiated with a MLC. The points that have two or more direct unused neighbors are called edge points and are not clustered to preserve the possibility to produce sharp gradients at the tumor border. The other points are clustered into 6 different groups, denoted by the letters A to F, which have a maximal member count of 9. By using a MLC each of these groups can be irradiated within a single laser shot. In this example the total number of used dose delivery points is 45, there are 9 edge points and 6 groups with a total number of 36 members. Therefore, with clustering one needs 15 instead of 45 dose spots. Alternatively, one could define edge points to be the points with 1 or more direct unused neighbors. This would lead to 24 edge points instead of 9 and therefore a higher total number of dose spots. It has to be determined which setting gives rise to the best tradeoff between plan quality and spot number reduction.

F. Axial spot clustering

Being able to generate the required energy spectrum for irradiating the whole axial tumor extent in one shot would

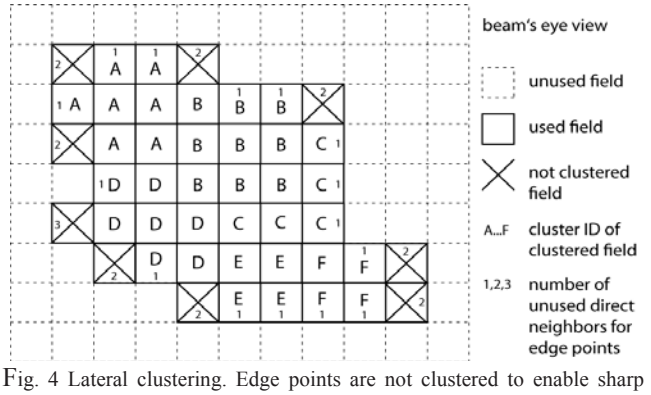

Fig. 4 Lateral clustering. Edge points are not clustered to enable sharp lateral gradients.

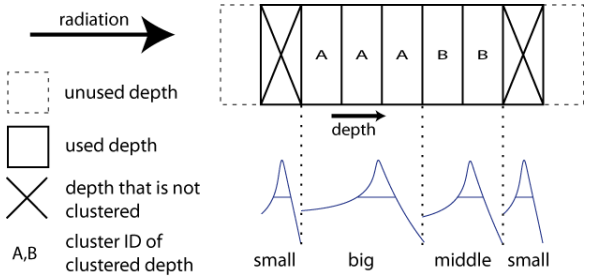

Fig. 3 Axial spot clustering. Edge points are not clustered to enable sharp gradients in depth.

be ideal. However, at least in the beginning, it will only be possible to choose the minimal and maximal energy of a given spectrum. Broader energy spectra can be used in the center of the target volume to increase particle efficiency. Figure 4 shows one possibility to cluster points in axial direction. Again, edge points (which have one unused neighbor) are not clustered to remain the possibility to create sharp gradients. The distal edge is most important since the sharp dose falloff of protons can only be utilized with monoenergetic beams. Therefore, the distal points certainly need to be independent. It has to be determined if the proximal points can be clustered safely without losing plan quality. The figure shows sketches of Bragg peaks for the different clusters. For larger clusters the 80% to 80% width is bigger than for the smaller ones (cf. figure 1).

G. Possibilities to reduce the number of dose spots

To obtain the highest reduction of dose spots a combination of lateral and axial clustering can be applied. As depicted in figure 2 not every spot shape can be delivered. In a two-dimensional plot of depth versus one lateral direction the allowed shapes are rectangles. Therefore, the two clustering methods are not independent from each other.

Beyond the clustering of dose points prior to the optimization there are further possibilities to reduce the overall number of necessary laser shots. The long term goal of our current research is to implement the following scheme into treatment planning for laser accelerated ions: First, as mentioned above, remove as many independent dose points as possible prior to the optimizations without significantly changing the treatment plan quality. Second, modify the objective function for the optimization to enforce solutions that have a minimal number of laser shots and therefore an efficient particle usage. This involves optimizing small and big points simultaneously with additional constraints. And third, posterior to the optimization, try to build additional clusters out of dose spots that have similar weights. After that an optional second optimization could be of advantage.

H. Treatment planning

To test the impact of different dose delivery methods on the treatment plan quality we use a modified version of the Matlab based experimental treatment planning tool CERR [6] that has been extended to enable dose calculation for protons with arbitrary energy spectra. The algorithm is pencil beam based and uses lookup tables for the depth dose curve and the lateral spread in matter.

III. Results

The first tests that have already been performed analyzed the influence of lateral clustering on the dose volume histograms (DVHs) of a proton treatment plan for a head and neck tumor. Figure 5 shows the DVHs for the target and the parotid gland for three different dose delivery methods. The solid line is calculated for a 0.4 cm lateral resolution of the dose delivery grid with no clustering. It needs about 11,000 dose spots. The dashed line uses the same resolution but applies lateral clustering as described above. Despite needing only about 2,000 dose spots it produces almost the same results than the not clustered plan. For comparison the dotted line is calculated for a non-clustered case with a lateral resolution of 0.93 cm corresponding to the same number of about 2,000 dose spots. There is certainly an advantage of high resolution clustering with an MLC compared to low resolution non-clustered rectangular fields. The difference in the parotid gland are small but regarding target coverage clustering is beneficial.

IV. Discussion and conclusion

Laser accelerated ions have certain distinct properties that make it necessary to develop alternative dose delivery methods for treatment planning. Two of them are dealt with in this work: broad energy spectra and dose quantization. As a consequence the reduction of the number of required dose spots compared to conventional spot scanning is essential. To obtain this, a method has been presented that clusters points in axial direction by the use of broader energy spectra and groups neighboring points in lateral direction. It has been shown that lateral clustering can already greatly reduce the number of spots without sacrificing plan quality. In the presented case the number could be reduced from 11,000 to 2,000.

By applying all presented clustering methods it should be possible to reduce the total number of dose spots to an amount that can be applied in the clinical use of future laser accelerated treatment machines. The treatment plan quality is potentially comparable to conventional plans and certainly better than photon plans [7].

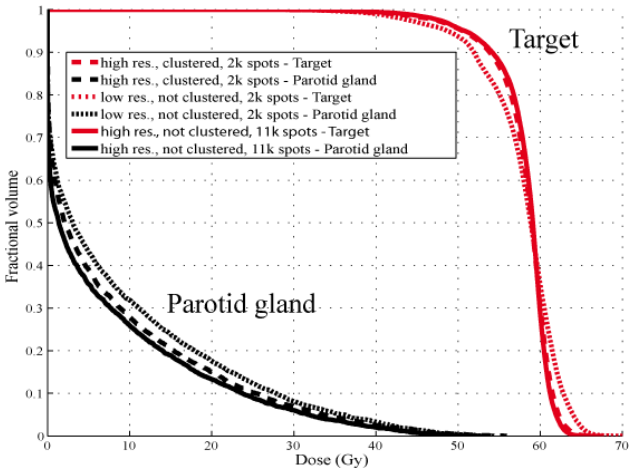

Fig. 5 Comparative dose volume histograms for clustered versus non-clustered dose delivery spots.

Acknowledgment

Supported by DFG Cluster of Excellence: Munich Centre for Advanced Photonics.

References

1. Ma CM, Veltchev I, Fourkal E et al. (2006). Development of a laser-driven proton accelerator for cancer therapy. Laser Phys 16:639-646
2. Luo W, Fourkal E, Li J et al. (2005). Particle selection and beam collimation system for laser-accelerated proton beam therapy. Med Phys 32:794-806
3. Fan J, Luo W, Fourkal E, Lin T et al. (2007). Shielding design for a laser-accelerated proton therapy system. Phys Med Biol 52:3913-3930
4. Bortfeld T (1997). An analytical approximation of the Bragg curve for therapeutic proton beams. Med Phys 24:2024-2033
5. Linz U, Alonso J (2007). What will it take for laser driven proton accelerators to be applied to tumor therapy? Phys Rev ST Accel Beams 10:094801
6. Deasy JO, Blanco AI, Clark VH (2003). CERR: A computational environment for radiotherapy research. Med Phys 30:979-985
7. Luo W, Li J, Fourkal E et al. (2008). Dosimetric advantages of IMPT over IMRT for laser-accelerated proton beams. Phys Med Biol 53:7151-7166

Author: Stefan Schell
Institute: Department of Radiation Oncology, Technische Universität München, Klinikum rechts der Isar
Address: Ismaninger Str. 22, 81675 München, Germany
Email: stefan.schell@tum.de

Causes, Detection and Characterization of Tumor Hypoxia

P. Vaupel

Klinik für Strahlentherapie und Radiologische Onkologie, Klinikum rechts der Isar, Technische Universität München, 81675 München, Germany

Abstract— **Tumor oxygenation is heterogeneous and severely compromised as compared to normal tissue. Hypoxia, i.e., oxygen depletion as a consequence of an imbalance between oxygen supply and cellular oxygen consumption, mostly results from inadequate perfusion and diffusion within tumors and from reduced O_2 transport capacity in anemic patients. Detection of tumor hypoxia has been performed using minimally invasive approaches, imaging PET and MRI techniques and immunohistochemistry on tissue biopsies. The development of tumor hypoxia is independent of a series of relevant tumor characteristics (e.g., clinical size, stage, histology, and grade) and various patient demographics. Overall median pO_2 in cancers of the uterine cervix, head and neck, and breast is about 10 mmHg with the overall hypoxic fraction ($pO_2 \leq 2.5$ mmHg) being approx. 25%. Metastatic lesions do not substantially deviate from the oxygenation status of (their) primary tumors. Identification of tumor hypoxia may allow an assessment of a tumor's potential to develop an aggressive phenotype or acquired treatment resistance, both of which lead to poor prognosis. Detection of hypoxia in the clinical setting may therefore be helpful in selecting high-risk patients for individual and/or more intensive treatment schedules.**

Keywords— **Tumor hypoxia, tumor oxygenation, hypoxia detection, causes of hypoxia, characterization of hypoxia.**

I. Introduction

The physiology of tumors ("*tumor pathophysiome*") is uniquely different from that of normal tissues. It is characterized *inter alia* by oxygen (O_2) depletion (hypoxia or anoxia), extracellular acidosis, high lactate levels, glucose and energy deprivation, significant interstitial fluid flow and interstitial hypertension [1,2]. This hostile microenvironment is largely determined by an abnormal tumor microcirculation. The tumor is characterized by vigorous proliferation leading to immature, structurally defective and, in terms of perfusion, ineffective microvessels which lack the signals to mature. Tumor vasculature is often described as an "aberrant monster" [3]. Consequently, tumor blood flow is chaotic, inadequate and heterogeneous [1,2,4,5].

II. Causes of tumor hypoxia

The pathogenesis of tumor hypoxia is multifactorial. Tumor hypoxia, i.e., critical O_2 levels below which clinical, biological, and/or molecular effects are progressively observed (e.g., slowing of proliferation rate, changes of the transcriptome, proteome and genome, metabolic hypoxic stress response, and development of an aggressive phenotype, ATP depletion, binding of hypoxic markers, acquired treatment resistance), predominantly results from the inadequate perfusion. *Perfusion-limited O_2 delivery* leads to *ischemic hypoxia* which is often transient. For this reason, this type of hypoxia is often called "acute" hypoxia, a term that does not take into account the mechanisms underlying this condition [6]. "Acute" hypoxia often results as a consequence of transient flow with plasma only due to the very low O_2 content in plasma.

Hypoxia in tumors can also be caused by an increase in diffusion distances, so that cells far away (>70μm) from the nutritive blood vessels receive less oxygen than required. This condition is termed *diffusion-limited hypoxia*, also known as "chronic" hypoxia. In addition to enlarged diffusion distances, an adverse diffusion geometry (e.g., concurrent vs. countercurrent tumor microvessels) can also cause hypoxia [7].

Tumor-associated or therapy-induced anemia can lead to a reduced O_2 transport capacity of the blood, a major (systemic) factor contributing to the development of hypoxia (*anemic hypoxia*). This type of hypoxia is especially pronounced in tumors or tumor areas exhibiting low perfusion rates. A similar condition can be caused by carboxyhemoglobin (HbCO) formation in heavy smokers, which leads to a *functional anemia*, since hemoglobin blocked by carbon monoxide (CO) is no longer capable of transporting oxygen.

Hypoxia can rapidly develop in (primary or metastatic) liver tumors that are preferentially supplied by branches of the portal vein (*hypoxemic hypoxia*).

There is abundant evidence for the existence of steep, fluctuating and unstable oxygen gradients leading to a substantial spatial and temporal heterogeneity (*"4D-heterogeneity"*) in the development and extent of tumor hypoxia

O. Dössel and W.C. Schlegel (Eds.): WC 2009, IFMBE Proceedings 25/XIII, pp. 32–35, 2009.
www.springerlink.com

due to pronounced intra-tumor (and inter-tumor) variabilities in vascularity and perfusion rates (for reviews see refs. [1,7,8]).

III. Detection of tumor hypoxia

A series of techniques have been suggested for the detection of tumor hypoxia (see Table 1). Direct measurement of oxygen tension (pO_2, O_2 partial pressure) can be performed using *polarographic O_2 needle electrodes* and this has often been referred to as the "gold standard". Numerous studies in patients have been performed in the clinical setting in a large variety of cancer types [9]. This minimally invasive approach, however, is limited to accessible tumors and needs experienced investigators.

Imaging techniques are of great interest in the clinical setting. Imaging offers the advantage of being noninvasive and repeatable but with the disadvantages of limited spatial resolution, and some approaches are not hypoxia-specific. Methods used to visualize regional hypoxia include *positron emission tomography* (PET), *dynamic contrast-enhanced MRI* (DCE-MRI) and *blood oxygen level-dependent MRI* (BOLD-MRI).

A number of hypoxia-specific agents for PET have been developed, of which ^{18}F-fluoromisonidazole (FMISO) has been the most widely studied molecule in patients. ^{18}F-labelled EF5 has recently been introduced for studies in humans. EF5 may be of interest since it can be used for both imaging and immunohistochemical detection in the same subject.

The bioreductive molecule ^{60}Cu-ATSM has also been proposed for tumor hypoxia imaging although some cell lines showed no hypoxic selectivity at all. Another PET hypoxia agent, ^{18}F-FAZA, has properties similar to those of ^{18}F-FMISO.

MRI methods for assessment of tumor oxygenation are attractive since they avoid the complications of short-lived radioactivity and MRI equipment is widely available. The BOLD/MRI signal is related to the oxygenation of the vascular compartment. This repeatable technique has the advantage of both high spatial and temporal resolution. However, BOLD may be confounded by flow effects, making the interpretation of the BOLD signal somehow difficult.

The use of exogenous markers of hypoxia has a wide application and can be carried out in any tumor where a routine diagnostic biopsy is taken. After administration, an exogenous drug (such as pimonidazole or EF5) is reduced in hypoxic cells and forms a stable product that can be detected in stained tumor samples using immunohistochemistry.

Assessing the expression of hypoxia-inducible proteins ("endogenous hypoxic markers") has received great interest because these downstream proteins can be detected on archived paraffin-embedded tissue material. The disadvantage of using such surrogate markers is: they are not hypoxia-specific and the proteins can be induced by several other, non-hypoxia-related factors. For this reason interpretation of the data can be difficult [12].

Table 1 Methods currently available or undergoing development for detection of tumor hypoxia in the experimental and clinical setting (selection, modified from [10,11])

1. Minimally invasive microsensor techniques for direct tissue pO_2 measurements
   - polarographic O_2 sensors
   - luminescence-based optical sensors
2. Noninvasive detection of sensitizer adducts
   - ^{18}F-fluoromisonidazole, ^{18}F-FMISO (PET)
   - ^{18}F-azomycin-arabinoside, ^{18}F-FAZA (PET)
   - ^{60}Cu-ATSM (PET)
   - ^{18}F-EF5 (PET)
   - ^{123}I-Iodoazomycin-arabinoside (SPECT)
   - ^{99m}Tc-HL91 (SPECT)
3. Nuclear magnetic resonance spectroscopy and imaging techniques
   - blood oxygen level dependent (BOLD) MRI
   - dynamic contrast-enhanced (DCE) MRI
   - ^{19}F-MR relaxometry (^{19}F-MRI-oximetry)
4. Techniques for intravascular O_2 detection
   - cryospectrophotometry (HbO_2 saturations)
   - near-infrared spectroscopy (HbO_2 saturations)
   - phosporescence imaging
5. Electron paramagnetic resonance (EPR) oximetry
6. Immunohistochemistry (IHC) with exogenous hypoxic markers
   - misonidazole (^{3}H-MISO)
   - pimonidazole (PIMO)
   - etanidazole (EF5)
   - nitroimidazole-theophylline (NITP)
7. Immunohistochemistry with "endogenous hypoxia markers" (secondary downstream effects; biomarkers are not hypoxia-specific)
   - hypoxia-inducible factor-1α (HIF-1α)
   - carbonic anhydrase-IX (CA-IX)
   - glucose transporter-1 (GLUT-1)
   - vascular endothelial growth factor (VEGF)
   - urokinase-type plasminogen activator system

IV. Characterization of tumor oxygenation

Current knowledge concerning the oxygenation status of tumors in terms of O_2 partial pressure distributions are predominantly derived from clinical studies on the pretreatment O_2 status of solid tumors using minimally invasive oxygen microsensors [9]. This technique allows the direct and reliable measurement of O_2 partial pressures (pO_2 values) in accessible tissues. It provides quantitative measures.

Investigations carried out in the clinical setting over the last two decades demonstrated that the presence of hypoxic tissue areas with pO_2 values $\leq$ 2.5 mmHg is a characteristic

Table 2 Pretherapeutic oxygenation status of locally advanced human tumors (selection of data [9]).

Tumor type	median pO_2 (mmHg)	HF 2.5 (%)	HF 5 (%)	HF 10 (%)
Cervix cancers	9	28	44	59
Head and neck cancers	10	21	32	
Soft tissue sarcomas	14	13	12	59
Breast cancers	10	30	47	50
Prostate cancers	10	45	55	
Gliomas	13	26	30	49

HF 2.5 = fraction of pO_2 values ≤ 2.5 mmHg; HF 5 = fraction of pO_2 values ≤ 5 mmHg; HF 10 = fraction of pO_2 ≤ 10 mmHg

Table 3 Oxygenation status of normal tissues [12,13].

Tumor type	median pO_2 (mmHg)	HF 2.5 (%)	HF 5 (%)	HF 10 (%)
Cervix	42	0	13	20
Subcutis	51	0	0	4
Skeletal muscle	25-30	0	4	12
Breast	52	0	0	0
Brain	24-27	0	3-8	13

pathophysiological property of locally advanced solid tumors, and such areas have been found in a wide range of human malignancies. Evidence has accumulated showing that at least 50-60% of locally advanced solid tumors may exhibit hypoxic and/or anoxic tissue areas that are heterogeneously distributed within the tumor mass [9]. (Anoxia describes the pathophysiological state where no O_2 is detectable (measurable) in the tissues (pO_2 = 0 mmHg)).

Relevant parameters of the pretherapeutic oxygenation status of locally advanced human tumors are presented in Table 2. There is clear evidence that the oxygenation of solid tumors is distinctly poorer than that of the respective normal tissues (see Table 3).

When the available data on pretreatment tumor oxygenation of 150 locally advanced cancers of the uterine cervix is summarized [8,9], there is evidence that:

a) Oxygenation in tumors is heterogeneous and compromised as compared to normal tissues.
b) Tumor oxygenation is not regulated according to the metabolic demands as is the case in normal tissues.
c) On average, the median pO_2 values in primary cancers of the uterine cervix are lower than those in the normal cervix.
d) Many cervical cancers contain hypoxic tissue areas (at least 60%).
e) There is no characteristic topological distribution of O_2 tensions within cervix cancers.
f) Tumor-to-tumor variability in oxygenation is greater than intra-tumor variability.
g) Tumor oxygenation is independent of various patient demographics (e.g., age, menopausal status, parity).
h) Anemia (found in approximately 30% of patients at diagnosis) considerably contributes to the development of hypoxia, especially in low-flow tumor areas.
i) In cervix cancers of moderately/severely anemic patients, hypoxic areas are more frequently found than in non-anemic patients.
j) Tumor oxygenation and the extent of hypoxia are independent of clinical size, FIGO stage, histological type (squamous cell carcinomas vs. adenocarcinomas), grade, and lymph node status.
k) Tumor oxygenation is weakly dependent on the pathological tumor stage (pT stage).
l) Local recurrences of cervix cancers have a higher hypoxic fraction than the primary tumors.
m) Hypoxia in cervical cancers has been found to be of prognostic significance in many investigations.

V. Clinical importance of tumor hypoxia

Cells exposed to hypoxia respond by reducing their overall protein synthesis, which in turn leads to restrained proliferation and a change in the cell cycle distribution. Under anoxia, most cells undergo immediate arrest in whichever cell cycle phase they are currently in. Additionally, hypoxia can induce apoptosis and - below a critical energy state - hypoxia may result in necrotic cell death.

In contrast, hypoxia has been recognized as an important driving force in *malignant progression.*[8,13,14]. Hypoxia – as an inherent consequence of unregulated growth – can promote local invasion, intravasation of cancer cells and finally metastatic spread to distant sites whereby this occurs in a cooperative manner:

- on the *transcriptome* level leading to hypoxia-induced *changes in gene expression* coordinated by a special set of transcription factors, such as HIFs, NF-κB, AP-1, indicating redundancy in biological mechanisms in malignant tumors below 1% O_2 [8],
- on the *proteome* and *metabolome* level via adaptive gene expression, post-transcriptional and posttranslational modifications [15],
- on the *genome/epigenome* level by increasing genomic and epigenomic instability (below 0.1% O_2) and
- on the level of cell populations by *clonal selection* and *clonal expansion* according to phenotype fitness [14].

Tumor cell variants with adaptations favorable to survival under hypoxic stress may have growth advantages over non-adapted cells in the hypoxic microenvironment and may subsequently develop a more aggressive phenotype which in turn is responsible for malignant progression. Cyclic hypoxia and pronounced spatio-temporal heterogeneities (4D-

heterogeneities) in hypoxia may be the most powerful factors promoting an aggressive tumor phenotype.

Hypoxia is known to restrict the success of tumor therapy. Hypoxia-driven resistance to therapy – like that triggered by other microenvironmental factors – adds to the "classical" treatment resistance based on the molecular biology of tumors. Tumor hypoxia plays a pivotal role in *acquired treatment resistance*, since O_2 depletion in solid tumors is classically associated with *resistance to radiotherapy*, but has also been shown to reduce the efficacy of certain forms of *chemotherapy*, *photodynamic therapy*, *immunotherapy* and *hormonal therapies* [16]. Hypoxia directly and/or indirectly confers resistance to therapy. Direct effects are mediated through reduced generation of free radicals (some chemotherapy, photodynamic therapy) or lacking fixation of DNA damage (X- and γ-rays). Indirect hypoxia-driven effects are mostly based on cell cycle effects and on slowing of cellular proliferation kinetics, on changes in the transcriptome, on differential regulations of gene expression, on alterations of the proteome, on enhanced mutagenesis, genomic instability and clonal selection, i.e., on hypoxia-associated tumor progression [13].

There is increasing evidence that tumor hypoxia – through favoring malignant progression and reducing the therapeutic response – may act as an *adverse prognostic factor* [10,13]. Independent of standard prognosticators, such as tumor stage and nodal status, hypoxia has been suggested as a negative prognostic factor for patient outcome. Studies of tumor hypoxia involving the direct assessment of the oxygenation status have suggested worse disease-free survival for patients with hypoxic cancers of the uterine cervix or soft tissue sarcomas. In head and neck cancers, available studies suggest that hypoxia is prognostic for survival and local control. In many – albeit not in all – studies endogenous markers (HIF-1α, GLUT-1, CA IX) also showed prognostic significance for patient outcome. Noninvasive assessment of hypoxia using imaging techniques (e.g., PET, MRI) with regard to patient prognosis is so far limited. In the clinical studies performed up until now, the lack of homogeneous patient cohorts and of standardized treatment protocols, inconsistencies of the endpoints characterizing the oxygenation status and methodological differences may compromise the power of the prognostic parameter used.

REFERENCES

1. Vaupel P, Kallinowski F, Okunieff P (1989) Blood flow, oxygen and nutrient supply, and metabolic microenvironment of human tumors: A review. Cancer Res 49:6449-6465
2. Vaupel P (2004) Tumor microenvironmental physiology and its implications for radiation oncology. Semin Radiat Oncol 14:198-206
3. Shchors K, Evan G (2007) Tumor angiogenesis: cause or consequence of cancer? Cancer Res 65:7059-7061
4. Vaupel P (2006) Abnormal vasculature and defective microcirculatory function in solid tumors. In: Siemann DW (ed) Vascular-targeted Therapies in Oncology, Wiley & Sons, Chichester, UK, pp 9-29
5. Molls M, Vaupel P (eds) (2000) Blood Perfusion and Microenvironment of Human Tumors. Implications for Clinical Radiooncology. Springer, Berlin Heidelberg, New York
6. Vaupel P, Mayer A, Höckel M (2004) Tumor hypoxia and malignant progression. Methods Enzymol 381:335-354
7. Vaupel P, Harrison L (2004) Tumor hypoxia: Causative factors, compensatory mechanisms, and cellular response. Oncologist 9 (suppl 5):4-9
8. Vaupel P (2009) Pathophysiology of solid tumors. In: Molls M, Vaupel P, Nieder C, Anscher MS (eds) The Impact of Tumor Biology on Cancer Treatment and Multidisciplinary Strategies. Springer, Berlin, Heidelberg, New York, pp 51-92
9. Vaupel P, Höckel M, Mayer A (2007) Detection and characterization of tumor hypoxia using pO_2 histography. Antioxid Redox Signal 9:1221-1235
10. Vaupel P, Mayer A (2007) Hypoxia in cancer: significance and impact on clinical outcome. Cancer Metastasis Rev 26:225-239
11. Krohn KA, Link JM, Mason RP (2008) Molecular imaging of hypoxia. J Nucl Med 49:129S-148S
12. Mayer A, Höckel M, Vaupel P (2006) Endogenous hypoxia markers in locally advanced cancers of the uterine cervix: reality or wishful thinking? Strahlenther Onkol 182:501-510
13. Vaupel P (2004) The role of hypoxia-induced factors in tumor progression. Oncologist 9 (suppl 5):10-17
14. Giaccia AJ (1996) Hypoxic stress proteins: survival of the fittest. Semin Radiat Oncol 6:46-58
15. Höckel M, Vaupel P (2001) Tumor hypoxia: Definitions and current clinical, biologic and molecular aspects. J Natl Cancer Inst 93:266-276
16. Vaupel P (2009) Physiological mechanisms of treatment resistance. In: Molls M, Vaupel P, Nieder C, Anscher MS (eds) The Impact of Tumor Biology on Cancer Treatment and Multidisciplinary Strategies. Springer, Berlin, Heidelberg, New York, pp 273-290

Univ.-Prof. Dr. med. Peter Vaupel, M.A./Univ. Harvard
Klinik für Strahlentherapie und Radiologische Onkologie
Klinikum rechts der Isar der Technischen Universität
Ismaninger Str. 22
81675 München
Germany
peter.vaupel@lrz.tum.de
vaupel@uni-mainz.de

Experiences of in-field and remote monitoring of diagnostic radiological quality in Ghana using an equipment and patient dosimetry database.

M.A. Ward[1], E. K. Ofori[2], D. Scutt[3], B.M. Moores[1]

[1] Integrated Radiological Services Limited, Liverpool, UK

[2] School of Allied Health, University of Ghana, Accra, Ghana

[3] School of Health Sciences, University of Liverpool, Liverpool, UK

Abstract — **A review of diagnostic radiological equipment performance and resultant patient dose values in Ghana has been undertaken. Equipment survey data was taken from 10 x-ray rooms across 7 individual hospitals in southern and central Ghana in order to establish basic equipment performance levels against IPEM standards. The x-ray kerma output data for a range of kVp values was transferred to an online relational database in order that a comprehensive dose audit could be undertaken using exposure factors emailed back to the UK using conventional data entry forms. Analysis was undertaken of the key tube performance parameters. This established a baseline level of equipment acceptability and allowed entrance surface dose values to be verified and calculated using proprietary software.**

Data was collected on 1968 patients who underwent a total of 2838 radiographic projections comprising chest, pelvis, lumbar spine (AP and lateral), abdomen and skull (PA and lateral). Entrance surface doses were calculated by operators and analysts inputting the data into the database containing basic output data which then corrected for the applied kVp, mAs, focus-to-skin distance and backscatter variables. The results have been analyzed and compared with IAEA Basic Safety, European and UK quality standards in patient dosimetry. Chest PA and lumbar spine lateral results are presented.

A narrow range of performance variation between the radiographic equipment in the sample was found. The tube and generator performance is acceptable. However, the wide range of ESD values presented highlights that a prioritized approach is needed to address areas of investigation and non-compliance, especially where values exceed basic safety standards. The Chest PA results serve as an example of how standardization of technique could contribute to optimization. A program of patient dose monitoring is proposed, provided that a basic level of practical, cost-effective, ongoing routine equipment quality control can be undertaken.

Keywords— **quality control, radiation protection, audit.**

I. Introduction

Assessment of patient doses in diagnostic radiology is widely accepted as necessary to ensure that doses are ALARP [1]. Furthermore, in the absence of specific resources for quality control checks of the relevant parts of the imaging chain (tubes and generators, automatic exposure controls, processors), patient dosimetry offers the potential to provide ongoing quality measures. Remote monitoring of entrance surface dose (ESD) values is possible where the analyst has access to both patient exposure data for a range of examinations and efficiently acquired baseline tube output and kVp values [2]. Numerous studies with thermoluminescent dosimeters (TLDs) have demonstrated patient dosimetry outcomes with data acquired on a subject-by-subject or location-by-location basis across African nations [3, 4, 5]. Prime drivers to perform an audit using direct exposure factors rather than TLD methods were the need to minimize costs and time, to establish basic equipment performance standards, and to allow all radiographers and physics staff in the study to be able to view their results online after verification in the UK.

It was postulated that tube performance in Ghana would not be the governing factor giving rise to any deviation or unexpected results from IAEA, EU or UK reference dose standards, but rather a wider mix of training, technique and film processing resource limitations. In order to confirm this, the following specific objectives were established:

· carry out quality control test on the x-ray equipments in the selected examination rooms.

· compare the results obtained to recognized standards [6].

· measure the X ray tube outputs in μGy per mAs measured at 1 meter for the radiographic equipment in the selected examination rooms.

O. Dössel and W.C. Schlegel (Eds.): WC 2009, IFMBE Proceedings 25/XIII, pp. 36–39, 2009.
www.springerlink.com

· estimate air kerma at different settings from the radiographic equipment in the selected examination rooms according to the clinical settings used on each site.

· measure and record patient's anatomical data and exposure parameters used for the specific examination selected for the study.

· calculate and store patient doses using the Quality Assurance Dose Data Software (QADDS) developed by IRS Ltd, Liverpool, UK.

· compare the data with internationally recommended reference values

II. Materials and methods

In this study, field measurements were undertaken using an Unfors Xi Platinum series semiconductor detector type field kit (Unfors Inc., Bildal, Sweden). 7 hospital sites were chosen, comprising 10 x-ray tubes and generators in total. Appropriate field measurements were undertaken of the IPEM "level B" type according to recognized UK protocols [6]. Outputs in terms of µGy/mAs at were ascertained at kV_p settings from 50-120 during the survey.

Following the equipment surveys, radiographic staff were issued with patient dose audit forms in order that patient weight, sex, height, thickness (AP or coronal plane width), examination type, projection, focus-to-skin distance, focus to film distance, applied kVp and mAs could be logged. The remit for each site was to obtain at least 20 patients per x-ray room per examination/projection category at each site for the most commonly employed examinations.

Patient radiation dose assessments were conducted on patients who underwent the 5 most common radiographic examinations (chest, lumbar spine, pelvis, abdomen and skull) in selected hospitals during the study period. The selection of the above examinations was based on their frequencies and contribution to the collective dose to the population. In particular, chest PA was selected because it is the most frequent x-ray examination among the hospitals [7], lumbar spine, particularly the lateral projection, because it is associated with higher ESD values than all other X-ray plain film examinations [8]. It should be noted that pelvis AP data is stored and may offer useful investigation into effective and organ dose studies owing to the critical organs irradiated.

Each patient was weighed, bare-footed and in an upright position. A specially designed caliper was used to measure the patient anatomical thickness for the body part under examination that was then used to deduce the focus-skin distances for the examination. It was therefore agreed among the radiographers in consultation with the participating radiologists that, for consistency in measurements, the anatomical thickness of the patient for each projection in this study was to be measured at the following anatomical levels:

(i) Chest PA projection: in the sagittal plane at the level of inferior angle of scapula.

(ii) Lumbar spine lateral projection: in the coronal plane at the level of the lower costal margin.

A domestic tape measure was used to measure the focus–film-distances (FFD). All FFD measurements were from the center of the tube to the film or the tabletop. The datasheets were placed near the console of the X-ray room and were completed when a patient entered requiring one of the specified examinations.

Entrance surface dose (ESD) were calculated using the formula:

$$\mathrm{ESD} = \mathrm{R}_{100} \cdot \left(\frac{100}{\mathrm{FFD} - \mathrm{t}} \right)^2 .mAs.BSF \qquad (1)$$

Where:

ESD is the entrance surface dose in milli-Gray, R_{100} is the radiation output per mAs, at 100 centimeters from the x-ray source. Between 10 keV intervals not directly measured on the survey, R_{100} was calculated by linear interpolation between the nearest upper and lower intervals to the nearest 10 keV. mAs denotes the applied tube mAs used for the radiograph, FFD is the focus-to-film skin distance, t is the patient thickness and BSF is a backscatter factor.

III. Results and discussions

A summary of equipment performance values is shown in Table 1. The rooms selected show the best and worst performing tubes in terms of kVp and timer accuracy. The selection also corresponds to sites using the same FFD and film/screen speeds, but four different kVp ranges (Range values here) for chest examinations.

Mean Chest PA ESD values at KR2, 37M, KBUA and RR1 were 0.2, 0.2, 04 and 0.7 mGy respectively. The mean value across all ten locations was 0.5 mGy. Mean Lumbar Spine LAT values were 12.1, 13.2, 23.2, 6.1 mGy respectively. The mean value across all ten locations was 13.3 mGy. ESD range factors were defined as the ratio of the maximum ESD value to the minimum for each exam at each site. The intra-room values for chest examinations ranged from 2.9-10.8, and for Lumbar LAT values, from 1.9-2.8.

A wider selection of all 10 rooms surveyed and audit for dosimetry has been defined as GHANASET. The range factors across these ten rooms for chest and spine exams were 6.8 and 12.5 respectively using the ratio of the ESD means. The range factors across the whole data set for chest and spine exams increased to 38.4 and 32.0 respectively when the using the ratio of the absolute maximum and minimum ESD values.

Table 1. Results of QC checks on x-ray equipment at four selected hospitals (maximum value of performance indicated)

Parameters	KR2	37M	KBUA	RR1
KV accuracy (%)	2.4	4.2	3.1	1.5
HVL_{80kVp}, mm Al	2.8	3.5	3.1	3.1
Total Filtration, mm Al.	2.42	3.7	2.9	2.9
Timer reproducibility (%)	9.0	1.8	N/A	0.3
Output Linearity	1.8	1.9	1.8	1.9
Radiation Output Repeatability (%)	0.1	0.3	0.6	3.1
Radiation Output Reproducibility (%)	6.6	5.0	1.5	0.5

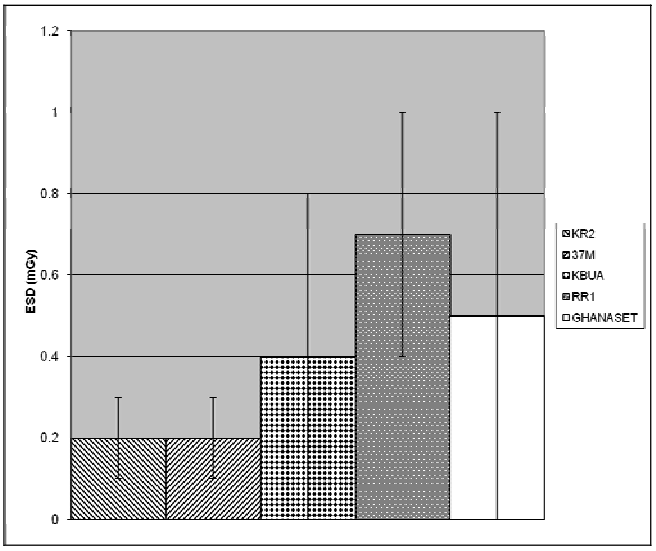

Fig. 1 Mean Chest PA Entrance Surface Doses for 4 locations in the study, together with the mean ESD values for the 10 rooms in total (GHANASET). The error bars shown represent one standard deviation in both the positive and negative direction.

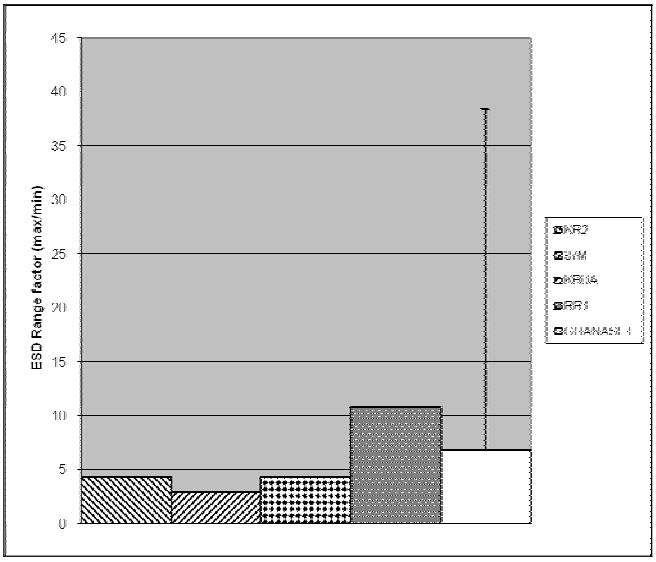

Fig. 2 Chest PA Entrance Surface Dose intra-room range factors (ESD) for 4 locations in the study, together with the mean inter-room range factor for the 10-room GHANASET. The positive error bar value represents the absolute range factor for the maximum and minimum ESD in the examination dataset.

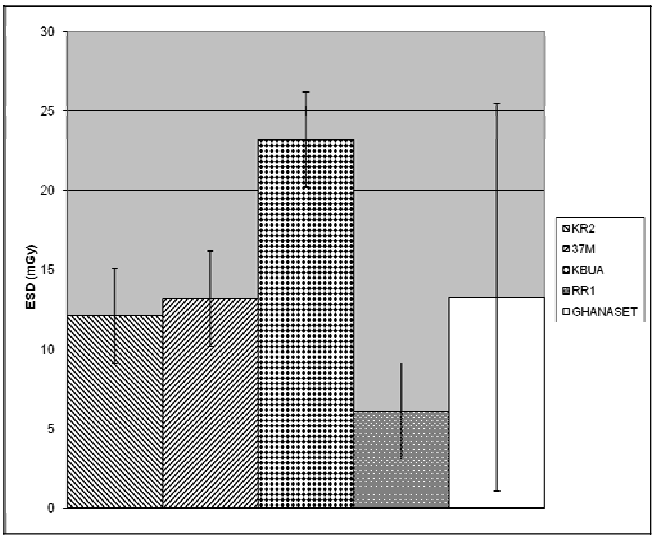

Fig. 3 Mean Lumbar Spine LAT Entrance Surface Doses for 4 locations in the study, together with the mean ESD values for the GHANASET. The error bars shown represent one standard deviation in both the positive and negative direction.

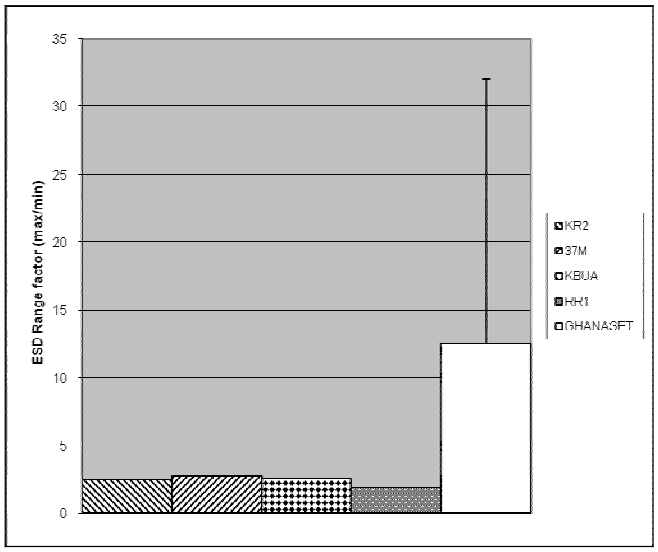

Fig. 4 Lumbar Spine LAT Entrance Surface Dose range factors (ESD) for 4 locations in the study, together with the mean range factor for all GHANASET sites, based on the mean ESD obtained in each room. The positive error bar value represents the absolute range factor for the maximum and minimum ESD in the examination dataset.

The four centers sampled for this audit submitted the same FFD and speed class parameters. They all used AEC and grid techniques. The third quartile ESD value for Chest PA is 0.8 mGy, 0.2 mGy lower than a published value [3]. Mean ESD values for Lumbar Spine LAT exams are available from Nigeria [5], in a reported range of approximately 5-24 mGy, with an overall range factor of approximately 17. The GHANASET lumbar LAT mean ESD in this study is 13.3 mGy. Individual intra-room Ghana range factors are lower than those published in [5], but the overall inter-room range is approximately twice that of Nigeria. It is observed that different audit methods and total patient numbers are employed in each study.

IV. CONCLUSIONS

The results contained herein suggest that improvements have been made in the past ten years in terms of dose reduction in chest radiography. However, the spread of dose values remains similar to or greater than that encountered in Ghana and other African nations [3, 4, 5]. Review and prioritized areas for action in terms of patient dose are still needed.

The methodology contained in this study suggests that a basic local QC program could serve to show consistent x-ray tube compliance and thus allow for more users to update and review performance via the web or other database technologies with little or no requirement for TLDs. It has already been shown that QC programs serve to improve reject analysis figures and reduce patient dose. [3, 8]

It should be considered through review of training and exposure protocols whether the use of appropriate kV_p ranges and grids and other technique factors in are employed optimally according to specific examinations. The results from this study support this. X-ray tube performance is satisfactory.

The large amount of data stored from this study should allow more sensitive analysis than may have been possible previously. In particular, analyses with respect to demographic parameters, or moving-average studies over time as has been demonstrated elsewhere [2] are possible.

ACKNOWLEDGMENT

Thanks must be offered to the radiographic staff at each hospital, and at IRS Ltd. for data collection and IT support.

REFERENCES

1. International Commission on Radiological Protection. 1990 recommendations of the International Commission on Radiological Protection. ICRP publication no. 60. Ann ICRP 1991; 21:1-201.
2. Vano, E., Fernandez, J.M., Ten, J.I., Guibelalde, E., Gonzalez, L and Pedrosa, C.S. (2002). Real-Time Measurement and Audit of Radiation Dose to Patients Undergoing Computed Radiography. Radiology vol . 225 pp 283-288. DOI: 10.1148/radiol.2243011331.
3. Schandorf, C. and Tetteh, G.K. (1998). Analysis of dose and dose distribution for patients undergoing selected x ray diagnostic procedures in Ghana Rad. Prot. Dosim. Vol. 76, No. 4, pp. 249–256 (1998)
4. Muhogora, W.E., Nyanda, A.M., Lema, U.S., Ngaile, J.E. (1999). Typical radiation doses to patients from some common x-ray examinations in Tanzania. Radiation Protection Dosimetry, vol. 82, no. 4, pp 301-305.
5. Ogundare, F.O., Uche, C.Z., Balogun, F.A. (2004). Radiological parameters and radiation doses of patients undergoing abdomen, pelvis, and lumbar spine X-ray examinations in three Nigerian hospitals. Br. J. Radiol. Vol. 77, pp 934-940.
6. IPEM 91
7. Schandorf, C. and Tetteh, G.K. (1998). Analysis of the status of X-ray diagnosis in Ghana. Br. J. Radiol. Vol. 71. pp 1040-1048.
8. European guidelines on quality criteria for diagnostic radiographic images. Brussels: EUR16260EN CEC, 1996.

Address of the corresponding author:

Author: M.A. Ward
Institute: Integrated Radiological Services Limited
Street: 188 Tower Street
City: Liverpool
Country: UK
Email: mattward@irs-limited.com

New Frontiers in Pre-clinical Small Animal Radiation Research*

John W. Wong

Department of Radiation Oncology and Molecular Radiation Sciences, Johns Hopkins University, Baltimore, USA

Small laboratory animals are invaluable in pre-clinical studies. For radiation therapy, the significant technological disparity between methods used for human treatment and those for laboratory animal irradiation brings into question the effectiveness of the latter to represent the clinical environment. In an effort to bridge the gap, we have constructed a small animal radiation research platform (SARRP) with the capabilities of a modern human machine. The SARRP is equipped with on-board cone-beam CT (CBCT) to guide focal irradiation. Under CBCT guidance, the SARRP is capable of delivering radiation dose from beams as small as 0.5 mm in diameter to a target with accuracy of 0.2 mm; at a dose rate of 2.5 Gy per min from gantry angles that ranged from the vertical to 30^{o} below the horizontal directions. In use for nearly two years, the system has enabled previously unfeasible focal irradiation studies with mice. These include studies of the response of neural stem cells to focal irradiation; vaccine mediated immunotherapy in combination with radiation in orthotopic tumor models; positron-emission-tomography markers for early assessment of radiation induced lung toxicity. While the advantages of anatomic guided pre-clinical small animal irradiation are apparent, the next frontier clearly points to the use of functional and molecular imaging to study radiation response in the small animal experiments. At present, MRI or PET imaging for small animal radiation research are performed via off-line image registration and analysis. Taking advantage of the "open" architecture of the SARRP, we have embarked on the implementation of on-board high resolution ultrasound imaging for functional studies and on-board optical imaging of bioluminescent and fluorescent markers in tumor models. With the rapid advances made in contrast-enhanced 3D ultrasound imaging and 3D optical imaging, the capabilities of focal irradiation of functional and molecular targets with the SARRP creates new exciting opportunities to conduct mechanistic studies of tumor response to radiation in the in vivo small animal models.

* Supported in part by the NCI Bioengineering Research Partnership grant R01 CA 108449.

O. Dössel and W.C. Schlegel (Eds.): WC 2009, IFMBE Proceedings 25/XIII, pp. 40, 2009.
www.springerlink.com

Size Matters – Revealing Small Scale Structures in Large Datasets

T. Fogal, J. Krüger

Scientific Computing and Imaging Institute, University of Utah

ABSTRACT

The size of datasets generated in the medical imaging community is increasing faster than additional processing resources are made available. Even if we can surmount the hurdles in large data handling and processing, the amount of information encoded in these datasets is overwhelming. Therefore effective visualization techniques must allow a user to identify and focus on scientifically interesting subsets of the data. We describe a system for generating high-quality renderings of large volumetric data, and discuss the importance of scalable systems in the medical community.

Index Terms— volume, visualization, scalable, rendering

1. INTRODUCTION

There are two additional challenges that are presented once data grow beyond a certain size: first and foremost, we must be able to process and work with data using hardware resources that cannot advance as quickly as the size of our datasets. Secondly, the tools we create for processing these data must provide more efficient means to identify and focus on interesting structures within the data. The resolution obtained through modern data acquisition techniques is staggering, and therefore our tools must avoid presenting all of the information at once. It follows that those tools must allow users to efficiently focus their attention on interesting features of the dataset.

Aesthetics is an important and often overlooked secondary concern. While it is true that our primary motivation for using visualization tools is to create informative and useful visualizations, we argue that one should consider how the viewer will receive the generated media. Important considerations are ensuring the viewer is drawn to the feature of interest, is not distracted by extraneous information, and can immediately grasp the topic or issue that the visualization brings to light.

These concerns are frequently at odds with the challenges large data present. As the resolution of measured data improves, we begin to note many small scale structures that were not previously evident. In this paper, we describe a volume rendering system that addresses these concerns for large scalar data.

2. MOTIVATION

It is important to visualize data at their native resolution, despite the technical challenges in doing so. High resolution data can reveal features in a dataset which were not visible at lower resolutions. For example, the visible human male [1] was originally released in 1994, yet to date few people know about the tattoos which the male had on his chest and arms (see Figure 1). This was due to the difficulty processing and rendering the data at its full resolution. While a set of tattoos is arguably not a critical feature in a dataset, resolving structures on the same scale as a tattoo may be important for recognizing anomalies among the data, or useful in identifying components among a larger whole.

3. METHODS

3.1. Volume Rendering

We chose to implement our visualization tool based on the direct volume rendering method [2], to give the greatest flexibility to the user. Volume rendering allows users to map data values to colors and opacities of their choosing. This creates an empowering ability to create renderings which highlight areas of interest in exactly

Thanks to the NIH/NCRR Center for Integrated Biomedical Computing for funding.

O. Dössel and W.C. Schlegel (Eds.): WC 2009, IFMBE Proceedings 25/XIII, pp. 41–44, 2009.
www.springerlink.com

Fig. 1. Full-color visible human male dataset, with close-ups of the high-resolution tattoos visible on the chest and arms.

the manner that the user desires.

Unfortunately this flexibility comes with a price: volume rendering is one of the most computationally complex visualization techniques available [3]. We employ standard volume rendering techniques, such as empty space skipping and early termination [4], yet these techniques alone are not enough to achieve the real time rendering performance required for an exploratory visualization tool. To achieve this level of performance, we take advantage of the 3D texturing capabilities [5, 6, 7] and programmable shaders [8] of current graphics processing units.

3.2. Large Data

'Large Data' is a relative term. Such a term might refer to the physical extents of the domain under study, even if the dataset itself requires little disk space. It might refer strictly to the sampling rate used when acquiring that data. Or we might label data 'large' when it exceeds a particular threshold as stored on disk.

For our purposes, we use the following definition of large data:

- Data sets which are larger than the memory available on the computer used for visualization, or
- Data sets with a significant number of high frequency features.

These serve as our general guidelines, in that they imply all of the issues we encounter with large data. For example, large data might technically fit in the amount of memory available on a new workstation, yet conventional 32-bit computing architectures cannot handle data larger than two gigabytes. Further, the time to render datasets of this size would be prohibitively long for an interactive system. Yet data with high frequency components must be rendered at full resolution to effectively capture fine structures such as tattoos or bone texture. Clearly, these two issues represent competing design challenges for a visualization tool.

There are numerous solutions to these problems. The first and most popular approach is to downsample the data to a size which is manageable given the current

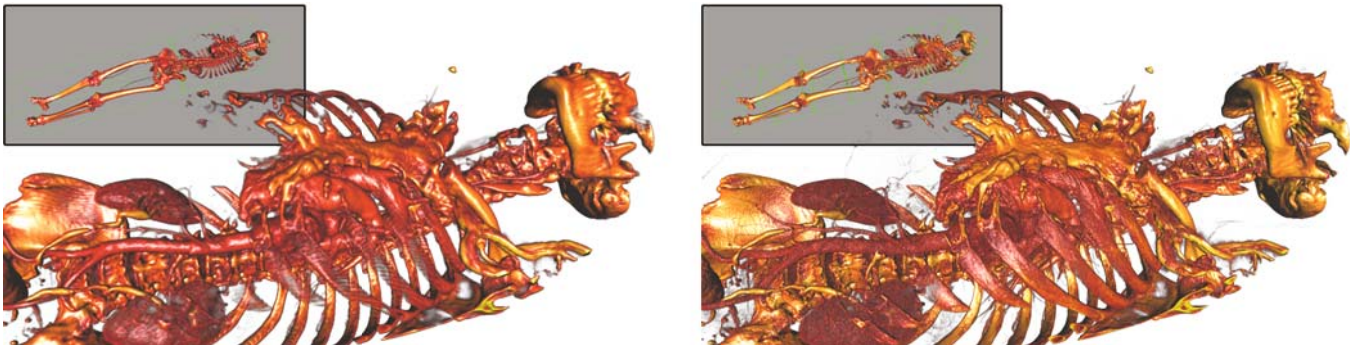

Fig. 2. Renderings at low (left) and high (right) resolutions reflect the importance of viewing data at native resolution. Note the additional texture available in the high-resolution rendering. The full dataset is shown in the background, with green outlines depicting bricks.

computing resources. This is undesirable for many reasons, the most important of which is the loss of important, high frequency features in the source dataset (see Figures 2 and 3) .

Another solution is to crop or extract a subset of the data. A dataset would be split into multiple parts, for example by extracting only the head and shoulders. While this can significantly impact the size of the data to be visualized, we argue that potentially important context information may be lost in this process. Furthermore, used exclusively this strategy is unable to cope with the largest of datasets: a third of the visible human female is around twelve gigabytes, too large for even the most capable current workstations.

3.3. Scalable Tools

The solution we have implemented is a bricked, level of detail volume renderer. Bricking the dataset involves dividing it into chunks of a predefined size, and committing to working with only one such chunk at a time. The advantage of this scheme is that it scales independently of the dataset size. Our system can render datasets up to tens of gigabytes as easily as it renders datasets comprised of only tens of megabytes.

Using level of detail techniques allows real time performance, even for datasets on the size of the visible human male. By presenting the user with a reduced resolution rendering of the dataset during interaction, immediate feedback is given when rendering parameters change. We emphasize that this feature is critical for identifying regions and features of interest. While visualization systems should encourage an exploratory style of interaction, without real time feedback for the available parameters users will inevitably resort to a guess and check style of interaction.

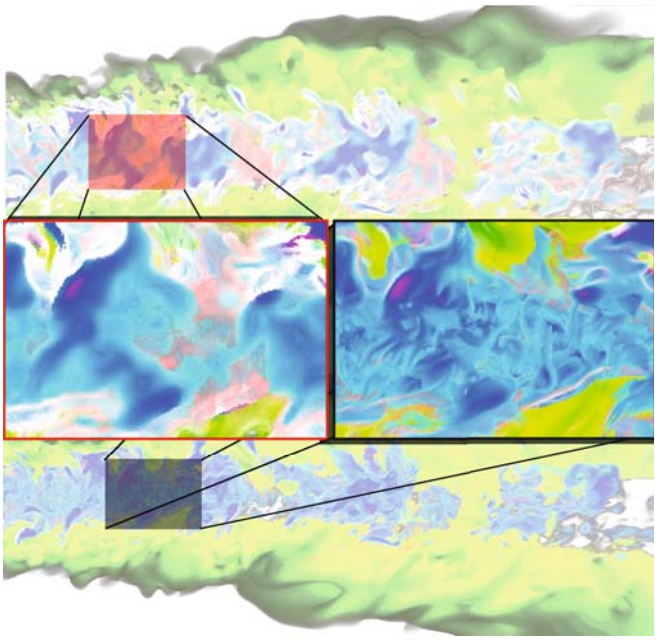

Fig. 3. Low (top) and high (bottom) resolution results from a combustion simulation. Some of the larger structures implied in the low resolution version (left) are not present in the data at its native resolution (right).

Conclusions

Analyzing and rendering data at their native resolution is paramount for gaining insight into fine structures

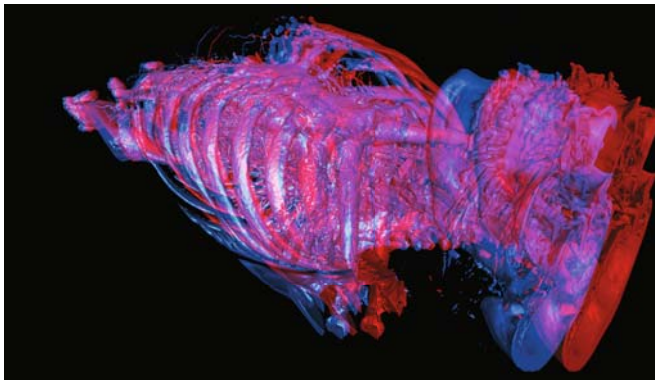

Fig. 4. Stereo rendering of a CT scan. Using anaglyph glasses increases the information presented by offering an illusion of depth.

that frequently go unnoticed. Despite the importance, many if not most tools cannot cope with the size of data currently being generated. To ensure that data size does not become a limiting factor in future research, new tools must be developed, or existing tools retrofitted, to explicitly cope with large data.

As we move forward with larger datasets, tools which can only load and render the data will become obsolete. Since the number of scientifically interesting features of a dataset scales with the dataset size, it follows that the limits of human analysis and cognition will soon become the limiting factor [9]. Therefore scientific visualization tools of the future must embrace a human-assisted computational analysis pattern, to help focus the rare resource of human analysis on the components of a dataset which are most interesting.

Acknowledgements

We thank Jacqueline Chen for the combustion dataset pictured in Fig. 3, and the visible human project for the dataset pictured in Fig. 1. This work was made possible in part by the NIH/NCRR Center for Integrative Biomedical Computing, P41-RR12553-07.

References

[1] V.M. Spitzer, M.J. Ackerman, A.L. Scherzinger, and D.G. Whitlock, "The visible human male: a technical report," *J. Am. Med. Inform.*, pp. 118–130, 1996.

[2] Robert A. Drebin, Loren Carpenter, and Pat Hanrahan, "Volume Rendering," in *SIGGRAPH '88: Proceedings of the 15th annual conference on Computer graphics and interactive techniques*, New York, NY, USA, 1988, pp. 65–74, ACM.

[3] Nelson Max, "Optical Models for Direct Volume Rendering," *IEEE Transactions on Visualization and Computer Graphics*, vol. 1, no. 2, pp. 99–108, 1995.

[4] Marc Levoy, "Efficient Ray Tracing of Volume Data," *ACM Trans. Graph.*, vol. 9, no. 3, pp. 245–261, 1990.

[5] Brian Cabral, Nancy Cam, and Jim Foran, "Accelerated volume rendering and tomographic reconstruction using texture mapping hardware," in *VVS '94: Proceedings of the 1994 symposium on Volume visualization*, New York, NY, USA, 1994, pp. 91–98, ACM.

[6] Timothy J. Cullip and Ulrich Neumann, "Accelerating volume reconstruction with 3D texture hardware," Tech. Rep. TR93-027, University of North Carolina at Chapel Hill, 1994.

[7] R. Westermann and T. Ertl, "Efficiently using graphics hardware in volume rendering applications," in *ACM SIGGRAPH 1998*, 1998.

[8] Jens Krüger and Rüdiger Westermann, "Acceleration Techniques for GPU-based Volume Rendering," in *Proceedings IEEE Visualization 2003*, 2003.

[9] Hank Childs and Mark Miller, "Beyond meat grinders: An analysis framework addressing the scale and complexity of large data sets," in *SpringSim High Performance Computing Symposium (HPC 2006)*, 2006, pp. 181–186.

Focus and Context—Visualization without the Complexity

J. Krüger, T. Fogal

Scientific Computing and Imaging Institute, University of Utah

ABSTRACT

Attempting to display the entirety of a large volumetric dataset at one time would result in an overwhelming amount of information. Furthermore, visualization tools based on volume rendering present the user with a host of confusing options. We present ClearView, which provides a simplified volume visualization tool with a focus on doing what matters most: looking at your data. Users frequently want to direct the viewer's attention to a particular region of their volumes. With many volume rendering tools, this means setting up complex transfer functions to highlight the region of interest, with the unfortunate side effect of potentially affecting the larger image. ClearView allows the user to focus their visualization efforts on the area of their choice, while separating parameters for visualizing of surrounding data. This provides not only a simplified user interface, but finer-grained control over the final publication-quality visualization. Through advanced GPU rendering techniques, ClearView presents all of this to the user at highly interactive frame rates.

Index Terms— focus, context, volume, visualization

1. INTRODUCTION

As data sizes grow, the amount of information resident in those data grows proportionally. Visualizations of these large datasets are correspondingly dense in their complexity, causing the viewer to be lost in a sea of data. This can cause important features to be drowned out by surrounding data, making the viewer focus on aspects of the data which are relatively unimportant.

'ClearView' is a reaction to the complexities of the images generated by modern volume rendering tools. It was designed to follow the 'focus and context' model of visualization, in which we focus our attention on an area of interest while maintaining the relevant context of spatially related data [1]. The result is a very simple tool which users can grasp, manipulate, and use to understand their data quickly and easily.

Images are generated based on the ClearView lens, which the user moves through the dataset to look inside at values of interest. Even though context information is dissolved to allow viewing inner portions of the dataset, small scale structures of the context data are preserved to allow one to easily infer the relationship between the 'focus' and 'context' data.

Fig. 2. ClearView rendering of the visible human male torso.

Thanks to NIH/NCRR Center for Integrated Biomedical Computing for funding.

O. Dössel and W.C. Schlegel (Eds.): WC 2009, IFMBE Proceedings 25/XIII, pp. 45–48, 2009.
www.springerlink.com

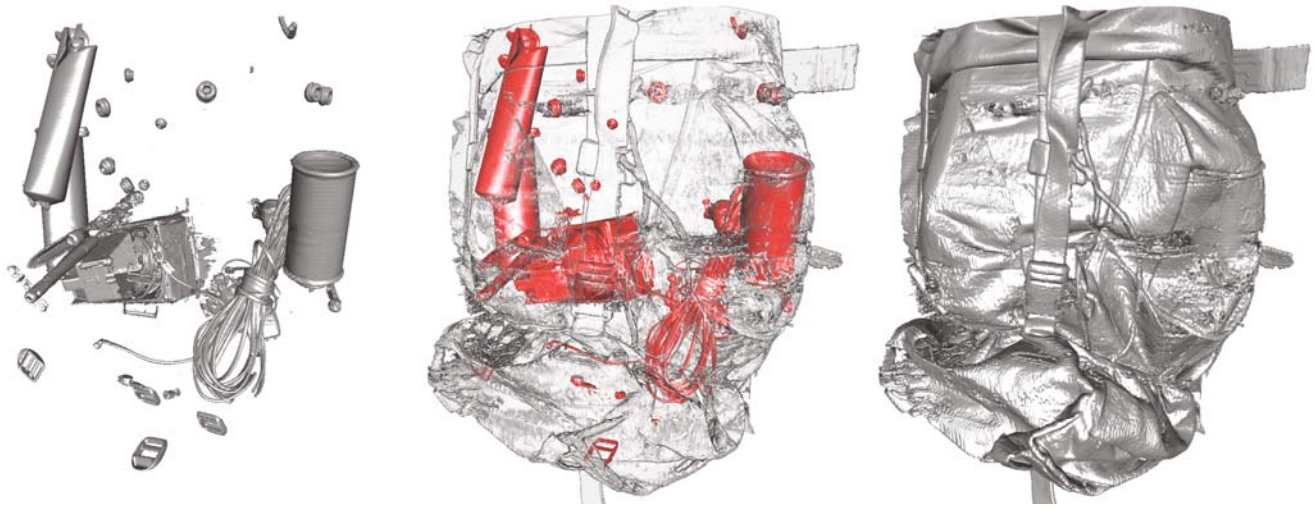

Fig. 1. Internal (left) and external (right) views of a backpack, with the ClearView rendering in the center.

2. Methods

At its core, ClearView is a rendering mode which allows the simultaneous viewing of two isosurfaces: an inner, or 'focus' isosurface, and an outer, or 'context' isosurface. ClearView renders the two surfaces independently and then composites them together based on the position of the ClearView lens. The lens dictates the behavior of the compositing: near the center of the lens, the 'focus' isosurface dominates the rendering. As the distance increases radially from the center of the lens, the 'context' isosurface is weighted more prominently. Thus it appears as if the 'focus' isosurface is gradually occluded by the 'context' isosurface.

Yet ClearView provides more than just a rendering of two isosurfaces. To better highlight the important context information available in the dataset, distinct features in the context isosurface are preserved even if the lens is focused on those features. In the depicted implementation, areas of high curvature are preserved. This is represented well in Figure 2; note that one can still recognize creases in the neck, as well as the location of the ears, despite the ClearView lens being centered around the jaw.

Real time feedback of malleable rendering parameters is critical for exploratory visualization systems [2]. Due to the importance of this style of interaction, ClearView is implemented to take advantage of the advanced parallel computation capabilities of modern graphics processing units [3, 4, 5]. This design choice, coupled with an appropriate out of core renderer [2], allows ClearView to render data of immense sizes at hundreds of frames per second.

3. Discussion

To use ClearView, the user selects an outer isovalue, which determines the surface rendered for the 'context' isosurface. Then the user places a lens over the data which depicts the location where the inner surface will show through. Finally, the user customizes a second isovalue, in turn selecting the inner or 'focus' isosurface. This makes an intuitive interface to create informative visualizations, as has been shown in previous work [6, 7].

The ease of explanation is one of the strengths of ClearView. Unlike some volume rendering tools, users can immediately grasp the concept behind ClearView and focus on looking at their data. Further, users do not need to become volume rendering experts to explain to a colleague what a ClearView visualization is conveying—in many cases, no explanation is required, as the focus of the image is self-evident.

4. Conclusions

Advances in state of the art visualization can enable and empower users to create new and informative visualizations. However non-experts may lack the time required to penetrate the background material needed to under-

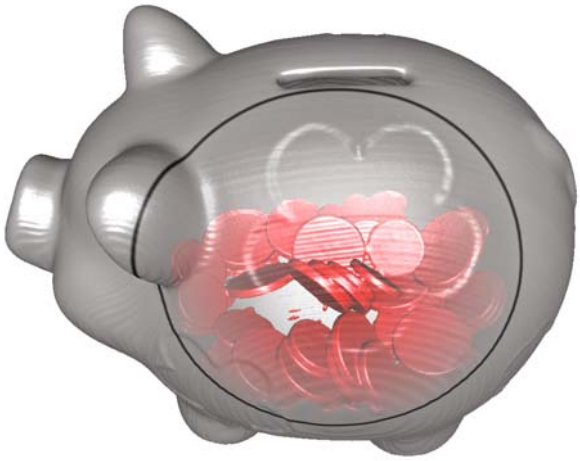

Fig. 3. The rendering provided by ClearView allows us to count the change in this piggy bank, saving the fortuitous piggy from untimely destruction.

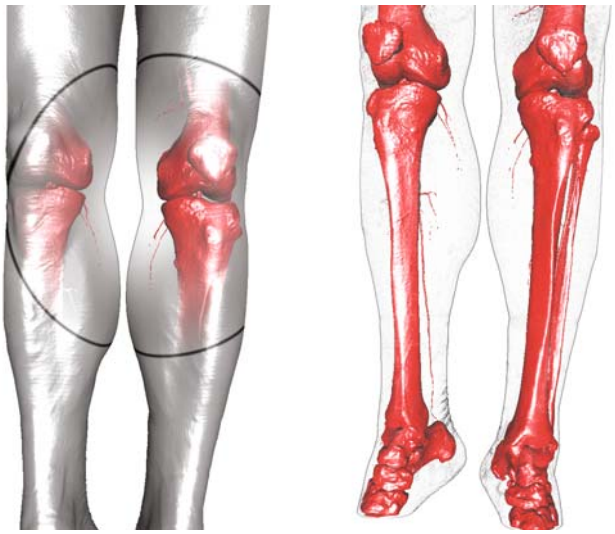

Fig. 4. ClearView renderings of the knee area clearly show the relative size and alignment of bone and flesh.

stand a new method. For the most part, researchers should not be expected to become experts in visualization technologies if they only desire to use a specific tool. In the end, what matters most is the ability to create informative media with minimum effort.

ClearView provides a simplified rendering mode which sacrifices complexity to focus on what the majority of users require: a method to highlight a feature of interest without removiing potentially relevant context information. In contrast to typical volume rendering tools, ClearView has few parameters, and the default settings work surprisingly well; this allows users to rapidly discern the interesting features of their data.

Acknowledgements

We thank the visible human project for providing the visible male dataset. This work was made possible in part by the NIH/NCRR Center for Integrative Biomedical Computing, P41-RR12553-07.

References

[1] Jens Krüger, Jens Schneider, and Rüdiger Westermann, "ClearView: An interactive context preserving hotspot visualization technique," *IEEE Transactions on Visualization and Computer Graphics (Proceedings Visualization / Information Visualization 2006)*, vol. 12, no. 5, September-October 2006.

[2] Thomas Fogal and Jens Krüger, "Size matters—revealing small scale structures in large datasets," in *International Union for Physical and Engineering Sciences in Medicine World Congrees 2009*, September 2009, To Appear.

[3] Brian Cabral, Nancy Cam, and Jim Foran, "Accelerated volume rendering and tomographic reconstruction using texture mapping hardware," in *VVS '94: Proceedings of the 1994 symposium on Volume visualization*, New York, NY, USA, 1994, pp. 91–98, ACM.

[4] Timothy J. Cullip and Ulrich Neumann, "Accelerating volume reconstruction with 3d texture hardware," Tech. Rep. TR93-027, University of North Carolina at Chapel Hill, 1994.

[5] Jens Krüger and Rüdiger Westermann, "Acceleration Techniques for GPU-based Volume Rendering," in *Proceedings IEEE Visualization 2003*, 2003.

[6] Milan Ikits and Charles D. Hansen, "A focus and context interface for interactive volume rendering," May 2004.

[7] Eric A. Bier, Maureen C. Stone, Ken Pier,

WILLIAM BUXTON, AND TONY D. DEROSE, "TOOLGLASS AND MAGIC LENSES: THE SEE-THROUGH INTERFACE," IN *SIGGRAPH '93: Proceedings of the 20th annual conference on Computer graphics and interactive techniques*, NEW YORK, NY, USA, 1993, PP. 73–80, ACM.

Electroporation and Behind: The Action of Nanosecond Pulsed Electric Field

U. Pliquett

[1] Institut für Bioprozess- und Analysenmesstechnik e.V., 37308 Heilbad Heiligenstadt, Germany

Abstract **The electrical properties of cells and tissue during electroporation at moderate field strength (E < 2 kV/cm) and its recovery after high voltage application is compared to the behavior due to nanosecond pulsed electric field (nsPEF) with a field strength exceeding 10 kV/cm. Key features at nsPEF are the extremely high conductivity and the fast decay in conductivity after the pulse.**

Based on experimental results a hypothetical mechanism for the action of extremely high field strength on the level of bilayer membranes is given. This involves the disintegration of membrane structures so that lipid molecules form micellar structures. The extremely fast recovery is due to self organization in the absence of stable pore structures.

Keywords **electroporation, nsPEF, electrical behavior, impedance, lipid bilayer, micelle**

I. Introduction

Electroporation is a physical phenomenon rendering biological membranes permeable in the presence of an outer electric field. Once the membranes are charged to several hundred millivolt, they become instable due to water entering the membrane structure. With water inside the membrane, the head groups of the lipid molecules turn into the membrane, thereby forming a hydrophilic pore (electroporation). Such pores with a radius on the order of 1 nm are stable during the presence of the electric field due to the polarization of the water. As soon as the field ceases, pores below a critical radius start to shrink and finally reseal which reestablishes the low permeability of the membrane. Larger pores are stable even without the electric field and persist up to seconds or even hours. If the outer electric field strength equilibrates with the field inside the membrane, i.e. the time duration of the electrical stimulus is long compared to the charging time constant of the membrane (μs-range), electroporation proceeds near the thermodynamic equilibrium.

Numerous applications of electroporation have been explored. Mostly, the high permeability during the presence of the electric field is employed for facilitating molecular transport across the plasmamembrane of cells like for instance in electrochemotheraphy or electrotransfection . By application of pulsed electric field even the multilamellar systems of the stratum corneum, the outer highly insulating layer of the skin, can be transiently permeabilized. This is a candidate approach for transdermal delivery of large, charged molecules.

One of the first demonstration of the action of electric field at cells was the inactivation of bacteria and yeast [1]. During the last years, several applications for electrically mediated cell killing were established. The cell death is interpreted as a result of irreversible breakdown of the plasma membrane. Other applications for irreversible breakdown or even disintegration of the plasmamembrane are developed for food processing. A very successive approach is the extraction of sugar from beets [2]. It was found, that cell killing and electrically mediated extraction processes with short pulses but therefore very high electric field strength are more efficient.

Basically, pulsed electric fields are used for two distinct purposes: electrically mediated transmembrane transport where irreversible breakdown of the membrane should be avoided and cell killing or cell destruction which bases on irreversible breakdown of membranes.

II. Time course of electroporation

For kinetic studies of electroporation both imaging and electrical measurements [3] were used. While the optical measurements show clearly the transmembrane voltage with local resolution, electrical measurements reveal the transport of charged species across the membrane. The conductivity increase exhibits two distinguishable phases. In a first phase on the order of several microsecond most of the pores are created. Especially in cells with membranes supported by structure proteins, which creates stress and tension within the plasma membrane, pore expansion is probably the reason for a second, much slower phase (10 ms-range). Further increase of the membrane conductivity involves Joule heating or the disintegration of the membrane.

Besides the both phases showing kinetics of first order, an additional phase appears when the field strength exceeds 2 -5 kV/cm, depending on the system under investigation. This phase is a sudden step of conductivity. Even more interesting, the conductivity immediately after the high voltage pulse (< 10 ms) was elevated by almost

O. Dössel and W.C. Schlegel (Eds.): WC 2009, IFMBE Proceedings 25/XIII, pp. 49–52, 2009.
www.springerlink.com

the same value as the sum of the amplitudes of phase 1 and 2. The extent of conductivity increase did not depend on the additional conductivity step at the beginning of a very high pulse. The explanation for this step involves a Wien effect but is not fully justified yet.

Moreover, the conductivity jump was even more pronounced during the application of ns-pulses (t_{pulse}<300 ns) with a field strength exceeding 10 kV/cm [4].

For a candidate explanation one should recall the behavior of electrolytes and supramolecular structures in an electric field.

III. Wien effect

The electrolytic conductivity is highly dependent on the ionic strength, temperature and the degree of dissociation. Especially at high ionic strength, the counter ion cloud shields the central ion which results in decreased molar conductivity. The molar conductivity is the conductivity with respect to the concentration of the dissolved molecules. According to the experimental results of Kohlrausch and the theoretical explanation of Debye, Hückel, and Onsager the molar conductivity depends on the square root of the concentration (Kohlrausch's law).

Besides these factors, high frequency and electric field strength influences the conductivity as well. In a high electric field ($E > 10^6$ V/m) an increase in molar conductivity is observed. A candidate explanation is the loss of the counterion cloud due high electric field, which prevents the immobilization of the central ion (I. Wien effect). Theoretically, the molar conductivity can reach the limiting molar conductivity, which is the conductivity at infinite dilution or where no electrostatic interactions take place. This affects mostly strong electrolytes. Week electrolytes, showing a low level of dissociation, are affected at even higher field strength. The increase in conductivity cannot be explained by the loss of the counter ion cloud, because of the low concentration of dissociated molecules. It is likely that the high electric field ($E > 10^7$ V/m) overcomes the electrostatic binding forces within the molecule and shifts the dissociation equilibrium towards the ions (field dissociation) which in turn creates new movable charge carriers (II. Wien effect).

In experiments up to $3 \cdot 10^6$ V/m, a conductivity increase for strong electrolytes (KCl, NaCl) on the order of less 2 % was found. For a week electrolyte (acetic acid) with low initial conductivity only a trend of conductivity increase was seen. Because of the scattered data, these results have not been significant (unpublished).

However, the conductivity step in cell suspensions, or even more pronounced, in tissue at the beginning of very high pulses [4] can be up to several times. This is not compatible with the Wien effect for pure electrolytic solutions.

IV. Effect of electric field on supramolecular structures

By involving macro molecules, like collagen or agarose gel, an increase up to 2.5 % for 2 mM NaCl at 30 kV/cm was found. This suggests that the involvement of supramolecular structures can enhance the Wien effect.

An even higher effect, up to 100 % was found for micelle forming molecules such as SDS (sodium dodecyl sulfate). Usually, SDS showed a CMC (critical micelle constant) around 9 mM measured by using the conductivity κ depending on the concentration c at room temperature. In brief, if no micelles are created, the κ/c – curve is almost linear (still fulfilling Kohlrausch's law). When micelles are created, the mobility of the SDS molecules decreases significantly which results in less conductivity increase with increasing concentration. The CMC will be found where the curve kinks (Fig.1. right diagram).

A special experiment was designed for the investigation of the role of the electric field for micelle creation. First, the CMC has been determined using a conductometer as control (Fig.1. red curve). Further experiments were done in a high voltage pulse chamber machined from Plexiglas with parallel stainless steel electrodes with a distance of 1 mm.

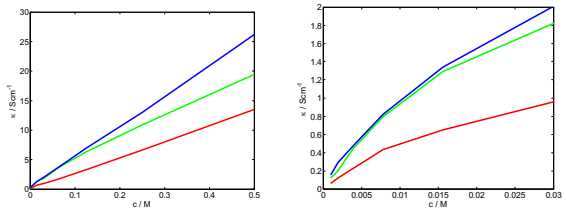

Fig.1. Conductivity of a SDS-solution. (Red : conductometer, green : 1 kV/cm, blue : 100 kV/cm)

Instead of using low voltage AC-measurements, a pulsed electric field (PEF) was applied. The maximum voltage applied was 10 kV and the length of the pulses was 400 ns, generated by means of cable discharge. Due to the cable impedance, only 4 kV were reached for the highest concentrations (c > 0.2 M).

The current was determined using a pickup coil. It was checked that the electrode impedance was negligible using NaCl – solution of different concentration.

Under the influence of a high electric field, a shift of CMC to higher concentration, i.e.16 mM for 100 kV/cm, was found. The most important outcome of this study was

the increase of the conductivity which reached up to 190 % for the highest field strength, which suggests that the SDS-molecules do not form stable micelles under the influence of a high electric field.

V. Electrical Behavior of Cells and Tissue During and After nsPEF

At least two phases of conductivity increase could be distinguished during the presence of moderate electric field. Experimentally, it is much more complicate for the ultrashort pulses. Independent on the first step of conductance increase, even during the presence of ns-pulses a further increase takes place. This is even more pronounced for highly insulating tissue like stratum corneum. For instance, for mouse skin a dramatic increase during a 300 ns-pulse by up to 30 % was found [4]. Unfortunately, due to the noisy signals, no kinetic information could be derived. So far, nsPEF and pulses at moderate voltage show similar action on biological matter.

However, quantitatively, the conductivity increase due to very high electric field exceeds the limits of electroporation (Fig.2). If an insulating membrane experiences electroporation, the membrane conductivity increases. The limits are expected between no changes (no pores are created) and membrane conductivity equal to the conductivity of the surrounding electrolytes (100% electropores). The upper limit can be estimated by the electrical impedance. Since the β-dispersion is caused by membrane structures, at any frequency above this dispersion all membranes show a negligible resistance. Therefore, the magnitude of the impedance at 3 MHz is a good estimation for the upper limit of the conductivity during high voltage application.

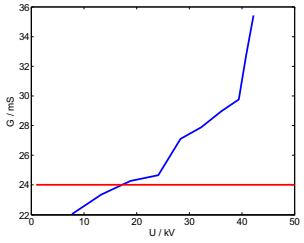

Fig.2. Conductivity (blue line) of a cell suspension (Jurkat, cell volume fraction = 15 %). The red line shows the magnitude of the conductance, $Y = 1/Z$, at f = 3 MHz.

The increased conductivity at moderate field strength can be explained using the pore concept. However, at a field strength, exceeding 20 kV/cm the membrane conductivity exceeds the conductivity of the surrounding electrolytes, which is hard to explain with creation of electrolyte filled pores [4].

Immediately after a moderate electric field ceases, the recovery of the membrane integrity takes place in several phases. It lasts from milliseconds up to seconds or even minutes. Using the single shell model for cell suspensions, elevated membrane conductivity on the order of magnitudes was found immediately (10 to 50 ms) after the pulse. It should be noted, that the single shell model is only an approximation due to the high cell concentration used in these experiments.

After the application of nsPEF with a field strength exceeding 20 kV/cm, however, a very fast recovery was found. Despite persistent changes during several minutes [5] were found, a very fast recovery from the extremely high conductivity during the pulse to about 2-3 times of the membrane conductivity before pulsing happens within less than 50 ms. This is in contrast to the expectation that a greater disturbance of the membrane should be followed by a slower recovery. It should be noted, that in [5] patch-clamp technique at a single cell was used while the fast recovery was found with fast impedance measurements after the high voltage application (submitted for publication). Therefore, both results are not directly comparable.

V. Discussion

The marked difference in the action of high voltage pulses at moderate (E < 2 kV/cm) and very high (E > 20 kV/cm) is the very different conductivity during the pulse and the quite different recovery after the pulse.

While the conductivity increase at moderate field strength is compatible to the pore concept, the high conductivity at higher field strength exceeds the limits of pore creation. A candidate explanation is the disintegration of the membrane structure. It should be recalled that double tailed lipids form bilayer structures rather than micelles because of the space requirement due to the two tails. In case of micelle forming, it would yield a relatively large angle between neighboring molecules and therefore an exposure of the hydrophobic tails to the water, which is energetically not favorable. In the presence of a high electric field however, water is forced into these regions, which in turn will stabilize micelle structures. As found experimentally, even micelle structures can break down in the presence of a high electric field (Fig.1), yielding freely movable charge carriers. This is behind the Wien effect as understood for pure electrolytic solutions. However, it is similar to the field dissociation and will considerably increase the conductivity of supramolecular structures such as membranes or micelles. Since

most of the cells consist of electrolytes surrounded by membrane systems (endoplasmatic reticulum, Golgi apparatus, mitochondria, lysosomes, ribosomes, peroxysomes etc.) even the cell plasma will exhibit an increase in conductivity due to an applied electric field.

The time required for the disintegration is extremely short due to the fact that the system is far from thermodynamic equilibrium. In experiments, where the applied field strength is just sufficient for charging the membrane to condition where electroporation takes place, a negative feedback saves the membrane structure. Once electroporation happens, the increase in membrane conductivity will lower the field within the membrane due to the voltage divider between the membrane and the surrounding electrolytes. This in turn prevents further pore creation or can force already existing pores to shrink or even reseal.

A very rapid charging of the membrane (ps – ns) does not leave the time for pore creation which yields a somehow 'overcharged' membrane. Under this condition, thermodynamic equilibrium is far and extremely fast structural changes become likely.

In the extreme case of complete disintegration of the membrane structures, a homogeneous mixture of lipids and electrolyte appears. Immediately after the pulse, self organization would force the reestablishment of bilayer structures. Interestingly, this is a very fast process on the order of nanoseconds as suggested by molecular dynamics [6]. Despite of numerous defects after about 5 ns, a mostly defect free membrane was found in simulation after 15 ns which is quite compatible with the fast recovery process ($t_{recover} < 10$ ms) found experimentally.

The membrane structures recreated in this way may have a different composition due to phase separations. Moreover, it is expected that the leaflets are mixed up that for instance phosphatidylserine appears at the non cytosolic side. Besides this, the loss of membrane material becomes likely.

The biological significance is not completely clear. It is evident, that ultrashort but very intense pulses kill cell more efficiently than long lasting pulses with moderate field strength. On the other hand, cell survival has been reported for nsPEF as well. Finally, it is important what structures of the cell are altered so that their function is non recoverable. If for instance the plasma membrane is disturbed, most cells will reestablish it within seconds to minutes. Other than a mixture of lipids and electrolyte, a disintegrated biological membrane is still supported by structure proteins which prevent the free diffusion of membrane material and proteins anchored within the membrane and the cell cortex.

Only if essential parts of the cell, like the DNA are altered, the cell will die.

VI. Conclusion

A hypothetical, mechanistic model for the action of ultrashort but very intense electrical pulses at living cells is presented. Although the pore model [7] cannot be ruled out, a disintegration of membrane structures is likely as well. Especially the extremely high conductivity during the field application will exceed the pore model and Wien effect as known for pure electrolytes. Other features, like loss of membrane material after nsPEF or the externalization of molecules like phosphatidylserine, hint to a greater disturbance of the membrane.

References

[1] A. J. H. Sale and W. A. Hamilton, Effects of high electric fields on microorganisms. I. Killing of bacteria and yeasts, Biochim. Biophys. Acta 148 (1967) 781-788.

[2] C. Schultheiss, H. Bluhm, H.-G. Mayer, M. Kern, Y. Michelberger, and G. Witte, Processing of sugar beets with pulsed-electric fields, IEEE Transactions on Plasma Science 30 (2002) 1547-1551.

[3] M. Schmeer, T. Seipp, U. Pliquett, S. Kakorin, and E. Neumann, Mechanism for the conductivity changes casued by membrane electroporation of CHO-cell pellets, Phys. Chem. Chem. Phys. 6 (2004) 5564-5574.

[4] U. Pliquett, R. P. Joshi, V. Sridhara, and K. H. Schoenbach, high electrical field effects on cell membranes, Bioelectrochemistry 70 (2007) 275-282.

[5] A. G. Pakhomov, J. F. Kolb, J. A. White, R. P. Joshi, S. Xiao, and K. H. Schoenbach, long-lasting plasma membrane permeabilization in mammalian cells by nanosecond pulsed electric field (nspef), Bioelectromagnetics 28 (2007) 655-663.

[6] Marrink S.J., E. Lindahl, O. Edholm, and A. E. Mark, Simulation of the spontaneous aggregation of phospholipids into bilayers, J. Am. Chem. Soc. 123 (2001) 8638-8639.

[7] T. R. Gowrishankar and J. C. Weaver, electrical behavior and pore accumulation in a multicellular model for conventional and supra-electroporation, Biochem. Biophys. Res. Commun. 349 (2006) 643-653.

Corresponding author:

Author: Uwe Pliquett
Institute: Institut für Bioprozeß- und Analysenmesstechnik e.V.
Street: Rosenhof
City: Heilbad Heiligenstadt

Country: Germany
Email: uwe.pliquett@iba-heiligenstadt.de

APPLICATION OF MORPHOMETRIC ANALYSIS FOR QUONTITATIVE EVALUATION OF LIVER BIOPSIES IN THERAPEUTIC TRIALS

I.B. TOKIN[1], I.I. TOKIN[2], G.F. FILIMONOVA[2], P. HUSSAR[3], V.M. BURE[1], Yu. M. MOTUSENKO[1]

[1]Department of Computer Microscopy, Faculty of Applied Mathematics, State University, University Ave 35, St.-Petersburg, 198504 Russia (ivan.tokin@pobox.spbu.ru); [2]Department of Histology, State Medical Academy, St.-Petersburg, Russia; [3]Department of Histology, Estonian University of Life Sciences, Tartu, Estonia

Abstract: Quantitative stereological morphometric analysis of liver biopsy was used for more correct evaluation of dynamic of liver damages in patients with chronic viral hepatitis C. The analysis allows to estimate the area (%) of non-parenchymal elements such as portal tracts, bridging and piecemeal necrosis, intralobular focal infiltrates. That is important for estimation of efficiency of antiviral therapy. The investigation showed that the portion of the area of non-parenchymal elements of different patients strongly varied; the interrelations between some morphological parameters and level of serum alanine aminotransferase were established. This study demonstrates that the ratio of the area of non-parenchymal elements to that of entire tissue specimen in the initial biopsy might be a predictive factor for prognosis.

Introduction

Information on the stage of fibrosis in chronic hepatitis C (HCV) is essential to make prognosis and decide antiviral treatment (Koda et al., 2007). Liver biopsy is the gold standard for fibrosis staging in chronic hepatitis. However, recent studies have reported that the estimation of fibrosis by semi-quantitative scoring system is not always accurate and high rate of inter- and intraobserver discrepancies takes place (Rousselet et al., 2005).

We used quantitative stereological analysis of liver biopsy for more correct estimation of stage of fibrosis in patients with chronic hepatitis C. We also performed comparative analysis of development of fibrosis and level of serum alanine aminotransferase (ALT).

Material and methods

All liver biopsies were performed according to the routine medical follow up program, using the standard Mengini procedure. Samples were formalin-fixed and paraffin-embedded. Hematoxylin-eosin stain was used. Each biopsy for necro-inflammatory activity and fibrosis was assessed by two hepatologists. Knodell Histology Activity Index (HAI) was used to grade histopathological lesions. METAVIR group scoring system was used for detecting the stage of fibrosis. Fibrosis was staged on a scale from F0 to F4, as follows: F0 = no fibrosis, F1 = portal fibrosis without septa, F2 = few septa, F3 = numerous septa without cirrhosis, and F4 = cirrhosis. None of the included patients showed any signs of cirrhosis.

The stereological method of morphometry is based on counting the points or intersections at the standard unit as the field of microscope at the magnification of x 400. This method was used either for measurement of portions (%) of non-parenchymal elements (portal tracts, piecemeal and bridge necrosis, hepatic vessels) and for estimation of foci of intralobular necrosis at the magnification of x 400. All liver sections were considered adequate and based on specimen size (about 10 mm) and number of portal tracts (no less than 5). HCV infection was defined as positive HCV-RNA by polymerase chain reaction. Serum level of ALT was expressed. The upper limit of normal (ULN) of ALT was 41 U/L for men and 31 U/L for women.

Variables, differing significantly according to quantity of non-parencymal elements in the estimation group were identified by univariate analysis. Therefore, all variates were included in a multivariate forward stepwise regression analysis to determine the morphometric data. Spearman correlation coefficients were used to evaluate whether changes in morphometric data were correlated with ALT. Statistical analysis was performed by tabulated processor MS Excel, package STATISTICA.

Results

Typical histological features of chronic hepatitis C are variable degrees of hepatocellular necrosis and fibrosis as non-parencymal elements. For measurement of the area of non-parencymal elements the field of vision of a microscope at the magnification of x400 as a standard unit (SU) of accounting was accepted. The number of investigated SU changed from 58 to 290 and on the average was 173.3 ± 16.8. Accordingly, the total volume of morphometry (the number of points or intersections) varied from 17980 to 89900, average value 53339.7 ± 5211.6. The amount of investigated material was enough and statistically significant.

The analysis showed that the portion of the area of non-parenchymal elements of different patients strongly varied, from 2.16 % to 11.93 %. Comparative estimations of morphological pictures, semi-quantitative evaluation of HAI and staging of fibrosis, quantitative stereological morphometric analysis of non-parenchymal parameters showed

O. Dössel and W.C. Schlegel (Eds.): WC 2009, IFMBE Proceedings 25/XIII, pp. 53–54, 2009.
www.springerlink.com

specific interaction. So, if the portion (%) of non-parenchymal elements varied from 2.26 % to 4.30 %, fibrosis was absent (F0). The portion of non-parenchymal elements from 4.63% to 6.64% corresponded to weak fibrosis (F1). The portion of non-parenchymal elements from 8.67% to 11.93% was typical for patients with the picture of moderate and heavy fibrosis (F2, F3).

It is also essential that, as a rule, the patients with a high index of non-parenchymal elements were discovered with bridging and piecemeal necrosis and chains of lymphocytes in sinusoids.Correlations between focal intralobular infiltrates and the presence of chains of lymphocytes inside sinusoids were discovered (r = 0.7104), that important for estimation of severity of necroinflammatory activity with HCV.

We supposed that evaluation of index of non-parenchymal elements had important predicting value. As a rule, the increasing of index higher than 6% was connected with the activation of necro-inflammatory lesions.

With the help of correlation and regression analysis the interrelations between level of serum ALT and morphological parameters of non-parenchymal elements were established (coefficient of correlation r_{xy} = 0.74124499, p = 0.0025; coefficient of determination R^2 = 0.54944413, F-statistic F = 14.63376674 at the level p = 0.0025). Interrelation appeared more strongly at light increase of level ALT.

Statistically significant correlation and regression dependences of specific area focal intralobular necrosis and level of ALT were also considered (coefficient of correlation r_{xy} = 0.7807727, p = 0.00025; coefficient of determination R^2 = 0.609613146, F-statistic F = 23.42342499 at the level p = 0.0003). These findings support the clinical usefulness of monitoring ALT levels in assessing of disease progression.

Conclusion

Stereological quantitative morphometry allows to getting more correct evaluation of some morphological parameters of pathologically changed liver in patients with chronic viral hepatitis. It is very important for establishment of either positive or negative dynamic changes in liver, especially during estimation of efficiency of antiviral treatment. We supposed that the stereological morphometry is a suitable tool for quantitative avaluation of liver biopsies in therapeutic trials.

References

Koda M, Matunaga Y, Kawakami M. et al. (2007). Fibroindex, a practical index for predicting significant fibrosis in patients with chronic hepatitis C. *Hepatology,* **45**: 297-306.

Rousselet MC, Michalak S, Dupre F. et al. (2005). Hepatitis Network 49. Sources of variability in histological scoring of chronic viral hepatitis. *Hepatology*, **41**:257-264.

IMAGE-GUIDED STEREOTACTIC SMALL ANIMAL IRRADIATOR

Pidikiti R[1], Stojadinovic S[1], Song K[1], Speiser M[1], Seliounine S[1], Saha D[1], Solberg TD[1]

[1]University of Texas Southwestern Medical Center, Dallas, TX, USA

Abstract— **Stereotactic body radiation therapy (SBRT) is a promising modality in the treatment of cancer. Despite success in early clinical applications and in subsequent clinical trials, there remains much to learn to understand and optimize the effects in tumors and normal tissues. In this study, we develop and characterize an image-guided small animal stereotactic body irradiator capable of delivering a highly localized radiation beam accurately to a small target. The irradiator employs a commercial X-ray device (XRAD 320, Precision X-Ray, Inc.) and a modular collimation system, consisting of a brass collimator holder and variable tungsten alloy collimators with apertures ranging from 1 to 10 mm in diameter. The unit is typically operated at 30 kVp for image guidance and at 250 kVp for therapy. To characterize the radiation beam, we measured percent depth dose (PDD), off-axis ratios (OARs), and absolute dose rate for each collimator using radiochromic film (Gafchromic EBT, International Specialty Products, Wayne, NJ). For all collimators the penumbra, defined as distance between 80% and 20% isodoses, was measured at a source-to-surface distance (SSD) of approximately 20 cm. For a 5 mm collimator, in-plane and cross-plane measurements of penumbra were 0.7 and 1.1 mm, respectively. Absolute dose rates ranged from 6.7 to 11.6 Gy/min for the 1 to 10 mm collimators. The image guidance system provided accuracy commensurate with stereotactic localization in small animals. We have demonstrated the capability of an image-guided stereotactic radiotherapy by the animal studies. Subsequent studies in a variety of pre-clinical tumor and normal tissue models suggest that use of the irradiator can significantly contribute to the understanding of new clinical therapies such as SBRT.**

Keywords— **SBRT, Small animal irradiation, kV dosimetry, Image guided radiotherapy**

I. Introduction

With the advent of advanced image-guidance technologies, stereotactic body radiation therapy (SBRT), the application of an ablative dose of radiation given in one or few fractions and delivered with high accuracy, has emerged as a promising modality in the treatment of cancer[1-2]. despite this success, there remains room in optimizing delivery and understanding response. In this regard, pre-clinical studies can be very beneficial in systematically evaluating response and predicting and validating clinical protocols [3]. To be most effective, pre-clinical experiments must mimic clinical application as closely as possible; in the case of SBRT, it is critical to deliver a highly localized radiation dose to the desired target while sparing normal tissue. Due in part to the lack of sophisticated equipment necessary to provide precise stereotactic radiation delivery to mice and rats, systemic small animal SBRT studies have thus far been limited.

In this work, we describe the development and application of a small animal irradiator, which provides high accuracy in target localization and radiation delivery in a manner that mimics clinical SBRT delivery. The essential characteristics of the irradiator include: a high dose rate (≥ 10 Gy/min), allowing high dose delivery in a clinically-relevant time frame; precise target localization (≤ 1 mm) to optimize irradiation to a tumor with respect to normal tissue sparing; and small radiation fields (1 to 10 mm) needed to implement the technology in small animals. The irradiator is based on a commercial X-ray device (XRAD 320, Precision X-ray, Inc.). The system can be operated at low energies (20-30 kVp) for high contrast imaging (essential for precise localization), and at high energies (≥ 250 kVp) for therapeutic delivery. Characterization of radiation beam parameters, including energy specification (characterized by the half-value layer - HVL), depth dose characteristics, and off-axis ratio, are essential for accurate treatment planning and delivery. Absolute calibration, following the TG 61 protocol [4], is also necessary for delivering the desired dose. In this study, we have described the design and characterized the radiation beam of a prototype small animal irradiator, and demonstrated the capabilities of image-guided stereotactic radiotherapy in a rat orthotopic lung tumor model.

II. Materials & Methods

The irradiator consists of four main components: a small field collimation system, a digital imaging system, a 3D animal positioning device, and a commercial x-ray tube which provides beam for both imaging and therapy.

Collimation and beam characterization: The current collimation assembly consists of different sizes of collimators and a disk-shaped collimator holder shown in Figure 1. The collimators are made of high density (14.7 g/cm^3) tungsten and copper alloy and are interchangeable with five different collimator apertures: 1.0, 3.5, 5.0, 7.5, and 10.0 mm in diameter. The collimator holder is made of brass (8.4 g/cm^3), 2.3 cm in thickness and 12.3 cm in diameter. The holder also has 2.3 cm

O. Dössel and W.C. Schlegel (Eds.): WC 2009, IFMBE Proceedings 25/XIII, pp. 55–58, 2009.
www.springerlink.com

circular opening at the center into which the variable-aperture collimators are inserted. The appropriate aperture is selected based on the target volume of interest. For imaging, the required field of view is obtained by simply removing the collimator assembly. The source to surface distance is adjusted based on imaging and therapy requirements, on animal size (mice versus rats), and on desired dose rate. Imaging is performed at the tube potential of 30 kVp and 10 mA while treatment is performed at 250 kVp and 15 mA with the addition of 1.65 mm Al filtration.

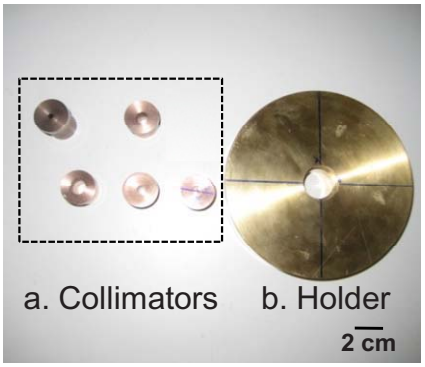

Fig 1 The collimator components, with apertures of 1.0, 3.5, 5.0, 7.5, and 10.0 mm. Apertures are manually inserted into the brass collimator holder, which measures 2.3 cm in thickness by 12.3 cm in diameter.

Imaging system: The image guidance system (Figure 2) consists of a high resolution x-ray intensifying screen (Kodak Min-R2) coupled to a computer-controlled digital camera. The camera parameters and image acquisition are controlled by a PC through a USB port**.** For image-guided positioning of an animal, a 3D manual translational stage is employed.

III. Results

Dosimetry: Initial dosimetric measurements have been performed using radiochromic film (Gafchromic EBT, International Specialty Products, Wayne, NJ). Dose analysis is conducted with commercially available FilmQA software (3cognition LLC, Great Neck, NY). Film calibration was performed by exposing a reference set of films to known doses, using a 6 MV linear accelerator (Varian Medical Systems, Palo Alto, CA). Radiochromic film is a preferred dosimeter since its response is energy independent at clinically-relevant X-ray energies [5]. For an accurate dose calculation and treatment planning, a systematic characterization of beam parameters (depth dose, off axis ratios, dose rate and relative output) must be performed for a range of source-to-surface distances and field sizes.

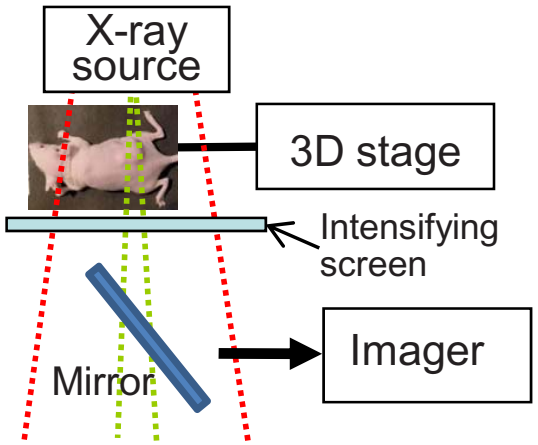

Fig 2. Diagram showing components and operation of the imaging subsystem.

Transmission through the collimator, measured in narrow beam geometry at 250 kVp, was less than 2%. Beam quality at a nominal potential of 250 kVp is 0.73 mm Cu (Figure 3). Absolute dose rates at a distance of 19.76 cm from the source, measured using radiochromic film, range from 6.75 to 11.65 Gy/min for 1 to 10 mm diameter collimators (Figure 4).

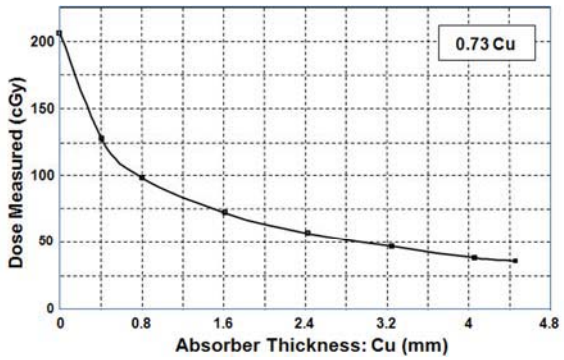

Fig 3 Beam Quality at 250kVp setting (1.65 mm Al additional filtration) specified by HVL of Cu.

Corresponding percent depth dose (PDD) and off-axis ratios (OARs) at 250 kVp are shown in Figures 5-7. Depth dose characteristics, 55% and 20% at depths of 25 and 50 mm for the 5 mm collimator, provide more than adequate penetration for targeting deep seated targets in small animals, particularly when multiple beam directions are employed. PDD data show the familiar relationship of increasing penetration with increasing field size.

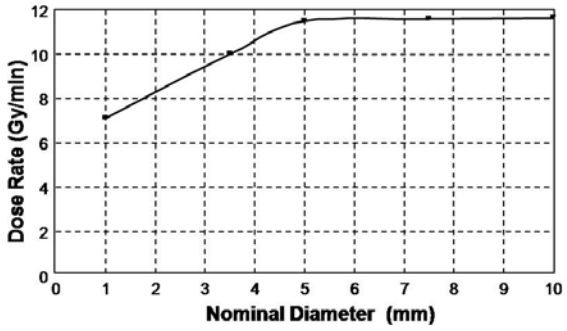

Fig 4 Absolute dose rate as a function of collimator size measured at an SSD of 19.76 cm.

The rectangular nature of the focal spot creates a beam that is slightly elliptical in shape, and thus in-plane and cross-plane profiles are significantly different. Penumbra, measured between 80% and 20%, is shown as a function of field size in Table 1.

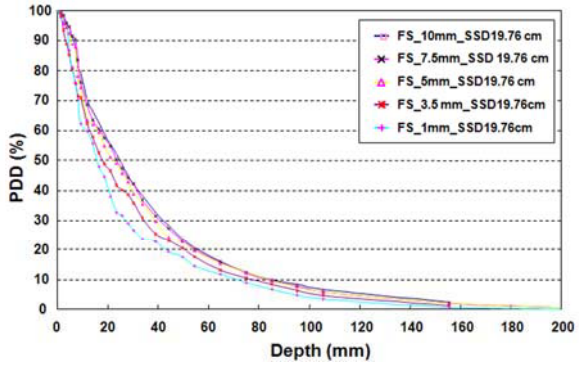

Fig. 5 Percent Depth Dose curves at 250 kVp (with 1.65 mm Al additional filtration) at an SSD of 19.76 cm. PDD curves.

To validate dosimetric measurements and in anticipation of Monte Carlo-based treatment planning, a Monte Carlo beam model of the treatment beam has been created. The unmodified 250 kVp energy spectrum produced by the XRAD 320 was determined using the SpekCalc GUI program by Poludniowski and Evans [6-7].

The resulting energy spectrum as well as the beam collimation system and experimental geometries were subsequently modeled using the MCNPX program (Los Alamos National Laboratories). Monte Carlo calculations are in excellent agreement with measured data (Figure 8).

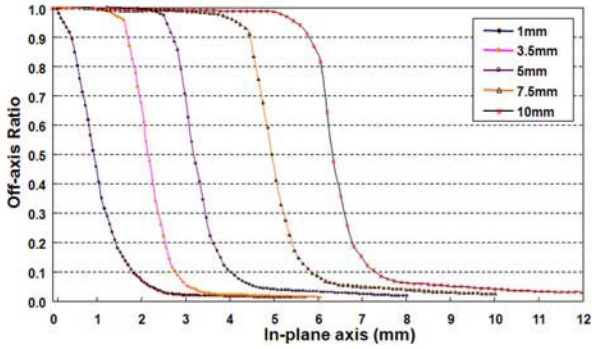

Fig. 6 Off-axis ratio as a function of distance along the in-plane axis.

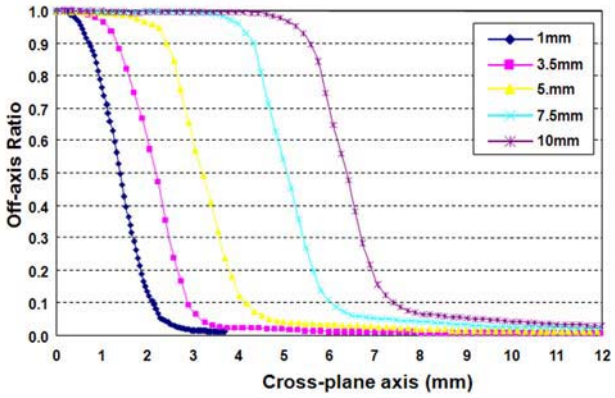

Fig. 7 Off-axis ratio as a function of distance cross to the cross-plane axis

Table 1: Beam penumbra along in plane axis and cross plane axis

Nominal Aperture Diameter	Penumbra (mm) in-plane axis	Penumbra (mm) Cross-plane axis
1.0 mm Collimator	0.79	0.91
3.5 mm Collimator	0.71	1.05
5.0 mm Collimator	0.73	1.10
7.5 mm collimator	0.60	1.16
10.0 mm Collimator	0.75	1.33

Operation of the Image Guidance System: Image guided stereotactic irradiation has been successfully performed in a variety of tumor and normal tissue models, including: subcutaneous lung tumors in mice, orthotopic human brain tumors in mice, orthotopic human lung tumors in rats, and normal mouse. The process is shown in Figure 9 as follows: microCT are obtained, from which digitally reconstructed radiographs (DRR) are calculated to visualize the region of interest (Figure 9A). Animals are subsequently positioned on the irradiation device, and a diagnostic (20-30 kVp) X-ray image is acquired which shows the anatomy of interest relative to the center of radiation field (Figure 9B). The radiation field center can be visually identified based on fiducial markers imbedded

above the X-ray intensifying screen; the markers are spaced 1 and 2 cm apart. Subsequently, the animals are repositioned according to the target location on DRRs. Proper localization is verified on subsequent imaging (Figure 9C). The desired collimator is then inserted, the tube potential is changed to 250 kVp, and irradiation delivery is performed. During delivery, a beam's eye view image with the chosen collimator can be superimposed on the prior localization images (Figure 9D). The double exposure of the animal with and without the collimator provides verification of the beam position as well as documentation of the irradiated structure**.**

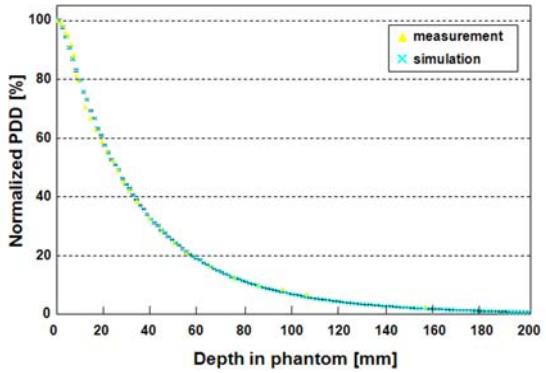

Fig. 8 PDD for a 10 mm collimator at a nominal potential of 250 mkVp calculated using MCNPX and measured with radiochromic film.

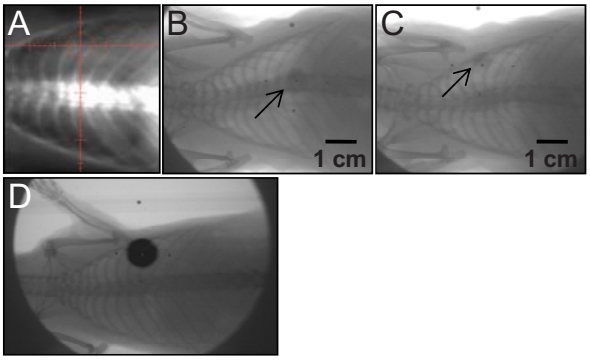

Fig. 9 Image-guided SBRT in a rat with orthotopic lung tumor. (A) A digitally reconstructed radiograph (DRR) obtained from micro CT. (B) and (C) X-ray images before and after position adjustment. (D) X-ray image overlaid on treatment image. Arrows indicate a center of the radiation field.

IV. Conclusions

We have successfully developed a small animal stereotactic body irradiator which utilizes image guidance capabilities for targeting. The irradiator provides a good spatial resolution and high contrast images for accurate localization and targeting tumor. We have characterized the beam parameters, such as PDD, OAR, and dose rate, and compared PDD with Monte Carlo computed data. The measured parameters can be used in treatment planning system. We believe that the irradiator can contribute to the various pre-clinical studies to assess and optimize current treatment strategies.

References

1. Potters, L., M. Steinberg, et al. (2004) American Society for Therapeutic Radiology and Oncology and American College of Radiology practice guideline for the performance of stereotactic body radiation therapy. Int J Radiat Oncol Biol Phys 60(4): 1026-32.
2. Solberg, T. D., B. D. Kavanagh, et al. (2008) Stereotactic body radiation therapy: a new paradigm in radiotherapy management of cancer. J Am Coll Radiol 5(5): 673-7.
3. Stojadinovic, S., D. A. Low, et al. (2007) MicroRT: Small Animal Conformal Irradiator" Medical Physics, 34 (12):4706-16.
4. Ma, C. M., C. W. Coffey, et al. (2001) AAPM protocol for 40-300 kV x-ray beam dosimetry in radiotherapy and radiobiology. Med Phys 28(6): 868-93.
5. Niroomand-Rad, A., C. R. Blackwell, et al. (1998) Radiochromic film dosimetry: recommendations of AAPM Radiation Therapy Committee Task Group 55. American Association of Physicists in Medicine. Med Phys 25(11): 2093-115.
6. Poludniowski G, Evans P (2007) Calculation of x-ray spectra emerging from an x-ray tube. Part I. electron penetration characteristics in x-ray targets. Med Phys. (6):2164-74.
7. Poludniowski G (2007) Calculation of x-ray spectra emerging from an x-ray tube. Part II. X-ray production and filtration in x-ray targets. Med Phys 34(6):2175-86.

Author: Rajesh Pidikiti
Institute: University of Texas Southwestern Medical Center
Street: 5323 Harry Hines Boulevard
City: Dallas
Country: USA
Email: raejsh.pidikiti@utsouthwestern.edu

Electric Field Redistribution due to Conductivity Changes during Tissue Electroporation: Experiments with a Simple Vegetal Model

A. Ivorra[1], L.M. Mir[2,3] and B. Rubinsky[1,4]

[1] Depts. of Mechanical Eng. and Bioengineering, University of California at Berkeley, Berkeley, CA, USA
[2] UMR 8121 CNRS-Institut Gustave-Roussy, Villejuif, France
[3] Univ. Paris-Sud, UMR 8121
[4] Center for Bioengineering in the Service of Humanity and Society, Hebrew University of Jerusalem, Jerusalem, Israel

Abstract— **Electroporation, or electropermeabilization, is the phenomenon in which cell membrane permeability to ions and macromolecules is increased by exposing the cell to short high electric field pulses. In living tissues, such permeabilization boost can be used in order to enhance the penetration of drugs (electrochemotherapy) or DNA plasmids (electrogenetherapy) or to destroy undesirable cells (irreversible electroporation). During the application of the high voltage pulses required for *in vivo* electroporation treatments, the conductivity of the involved tissues increases due to the electroporation phenomenon. This alteration results in a redistribution of the electric field magnitude that should be taken into account at treatment planning in order to foresee the areas that will be treated by electroporation. In the last five years some authors have indeed started to include such conductivity alteration in their simulation models. However, little experimental evidence has been provided to support the fact that conductivity changes really have a significant role on the electric field distribution. By reporting experiments on potato tuber, here we show that conductivity increase due to electroporation has indeed a significant physiological effect on the result of the application of the pulses. For instance, we noticed that by taking into account such conductivity alteration during simulations the error in electroporated area estimation went down from 30 % to 3 % in a case in which electroporation was performed with two parallel needles. Furthermore we also show that the field redistribution process occurs in two stages: an immediate and fast (<5 μs) redistribution after the pulse onset, probably only held up by the cell membrane charging process, and a slower, and less significant, redistribution afterwards probably related to slow, and moderate, changes in tissue conductivity during the pulse.**

Keywords— **Electroporation, Tissue Conductivity, Electric Field, Potato, Finite Element Method.**

I. Introduction

Electroporation, or electropermeabilization, is the phenomenon in which cell membrane permeability to ions and macromolecules is increased by exposing the cell to short (microsecond to millisecond) high electric field pulses. Reversible electroporation of living tissues is the basis for different therapeutic maneuvers on clinical use or under study [1] such as the in vivo introduction of genes into cells (electrogenetherapy) and the introduction of anti-cancer drugs into undesirable cells (electrochemotherapy). More recently, irreversible electroporation (IRE) has also found a use in tissues as a minimally invasive surgical procedure to ablate undesirable tissue without the use of adjuvant agents [2-4].

Electroporation is a dynamic phenomenon that depends on the local transmembrane voltage. It is generally accepted that, for a given pulse duration and shape, a specific transmembrane voltage threshold exists for the manifestation of the electroporation phenomenon (from 0.5 V to 1 V). This leads to the definition of an electric field magnitude threshold for electroporation (E_{rev}); only the cells within areas where $|\mathbf{E}| > E_{rev}$ are electroporated. If a second threshold (E_{irrev}) is reached or surpassed, electroporation will compromise the viability of the cells because electroporation becomes irreversible (cells do not reseal). A larger threshold can also be defined ($E_{thermal}$) for the manifestation of thermal damage caused by the Joule effect. This is particularly relevant in the case of IRE ablation techniques: if irreversibility threshold is surpassed but thermal threshold is not reached then cells are destroyed but tissue scaffold is spared and that facilitates post-treatment healing [4].

For more than ten years [5] researchers have been employing numerical methods (e.g. the Finite Element Method (FEM)) for computing the electric field magnitude distribution and therefore for predicting the tissue volumes that will be effectively electroporated under a certain sample and electrode configuration. The most common model consists of one or multiple regions with constant electrical conductivities. Although this sort of models has been validated empirically with reasonably positive results [6, 7], recently it has been introduced a refinement [8, 9]: the electrical conductivity of the tissue is not constant but depends on the electric field magnitude it is experiencing. This feature models the fact that when electroporation occurs the conductivity increases abruptly and significantly. The conductivity increase results in a field redistribution which in turn results in a new conductivity redistribution and so on.

O. Dössel and W.C. Schlegel (Eds.): WC 2009, IFMBE Proceedings 25/XIII, pp. 59–62, 2009.
www.springerlink.com

Although this new refinement sounds perfectly logical, in our opinion, and to the best of our knowledge, no valid empirical evidence has been provided to support it against the more common and simpler models based on constant conductivities. It is precisely the purpose of the present study to provide evidences in this sense. It is also an objective of this paper to analyze how fast the field redistribution evolves.

Following the replacement concept of the 3 Rs approach for animal testing (**r**eduction of the number of animals, **r**efinement of procedures to reduce distress, and **r**eplacement of animal with non-animal techniques [10]), it is convenient to note here that some vegetables can be a proper alternative for studying bioelectrical aspects of tissue electroporation. In particular, raw potato tuber is a good choice because any irreversibly electroporated area will be distinctively darker about 5 hours after electroporation. Such darkening is probably due to an accelerated oxidation of chemical constituents caused by a decompartmentalization of certain enzymes and substrates [11] that occurs at cell lysis caused by electroporation. Here we have chosen to wait for 12 hours before observing the effects of the high voltage pulses.

II. Methods

A. Uniform field electroporation

Sixteen potato tuber cylinders of 5 mm in diameter and approximately 5 mm in height were electroporated between two large plate electrodes made of aluminum (Fig 1.a) attached to a dielectric digital caliper (Digimatic by Mitutoyo Corp., Kawasaki, Japan) for accurate assessment of cylinder height. The electroporation protocol consisted of a single pulse of 400 µs. Multiple voltages, ranging from 50 V to 500V, were selected in the electroporation generator (ECM 830 by BTX-Harvard Apparatus Inc., Holliston, MA, USA). Voltage and current waveforms were recorded with a digital oscilloscope (WaveRunner 44Xi by LeCroy Corp., Chestnut Ridge, NY, USA).

This electrode and sample configuration produces a uniform electric field magnitude distribution ($|\mathbf{E}|=\Delta V/d$), without edge effects, if the sample is homogeneous.

After the electroporation pulse, the samples were kept in Petri dishes (for minimizing dehydration) for 12 hours at room temperature. Then a single picture of all the samples on a white sheet was taken with a digital camera (C-7070 by Olympus Corp., Tokyo, Japan). The obtained color image was converted to a grayscale image and brightness and contrast were adjusted (software Photoshop 8.0 by Adobe Systems Inc., Mountain View, CA, USA) so that the white paper had a 0% black content ("K"), the non treated potato cylinder had a K of about 60% and the darkest cylinders ($|\mathbf{E}| > 800$ V/cm) had a K of about 95%. The black content of the samples was represented against the electric field magnitude each one of them experienced (Fig 1.c) and a linear piecewise function was obtained for the relationship between K and $|\mathbf{E}|$.

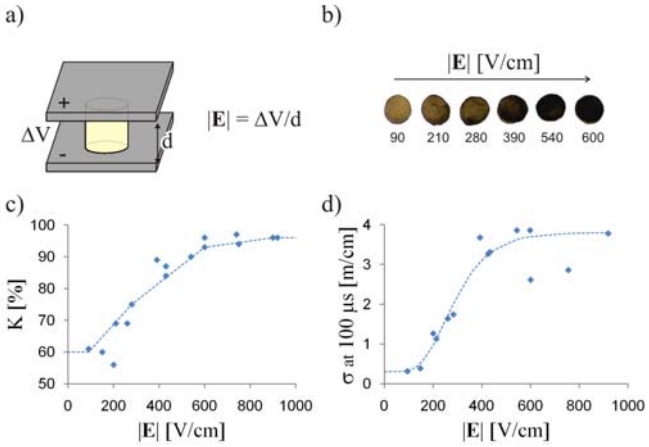

Fig. 1 a) Potato tuber cylinders are electroporated between two large plates. b) After 12 hours the cylinders exposed to higher fields are clearly darker. c) The "black contents" after 12 hours is represented against the field magnitude. d) Conductivity values at the 100th µs of the pulse and the sigmoid function used to model these values.

B. Ununiform field electroporation

A two needle electroporation array (5 mm separation, 0.3 mm in diameter, model 533 by BTX-Harvard Apparatus Inc., Holliston, MA, USA) was inserted across the center of a rectangular piece (20 mm × 20 mm × 5 mm) of potato tuber (similarly to what is shown in Fig. 2). Then a single pulse of 400 µs and 300 V was applied with the ECM 830. The same process was repeated with a 500 V pulse.

Both pieces were kept in Petri dishes for 12 hours and pictures were obtained and processed as it is described in the previous subsection (result images are subfigures a and b of Fig 3; only the central 15 mm × 15 mm section is displayed).

C. Finite Element Method simulations

Bidimensional FEM simulations of a model equivalent to the case described in subsection B were performed with COMSOL Multiphysics 3.4 (Comsol AB, Stockholm, Sweden). A very similar simulation process is described in [9].

Two conductivity models for the potato tissue were considered here: 1) constant conductivity ($\sigma(|\mathbf{E}|)=0.3$ mS/cm) and 2) conductivity according to the values obtained at the

100^{th} μs of the pulse (Fig 1.d), which are approximated with the following sigmoid function (fitted automatically with the *Curve Fitting Toolbox* of Matlab 7.6 by The Mathworks, Inc., Natick, MA, USA):

$$\sigma(|\mathbf{E}|) = 3.5\, e^{-e^{-0.01(|\mathbf{E}|-250)}} + 0.3 \quad [\text{mS/cm}] \qquad (1)$$

In the second conductivity model, field dependent, the simulation was solved as an iterative process with a sequence of steps in which the conductivity for each step was defined by the field in the previous step.

The simulated electric field magnitude was then displayed with the gray scale obtained with the samples of subsection A (Fig. 1.c)

D. Voltage recordings for assessing redistribution speed

From the above referred simulation at 500 V with field dependent conductivity, two points were selected (Fig. 2): p1) a point in which the potential is constant (ΔV/2= 250 V) across all the simulation steps and p2) a point in which there is a significant difference between the voltage at the first step, $V_{STEP\ 0}$ (i.e. before conductivity has been modified according to electric field magnitude), and the voltage at the step in which a stable solution has been reached, $V_{STEP\ \infty}$.

In principle, immediately after the onset of the pulse, the recorded potential at p2 should be equal to $V_{STEP\ 0}$ whereas after the whole redistribution process is finished it should be equal to $V_{STEP\ \infty}$.

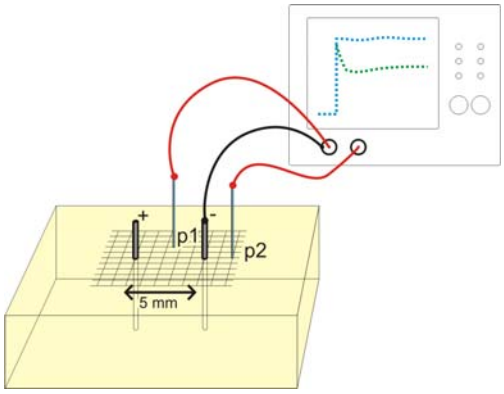

Fig. 2 Voltage recordings (at points p1 and p2) for analyzing the dynamics of electric field redistribution. A 500V and 400μs pulse is applied between the needle electrodes + and -. Recording electrodes at p1 and p2 are stainless steel hypodermic needles (diameter = 0.28 mm).

III. Results and Discussion

A. Uniform field electroporation

See Fig. 1.

B. Comparison of simulation results and electroporated areas according to conductivity models

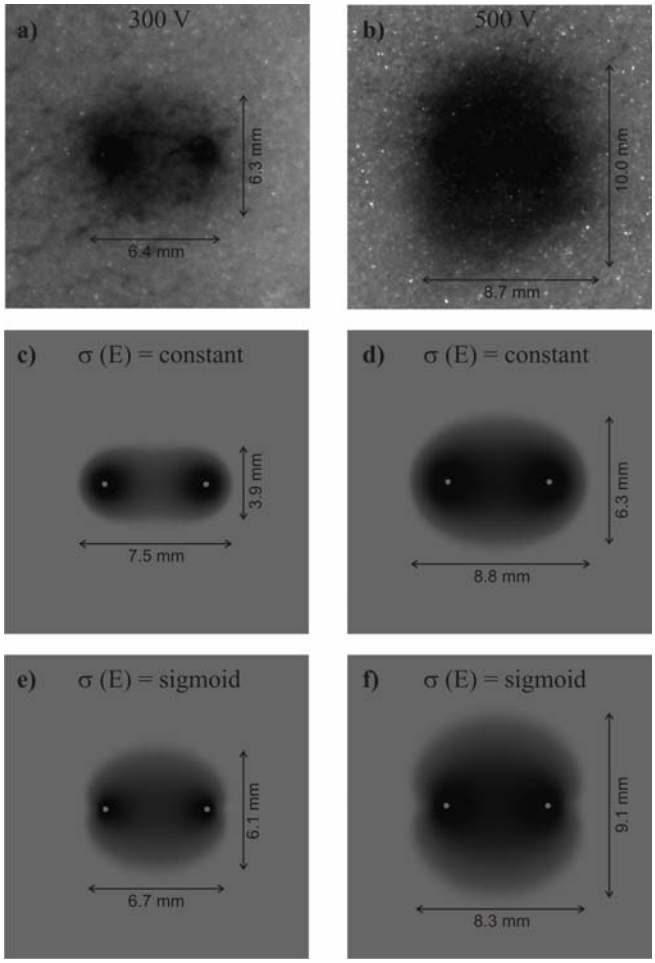

Fig. 3 a) Processed black and white picture (brightness and contrast adjustment) of a potato tuber slice 12 hours after electroporation with two parallel needles at 300 V(separation = 5 mm). b) the same with ΔV= 500V. c) and e) simulation of the 300 V case with constant conductivity (c) and with field dependent conductivity according to eq. 1 (e). d) and f) the same than e and f but for the case ΔV= 500V. The area represented in all the subfigures is a 15 mm × 15 mm section.

Fig. 3 shows that by including the dependence of the conductivity on the field the simulations are indeed closer to the actual effect of the pulses. With the aid of Engauge Digitizer (http://digitizer.sourceforge.net) we computed the

electroporated areas for all the subfigures shown in Fig. 3: a) 33 mm^2, b) 83 mm^2, c) 23 mm^2, d) 45 mm^2, e) 32 mm^2 and f) 62 mm^2. Therefore, by including the conductivity dependence effect, the area error for the 300 V case goes down from 30% to 3% whereas for the 500 V case the area error goes down from 46 % to 25 %.

Here it is necessary to note that potato tuber is a special case of biological tissue in the sense that its extracellular conductivity is exceptionally lower than its intracellular conductivity and that induces a huge increase of conductivity when electroporation occurs (approx. ×12 in Fig. 2.d). Soft animal tissues only augment their conductivity during electroporation pulses in ×3 to ×6 factors [12-14]. Therefore, in those cases the effect of the conductivity dependence on the electric field should not have such significant consequences as the ones displayed in Fig. 3.

C. Dynamics of field magnitude redistribution

In Fig. 4 it can observed that, as expected, voltage at point p1 is almost constant during the first quarter of the pulse and almost equal to $\Delta V/2 = 250$ V (error is probably caused due to location inaccuracy). However, voltage at p2 seems to show that the field redistribution behaves as a two stage process: an immediate and fast (<5 µs) phase after the pulse onset in which the voltage drops almost 50 V (as expected by the difference between $V_{STEP\ 0}$ and $V_{STEP\ \infty}$), probably only held up by the cell membrane charging process, and a slower, and less significant, redistribution phase afterwards probably related to slow, and moderate, changes in tissue conductivity during the pulse; note that the simulated $V_{STEP\ \infty}$ was obtained with conductivity values at 100 µs but that the conductivity of the uniform field samples increased moderately across the pulse (details not reported here due to space constrains).

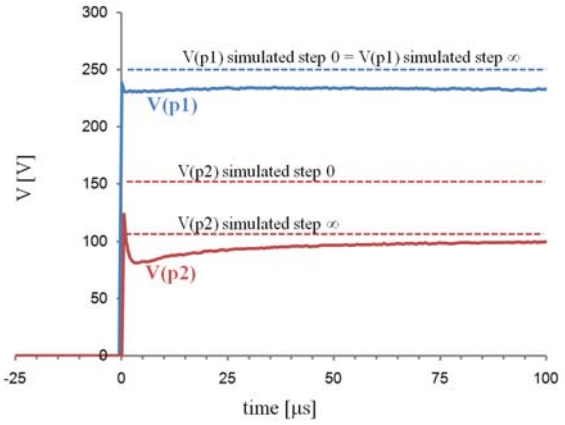

Fig. 4 Voltage recordings at points p1 and p2 during the first 100 µs of a 500 V pulse (see Fig. 1).

Acknowledgment

This work was supported in part by U.S. National Institutes of Health (NIH) under Grant NIH R01 RR018961.

BR has a financial interest in Excellin Life Sciences and Oncobionic which are companies in the field of *in vitro* electroporation and *in vivo* IRE, respectively.

References

1. L. M. Mir, "Therapeutic perspectives of in vivo cell electropermeabilization," Bioelectrochemistry, vol. 53, pp. 1-10, 2000.
2. R. V. Davalos, L. M. Mir, and B. Rubinsky, "Tissue Ablation with Irreversible Electroporation," Ann. Biomed. Eng. , vol. 33, pp. 223, 2005.
3. B. Al-Sakere, F. André, C. Bernat, E. Connault, P. Opolon, R. V. Davalos, B. Rubinsky, and L. M. Mir, "Tumor ablation with irreversible electroporation," PLoS ONE, vol. 2, pp. e1135, 2007.
4. B. Rubinsky, "Irreversible electroporation in medicine," Technology in Cancer Research and Treatment, vol. 6, pp. 255-260, 2007.
5. D. Miklavcic, K. Beravs, D. Semrov, M. Cemazar, F. Demsar, and G. Sersa, "The Importance of Electric Field Distribution for Effective in Vivo Electroporation of Tissues," Biophys. J., vol. 74, pp. 2152-2158, 1998.
6. J. Edd, L. Horowitz, R. V. Davalos, L. M. Mir, and B. Rubinsky, "In-Vivo Results of a New Focal Tissue Ablation Technique: Irreversible Electroporation," IEEE Trans. Biomed. Eng. , vol. 53, pp. 1409-1415, 2006.
7. D. Miklavcic, D. Semrov, H. Mekid, and L. M. Mir, "A validated model of in vivo electric field distribution in tissues for electrochemotherapy and for DNA electrotransfer for gene therapy," Biochimica et Biophysica Acta, vol. 1523, pp. 73-83, 2000.
8. D. Sel, D. Cukjati, D. Batiuskaite, T. Slivnik, L. M. Mir, and D. Miklavcic, "Sequential finite element model of tissue electropermeabilization," IEEE Trans. Biomed. Eng., vol. 52, pp. 816-827, 2005.
9. A. Ivorra, B. Al-sakere, B. Rubinsky, and L. M. Mir, "Use of conductive gels for electric field homogenization increases the antitumor efficacy of electroporation therapies," Physics in Medicine and Biology, vol. 53, pp. 6605-6618, 2008.
10. W. M. S. Russell and R. L. Burch, The Principles of Humane Experimental Technique. London: Methuen & Co. Ltd., 1959.
11. I. N. A. Ashie and B. K. Simpson, "Application of high hydrostatic pressure to control enzyme related fresh seafood texture deterioration," Food Research International, vol. 29, pp. 569-575, 1996.
12. A. Ivorra and B. Rubinsky, "In vivo electrical impedance measurements during and after electroporation of rat liver," Bioelectrochemistry, vol. 70, pp. 287-295, 2007.
13. A. Ivorra, L. Miller, and B. Rubinsky, "Electrical impedance measurements during electroporation of rat liver and muscle," in 13th International Conference on Electrical Bioimpedance, vol. IFMBE Proceedings 17, H. Scharfetter and R. Merva, Eds. Berlin: Springer-Verlag, 2007, pp. 130-133.
14. D. Cukjati, D. Batiuskaite, F. Andre, D. Miklavcic, and L. M. Mir, "Real time electroporation control for accurate and safe in vivo non-viral gene therapy," Bioelectrochemistry, vol. 70, pp. 501-507, 2007.

Author: Antoni Ivorra
Institute: University of California at Berkeley
Street: 6124A Etcheverry Hall
City: Berkeley, CA 94720
Country: USA
Email: antoni.ivorra@gmail.com

Nanoparticle-mediated radionuclide-gene therapy of liver cancer

Mu-Hua Cheng[1,2], Yao-Xiong Huang[1]*

1. Department of Biomedical Engineering, JinNan University, Guangzhou, China. 510632
2. Dept. of Nuclear Medicine. Third hospital affiliated Sun Yat-sen University, Guangzhou, China. 510630
* tyxhuang@jnu.edu.cn

Abstract-- **The technique of nanoparticle-mediated radionuclide-gene therapy has been developed to promote targeted gene therapy of liver cancer. The AFP gene antisense oligonucleotide labeled with radioactive iodine-125 ^{125}I-AFPasON was encapsulated with chitosan nanoparticle. Then the nanoparticles were transfected into the Hepatic cell cancer (HepG2 cell) to interfere its AFP gene expression. The transfection efficiency of the Nanoparticle-mediated radionuclide-gene, the target site of the gene, the AFP gene expression in the cell and its DNA damage were investigated using the techniques of nanoscale measurements such as confocal Raman scattering microscopy and multi-dimensional microscopy. All the parameters were measured as functions of the radiation intensity, the time of the transfection, and the size of the nanoparticle. It was found that Auger electron emitted from iodine-125 could damage the helical conformation and structure of DNA, and depress the AFP gene expression. The DNA damage increased with the radiation intensity. The asON is an effective specific carrier of the radionuclide iodine-125 into the target DNA. Mediated by chitosan nanoparticles, the effect of the ^{125}I-AFPasON on the DNA damage of the HepG2 cell can be enhanced to over twice.**

Keywords--**Nanoparticle, Radionuclide, Antisense oligonucleotide, Raman spectra, Cancer**

I. INTRODUCTION

Hepatocellular carcinoma (HCC) is a primary malignancy (cancer) of liver, early prevention and therapy of HCC is important, for only 10 - 20% of hepatocellular carcinomas can be removed completely by surgery [1]. If the cancer cannot be completely removed, the disease is usually dead within 3 to 6 months. However, in the early stage of HCC, there is no focus found in liver. Therefore, HCC has a poor early prognosis, what people can do is to wait for the growth of the cancer, even if there is a high level of AFP protein.

It may be possible to exploit RNA interference for early cancer therapy [2]. The target gene silence is one of the efficient methods of gene therapy with antisense oligonucleotide (asON) or siRNA for RNA interference. The antisense technology which is relatively straightforward to a specific mRNA can inhibit the gene expression and then induce a blockade in the transfer of genetic information from DNA to protein. The antisense approach involves injecting an organism with RNA sequence complementary to mRNA transcribed from a target gene. Among the first applications to reach clinical trials were the treatment of macular degeneration and respiratory syncytial virus. There are numerous examples of human diseases in which even short-term suppression of the underlying genes can result in therapeutic benefit and in which RNAi remain an utmost viable and potent reagent[2].

AsON may also function as specific carriers of radionuclides into cells, if the target sequence is specifically expressed in that particular cell type. Theoretical studies and experimental evidence suggest that short range Auger electron-emitters such as iodine-125 may be suitable for delivery of radiation confined to the cell nucleus. The primary target for the ionizing radiation is the nuclear DNA, since the radiation source is in close proximity to the DNA, it can induce DNA strands damage. Therefore, the radiolabeled asON can specifically inhibit the cell growth and destroy melanoma cells.

In order to perform these functions using an asON, the asON must penetrate into the targeted cells. Numerous reports have demonstrated that naked oligonucleotides are internalized poorly by cells whether or not they are negatively charge [3]. To improve cellular uptake and oligonucleotide's spatial and temporal activity, a range of techniques and transporters have been developed, in which the synthetic nanoparticles show unprecedented biophysical and biochemical properties. In recent years, the potential of chitosan as a polycationic gene carrier has been widely used in biomedical research due to its advantages such as low toxicity, biodegradability and biocompatibility [4].

Accordingly in this study, we developed a technique using the nano-particle of chitosan to encapsulate ^{125}I labeled antisense oligonucleotide for the radionuclide-gene therapy of liver cancer. To evaluate the potential of the nanoparticle mediated radiolabeled asON in the treatment of Hepatic cell cancer (HepG2 cell), the transfection rate of the nanoparticle-mediated radiolabeled asON, the target site of the gene, the AFP gene expression in the cell, the secondary or tertiary structure changes of the DNA and the DNA damage of the cell were investigated as functions of the radiation intensity, the time of the transfection, and the size of the nanoparticle. Some techniques which can perform non-invasive and nano-scale measurements on living cells such as confocal Raman scattering microscopy and multi-dimensional microscopy were employed for the study.

---

*: Corresponding author.

O. Dössel and W.C. Schlegel (Eds.): WC 2009, IFMBE Proceedings 25/XIII, pp. 63–65, 2009.
www.springerlink.com

II. MATERIALS AND METHODS

Materials: Radioactive iodine-125 was purchased from China Atom High Technique Limited Company. 5-iodine-deoxyurime (5-IdU) was obtained from sigma limited company (China). The asON of AFP gene was devised and synthesized by the Biosciences and Technique Limited Company in Shenzhen city of China. The HepG2 cells were obtained from the center laboratory of medical science academy of Sun Yat-sen University, China. Our *in vitro* studies on the cells were approved in advance by the Institution Animal Care and Use Committee of Ji Nan University and conformed to the Chinese Public Health Service Policy on Human Care and Use of Laboratory Animals.

Methods: The 5-IdU was labeled with radioactive iodine-125 (^{125}I-IdU) using the methods reported by Schaffland et al. Briefly, a mixture of Bu3SndUrd (100 mg) in ethanol (20 ml), 0.1M phosphate buffer pH 8 (70 ml) and sodium [^{125}I] iodide was prepared. Then ^{125}I-IdU was linked with the AFP asON using the terminal transferase (^{125}I-AFPasON). Different doses of ^{125}I-AFPasON were combined with the target AFP gene in vitro in the way simulating the PCR condition.

The ^{125}I-AFPasON-Chitosan nanoparticles were prepared simply by mixing the radiolabeled asON and chitosan phosphonate. Their size and size distribution were determined using the techniques of dynamic light scattering and transmission electron microscope. Then the nanoparticle complexes were transfected into the HepG2 cell by incubating the cells with the ^{125}I-AFPasON-chitosan nanoparticles. During the first 24 h of incubation with different doses of ^{125}I-AFPasON, the cells accumulated iodine-125 to activities of approximately 18.5, 37, 74, 148, 296 k Bq/μl respectively. Then the structure, conformation, and the functional groups of their DNA were evaluated by laser Raman microspectroscopy using a Horba JY LabRam INV. The spectra were collected on a triple spectrograph equipped with an intensified diode array detector. The effective spectral resolution was 1 cm^{-1}. In order to improve the ratio of Raman signal to noise, up to several hundred accumulated spectra, each of 15 s exposure time, were averaged over the spectral interval 400-1800cm^{-1}. The cell growth and damage were monitored by a multi-dimensional microscopy which was described previously [3, 5].

All the measurements were carried out as functions of the radiation intensity, the time of the transfection, and the size of the nanoparticle. After incubating the HepG2 cells with the ^{125}I labeled AFPasON-chitosan nanoparticles for 48 hours, we also employed PCR examination to investigate the AFP gene expression in the cell and the cell's DNA damage, besides using the techniques of confocal Raman scattering microscopy.

III. RESULTS AND DISCUSSION

It was found that the nanoparticle formation was influenced by several factors, especially the concentration of chitosan. The more amount of the chitosan was used, the larger size of the nanoparticles was. The optimal condition for the nanoparticle formation in the molar proportion of chitosan to asON is 2:1. In this circumstance, the size of the chitosan-asON nanoparticles was 112.6±32.0nm, its zeta potential was 1.45 ± 0.75 mV, and the encapsulated ratio of the chitosan crosslinked asON was 87.6 ± 3.5 ／. The transmission electron microscope displayed that the nanoparticles was well-proportioned and the chitosan can link the asON (Figure 1).

The confocal Raman microspectroscopy showed that the Auger electron emitted from iodine-125 could damage the conformation of DNA backbone and DNA structure. The changes in the characteristic Raman vibration band of DNA were extensive and their peak intensities were reduced obviously after the target DNA exposed to the Auger electron for 24 hours. The Raman intensities of all the peaks in the spectra of the functional groups of pyridine and purine bases, the ribosome, phosphate bond, and the helical conformation of DNA backbone became weak, indicating DNA damage. The DNA damages increased with the radiation intensity. On the other hand, the characteristic peak of Raman spectra of the DNA segments gradually emerged when the accumulated radioactive dose of iodine-125 increased to 74 k Bq/μl. The pyridine and purine bases in the target gene dissociated and stacked, and the peak intensities of their Raman spectra increased with the accumulated radioactive dose as shown in figure 2. Though in the previous researches, it was hypothesized that the Auger electron cascades from the incorporated iodine atoms were the cause of irreparable damage to the DNA, and could destabilize the DNA structure and raise the initial level of DNA damage [6-8], there were no direct evidence to prove it. In our experiment, since the radiation source is in close proximity to the back bone of the DNA, and the damages of the DNA structure in different extents were directly detected *in situ* using the laser Raman spectroscope technique, therefore, our finding can be the direct evidence provided the first time for the effect of the Auger electron cascades on the damages of the DNA structure of cancer cells.

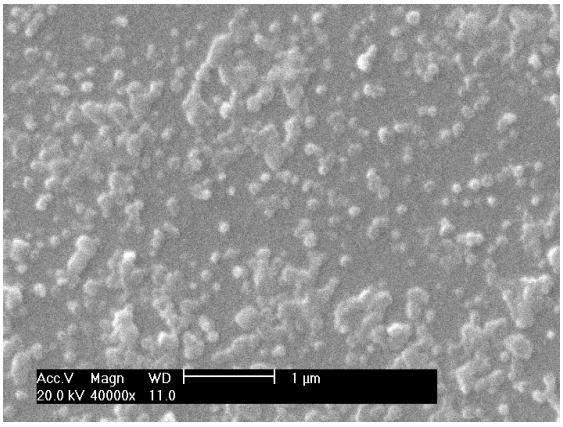

Fig 1. The electron microscope photograph of the AFPasON-Chitosan nanoparticles. The mean size of chitason-asON nanoparticles is 112.6±32.0nm.

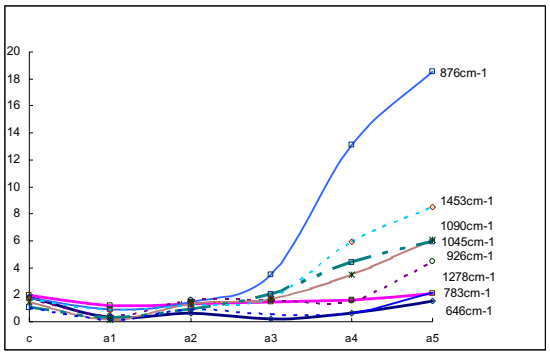

Fig 2. The Raman intensity of DNA spectra after auger electron radiation as functions of radioactive dose.

The a1,a2,a3,a4,a5 respectively represent the radioactive doses of 18.5, 37, 74, 148, 296 k Bq/μl,

To enhance its effect, the iodine-125 must be taken into the targeted cell and approach the targeted DNA. The nanoparticles of chitosan have been proved to be a good mediated carrier, which can promote the transfection efficiency of the gene drug in target cell [4]. Our results showed that the transfection efficiency of the ^{125}I-AFPasON mediated by the chitasan nanoparticles in HepG2 cells was enhanced over twice compared with that of naked AFPasONs. After the nanoparticle mediated ^{125}I-AFPasON was taken into the HepG2 cell and radiated the target DNA for 48 hours, the characteristic peak of Raman spectra of the DNA segments was found, and the AFP gene expression was also depressed down over twice compared to that without nanoparticle mediation. The primary biomedical effect of the Auger electron radiation had been reported by other researchers previously[6-7], however, in our study, not only the damage of the target DNA was found, but also the discrimination of the structure and conformation of the target DNA before and after the radiation was detected. These findings can provide detail information about the changes of the secondary or/and tertiary structure of the target DNA, thus help to understand the mechanism of the DNA damage [8-10], and would be beneficial to the efficiency of RNA interference. As for the means to control the secondary or tertiary structure of DNA with local radiation by Auger electron, further research is needed.

IV. CONCLUSIONS

Auger electron emitted from iodine-125 is proved can damage the helical conformation and structure of the DNA in HepG2 cell, depress the target gene expression. The DNA damage increases with the radioactivity. The asON is an effective specific carrier of the radionuclide iodine-125 into the target DNA. Satisfied transfection rate can be obtained when the transfection(incubating) time reaches 24 hours. Mediated by chitosan nanoparticles, the ^{125}I-AFPasON can enhance its effect on the DNA damage in the HepG2 cell to over two fold.

ACKNOWLEDGMENT

This project was supported in part by the Chinese National Natural Science Foundation (grant No.:30227001 and 60377043).

REFERENCES

1. Hashimoto T, Minagawa M, Aoki T, et al. (2008) Caval invasion by liver tumor is limited [J]. J Am Coll Surg. 207(3):383-92.
2. Kurreck J. (2009)RNA interference: from basic research to therapeutic applications [J]. Angew Chem Int Ed Engl. 48(8):1378-98.
3. Lee D, Mohapatra SS. (2008)Chitosan nanoparticle mediated gene transfer [J]. Methods Mol Biol. 433:127-40.
4. Jayakumar R, Selvamurugan N, Nair SV, et al. (2008)Preparative methods of phosphorylated chitin and chitosan--an overview [J]. Int J Biol Macromol. 43(3):221-5
5. Huang YX. (2005) A novel multi-dimensional microscope & its applications to nano-material measurements. *Current Applied Physics,* 5**:**553-556.
6. Datta K, Neumann RD, Winters TA, et al. (2005) Characterization of a complex 125I-induced DNA double-strand break: implications for repair [J]. Int J Radiat Biol, 81(1):13-21.
7. Panyutin IV, Sedelnikova OA, Bonner WM, et al. (2005)DNA damage produced by 125I-triplex-forming oligonucleotides as a measure of their successful delivery into cell nuclei [J]. Ann N Y Acad Sci, 1058:140-50.
8. Gelder JD, Gussem KD, Vandenabeele P, et al. (2007)Reference database of Raman spectra of biological molecules[J]. J Raman Spectrosc, 38: 1133-1147.
9. Vrána O, Masek V, Drazan V, et al. (2007)Raman spectroscopy of DNA modified by intrastrand cross-links of antitumor Cisplatin [J]. J Struct Biol, 159(1):1-8.
10. Barhoumi A, Zhang D, Tam F, et al. (2008,Surface-enhanced Raman spectroscopy of DNA [J]. J Am Chem Soc, 130(16):5523-9.

The address of the corresponding author:

Author: Yao-Xiong Huang
Institute: Department of Biomedical Engineering, JinNan University
City: Guang Zhou
Country: China
Email: tyxhuang@jnu.edu.cn

Development of Laser Accelerated Proton Beams for Radiation Therapy

C.-M. Ma, E. Fourkal, I. Veltchev, J.S. Li, J. Fan, T. Lin, and A. Tafo

Department of Radiation Oncology, Fox Chase Cancer Center, Philadelphia, USA

Abstract— **Recent advances in laser technology have made proton (ion) acceleration possible using laser induced plasmas. In this presentation we will review the theoretical and experimental results of laser-proton acceleration for radiotherapy applications. We will report on our work progress in the development of a laser-proton therapy system at Fox Chase Cancer Center. The new proton therapy system is designed as a compact and cost-effective alternative to conventional accelerator based proton systems capable of delivering intensity-modulated proton therapy (IMPT). The specific aims of our research are: (1) target design for laser-proton acceleration, (2) system design for particle/energy selection and beam collimation, and (3) dosimetric studies on the use of laser-accelerated protons for cancer therapy. We have established a 150 TW laser system for preliminary experimental studies. We also patented a compact particle selection and beam collimating system for IMPT beam delivery and a new gantry design to make the whole system compact and easy to operate with adequate shielding considerations. Our Monte Carlo results show that IMPT using laser protons provided superior target coverage and much reduced critical structure dose and integral dose. IMPT is more dosimetrically advantageous than photon IMRT or conventional proton beams.**

Keywords— **Laser plasmas, particle acceleration, proton therapy, radiation oncology.**

I. Introduction

Proton beams have superior dosimetric properties for radiation therapy to improve target dose coverage and normal tissue sparing compared to commonly used photon and electron beams [1]. Protons and heavier ions were studied in the early 1950s and the first human patient was treated for a pituitary tumor in 1954 [2,3]. So far about 55000 patients have been treated with proton beams worldwide. Light ion and other particle beams have also been investigated showing encouraging results particularly for well-localized radiation resistant lesions [4,5].

Despite its potential dosimetric advantages, particle therapy has lagged behind photon and electron beam therapy because of the prohibitively high cost of a conventional particle therapy system based on the cyclotron or synchrotron technology. An accelerator that is big enough to accelerate protons to the required therapeutic energies can cost 5-10 times more than a clinical linac. Currently available proton gantries are roughly three times the radius and three times the length of typical linac gantries. The amount of concrete and steel used to shield a proton treatment room will thus be approximately nine times or greater than for a linac room. Although the use of an expensive accelerator is maximized by sharing the accelerator in multiple treatment rooms this also requires additional space for a switchyard, which houses the vacuum beam lines, dipole bending magnets, steering magnets, focusing quadrapole magnets, power supplies, and cooling equipment. Even if a proton or ion facility can be amortized for 30 years or longer its maintenance, upgrade and operational cost will be significantly higher than that for a linac-based facility of similar treatment capacity. Alternative solutions are being sought for widespread applications of particle therapy including superconductor-based accelerators, dielectric wall accelerators and laser driven proton accelerators [6-19].

In this paper, we present our work on laser-accelerated proton beams for radiation therapy with a focus on the basic design of a laser-proton therapy system and our studies on particle selection and beam collimation, energy- and intensity-modulation, and shielding designs for a compact treatment gantry for laser-accelerated proton beams.

II. System development

A. The laser system

Figure 1 shows the 150 TW laser system developed for the Fox Chase laser-proton therapy facility [18]. The front end laser is a 10 Hz, 25 TW laser starting with a conventional mode-locked Mira Ti:sapphire oscillator pumped by a 5 watt CW Verdi laser at 532 nm. A stream of 20 femtosecond pulses is generated at a repetition rate of 80 MHz that feeds into a Legend regenerative amplifier, operating at 1 kHz, pumped by a 10-watt Q-switched Evolution laser at 527 nm. The 10 Hz TW multipass amplifier is pumped by the 4.0 J/pulse output of a custom-built TEM00 Nd:YAG laser, and delivers output pulses with energy >1 J. Finally, the 800nm output is stepped up to 5-15 J/pulse levels in a second stage multipass amplifier, which is pumped by a 60 J/pulse frequency-doubled output of an Nd:glass laser. After

O. Dössel and W.C. Schlegel (Eds.): WC 2009, IFMBE Proceedings 25/XIII, pp. 66–69, 2009.
www.springerlink.com

leaving the Nd:glass-pumped amplifier, the output pulses are compressed to between 40 and 50 fs in a custom-made vacuum pulse compressor, which incorporates large diameter gratings in order to handle the high pulse energy. The laser parameters are listed in table 1 for the FCCC system.

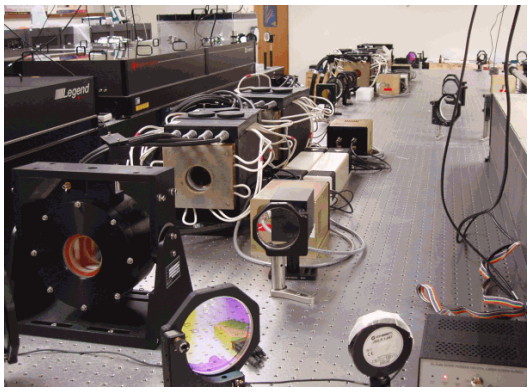

Fig. 1 The laser system for the FCCC laser-proton radiotherapy facility.

Table 1 Physical characteristics of the FCCC laser system.

Energy per pulse (E)	5~21 Joule
Pulse duration (T)	35~50 x 10^{-15} sec
Focal spot size (A)	15~75 mm^2
Power (P) = E/T	100~600 TW
Intensity (I) = P/A	0.13~4 x 10^{20} W/cm^2

Fig. 2 The shielding structure for the laser-proton acceleration investigation at FCCC.

B. The Target assembly and the particle selection system

For the experimental studies on particle acceleration with laser plasmas we have established a shielding structure (Fig. 2) that houses the target chamber and bean diagnostic instruments. The target chamber contains the target assembly that consists of the final focusing system and the target holder (Fig. 3). Previous studies have shown that the target configuration plays an important role in laser-proton acceleration. We have performed particle-in-cell (PIC) simulations to study optimal laser parameters and target geometry to guide our experimental studies [20-22]. Different laser parameters and target configurations have been simulated. The results of PIC simulations have been used to derive particle phase space data for further dose calculation and treatment optimization studies. Bi-layer targets are primary options where the front, thick layer provides a large number of heavy ions to form an intense electric field after relativistic electrons are expelled and the back, thin layer provides light ions to be accelerated by the electric field. The materials and thicknesses of the bi-layer target or multiple targets must be optimized based on the laser parameters and acceleration requirements [16,24,26].

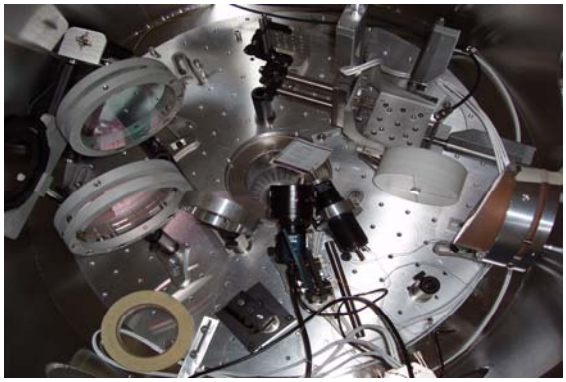

Fig. 3 The target assembly inside the target chamber.

A compact device for particle selection and beam modulation has been investigated, which utilizes a magnetic field to spread the laser-accelerated protons spatially, based on their energies and emitting angles, and apertures of different shapes to select protons within a therapeutic window of energy and angle [12,18,23]. Such a compact device will eliminate the massive beam transportation and collimating equipment in a conventional proton therapy system. The laser-proton target assembly and the particle selection and collimating device can be installed on the treatment gantry to form a compact treatment unit, which may be installed in a conventional radiotherapy treatment room [18].

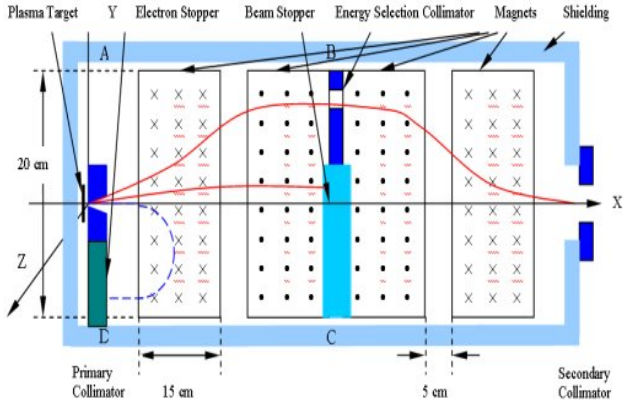

Fig. 4 The particle selection and beam collimation system for energy- and intensity-modulated proton therapy.

A schematic diagram of the particle selection and collimation system is shown in figure 4. A beam stopper will stop the uncharged particles from the target and the primary collimator. Electrons will be stopped by an electron stopper. Theoretical proton tracks in high magnetic fields (moving from left to right) are displayed. Only protons of energies within an energy range will be allowed to pass through the beam stoppers and refocused through an exit collimator. Collimators of different shapes, sizes and locations can be used to select particles of desired energies. Other protons will be stopped or scattered by the energy selection collimator so that they will not be able to reach the exit collimator. Superconducting magnets were investigated to reduce the size of the device [23]. The shielding for the whole system has been designed to reduce the radiation leakage (from protons, electrons and other radiation particles) to the level required by state regulations [25].

III. Dosimetric studies

The use of proton therapy for prostate cancer has been controversial. Conventional proton therapy has typically used two lateral beams with large margins, leading to significant rectal toxicities compared to intensity modulated radiation therapy (IMRT). We have performed Monte Carlo simulations of laser-accelerated protons for intensity modulated proton therapy (IMPT). We compared IMPT dose distributions with those from conventional proton therapy and IMRT for prostate treatment using realistic clinical cases. The same contours were used in the plan generation and our clinical acceptance criteria were used in the plan evaluation. We further investigated different dose delivery techniques for laser-accelerated proton therapy including an aperture-based optimization and treatment technique [18].

Our results clearly show that IMPT using laser-accelerated protons is superior to that using x-ray IMRT in terms of target coverage and normal tissue sparing [22,28]. This can be explained by the fact that the dose distribution in the depth direction cannot be modulated for photon beams while this can be achieved by energy modulation with proton beams. We have used 6-9 gantry angles for prostate treatment planning. The isodose distributions from IMPT are more conformal to the prostate target compared to those from IMRT using the same beam angles and optimization parameters. The same conclusion can be drawn on the dose-volume histograms (DVHs) for the target and the rectum using IMPT and IMRT. Laser-proton IMPT is clearly superior to X-ray beams. The target dose is more uniform and the rectum dose is much reduced with laser-proton therapy compared to x-ray IMRT. The combination of a compact particle selection and collimation device and an associated treatment optimization algorithm will make IMPT possible using laser-accelerated proton beams. In fact, the polyenergetic nature of a laser proton beam makes it ideal for IMPT since it is convenient for both energy modulation (using a spectrum) and intensity modulation (through beam scanning or aperture integration as shown in figure 5).

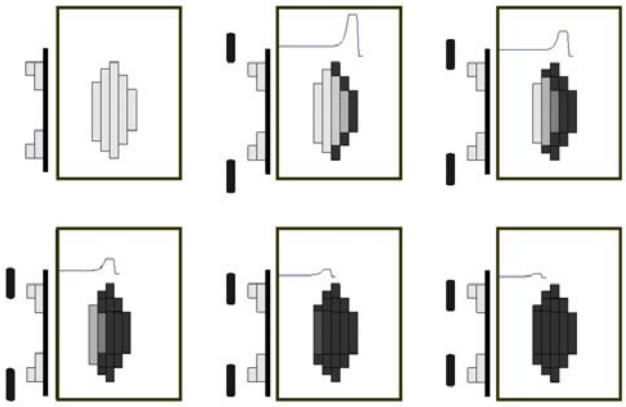

Fig. 5 A schematic diagram showing how to delivery aperture based conformal proton dose distributions. The dose is conformed to the cross-section of the target volume at each depth with the use of a compensator.

IV. Future plans

The FCCC laser-proton accelerator facility has been established in 2006 and we have attained regulatory approval to use it as a research accelerator by the Commonwealth of Pennsylvania's Department of Environmental Protection Bureau of Radiation Protection. Our future work plans are as follows:

(1) To prove the scalability of laser proton acceleration using our existing laser system (we plan to upgrade our laser to a PW laser with >1Hz rap rate).
(2) To demonstrate the effectiveness and efficiency of a compact proton selection and beam collimating device. This is the key element for a laser-proton therapy system, which also serves as an independent dose monitoring system.
(3) To perform ion-biology studies for laser-accelerated ion beams for radiotherapy applications. These experiments are necessary prior to clinical applications, which may lead to more research funding.

REFERENCES

1. Wilson R R. (1946) Radiological use of fast protons Radiology, 47: 487
2. Tobias C.A., Anger H.O. and Lawrence, J.H. (1952) Radiological use of high energy deuterons and alpha particles, Am. J. Roentgenol, 67: 1-27
3. Lawrence J.H. (1957) Proton irradiation of the pituitary, Cancer, 10: 795-98
4. Smith AR. (2009) Vision 20/20: Proton therapy, Med. Phys. 36: 556-568
5. Jakerl O, Karger CP and Debus J. (2008) The future of heavy ion radiotherapy, Med. Phys. 35: 5653–63
6. Ma C-M, Maughan RL and Orton CG. (2006) Within the next decade conventional cyclotrons for proton radiotherapy will become obsolete and replaced by far less expensive machines using compact laser systems for the acceleration of the protons, Med. Phys. 33: 571-573
7. Caporaso GJ, et al. (2008) A compact linac for intensity modulated proton therapy based on a dielectric wall accelerator, Phys. Medica 24: 98–101
8. Chen YJ and Paul AC. (2007) Proceedings of PAC07, Albuquerque, New Mexico, USA, edited by S. Hardage and C. Petit-Jean-Genaz, Piscataway, IEEE, pp. 1787-1789
9. Mackie TR, et al. (2007) A proposal for a novel compact intensity modulated proton therapy system using a dielectric wall accelerator, Med. Phys. 34: 2628
10. Tajima T and Dawson J M （1979）Laser electron accelerator Phys. Rev. Lett., 43： 267
11. Tajima T. (1999) Compact Laser Proton Accelerator beyond 100 MeV for Medicine, Livermore, LLNL
12. Ma C-M. (2000) Compact Laser Proton Accelerator for Medicine (SPO #22962), Stanford, Stanford University
13. Snavely R A, Key M, Hatchett S, et al, (2000) Intense high energy proton beams from Petawatt Laser irradiation of solids, Phys. Rev. Lett. 85: 2945-8
14. Ma C-M, Tajima T, Shahine B, et al. (2001) Laser accelerated proton beams for radiation therapy, Med. Phys. 28: 1236
15. Bulanov SV and Khoroshkov V. (2002) Feasibility of using laser ion accelerators in proton therapy, Plasma Phys. Rep. 28: 453-456
16. Esirkepov T, et al. (2002) Proposed double-layer target for the generation of high quality laser accelerated ion beams, Phys. Rev. Lett. 89, 175003
17. Malka V, Fritzler S, Lefebvre E, et al. (2004) Practicability of protontherapy using compact laser systems, Med. Phys. 31: 1587-92
18. Ma C-M, et al. (2006) Development of a laser-driven proton accelerator for cancer therapy, Laser Phys., 16: 639-646
19. Schwoerer H, Pfotenhauer S, Jäckel O, et al. Laser-plasma acceleration of quasi-monoenergetic protons from microstructured targets, Nature 439: 445-448
20. Fourkal E, Tajima T, Ding M and Ma C-M. (2002) PIC simulation of laser proton acceleration for radiotherapy, Med. Phys. 29: 2788-96
21. Fourkal E, Li JS, Ding M, Tajima T and Ma C-M. (2003) Particle selection for laser-accelerated proton therapy feasibility study, Med. Phys. 30: 1660-70
22. Fourkal E, Li JS, Xiong W, Nahum A and Ma C-M. (2003) Intensity modulated radiation therapy using laser-accelerated protons: a Monte Carlo dosimetric study, Phys. Med. Biol. 48: 3977-4000
23. W. Luo, E. Fourkal, J. Li and C.-M. Ma C-M. (2005) A laser-accelerated proton therapy unit with a superconducting magnet system, Med. Phys. 32: 794-806
24. E. Fourkal, I. Velchev, and C.-M. Ma. (2005) Coulomb explosion effect and maximum energy of protons accelerated by high-power lasers, Phys. Rev. E17, 036412 :1-11
25. Fan J, Luo W, Fourkal E, Lin T, Li JS, Veltchev I, Ipe NE, and Ma C-M. (2007 Shielding design for a laser-accelerated proton therapy system, Phys. Med. Biol. 52: 3913-3930
26. Veltchev I, Fourkal E, and Ma C-M. (2007) Laser-induced Coulomb mirror effect: Applications for proton acceleration, Physics of Plasmas 14, 033106
27. Fourkal E, Veltchev I, Fan J, Luo W, Ma C-M. (2007) Energy optimization procedure for treatment planning with laser-accelerated protons. Med. Phys. 34:577-84
28. W. Luo, J. Li, E. Fourkal, J. Fan, X. Xu, Z. Chen, L. Jin, R.A. Price, and C.-M. Ma. (2008) Dosimetric advantages of IMPT over IMRT for laser-accelerated proton beams, Phys. Med. Biol. 53: 7151-66

Address of the corresponding author:
Author: C-M Charlie Ma, Ph.D.
Institute: Fox Chase Cancer Center
Street: 333 Cottman Avenue
City: Philadelphia
Country: Pennsylvania
Email: Charlie.ma@fccc.edu

An Initial EFOMP Position on the Tuning Process for Masters Programs in Medical Physics in Europe

S. Christofides[1], W.Schlegel[1], R. Padovani[1], P. F. Sharp[1], A. Torresin[1], M. Wasilewska-Radwanska[1], W. van der Putten[1], E. Guibelalde[1], K.-U. Kasch[1], and C. J. Caruana[2]

[1] European Federation of Organisations for Medical Physics (EFOMP)
[2] Biomedical Physics, Institute of Health Care, University of Malta, Msida, Malta

Abstract— **The EFOMP (European Federation of Organisations for Medical Physics) Council at its September 2008 meeting in Krakow set in motion the 'Tuning Educational Structures in Europe' process for Masters' programmes in Medical Physics in Europe. For the medical physics profession a fundamental component of Tuning would be the setting up of an inventory of agreed pan-European learning outcome competences for such programs. This would represent the minimum set of competences that a student should acquire at the exit point of the program. An initial form of this inventory is presented. The inventory was set up on the basis of a thorough analysis of Tuning documentation, lists of medical physics competences used by universities in the various EU states and other competence inventories such as those of ESTRO (European Society for Therapeutic Radiology and Oncology) for radiotherapy physicists. Best-practice elements of these inventories were identified and used as inputs for the inventory. The final form of the inventory must be acceptable for the medical physics profession and associated stakeholders on a European scale. It is important to ensure that this inventory dovetails seamlessly with any EFOMP policy statements regarding the competences of the Qualified Medical Physicist (QMP) and Specialized Medical Physicist (SMP). It is also suggested that in future EFOMP would use the inventory to propose a system of accreditation for programs in Europe similar to that used by CAMPEP (Commission on Accreditation of Medical Physics Educational Programs) in the US.**

Keywords— **Qualified Medical Physicist, Bologna process, Tuning, curriculum development, competence inventories.**

I. Introduction

The EFOMP Council at its meeting of September 2008 in Krakow set in motion the 'Tuning Educational Structures in Europe' process for the Masters' programmes in Medical Physics in Europe. The Tuning process is an initiative within the framework of the Bologna agreement (one aim of which is the facilitation of students, professional and researcher mobility through increased mutual recognition of qualifications). The Tuning process offers a tangible approach for the implementation of the Bologna process in higher education. The Tuning approach consists of a methodology to "re-design, develop, implement and evaluate study programmes for each of the Bologna cycles" [1]. It is important to note that 'Tuning' *does not mean uniformity*. "The name Tuning is chosen for the process to reflect the idea that universities do not and should not look for uniformity in their degree programs or any sort of unified, prescriptive or definitive European curricula but simply look for points of reference, convergence and common understanding" [1] Tuning promotes convergence (which is essential for a system of easily comparable, compatible and transparent degrees) *whilst encouraging diversity in curricular delivery methods and learning paths according to the principle of autonomy and local culture and conditions*. For the medical physics profession two fundamental 'points of reference' would be the sets of outcome learning competences for Masters programs in Medical Physics and those at the end of the two year clinical training period mandated by EFOMP for the Qualified Medical Physicist (QMP). These learning outcomes should be stated in terms of an inventory of the minimum set of competences (including the required level) that a student should acquire. *This study addresses the outcomes for the Masters program.*

II. Materials and methods

A. Principles of the Tuning methodology

Tuning is a university driven project. Groups of EU universities would be the drivers for determining the learning outcome student competences (including level of competence). This has to be done in consultation with future employers, recent graduates and professional organizations (e.g., EFOMP and EFOMP National Member Organizations) to ensure relevance to society and employability of graduates. Competences refer to learner knowledge and understanding, interpersonal, intellectual and practical skills, ethical values and attitudes. Tuning recognizes two types of competences: Generic Competences (meaning transferable across disciplines) and Subject Specific Competences (specific to a particular discipline). Tuning recognizes three types of generic competences: instrumental

O. Dössel and W.C. Schlegel (Eds.): WC 2009, IFMBE Proceedings 25/XIII, pp. 70–73, 2009.
www.springerlink.com

competences (cognitive, methodological, technological and linguistic abilities), interpersonal competences (such as social interaction and co-operation) and systemic competences (abilities and skills concerning combinations of various competences). Once an inventory of competences is developed the opinions of academics, employers, recent graduates and professional bodies should be surveyed regarding the importance and desired level of achievement of each competence. The ultimate objective is for the stakeholders to identify and reach consensus on the learning outcome competences considered as essential for students to be well prepared for their future profession.

B. Our approach

The Education and Training Committee of EFOMP analyzed documentary material regarding the Tuning process from the official Tuning site. We also collected medical physics curricula and lists of competences from EFOMP National Member Organizations for an insight into the current situation regarding medical physics education and training across Europe. An initial version of an inventory of competences was set up on the basis of a thorough analysis of documentation authored by the Tuning physics group [2], competence inventories for healthcare professions [3], lists of medical physics competences used by universities in Latvia, Macedonia, Netherlands, Poland, Ukraine and the United Kingdom and an ESTRO radiotherapy physics competence inventory [4]. The latter is presently being further developed by an ESTRO-EFOMP working group. Best-practice elements of these inventories were identified and used as inputs for the inventory.

III. Results

An initial version of the inventory is shown in Appendix 1. The competences are divided into Generic Competences and subject Specific Competences as required by Tuning. The Generic competences are further subdivided into Instrumental, Interpersonal and Systemic competences as suggested by Tuning [1]. The Subject Specific Competences are grouped into four sub-sections namely:

1. Competences required of a physicist at Masters level
2. Competences required by a medical physicist as a healthcare professional
3. Core medical physics competences which would be expected of *all* medical physics graduates.
4. Competences required for the various specialisations of medical physics. At the moment we have limited ourselves to a study of the following specialisations: Radiotherapy, Diagnostic Radiology, Nuclear Medicine, Magnetic Resonance Imaging, Ultrasound, Physiological Measurement and Audiology.

The Generic Competences and the competences in the first three sections of the Subject Specific Competences *should be included in all programme outcomes and acquired by all students*. It is suggested that students should then be required to choose *three* areas of specialization. The programme should also include a research project which would have a clinical and / or basic research orientation according to the future career direction of the student

IV. Discussion

In this article we have presented an initial version of an inventory of learning outcome competences for the Masters in Medical Physics in Europe. It is by no means complete and the wording of the competences still needs to be improved, however it does provide a robust structure on which a further refined inventory can be built. It is important to ensure that the final form of the inventory dovetails seamlessly with any present and future EFOMP policy statements regarding the competences of the Qualified Medical Physicist (QMP) and Specialized Medical Physicist (SMP). An improved version of the inventory will be eventually sent to university and clinical medical physics, professional bodies (National Member Organizations of EFOMP), recently graduated students and employers for their feedback. The final form of the inventory must be acceptable for the medical physics profession and associated stakeholders on a European scale. It will provide an important point of reference for curriculum developers in Medical Physics departments in Europe. In future we need to work on similar lines for the competences for the two-year post-qualification clinically-based training period for the QMP.

V. Conclusions

The main conclusions of this initial phase of the process are:

1) Although the inventory is still in an initial form it does provide a robust structure on which a further refined inventory can be built.
2) The final form of the inventory must be agreed upon by the European medical physics community and associated stakeholders

It is suggested that in future EFOMP would use the final form of the inventory to propose a system of accreditation for academic programs in Europe similar to the system used by CAMPEP in the US.

APPENDIX 1

Generic Competences

A. Instrumental

1. Demonstrate a capacity for analysis and synthesis.
2. Demonstrate ability for organisation, planning and management of one's workload.
3. Demonstrate ability to retrieve and analyse information from different sources.
4. Display effective oral and written communication in the native language.
5. Be able to use general productivity software.
6. Demonstrate problem solving skills.
7. Demonstrate decision taking skills.
8. Demonstrate knowledge of a second language.

B. Interpersonal

1. Be able to be critical and accept criticism.
2. Demonstrate ability to work in both mono-disciplinary and multi-disciplinary teams.
3. Be able to communicate orally and in writing with both experts in the field and non-experts.
4. Demonstrate respect for diversity and multiculturality.
5. Be able to work in an international context.
6. Demonstrate ethical commitment.

C. Systemic

1. Demonstrate an ability to apply knowledge in practice
2. Demonstrate a capacity to learn.
3. Be able to apply research skills.
4. Demonstrate a capacity to adapt to new situations.
5. Demonstrate ability to generate new ideas (creativity).
6. Demonstrate leadership and initiative.
7. Be able to work autonomously.
8. Be able to design and manage projects.
9. Demonstrate an ongoing concern for quality.
10. Demonstrate reflection and evaluation of own practice.
11. Take responsibility for one's own learning.
12. Demonstrate an entrepreneur spirit.
13. Demonstrate a will to succeed.

Subject Specific Competences

A. Physics Competences at Master Level

1. Have advanced knowledge and understanding of theoretical areas of physics relevant to medical physics at the level of Masters.
2. Demonstrate skill in physics laboratory techniques and use of equipment at the level of Masters.
3. Use mathematical and modeling techniques appropriate for medical physics at Masters level.
4. Demonstrate research communication skills (poster, article and oral) at the level of Masters.

B. Competences as a Healthcare Professional

1. Understand the functions of healthcare organizations, the way healthcare is organized and principles of clinical governance.
2. Understand those sections of the human biological sciences (anatomy, physiology, pathology, cellular and biomolecular science, medical imaging) to a level appropriate to the profession.
3. Appreciate the importance of quality and safety in healthcare.
4. Be aware of those ethical issues in healthcare relevant to the scope of the profession (including data protection issues).
5. Understand those aspects of Healthcare Psychology and Sociology relevant to the profession.
6. Be able to practise within the legal and ethical boundaries of the profession
7. Understand the obligation to maintain fitness to practise.
8. Be able to work, where appropriate, in partnership with other healthcare professionals, support staff, service users and their relatives and carers
9. Be able to demonstrate effective and appropriate skills in communicating information, advice, instruction and professional opinion to colleagues, service users, their relatives and carers.

C. Core Medical Physics Competences

1. Demonstrate knowledge and understanding of medical device terminology.
2. Appreciate the need for quality in healthcare and in particular the role of the medical physicist with respect to the clinically-effective, evidence-based, safe and economical use of medical devices.
3. An appreciation of the importance of patient and occupational safety and in particular the role of the medical physicist with respect to risk assessment, optimisation and protection from physical agents (ionising radiation, electromagnetic fields, electricity, laser etc) in the hospital environment.
4. Understanding relevant EU, national and local legislation and documentation regarding medical devices and

risk from physical agents within the hospital environment.
5. Understand at the expert level the principles of device management including procurement, acceptance testing, commissioning, constancy testing and calibration.
6. Understand at the expert level the principles of assessment of quality in the use of medical devices.
7. Understand at the expert level the use of instrumentation for the measurement of doses from physical agents associated with patient and occupational risk.
8. Know and understand basic biomedical electronics and signal processing.
9. Able to apply research methodologies and statistical techniques used at the interface between physical and biomedical science.
10. Know and understand the basic principles of medical device design.
11. Be able to apply the principles of Health Technology Assessment to medical devices.
12. Have a basic understanding of frontier research in biomedical physics.

D. Competences for Medical Physics Specializations

Owing to word-count limitations we cannot present detailed competence inventories for each specialisation, however, we give a brief indication of the requirements for each area.

Radiotherapy: physics, the various forms of teleradiotherapy, radiosurgery and brachytherapy devices, quality control, treatment planning and associated imaging simulation systems, clinical application, patient and occupational ionising radiation risk assessment, optimisation, protection and dosimetry with respect to external kV and MV beams.

Diagnostic Radiology: physics, devices for film / digital projection imaging, interventional radiology devices, conventional / spiral / multidetector / cone-beam CT, quality control, clinical application, patient and occupational ionising radiation risk assessment, optimisation, protection and dosimetry with respect to external kV beams.

Nuclear Medicine: physics, devices for planar imaging / SPECT and PET, dose calibrators, quality control, clinical application, patient and occupational ionising radiation risk assessment, optimisation, protection and dosimetry with respect to unsealed sources including decontamination techniques and internal dosimetry calculations.

Magnetic Resonance Imaging: physics, devices, SD / T1 / T2 weighted images, pulse sequence design, functional MRI, clinical application, quality control, patient and occupational electromagnetic risk assessment, protection, optimisation and dosimetry.

Ultrasound: physics, the various forms of US scanning devices, quality control, clinical application, patient ultrasound risk assessment, optimisation, protection and dosimetry.

Physiological Measurement: measurements of electrical, magnetic, pressure, temperature and other physical variables arising from physiological processes, devices, quality control, patient and occupational safety.

Audiology: acoustic physics, structure and function of the auditory system, pathologies of the auditory system, screening auditory function, diagnostic audiological testing, hearing aids, implants.

Acknowledgment

We thank Dag R. Olsen (ESTRO), Yuri Dekhtyar (Latvia), Zoran Stefanovski (Macedonia)., Herman J van Kleffens (Netherlands), Valery Orel (Ukraine), and Cornelius Lewis (UK) for sending us the competence inventories used in their respective countries.

References

1. Tuning (2008) Universities' contribution to the Bologna Process. 2nd ed. Available from http://www.tuning.unideusto.org/tuningeu/
2. Tuning physics group (2005) Tuning summary or common reference points for Physics. Available from http://tuning.unideusto.org/tuningeu/images/stories/template/Template_Physics.pdf
3. Health Professionals Council UK (2007) Standards of proficiency for clinical scientists.
4. Eudaldo T et al (2004) Guidelines for Education and Training of Medical Physicists in Radiotherapy - Recommendations from an ESTRO-EFOMP working group. Radiother Oncol 70:125-35 (presently under update).

Author: M. Wasilewska-Radwanska
Institute: EFOMP
Street: Fairmount House, 230 Tadcaster Road
City: York YO24 1ES
Country: United Kingdom
Email: ETP@efomp.org

The influence of intracellular connections on the electric field induced membrane voltage and electroporation of cells in clusters

G. Pucihar and D. Miklavčič

University of Ljubljana, Faculty of Electrical Engineering, Ljubljana, Slovenia

Abstract— **In this paper we examine the influence of gap junction inhibition on the amplitude and distribution of the induced transmembrane voltage (ITV) and electroporation of cells in clusters. Cell clusters were used as they represent simple models of cells in tissues and thus enable the study of the effects of the external electric field on the level of individual cells. We demonstrated that cells in clusters respond differently to the electric field exposure, depending on the field parameters. Namely, when exposed to long, low voltage pulses (such as during the measurements of the ITV) cells in clusters behave as one giant, single cell. At short, high voltage pulses (such as during electroporation) they behave as individual cells. Different response of cells in clusters was attributed to the changes in the properties of gap junctions, specifically, their opening and closing. This was demonstrated by pre-treating the cells with gap junction inhibitor, which caused the cells in clusters to respond as individual cells, regardless of the pulse parameters.**

Keywords— **Gap junctions, Transmembrane Potential, Electropermeabilization, Lucifer Yellow, di-8-Anepps**

I. Introduction

Clusters of cells grown in monolayers present a simple model system for examining the behavior of cells in tissues. Namely, similar to cells in tissues, cells in clusters have complex geometrical shape, they are densely packed and are also connected with intracellular pathways.

Exposure of tissue to an external electric field induces a voltage on membranes of individual tissue cells, termed the induced transmembrane voltage (ITV). However, the amplitude and the spatial distribution of the ITV on these cells can vary considerably from the ITV observed on single isolated cells. This is because: (i) dense cell packing can to some extent electrically shield cells from the electric field, and/or (ii) intracellular pathways can electrically connect adjacent cells. Due to the nature of the tissue structure it is difficult to experimentally observe these effects on the level of individual tissue cells. Alternatively, we can use simple models of tissue, such as clusters of cells in monolayers.

Cell clusters were already utilized to study the effect of cell shape and cell density on the amplitude and distribution of the ITV [1-3]. Here, we focus on the role of intracellular pathways. Intracellular pathways, also termed gap junctions, are small protein channels, which allow the flow of ions between neighboring cells. Opened or closed state of these channels would render these cells as electrically connected or insulated, respectively, and could therefore considerably affect the distribution of the ITV on cells in clusters.

Understanding the influence of gap junctions on the distribution of the ITV can be of interest in many theoretical and experimental settings, such as activation of voltage-dependent membrane channels and cell membrane electroporation [4]. In the later case a strong electric field applied to the tissue induces a supracritical ITV on cell membranes, which results in a transiently increased permeability of the cell membrane. Despite the fact that electroporation is nowadays frequently applied to tissues for e.g. electrochemotherapy [5] or tissue ablation [6], the course of electroporation of individual tissue cells remains to be explained.

To investigate the influence of gap junctions on the distribution of the ITV we measured the ITV on cells in clusters with inhibited and uninhibited gap junctions. In addition, the same cells were then exposed to the supracritical ITV leading to electroporation and the course of electroporation of cells in clusters was investigated.

II. Materials and methods

A. Cells

Chinese Hamster Ovary (CHO K1) cells were grown in flasks in culture medium (HAM-F12, Sigma-Aldrich, Germany) with added Fetal calf serum (8%, Sigma-Aldrich, Germany), L-glutamine (0.15 mg/ml, Sigma-Aldrich, Germany), and antibiotics (crystacillin 200 units/ml, gentamicin 16 μg/ml) in an incubator at 37°C, 5% CO_2. One day prior to experiments the cells were trypsinized and 10^5cells/ml were plated in LabTek II chambers (Nunc, Denmark).

B. Measurements of the induced transmembrane voltage

The induced transmembrane voltage (ITV) was measured with a fast potentiometric fluorescent dye di-8-Anepps. The dye becomes fluorescent when it binds to the cell membrane with its fluorescence intensity varying linearly with the change of ITV. The culture medium was replaced with SMEM (Spinner's modification of the MEM, Gibco, USA)

O. Dössel and W.C. Schlegel (Eds.): WC 2009, IFMBE Proceedings 25/XIII, pp. 74–77, 2009.
www.springerlink.com

containing 30 μM of di-8-Anepps and 0.05% of Pluronic (both Molecular Probes, Netherlands). After staining for 12 min at 4°C, cells were washed with pure SMEM to remove the excess dye. The cells were then exposed to a 40 V, 50 ms pulse applied on two parallel electrodes with a 4 mm gap (voltage-to-distance ratio 100 V/cm). During the pulse, the fluorescence image of the cell cluster was acquired (ex: 490 nm, em: 605 nm) with a CCD camera (VisiCam 1280, Visitron, Germany) mounted on a fluorescence microscope (AxioVert 200, Zeiss, Germany). Four consecutive pulses were applied with a delay of 4 s and during each pulse the image was acquired. The control image was acquired before the pulses and was subtracted from the images with pulse. The corrected images were then averaged to increase the signal-to-noise ratio. The changes in the fluorescence of the dye were quantified by measurements of gray levels of the region of interest, which was a line encircling the outermost membranes of cells in clusters, using MetaMorph 5.1 (Molecular Devices Corp., PA, USA). With a calibration curve obtained in a separate experiment (a 6% change in fluorescence intensity corresponds to app. 100 mV change in ITV [1]), the fluorescence changes were transformed to the values of the ITV, which were plotted on a graph as a function of the relative arc length.

C. Test for gap junctions

To verify if CHO cells were forming gap junctions, we used the Scrape-loading test [7]. Cells (5×10^5 cells/ml) were grown in Lab Tec chambers to ~70% confluence, which took app. two days. The culture medium was then replaced with SMEM containing 1 mM of a membrane-impermeant fluorescent dye Lucifer Yellow (Sigma-Aldrich, Germany). A tip of a needle was used to scratch cells from the bottom of the chamber. After 5 min of incubation, the dye was washed away with pure SMEM and fluorescence from cells was observed with the imaging system described in Section B. The dye was excited with 425 nm and emission was detected at 605 nm. To inhibit gap junctions, a 200 μM of gap junction inhibitor Oleamide (Sigma-Aldrich, Germany) was added to the cell culture 45 min before the experiments. The concomitant cell handling, dye addition and fluorescence observation were the same as described above.

D. Monitoring the course of electroporation

The same cell clusters, which were used in measurements of ITV (Section B) were then exposed to supracritical electric pulses, leading to electroporation. The course of electroporation was monitored with a membrane-impermeant fluorescent dye Propidium Iodide (PI, Sigma-Aldrich, Germany), which was added to SMEM in a quantity leading to 100 μM final concentration of PI. The fluorescence of the dye increased considerably after it entered electroporated cells. A single 400 V, 200 μs rectangular pulse was delivered to the electrodes, and fluorescence of the cluster was monitored (ex: 515 nm, em: 605 nm) in 100 ms time steps with the same imaging system as described in Section B.

III. Results and Discussion

A. Test for gap junctions

Before we started measuring the induced transmembrane voltage (ITV) and monitoring the course of electroporation, we demonstrated that cells in our study are forming gap junctions. Figure 1A shows a monolayer of CHO cells, which was partially damaged with the tip of the needle (black line in the center of Figures 1A and C). Membrane impermeant fluorescent dye Lucifer Yellow entered the damaged cells rendering them fluorescent and slowly diffused through gap junctions into adjacent, intact cells (Figure 1B). During the five minutes of incubation, the dye diffused through 4 or 5 layers of adjacent cells (Figure 1B) thereby confirming the existence of gap junctions. If cells were pre-incubated with a gap junction inhibitor Oleamide, the fluorescence was confined only to the cells, which were damaged during scraping (Figure 1D).

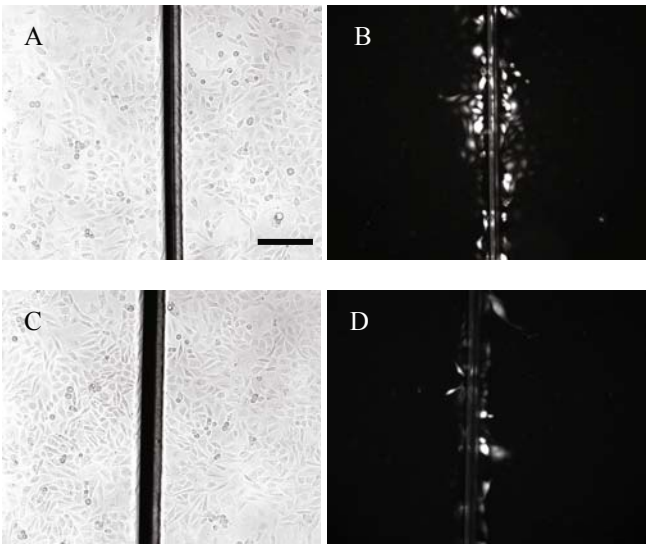

Fig. 1 Scrape loading test with Lucifer Yellow. CHO cells were scraped with a needle (black line in the middle of the figure) and then incubated for 5 minutes in presence of the dye (1 mM). (A) Phase contrast of the monolayer. (B) Fluorescence of cells. (C) Same as A except that cells were pre-incubated for 45 min with 200 μM Oleamide, a gap junction inhibitor. (D) Fluorescence of cells pre-incubated with Oleamide. Bar represents 100 μm.

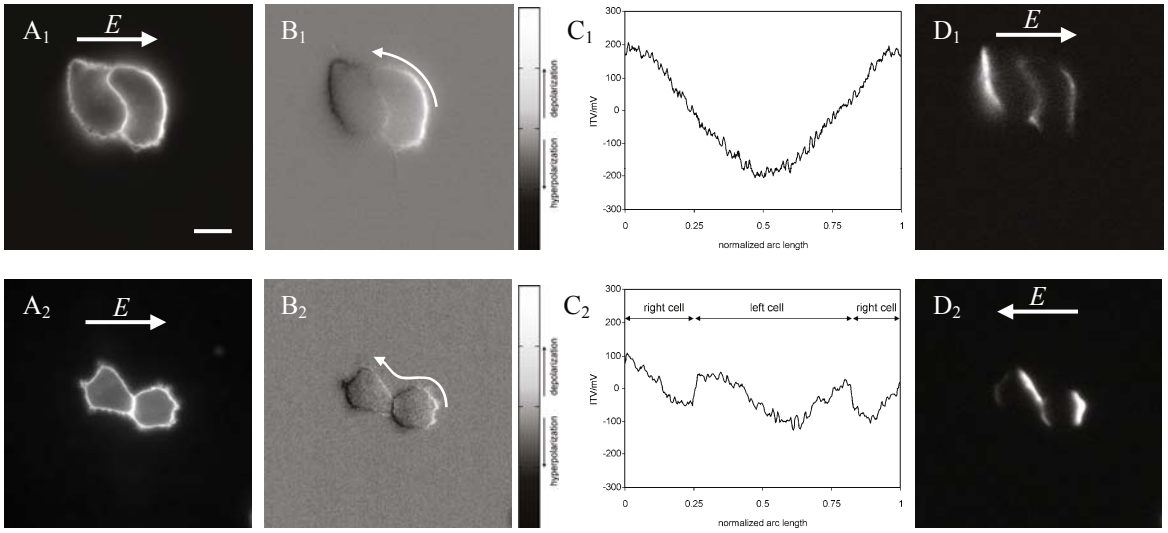

Fig. 2 Measurements of the induced transmembrane voltage (ITV) on a cluster of two CHO cells with uninhibited (upper row) and inhibited (lower row) gap junctions. (A) Fluorescence images of a cluster acquired during the exposure to 40 V (100 V/cm), 100 ms rectangular pulse. (B) Changes in fluorescence reflecting changes of the ITV. (C) ITV as a function of normalized arc length. (D) Electroporation, 100 ms after the cluster was exposed to a single 400 V (1000 V/cm) rectangular unipolar pulse (200 µs). Bar represents 10 µm.

B. Measurements of the induced transmembrane voltage

Measurements of the induced transmembrane voltage (ITV) were performed on different cell clusters, with varying complexity and size, but due to the limited space, the results of only two representative cases are presented. The fluorescence images acquired during the exposure to the external electric field of 100 V/cm are shown in Figures $2A_1$ and $2A_2$ for cells with uninhibited and inhibited gap junctions, respectively. Changes in fluorescence, resulting from changes in ITV, became visible after subtraction from the control image (not shown) and subsequent contrast enhancement (Figures $2B_1$ and B_2). The results for the uninhibited cells show that the right cell in the cluster experienced an increase in fluorescence (white color - depolarization), and the left cell a decrease (black color - hyperpolarization). The two cells in the cluster therefore acted as one interconnected giant cell, during the exposure to the external electric field (Figure $2B_1$). The ITV measured along the outermost membranes of cells in a cluster is presented in Figure $2C_1$ as a function of normalized arc length. The measurements show that the ITV gradually decreased from approximately 200 mV, measured on the farthest right part of the cluster, to -200 mV, measured on the farthest left part of the cluster, and then gradually increased back to 200 mV (Figure $2C_1$). Such a behavior implies that the gap junctions of cells in the cluster are in the open state and the two cells are electrically connected.

A different situation was observed for cells with inhibited gap junctions (Figure $2A_2$). In this case, each of the two cells in the cluster was depolarized on one side and hyperpolarized on the other side (Figure $2B_2$). The two cells in the cluster therefore acted as two individual cells during the exposure to the external electric field. As a result, ITV measured on the cluster changes in a discontinuous fashion. Namely, ITV gradually decreased from approximately 100 mV to -50 mV on the right cell of the cluster, followed by a sudden increase in ITV to 60 mV as we moved to the left cell of the cluster, and then again gradually decreased to -120 mV, on the outmost left part of the left cell. Such a behavior implies that the gap junctions of cells in the cluster are in the closed state and the two cells are electrically insulated.

The measurements of ITV on uninhibited clusters are in agreement with observations reported by Gross on clusters of A-431 nonexcitable human carcinoma cells and with observations of Hassan on clusters of excitable bovine adrenal cromaffin cells [8,9]. They observed depolarization of one part of a cluster and a complete hyperpolarization of the other part in case of small clusters. For larger clusters, they reported a more complex behavior, where some cells inside the cluster exhibited both hyperpolarization and depolarization.

C. Electroporation

In the presence of a membrane-impermeant fluorescent dye Propidium Iodide, the same clusters of cells were then exposed to a single rectangular 400 V pulse (1000 V/cm) of 200 µs duration, pulse parameters, which are known to

cause cell membrane electroporation. The fluorescence of the dye increased several fold after entering the cell through electroporated membrane, which enabled the observation of the electroporated parts of the membrane. Regardless of the treatment of cells with gap junction inhibitor, electroporation was always observed on both sides of each of the cells in the cluster (Figures $2D_1$ and $2D_2$). Clearly, cells in clusters were electroporated individually. This is in agreement with the measurements of ITV, but only for the case of clusters treated with a gap junction inhibitor (cf. Figures $2B_2$ and $2D_2$).

For uninhibited cells, two opposing behavior of cells in clusters were observed. During the measurements of ITV, which were performed at long pulse durations and lower pulse amplitudes (50 ms, 100 V/cm), cells in clusters behave as one giant cell, while during electroporation, which was performed at short pulse durations and higher pulse amplitudes (0.2 ms, 1000 V/cm) cells behave as individual cells. We attribute these observations to the changes in properties (closing) of gap junctions as a response to different parameters of electric pulses. Opening and closing of gap junctions is a stochastic process, occurring on a time interval of hundreds of milliseconds to seconds [10,11]. It is therefore plausible that the average conductivity of these channels on a shorter time interval (such as during electroporation) is different than the conductivity on a longer time interval (such as during measurements of ITV). Besides, higher pulse amplitude in electroporation experiments could change the structure of gap junctions, by rendering them less conductive. In addition to pulse parameters, the properties of gap junctions can also be modified by the change in intracellular Ca^{2+} concentration [12]. It was shown that elevated intracellular concentration of Ca^{2+} closes the gap junctions [11,13] and this is very likely to occur during electroporation.

IV. Conclusions

In our study we demonstrated that the state of gap junctions (opened or closed) considerably affects the amplitude of the ITV and also its distribution on cells in clusters if the pulse amplitude is relatively low and the pulses are long. In this case, cells in clusters behave as a giant, single cell if gap junctions were uninhibited, or as individual cells if gap junctions were inhibited. On the other hand, with short, high voltage pulses, such as used in electroporation, the state of gap junctions does not seem to have any influence on electroporation of these same cells. On the basis of these observations, we can assume that cells in tissues exposed to long, low voltage pulses act, at least to some extent, as one large interconnected unity, while electroporation of the same cells in tissues occurs on many individual tissue cells simultaneously.

Acknowledgment

This work was supported by the Slovenian Research Agency (project No: Z2-9227 and program No: P2-0249).

References

[1] Pucihar G, Kotnik T, Valič B et al. (2006) Numerical determination of transmembrane voltage induced on irregularly shaped cells. Ann Biomed Eng 34:642-652

[2] Pavlin M, Pavšelj N, Miklavčič D (2002) Dependence of induced transmembrane potential on cell density, arrangement and position inside a cell system. IEEE T Biomed Eng 49:605-612

[3] Canatella P J, Black M M, Bonnichsen D M et al (2004) Tissue electroporation: quantification and analysis of heterogeneous transport in multicellular environments. Biophys J 86:3260-3268

[4] Tsong T Y (1991) Electroporation of cell membranes. Biophys J 60:297-306

[5] Mir L M, Glass L F, Serša G et al (1998) Effective treatment of cutaneous and subcutaneous malignant tumours by electrochemotherapy. Br J Cancer 77:2336-2342

[6] Lavee J, Onik G, Mikus P et al (2007) A novel nonthermal energy source for surgical epicardial atrial ablation: irreversible electroporation. Heart Surg Forum 10:92-101

[7] El-Fouly M, Trosko J E, Chang C. C. (1987) Scrape-loading and dye transfer. A rapid and simple technique to study gap junctional intercellular communication. Exp Cell Res 168:422-430

[8] Gross D, Loew L M, Webb W (1986) Optical imaging of cell membrane potential changes induced by applied electric fields. Biophys J 50:339-348

[9] Hassan N, Chatterjee I, Publicover N G et al (2002) Mapping membrane-potential perturbations of chromaffin cells exposed to electric fields. IEEE T Plasma Sci 30:1516-1524

[10] Brink P R (1996) Gap junction channel gating and permselectivity: their roles in co-ordinated tissue function. Clin Exp Pharmacol P 23:1041-1046

[11] Marino A A, Kolomytkin O V, Frilot C (2003) Extracellular currents alter gap junction intercellular communication in synovial fibroblasts. Bioelectromagnetics 24:199-205

[12] Kumar N M, Gilula N B (1996) The gap junction communication channel. Cell 84:381-388

[13] Loewenstein W (1981) Junctional intercellular communication: The cell to cell membrane channel. Physiol Rev 61:829-913

Author: Gorazd Pucihar
Institute: University of Ljubljana, Faculty of Electrical Engineering
Street: Tržaška 25
City: Ljubljana
Country: Slovenia
Email: gorazd.pucihar@fe.uni-lj.si

MEDICAL PHYSICS DEGREE: A MATURE CHOICE FOR GREECE

C. Koutsojannis[1], S. Kaplanis[1]

[1] Technological Educational Institute of Patras/ Department of Physiotherapy/ Medical Physics Lab, Patras, Greece

Abstract— **Almost all major engineering university schools now have a department of biomedical engineering. Biomedical engineering is now an equal to electrical, mechanical, civil and chemical engineering. Additionally the industrial sector in medical physics on ionizing and non-ionizing radiation as well as on biomedical engineering is also advancing and evolving quickly. Physicists as engineers can find numerous and lucrative opportunities with companies. Consequently medical physics is currently the most rapidly growing field of physics. Numerous academic, clinical and industrial opportunities are open to physicists in the medical world. In Europe today a number of physics and engineering undergraduates proceed to postgraduate programs to become professional medical physicists. Students are interested in medical physics for a number of reasons. There are equally good reasons for the faculty to provide a course in medical physics. This is another motivation for the development of an undergraduate medical physics course. Finally according to latest EU directives for education and professions undergraduate education is of major importance. This the first report of a higher degree level course on medical physics developed and introduced at Technological Educational Institute of Patras in Greece partly due to student interest, and partly due to the faculty's desire to provide interesting courses, resulting the tight cooperation of Health Science and Engineering Schools. While this is certainly good news, the curriculum have been designed with extreme care. If too much of the core physics material is removed to free up time for the discipline-specific material, there's a serious risk of graduating students that do not have a sufficiently strong foundation on which to build a career as a professional medical physicist. More discussion under national and international organizations will also improve this choice of TEI of Patras.**

Keywords—**Medical. Physics, education, undergraduate, Greece**

I. Introduction

Almost all major engineering university schools now have a department of biomedical engineering. Biomedical engineering is now an equal to electrical, mechanical, civil and chemical engineering. Additionally the industrial sector in medical physics on ionizing and non-ionizing radiation as well as on biomedical engineering is also advancing and evolving quickly. Physicists as engineers can find numerous and lucrative opportunities with companies. Consequently medical physics is currently the most rapidly growing field of physics. Numerous academic, clinical and industrial opportunities are open to physicists in the medical world. According to a number of authors just a medical physics course should be looked upon as a beneficial addition to the undergraduate physics curriculum. The course should be considered as an ideal addition to the intermediate level physics curriculum, as it covers almost all of the major subjects that physics undergraduates should see. [1] Three Canadian universities currently offer undergraduate medical physics degrees. Those institutions offer four-year BSc honours programmes that are primarily intended to prepare students for graduate studies in medical physics. The specifics of the curricula associated with these degree programmes vary. Depending on the relative proportions of traditional physics and mathematics courses, in comparison to life sciences content, these qualifications may also suffice to prepare the student for graduate work in other fields of physics, thereby maximizing the options available on graduation. [2] Following the Bologna process of transforming European educational area the new curricula in medical physics and bio/physics for medicine and medicine specialists in Serbia, has already introduced on Belgrade and Novi Sad University starting in 2004. [1] The new courses were aimed to fulfil the existing gap in education of physicists and medicine and medicine specialists as according to EFOMP recommendations holding a university Master's Degree in Medical Physics, is not a sufficient qualification to work as a medical physicist or a medical engineer in hospital environment. [4,5] To manage patients without supervision the Recommendations hold necessary to have basic university degree, master degree and hospital practice. In 2006, a new program for Specialist Study for Medical Physics and Medical Engineering was established at ACIMSI, integrating other programs in the area. [6,7] At the same time, new courses on Bio/Physics/Medical Physics within Medicine curricula were introduced at the Faculty of Medicine, University of Belgrade in 2004: those were the Core Course in Biophysics/Medical Physics and an Elective Course on Physical Methods, Instrumentation and Techniques. [1] In Europe today all countries, the basic requirement to enter the Medical Physics education is a university degree. The length of this university education

O. Dössel and W.C. Schlegel (Eds.): WC 2009, IFMBE Proceedings 25/XIII, pp. 78–81, 2009.
www.springerlink.com

ranges from 2 to 5 years. Concerning the Post-graduate education in Medical Physics:

- A nationally approved educational programme is in operation in 16 of the 25 countries.
- Postgraduate education takes place essentially within 3 different approaches and the total length of Medical Physics education and training ranges from2½ years to 9 years. [5]

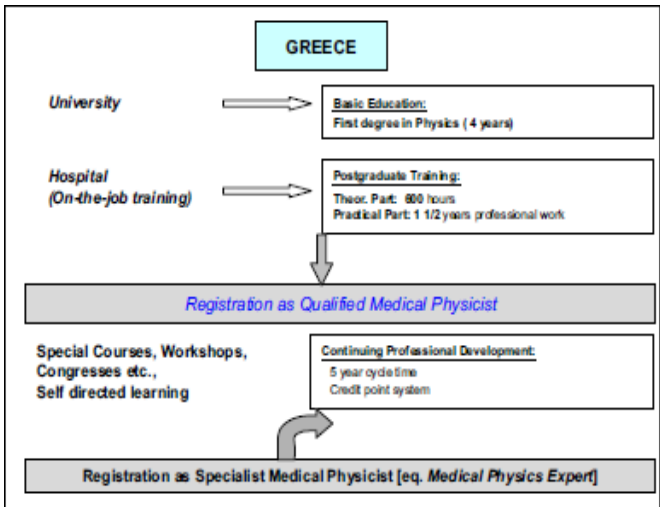

Fig. 1 Education and Training Scheme in Greece *(EFOMP survey 2008)*

In Greece today a number of physics and engineering undergraduates proceed to postgraduate programs to become professional medical physicists. (fig. 1) Students are interested in medical physics for a number of reasons. According to perception results there are equally good reasons for the faculty to provide a course in medical physics. [2,5] This the first report of a higher degree level course on medical physics developed and introduced at Technological Educational Institute of Patras in Greece partly due to student interest, and partly due to the faculty's desire to provide interesting courses, resulting the tight cooperation of Health Science and Engineering Schools. [6]

II. Medical Physics in Greece

A. Generally

Medical Physicist/Engineer is generally involved in three basic hospital activities: *health care services; consulting; and training.* [2,3,5]

Medical Physicist is a professional with clearly defined competences and responsibilities in health care service and consulting, patient dosimetry, development and implementation of complex equipment as well as in optimization and radiation protection.

He works in the same environment with *Medical (Clinical) Engineer* who is also a professional with the same competences and responsibilities in health care service. This also requires similar adequate theoretical and practical knowledge, as well as permanent education and training.

B. Current state of Education and Licensing of Medical Physicists in Europe and Greece

According to international recommendations of EU, EFOMP (European Federation of Organizations for Medical Physics) and IFMBE (International Federation for Medical and Biological Engineering) Greece recognized following professional categories in Medical Physics and Medical (Clinical) Engineering: [2,3,4]

1. *Qualified Medical Physicist/Medical (Clinical) Engineer (*QMP/QME) should have a bachelor and a master university degree and at at least 2 years' training experience on the job, that is essential to achieve the competencies to work as QMP
2. *Specialist Medical Physicist/Engineer* (SMP/SME) must fulfill all requirements defined in point 1. and must successfully complete a 5 years CPD cycle
3. *Expert in Medical Physics/Engineer* (EMP/EME) besides the requirements defined in point 2. should complete a Specialist study program and have at least 3 years of working experience, or should have a PhD degree in Medical Physics.

The certification is in responsibility of the National Certification Board, (for Greece is Hellenic Medical Physics Association) within the Ministry for Health, which forms a National Register of Medical Physicists/Engineers. [2,4] Academic (University) education of medical physicists and preferences (university titles) are divided in tree basic stages: (fig. 1)

I stage – Basic University Study in Physics, duration: 4 years. University title: *l Physicist*

II stage – Master University Study in Medical Physics at the Department of Physics, Faculty of Science, University title: *Master in Medical Physics.*

III stage – Postgraduate University Study .Doctorial study in Medical Physics, duration: 3 years, University degree: *PhD in Medical Physics.* [7,8]

Postgraduate studies for medical physicists are aimed at training professional and research personnel for successful team work in medical institutions, as rapid development of medical diagnostics and therapy, as well as medical equipment of advanced technology, require a team work of experts who, apart from being competent in their profession,

have to demonstrate knowledge in the field of medicine and physics. The concept of such multidisciplinary studies enables physicists who decide to work in medical institutions, to use the existing equipment successfully, modernize it rationally and continually work on its improvement. [9]

C. Program for Undergraduate Study in Medical Physics

Higher education consists of two parallel sectors: the University sector (Universities, Polytechnics, Fine Arts Schools) and the Technological sector (Technological Education Institutions and the School of Pedagogic and Technological Education). Higher Education Institutes are self-governing legal entities under public law, supervised and subsidized by the state through the Ministry of National Education and Religious Affairs. The main source of funding is the state budget through the Ministry of Education and European funds. Additional funding is provided by National and European Framework research projects (RTD), through other ministries and third bodies that receive services provided by the Higher Educational Institutions. Greece has a binary system of Higher Education, designed to ensure maximum flexibility and to respond to the wide variety of social and economic requirements. [6] The Greek Higher Education system is highly diversified offering a wide range and type of courses. The universities are essentially involved with undergraduate and postgraduate programmes, along with basic and applied research. The main responsibility of the T.E.I.'s is in undergraduate programmes with a smaller number of post graduate programmes developed with Greek or other European universities and a growing involvement in European Framework research projects (RTD). The internal structure, organization, and operation of administrative, financial and technical services; overall teaching and research policy; planning; the procedures and requirements for hiring personnel for such positions; the allocation of funds, etc, are determined by the respective provisions and the internal regulations of each university or T.E.I.. Greek Higher Education Institutes develop their own curricula which are published in the Official Journal of the Greek Government and come up for review every two years, 5 by law. Course validation and accreditation is subject to the advisory body of The National Council of Education (ESYP). However, Greek Higher Education Institutes award their own qualifications (Degree, Diploma, MSc, Doctorate). Greek educational institutes are entitled to formulate autonomous policies for achieving their specific educational goals and in fulfilling their mission. [6] In T.E.I of Patras in Greece partly due to student interest, and partly due to the faculty's desire to provide interesting courses, was recently developed a new curriculum as the result of tight cooperation of Health Science and Engineering Schools a undergraduate program for Medical Physics degree under the title "Technologists of Medical Physics" (T.M.P). In T.M.P. program the relative content of physics/mathematics compared with life sciences courses is necessarily strongly dependent on the goal of the degree programme. It should be stressed, however, that an honours undergraduate programme with a strong emphasis on physics and mathematics is crucial for any student who wishes to pursue graduate studies in medical physics on the path to an exciting and rewarding career as a professional medical physicist. [2, 9] Consequently the 1st education-stage presented in *B* section will be replaced with: I stage– Basic University Study in Medical Physics/Physics, duration: 4 years. University/T.E.I. title: *Medical Physicist/Physicist.*

The T.M.P. program has been designed as to incorporate the contemporary scientific and professional findings in the field of medical physics, medical diagnostics and therapy as well as modern technological achievements regarding medical instruments. The curriculum offers a flexible approach to students' preference for studying particular specialized areas of medical physics through core subjects of Health Science and Engineering Schools as well elective subjects regarding applications in current medical practice. The studies are multidisciplinary, since experts from different fields carry out the process of teaching: medical physicists, mathematicians, doctors, biologists, biochemists, biomedical engineers and others. The educational basis are Faculty of Physiotherapy and Optics Departments, and the clinical one are the Faculty of Health Sciences School of T.E.I of Patras. International Aspects of the Program intend to be recognized regarding the Bologna declaration, EFOMP (European Federation of Organizations for Medical Physics) Program. [3,4,5] The program offers 48 courses divided in two categories: core mandatory subjects and elective subjects. The students are recommended to choose the mentor and to select the group of subjects which is in the best correspondence with his/her job. *Core subjects* includes the topics in physics; mathematics, anatomy, physiology; biochemistry and biology; principles of biomedical engineering; medical facilities; health informatics; biological mechanics; principles and safety standards; biostatistics; Quality Assurance in various branches of medicine; Electromagnetic theory; signal analysis; Information technologies; etc. *Elective subjects* are divided in two groups as follows: 1st group includes Medical facilities in radiological diagnostics and safety aspects; Medical facilities in Nuclear Medicine and safety aspects; Medical Facilities in Radiotherapy and safety aspects; Dosimetry and Radiation protection in Radiological diagnostics, Nuclear Medicine and Radiotherapy; Nonionizing techniques in medicine and

safety aspects; 2nd group includes *subjects of general interest* as: ethics and deontology; health psychology; health economics; international terminology; etc. Within Health Sciences and Engineering (Mechanical and Electrical) studies at T.E.I of Patras, physics/and mathematics as well as biomedical technology/health informatics etc, are incorporated in the curriculum at the faculties of Optics, Physiotherapy, Nurse and Speech Therapy. For decades, physics was considered rather as sort of "cook book" of technical terms than as an essential tool for understanding and interpreting the basic laws of nature, and should it be presented as a fundamental part of today's culture or give only elementary scientific facts and technical data for core biomedical subjects and diagnostics and therapeutic methods and instrumentation for the clinics. [7] The new program developed at the Faculty of Health Sciences, at T.E.I of Patras offers a Core Course in Biophysics/Medical Physics in the first two years of the study and an Elective Course dealing with physical methods, instrumentation and techniques applied in medicine research and practice. The courses are aimed to reflect the interest of medicine specialist and future researchers, as well as to provide information on new physical methods and techniques to be used in biomedical sciences and practice. Their main goal is to present physics both on formal cognitive level and to instigate logical reasoning and abstract thinking, as well as to encourage future biomedical community to take a closer look into physic/biophysics /medical physics theories and methodology. The courses try to promote a new understanding of the living matter, to enabled students *to observe*, *to categorize* and *to quantify* the natural phenomena, to read formulae as a phenomenon or a process and not just a sequence of signs, and finally *to get a grip of the totality of nature itself.* [8]
The Core Courses present basic concepts and issues in biophysics/medical physics relevant in understanding essential physiological functions of the living systems and to present basic contemporary aspects on the transport and transformation of matter and energy, both within living and non-living environment. The Elective Courses are aimed to presents operative and practical knowledge on the principles and functioning of biomedical instrumentation and techniques used in medicine practice. [6,7,8] T.M.P. will be largely founded on practical exercises and experimental work. Physics workshop will be an integral part of laboratory workshops and will be focused on examples from clinical praxis. The syllabus is divided into modules and students are enabled to pass the course *step by step*, passing the test following the modules. The *ex cathedra* presentations will be avoided as much as possible, and laboratory, e-learning as well on-the-job presentations are complementary with the theoretical part of the courses. Students will be encouraged to search for literature and present seminars as a result of individual or teamwork.

IV. Conclusions

This the first report of the first higher degree level course on Medical Physics developed at Technological Educational Institute of Patras in Greece partly due to student interest, and mainly due to the faculty's desire to provide interesting courses, resulting the tight cooperation of Health Science and Engineering Schools. While this is certainly good news, the curriculum has been designed with extreme care. If too much of the core physics material is removed to free up time for the discipline-specific material, there's a serious risk of graduating students that do not have a sufficiently strong foundation on which to build a career as a professional medical physicist. More discussion under international organizations will also improve this choice of TEI of Patras. There is already strong interest among graduate at postgraduate students to apply for the new programs, as well as among professionals already working in the field. The T.M.P. program, as well as the teaching stuff obtained higher evaluations for content of the courses, as well as for the clearness of presentations and good organization.

References

1 Christensen N Medical Physics: the perfect intermediate level physics class, Eur. J. Phys. Vol22 2001, pp. 421–427
2 Spasic-Jokic V, Popovic D, Stankovic S and Zupunski I New courses in medical engineering, medical physics and bio/physics for clinical engineers, medicine and medicine specialists in Serbia, T. Jarm, P. Kramar, A. Županič (Eds.): Medicon 2007, IFMBE Proceedings Vol16, 2007, pp. 310–312
3 EFOMP at www.efomp.org/policy/policy5.html
4 O' Meara J. Medical physics degrees: too much too soon? http://medicalphysicsweb.org/cws/article/opinion/26135 (10/17/2006)
5 Eudaldo T, Olsen K, The present status of Medical Physics Education and Training in Europe: An EFOMP survey, Physica Medica Vol24, 2008, pp. 3-20
6 T.E.I of Patras, www.teipat.gr
7 Faculty of Technical Science at University of Novi Sad at http://www.ftn.ns.ac.yu/studije/specijalisticke/biomedicinska.pdf
8 ACIMSI at www.medfiz.ns.ac.yu
9 Brown H, Smallwood RH, at al. (1999) Medical Physics and Biomedical Engineering. Inst.of Physics Publ. Bristol and Philadelphia

Author: C. Koutsojannis
Institute: Technological Educational Institute of Patras, Branch Department of Aigion, Department of Physiotherapy
Street: Psaron 6, Myrtia
City: 25100 Aigion
Country: Greece
Email: ckoutsog@teipat.gr

Plasma medicine - therapeutic application of physical plasmas

Thomas von Woedtke[1], Michael Jünger[2], Thomas Kocher[2], Axel Kramer[2], Jürgen Lademann[3], Ulrike Lindequist[2], Klaus-Dieter Weltmann[1]

[1]Leibniz Institute for Plasma Science and Technology (INP) Greifswald,
[2]Ernst Moritz Arndt University Greifswald, [3]Charité – University Medicine Berlin, Germany

Abstract— **Plasma medicine is an innovative and emerging field combining plasma physics, life science and clinical medicine to use physical plasma for therapeutic applications. Initial experiments confirm that plasma can be effective in *in vivo* antiseptics without affecting surrounding tissue and, moreover, stimulating tissue regeneration. Based on sophisticated basic research on plasma-tissue interaction, first therapeutic applications in wound healing, dermatology and dentistry will be opened.**

Keywords— **physical plasma, plasma medicine, wound healing, dermatology, dentistry**

I. Introduction

Progress in life sciences is increasingly caused by utilization of unrelated technologies and knowledge. In this spirit, microelectronics, optics, material sciences or nanotechnology became key technologies in modern medicine. A similar trend is expected now concerning plasma technology. Actually, plasma medicine is emerging worldwide as an independent medical field - comparable to the launch of laser technology into medicine years ago. Plasma medicine can be subdivided into three main fields: plasma-assisted modification of bio-relevant surfaces, plasma-based biodecontamination/sterilization, and – as the central field – direct therapeutic plasma application. Especially for this last-mentioned field, a fundamental knowledge of the mechanisms of plasma interaction with living cells and tissue is essential as a scientific basis (Fig. 1).

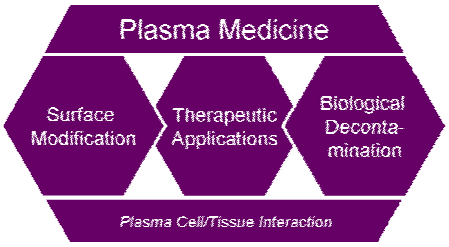

Fig.1 Plasma medicine: scientific basis and main fields [1]

II. Direct Application of Non-Thermal Atmospheric Pressure Plasmas in Medicine

Plasma-assisted modification of bio-relevant materials is an established technique to optimize the biofunctionality of implants or to qualify polymer surfaces for cell culturing and tissue engineering. Plasma-based methods and processes for sterilization, decontamination or reprocessing of medical and diagnostic devices, pharmaceutical products or packaging materials are under development worldwide. Both fields are more or less indirect medical plasma applications. The main challenge now is the application of physical plasmas directly on or in the human body. Whereas for surface modification and biological decontamination both low-pressure and atmospheric pressure plasmas can be used, for direct therapeutic plasma applications only atmospheric pressure plasma sources are applicable. The high reactivity of plasma is a result of different plasma components: electromagnetic radiation (UV/VUV, VIS, IR, high-frequency electromagnetic fields, etc.) on the one hand and ions, electrons and reactive chemical species, primarily radicals, on the other. Besides surgical plasma application like argon-plasma coagulation [2], which is based on high-intensity lethal plasma effects, first and sporadic non-thermal therapeutic plasma applications are documented in literature [3]. However, the basic understanding of mechanisms of plasma effects on different components of living systems is in the early beginning (Fig. 2).

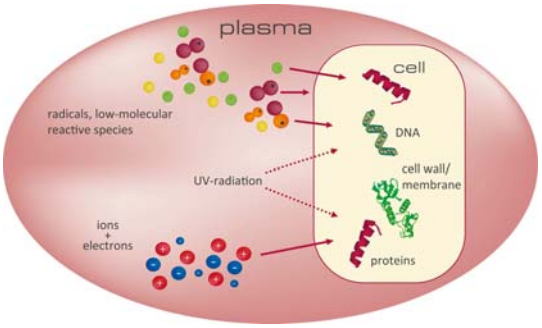

Fig.2 Schematic of effective plasma components and assumed target structures in a living cell

O. Dössel and W.C. Schlegel (Eds.): WC 2009, IFMBE Proceedings 25/XIII, pp. 82–83, 2009.
www.springerlink.com

III. INTERDISCIPLINARY BASIC RESEARCH ON PLASMA INTERACTION WITH LIVING MATTER

Based on several knowledge about mechanisms of antimicrobial plasma activity, actual research in plasma medicine is mainly focussed on the following fields:

- selective inactivation of infectious agents in the close presence of living tissue (*in vivo* antisepsis)
- direct interaction of active plasma components with biochemical and physiological processes influencing growth and vitality of cells and tissue
- indirect influencing of cells and tissue via changes of the vital environment (physiological liquids) of cells and tissue through physical plasma

Combination of plasma technology and plasma diagnostics with cell biological, biochemical and chemical analytical techniques based on *in vitro* models using microorganisms as well as cell and tissue cultures, will facilitate a sophisticated evaluation of biological plasma effects.

To achieve sustained success of plasma medicine, for any potential therapeutic application optimal plasma composition (radicals, irradiation, temperature, etc.), useful application rate and acceptable relation between desired therapeutic effects and adverse reactions have to be found. This can be realized only in close collaboration between plasma physicists, life scientists and clinical physicians. With the Greifswald Campus PlasmaMed (www.campus-plasmamed.de) an optimal organization framework bringing together non-university research institutes, universities and universities of applied sciences, has been established to realize this.

IV. FIRST THERAPEUTIC APPROACHES OF PLASMA MEDICINE: DERMATOLOGY AND WOUND HEALING

Initial experiments confirm the fact that infectious agents can be killed without adverse reactions on surrounding healthy body cells. Furthermore, it is possible to stimulate physiological and biochemical processes in living tissues by plasma treatment under special conditions. This opens the possibility to use plasma to support wound healing as well as to treat several skin diseases. Therefore, application-oriented research is directed to develop an integrated concept of plasma-based wound treatment comprising both superficial wound cleaning and antiseptics and stimulation of tissue regeneration in deeper tissue layers (Fig.3). On a solid scientific basis, further therapeutic plasma applications e.g. in dentistry, or surgery, will be opened during the next years [4].

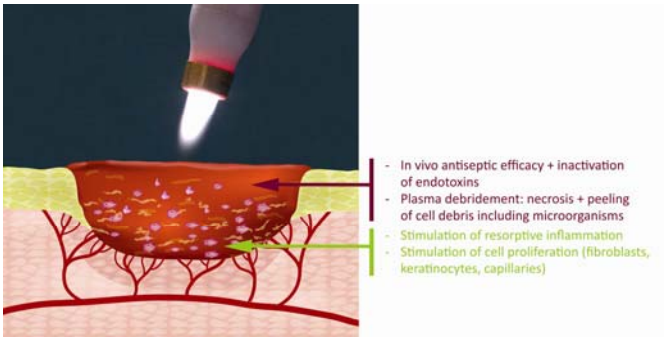

Fig.3 Integrated concept of plasma-based wound healing

ACKNOWLEDGMENT

The Campus PlasmaMed is supported by the BMBF program “Spitzenforschung und Innovation in den Neuen Ländern” (PROSIN 5).

REFERENCES

1. Brandenburg R, Lanhe H, von Woedtke Th, Stieber M, Kindel E, Ehlbeck J, Röpcke J, Weltmann K-D. Antimicrobial effects of UV and VUV radiation of nonthermal plasma jets. IEEE Trans Plasma Sci, revised
2. Zenker M (2008) Argon plasma coagulation. GMS Krankenhaushyg Interdiszip 3:Doc15; http://www.egms.de/en/journals/dgkh/2008-3/dgkh000113.shtml
3. Fridman G, Friedman G, Gutsol A, Shekter AB, Vasilets VN, Fridman A (2008) Applied Plasma Medicine. Plasma Process Polym 5:503-533
4. Kramer A, Lindequist U, Weltmann K-D, Wilke C, von Woedtke Th (2008) Plasma Medicine – its perspective for wound therapy. GMS Krankenhaushyg. Interdiszip. 3:Doc16; http://www.egms.de/en/journals/dgkh/2008-3/dgkh000114.shtml

Corresponding author:

Author: PD Dr. Thomas von Woedtke
Institute: INP Greifswald e.V.
Street: Felix-Hausdorff-Str. 2
City: 17489 Greifswald
Country: Germany
Email: woedtke@inp-greifswald.de

Numerical models of microneedle electrodes for gene electrotransfer in skin

N. Pavšelj[1] and D. Miklavčič[1]

[1] University of Ljubljana, Faculty of Electrical Engineering, Ljubljana, Slovenia

Abstract— **Most widely used electrodes in gene electrotransfer in the skin are external plate electrodes of different geometries where we first have to cause the electrical breakdown of the stratum corneum, in order to reach the viable layers underneath. Therefore, painless microneedle electrodes for transdermal drug delivery and electrogene transfection in skin were proposed and are under development. Their depth of penetration is small enough not to cause any pain for the patient. A preliminary comparison, by means of numerical models, between different settings of microelectrode arrays was made. Comparison with external plate electrodes showed that the volume of the tissue exposed to electric fields exceeding the irreversible electroporation threshold, is smaller when needle microelectrodes are used. Further, as the areas of high (irreversible) electric field coincide with the areas of DNA injection, (both near the electrode tips), it may be sensible to alternate the role of the microneedles, using half of them (every second) as electrodes and the other half as DNA delivery device.**

Keywords— **electroporation, electrogene transfer, skin, finite element method, microneedles.**

I. Introduction

Cell membrane is, in general, impermeable for larger molecules; however, the application of electric pulses to cells results in electroporation of cell membrane, increasing its permeability and making possible for molecules, such as drug molecules or DNA, to enter the cell [1]. After treatment, cell membrane reseals provided the applied voltage was, although high enough to cause cell membrane permeabilization (the electric field is above reversible threshold), still low enough not to cause irreversible permeabilization (irreversible threshold), hence permanent damage. Skin is an attractive target tissue for gene therapy for a variety of reasons. Its size and accessibility facilitates gene delivery. Electroporation seems particularly effective to improve DNA transfection after intradermal and topical delivery without any significant alteration of skin structure and can be used to create aqueous pathways across the skin's outermost layer, the stratum corneum to enhance transdermal drug delivery [2]. Skin is also a very good target organ for DNA immunization because of the large number of potent antigen presenting cells, critical for an effective immune response [3].

The most widely used electrodes in gene transfection in the skin are external plate electrodes of different geometries. They are also used for the treatment of the subcutaneous tumors and for transdermal drug delivery. However, using external electrodes, we first have to cause the electrical breakdown of the highly resistive outermost layer, the stratum corneum, which could pose a safety issue and cause discomfort for the patient. Therefore, new electrode geometry for transdermal drug delivery and electrogene transfection in skin was proposed – painless microneedle electrodes [4-8]. Namely, in order to breach the high electrical resistance and non-permeability of skin, only its outermost layer, the stratum corneum needs to be pierced. The depth of penetration does not exceed 50 μm, which causes no pain for the patient, since epidermis contains no nerves or nerve endings.

A preliminary comparison, by means of numerical models, between different settings of microelectrode arrays was made. The microelectrodes were modeled hollow to be used as microneedles, allowing the DNA to be injected into the skin.

II. Materials and methods

The numerical models were made by means of commercially available computer program COMSOL Multiphysics 3.3 (COMSOL, Los Angeles, CA, USA) based on the finite element method. This method solves partial differential equations by dividing the model into smaller elements where the quantity to be determined is approximated with a function or is assumed to be constant throughout the element. Finite elements can be of different shapes and sizes, which allows modeling of intricate geometries. Nonhomogeneities and anisotropies can also be modeled and different excitations and boundary conditions can be applied easily.

III. Numerical models of microelectrode arrays

Three different settings of the microneedle arrays were modeled, all consisting of arrays of 10x10 needles 1 mm apart. All three geometries are shown in Figure 1 where

O. Dössel and W.C. Schlegel (Eds.): WC 2009, IFMBE Proceedings 25/XIII, pp. 84–87, 2009.
www.springerlink.com

black and white dots denote electrodes of different polarities.

The microelectrodes were modeled hollow, namely, they can be used as microneedles, delivering the DNA into the skin. Electrode length is 500 μm, however, their modeled penetration depth is 400 μm. The outer and the inner diameter of the hollow microneedle are 150 μm and 60 μm, respectively. The content of the hollow needle array (DNA with its properties) was not modeled at this stage.

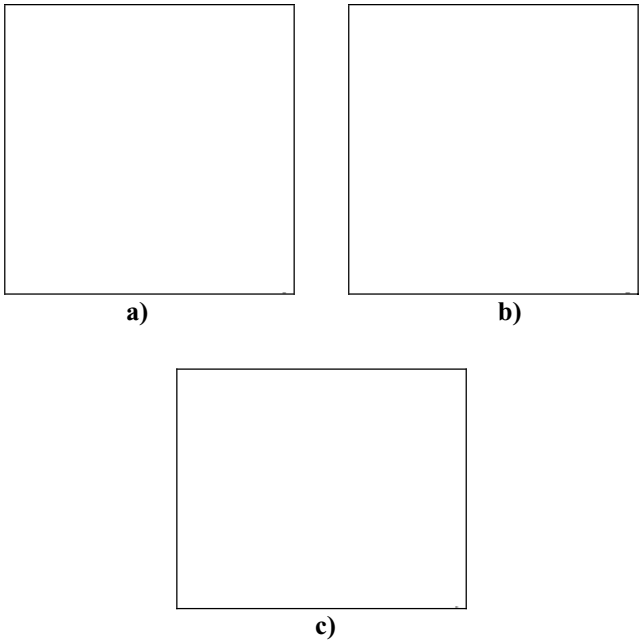

Fig 1 Different settings of microneedle arrays: a) lined; b) crossed; c) hexagonal. Black and white dots denote electrodes of different polarities.

Modeling the whole array would be a wasteful task from both the modeler's and computer time point of view. Therefore, using the symmetry, only a small portion of the whole array, a unit cell, needs to be modeled by applying appropriate periodic boundary conditions [9]. However, the calculation thus made will only hold true for the microneedles inside the array which are surrounded by neighboring microneedles, and not on the edges of the array. Figure 2 shows unit cells for each of the microelectrode arrays presented in Figure 1, along with the dimensions and the boundary conditions to model an infinite array of microelectrodes. The unit cells are shown in black, while the surrounding needles are grayed out. Although the unit cell of the "crossed" geometry Figure2b) can be chosen differently (even smaller, with each corner of the unit cell containing a quarter of a microelectrode and the electric insulation boundary condition on all edges), we used the one on Figure 2b for easier comparison of the results.

Skin layers were not modeled in the microneedle array models. Instead, skin was modeled as a homogeneous structure with the initial conductivity of 0.002 S/m and an 80-fold increase in the conductivity when in a permeabilized state. Namely, as observed from in vivo experiments, a nonlinear current/voltage dependence is measured during pulse delivery. This suggests tissue conductivity change during tissue electropermeabilization (the tissue conductivity depends on the strength of the electric field: $\sigma=\sigma(E)$), that needs to be included in the numerical models [10-12].

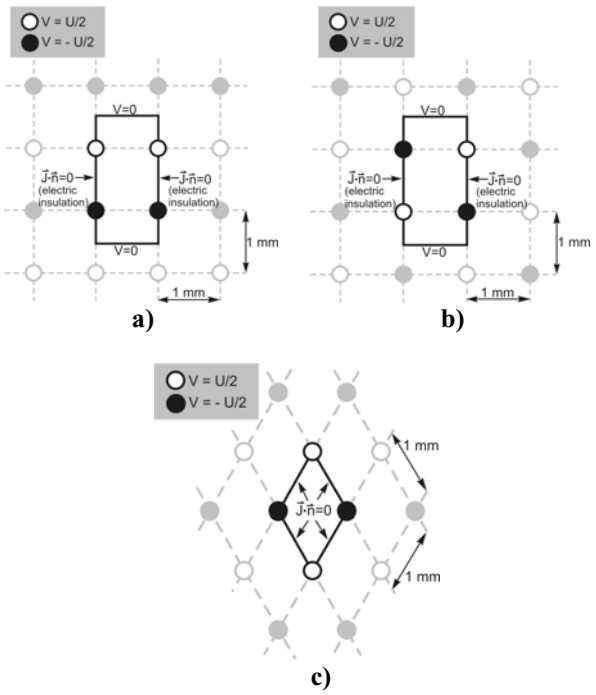

Fig 2 Dimensions, unit cells and boundary conditions of the microelectrode array geometries: a) lined geometry; b) crossed geometry; c) hexagonal geometry

IV. Results

The electric field distributions in skin where pulses of 60 V between the negative and the positive electrodes are delivered through different setups of microneedle electrode arrays are shown in Figure 3. Colored areas denote reversibly permeabilized tissue, thus regions in the model where the electric field is between the reversible and the irreversible thresholds (400 V/cm<E<900 V/cm) [10]. The distributions are shown in 3-dimensional view and on the vertical section plane cut through the middle of the electrodes.

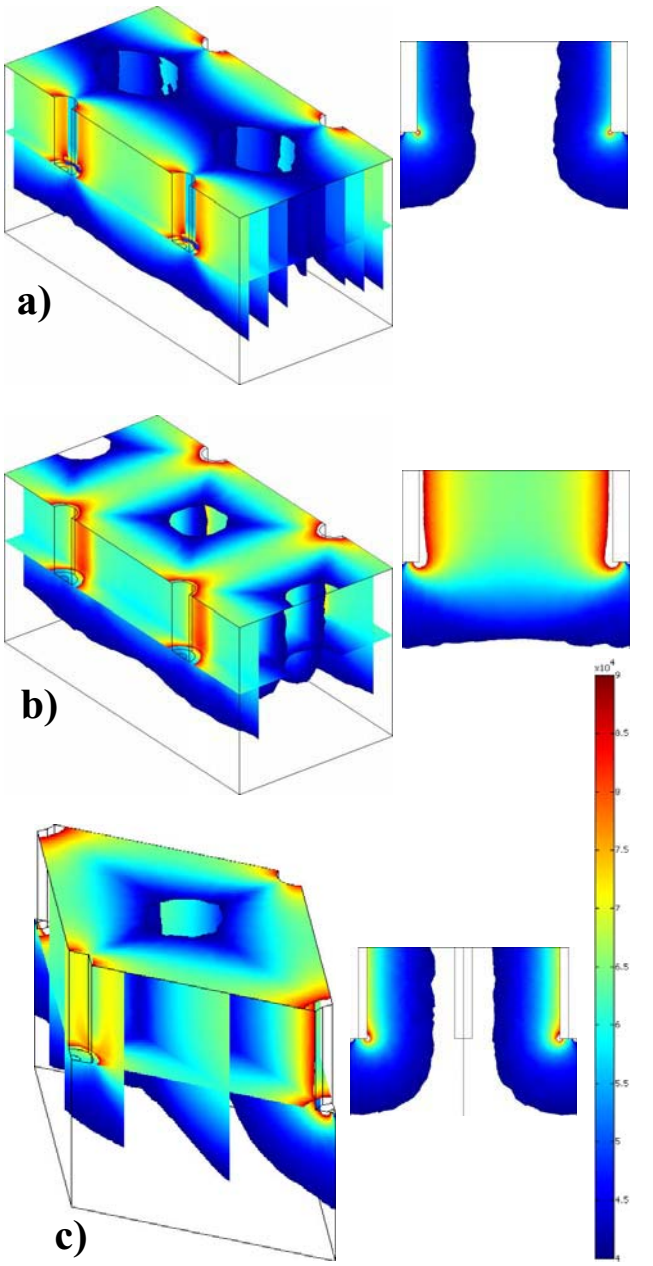

Fig 3 The electric field distributions in a) lined, b) crossed, c) hexagonal microelectrode array. The colored areas denote regions where the electric field is between the reversible and the irreversible electric field thresholds, hence between 400 V/cm < E < 900 V/cm. The electric field in the non-colored areas is either above 900 V/cm (near the electrodes), or below 400 V/cm (elsewhere). The distributions are shown in 3-dimensional view (left) and on the vertical section plane cut through the middle of the electrodes (right).

Comparing the portions of skin tissue above the reversible and the irreversible thresholds, respectively, and the electric currents through different microelectrode arrays, very small differences can be observed (Table 1). Although the calculated tissue volumes where the reversible and the irreversible electric field thresholds are exceeded might seem somewhat low, one has to take into account the tissue volume below the electrode tips that was included in the calculation. Namely, enough tissue volume was modeled below the electrode tips in order not to restrain the natural current flow, which would lead to an incorrect representation of the process.

Table 1 Electric currents, percentages of the reversibly and the irreversibly permeabilized tissue, and the difference between the two for the applied voltage of 60 V.

U=60 V	●● ○○	●○ ○●	●● ○○
Electric current	0.117 A	0.118 A	0.122 A
Volume above E_{rev}	54.7 %	64.4 %	64.8 %
Volume above E_{irrev}	0.125 %	0.45 %	0.5 %

V. CONCLUSIONS

Using external electrodes on skin is problematic, due to the high resistivity of its outermost layer, the stratum corneum. Therefore, a new electrode design, arrays of microneedle electrodes, was proposed. Modeling different settings of the microneedle arrays, only small differences were observed between them. The portions of the volume between the reversible and the irreversible electric field thresholds were comparable, as well as the electric currents through the arrays. However, the electric field distributions seem more favorable in the "crossed" and the "hexagonal" setting, where the electropermeabilized regions are more symmetrically distributed around the electrodes.

Since the electrical barrier of the stratum corneum when using the microneedles is breached by piercing it, no layers were modeled in the microelectrode array models. Namely, the error made when using average skin conductivity instead of modeling different skin layers is lower in this electrode-tissue setting. Also, as we had no current-voltage experimental data, nor any data on transfection rates, the model of the electropermeabilization process in the skin using microelectrode arrays could not be validated. Therefore, the currents through the models and the percentages of the volume exposed to electric field magnitude above the

permeabilization threshold were used only to compare the different microelectrode array settings modeled.

Another point to be taken into account when using such electrodes for gene electrotransfer is the presence of a very high electric field (above the irreversible threshold) in the immediate vicinity of the electrodes, especially the electrode tips. Namely, in gene electrotransfer, caution must be taken not to exceed the irreversible electric field value in the target tissue, causing cell death, as gene therapy will be successful only if there are enough viable transfected cells. In the case of hollow microneedles that are used to deliver both, the DNA and the electric pulses, the areas of high (irreversible) electric field coincide with the areas of DNA injection, both near the electrode tips. Therefore it may be sensible to alternate the role of the microneedles, e.g. using half of them (every second) as electrodes and the other half for DNA delivery.

We compared the electric field distributions in the models of the microneedle arrays with models where external plate electrodes are used [11, 12]. The volume of the tissue exposed to electric fields exceeding the irreversible threshold seems to be smaller when using microneedle arrays. Despite the lack of experimental data on microneedle arrays, the microneedle array models made are good first approximation and useful for comparison with the skin fold model. As the first prototype of microneedle arrays has been made, the presented models will in the future be validated and improved with the help of experimental data.

Acknowledgment

This research was supported by the European Commission under the FP6 grant Angioskin LSH-2003-521217 and by the Slovenian Research Agency.

References

1. Mir LM (2000) Therapeutic perspectives of in vivo cell electropermeabilization. Review article, Bioelectrochemistry 53: 1-10
2. Denet A-R, Vanbever R, Préat V (2004) Skin electroporation for transdermal and topical delivery, Adv Drug Deliv Rev 56: 659-674
3. Zhang L, Widera G, Rabussay D (2004) Enhancement of the effectiveness of electroporation-augmented cutaneous DNA vaccination by a particulate adjuvant. Bioelectrochemistry 63: 369-373
4. Henry S, McAllister DV, Allen MG et al. (1998) Microfabricated microneedles: a novel approach to transdermal drug delivery. J Pharm Sci 87(8):922-925
5. Davis SP, Landis BJ, Adams ZH et al. (2004) Insertion of microneedles into skin: measurement and prediction of insertion force and needle fracture force. J Biomech 37:1155-1163
6. Davis SP, Martanto W, Allen MG et al. (2005) Hollow metal microneedles for insulin delivery to diabetic rats. IEEE Trans Biomed Eng 52:909-915
7. Mukerjee EV, Collins SD, Isseroff RR et al. (2004) Microneedle array for transdermal biological fluid extraction and in situ analysis. Sensor Actuator 114(1-2):267-275
8. Prausnitz MR (2004) Microneedles for transdermal drug delivery; Adv Drug Deliv Rev 56:581-587
9. Susil R, Šemrov D, Miklavčič D (1998) Electric field induced transmembrane potential depends on cell density and organization; Electro and Magnetobiology 17(3):391-399
10. Pavšelj N, Bregar Z, Cukjati D et al. (2005) The course of tissue permeabilization studied on a mathematical model of a subcutaneous tumor in small animals. IEEE Trans Biomed Eng 52(8): 1373-1381
11. Pavšelj N, Préat V, Miklavčič D (2007) A numerical model of skin electropermeabilization based on in vivo experiments. Annals Biomed Eng 35: 2138-2144
12. Pavšelj N, Miklavčič D (2008). Numerical models of skin electropermeabilization taking into account conductivity changes and the presence of local transport regions. IEEE Trans Plasma Sci 36: 1650-1658

Author: Nataša Pavšelj
Institute: University of Ljubljana, Faculty of Electrical Engineering
Street: Tržaška 25
City: Ljubljana, SI-1000
Country: Slovenia
Email: natasa.pavselj@fe.uni-lj.si

Small Animal Imaging with Micro, Flat-panel and Clinical CT-Scanners: An Applicability Analysis

W. Stiller[1], F. Kiessling[2] and W. Semmler[3]

[1] Department of Radiology (G030), German Cancer Research Center (DKFZ), Heidelberg, Germany
[2] Institute of Biomedical Engineering/Chair of Experimental Molecular Imaging, University Hospital Aachen, Aachen, Germany
[3] Department of Medical Physics in Radiology (E020), German Cancer Research Center (DKFZ), Heidelberg, Germany

Abstract— **An analysis which technical concept of CT is best suited for addressing the problems of in-vivo small animal CT imaging is presented. Imaging properties of three CT scanner designs most commonly employed for the task have been studied in view of small animal imaging using custom-designed small animal phantoms as well as in vivo. The presented applicability analysis provides a scientific basis for the decision which scanner concept is most suited for addressing a specific problem of in-vivo small animal CT imaging.**

Keywords— **Computed tomography (CT), small animal imaging, phantoms, technical scanner concepts, in-vivo imaging.**

I. Introduction

Over the past decade, pre-clinical research has increasingly relied on the use of laboratory animals due to an increased availability of animal models of human disease. In consequence, the interest in non-invasive small animal imaging *in vivo* has risen since it facilitates longitudinal study designs in which the same animal can be measured repeatedly at different time points acting as its own control. Thus, required cohort size can be reduced.

With the rise of small animal imaging, CT has commonly been employed, e.g. for phenotyping different animal models, characterizing morphology or monitoring changes thereof, mainly because of the modality's wide-spread use, good availability, and – with spatial resolution down to the order of 10 µm – highly detailed anatomical information [1].

While clinical multi-slice CT (*MSCT*) has been used for small animal imaging [2], scanner systems like micro- and flat-panel detector Volume-CT (*µCT* and *fpVCT*, resp.) have come to the fore to meet the requirements of small animal imaging in pre-clinical studies by a down-scaling of clinical CT accounting for the difference in size between humans and small animals, e.g. by offering higher spatial resolution.

Several design factors of CT scanners such as geometry, x-ray source and detector technology influence the CTs' fundamental imaging characteristics, and complex inherent relationships between imaging parameters such as resolution, noise, gantry rotation time and applied x-ray dose imposed by the fundamental laws of physics exist [3]. No single scanner design is able to optimize all fundamental imaging characteristics; instead, several different scanner designs exist which are more or less suited to address a certain imaging problem.

The goal of this study has been to determine which of the three aforementioned technical concepts of CT currently most commonly employed for small animal imaging [1], i.e. MSCT, fpVCT, and µCT, is best applicable for addressing a specific problem of in-vivo small animal CT imaging. To this end, custom-designed small animal phantoms have been developed along with methods for an applicability analysis of different physical scanner concepts in view of small animal CT imaging, and a complete and systematic assessment of all decisive imaging parameters with respect to in-vivo imaging of small laboratory animals has been undertaken with phantom and animal studies.

II. Material and methods

A. CT scanner systems

Technical scanner concepts studied in the applicability analysis comprise MSCT, fpVCT and µCT.

The clinical MSCT scanner has been a conventional 16-slice MSCT scanner of the *Aquilion*™16 series (Toshiba Medical Systems Corporation (TMSC), Nasu, Japan). It features a multi-row detector of 40 rows (16×0.5 mm (isocenter (IC)) enclosed by twice 12×1.0 mm (IC)) with a maximum axial coverage of 32 mm. Detector elements consist of a fast ceramic scintillator of praseodymium-doped gadolinium-oxysulfide (Gd_2O_2S:Pr) combined with photodiodes to detect scintillation light. The smallest detector field of view (FOV) available covers 180 mm (FOV SS). It has been employed for all measurements. For the chosen FOV, small focal spot together with small beam-shaping wedge filter are applied throughout all measurements in order to achieve highest spatial resolution possible. A standard rotating anode x-ray tube (MegaCool™) and a 60 kW generator are used in the scanner. Gantry rotation time can be selected from 0.4, 0.5, 0.6, 0.75, 1.0, and 1.5 s/rot.; maximum scan time is 100 s per image series. Both sequential acquisition as well as standard helical scanning is avail-

O. Dössel and W.C. Schlegel (Eds.): WC 2009, IFMBE Proceedings 25/XIII, pp. 88–91, 2009.
www.springerlink.com

able. The latter mode with a pitch of 0.9375 and a collimation of 16×0.5 mm (IC) has been used for all phantom and animal scans. Image reconstruction is based on a helical 3D-Feldkamp backprojection algorithm.

The fpVCT has been an experimental scanner prototype (Siemens Medical Solutions, Forchheim, Germany). The system is based on a clinical MSCT gantry in which the multi-row detector block has been replaced by a digital flat-panel detector (PaxScan™ 4030CB, Varian Medical Systems, Palo Alto, CA, USA). The detector features an active area of 40×30 cm^2 with 2048×1536 pixels of 194 µm edge length. Incident x-ray photons are converted to scintillation light in a crystal layer of thallium-doped caesium-iodide (CsI(Tl)) and subsequently detected in an amorphous silicon wafer of photodiodes. For detector readout three combinations of pixel binning and frame rate are available (1×1 at 30 fps and 2×2 at 30 or 120 fps). True cone-beam geometry over the full z-coverage is achieved by enlargement of the anode angle of a rotating anode x-ray tube to ~16°. Additionally, the tube filament has been shortened to reach a focal spot size of ~0.5 mm. Thus, the penumbra effect in high-resolution imaging is minimized while an x-ray beam of sufficient photon flux and energy can still be warranted. The resulting cone-beam geometry of the prototype makes scan FOVs of either 25×25 (transaxial) ×18 cm^3 (axial) or 25×25×5 cm^3 available. Gantry rotation times can be varied from 2 to 19 s in steps of 1 s; a maximum scan time per image series of 80 s thus allows for multiple rotations. Image reconstruction is based on a modified Feldkamp algorithm.

The micro-CT has been a pre-series *LaTheta*™ LCT-100A (Aloka Co., Ltd.; Tokyo, Japan). It is based on a fully x-ray shielded dolly. The scanner features a single detector row consisting of a photodiode array with 512 pixels of 0.45×0.6 mm^2. A micro-focus x-ray tube with focal spot size of 50 µm is used; it supports operation at either 35 kV or 50 kV with a constant current of 1 mA. The size of the transaxial FOV can be varied depending on the diameter of the object to be imaged: the pre-series system allowed setting FOV diameters of 30 (S), 48 (M) or 120 (L) mm. Data is acquired sequentially through step-and-shoot half-scanning. Gantry rotation time can be set to 4.5 s (fast), 18 s (slow) and 36 s (ultra-slow); up to 80 consecutive transaxial slices with a minimum spacing of 30 µm can be acquired in one scan sequence. Alternatively, dynamic scanning of up to 80 scans at the same slice position with a time resolution corresponding to selected rotation time is possible.

B. Small-animal phantom and in-vivo studies

A set of dedicated small animal CT phantoms has been custom-designed and manufactured [4]. It facilitates measurement of the imaging parameters most important for small animal CT: image homogeneity and noise, temporal stability and CT number scaling, spatial and low-contrast resolution as well as radiation exposure.

The cylindrical phantoms of 10 cm length have a diameter of 4.5 cm (rats) and 2.5 cm (mice), respectively, mimicking realistic cross-section sizes of these animals. Phantoms were manufactured from polymethyl methacrylate (PMMA, acrylic) which is very homogeneous and has x-ray absorption and scattering properties similar to those of water.

Solid cylinder phantoms have been used to study CT number homogeneity and pixel noise; temporal stability as well as CT number scaling have been measured with hollow cylinder phantoms filled with either distilled water or solutions of an iodine contrast agent (Ultravist© 300, Schering AG, Berlin, Germany) with iodine concentrations in the range of 0.0–150.0 mg/ml. Spatial resolution of MSCT and fpVCT has been measured with the spatial resolution module of a standard CT phantom (Siemens Cone-Beam Phantom, QRM GmbH, Möhrendorf, Germany); for µCT an acrylic block with air-filled bore hole groups of decreasing diameter (3.0–0.1 mm) was employed. Low-contrast resolution has been determined in a phantom of 4.5 cm diameter featuring 4 water-filled bores of 8, 4, 2 and 1 mm diameter whose centers are located 5 mm below the phantom surface. To measure radiation exposure, two “rat”-sized phantoms of an outer diameter of 5.1 cm and a “mouse”-sized phantom with an outer diameter of 3.1 cm have been employed. Both “rat”-sized phantoms feature a bore of 8 mm diameter, located centrally in one and 2 mm below the surface in the other phantom; the “mouse” phantom only has a central bore. An ionization chamber (CT chamber type 30009, PTW-Freiburg GmbH, Freiburg, Germany) exactly fitting the phantom bores and fully covering their length has been used for MSCT and fpVCT; it has been replaced by TLDs (UD-200S, Matsushita Electric Industrial Co., Ltd.; Osaka, Japan) for the µCT.

For the phantom study, data has been acquired for every combination of scan parameters – i.e. x-ray tube high voltage, gantry rotation time, detector readout mode or FOV – sensible with respect to CT imaging of small animals. Data analysis was based on large measurement statistics and conducted in a uniform manner for all three scanners. Therefore, direct comparison of phantom study results in view of small animal imaging is possible across CT systems for each of the imaging parameters studied.

To test and support the results of the comprehensive phantom study, dynamic contrast-enhanced (DCE) CT of mice and rats has been performed to test temporal stability, homogeneity, noise and low-contrast resolution in vivo. Animals were anesthetized by inhalation narcosis, catheterized for application of contrast agent during DCE scanning

via their tail vein, and placed in the scanners in prone position. Gaseous anesthetic ($C_4H_3F_7O$, 3.0 %; Sevorane©, Abbott Laboratories, Abbott Park, IL, USA / O_2, 97.0 %) was supplied by a gas nozzle; the animals were left "free-breathing".

III. Results

A. Homogeneity

Phantom studies show that CT number homogeneity of MSCT is independent of gantry rotation time and almost independent of phantom diameter (±2.5 HU) as well as tube voltage (15 HU max. difference) across the FOV. Homogeneity measurements for fpVCT reveal small dependence on gantry rotation time (±(2–5) HU) but strong d ependence on tube voltage or selected detector mode (up to ~180 HU difference, see **Fig. 1**). Cupping leads to differences between CT numbers measured centrally and in the periphery of 40 HU or 75 HU (objects of "mouse"- or "rat"-sized phantom cross-section, resp.), cf. **Fig. 2**. The µCT scanner exhibits good CT number homogeneity (±1 HU) independent of gantry rotation time but slightly dependent on FOV size (variation by 3 HU) and strongly on tube voltage – a shift of +50 HU is observed between 35 and 50 kV.

B. Noise

All studied CT systems show image noise proportional to the inverse square root of gantry rotation time *t* in good approximation as expected, for all other acquisition parameters influencing x-ray tube photon output kept constant. Noise of MSCT is low (4−14 HU), fpVCT noise is ~6 times higher; µCT noise reaches worst MSCT noise level at best.

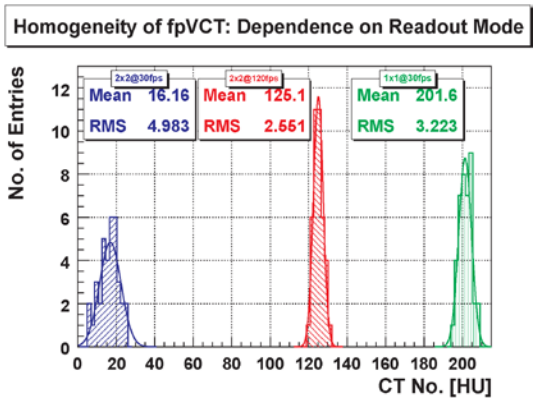

Fig. 1 Dependence of measured CT number on readout mode (detector binning and acquisition frame rate) for fpVCT.

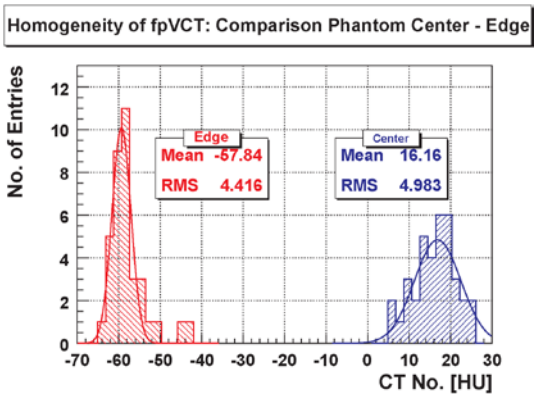

Fig. 2 FpVCT homogeneity impaired by cupping: comparison of CT numbers measured at the center (*blue*) and in the periphery (*red*) of a rat-sized specimen.

C. Temporal stability

Temporal stability of MSCT is ±(2−4) HU over 80 s of scan time with 0.5 s temporal resolution. With ±(1−6) HU temporal stability is slightly worse for fpVCT (scan time of 80 s); reconstructed temporal resolution lies between 2−5 s. Temporal stability of µCT is good (±1 HU over 360 s scan time); however, best temporal resolution of 4.5 s/rot is low.

D. CT number scaling

Due to beam hardening, CT number scaling is non-linear for iodine concentrations of 0.0–150.0 mg/ml for all CT systems studied. Two linear regimes can be made out for low (0.0–30.0 mg/ml) and high (100.0–150.0 mg/ml) iodine concentrations. These regimes can be calibrated to conform to the Hounsfield scale by double-linear fitting. Whereas MSCT and µCT have a CT number scale extending beyond +3071 HU, the scale of fpVCT is cut off at that value.

E. Spatial resolution

Spatial resolution of 360 µm (MSCT), 200 µm (fpVCT) and 100 µm (µCT) can be achieved at best. In case of MSCT it is noise-limited and thus slightly dependent on gantry rotation time, but independent of tube voltage. For fpVCT it shows dependence on rotation time and detector mode as well as slight dependence on high voltage. Spatial resolution of µCT in turn is independent of tube voltage and rotation time, it depends on FOV size because of increasing geometric magnification with decreasing FOV size.

F. Low-contrast resolution

All systems allow detecting low-contrast lesions of ~1mm: MSCT is most reliable, fpVCT requires longer gan-

try rotation times (e.g. ≥ 14 s at 80 kV). So does μCT, where contrast increases if tube voltage is lowered. In general, low-contrast visibility increases with detector statistics, i.e. with rotation time and – apart from μCT – tube voltage.

G. Radiation dose

Table 1 lists ranges of small animal whole body radiation exposure for each of the scanner concepts studied. Dose has been measured for tube voltages of 80, 100, 120, and 135 kV for MSCT (50 mA, 1 s) as well as fpVCT (50 mA, 10 s). It rises with tube voltage since beam penetration and tube photon output increase. Exposure of mouse-sized specimen measured at their center is at max. 7% higher than of rat-sized specimen; exposure difference between center and periphery of rat-sized objects also amounts to 7% at max.. For μCT radiation exposure can be as low as 50 mGy·cm (50 kV, 4.5 s/rot., 58 slices) for fast scanning and low number of slices with large scan increment; here the exposure difference between mouse- and rat-sized specimen is ~10%. For all systems acquisition parameters can be chosen such that exposure stays below the threshold of 100−300 mGy, an exceedance of which is believed to induce radiation effects, but care must be taken to avoid excessive exposure – especially for fpVCT and μCT scans.

Table 1 Small animal radiation exposure per whole body scan

CT System	MSCT	fpVCT	μCT
Dose [mGy·cm]	70 – 230	100 – 980	40 – 440

H. DCE imaging in vivo

Results of liver perfusion and blood flow measurement in rats gained through in-vivo DCE scans with MSCT and fpVCT are tabulated in **Table 2**. Results are stable and consistent with phantom study results; thus, quantitative parameters can be determined. Compared to MSCT, parameters determined using fpVCT have limited precision because of lower temporal resolution of the system. DCE scanning is also possible with μCT; here feasibility is limited to the recording of slow enhancement dynamics (e.g. for differentiation of tumor and muscle tissue) since temporal resolution of the system is too low for imaging of fast dynamic processes.

Table 2 Rat liver perfusion and blood flow determined in vivo

CT System	Perfusion (Miles) [min^{-1}]	Blood flow [ml/min]
MSCT	0.0752–0.0782	0.72–0.75
fpVCT	0.0346–0.0435	0.33–0.42

IV. Discussion

The results of the applicability analysis show that clinical MSCT is best suited for quantification of DCE small animal studies because of its good homogeneity, low noise level, high temporal resolution and low-contrast resolution; spatial resolution is limited in view of small animal CT but of secondary importance in DCE studies.

FpVCT offers increased spatial resolution and is thus suited for studies of small animals of the size of a rat; in addition, large volume coverage makes it an ideal choice for high throughput imaging and for gated scans requiring good volume coverage per rotation. However, its non-uniform behavior is a hindrance for quantitative studies.

Highest spatial resolution in combination with good overall stability of imaging parameters has been found for μCT; it should thus be employed for quantitative studies of small animal morphology for which high temporal resolution is not required.

V. Conclusions

Out of the three CT scanner designs most commonly employed for small animal imaging no single scanner design is able to meet all imaging performance requests raised by small animal CT yet. Instead, a careful selection of a suitable scanner system depending on clinical problem is required.

The decision if a particular scanner concept is sufficiently suited for addressing a specific problem of in-vivo small animal CT imaging should be based on its quantitative evaluation with regard to the key image quality parameters of small animal imaging, i.e. through an applicability analysis with dedicated small animal phantoms.

References

1. Bartling* S, Stiller* W et al. (2007) Small animal computed tomography imaging. CMIR 3:45–59 *Equal contribution first authorship
2. Plathow C, Li M et al. (2004) Computed tomography monitoring of radiation-induced lung fibrosis in mice. Invest Radiol 39:600-609
3. Ford N et al. (2003) Fundamental image quality limits for microcomputed tomography in small animals. Med Phys 30:2869-2877
4. Stiller W, Kobayashi K et al. (2007) Initial experience with a novel low-dose micro-CT system. Rofo 179:669-676

Author: Dr. W. Stiller, PhD, Dipl.-Phys.
Institute: Department of Radiology (G030), German Cancer Research Center (DKFZ)
Street: Im Neuenheimer Feld 280
City: D-69120 Heidelberg
Country: Germany
Email: w.stiller@dkfz-heidelberg.de

Intramuscular fat content estimation in the loin muscle of pig carcasses by ultrasound spectral parameter analysis

S Lakshmanan[1,2], T Koch[3], D Mörlein[3], S Brand[1] and K Raum[1,2]

[1] Q-BAM Group, Department of Orthopedics, Martin Luther University of Halle - Wittenberg, Germany
[2] Julius Wolff Institute and Berlin-Brandenburg School for Regenerative Therapies, Charité-Universitätsmedizin Berlin, Germany
[3] Department of Animal Sciences, Georg August University Göttingen, Germany

Abstract— **The aim of this study was to estimate the intramuscular fat content (IMF) of porcine longissimus muscle using a handheld ultrasound device with a centre frequency of 3.2 MHz. The IMF estimation method from acoustic parameters obtained by the spectral analysis of ultrasonic echo signal is described. System specific effects and sound propagation effects on the spectral analysis were analyzed and corrected. RF data acquisition was performed at a commercial abattoir at 54 warm carcasses approximately 45 min post-mortem. Muscle specific acoustic parameters, i.e. attenuation, spectral slope, midband fit, apparent integrated backscatter, and cepstral parameters were extracted from the measured rf echoes.**

The cepstral parameters, i.e. integrated cepstrum and cepstral first peak value were the strongest indicators of IMF content changes (R^2 = 0.36). By multivariate regression analysis 66 % of the IMF variation (range 0.63 to 3.16 %) could be predicted with the proposed method (RMSEP = 0.35 %). The results suggest that this method is directly adaptable for utilization in a commercial abattoir for a non-invasive IMF estimation.

Keywords— **Intramuscular fat, Muscle, Ultrasound, Spectral parameters, Apparent Integrated Backscatter, Integrated cepstrum**

I. Introduction

The IMF content in pig muscle is an important parameter for the eating quality of pork. To date, there is no instrument for non-invasive IMF estimation at slaughter, yet. Ultrasound has repeatedly been applied to predict the IMF. Ultrasonic velocity (ex vivo) was reported to have limited precision [1, 2]. Conventional B-mode ultrasonic devices were successfully used to predict bovine IMF or marbling score in living animals [3, 4] but less precise when used at pigs [5]. However, conventional B-mode images created from the envelope of the rf signal represent only the morphology of tissue. Additional information can be obtained by estimating frequency dependent acoustical parameters by spectral analysis of rf echos. Spectral parameters, e.g. attenuation and backscatter parameters provide more detailed information about tissue contribution compared to image analysis. Therefore spectral analysis of ultrasonic echo signals has become one of the prominent tools for quantitative characterization and differentiation of soft tissue in medical research [6, 7, 8, and 9].

However, those parameters are affected by system specific effects (time gain compensation (TGC) and sound field geometry) and sound propagation effects (sound velocity and attenuation alterations in backfat and intermediate muscle) [10]. The IMF estimation from spectral parameters has been reported with a coefficient of correlation of 76 % with a RMSE of 0.36 % [11]. That study used a clinical ultrasound scanner and a large number of spectral parameters have been used in a multiple regression model for IMF estimation.

The aim of this study was to develop a method to predict the IMF content of porcine loin muscle non-destructively by means of tissue characterizing parameters calculated from unprocessed ultrasound echo-signals of a commercial ultrasound device that is already used at slaughter for backfat and muscle thickness estimation. This system was optimized for the acquisition of backscatter signals. Moreover, compensation function for system transfer function and intermediate medium effect corrections have been improved.

II. Materials and Methods

Samples: 54 pig carcasses of highly varying IMF (0.63 – 3.16 %) were selected at a commercial slaughter plant according to carcass weight and fat to lean ratio. Mean carcass weight was 95.0 ± 7.1 kg. The ultrasonic measurements were made at the abattoir 45 min post mortem at suspended carcasses including skin and subcutaneous fat layers. Average muscle temperature was 38°C. Scanning localization was chosen with respect to the official site of carcass classification at $2^{nd}/3^{rd}$ last rib, 7 cm off the carcass split line. Per carcass three replicate scans were performed parallel to the split line using ultrasound contact gel. The IMF content was determined at excised loin samples by means of petroleum ether extraction with prior acid pretreatment [12].

O. Dössel and W.C. Schlegel (Eds.): WC 2009, IFMBE Proceedings 25/XIII, pp. 92–95, 2009.
www.springerlink.com

Experimental setup: For rf data acquisition, the Ultrafom300 (SFK Technology A/S, Denmark) was used. It

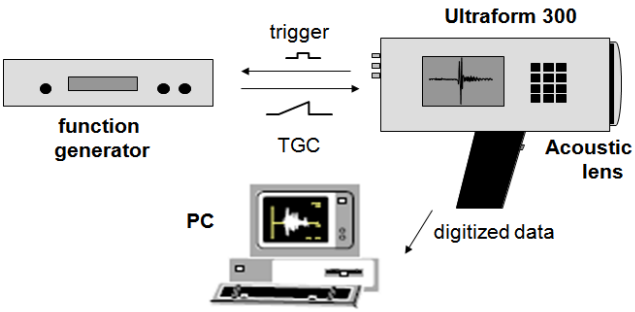

Fig. 1 Block diagram of measurement system.

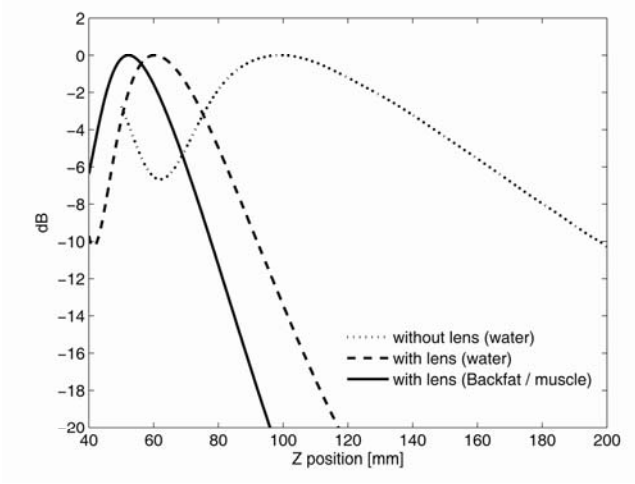

Fig. 2 Sound field plots along the depth with and without acoustic lens.

is equipped with a linear array of 64 unfocused transducer elements with central frequency 3.2 MHz with a nominal focus at 100 mm. In order to acquire desired rf signal from the muscle region, some hardware modifications had to be implemented. An acoustic lens was attached in front of the transducer to focus the sound in the central part of the muscle region (~ 55 mm) (Fig 2). TGC was adjusted by a function generator (HAMEG HM 8150) to optimize the signal to noise ratio over the entire depth to the muscle/rib boundary (Fig 1). After hardware modification, the centre frequency is 2.7 MHz and corresponding -6dB frequency bandwidth ranges from 2.1 MHz to 3.5 MHz. The rf data from all 64 elements were digitized with a sampling frequency of 10 MHz and stored on an PC. The effect of the TGC was corrected prior to any kind of spectral analysis. A procedure was developed to correct the system specific effects and to determine the tissue acoustic parameters. For several gaussian time windows along the depth of the scan lines in a region of interest (ROI), the logarithmic power spectra were calculated. The power spectra all 64 elements were averaged. Then, system and sound field effects were corrected by subtracting from the averaged logarithmic spectra a reference spectrum (obtained from a plane reflector positioned in a water bath the same depth). Finally, the attenuation of the overlaying fat tissue was compensated.

Sound field correction: The direct measurement of a sound field for a particular transducer inside the carcass is not possible, so commonly measurements in water are carried out. However, water is not a scattering medium, its attenuation is much lower than that of biological tissue, and the sound velocity is not necessarily equivalent to the tissue. Therefore, the measured sound field in water is only an approximation of the real sound pressure distribution. For sound field correction verification, a tissue mimicking phantom with known acoustic parameters was used. This phantom is made of graphite powder immersed in agar. The phantom was investigated using the same device settings as for the muscle measurements and spectral analysis was carried out with sound field and intermediate medium attenuation compensations. The apparent integrated backscatter amplitude (AIB) was estimated as a function of depth (-6dB range). For a valid sound field correction, AIB is supposed to be constant along the depth. Due to the curvature of the focused beam before and after the focal plane, AIBs were higher in the regions below and above the focus position (Fig. 3a). This sound field deviation was corrected from the known phantom's normalized AIBs deviation along the depth (Fig. 3b). The position of the reference spectrum for the corresponding gated signal was determined from the backfat and muscle SOSs as given in Eq. (1). The speed of sound in muscle ν_m of 1620 m/s was obtained from [13].

$$z_{\text{ref}} = d_{BF} + (TOF_{Gateposition} - TOF_{BF/Muscle}) \times \nu_m / 2 \quad (1)$$

The linear correlation between thickness, d_{BF} and SOS, ν_{BF} of backfat [13] was used to estimate backfat SOS from the automatically detected backfat time of flight (TOF) from the Ultrafom300 data using an iteration method.

The parameters used for the characterization of the IMF are summarized in Table 1.

Muscle attenuation: For muscle attenuation estimation, the power spectra $\langle S_m(f,z)\rangle$ were calculated from gated rf signal using a sliding window (gate length: 2 pulse duration, 50 % overlap) within ROI. The sound field correction was done by normalizing the muscle spectrum with their corresponding modified reference spectrum $\langle S_{ref}(f,z)\rangle$ as given in (2).

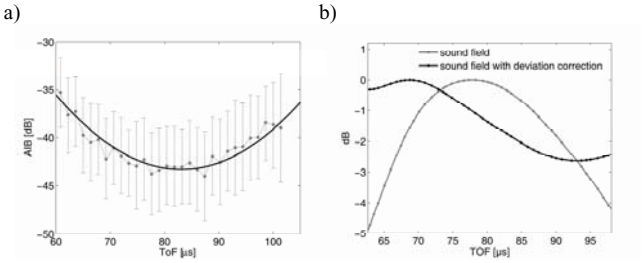

Fig. 3 Sound field correction, a) AIB in phantom before deviation correction and b) sound field with deviation correction.

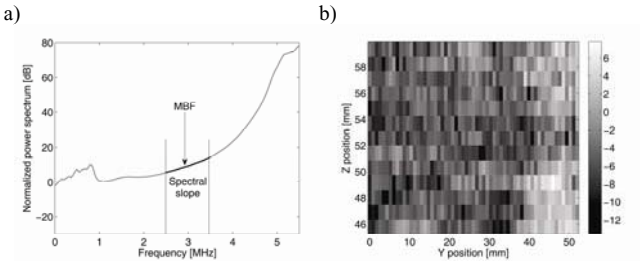

Fig. 4 Apparent integrated backscatter estimation, a) spectral slope and midbandfit estimation and b) AIB distribution in muscle ROI.

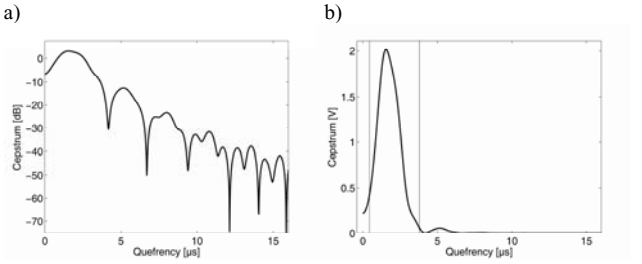

Fig. 5 Cepstral parameters estimation, a) logarithmic and b) linear cepstrum plots.

$$\langle S_{cor}(f,z)\rangle = \frac{\langle S_m(f,z)\rangle}{\langle S_{ref}(f,Z)\rangle} \tag{2}$$

The attenuation in muscle is independent on the intermediate tissue effects. The logarithmic spectral amplitudes versus depth position slopes (dB/cm) were calculated for discrete frequencies from 2.5 MHz to 3.5 MHz. Linear regression was applied between discrete frequencies and their corresponding amplitude-depth slopes. The slope of the linear regression provides the attenuation, $\alpha(f,z)$ in dB/MHz/cm. 15 sub ROIs within a muscle region of 54 x 26 mm were always selected to get sufficient data for the amplitude versus depth position slope estimation.

Spectral parameters: To estimate the backscatter properties of tissue within a ROI it is necessary to compensate for the attenuation of the intermediate tissue (tissue between transducer and ROI). ROI size for backscatter properties estimation is 54 x 15 mm (-6dB range size along the depth). The normalized power spectra were estimated as described above with intermediate tissue attenuation compensation. Then, the AIB was estimated by taking the integral of the logarithmic compensated power spectrum $10\log_{10}\langle S_{comp}(f,z)\rangle$ within the frequency bandwidth of the transducer:

$$AIB = \frac{1}{\Delta f}\int_{\Delta f} 10\log_{10}\langle S_{comp}(f,z)\rangle df \ . \tag{3}$$

This was done for all signals along the element positions and depths within the ROI. This yields the AIB distribution within the muscle region (Fig. 4b). Linear regression analysis was applied to the mean normalized spectral data of the entire ROI. Backscatter power spectral slope (BPSS), the slope of the linear regression and midband fit (MBF), i.e. the value of regression fit at the centre frequency, were estimated (Fig 4a).

Cepstral parameters: For the cepstrum parameter calculation, the normalized power spectra were estimated like before with a sliding window length 5 pulse duration and overlap 90 %. The cepstrum (Fig 5) was calculated by taking the FFT of the logarithmic power spectrum within the frequency bandwidth of the transducer. Prior to the FFT the power spectrum was preconditioned by subtracting a reference spectrum, as described before, and by removing DC and linear components. The cepstrum parameters used for IMF estimation are, the cepstrum first peak (CFP), corresponding quefrency (CFPP) and integrated cepstrum (IC) for time range 0.5 – 4 µs:

$$IC = \frac{1}{\Delta\tau}\int_{\Delta\tau} \mathrm{FFT}(10\log_{10}\langle S_{comp}(f,z)\rangle)d\tau \ . \tag{4}$$

III. Results

The IMF of the loin samples under investigation ranged from 0.63 – 3.16 % (1.26 ± 0.58 %). They reasonably represent the commercial pig populations. To investigate the relation between the acoustical parameters and the IMF, acoustic parameters of three replicate measurements per carcass were averaged.

Results of linear regressions analysis are given in Table 1. Highest correlations were observed for the cepstral parameters (Linear CFP and IC; $R^2 > 0.3$). It should be noted that these parameters are independent of the any intermediate mediums effect compensation. Cepstral parameters alone predicted 38 % of the IMF variation (RMSE = 0.46 %). Moderate correlations to IMF were observed for AIB, its variability within the evaluated ROI, and MBF.

Table 1 Linear correlation coefficient between IMF and acoustic parameters. The contributing parameter for the multivariate IMF prediction model is written in bold letters.

Parameters	R^2
Backfat thickness [mm]	0.09
Muscle attenuation [dB/MHz/cm]	0.07*
Spectral slope [dB/MHz]	0
Midband fit [dB]	**0.18***
Apparent Integrated Backscatter [dB]	**0.17***
Apparent Integrated Backscatter std [dB]	**0.12***
Linear Cepstrum first peak [V]	**0.32***
Linear Cepstrum first peak position [µs]	0
Integrated Cepstrum [V]	**0.36***
Log Cepstrum first peak position [dB]	0.15*
Log Cepstrum first peak position [µs]	0

* significant at the 0.05 level

Multiple stepwise regression analysis to estimate IMF from a combination of acoustic parameters was applied. With the parameters selected (Table 1) the multiple R^2 was 0.66 yielding an average prediction error (RMSE) of 0.35 %.

IV. Discussion

Ultrasound B-mode image analysis techniques have repeatedly been shown to be feasible for non-destructive prediction of IMF content at beef but less precise when used at pigs [5]. Spectral analysis of rf signals is supposed to provide additional information on tissue composition. In an earlier study [11] we reported the use of a sophisticated medical ultrasound scanner to predict the IMF at pork loin. With a high number of spectral parameters a multiple R^2 of 0.58 was obtained (RMSEP = 0.36 %).

In the present study, using a modified hand held device used for pig carcass classification the IMF estimation has been increased by improving the system specific defect corrections compare to the previous study. Instead of using the fixed value for the backfat correction, the backfat thickness and speed of sound are predicted from the time of flight measurement using an iteration method. The number of spectral parameters in the model is remarkably reduced.

V. Conclusions

Non-destructive IMF estimation using a modified handheld device and ultrasound spectral analysis of rf data obtained at pig carcasses in a commercial slaughter plant is described. Multivariate regression analysis yields an average prediction error of 0.35 % (R^2 = 0.66). System specific corrections, TGC and sound field were analyzed at hot carcass (38°C). Medium dependent effect correction has been improved by calculated backfat parameters from the ultrasound spectroscopy rf data itself. The results suggest that the proposed method is feasible for non-invasive IMF estimation.

Acknowledgment

This work was supported by the German Research Council (DFG; grants Mo 1746/1 and Ra 1380/3), PRO INNO (grant KF0380401LF6) and SFK Technology GmbH.

References

1. Park B, Whittaker A D, Miller R K. et al (1994) Predicting intramuscular fat in beef longissimus muscle from speed of sound, J. Ani. Sci. 72 (1), pp 109 – 116
2. Whittaker A D, Park B, Thane B R. et al (1992) Principles of ultrasound and measurement of intramuscular fat, J. Ani. Sci., 70 (3), pp 942 – 952
3. Brethour J R. (1994) Estimating marbling score in live cattle from ultrasound images using pattern recognition and neural network procedures, J. Ani. Sci., 72 (6), pp 1425 – 1432
4. Hasssen A, Wilson D E, Amin V R. et al (2001) Predicting percentage of intramuscular fat using two types of real-time ultrasound equipment, J. Ani. Sci, 79 (11), pp 11 – 18
5. Newcom DW, Baas TJ, and Lampe JF (2002) Prediction of intramuscular fat percentage in live swine using real-time ultrasound, J. Anim. Sci., 80, pp 3046-3052
6. Raum K, Gottwald M, Wohlrab D. et al (2007) Depth dependent high frequency backscatter analysis of degenerated cartilage, IEEE Ultrasonics Symposium Proceedings, 2007, 1, pp 1109 – 1112
7. Raju B I, Srinivasan M A, (2001) High-frequency ultrasonic attenuation and backscatter coefficients of in vivo normal human dermis and subcutaneous fat, Ultra.in Med. and Bio., 27 (11), pp 1543 – 1556
8. Banihashemi B, Vlad R, Debelijevic B. Et al (2008) Ultrasound imaging of apoptosis in Tunmor response: novel preclinical monitoring of photodynamic therapy effects, Cancer Research, 68 (20), pp 8590 – 8596
9. Scheipers U, Ermert H, Sommerfeld H. et al (2003) Ultrasonic multifeature tissue characterization for prostate diagnostics, Ultra. in Med. and Bio. 29 (8), pp 1137 – 1149
10. Brand S, Mörlein D, Rosner F. et al (2002) Estimation of intramuscular fat content (IMF) in the muscle longissimus dorsi (LD) of pigs by analysis of Rf echo signals obtained from a clinical B-mode device, IEEE Ultrasonics symposium, pp 8 – 11
11. Mörlein D, Rosner F, Brand S. et al (2005) Non-destructive estimation of the intramuscular fat content of the logissimus muscle of pigs by means of spectral analysis of ultrasound echo signals, Meat Science, 69, pp 187 – 199
12. LFGB (2005). Amtliche Sammlung von Untersuchungsverfahren nach §64 LFGB: L 06.00 6
13. Koch T, Lakshmanan S; Raum K, Wicke M, Mörlein, D, and Brand, S. (2009). Ultrasound velocity and attenuation of porcine loin muscle, backfat and skin. Proceedings of World Congress on Med. Phys. Biomed. Engin. (submitted)

Sound velocity and attenuation of porcine loin muscle, backfat and skin

Koch, T.[1], Lakshmanan, S.[2,3], Raum, K.[2,3], Wicke M.[1], Mörlein, D.[1] and Brand, S.[2]

[1]Department of Animal Sciences, University of Goettingen, Germany
[2]Q-BAM Group, Department of Orthopedics, University of Halle-Wittenberg, Germany
[3]Julius Wolff Institute and Berlin-Brandenburg School for Regenerative Therapies, Charité-Universitätsmedizin Berlin, Germany

Abstract— **Sound velocity and attenuation of porcine loin muscle, backfat and skin have been investigated. Experiments were performed in vitro at 38°C using a scanning acoustic microscope. With respect to the known anisotropy of muscle, the direction of the incident sound waves relative to the muscle fiber orientation was realized comparable to conditions when using an ultrasound handheld device at suspended carcasses at the abattoir. Muscle samples have been investigated 24 h and 48 h post mortem. An effect of the storage duration has not been found for sound velocity (~ 1620 m/s) however, attenuation showed slightly higher values at 48 h p.m. (1.02 to 1.16 dB/(MHz/cm)). Sound velocity and attenuation of fat ranged from 1435 to 1470 m/s and 1.5 to 2.7 dB/(MHz/cm), respectively. The skin proportion of the total backfat thickness significantly affected sound velocity (r = .88) and attenuation (r = .44) of the compound backfat. The data provided in this paper are the first ones published for porcine loin muscle for the chosen conditions.**

Keywords—**ultrasound, pig, muscle, attenuation, sound velocity**

I. Introduction

In Germany pork had the largest stake in the meat processing - in 2007, 50 million heads were slaughtered. With about 39 kg eaten meat per year and person it is the by far largest part of meat consumption (about 60%). Many factors like breed, gender, feeding or the handling pre- and post mortem have been shown to affect the final meat quality [1]. The intramuscular fat content (IMF) is widely regarded to influence the sensory characteristics of the pork loin.

However, to date, there is no instrument for non-invasive IMF estimation at intact carcasses in the slaughter environment. Ultrasound has increasingly been investigated as a non-destructive method to analyze tissue. Several studies indicate the potential of ultrasound techniques to predict bovine IMF or marbling score in living animals. Most investigations have been conducted on the analysis of digitized B-mode images [2, 3]. With pigs however, B-mode image analysis turned out to be less feasible for estimation of IMF [4]. In medical research, ultrasonic spectral analysis is widely investigated for enhanced tissue characterisation [5, 6]. Spectral parameters, e.g. attenuation and backscatter parameters provide more detailed information about tissue composition compared to image analysis. In a previous study a sophisticated diagnostic ultrasound B-mode device was successfully used to acquire ultrasonic rf data from the loin muscle in pig carcasses. Spectral analysis and multivariate modelling was performed to predict the IMF of the loin muscle with an average prediction error of 0.36 % [7]. The aim of our present work is to transfer that proof of principle to a hand held ultrasound device originally build for pig carcass grading based on fat and muscle thickness measurement [8]. However, prior to spectral analysis of the ultrasonic echo signals, system specific transfer properties of the ultrasonic device (time gain compensation and diffraction pattern) and sound propagation effects (sound velocity and attenuation in backfat and intermediate muscle) have to be corrected for. Thus, the propagation properties of a layered medium have to be considered, i.e. backfat consisting of skin, three subcutaneous fat layers, and muscle.

Acoustic attenuation and sound velocity of soft tissues have been studied extensively. However, there is little data available concerning porcine tissues obtained at common slaughter conditions which are required for system calibration of an ultrasonic set-up

It is known that ultrasound properties are affected by several factors which have to be considered for calibration. The temperature has been reported to be reversely related to sound velocity in fat and muscle, respectively [9]. A linear increasing attenuation with decreasing temperature has been stated for beef muscle [10]. Also, an influence of the fibre orientation of the muscle in accordance to the sound field, known as acoustic anisotropy has already been reported. An increase of attenuation has been found when the fibre direction is turned from 90° to 45° to the sound field [10]. Furthermore, the diameters of the muscle fibres and bundles have shown an influence on acoustic attenuation [10]. Finally, the tissue composition has to be considered. The speed of sound inside the tissue is not only affected by the IMF [11] but shows also correlations to the water content [10].

The current study aimed at collecting reference data needed for optimization of the correction algorithms required for an un-biased rf data processing. For data acquisi-

O. Dössel and W.C. Schlegel (Eds.): WC 2009, IFMBE Proceedings 25/XIII, pp. 96–99, 2009.
www.springerlink.com

tion a UF300 device has been modified for non-invasive estimation of intramuscular fat content [8]. By means of acoustic microscopy it was intended to estimate values for attenuation and sound velocity of porcine muscle and backfat of a representative set of pig carcasses. Experimental settings were realized according to tissue conditions found at the hot carcass at slaughter (45 min. post mortem). This includes not only the temperature, but also the direction of the incident ultrasound relative to the muscle fiber orientation.

II. Materials and Methods

Muscle Samples: At a commercial abattoir, 27 pig carcasses (left half each) were selected according to their body weight and lean meat proportion. Muscle and fat thicknesses were determined with a Fat-o-Meat'er (SFK Technology, Denmark) at $12^{th}/13^{th}$ rib. After refrigerating of the carcasses over night, two adjacent samples were excised approx. 24 h p.m. from the Longissimus dorsi muscle at the $12^{th}/13^{th}$ and $14^{th}/15^{th}$ rib. Backfat samples were obtained at the $13^{th}/14^{th}$ rib. One sample (including backfat) was photographed for further analysis of total backfat and individual layer thickness. The muscle samples were stored in plastic bags at 4 °C until subsequent ultrasound measurements.

Ultrasonic data aquisition: Prior to ultrasonic data acquisition, one subsample with an edge length of about 15 mm (approx. 10 – 15 g each) was prepared from each excised sample. The first sample ($12^{th}/13^{th}$ rib) was measured 24 h p.m. while the other sample ($14^{th}/15^{th}$ rib) was kept at 4°C for another 24 hours to be measured 48 h p.m.. The backfat samples were investigated approx. 72 h p.m. after storage at 4°C. The backfat was inspected as both, as a compound sample (including the skin) followed by data acquisitions of each individual fat layer, and skin separately.

Scanning acoustic microscopy: A custom made scanning acoustic microscope (SAM; Figure 1) equipped with a 10 MHz central frequency transducer (V311, PANAMETRICS, Waltham, USA) was used for acquiring ultrasonic data. The SAM consisted of a pulse-receiver unit (5900PR, PANAMETRICS, Waltham, USA), a x-y-z-scan stage including a motion controller (MICOS, Eschbach, Germany) and a computer containing an 12-bit analogue-to-digital converter (ADC) (8500, Lockport, USA). The received echo signals were digitized at 50 MS/s and the input range of the ADC was set to ±500 mV, respectively.

Each sample was placed in a custom made multi-chamber-holder made of stainless-steel enabling a plane target reflection (fig. 1). The scanning of the muscle samples was performed with an angle of the incident ultrasound of about 30° to 45° relative to the muscle fiber orientation, comparable to ultrasound the data acquisition with the handheld device when used at the abattoir. The scans were performed with a step increment of 400 µm horizontal (x-axis) and 1 mm vertical (y-axis) resulting in ~ 150 A-scans per chamber. For acoustic coupling, the sample and the transducer were submerged in degassed phosphate-buffered-saline (PBS) which also acted as an isotonic medium to prevent the muscle samples from swelling. The sound velocity of the PBS was measured before scanning each sample. Estimates ranged from 1535 m/s to 1545 m/s. The specific SOS values were included in the further calculations. The temperature was kept constant at 38°C. Prior to each measurement the samples were allowed to equilibrate.

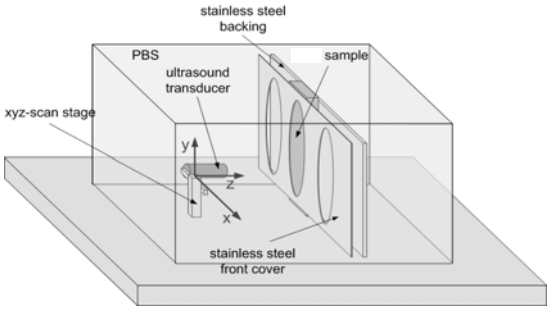

Fig. 1: Scan set-up of the Scanning acoustic microscope. Samples were placed in the middle chamber and approx. 150 A-scans were performed each in the sample and the reference chambers.

Data analysis: For estimating sound velocity and acoustic attenuation ultrasonic echo signals were analyzed using a custom made MATLAB (The Mathworks, Natick, USA) software. The ultrasonic echo positions were estimated as the pulse-maximum-position of the Hilbert transformed of the radio frequency signal. Thickness and sound velocity has been calculated using the measured time of flight (TOF) with respect to the TOF in the PBS. The TOF in the PBS was measured in the reference chambers as illustrated in figure 2 and calibrated for each sample individually to avoid changes in PBS falsifying the resulting parameter estimates.

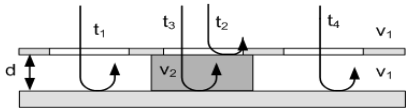

Fig. 2: Recorded echo positions and calculation of the sound velocity by evaluating time delays between sound propagation in the PBS and the sample.

Sound velocity was calculated by analyzing differences in time of flight when propagating through the sample vs. PBS, as illustrated in figure 2. TOF values t_1 and t_4 estimated from the reflection at the substrate-reflector were used to account for a potential tilt between the transducers

lateral motion and the substrate reflector. The tilt-compensated values for t_1, t_4 and t_3 were used for all further computations. In the first step the sample thickness was computed locally using the time delay between the tilt compensated t_1 (t_4) and t_3 and the sound velocity of the PBS ($d = V_{PBS}(t_2 - t_4)$). By evaluating the delay ($t_3 - t_2$) with respect to the sample thickness the sound velocity was computed applying the following equation:

$$v_{sample} = \frac{v_{PBS}(t_2 - t_4)}{(t_3 - t_2)} = \frac{d}{(t_3 - t_2)}$$

Acoustic attenuation was estimated by analyzing the logarithmic power spectra of pulses obtained at the substrate-reflector. Spectra recorded inside the sample chamber were subtracted from power spectra computed in the reference chambers. Difference spectra were then normalized to the local sample thickness prior to performing a linear fit. The slope of the linear fit provided the attenuation coefficient in dB/(MHz cm). The attenuation analysis was performed in the frequency range from 3 MHz to 6 MHz. In preparation for signal analysis a region of interest (ROI) was selected inside the sample chamber, containing approx. 100 A-lines. For each A-line the local sound velocity was estimated. Following, A-lines showing a discrepancy of more than 1.5 times the standard deviation from the mean of all velocity estimates were excluded from further analyses. The mentioned discrepancy in sound velocity indicates a certain sample unevenness at the back-side. The unevenness was caused by the sample not being in contact with the substrate reflector. Finally, about 75 A-lines per sample remained and were used for estimating the ultrasonic parameters. Each muscle sample was analyzed by two independent (both trained) users and the mean values of both users were used for evaluation.

Statistics: The statistical analysis was performed with the program SAS 9.1 (SAS Institute, Cary, USA). For comparison of the individual tissue types an ANOVA was performed with PROC GLM of SAS.

III. Results

A considerable variation for the carcass traits was realised due to the selection at slaughter, resulting in range from 80 kg to 108 kg for slaughter weight and 45.9 % to 61.0 % for lean meat percentage. The muscle and fat thickness ranged from 42.7 to 73.0 mm and 11.2 to 25.9 mm. Mean values and variation of ultrasound velocity is given in Table 1. The sound velocity of muscle was slightly above 1620 m/s and no significant difference was observed when measured at 24 h or 48 h p.m.. The sound velocity of fat ranged from 1435 m/s to 1470 m/s. Skin showed a significantly higher velocity (1680 m/s) compared to fat. The mean value of the compound sample was about 1502 m/s. No significant differences were found between the outer and middle fat layer, while the inner layer was significantly different from the two other layers.

Table 1: Mean values and variation of ultrasound velocity of porcine muscle, backfat and skin (n=27; s.d., standard deviation); different letters indicate significant differences.

	Mean	s.d.	Min	Max
compound backfat	1502.39[a]	20.76	1473.36	1537.04
skin	1682.26[b]	23.36	1631.60	1720.19
outer fat layer	1435.96[c]	9.58	1425.59	1476.49
middle fat layer	1450.47[c]	22.25	1426.86	1519.30
inner fat layer	1469.84[d]	37.09	1441.47	1562.29
muscle (24 h p.m.)	1620.50[e]	4.63	1610.65	1628.41
muscle (48 h p.m.)	1622.40[e]	5.19	1612.43	1632.11

Attenuation values are shown in Table 2. The attenuation of muscle was found to be 1.02 and 1.16 dB/(MHz/cm) at 24 h and 48 h p.m. (difference not significant). The attenuation of the fat ranged from 1.5 to 2.7 dB/(MHz/cm). Attenuation of the inner fat layer was significantly higher compared to the two other layers. Average attenuation of the compound backfat was found to be 2.46 dB/(MHz/cm).

Table 2: Mean values and variation of ultrasound attenuation of porcine muscle, backfat and skin (n=27; s.d., standard deviation); different letters indicate significant differences

	Mean	s.d.	Min	Max
compound backfat	2.46[a]	0.60	1.46	3.96
skin	2.60[a]	1.10	0.78	4.42
outer fat layer	1.62[b]	0.67	0.79	3.37
middle fat layer	1.59[b]	0.70	0.63	4.01
inner fat layer	2.72[a]	1.47	1.24	6.75
muscle (24 h p.m.)	1.02[b]	0.26	0.54	1.55
muscle (48 h p.m.)	1.16[b]	0.34	0.70	2.17

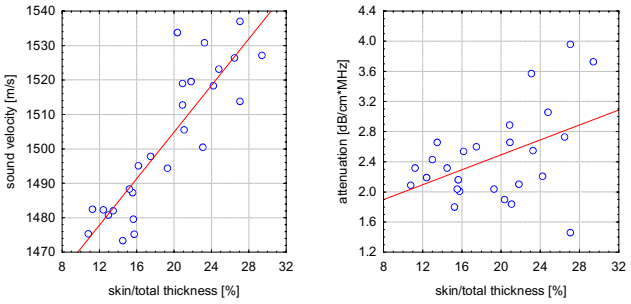

Fig. 3: Effect of skin proportion on total backfat thickness on sound velocity and attenuation.

The relationship between the skin proportion of total compound thickness and acoustic parameters is shown in Fig 3.

Both attenuation and velocity increase significantly with the proportion of skin on the complete sample.

IV. Discussion

The results found in literature for sound velocity of the muscle show a wide range from 1540 m/s up to 1680 m/s dependent on species, muscle type, temperature, fibre orientation and ultrasonic data acquisition technique. Sound velocity in beef skeletal muscle immediately post mortem has been reported to range from 1590 – 1630 m/s [12] and from 1644 – 1681 m/s [10] supporting the findings of the present study. However, structural and compositional differences of beef compared to porcine muscle, e.g. amount of connective tissue and IMF have to be considered.

An increased attenuation of the muscle samples measured 48 h p.m. compared to 24 h p.m. was observed. That increase is assumed to be caused by post mortal changes in the muscle tissue. Most probably the drip loss during storage may have changed the ultrasonic propagation properties. Previous studies on the sound velocity of beef fat tissue confirm the values reported herein [11, 13]. Comparing the fat layers, the inner one showed a significantly higher sound velocity and attenuation compared to both other layers. This is suggested to be caused by a higher amount of water in the inner fat layer. Differences in the fatty acid composition may also have affected the ultrasound propagation properties [13]. Sound velocity of pig skin at 25 °C has been reported in the range of 1710 ± 60 m/s [14] supporting our findings while attenuation was considerably lower in that study. However, the data were obtained from as little as two animals. Variation of sound velocity due to fat composition seems to be less important in the light of the following: sound velocity of skin is much higher compared to the fat layers. Thus, the proportion of skin thickness relative to the compound backfat determines its sound propagation properties.

V. Conclusions

Attenuation and sound velocity of the porcine Longissimus dorsi muscle, backfat and skin samples from 27 representative samples with respect to commercial slaughter pigs have been estimated. Care was taken to ensure measurement setups comparable to conditions found at hot carcasses. All parameters revealed slight differences compared to published values. Significant differences were found between the tissue types. Sound velocity of skin was considerably higher compared to the subcutaneous fat layers, resulting in a large influence of the proportion of skin compared to the total backfat thickness on sound velocity (r = .88). The correlation was not as strong for attenuation and total thickness (r = .44). These finding have to be considered when correcting for sound diffraction and attenuation during rf spectroscopy to estimate the IMF at carcasses.

Acknowledgment

This work was supported by the German Research Council (DFG; grants Mo 1746/1 and Ra 1380/3), PRO INNO (grant KF0380401LF6) and SFK Technology GmbH.

References

Fischer, K., M. Reichel, J. P. Lindner, M. Wicke, and W. Branscheid. 2000. Eating quality of pork in well-chosen crossbreds. Archives of Animal Breeding 43:477-485.

Brethour, J.R. 1994. Estimating marbling score in live cattle from ultrasound images using pattern recognition and neural network procedures. J. Anim. Sci. 72: 1425-1432

Hassen, A., Wilson, D.E., Amin, V.R., Rouse, G.H., Hays, C.L. 2001. Predicting percentage of intramuscular fat using two types of real-time ultrasound equipment. J. Anim. Sci. 79: 11-18

Newcom, D.W., Baas, T.J., Lampe,J.F. 2002. Prediction of intramuscular fat percentage in live swine using real-time ultrasound J. Anim. Sci. 80: 3046-3052.

Scheipers, U., Ermert, H., Sommerfeld, H.J., Garcia-Schurmann, M., Senge, T., Philippou, S. 2003. Ultrasonic multifeature tissue characterization for prostata diagnosis. Ultras. in Med. & Biol. 29: 1137-1149

Nair, A., Kuban, B.D. Obuchowski, N., Vince, D.G. 2001. Assessing spectral algorithms to predict atherosclerotic plaque composition with normalized and raw intravascular ultrasound data. Ultras. in Med. & Biol. 27: 1319-1331

Mörlein, D., F. Rosner, S. Brand, K. V. Jenderka, and M. Wicke. 2005. Non-destructive estimation of the intramsucular fat content of the *longissimus* muscle of pigs by means of spectral analysis of ultrasound echo signals. Meat Science 69:187-199.

Lakshmanan, S., Koch, T., Mörlein, D., Brand, S., and Raum, K. 2009. Intramuscular fat content estimation in the loin muscle of pig carcasses by ultrasound spectral parameter analysis. Proceedings of World Congress on Med. Phys. Biomed. Engin. (submitted).

Benedito, J., J. A. Carcel, C. Rossello, and A. Mulet. 2001. Composition assessment of raw meat mixtures using ultrasonics. Meat Science 57:365-370.

Smith, N. B. 1996. Effect of myofibril length and tissue constituents on acoustic propagation properties of muscle. Ph. D. Thesis, University of Illinois.

Park, B., Whittaker, A.D., Miller, R.K., and Hale, D.S. 1994. Predicting intramuscular fat in beef longissimus muscle from speed of sound. J. Anim. Sci. 72: 109-116.

Miles, C. A. and G. A. Fursey. 1974. A note on the velocity of ultrasound in living tissue. Anim. Prod. 18:93.

Ninoles; L., Clemente,G., Ventanas,S., Benedito,J. Quality assessment of Iberian pigs through backfat ultrasound characterization and fatty acid composition. Meat Science 76:102-111

Cantrell, J.H., Goans, R.E., and Roswell, R.L. 1978. Acoustic impedance variations at burn-nonburn interfaces in porcine skin. J. Acoust. Soc. Am. 64(3): 731-735.

Design and Synthesis of A Novel Inhibitor of 5-Enolpyruvylshikimate -3-phosphate Synthase

Jianhua Wang Zhengjian Lv

College of Bioengineering, Chongqing University, Chongqing, China

Abstract—**EPSP Synthase is an enzyme in the shikimate acid pathway1 found only in plants, fungi and bacteria. A novel 5-enolpyruvylshikimate-3-phosphate (EPSP) synthase inhibitor has been prepared by one step reaction using 2-chloroethylphosphonic acids with amino acid in a dilute alkaline solution below 100C , It has been found that these compounds have herbicidal activities.**

Keywords—**5-Enolpyruvylshikimate-3-phosphate synthase inhibitor, Synthesis, Herbicidal activity.**

One strategy for designing an enzyme inhibitor is to synthesize a chemical entity that mimics the high-energy intermediate involved in the reaction mechanism. EPSP Synthase is an enzyme in the shikimate acid pathway1 found only in plants, fungi and bacteria and is the target of glyphosate 1, the active ingredient in one broad spectrum herbicide. Recent investigations2 of this unique enzyme reaction confirmed an addition-elimination mechanism, in which the 5-OH of shikimate-3-phosphate (S3P) adds to phosphoenolpyruvate (PEP) to give a tetrahedral intermediate, followed by the extrusion of the phosphate group to give the product EPSP, a key intermediate in the biosynthesis of phenylalanine, tyrosine, tryptophan and other important secondary metabolites (Scheme 1). This and other studies3 implicate the involvement of the carbonium ion of PEP as the transient intermediate during the addition reaction (see Fig.1a).

Scheme 1

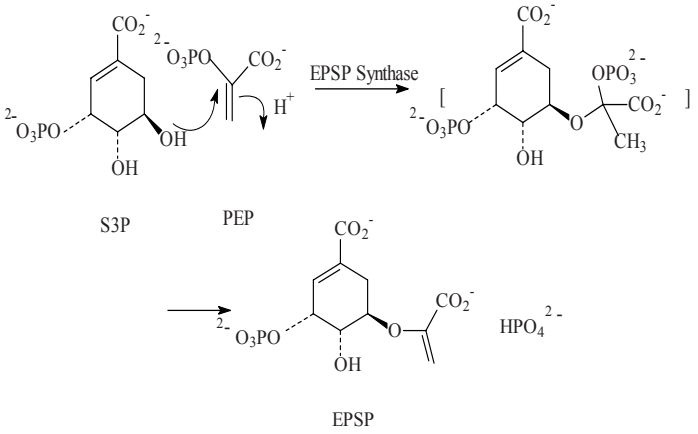

Fig.1

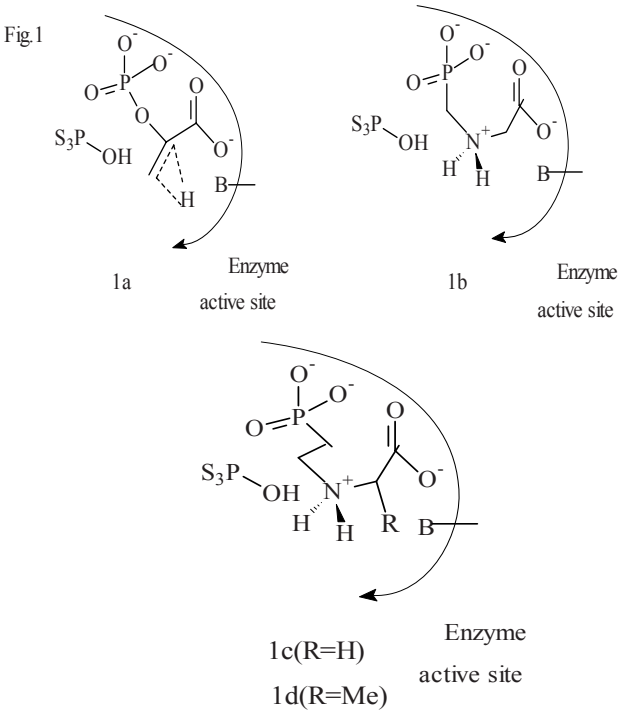

An ammonium functionality can mimic a carbonium ion in enzyme inhibitor design 4. Glyphosate is a competitive inhibitor of PEP5 in this reaction probably because its protonated nitrogen atom resembles the transient carbocationic centre of PEP (see Fig.1b). Intrigued by this hypothesis and the opportunity to discover novel inhibitors of EPSP synthase, we have synthesized a new analogue of glyphosate. Like the glyphosate the ammonium function is still tetrahedral, but the available induction of ethylene and (or) methyl at the enzyme active site would further strengthen this mimicking ability of the ammonium function (see Fig.1c, 1d).

Synthesis of 1c and 1d has been described as follow6. 0.2mol of 2-chloroethylphosphonic acid (CEPA, 40% solution), 300g of ice water, 0.25mol of amino acid and 0.3g of KI were mixed and stirred at room temperature, followed by addition of 160 ml of 10% cold NaOH solution. The reaction temperature was controlled below 200C by cold water bathe

O. Dössel and W.C. Schlegel (Eds.): WC 2009, IFMBE Proceedings 25/XIII, pp. 100–101, 2009.
www.springerlink.com

The reaction solution was stirred for 140 to 150 hours. Every half a day checked the pH value of the solution and about 10ml of 10% cold NaOH solution was added, in order to maintain the pH value of the solution above 8, until the pH value of the solution no longer changed. The reaction solution was standed for another 24 hours and then evaporated under reduced pressure. The most of water was removed, the compound were obtained from the aqueous solution by acidified with 6N HCl to pH=4 and crystallized from water. N-(2-phosphonoethyl)glycine Hydrochloride (1c): m.p.180-1820C, HNMR(D2O): δ6.72(s,1H), 3.75(s,2H), 2.86-2.56(m,44); IR(KBr): ν3350(NH), 1700(CO), 1235(PO), 1030(POC); MS(m/z): 220 (M+ 20.1); Anal. Found: C 21.55, H 4.88, N 6.74, Cacl. For C4H10NO5P•HCl: C 21.82, H 5.00, N 6.36 . N-(2-phosphonoethyl)alanine Hydrochloride (1d): m.p.165-1680C, HNMR (D2O): δ6.70(s,1H), 3.65(m,1H), 2.85-2.54(m,4H),1.12(d,3H); IR(KBr): ν3340(NH) , 1710(CO) , 1230(PO), 1035(POC); MS(m/z): 234(M+ 12.5); Anal. Found: C 25.45, H 5.84, N 5.64, Cacl. For C5H12NO5P•HCl: C 25.64, H 5.55, N 5.98 .

Enzyme assays were performed by HPLC radio-assay described previously 7. The results are described in Table 1.

Table 1 Inhibition of EPSP synthase

Inhibition	K_i/μmol.ml^{-1}
1b	0.30
1c	0.51
1d	0.72

The preliminary result of enzyme assays indicates that 1c and 1d were a potent inhibitor of EPSP synthase. Like glyphosate, the inhibition appears competitive with respect to PEP. Furthermore, 1d assayed is a racemic mixture and presumably the herbicidal activity of the pure enantiomer with the correct juxtaposition may be much higher.

ACKNOWLEDGMENT

The invaluable support by the National Natural Science Foundation of China (No. 30670496) and the Scientific Research Foundation for the Returned Overseas Chinese Scholars, State Education Ministry (2006-331) and the Natural Science Foundation Project of CQ CSTC (2006BB5017) , is gratefully acknowledged.

REFERENCES

1 Amrhen N. *Recent Adv in Phytochem*, 1986, 20, 83.

2 Anderson K S, Sammons G C, Sikorski J A. *Biochemistry*, 1990, 29, 1460.

3 Asano Y, Lee J J, Shieh L T. *J Am Chem Soc*, 1985, 107, 4314.

4 Sandifer R M, Thompson M D. *J Am Chem Soc*, 1982, 104, 7376/

5 Steinrucken H C, Amrhein N. *Eur J Biochem*, 1984, 143, 341.

6 Xiangkai F, Chengbin G. *Synth Commun*, 1998, 28, 2659.

7 Padgette S R, Huynh Q K, Borgmeyer J . *Arch Biochem Biophys*, 1987, 258, 564.

Author: Jianhua Wang Zhengjian Lv
Institute: Bioengineering College at Chongqing University
City: Chongqing
Country: P R China
Email: wjh@cqu.edu.cn

Introduction of Apoptosis and Inhibition of SMMC-7721 Growth by 2-Arsonoacetic Acid

J.H. Wang, Y.L Wei and Z.J. Lv

College of bioengineering, Chongqing University, Chongqing City, China

Abstract—**2-Arsonoacetic acid (ASAC) is an organic arsenic compound synthesized by complexing As_2O_3 , which has been shown to inhibit tumour cell proliferation via apoptosis and cell cycle arrest. In this study, we investigated the effects of ASAC on cell proliferation, cell cycle phases distribution and apoptosis. The antiproliferative effects of ASAC against SMMC-7721 cells were tested in vitro using MTT assays. The changes of morphological features of cells such as cell shrinkage, chromatin condensation, plasma membrane blebbing, and finally the breakdown of the cell into smaller units (apoptotic bodies) were observed by transmission electronic microscopy and lighting microscopy. Flow cytometry showed that ASAC leads to G_2/M arrest and the mitochondrial membrane potential loss. Taken together, the resulets indicated that ASAC inhibits the growth of SMMC-7721 cells via cell cycle arrest or apoptosis.**

Keywords—**Apoptosis, ASAC, The mitochondrial membrane potential, Cell cycle, SMMC-7721**

I. Introduction

Arsenic trioxide (As_2O_3) has recently been reported to induce complete remission in the patients with relapsed or refractory acute promyelocytic leukemia (APL) without severe marrow suppression [1].Resent preliminary reports suggest that the apoptosis of As_2O_3 is not specific for APL cells but can be observed in various cells lines of solid tumour [2-4]. Organic arsenicals such as melosporal,although more potent then As_2O_3 in inducing apoptosis in NB_4 cells, are clinically too toxic to be used in the treatment of APL [5]. This prompted us to synthesized a serial organic arsenic compounds with strong apoptosis-inducing activity but minimal toxicity.

Apoptosis, also known as programmed cell death, is characterized by distinct morphological features such as cell shrinkage, chromatin condensation, plasma membrane blebbing, oligonucleosomal DNA fragmentation, and finally the breakdown of the cell into smaller units (apoptotic bodies) [6]. It has been shown recently that mitochondria play essential roles in certain forms of apoptosis through the mitochondrial permeability transition (PT). Induction of the mitochondrial PT leads to dissipation of inner transmembrane potential ($\Delta\psi_m$) and is one of putative mechanisms triggering cytochrome c translocation, resulting in activation of caspase cascades [7].

Arsenic trioxide (As_2O_3) with an apoptosis–inducing activity are used in cancer chemotherapy, Therefore, organic arsenic compounds with strong apoptosis-inducing activity but minimal toxicity would be expected to have potential utility as anticancer drugs. ASAC is one of organic arsenic compounds. Thus, as a part of our screening program to evaluate the potential effect of organic arsenic compounds, In this paper, we have investigated the effects of ASAC on SMMC-7721cell proliferation, cell cycle phases distribution and apoptosis.

II. Materials and methods

Chemically synthesized ASAC was provided by the department of Pharmaceutical Chemistry, Chongqing university. A stock solution was made with phosphate-buffered saline (PBS) at a stock solution of 0.01mol/l. Prior to use in experiments, it was diluted with RPMI-1640 medium containing 10% fatal bovine serum (FBS), penicillin (100u/ml), streptomycin (100μg/ml) to the required concentrations. Trypan blue, propidium iodide, MTT and ribonuclease A were purchased from Sigma (St Third Medical University of China, Chongqing), RPMI 1640 medium were obtained from Gibco (Third Medical University of China, Chongqing), penicillin/streptomycin,fetal calf serum (FCS) were obtained from Hyclone (St Third Medical University of China ,Chongqing), and trypsin were obtained from Gibco (St Third Medical University of China, Chongqing), .All chemicals used were reagent grade.

III. conclusions

A. Effect of ASAC on growth inhibition in SMMC-7721 cells

We examined the effect of ASAC on the cell proliferation of SMMC-7721 cell using MTT assay. Dose- and time- dependent inhibition of cell growth was observed following the treatment of ASAC (0.01-10μmol/l) for various times(Fig. 1).

O. Dössel and W.C. Schlegel (Eds.): WC 2009, IFMBE Proceedings 25/XIII, pp. 102–105, 2009.
www.springerlink.com

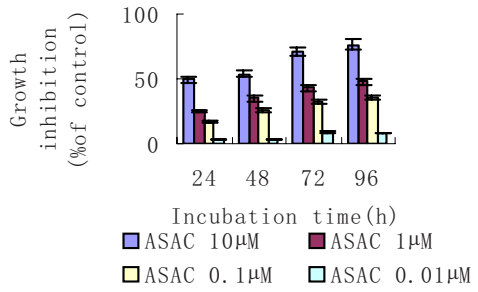

Fig1. Effect of ASAC on the growth inhibition of SMMC-7721 cell in vitro. Exponentially growing cells were treated with the indicated concentration of ASAC for various times. Cell growth inhibition was assessed by MTT assay as described in ‘‘Materials and methods.’’ The cellular growth of the cells was significantly inhibited in a dose- and time-dependent manner. Results represent means of at least three independent experiments; bars, SD.

B. Apoptotic morphology study with microscope

Morphological pictrures of SMMC-7721 cells at 48h after the addition of ASAC at various concentrations were examined under a phase contrast microscope and photographed.It show damidged cells which had become round and shrunken, while the control SMMC-7721 cells were well spread (Figure 2).The cell damage appeard after treated with 0.01-10μmol/l ASAC; however, 0.01μmol/l ASAC treatment had no significant difference with the control regimen.

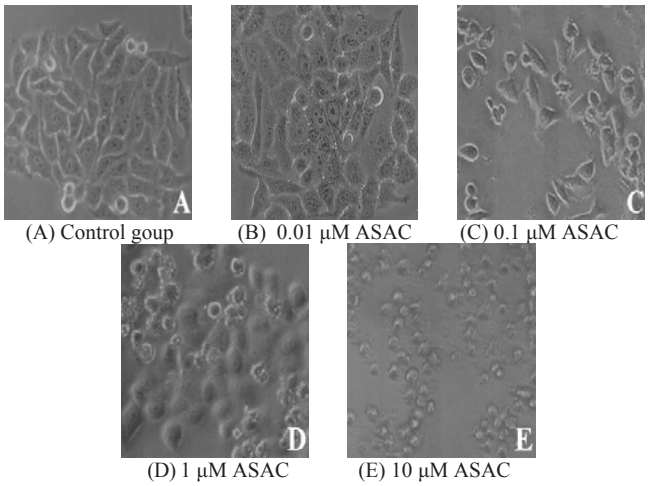

(A) Control goup (B) 0.01 μM ASAC (C) 0.1 μM ASAC

(D) 1 μM ASAC (E) 10 μM ASAC

Figure 2. Morphological study with phase contrast microscope.Cells were seeded in 24-well plates at a density of 1×10^4cells/well and grown 48h to be attached to the surface of the plates completely. They were then added to different concentrations of 0.01-10μmol/l ASAC and grown at 37℃ and then observed by phase contrast microscopy. At the consentrations of 0.01, 0.1 1,10μmol/l ASAC the cell became round and shrunken while the control SMMC-7721 cells were well spread.

C. Transmission electron microscopic observation

After treatment with 0.1 μmol/l ASAC for 24h, 48h, 72h, SMMC-7721 cells showed morphological changes characteristic of apoptosis, such as cell shrinkage, blebbing, chromatin condensation, fragmentation of nuclei and formation of apoptotic bodies. The chromatin of some SMMC-7721 cells was located along the nuclear edges or formed irregularly shaped crescents at the nuclear edges, or became condensed or fragmented; Some cells nuclear membrane became irregular; The vacuole in some cytoplasma could be observed (Figure 3).

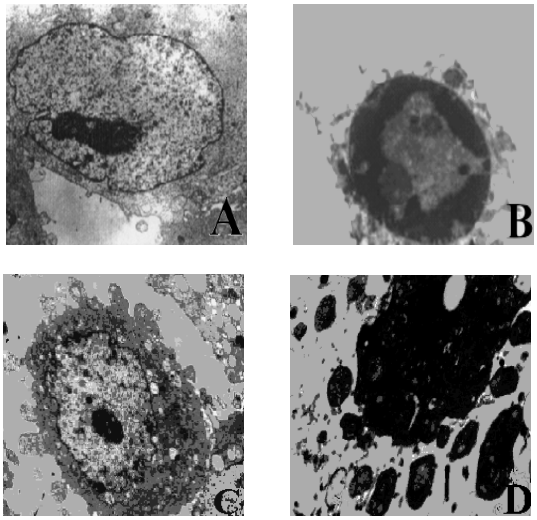

Fig.3 SMMC-7721 cells were seeded in flasks at a density of 10^5 cells per well and grown 24h to be attached to the surface of the flasks completely. They were then added to different concentrations of ASAC (0.01-10μmol/l) and grown at 37℃, in humidited 5% CO2 for24h,48h,72h, and then observed by transmissional electron microscopy as described in ‘‘Materials and methods.’’ A Control cells (×8,000) ; B treatment with 0.01 μmol/l ASAC for24h (×5,000) ; C treatment with 0.01 μmol/l ASAC for48h (×5,000) ; D treatment with 0.01 μmol/l ASAC for 72h (×15,000)

D. DNA lader formation in ASAC-treated SMMC-7721 cells

We performed agarose gel electrophoresis of low molecular DNA from SMMC-7721 cells. DNA ladder formation, characteristic for apoptosis, was induced in cells treated with 0.1μmol/l ASAC for 48,72,96h.(Fig. 4)

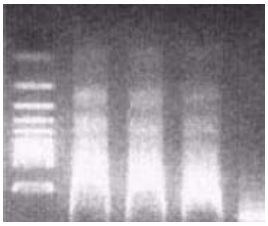

Fig. 4 ASAC induced DNA fragmentation insmmc-7721 cells. Cells were incubated with the indicated concentrations of ASAC for an additional 48, 72,96 h; then DNA degradation was analyzed by gel electrophoresis as described in Materials and Methods. M, DNA marker. Lane 1-3, treatment regimens. Lanes 4,control regiment. The results indicate that increasing amounts of DNA fragments were found in cells treated with 0.1μmol/l of ASACfor 96h.

E. Effects of ASAC on the SMMC-7721cell cycle

As shown in Fig. 5, DNA flow cytometric analysis indicated that ASAC induced a G2-M phase arrest in SMMC-7721cells following 24-72 h of exposure. SMMC-7721cells showed a few increased cells in the G2-M phase.

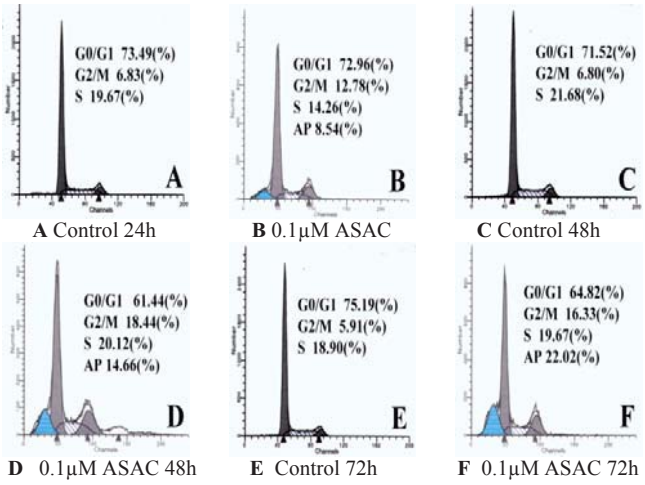

A Control 24h **B** 0.1μM ASAC **C** Control 48h

D 0.1μM ASAC 48h **E** Control 72h **F** 0.1μM ASAC 72h

Fig. 5. Flow cytometry analysis following treatment with ASAC. SMMC-7721 cells were treated with 0.1μM ASAC as indicated. Both attached and detached cells were collected 24h, 48hor 72 h after treatment with ASAC, fixed,stained with propidium iodide, and subjected to flow cytometry cell cycle analysis.

F. The loss of mitochondrial transmembrane potential (Δψm)

Increasing evidence suggest that altered mitochondrial function is linked to apoptosis and a decreasing mitochondrial transmembrane potential is associated with mitochondrial dysfunction. Thus, we next evaluated the effect of ASAC on the $\Delta\psi_m$ .We measured $\Delta\psi_m$ with flow cytometry using the fluorescent probe Rhodamine123. As shown in Fig. 6, In compared to control, SMMC-7721 cells exposed to ASAC (0.1μM) for 12h showed a decline in Rhodamine123 fluorescence. Cells exposed to ASAC (0.1μM) for 24h showed a sharp decline in Rhodamine123 fluorescence. (Fig. 6)

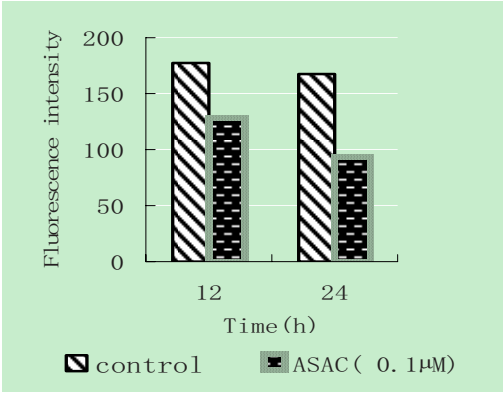

Fig 6. Effect of ASAC(0.1μM) on the loss of mitochondrial transmembrane potential ($\Delta\psi_m$).

IV. DISCUSSION

Cell death can be divided into two types: apoptosis and necrosis. The main difference between apoptosis and necrosis is the active participation of cells in the process [8, 9]. Recent accumulating evidence suggests that defects in the process of apoptosis may be closely associated with carcinogenesis and that many cancer cells have defective machinery for self-destruction [10]. It is suggested that the susceptibility to apoptosis–inducing effects of chemotherapeutic drugs may depend on the intrinsic ability of tumor cells to respond to apoptosis In the signal transduction pathway of apoptosis, it has been shown that some cellular processes in the cell cycle may play important roles. Some of the antitumor drugs, which have been showed to be able to intercalate with DNA in tumor cells after applied at optimal doses in vivo, do arrest tumor cells in the cell cycle [11-13]. In some cases, such an optimal regimen would diminish unfavorable toxic effects observed during cell killing by necrosis.

In the present study, we used MTT to observe the effect of ASAC (0.01-10μM) on the growth of the human hepatocellular carcinoma SMMC-7721 cells in vitro, indicating that ASAC can inhibit the SMMC-7721 cells growth and in time and dose- dependent manners. Also the flow cytometry showed that ASAC causes SMMC-7721

cells apoptosis at a low dose (0.01-10μM), which was confirmed by phase contrast microscope, transmission electron microscope, DNA lader formation .and a marked G2/M phase arrest with apparent apoptosis, this phenomenon seems to suggest that ASAC can induce apoptosis and G2/M phase arrest in SMMC-7721 cells. Moreover, either the G2/M phase arrest or apoptosis of hepatoma cells induced by ASAC was clearly dose and time- dependent. To confirm and quantitate the apoptosis-inducing property of ASAC, cell cycle distribution was measured by flow cytometry after treatment of 0.1μM ASAC for various times. As demonstrated in Figure 5,When the SMMC-7721 cells were treated with 0.1μM ASAC for 24h the G2/M phase cells was increased from 6.83% to 12.78 % and the AP cells was increased from 0 to 8.54%. following treatment with 0.1μM ASAC for 72h, the G2/M phase cells was increased from 5.91% to 16.3 % and the AP cells was increased from 0 to 22.02 %. This result indicates that ASAC blocks cell cycle at G2/M phase, disturbs mitosis and inhibits SMMC-7721 cells growth.

Increasing evidence suggest that altered mitochondrial function is linked to apoptosis and a decreasing mitochondrial transmembrane potential is associated with mitochondrial dysfunction [14-18]. Thus, in order to elucidate the mechanism underlying this phenomenon,we next evaluated the effect of ASAC on the $\Delta\psi_m$ with flow cytometry using the fluorescent probe Rdm123 .Our results indicated that 0.1μM ASAC could lead to the loss of mitochondrialtrans membrane potential, compared with those of the control.

In conclusion, this is the first report of the anti-hepatoma effect of ASAC, its mechanisms, and the relationship between the mitotic arrest and apoptosis in vitro .Our results not only provide the basis for further in vivo and clinical research in hepatocellular carcinoma, but also contribute to understanding of the pharmacology of ASAC further.

Acknowledgment

Supported by the National Natural Science Foundation of China (No.30670496) and the Scientific Research Foundation for the Returned Overseas Chinese Scholars, State Education Ministry (2006-331) and the Natural Science Foundation Project of CQ CSTC (2006BB5017)

References

1. Soignet S L, Maslak P, Wang Z G, Complete remission after treatment of acute promyelocytic leukemia with arsenic trioxide, N. Engl. J. Med. 339 (1998) 1341–1348
2. Woo Hyun Park, Yeon Hee Cho, Chul Won Jung, Arsenic trioxide inhibits the growth of A498 renal cell carcinoma cells via cell cycle arrest or apoptosis, Biochemical and Biophysical Research Communications 300 (2003) 230–235
3. Vanina B, Patterns of gene expressions induced by arsenic trioxide in cultured human fibroblasts, Toxicology Letters 143 (2003) 155-162
4. Zhang T C, Cao E H, Induction of Apoptosis and Inhibition of Human Gastric Cancer MGC-803 Cell Growth by Arsenic Trioxide European Journal of Cancer, 35(1999)1258-1263
5. Konig A,Wrazel L,Warrell R P, Comparative activity of melarsoprol and arsenic trioxide in chronic B-cell leukemia lines.Blood 90(1997) 562
6. Earnshaw W C, Nuclear changes in apoptosis, Curr Opin Cell Biol 7 (1995) 337–343
7. Petit P X, Lecoeur H, Alterations in mitochondrial structure and function are early events of dexamethasone-induced thymocyte apoptosis, J Cell Biol 130 (1995) 157–167
8. McGill, G, Fisher, D E, 1997. Apoptosis in tumorigenesis and cancer therapy. Frontiers in Bioscience 2, 353–397
9. Steller H, Mechanisms and genes of cellular suicide, Science 267 (1995) 1445–1449
10. Yano H, Mizoguchi A, Fukuda K, The herbal medicine sho-saiko-toinhibits proliferation of cancer cell lines by inducing apoptosis and arrest at the G0/G1 phase. Cancer Research 1994. 54, 448–454
11. Tseng C J, Wang Y J, Liang Y C, Microtubule damaging agents induce apoptosis in HL 60 cells and G2/M cell cycle arrest in HT29 cells. Toxicology 175, 123–142
12. Pignatti C, Schemia/ reperfusion-induced apoptosis: connecting nitric oxide andcell cycle regulators.Cardiovascular Research 59 (2003) 268–270
13. Myung-Ae B, Herman R, Byoung J ,Troglitazone but not rosiglitazone induces G1 cell cycle arrest and apoptosis in human and rat hepatoma cell lines.Toxicology Letters 139 (2003) 67-75
14. Bradham C A, Qian T, Streetz K, The mitochondrial permeability transition is required for tumor necrosis factor alpha-mediated apoptosis and cytochrome c release, Mol Cell Biol 18 (1998) 6353–6364
15. Hyeon K, Hee-Juhn Park, Cinnamaldehyde induces apoptosis by ROS-mediated mitochondrial permeability transition in human promyelocytic leukemia HL-60 cells. Cancer Letters 196 (2003) 143–152
16. Saeko Tada-Oikawa, Yusuke Hiraku, Michiko Kawanishi, Mechanism for generation of hydrogen peroxide and change of mitochondrial membrane potential during rotenone-induced apoptosis Life Sciences 73 (2003) 3277–3288
17. Renner K, Amberger A, Changes of mitochondrial respiration, mitochondrial content and cell sizeafter induction of apoptosis in leukemia cells. Biochimica et Biophysica Acta 1642 (2003) 115–123
18. Borutaite V, Jekabsone A, Morkuniene R, Inhibition of mitochondrial permeability transition prevents mitochondrial dysfunction, cytochrome *c* release and apoptosis induced by heart ischemiaJournal of Molecular and Cellular Cardiology 35 (2003) 357–366

Author: J.H Wang, Y.L. Wei and Z.J. Lv
Institute: College of bioengineering, Chongqing University
Street: No 174, Shazhengjie Street, Shapingba District
City: Chongqing City
Country: P R China
Email: wjh@cqu.edu.cn

Laser-accelerated ion beams for future medical applications

S. D. Kraft, K. Zeil, S. Bock, M. Bussmann, T. Kluge, J. Metzkes, T. Richter, T. E. Cowan, R. Sauerbrey, and U. Schramm

Forschungszentrum Dresden-Rossendorf, Dresden, Germany

***Abstract*— Recent success in laser-driven particle acceleration has increased interest in laser-generated "accelerator-quality" beams. For example, protons and ions have been produced with up to several tens of MeV per nucleon and monoenergetic features could be generated. Compact, high-gradient laser-accelerators are therefore now being discussed as a potentially viable technology for a host of particle-beam applications, including future compact medical accelerators for medical diagnostics and therapy. For this purpose, a new center for radiation therapy in oncology is founded in Dresden. Following the commissioning of a 150 TW laser system at the Forschungszentrum Dresden-Rossendorf the first acceleration of ion beams has been performed. In this test experiment proton beams with energies up to 6 MeV could be reached.**

***Keywords*— Laser-acceleration; protons**

Introduction

Radiation therapy plays an important role in cancer treatment, about two thirds of the patients are treated this way. Besides the conventional therapy with photons, hadron therapy became more and more important during the last years.

Despite the excellent clinical results the huge dimensions and hence the high costs of the apparatus prevent a wider spread of this method. A large contribution to this cost is caused by the gantry needed to rotate the beam around the patient and the overall radiation shielding. Hence, the development of an accelerator small enough to be rotated around the patient would therefore be a great step ahead.

Laser driven ion acceleration

Laser driven ion acceleration is a promising candidate in this direction [1,2]. For the acceleration ultrahigh intensity laser with pulse energies of a few Joule and pulse durations of some femtoseconds resulting in a power of up to a Petawatt are used. The laser light is focused onto a thin target (see Fig. 1) where focus intensities of up to 10^{21} W/cm^2 can be created. In theory the acceleration is described by the Target Normal Sheath Acceleration (TNSA) mechanism. The rising edge of the laser pulse ionizes the target and heats the electrons in the formed plasma. The hot electrons penetrate through the target, leave it at the backside and form a negative charged cloud at the backside. Together with the remaining positively charged ions of the target enormous electrical fields in the order of 10^{12} V/m are build up, many orders of magnitude higher than in an conventional RF accelerator. Even after the laser pulse has dyed out the field still remains for some picoseconds. Protons or other ions located at the surface of the target are accelerated within a few micrometers by this field, after penetrating the electron cloud ions with energies of up to several MeV leave perpendicular to the target together with low energetic electrons [3,4].

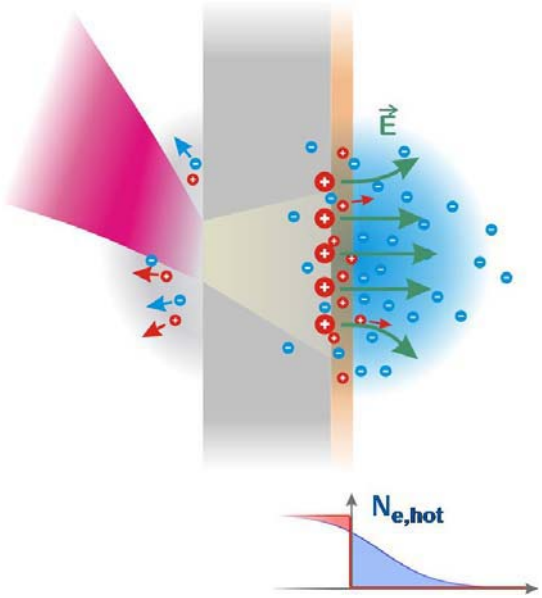

Fig. 1 Laser driven ion acceleration: The frontside of a target is illuminated by an ultrahigh intensity laser pulse. This pulse drives the electrons out of the target leaving behind the positively charged ions. Together with the electron cloud these ions form an enormous electrical acceleration field.

O. Dössel and W.C. Schlegel (Eds.): WC 2009, IFMBE Proceedings 25/XIII, pp. 106–107, 2009.
www.springerlink.com

In order to further investigate the ion acceleration mechanism and to perform first irradiation studies of biological tissue, the Ti:Sapphire laser system DRACO has been set up at the Research Center Dresden-Rossendorf during the last year. This laser delivers light pulses with a duration of 25 fs and up to 4 Joule of energy at a repetition rate of 10 Hz resulting in a peak power of 150 TW. Measurements of the laser contrast, i.e., the ratio of the intensity in the pulse maximum to the intensity before the main pulse arrives, showed a relative contrast of below 10^8 in the nanosecond and 10^{10} in the picosecond range. Hence the laser is well suited for ion acceleration experiments with thin foils.

In a first step investigations on different target types such as foils with various thicknesses are performed in order to find efficient ways to produce ion beams with appropriate energy spectra to irradiate biological tissue. As a second step cell irradiation studies with laser-accelerated ions will be compared to studies with ions from conventional accelerators.

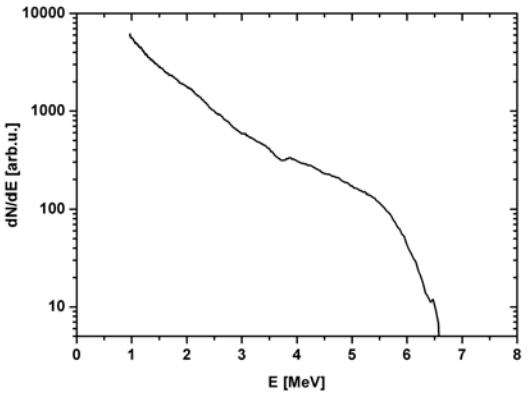

Fig. 2 Measured proton spectrum from a 13 µm thick aluminum foil. Protons up to an energy of 6 MeV are visible.

For ion acceleration, the laser beam with a diameter of 10 cm was focused by an off-axis parabola with a focal length of 25 cm onto a spot of 4.5 µm diameter. The target was formed by a 13 µm thick aluminum foil and was tilted under an angle of 45° to the laser propagation direction in order to prevent any back reflections of the light into the lasersystem.

The accelerated ions form a beam with a divergence of approximately 10° and fly perpendicular to the foil into an online energy spectrometer consisting of a Thomson parabola and a microchannel plate read out by a CCD Camera. Fig. 2 shows a proton spectrum recorded during the first ion acceleration experiments at DRACO. Protons originating from a water contamination layer up to an energy of 6 MeV are visible. This cutoff energy is in good agreement with the expectations for laser-acceleration from a thick aluminum foil, nevertheless it is not sufficient for the radiation of biological tissue [5]. As suggested by recent theoretical investigations, the energy spectrum does not only depend on the laser pulse but can be influenced by the target design as well. Therefore it is planned to perform further runs of experiments with thin foils ($d < 1$ µm) as well as with micro structured targets. In this case theory predicts proton energies of up to 20 MeV for the TNSA mechanism and thus high enough to perform cell irradiation studies. For ultrathin targets which become transparent to the laser light, theory predicts even higher energies due to new acceleration mechanisms [6,7].

CONCLUSIONS

We report on the first proton spectra with laser accelerated ions at the research center Dresden-Rossendorf, measurements with a 13 µm thick aluminum foil show proton energies up to 6 MeV. To increase the energy further experiments with ultra thin foils and structured targets are being set up.

For the future, cell irradiation experiments together with Oncoray and the Universitätsklinikum Dresden are planned.

Acknowledgment

The authors like to acknowledge financial support from the BMBF through the joint research project OnCOOPtics.

References

1. K.W.D. Ledingham, (2006) Nature Physics 2, 11
2. V. Malka, et al., (2008) Nature Physics 4, 447
3. S. P. Hatchett et al., (2000) Phys. Plasmas 7, 2076
4. S.C. Wilks et al., (2001) Phys. Plasmas 8, 542
5. J. Schreiber et al., (2006) Phys. Rev. Lett. 97, 045005
6. A. P. L. Robinson, et al.,(2008) New J. Phys. 10, 013021
7. B. I. Cho, et al., (2008) Phys. Plasmas 15, 052701

Author: Stephan Kraft
Institute: Forschungszentrum Dresden-Rossendorf
Street: Bautzener Landstraße 400
City: Dresden
Country: Germany
Email: s.kraft@fzd

Medical Physics Status in the Middle East Countries

I. Duhaini[1]

[1] Rafik Hariri University Hospital/ RT Department, Beirut, Lebanon

Abstract— **Middle East Federation of Medical Physics (MEFOMP) has passed in different stages. During the ISEP – 2007 conference held in Bahrain in November 2007, a meeting was arranged among representative physicists from the region and was decided to move ahead with the establishment of IOMP Middle East chapter. This follows more discussion among local physics societies in ME to further collect support and encouragement for such initiative. During the 16 th International Conference on Medical Physics 2008 that was held in Dubai in April 2008, there was a meeting for all the medical physics societies in the Middle East and the delegates signed a "Motion of Intent" which stated that all the delegates approve to form the Middle East Federation of Medical Physics (MEFOMP) which is part of the International Organization of Medical Physics IOMP and Ibrahim Duhaini was appointed the Secretary General of this federation by the President of IOMP professor Barry Allen. The following countries have signed up for the chapter: Bahrain, Iran, Iraq, Jordan, KSA, Lebanon, Oman, Qatar, Syria, and UAE.**

Keywords— **IOMP, MEFOMP, Middle East, Medical Physics**

I. Introduction

The Establishment of MEFOMP is part of the IOMP effort to organize societies under its umbrella to further enhance and improve the status of medical physics in all regions across the Globe.

The main goals of this chapter are to promote advancement in medical physics, to educate and train local society members for new procedures and technologies, to encourage exchange of expertise and information among societies and organize regional conferences and symposiums.

II. The Establishment Process

A. Bahrain Meeting: Nov 07

After the ISEP-2007 conference was adjourned, 12 members representing six ME countries and AAPM (e.g. Table 1) organized a meeting to discuss the status of Medical Physics in the region and what International organizations like AAMP and IOMP would do to help in promoting this field.

Table 1 Bahrain Meeting

Name	Country / Organition
Dr. Muthanna AlGhazi	USA, AAMP
Dr. Adel Mustafa	USA, AAMP
Mr. Adel G. Mohammed	Bahrain, BSMPBE
Mr. Jaffar Mattar	Bahrain, BSMPBE
Dr. Lama Sakhnini	Bahrain, BSMPBE
Dr. Ahmed Outaif	Saudi Arabia, SAMP
Dr. AbdullaAlHaj	Saudi Arabia, SAMP
Mr. Ibrahim Duhaini	Lebanon, LAMP
Mr. Osama El Natsheh	Jordan, JMPS
Ms. Abeer Ibrahim	Kuwait
Dr. Mohamed Bayoumi	UAE/EMPS
Dr. Jamila AlSuwaidi	UAE/EMPS

The meeting started by brief explanation from the countries' delegates about their local physics societies and the problems each one is facing. Some of the important points this meeting achieved was submitting request to IOMP for initiation of ME chapter since there was at least three established societies requested so. Also, all members agreed to carry out meetings among local societies to enhance the image of MP and to show its crucial role among hospitals, administration and physicians.

B. Dubai Meeting: April 08

During a poster session at the 16th International Conference on Medical Physics held in Dubai on April 2008, Dr. Barry Allen, IOMP President, called on for a meeting for all physics delegates representing ME countries to talk about the progress of establishing the chapter. In that meeting, every delegate sighed the "Motion of Intent" which states that:

O. Dössel and W.C. Schlegel (Eds.): WC 2009, IFMBE Proceedings 25/XIII, pp. 108–110, 2009.
www.springerlink.com

"The undersigned agree to inform their national societies of an invitation to form the Middle East Federation of Medical Physics (MEFOMP) for the purpose of supporting the development of Medical Physics in the region.
Following SEAFOMP, EFOMP, and AFOMP the IOMP encourages the formation of this regional federation."
(See Fig. 1)

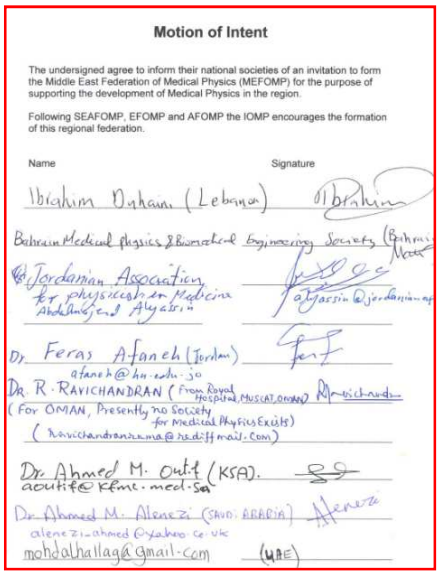
Motion of Intent

The undersigned agree to inform their national societies of an invitation to form the Middle East Federation of Medical Physics (MEFOMP) for the purpose of supporting the development of Medical Physics in the region.

Following SEAFOMP, EFOMP and AFOMP the IOMP encourages the formation of this regional federation.

Name Signature

Ibrahim Duhaini (Lebanon)
Bahrain Medical Physics & Biomedical Engineering Society (Bahrain)
Jordanian Association for physicists in Medicine Abdulmajeid Alyassin
Dr. Feras Afaneh (Jordan) afaneh@hu.edu.jo
Dr. R. RAVICHANDRAN (From Royal Hospital, MUSCAT, OMAN) (For OMAN, Presently no Society for Medical Physics Exists) (ravichandranrama@rediffmail.com)
Dr. Ahmed M. Outif (KSA). aoutif@kfmc.med.sa
Dr. Ahmed M. Alenezi (SAUDI ARABIA) alenezi_ahmed@yahoo.co.uk
mohdalhallag@gmail.com (UAE)

Fig. 1 Motion of Intent

After that, communication line was established to include all countries in the Middle East to join this chapter. Table 2 shows the list of MEFOMP and information about local societies. Three countries are in the progress of establishing their own society (Iraq, Kuwait, and Yemen).

Some countries lack resources and so it took more time to establish their own society, however, a lot of efforts are put with the help of Professional Medical Physicists from international organizations like IOMP, IAEA, AAMP and others.

In the following section, some detailed information about the status medical physics in the ME countries is included. Very few countries offer MS degree in Medical physics, so a lot of the graduates are coming from Europe or USA.

Table 2 MEFOMP List

Country	Society	No#	President / Contact
Bahrain	SMPBE	40	Dr. Lama Sakhini
Iran	IAMP	260	Alireza Mehdizadeh
Iraq	none		Ms. Alizabith Batyo
Jordan	JAPM	50	Dr. Abdalmajeid Alyassin
KSA	SAMPS	150	Dr. Ahmed Outif.
Kuwait	none		Mohamed Shaaban
Lebanon	LAMP	10	Ibrahim Duhaini
Oman	None		Dr. R. Ravichandran
QATAR	HMC	3	Dr. Huda Al Naemi
Syria	SAMP	30	Dr Mohammad Kharita
UAE	EMPS	38	Dr. Jamila Al Suwadi
Yemen	None		None

III. COUNTRIES INFORMATION

A. Bahrain

Bahrain Society of Medical Physics and Bio-engineering has been established in February 2008, and there are about 40 members. At present the Department of Physics at University of Bahrain is responsible for organizing Medical Physics courses for training students and professionals. The department offers a BS degree in Medical Physics, where at this time there are 30 students enrolled in the program. Moreover the department offers courses and workshops aimed for Physicians and Radiographers working in local Hospitals. For the names of the board members of the society and details of the activities please visit the website www.bsmpbe.org

B. Iran

The Iranian Association of Medical Physicists (IAMP) was established 10 years ago and at present is one of the most active non-governmental scientific associations among other scientific associations in this country. The president and committee in charge of IAMP are elected every 3 years by the members under auspices of the Ministry of Health and Medical Education of Iran. This committee has 7 members including the president. The association has 260 registered members working in different disciplines of Medical Physics, including 125 PhD holders (Nearly all of them university faculty members and professors) and 135 MS holders who are either PhD students at present or working in hospitals. This association runs a congress every two years about scientific achievements of researchers in Iran. At present 4 universities run Ph. D course and 7 uni-

versities run MS course involved in educating those interested in the field of Medical physics. For more information check this site http://www.iamp.hbi.ir/

C. Iraq

The Medical Physics society in Iraq is in the process of establishment.

D. Jordan

The Jordanian Association for Physicists in Medicine, JAPM, was founded in Dec 2006. Currently, JAPM consists of 50 members. Typically, JAPM conducts several scientific and social activities throughout the year. Yarmouk University offers an undergraduate degree in Biomedical Physics & Jordan University offers a master degree in Medical Physics. For more information: www.jordanianapm.org.

E. Kuwait

There is no medical physics society established yet, and there are around 15 medical physics.

F. Lebanon

In 2005, a group of physicists organized a conference for Radiation Protection and Safety in collaboration with IAEA in Beirut. A new committee called Medical Exposures Control Committee was formed. In 2007, the Lebanese Association of Medical Physics was established and a lot of efforts were made by writing the Constitution and opening the membership to other related field since there are only 7 medical physics working in Lebanon.

G. Oman

There is no Medical physics society established yet but there are 6 PhD level qualified Medical Physicists, 4 B.S level medical physicists, and 1 Dosimetrist. Regarding the formation of local society, it is believed that non-locals working in MOH cannot form such associations, and only local medical physicists only should initiate such society formation

H. Qatar

There is no local society for medical physicists established yet. However, a group of physicists trying to establish a local physics society at Hamad Medical Corporation (5 hospitals)

I. Saudi Arabia

The SAMPS was established in 2008 and it has more than 150 members.

J. Syria

The SAMP is in the process of establishment with more than 25 member.

K. United Arab Emirates

The EMPS was established in September 2005 under Emirates Medical Association. Member are now 38and a lot of educational activities in the field of MP were organized by EMPS.

L. Yemen

No Information provided yet.

IV. CONCLUSIONS

The final step of this new chapter is the official inauguration which will take place during the WC 2009 after approving the suggested constitution and the participating countries.

ACKNOWLEDGMENT

I would like to thank all country delegates for their updated information regarding their Medical Physics Societies.

Author: Ibrahim Duhaini, MS
Institute: Rafik Hariri University Hospital
Street: Semaan St. Mouseitbeh, Rayan Bldg. F#3
City: Beirut
Country: Lebanon
Email: Duhaini@yahoo.com

Locoregional hyperthermia in combination with chemotherapy for metastatic breast cancer patients: The Mammatherm- trial

J.K. Jueckstock[1], B. Eberhardt[2] and H.L. Sommer[1]

[1] Klinikum Innenstadt, Munich University, Gynecology and Obstetrics, Munich, Germany
[2] Kreiskrankenhaus Landshut-Achdorf, Gynecology and Obstetrics, Landshut, Germany

Abstract—**Treatment options for patients with metastatic breast cancer should be both as effective and preferably as little toxic as possible. However to date there is no standard therapy available but treatment regimens for metastatic breast cancer vary much. Locoregional hyperthermia might show additive effects to chemotherapy due to an increased perfusion and a simultaneous occurring of interstitial acidosis in tumor tissue. Primary objective of the multicenter prospectively randomized phase I/II German Mammatherm-trial is to evaluate if metastatic breast cancer patients regarding progression free survival benefit from locoregional hyperthermia given additionally to a chemotherapy regimen. Phase I of this study is a dose-finding-study for liposomal doxorubicin administered in combination with locoregional hyperthermia. Dose-escalation-levels are at 40/50/60 mg/m^2 and in each level 3 patients have to be treated without showing severe toxicity. The first eligible patient (i.e. metastatic lesions accessible to locoregional hyperthermia) entered the study in August 2007. Phase II (recruitment of 300 patients planned) will compare 2 different treatment regimens in a randomized setting: Arm A comprises 6 cycles of liposomal doxorubicin 40/50/60 mg/m^2 (final dose to be defined after phase I) i.v. d1 q22d x 6 and cisplatin 20 mg/m2 i.v. d1, 8, 15 q22d x 6 in combination with locoregional hyperthermia administered at d1, 4, 8, 11, 15, 18 q22d x 6. In arm B patients are treated according to the same chemotherapy regimen but without adding the hyperthermic treatment. Intentions of the study are that patients in the experimental arm will benefit from locoregional hyperthermia administered additionally to chemotherapy, i.e. that progression free survival as well as overall survival (as secondary study objective) can be prolonged significantly without being accompanied by increased toxicity or reduced quality of life. First results for phase I are expected by the end of 2010.**

Keywords— **hyperthermia, breast cancer, metastatic treatment, chemotherapy**

I. Introduction

Breast Cancer is the most common malignancy of females, responsible for 18% of cancer deaths in women. [1]

Unfortunately, a large proportion of patients develop metastatic disease and require chemotherapy to palliate symptoms and improve quality of life.[2] The median survival in this stage has been reported to be 18 to 24 months for most patients. The treatment is palliative in intent and the goals of treatment include improving quality of life and if possible prolongation of life. Treatment in metastatic cancer will usually involve hormone therapy and/or chemotherapy.

Anthracyclines are among the most active agents used in the treatment of advanced breast cancer, and doxorubicin and epirubicin can achieve response rates of around 20% to 40% (when used as single agents) and up to 60% (as part of combination regimens in the first-line setting).[3]

Various analogues and derivatives of doxorubicin were investigated, with the aim of finding chemotherapeutics with less cardiotoxic characteristics while providing the same, or better, cytostatic efficacy. An alternative approach besides the chemical variation of the agent is the variation of formulation.

Until now, non-pegylated liposomal doxorubicin has been investigated in five phase III studies for the treatment of metastatic breast cancer all showing less cardiotoxicity compared to conventional doxorubicin and equal efficacy. [4 - 9]

Concerning combination of liposomal encapsulated doxorubicin and hyperthermia Merlin showed already in 1993 that Thermosensitive liposome-encapsulated doxorubicin (TLED) yielded additive effects in the resistant cells while potentiation was observed in the sensitive cells, proclaiming that the possibility of obtaining additive cytotoxicity using TLED combined with hyperthermia may represent an alternative way of intensification of doxorubicin cytotoxicity.[9]

The origin of hyperthermia dates back to experiences in ancient days, when it was observed that endogenous fever had an antiproliferative effect on tumor growth. Since the second half of the 20th century, the methods of inducing hyperthermia are mainly based on the administration of exogenous energy. Since the 1930's, the hyperthermic water bath has been used as a source of energy (two-chamber hyperthermic tub).

Later, short wave radiation was applied with quartz lamps or various other sources of infra-red radiation. Since the 1980's adverse effects (mainly skin burns) have been decreased and tolerance rates have been improved by filtering the applied radiation either by water or gold-alloyed metal reflectors (wave length 0.75 - 1.40 µm). This type of

O. Dössel and W.C. Schlegel (Eds.): WC 2009, IFMBE Proceedings 25/XIII, pp. 111–113, 2009.
www.springerlink.com

filtered infra-red-A radiation is highly equivalent to natural sun-rays under the earth's atmosphere and is therefore better tolerated.

Various in-vitro and in-vivo experiments have shown that tumor circulation and oxygenation are increased by higher temperatures while an interstitial acidosis occurs.[10 - 12]

Several conditions might contribute to a potentially improved antiproliferative efficacy of cytostatic drugs combined with hyperthermia:

- Higher concentrations of the cytostatic drugs can be found in the regions of tumor, even in case of decreased perfusion.
- Cytostatic potency of various cytostatic drugs such as cisplatinum, ifosfamide, doxorubicin and bleomycin is increased.[13-15]
- The uptake of cisplatinum into the intracellular space can be improved under hyperthemic conditions.[16]
- Sensibilisation of previously cisplatinum-resistent cells under hyperthermic conditions was shown.[17]
- Under hyperthermia significantly higher concentrations of tumor necrosis factor and interleucins were observed.[18]

II. Patients and Methods

In this open-label, multicenter phase I / II study a total of 310 patients with metastatic breast cancer will be randomized into the experimental treatment group receiving chemotherapy in combination with locoregional hyperthermia or the control group receiving the same chemotherapeutic regimen but without hyperthermic treatment.

In order to assure adequate toxicity assessment, a phase-I-trial is preponed: At each dosage escalation level (Myocet 40, 50 and 60 mg/m^2) 3 patients have to be treated and complete 4 treatment cycles according to the protocol arm B without any severe side effect or limiting toxicity.

Primary objective of the study is to compare the time to progressive disease (TTPD) in a target volume amenable to locoregional hyperthermia in patients treated with liposomal-encapsulated Doxorubicin (Myocet®) and Cisplatin (MC) chemotherapy versus MC-chemotherapy combined with locoregional hyperthermia.

Secondary objectives of the study are to compare the following items in the two regimen arms:

- Response rate
- Survival time after randomisation
- Toxicity
- Changes in quality of life over time as defined by EORTC QLQ-C30 and QLQ-BR23 questionnaire

The first patient was recruited in August 2007 and a total of 10 patients will have to be treated without showing severe toxicity until the study can proceed into phase II.

In phase II 300 patients will be randomized into two treatment groups: The experimental arm will comprise a regimen of 6 cycles of liposomal-encapsulated Doxorubicin 40/50/60 mg/m² i.v. body surface area administered on day 1, repeated on day 22 and Cisplatin 20mg/ m² i.v. administered on day 1, 8 and 15, repeated on day 22 combined with locoregional hyperthermia d1, 4, 8, 11, 15, 18, repeated on day 22. In the control group patients will receive the same chemotherapy regimen without hyperthermia.

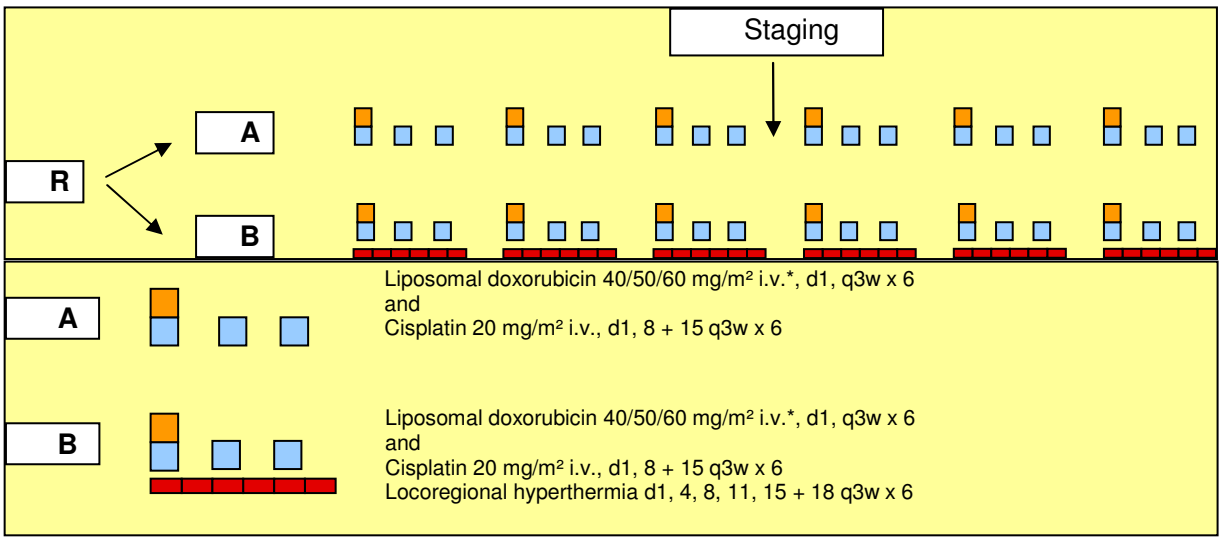

Fig. 1: Design of the Mammatherm-trial

Application of locoregional hyperthermia will be performed either by capacitive hyperthermia (Oncotherm©) or by Radiofrequency hyperthermia (BSD 2000© by the BSD Medical Corp.).

III. Results

Intentions of the study are that patients in the experimental arm will benefit from locoregional hyperthermia administered additionally to chemotherapy, i.e. that progression free survival as well as overall survival (as secondary study objective) can be prolonged significantly without being accompanied by increased toxicity or reduced quality of life. First results for phase I are expected by the end of 2010.

IV. Conclusions

The Mammatherm-trial will show if metastatic breast cancer patients have a prolonged progression free survival by adding locoregional hyperthermia to a chemotherapy regimen.

References

1. Jensen O.M., Estève J., Moller H., et al. (1993) Cancer in the European Community and its member states. *Eur J Cancer*26:1167-256.
2. Harris J, Morrow M, Norton L. Malignant tumors of the breast. (1997) In: DeVita VT, Hellman S, Rosenberg SA, editors. Cancer: Principles and practice of oncology. *Philadelphia: Lippincott-Raven Co.* 5th edition:1557-616.
3. Mouridsen HT. (1992) Systemic therapy of advanced breast cancer. *Drugs* 44 Suppl 4:17-28.
4. Batist G, Ramakrishnan G, Rao CS, et al. (2001) Reduced cardiotoxicity and preserved antitumor efficacy of liposome-encapsulated doxorubicin and cyclophosphamide compared with conventional doxorubicin and cyclophosphamide in a randomized, multicenter trial of metastatic breast cancer. *J.Clin.Oncol.* 19:1444-54.
5. Erdkamp F, Chan S, Davidson N, et al. (1999) Phase III study of TLC D-99 (liposome encapsulated doxorubicin) plus cyclophosphamide vs epirubicin (EPI) plus cyclophosphamide in patients with metastatic breast carcinoma. *Proc Ann Meet Soc Clin Oncol* 18:459a.
6. Harris L, Batist G, Belt R, et al. (2002) Liposome-encapsulated doxorubicin compared with conventional doxorubicin in a randomized multicenter trial as first-line therapy of metastatic breast cancer. *Cancer* 94:25-36.
7. Chan S, Davidson N, Juozaityte E, Erdkamp F, Pluzanska A, Azarnia N, Lee LW. (2004) Phase III trial of liposomal doxorubicin and cyclophosphamide compared with epirubicin and cyclophosphamide as first-line therapy for metastatic breast cancer. *Ann Oncol.* Oct;15(10):1527-34.´
8. O'Brien ME, Wigler N, Inbar M, Rosso R, Grischke E, Santoro A, Catane R, Kieback DG, Tomczak P, Ackland SP, Orlandi F, Mellars L, Alland L, Tendler C; CAELYX Breast Cancer Study Group. (2004) Reduced cardiotoxicity and comparable efficacy in a phase III trial of pegylated liposomal doxorubicin HCl (CAELYX/Doxil) versus conventional doxorubicin for first-line treatment of metastatic breast cancer. *Ann Oncol.* Mar;15(3):440-9
9. Merlin JL, Marchal S, Ramacci C, et al. (1993) Antiproliferative activity of thermosensitive liposome-encapsulated doxorubicin combined with 43 degrees C hyperthermia in sensitive and multidrug-resistant MCF-7 cells. *Eur J Cancer.* 29A(16):2264-8.
10. Engin K. (1996) Biological rationale and clinical experience with hyperthermia. *Control.Clin.Trials* 17:316-424.
11. Roszinski S, Wiedemann G, Jiang SZ, Baretton G, Wagner T, Weiss C. (1991) Effects of hyperthermia and/or hyperglycemia on pH and pO2 in well oxygenated xenotransplanted human sarcoma. *Int J Radiat.Oncol Biol.Phys.* 20:1273-80.
12. Song CW, Shakil A, Osborn JL, Iwata K. (1996) Tumour oxygenation is increased by hyperthermia at mild temperatures. *Int J Hyperthermia* 12:367-73.
13. Kuwano H, Sadanaga N, Watanabe M, et al. (1993) Clinical study of hyperthermia combined with chemotherapy in the treatment of carcinoma *Gan.To.Kagaku.Ryoho.*20:597-602.
14. Maymon R, Bar-Shira MB, Holzinger M, et al. (1994) Augmentative effects of intracellular chemotherapy penetration combined with hyperthermia in human ovarian cancer cells lines. *Gynecol Oncol.* 55:265-70.
15. Miller RC, Richards M, Baird C, et al. (1994) Interaction of hyperthermia and chemotherapy agents; cell lethality and oncogenic potential. *Int.J.Hyperthermia*10:89-99.
16. Ohtsubo T, Saito H, Tanaka N, et al. (1997) In vitro effect of hyperthermia on chemoenhancement and uptake of cisplatin in human pharyngeal carcinoma KB cells. *Chemotherapy* 43:43-50.
17. Katschinski DM, Wiedemann G, Mentzel M, et al. (1997) Optimization of chemotherapy administration for clinical 41.8 degrees C whole body hyperthermia. *Cancer Lett.* 115:195-9.
18. Robins HI, Kutz M, Wiedemann GJ, et al. (1995) Cytokine induction by 41.8 degrees C whole body hyperthermia. *Cancer Lett.* 97:195-201.

Corresponding author:

Author: J.K. Jueckstock
Institute: Frauenklinik am Klinikum Innenstadt Munich University
Street: Maistrasse 11
City: Munich
Country: Germany
Email: julia.jueckstock@med.uni-muenchen.de

The Future of Medical Physics
The Role of Medical Physics in Research and Development
An Opinion

S. Christofides

Medical Physics Department, Nicosia General Hospital, Nicosia, Cyprus

Abstract— **The convergence of technology in recent years within different fields of research has broadened the horizon for Medical Physics involvement both in basic research and in the clinical setting. These include and are not limited to the mapping of the entire human genome, tools to genetically manipulate cells or organisms, new treatment strategies, including molecular and cell based therapies, nanotechnology, and State-of-the-art imaging modalities with increased spatial and temporal resolutions. This convergence brings with it opportunities as well as threats to the traditional role of the Medical Physicist, both in the hospital environment and the research settings. This paper gives an opinion on the future role of the Medical Physicist the research as well as the clinical settings.**

Keywords—**Medical Physics, Research and Development, Education and Training, Clinical Setting**

I. Introduction

The convergence of technology in recent years within different fields of research has broadened the horizon for Medical Physics involvement both in basic research and in the clinical setting [1]. These include and are not limited to:

- The mapping of the entire human genome
- Tools to genetically manipulate cells or organisms
- New treatment strategies, including molecular and cell based therapies
- Nanotechnology, and
- State-of-the-art imaging modalities with increased spatial and temporal resolutions.

Physics underlines all the innovative techniques applied in both diagnosis and therapy. Core knowledge of the physics from quantum mechanics and solid state physics to molecular and computational physics are required to drive new developments in diagnostic and therapeutic medicine [2].

For Medical Physics to remain relevant, medical physicists have to become also actively involved in the task of health promotion and disease management, alongside the other healthcare professional. They have to begin learning about molecular biology, and take advantage of the opportunities available in the development of new therapeutic and diagnostic procedures.

Medical physicists can also contribute significantly by transforming scientific advances in the laboratory into clinical applications. Equipment that has been developed in the research setting can be integrated into cost effective and safe clinical applications for the benefit of the patient.

Currently though, the emphasis is on cost containment, optimisation with the limited resources available in healthcare. At the medical physicists' level, the emphasis is on enhancing specific skill development and competency, in both therapeutic and diagnostic physics. However, many opportunities created by translational and frontier research slips by because the profession is too focused on achieving greater competency and overspecialisation, which is, unfortunately, driven by economics and political pressure.

II. discussion

The focus on the above has raised serious concerns about the ability of the next generation of medical physicists to respond to new technology and the changing medical scene.

The majority of Medical Physicists work in the hospital environment and are occupied with routine work while a small proportion is conducting fundamental research. The former group, run the fear of downgrading their profession to that of an over specialised technologists [3]. The later run the fear of extinction if they do not adapt their knowledge and skills to compete in the increasingly blurred boundaries between disciplines.

If the current education and training curricula for Medical Physics remain unchanged, the profession runs the fear of being downgraded to an over specialised technological profession delivering routine therapeutic and diagnostic procedures.

III. conclusions

There is no future if the profession of Medical Physics is not refocused. Most Medical physicists spend too much

O. Dössel and W.C. Schlegel (Eds.): WC 2009, IFMBE Proceedings 25/XIII, pp. 114–116, 2009.
www.springerlink.com

time doing routine tasks such as quality control tests. The tasks of a Medical Physicists are to design processes, implement and monitor them. Medical Physicists should spend more time on development, assessment and implementation of new technologies. Medical physicists should do the work of a physicist and not that of a technologist.

IV. AN OPINION

Taking into consideration the present status of the education and training of the Medical Physicist in Europe [4, 5, 6] as well as the European recommendations on lifelong training [7, 8, 9], the author is of the opinion that in order for the Medical Physics profession to have a future, two directions should be aimed for:

- The introduction of the Medical Physics Technologist
- The introduction of the Medical Physics Researcher.

The following are given as food for thought and as a starting point for further discussion and development of the above opinion.

A. The Medical Physics Technologist

As it is evident from above, the Medical Physicist spent too much time carrying out routine work, such as quality control tests and radiotherapy treatment planning. Already Dosimetrists are employed in radiotherapy department (especially in the USA), to carry out routine work that in other coutries is done by Medical Physicists. The Medical Physics Technologist can take over the routine work of the Medical Physicist in other specialities (Nuclear Medicine, Radiology, etc) thus allowing the Medical Physicist to design, implement and monitor processes.

The education and training of the Medical Physics Technologist must be equivalent to level 3 or higher of the European Qualifications Framework [7]. Apart form the traditional subjects, the curriculum required should include new subjects such as biology, genetics, molecular engineering, nanotechnology, etc.

B. The Medical Physics Researcher

As it is evident from above, a number of new and emerging technologies appear regularly for possible applications in medicine that require the skill and knowledge of the Medical Physicist to be developed and applied into clinical practice. The Qualified Medical Physicist (QMP) and even the Medical Physics Expert (MPE) does not possess the necessary knowledge in biology, genetics and molecular engineering to be able to cope in this challenging development arena. To be involved in research is more difficult.

Currently in European countries the education and training of the QMP ranges between level 4 and 6 and that of the MPE ranges from level 5 to level 7 of the European Qualifications Framework [6].

A researcher should have an education and training equivalent to level 8 of the European Qualifications Framework [7]. Universities are encouraged to developed taught or semi taught PhD level programmes in Medical Physics so as to encourage the development of the Medical Physics Researcher to meet today's and the future's challenges.

C. Continuous Professional Development

Employers are encouraged to set up the necessary mechanisms to allow the continuous professional development of their employees in line with the European recommendations for lifelong learning. Through these mechanisms a Medical Physics Technologists can have the opportunity to became a Qualified Medical Physics or even a Medical Physics Research after gaining the necessary education and training qualifications prescribed at the deferent levels of the European Qualifications Framework [7].

An example is the effort of the United Kingdom's Health Departments to modernise the scientific careers in the healthcare environment [10].

REFERENCES

1. S. Christofides, "Molecular Imaging: a tool for Biotechnology", Central European Congress of Life Sciences, EUROBIOTECH 2008, Krakow, October 17-19, 2008, Acta Biochemica Polonica, vol. 55 Supplement 4/2008.
2. Ng K. H., "The Second John Cameron Memorial Lecture Delivered at SEACOMP'07, Manila, Nov 21-23, 2007 - Medical Physics in 2020: Will we still be relevant?", Australasian Physics & Engineering Sciences in Medicine Vol. 31, No 2, 2008, p. 85-89
3. European Medical Physics News, "The people behind Medical Physics: Cari Borrás, Medical Physicist, Chair of the IOMP Scientific Committee", www.efomp.org, winter 2008, p. 18-20.
4. S. Christofides, W.Schlegel, R. Padovani, P. F. Sharp, A. Torresin, M. Wasilewska-Radwanska, Wil van der Putten, E. Guibelalde and K. U. Kasch, "Education and Training of the Medical Physicist in Europe", These Proceedings.
5. EFOMP *Policy Statement 12:* The Present Status of Medical Physics Education and Training in Europe. New perspectives and EFOMP Recommendations. www.efomp.org
6. T. Eudaldo and K. Olsen, "The present status of Medical Physics in Europe: An EFOMP Survey", Physica Medica (2008), 24, p. 3-20.
7. Recommendation of the European Parliament and of the Council of 23 April 2008 on the establishment of the European Qualifications Framework for lifelong learning, (2008/C 111/01), OJ C111, p. 1-7
8. Resolution of the Council and of the Representatives of the Governments of the Member States, meeting within the Council of 21 November 2008 on better integrating lifelong guidance into lifelong learning strategies, (2008/C 319/02), OJ C319, p. 4-7

9. Decision no 1357/2008/EC of the European Parliament and of the Council of 16 December 2008 amending Decision No 1720/2006/EC establishing an action programme in the field of lifelong learning, OJ L350, p. 56-57
10. The Future of Healthcare Science Workforce. Modernising Scientific Careers: A Consultation", U.K. Healthcare Departments, www.dh.gov.uk/cso.

Author: S. Christofides
Institute: Medical Physics Department, Nicosia General Hospital
Street: 215 Old Nicosia Limassol Road
City: Nicosia 2029
Country: Cyprus
Email: cstelios@cytanet.com.cy

Application Potentials of Microwave in NanoMagnetic Particle Hyperthermia

M. Janmaleki[1], M. Mahmoudi[2], M. Rafienia [3], and H. Peirovi[1]

[1] Nanomedicine and Tissue Engineering Research Center, Shahid Beheshti University (M.C), Tehran, Iran
[2] Nano Research Center, Sharif University of technology, Tehran, Iran
[3] Tissue Engineering Lab., Faculty of Medicine, Isfahan University of Medical Science, Isfahan, Iran

Abstract—**Magnetic Nanoparticle Hyperthermia is a new auxiliary technique for cancer treatment, in which the temperature of tumor cells is elevated and maintained to a therapeutic level. Up to now a few researches have been done for Microwave Magnetic Hyperthermia. The authors have studied behavior of MNPs in Microwave field for hyperthermia application. The frequency and power of produced field was 915MHz and 25 Watts.**

Keywords— **Hyperthermia, MNP, Microwave, Nanoparticle.**

I. Introduction

Cancer hyperthermia is a treatment to increase the tissue temperature to a therapeutic level to kill tumor cells. Over the last three decades, much has been learned about the effects of heat on cells and the interactions between heat and radiation and chemotherapeutic agents [1-2,3-6]. Briefly speaking, by maintaining elevated temperatures (5–10◦C) on tumor cells for several minutes the apoptosis process could be induced. The foremost problem in hyperthermia, however, is the generation and control of heat in tumors. The clinical use of hyperthermia has been restricted by a lack of adequate equipment to effectively deliver heat to deep-seated and even large superficial lesions and by a lack of thermometry techniques that provide reliable information on heat distribution in the target tissues [1, 3-6].

Among several techniques for inducing heat, electromagnetic (EM) heating methods are preferable. The main reasons are ease of usage and producing and also controlling the fields. But there are some considerations; the energy deposition is a complex function of the frequency, intensity, and polarization of the applied fields, the applicator's size and geometry, as well as the size, depth, geometry, and dielectric property of the tumor. The material, thickness, and construction of a cooling bolus also influence the amount of energy deposition.

The EM energy used in hyperthermia is usually classified by frequency as either microwave energy (300 MHz and 300 GHz) or RF energy (300 KHz and 300 MHz). The most commonly used microwave frequencies in hyperthermia are 433, 915, and 2450 MHz, which are the designated ISM (industrial, scientific, and medical) Common RF frequencies are 13.56 and 27.12 MHz, which have also been widely used in diathermy. Frequencies higher than 2450 MHz have no practical value due to their limited penetrations. At lower frequencies field penetration is deeper, but the applicator must be larger and focusing is difficult. For the most part, MW applicators are used for treatment of tumors a few centimeters below the surface of the tissue [14-16]. MW techniques are the best candidate for intracavitary hyperthermia. There have been clinical and research studies on Microwave hyperthermia of the esophagus, rectum, cervix, prostate, nasopharyngeal, and bladder cancers. Some of these researches have been introduced to the market. The main frequency of the microwave applicators in the most research is 915MHz [6].

To overcome the mentioned difficulties, magnetically hyperthermia (MH) has been introduced. MH has the potential to address targeting and heat distribution shortcoming of other hyperthermia methods. The MH technique is defined as localizing magnetic nanoparticles (MNP) within tumor tissue and applying an external alternating magnetic field.

The coupling of an external RF magnetic field to magnetic particles in the body results transfer of energy to the tissue by: 1) eddy current heating, 2) hysteretic heating: heat generated when a magnetic material is forced around part or all of the hysteresis loop, 3) viscous heating: heat generated by the kinetic motion of a particle within a viscous fluid, and 4) magnetic resonance [4].

Except the first mechanism which has negligible effect the other mechanisms are frequency and amplitude dependent. Specific loss power (SLP) is an increasing function of frequency f and field amplitude H. According to the induction law the induced heating power is proportional to the square of $(H \cdot f \cdot D)$ were H is field amplitude, f frequency and D the induced current loop diameter [1-3].

According to Herget et al [1] for particles with mean size in the superparamagnetic regime losses increase with frequency in the range RF energy, and this parameter has to be over weighted against field amplitude.

There is a multitude of known magnetic materials which, however, for biomedical applications is strongly restricted by the demand of biocompatibility. Besides a few suggestions in the literature of using several spinel ferrites or special magnetic alloys for MPH the majority of investigations focused on magnetic iron oxides Fe_3O_4 (magnetite) and γ - Fe_2O_3 (maghemite) which have been proved to be well

O. Dössel and W.C. Schlegel (Eds.): WC 2009, IFMBE Proceedings 25/XIII, pp. 117–119, 2009.
www.springerlink.com

tolerated by the human body [1]. In spite of suitable results of the MW hyperthermia, there is a little research on its application with magnetic nanoparticle (MNP) for cancer therapy. In this work we study the response of iron oxide nanoparticles to 915MHz microwave.

II. Experimental methods

A. Chemical Synthesis for sample preparations

Based on the well known methods for producing Fe_3O_4 and Fe_2O_3 nanoparticles stabilized by PVA (polyvinyl alcohol), the main target in the our synthesis was to Optimize the synthesis parameters in order to produce pure Fe_3O_4 nanoparticles. By selecting different Stirring Rate and base Molarities 18 samples were produced. In the following table their specifications (phase and size) are shown. Sample's sizes are obtained by Scherrer Equation. The sizes of nanoparticles are in the region of superparamagnetic [1].

Table 1 MNP samples and sizes

Sample Number	Determined Phase	Sample Size (nm)
S1	Fe3O4	3.8
S2	Fe3O4, Fe2O3, FeO(OH)	3.6
S3	Fe3O4, Fe2O3	4.4
S4	Fe3O4, Fe2O3	4
S5	Fe3O4	4.9
S6	Fe3O4	4.1
S7	Fe3O4, Fe2O3	5
S8	Fe3O4, Fe2O3	3.7
S9	Fe3O4	4.7
S10	Fe3O4, Fe2O3	5.2
S11	Fe3O4, Fe2O3	3.9
S12	Fe3O4, Fe2O3	5.3
S13	Fe3O4	3.8
S14	Fe3O4	5.5
S15	Fe3O4, Fe2O3	4.1
S16	Fe3O4, Fe2O3	3.5
S17	Fe3O4, Fe2O3	5
S18	Fe3O4, Fe2O3, FeO(OH)	3.2

B. Experiment Setup for Microwave inducing Heat

A microwave signal generator was designed based on the theories of MW power amplifier. It generates and deliver a MW filed with a range of frequency between 850-1300MHz. The maximum output power of the device was 30 watt. The amplitude and frequency can be adjusted. In our experiments we fined the parameters of the amplifier to 915MHz and 30Watt. The device is illustrated in figure 1.

To Simulate the human body, we use a water bath with fixed temperature 37±2°C. after MW radiation the temperature of the sample would be increased. To minimize the effects of difference of temperatures between water bath and sample, a glass bottle filled with polyurethane used for increasing the time constant of convection process. The samples together with microwave probe (antenna) are placed in the glass. Then the glass would be introduced in the water for several minutes. This is needed for assuring the stabilization of the temperature. The temperature was measured with an IR thermometer (Fluke Corp.).

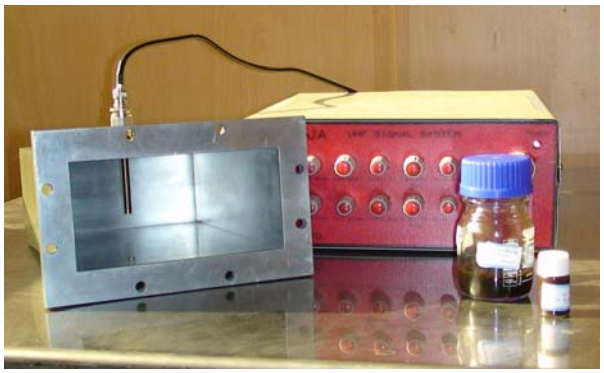

Fig. 1 Microwave Generator, 25Watts at 0.95 to 1.2GHz

III. Results and discussion

In all the experiments the power and frequency of the MW power amplifier were fixed. Tests were accomplished in 25 minutes. The following figure summarizes the results. It was not possible for us to monitor the temperature of samples during the experiments. We measure the temperature every 5 minutes. There is no significant differences between the interval measured temperature, So the final temperature which was recorded after 25 minutes are given.

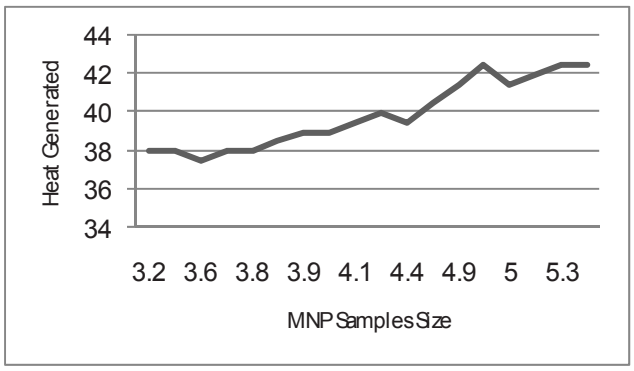

Fig. 2 Measured temperatures versus particle size of samples 1 to 18.

From the results we can see the best SLP attainable is from sample S7, S12 and S14. By considering the table 1 we can conclude that the main reason which led to this

result is the size of the particles. By increasing the size of the particles the amount of the induced heat is increased. On the other hand the samples including Fe_3O_4 and Fe_2O_3 response better.

IV. Conclusion

In this study, the effect of MW electromagnetic field on MNPs has been investigated. It was shown that the larger MNPs have larger SLP at the same frequency and intensity of the electromagnetic field. These results agree with the conclusion which Hergt et al had reported in the RF range.

References

1. R. Hergt, S. Dutz, J. (2006) Phys. Condens. Matter, 18: S2919–S2934
2. Kapp, D. S. (1994), Int. J Hyperthermia,10, 355
3. R. Hergt, W. Andra (1998) IEEE TRANSACTIONS ON MAGNETICS, VOL. 34
4. David Sellmyer (2006) Advanced Magnetic Nanostructure. Springer Science Inc., New York
5. V. Labhasetwa, (2007) BIOMEDICAL APPLICATIONS OF NANOTECHNOLOGY, Wiley InterScience, New York,
6. R. HABASH, (2008) BIOEFFECTS AND THERAPEUTIC APPLICATIONS OF ELECTROMAGNETIC ENERGY, CRC Press,

Author: M. Janmaleki
Institute: Nanomedicine and Tissue Engineering Research Center, Shahid Beheshti University (M.C), ,
Street: Velanjak
City: Tehran
Country: Iran
Email: janmaleki@sbmu.ac.ir

Thermographic measurements of allergen-induced skin reactions

E. Rokita[1,2], T. Rok[1] and G. Tatoń[1]

[1] Jagiellonian University Medical College/Department of Biophysics, Kraków, Poland

[2] Jagiellonian University/Institute of Physics, Kraków, Poland

Abstract— **The studies were performed to validate a thermographic (TH) technique for the evaluation of skin prick test results. The TH measurements of the skin allergic reactions are supplemented by a simple mathematical model based on the pathophysiology of heat generation. A set of new parameters are proposed to quantify intensity and kinetics of the skin reactions. There are possibilities to distinguish different susceptibility to histamine as well as to measure the intensity of the allergic response. The maximum radius of the heated region was applied to quantify different response to histamine. Three groups of patients were distinguished. The allergen-induced response was characterized by one parameter which is related to the heat generation rate. In agreement with clinical data, it was confirmed that the intensity of the allergic reaction does not correlate with the susceptibility to histamine. The values of the model parameters do not correlate well with the routine assessment based on wheal and erythema areas. The final verification of the proposed method needs to be addressed in future studies of the IgE antibody serum level.**

Keywords— **Allergy, skin testing, thermography.**

I. Introduction

The allergic response is commonly identified and assessed by skin testing [1]. Small amount of potential allergens and histamine (control) are introduced at the specific skin sites by superficial scratching. The usual method to quantify immediate allergic skin reactions is to mark wheal and erythema regions and assess the surfaces affected by the reactions using planimetry. Frequently, the results of skin testing are related to the size of the histamine control and are reported using a 0 to 5+ scale.

The advent of new imaging technologies offers possibilities to quantify the allergic reactions using a variety of the imaging modalities, the thermo-graphic (TH) camera being an example. It should be noted that the application of infrared imaging starts in breast cancer diagnosis about 50 years ago. Nowadays TH imaging is well established method for health monitoring and examinations s well as for assisting diagnosis [2-5].

In the present studies the TH measurements of the skin allergic reactions are supplemented by a simple mathematical model based on the patho-physiology of heat generation. A set of new parameters are proposed to quantify intensity and kinetics of the skin reactions. The main objective of this work is to describe and analyze a possible model mechanism for skin temperature distribution.

II. Materials and methods

A. Physical model of the allergic reaction

Here we are concerned in the development of a model to quantify the allergic reaction. The introduction of histamine and potential allergens (antigens) at sites on the skin induces a complex sequence of events known as the local inflammatory response [6-7]. If a person is allergic to the allergen, local mast cells de-granulate and release histamine. We assume that the reaction takes place in the thin skin layer. Moreover it is assumed in the model that histamine is the principal mediator of the allergic reaction. The involvement of other mediators in the process is neglected. Histamine penetrates the skin and binds to receptors on nearby capillaries and venules, causing vasolidation (increase in the diameter of the blood vessel). The engorged vessels are, in turn, responsible for skin redness and an increase in skin temperature. The novel feature of the model studied here is the description of the skin temperature measurements.

Due to the pivot role in the process, the administration of histamine is considered separately in the model. Suppose histamine is introduced, by superficial scratching, at the origin. A given amount of histamine is released and it is transported across the skin. The histamine transport is treated as a complex process (hereby called migration) which is probably mostly influenced by the blood perfusion within skin. As histamine migrates we assume it is additionally eliminated via first-order kinetics due to an interaction with the vessel network. The governing equation for the histamine concentration $c_H(r,t)$ is:

$$\frac{\partial c_H}{\partial t} = - v \frac{\partial c_H}{\partial r} - \gamma c_H \qquad (1)$$

where v is the histamine migration rate and γ is the elimination rate constant. The solution with a boundary condition

O. Dössel and W.C. Schlegel (Eds.): WC 2009, IFMBE Proceedings 25/XIII, pp. 120–123, 2009.
www.springerlink.com

$c_H(0,0) = c_{0H}$, representing a local introduction of histamine, is given by:

$$c_H(r,t) = c_{0H}\,\delta(t - \frac{r}{v})\exp(-\gamma\frac{r}{v}) \quad (2)$$

where δ is a Dirac delta function.

As histamine is moving across the skin, the vessel system reacts in response to local histamine level and a supplementary heat source (Q_R) is activated. The governing equation for the Q_R-c_H relationship is:

$$Q_R(r,t) = \Delta Q_O c_H(r,\frac{r}{v}) = \Delta Q_O\, c_{OH}\exp(-\gamma\frac{r}{v})) \quad (3)$$

where ΔQ_0 is the positive constant. Intuitively, we can see how the mechanism (3) can generate a skin temperature distribution. The histamine "wave" propagates with the velocity v and it exhibits a biochemical switch behavior. At point r a supplementary heat source appears after time t = r/v. The increase of heating is constant in time and is linearly related to the maximal histamine concentration at point r. Of course, there is a threshold histamine concentration (c_{TH}) to produce the heating effect. If over the region of the skin $c_H \geq c_{TH}$, then a domain of permanently nonzero values of heating is generated. We can calculate the maximal radius of the histamine-activated region given the threshold concentration c_{TH}. We want the maximum value of r (denote by R) such that $c_H = c_{TH}$. From (2) with $c_H = c_{TH}$ and t = r/v we have:

$$R = \frac{v}{\gamma}\ln(\frac{c_{OH}}{c_{TH}}) \quad (4)$$

The temperature distribution of the skin T(r,t) is given by the solution of the Pennes bio-heat equation [8]. In the model we make the approximations that the thermal diffusivity and the metabolic heat generation are neglected. Defining new variable:

$$\Delta T(r,t) = T(r,t) - T_S \quad (5)$$

where T_s is the skin temperature before examination it is possible to write equation for ΔT as:

$$\frac{d(\Delta T)}{dt} + \tau\Delta T = S \quad (6)$$

where τ and S and free parameters. The solution of (6) is:

$$\Delta T(r,t) = \frac{S(r)}{\tau}(1 - e^{-\tau t}) \quad (7)$$

Concerning modeling of the allergen action it is assumed that we are dealing with immunoglobulin E (IgE) mediated hypersensitivity [6]. A sensitization to an allergen was done some time ago. As a result, IgE antibodies occupy IgE receptors on skin mast cells, where they are ready to react promptly to the next encounter with an allergen. A subsequent exposure to an allergen, leads to cross-linking of the bound IgE molecules. The linking process, in turn, activates the mast cell and the cell releases histamine that directly generate allergic symptoms.

The overall mechanism is a conversion of the allergen, via the mast cell, into histamine consists of two steps. The first step relies on activation of mast cells. An inactivated mast cell (denoted by M_0) is activated by binding with molecules of allergen and the activated mast cells (denoted by B) are produced. Assuming that activation of the mast cells is very fast process (forward rate constant of the reaction >> 1), it follows that $B(t) \approx M_0$.

The second step of the histamine production relies on the degranulation of the activated mast cells. Suppose that the rate of degranulation of a mast cell is proportional to the amount of histamine present in the cell (radioactive decay) and that the degranulation rate is >> 1. The concentration of histamine (c_{HA}) at the origin after an allergen injection is equal to the amount of histamine accumulated in one mast cell times M_0. Therefore the solution (7) describes also the temperature distribution after an allergen injection. The difference between histamine and allergen relies on the value of constant S ($S \rightarrow S_A$).

B. Experimental procedure

24 patients were subjected to the skin prick test. Commonly used procedure was applied before and during examinations. All subjects gave informed consent before participation in the studies. Patients were allowed to adapt to room temperature for 30 minutes. The arms were placed on the special constructed table and fixed. The studies were performed using the commercial allergen panel (Allergopharma, Reinbek, Germany). The positive control was the solution of hydrochloride of histamine. A drop of the allergen was placed onto a marked area of skin. Using a sterile lancet a small prick through drop was vertically made. Thermo-camera was placed about 30 cm over the forearms.

The distributions of temperature of both forearms were acquired every 70 s from 0 up to 910 s after skin pricks. Thermograms were evaluated using the software developed in our laboratory. The first step of the calculations relies on the image subtraction according to formula (5). Next the heated region (HR) was approximated by a circle and $\Delta T(r,t)$ was determined. Assuming ΔT = experimental error (0.5^0C), the radius of the HR as a function of time was calculated. Final step of data elaboration produces $\Delta T(r,t)$ for r = constant. Fitting of the equation (7) to the histamine and

allergen data generates the parameters correlated to the temperature distribution (S, τ and S_A).

III. Results

In Fig. 1 an example of the radius of the HR after histamine injection at different time points is presented. The linear fits enable the determination of v and R parameters. The histogram of R values after histamine injection is given in Fig. 2. The performed analysis confirms the R value may

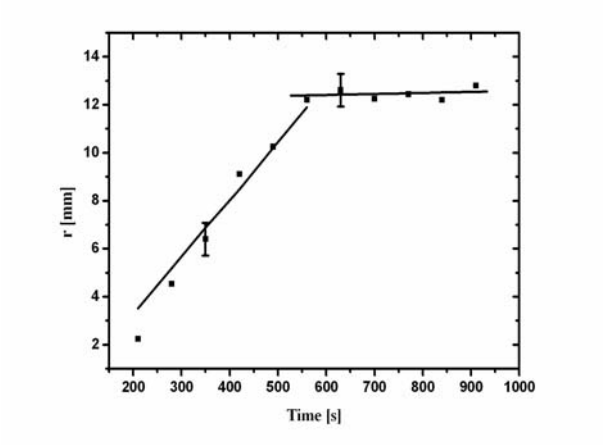

Fig. 1. The radius of the heated region at different time points. The error bars mark the experimental errors.

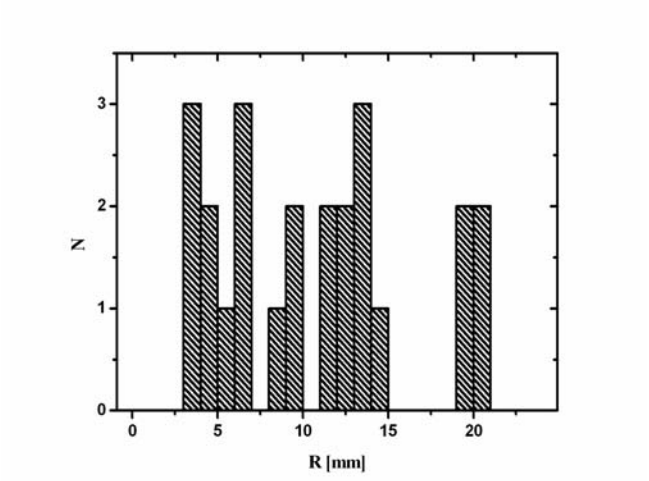

Fig. 2. The maximum radius of the heated region after histamine injection.

be treated as the best marker of organism response to histamine. Three groups of subjects are arbitrary distinguished on the basis of the histogram. The first group (GL - R < 7 mm) is characterized by a low response while for the second group (GH - 7 mm < R < 15 mm) a high response is observed. For a few cases a very high effect (GVH - R > 15 mm) is detected. It should be pointed out that we did not observe an increase of temperature after histamine injection in ~20% of patients under investigations. Such cases were excluded from further studies.

The temperature distributions after histamine and two allergens injections are presented in Fig. 3. It should be noted that the time constant τ was extracted from histamine data. Identical value was used for all allergens. It confirms that kinetics of heating is patient-dependent.

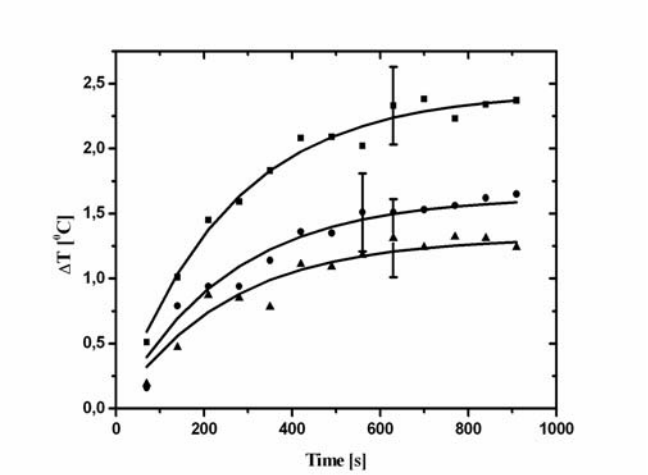

Fig. 3. Fits of the equation (7) to the experimental data. The results for histamine (■) and 2 allergens (●, ▲) are given. The error bars mark the experimental errors.

IV. Discussion

The collected results confirm unequivocally the usefulness of the TH measurements in the description of allergen-induced skin reactions. A simple model was proposed to quantify the intensity of the reactions. There are possibilities to distinguish different susceptibility to histamine as well as to measure the intensity of the allergic response. It should be emphasized that we proposed new approach to the quantification of the allergic reactions. The results reported so far [5] exploit the area of the HR or, so called, TH units (area times average rise in temperature) as markers of the allergic response.

The proposed model is the simplest description of the allergen-induced skin reactions. The skin reaction to allergens involves many patho-physiological steps which are not described in the model. For example, many inflammatory factors other than histamine are involved in the allergen-

induced reaction [6]. Additionally, diffusion process was neglected in case of histamine/allergen transport. The same pertain to the description of heating. In spite of simplifications, the model reproduces well measurement results.

It is interesting to note the different response to histamine. R values equal to 5.0±1.5 mm (mean±SD), 11.8±1.9 mm and 19.6±0.5 mm for GL, GH and GVH groups, respectively. The maximum radii of the HR correlate with S values (correlation coefficient = 0.9). The histogram of S values contains one broad peak and the separation of different groups was not possible. The precise mechanism of the reaction to histamine is not clear this time and awaits further studies.

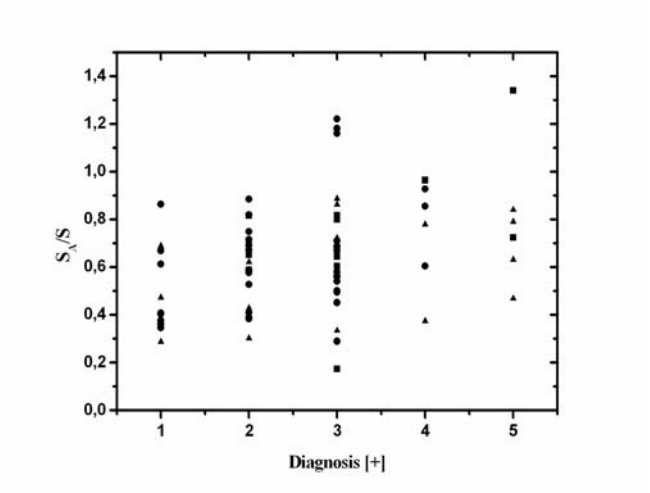

Fig. 4. The relation between classical planimetry and the model parameters. For details see text.

The comparison of the model calculations (S_A/S) with the results of the classical evaluation method is presented in Fig. 4. The surfaces affected by the reactions were determined using planimetry and were related to the size of the histamine control using a 0 to 5+ scale. The first grade of the scale (0) was not included since heating was not detected ($S = S_A = 0$). The results were presented separately for GL (■), GH (●) and GVH (▲) groups. It is clearly visible that the model calculations do not correlate well with the routine assessment. It should be noted that planimetry, although simple and fast, offers a rough estimation of the allergen response. To obtain the unequivocal verification of the reaction to allergen the IgE antibody serum level is required.

V. CONCLUSIONS

It was demonstrated that forearm thermography is non-invasive and sensitive method to study allergic response. The TH measurements supplemented by model calculations offer a new approach to quantification of allergen-induced skin reactions. The final verification of the proposed method awaits further studies of the IgE antibody serum level.

REFERENCES

1. Oppenheimer J, Nelson HS (2006) Skin testing: a survey of allergists. Ann. Allergy Asthma Immunol. 96:19-23
2. Jones BF (1998) A reappraisal of the use of infrared thermal image analysis in medicine. IEEE Transaction on Medical Imaging, 17:1019-1027
3. Larbig M, Burtin B, Martin L et al (2006) Facial thermography is a sensitive tool to determine antihistaminic activity: comparison of levocetrizine and fexofenadine. Br. J. Clin. Pharmacol. 62:158-164
4. Pabisiak K, Romanowski M, Myslak M et al (2003) Variations in temperature of the donor kidney during cold ischemia time and subsequent assessment of reperfusion using the application of thermovision camera. Transplant. Proc. 35:2157-2159
5. de Weck AL, Gluck U, Bahre M (2000) Investigation of the anti-allergic activity of azelastine on the immediate and late phase reactions to allergens and histamine using telethermography. Clin. Exp. Allergy 30:283-287
6. Goldsby RA, Kindt TJ, Osborne BA, Kuby J (2003) Immunology. W.H. Freeman & Company, New York
7. Scherer K, Grize L, Schindler C et al (2000) Reaction pattern to histamine and codeine in a human intra-dermal skin test model. Clin. Exp. Allergy 37:39-46
8. Pennes HH (1948) Analysis of tissue and arterial blood temperature in resting human forearm. J. Appl. Physiol. 2:93-122

Author: E. Rokita
Institute: Jagiellonian University Medical College Department of Biophysics
Street: Łazarza 16
City: Kraków
Country: Poland
Email: ufrokita@cyf-kr.edu.pl

Vascular Disrupting Action of Electrochemotherapy

G. Sersa, M. Cemazar, and M. Snoj

Institute of Oncology Ljubljana, Zaloska 2, SI-1000 Ljubljana, Slovenia

Abstract— **Electrochemotherapy has besides a direct cytotoxic effect on tumor cells also vascular disrupting effect. Application of electric pulses to the tumor induces transitory, but profound reduction in tumor perfusion and oxygenation of tumors. When bleomycin or cisplatin are present at the time of tissue electroporation, endothelial cells in tumor blood vessels are also affected, leading to their apoptotic death. As a consequence, blood flow in the treated tumor is abrogated, leading to extensive tumor cell necrosis and complete regression of the tumors. Therefore, electrochemotherapy can be beneficially used in treatment of bleeding metastases, as demonstrated in several reported cases.**

Keywords— **electrochemotherapy, vascular disrupting effect, bleomycin, cisplatin.**

I. Introduction

Functioning vascular supply is essential for solid tumor growth and metastasis. It is known that in the absence of angiogenesis, tumors are not able to develop beyond a few millimeters and therefore remain dormant. Angiogenic switch enables neovascularization of the tumors and consequently rapid tumor growth, metastasis and tumor progression [1]. The newly developed vessels have specific physiological and molecular features that distinguish them from normal vessels. Consequently, tumor vasculature is a specific target for tumor treatment.

There are two concepts of *vascular targeted agents* as cancer therapeutics that act on tumor blood vessels; those inhibiting the formation of new blood vessels - *anti-angiogenic agents*, and those that act on the established blood vessels - *vascular disrupting agents* [2].

II. Electrochemotherapy

Electrochemotherapy consists of chemotherapy followed by local application of electric pulses to the tumor to increase drug delivery into cells [3]. Drug uptake can be increased by electroporation for only those drugs whose transport through the plasma membrane is impeded. Among many drugs that have been tested so far, only bleomycin and cisplatin found their way from preclinical testing to clinical trials. In preclinical studies on several tumor models, electrochemotherapy either with bleomycin or cisplatin was elaborated and parameters for effective local tumor control were determined [4]. Furthermore, several clinical studies were performed, demonstrating that electrochemotherapy is effective in local tumor control of cutaneous and subcutaneous tumor nodules of different histology. So far, predominantly melanoma skin metastases were treated with ~70% long lasting complete responses of the treated nodules [5,6].

Besides membrane electroporation, which facilitates drug transport and its accumulation in the cell, other mechanisms that are involved in antitumor effectiveness of electrochemotherapy were described [4,7].

III. Tumor blood modifying effect of electric pulses

The application of electric pulses to the tissues induces a transient, but reversible reduction of blood flow. Several studies have investigated changes in tumor blood volume, perfusion and oxygenation in tumors and normal tissue after application of electric pulses. The first study, using albumin-(Gd-DTPA) contrast-enhanced magnetic resonance imaging (MRI) has demonstrated that 30 min after application of electric pulses to SA-1 tumors reduced tumor blood volume from 20% in untreated tumors to 0% in electroporated tumors [8]. Also a pharmacological study with ^{86}RbCl on the same tumor model was done, exploring time dependence of the perfusion changes. A significant reduction of tumor perfusion (~30% of control) was observed within 1 h following the application of electric pulses to the tumors. Thereafter, tumor blood flow slowly recovered, almost reaching the pretreatment level by 24 h. No change in perfusion was induced in untreated contra-lateral normal leg muscle [9].

The changes in tumor perfusion were demonstrated to correlate with changes in tumor oxygenation, as measured by electron paramagnetic resonance (EPR) technique. The maximal reduction in partial oxygen pressure (pO_2) level was observed at 2 h after the treatment (~40% of control), with recovery to the pretreatment level within 10 h after application of electric pulses to the tumor [10]. The latest

O. Dössel and W.C. Schlegel (Eds.): WC 2009, IFMBE Proceedings 25/XIII, pp. 124–127, 2009.
www.springerlink.com

study on tumors demonstrated that the changes in tumor blood flow are instantaneous, occurring during the application of electric pulses, as demonstrated by laser Doppler flowmetry [11].

In vitro studies have shown that application of electric pulses to endothelial cells resulted in a profound disruption of microfilament and microtubule cytoskeletal networks, loss of contractility, and loss of vascular endothelial cadherin formed cell-to-cell junctions immediately after electroporation, which recovered within 60 min of electroporation, without any significant loss of cell viability. The cytoskeletal effects of electroporation were paralleled by a rapid increase in endothelial monolayer permeability, indicating on putative mechanisms responsible for the observed increase in permeability and cessation of blood flow *in vivo* [12].

Tumor is a heterogeneous tissue consisting of tumor stromal cells and capillary network. When a tumor mass is exposed to an electric field that is used for electrochemotherapy, all cells in the tissue are exposed [13]. In a mathematical model it was validated whether endothelial cells in the lining of small tumor blood vessels are exposed to an electric field that can increase their permeability. The model predicted that endothelial cells lining the tumor blood vessels are even exposed to ~40% higher electric field than the surrounding tumor cells. This indicates that tumor endothelial cells are v valid target for electroporation [11].

Histological study of tumors exposed to electric pulse application examined blood vessel changes. Changes in endothelial cell shape were observed 1 h after application of electric pulses. Endothelial cells were rounded up and swollen and the lumen of blood vessels was narrowed [11].

The observed effects of tumor blood flow modification after application of electric pulses was observed also in normal muscle in mice. Similar effects on leg perfusion measured by Patent blue were observed in mice, with wide variety of electric pulse amplitudes and pulse duration (10-20 000 µs and 0.1-1.6 kV/cm) [14].

Based on all the gathered information on vascular effects of electric pulses in the tumor, a model of the sequence of changes is proposed (Fig. 1):

- Rounding up of endothelial cells due to the disruption of cytoskeletal networks.
- Increased leakage of plasma into the interstitial space.
- Increased interstitial fluid pressure and vascular resistance that lead to narrowed vascular lumen and reduced blood flow.
- The effect on endothelial cells and vascular permeability is reversible leading to restoration in tumor blood flow after 12 to 24 h.

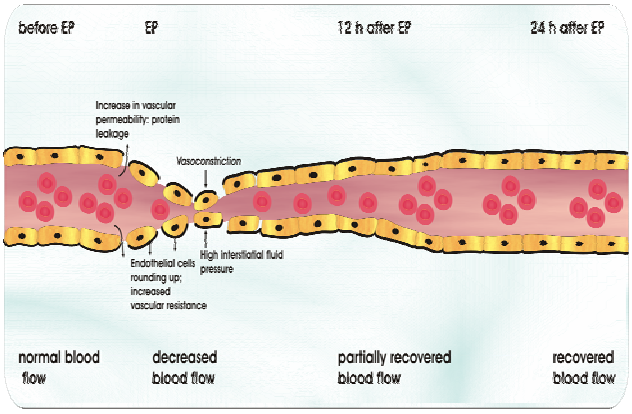

Fig. 1 Model of vascular changes in tumor blood vessels exposed to high intensity electric pulse as used in electrochemotherapy.

The studies indicate that vascular reactions induced by application of electric pulses to the tissue are important for the kinetics of the drug delivery used in electrochemotherapy or plasmid delivery in gene electrotransfer. Vascular lock causes drug entrapment by temporary cessation of tissue perfusion induced by electric pulses that leads to a prolonged exposure of the previously injected drug or plasmid DNA, as demonstrated in the case of electrochemotherapy with cisplatin [15].

IV. Tumor Blood Modifying Effect of Electrochemotherapy

Tumor blood modifying effects of electrochemotherapy, such as tumor perfusion, oxygenation and histological changes were studied in comparison to vascular changes observed after application of electric pulses [11]. Studies on electrochemotherapy with bleomycin as well as with cisplatin have demonstrated that initial changes within 2 h in tumor perfusion and oxygenation are identical to changes observed after the application of electric pulses only. Immediately after treatment, tumor perfusion in maximally reduced. Approximately 30 min later, the tumors started to reperfuse in both groups; in the tumors treated by electrochemotherapy, the reperfusion leveled at ~ 1 h and stayed at 20% up to 48 h after the treatment, whereas the tumors treated with application of electric pulses continued to reperfuse. The changes in tumor perfusion were demonstrated to be similar when using electrochemotherapy with bleomycin or electrochemotherapy with cisplatin. The degree of changes was demonstrated to be dependent on the drug dosage in electrochemotherapy; lower drug dosage resulted in lower reduction of tumor perfusion and gradual

reperfusion of the tumors, which was in all cases significantly delayed compared to perfusion changes after application of electric pulses only [10,11,16].

The perfusion changes after electrochemotherapy correlated with tumor oxygenation. EPR oxymetry demonstrated that electrochemotherapy induced instantaneous reduction in pO_2 level to ~25% of the pretreatment level, which was a more profound effect than application of electric pulses alone. The tumor oxygenation then correlated with changes after application of electric pulse up to 2 h post treatment; however, the recovery of tumor's oxygenation was much slower, returning to the pretreatment level with a delay as long as 2 days [10,11].

All these data indicate that *in vivo* electrochemotherapy, especially with bleomycin, may directly damage the vascular endothelium and account for its vascular disrupting effect. The detailed histological analysis of tumors after electrochemotherapy demonstrated that the same morphological changes in endothelial cells were found as after application of electric pulses to the tumors, endothelial cells were rounded up, and swollen, and the lumen of blood vessels was narrowed. However, at later time after electrochemotherapy (8 h) in some vessels apoptotic morphological characteristics were found. Furthermore, blood vessels were stacked with erythrocytes and extravasation of erythrocytes was also observed. Apoptotic endothelial cells were not observed in tumors treated with electric pulses alone, bleomycin alone or in the control group [11].

Based on all the gathered information on vascular effects of electrochemotherapy with bleomycin or cisplatin a model of the sequence of changes is proposed (Fig. 2) that shares initial changes with the model proposed for application of electric pulses and further changes due to the presence of chemotherapeutic drug:

- Rounding up of endothelial cells due to the disruption of cytoskeletal networks.
- Increased leakage of plasma into the interstitial space.
- Increased interstitial fluid pressure and vascular resistance that lead to narrowed vascular lumen and reduced blood flow and stacking of red blood cells.
- Apoptosis of endothelial cells due to the presence of increased amount of chemotherapeutic drug.
- Depending on the degree of the vascular disruption, no or significantly delayed vascular reperfusion is expected.

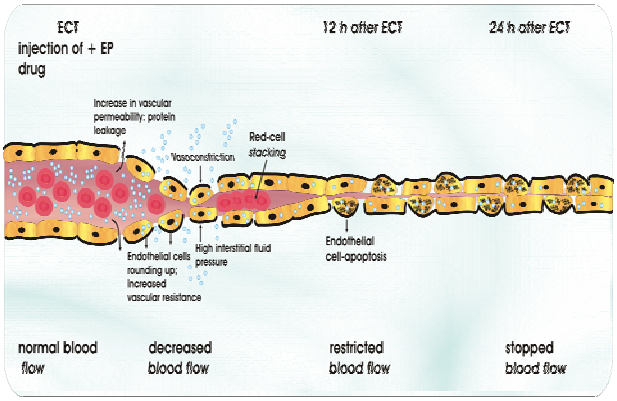

Fig. 2 Model of vascular disrupting action of electrochemotherapy.

V. Clinical Application

As hemorrhaging cutaneous metastases are a common clinical problem, several reports on successful treatment with electrochemotherapy have already been described. Kubota *et al.* revealed its palliative effect in the management of skin metastases from bladder cancer while Gehl *et al.* described two cases of successful management of bleeding melanoma skin metastases [17,18,19]. The first case established the effectiveness of electrochemotherapy in the treatment of nine bleeding, ulcerated nodules on the chest wall, with immediate cessation of bleeding after administration of electric pulses and 100% complete regression of nodules [18]. The second case demonstrated a palliative effect of electrochemotherapy in dealing with eight metastases on the head and scalp, with complete remission of all but one of the metastases (87%) [19]. Even bigger bleeding skin metastasis 3.5 x 3 cm in diameter was treated at our Institute of Oncology Ljubljana [20]. The metastasis was located on the leg and as a definitive cure was first considered amputation of the leg. Electrochemotherapy with bleomycin given intravenously was performed, and immediately after delivery of the electric pulses the bleeding stopped and did not recur. The lesion developed a crust and decreased in size in a matter of weeks. At the end of three weeks observation time, the lesion was in partial response. Therefore, electrochemotherapy represents a novel approach in the palliation of bleeding metastases.

VI. Conclusion

A comparison of the discussed treatment modalities for bleeding metastases to electrochemotherapy points to the many advantages of the latter. Regarding patients' poor physical condition it offers an excellent alternative due to its

once-only treatment strategy, high probability of immediate relief, its outpatient basis and modest patient discomfort. Currently, its main use remains restricted to palliative treatment of cutaneous and subcutaneous tumor nodules refractory to conventional treatment, but according to the presented cases, electrochemotherapy should also be considered as a modality treatment in patients with refractory bleeding tumor nodules.

Acknowledgment

The authors acknowledge the financial support from the state budget of the Slovenian Research Agency. The authors also acknowledge the help of dr. Simona Kranjc in preparation of figures.

References

1. Folkman J (1972) Anti-angiogenesis: new concept for therapy of solid tumors. Ann Surg 175:409-416
2. Siemann DW, Bibby MC, Dark GG, Dicker AP, Eskens F, Horsman MR, Marme D, LoRuso PM (2005) Differentiation and definition of vascular-targeted therapies. Clin Cancer Res 11:416-420
3. Sersa G, Miklavcic D, Cemazar M, Rudolf Z, Pucihar G, Snoj M (2008) Electrochemotherapy in treatment of tumors. EJSO 34:232-240
4. Mir LM (2006) Bases and rationale of the electrochemotherapy. EJC Suppl 4: 38-44
5. Marty M, Sersa G, Garbay JR, Gehl J, Collins CG, Snoj M, Billard V, Geertsen PF, Larkin JO, Miklavcic D, Pavlovic I, Paulin-Kosir SM, Cemazar M, Morsli N, Soden DM, Rudolf Z, Robert C, O'Sullivan GC, Mir LM (2006) Electrochemotherapy – an easy, highly effective and safe treatment of cutaneous and subcutaneous metastases: Results of ESOPE (European Standard Operating Procedures of Electrochemotherapy) study. EJC Suppl 4: 3-13
6. Quaglino P, Montera C, Osella-Abate S, Barberis M, Illengo M, Rissone M, Savoia P, Bernengo MG (2008) Electrochemotherapy with intravenous bleomycin in the local treatment of skin melanoma mestastases. Ann Surg Oncol 15:2215-2222
7. Sersa G, Cemazar M, Miklavcic D, Rudolf Z (2006) Electrochemotherapy of tumours. Radiol Oncol 40:163-174
8. Sersa G, Beravs K, Cemazar M, Miklavcic D, Demsar F (1998) Contrast enhanced MRI assessment of tumor blood volume after application of electric pulses. Electro Magnetobiol 17:299-306
9. Sersa G, Cemazar M, Parkins CS, Chaplin DJ (1999) Tumour blood flow changes induced by application of electric pulses. Eur J Cancer 35:672-677
10. Sersa G, Krzic M, Sentjurc M, Ivanusa T, Beravs K, Kotnik V, Coer A, Swartz HM, Cemazar M (2002) Reduced blood flow and oxygenation in SA-1 tumours after electrochemotherapy with cisplatin. Brit J Cancer 87:1047-1054
11. Sersa G, Jarm T, Kotnik T, Coer A, Podkrajsek M, Sentjurc M, Miklavcic D, Kadivec M, Kranjc S, Secerov A, Cemazar M (2008) Vascular disrupting action of electroporation and electrochemotherapy with bleomycin in murine sarcoma. Brit J Cancer 98:388-398
12. Kanthou C, Kranjc S, Sersa G, Tozer G, Zupanic A, Cemazar M (2006) The endothelial cytoskeleton as a target of electroporation based therapies. Mol Cancer Ther 5:3145-3152
13. Pavselj N, Miklavcic D (2008) Numerical modeling in electroporation-based biomedical applications. Radiol Oncol 42:159-168
14. Gehl J, Skovsgaard T, Mir LM (2002) Vascular reactions to in vivo electroporation: characterization and concequences for drug and gene delivery. Biochim Biophys Acta 1569:51-58
15. Cemazar M, Miklavcic D, Scancar J, Dolzan V, Golouh R, Sersa G (1999) Increased platinum accumulation in SA-1 tumor cells after in vivo electrochemotherapy with cisplatin. Brit J Cancer 79:1386-1391
16. Sersa G, Cemazar M, Miklavcic D, Chaplin DJ (1999) Tumor blood modifying effect of electrochemotherapy with bleomycin. Anticancer Res 19:4017-4022
17. Kubota Y, Mir LM, Nakada T, Sasagawa I, Suzuki H, Aoyama N (1998) Successful treatment of metastatic skin lesions with electrochemotherapy. J Urol 160:1426
18. Gehl J, Geertsen PF (2000) Efficient palliation of haemorrhaging malignant melanoma skin metastases by electrochemotherapy. Melanoma Res 10:585-589
19. Gehl J, Geertsen PF (2006) Palliation of haemorrhaging and ulcerated malignant cutaneous tumors using electrochemotherapy. EJC Suppl 4: 35-37
20. Snoj M, Cemazar M, Srnovrsnik T, Paulin Kosir S, Sersa G (2009) Limb sparing treatment of blooding melanoma recurrence by electrochemotherapy. Tumori in press

Author: Gregor Sersa,
Institute: Institute of Oncology Ljubljana
Street: Zaloska cesta 2,
City: Ljubljana
Country: Slovenia
Email: gsersa@onko-i.si

Construction of EGFP Expressing HepG2 Cell Line Using Electroporation

M. Cemazar[1], I. Hreljac[2], G.Sersa[1], and M. Filipic[2]

[1] Institute of Oncology Ljubljana/Department of Experimental Oncology, Zaloška 2, SI-1000 Ljubljana, Slovenia
[2] National Institute of Biology/Department for Genetic Toxicology and Cancer Biology, Ljubljana, Slovenia

Abstract— **The human hepatoma HepG2cell line has been extensively used as an experimental model in toxicological and pharmacological research. HepG2 cells, similar to primary hepatocytes, are difficult to transfect with traditional liposome-based methods. Electroporation is a physical method for cell transfection, where application of high voltage electric pulses is used to transiently permeabilize cell membranes allowing facilitated entry of plasmid DNA into the cells. An optimized electroporation protocol was developed for transfection of HepG2 cells stably expressing green fluorescent protein. Electric pulses of 600 V/cm yielded the highest transfection efficiency and stably transfected clones were selected after ~ 14 days incubation in selection medium. High correlation between emitted fluorescence and different cell densities were demonstrated. Such stably transfected cells HepG2-EGFP can be used for the development of rapid and simple cytotoxicity assay, that can be easily amenable for automation in high-throughput screening setups.**

Keywords— **Electroporation, HepG2 cell line, green fluorescent protein, stable transfection.**

I. Introduction

The human hepatoma HepG2cell line has been extensively used as an experimental model in toxicological and pharmacological research. With the new European legislature REACH (Registration, Evaluation and Authorisation of Chemicals; Official Journal No L 396, 2006) coming into action, and the Directive 86/609/EEC on the protection of animals used for experimental and other scientific purposes, there is an increasing need for the development of alternative toxicity tests utilizing *in vitro* models that would adequately reflect the effects of xenobiotics in living organisms. Compared to other *in vitro* cell based models for toxicity studies the advantages of HepG2 cells are their human origin, wide characterization and their retained activities of xenobiotic-metabolizing enzymes [1]. HepG2 cells, similar to primary hepatocytes, are difficult to transfect with traditional liposome-based methods. Electroporation is a technique widely used for introduction of different types of exogenous membrane-impermeable molecules into the cells *in vitro* or *in vivo*. A single electric pulse or a train of electric pulses in the range of kV/cm and at pulse duration of several microseconds causes a reversible permeabilization of plasma membrane which forms the basis of this technique [2]. Electroporation is now used routinely in many laboratories for electrotransfection due to its reproducibility and efficiency compared to other viral and chemical methods. Therefore, we optimized a method for transfection the HepG2 cells using electroporation. We constructed the HepG2-EGFP cell line, which constitutively expresses EGFP, and we showed that EGFP emitted fluorescence measured spectrofluorimetricaly on microplates correlates with the number of viable cells over a broad range of cell densities.

II. Materials and methods

A. Cell culture

HepG2 cells were a gift from Dr. Firouz Darroudi (Department of Radiation Genetics and Chemical Mutagenesis, University of Leiden, Netherlands). The cells were grown in William's medium E (Sigma, St. Louis, USA) without phenol red, containing 15% of fetal bovine serum, 2 mM L-glutamine and 100 U/ml penicillin/streptomycin at 37ºC in 5% CO_2 atmosphere.

B. Stable transfection of HepG2 cells using electroporation

HepG2 cells were trypsinized at 70% confluence and then centrifuged for 4 minutes at 200g. The cell pellet was resuspended in 125 mM saccharose in PBS buffer to a density of $2.2*10^5$ cells/µL. 20 µg of plasmid pEGFP-N1 (Clontech, Palo Alto, USA) was added per $1*10^6$ cells. A 50 µL drop containing cells and plasmid was then placed between the electrodes with 2 mm gap connected to the electroporator (developed at Faculty of Electrical Engineering, Ljubljana, Slovenia). For each electroporation, 8 square electric pulses, 50 ms long, were used. Electric field intensities were varied from 400 to 1000 V/cm, in 100 V/cm increments. After electroporation, the cells were placed in a well of a 6-well plate (Corning, New York, USA). After 5 min, 3 mL of antibiotic-free culture medium was added to the wells. 48 hours after transfection, the medium was ex-

O. Dössel and W.C. Schlegel (Eds.): WC 2009, IFMBE Proceedings 25/XIII, pp. 128–131, 2009.
www.springerlink.com

changed for complete medium with 1 mg/mL of antibiotic G418 (Sigma, St. Louis, USA). After 14 days of selection, positive clones were picked and transferred to 96 well plates. The positive clones were further grown in 400 µg/mL G418 and transferred to larger wells until they reached confluence. At that time, they were trypsinized, centrifuged and stored in liquid nitrogen.

C. Spectrofluorimetric EGFP fluorescence measurement

The cells were seeded on 96-well black plates with clear bottom (Corning, USA) and left overnight to attach. The fluorescence was measured (emission 515 nm, excitation 485 nm) after indicated time points using a microplate spectrofluorimeter (Tecan, Groedig, Austria).

D. MTT assay

MTT reduction assay [3] measures the conversion of MTT to formazan crystals by mitochondrial dehydrogenase enzymes in living cells. HepG2 cells were seeded onto 96-well microplates densities of 10000, 25000, 50000, 75000 and 100000 cells/well and left overnight to attach. MTT reagent (final concentration 0.5 mg/mL) was added and the plates and incubated (37°C, 5%CO_2) for additional 3 hours. The medium was then removed and the formazan crystals dissolved in DMSO. The optical density was measured at 590 nm (reference filter 690 nm), using a spectrofluorimeter.

III. Results

A range of different electric field intensities were tested in order to obtain efficient transfection of HepG2 cells. The lowest electric field intensities from 400 to 500 V/cm resulted in low transfection efficiency, as observed by fluorescence microscopy (Fig. 1) At 600 and 700 V/cm, the transfection efficiency were high and there were no visible signs of toxicity. High levels of toxicity were observed from 800 to 1000V/cm, with small number of fluorescent cells. Therefore, we concluded that 600 V/cm was the optimal electric filed intensity needed for transfection of HepG2 cells and was used for further experiments to prepare stably transfected HepG2 clones.

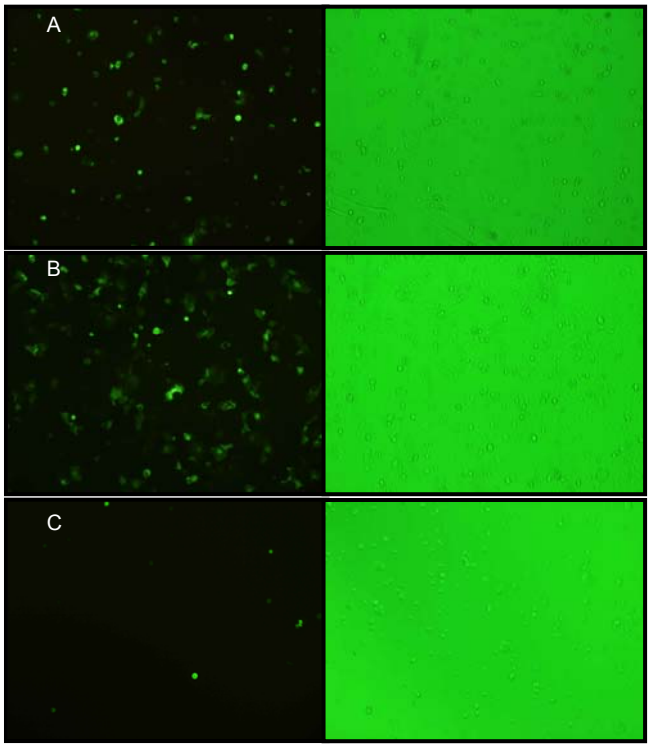

Fig. 1. HepG2 cells transfected with pEGFP-N1 6 days after electroporation. Left panel: images taken under fluorescence illumination; right panel: images taken under visible light condition (x10 objective) (**A** 400 V/cm, **B** 600 V/cm, **C** 800 V/cm).

Several samples of HepG2 cells were exposed to electric pulses of 600 V/cm and plated in selection medium to obtain stably transfected clones. Stably transfected colonies were picked and expanded up to 25 cm^2 plates. The clones with morphological differences from the parent cell line and/or changed population doubling time were discarded. Three clones were chosen for fluorescence measurements.

Clone 1 was chosen as the new cell line named HepG2-EGFP, because it showed higher fluorescence at the same cell number compared to other two clones.

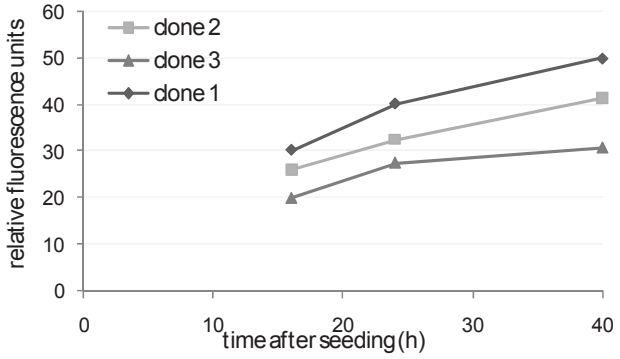

Fig. 2. Fluorescence increase with time of three stable EGFP transfected clones. Cells were seeded on a 96-well microplate at 40000 cells/well and the fluorescence was measured 16, 24 and 40 hours after seeding.

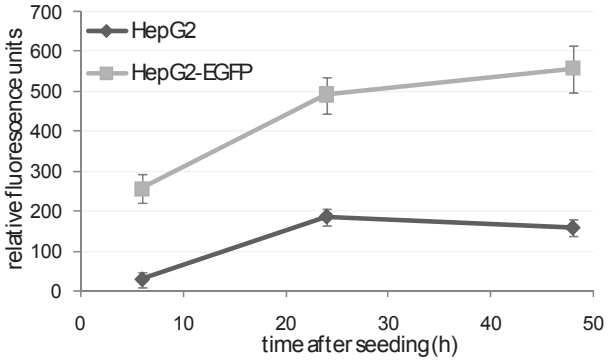

Fig. 3.Comparison of the fluorescence of HepG2 parent cell line and HepG2-EGFP stable cell line. Cells were seeded on a 96-well microplate at 40000 cells/well and the fluorescence was measured 8, 24 and 48 hours after seeding.

The background fluorescence of parental HepG2 cells grown in phenol red free medium was in the range of 30-200 relative fluorescence units. HepG2-EGFP cell line exhibits ~2.5 higher fluorescence intensity compared to parent cell line, which could be easily detected using a microplate spectrofluorimeter (Fig. 3).

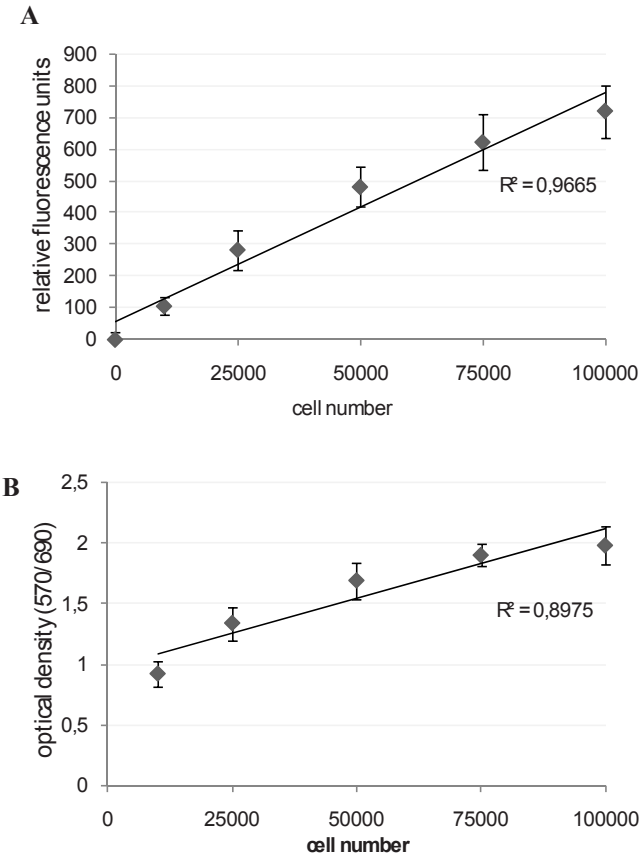

Fig. 4. Correlation between fluorescence intensity (A) or absorbance of dissolved formazan crystals (MTT assay) (B) and HepG2-EGFP cell number.

Fig. 4 shows the correlation between the cell number per well on 96-well plate and fluorescence (A) and absorbance measured with the standard MTT assay (B). Fluorescence measurement highly correlated with the cell number up to 100 000 cells per well (Fig. 4A), whereas Pearson correlation coefficient for formazan absorbance measurement was lower and a plateau was obtained at 50000 cells/well and higher (Fig. 4B).

IV. Discussion

We have optimized electroporation parameters to stably transfect human hepatoma HepG2 cells with pEGFP-N1 plasmid. HepG2 cells, which are similar to their normal counterpart hepatocytes, are difficult to transfect with standard transfection methods. Electroporation is widely used physical method for transfection of cells. Although physical parameters for effective electroporation are well defined,

due to different physiological properties of cells, the optimal parameters of electric pulses for efficient electrotransfection still need to be determined empirically. This was already demonstrated in several previous studies, where different mammalian cell lines were evaluated [4,5].

In the present study, we used electroporation for transfection of HepG2 cells with pEGFP-N1 to obtain stably transfected cells. We have obtained several highly fluorescent clones, and chose the most fluorescent one as the new cell line HepG2-EGFP. The emitted fluorescence measured on microplates correlated well with the number of cells per well over a broad range of cell densities. Several previous studies showed that decrease in the fluorescence of cells constitutively expressing EGFP can be used for cytotoxicity testing [6,7]. Compared to other cytotoxicity assays that are mostly based on measurement of general decrease of the metabolism of dying cells, such as MTT assay, or the uptake of vital dyes by dead cells, such as propidium iodide, EGFP based assay requires no addition of reagents or substrates. Because detection of fluorescence does not alter or damage the cells it permits real-time and kinetic measurements of cell death. Thus, HepG2-EGFP cells can be used for the development of rapid and simple cytotoxicity assay that can be easily amenable for automation in high-throughput screening setups.

Acknowledgment

The authors acknowledge the financial support from the state budget by the Slovenian Research Agency (project No M1-0151 and J3-9580)

References

1. Knasmuller, S., Parzefall, W., Sanyal, R., Ecker, S., Schwab, C., Uhl, M., Mersch-Sundermann, V., Williamson, G., Hietsch, G., Langer, T., Darroudi, F., and Natarajan, A. T. (1998) Use of metabolically competent human hepatoma cells for the detection of mutagens and antimutagens. Mutat Res 402: 185-202
2. Neumann E, Sowers AE, Jordan CA (1989) Electroporation and Electrofusion in Cell Biology. Plenum Press, New York and London
3. Mosmann, T. (1983) Rapid colorimetric assay for cellular growth and survival: application to proliferation and cytotoxicity assays. J Immunol Methods 65: 55-63
4. O'Hare MJ, Ormerod MG, Imrie PR, Peacock JH, Asche W (1989) Electropermeabilization and Electrosensitivity of Different Types of Mammalian Cells, in Electroporation and Electrofusion in Cell Biology, E. Neumann, AE. Sowers, CA. Jordan, eds., Plenum Press, New York and London, 319-330
5. Cemazar M, Jarm T, Miklavcic D et al (1998) Effect of electric-field intesity on electropermeabilization and electrosensitivity of various tumor-cell lines in vitro. Electro Magnetobiol 17: 261-270
6. Steff, A. M., Fortin, M., Arguin, C., and Hugo, P. (2001) Detection of a decrease in green fluorescent protein fluorescence for the monitoring of cell death: An assay amenable to high-throughput screening technologies. Cytometry 45: 237-243
7. Hellweg, C. E., Baumstark-Khan, C., and Horneck, G. (2001) Enhanced green fluorescent protein as reporter protein for biomonitoring of cytotoxic effects in mammalian cells. Analytica Chimica Acta 427, 191-199

Author: Maja Cemazar
Institute: Institute of Oncology Ljubljana
Street: Zaloska 2
City: SI-1000 Ljubljana
Country: Slovenia
Email: mcemazar@onko-i.si

Automated Laboratory of Electromagnetic Radiation for the Study of Biological Effects and Oncologic Hyperthermia

M.F.J. Cepeda, A. Vera and L. Leija

CINVESTAV-IPN Electrical Engineering Department, Bioelectronics Section, Mexico D.F., Mexico.
mcepeda@cinvestav.mx

Abstract— **The aim of this work is to describe the design and construction of an automated laboratory for electromagnetic radiation, which will be used in the study of the effects of radiation in living organisms, focusing the study in the effects of oncologic hyperthermia. For this purpose the laboratory was divided in several parts: the electromagnetic shielding system, temperature measurement using optical fiber sensors and analog signal conditioner, automated positioning temperature sensors inside the phantom, the communication and control stage using two personal computers, software for the visualization of the temperature distribution inside the phantom and the EM system.**

Keywords— **Hyperthermia, EM radiation, shielding system, automated laboratory.**

I. Introduction

Hyperthermia is a cancer treatment in which body tissue is exposed to high temperatures up to 42°C. Research has shown that high temperatures can damage and kill cancer cells, usually with minimal injury to normal tissues. Hyperthermia makes cancer cells more sensitive to radiation or harms other cancer cells that radiation cannot damage. Hyperthermia can also enhance the effects of certain anticancer drugs. Numerous clinical trials have studied hyperthermia in combination with radiation therapy and/or chemotherapy. These studies have focused on the treatment of many types of cancer, including sarcoma, melanoma, and cancers of the head and neck, brain, lung, esophagus, breast, bladder, rectum, liver, appendix and cervix [1]. Protein damage is the main molecular event underlying the biological effects of hyperthermia in the clinically relevant temperature range (39–45 ºC). The activation energies for protein denaturation and heat-induced cell death are within the same range [2]. This is the basis of the use of the hyperthermia in cancer therapies.

II. Proposed approach

The laboratory was divided in several parts: the electromagnetic shielding system, temperature measurement using optical fiber sensors and analog signal conditioner, automated positioning temperature sensors inside the phantom, the communication and control stage using two personal computers, software for the visualization of the temperature distribution inside the phantom and the EM system. Fig. 1 shows a block diagram of the system.

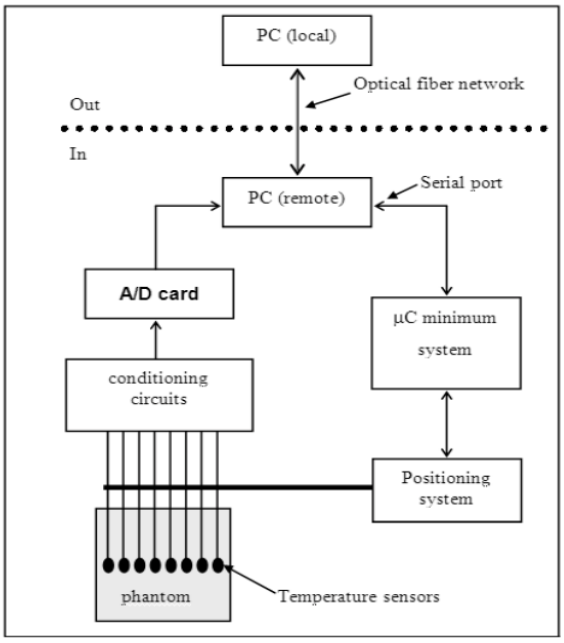

Fig. 1 Diagram of the automated laboratory. In the inner of the anechoic chamber, a PC controls the temperature sensors and the positioning system. A PC located outside the chamber for the visualization of the temperature distribution.

A. Electromagnetic Shielding system

In order to contain the Electromagnetic radiation, a Faraday Box was built. It allows have a free space of electromagnetic radiation from any external source. In addition, it delimits the space in which the radiation generated inside could act, assuring personal´s security.

In addition, the interior of Faraday's Cage is covered with microwave absorber, which allows that the radiation used on the biological material is originated only by the radiation source provided by the applicator, and not by reflections

O. Dössel and W.C. Schlegel (Eds.): WC 2009, IFMBE Proceedings 25/XIII, pp. 132–135, 2009.
www.springerlink.com

coming from metallic surfaces like the walls of the Faraday´s cage. This chamber has conductive walls and it´s geometric dimensions are Width=2.0 m, Length=2.0 m and Height=1.9 m, the inner walls of the cage are made of steel and the outer walls are made of copper, the use of both metals it´s because the steel absorbs the electromagnetic waves at low frequencies and copper those at high frequency [3]. A photograph of the created chamber is shown on Fig. 2.

Fig. 2 Anechoic chamber developed for electromagnetic radiation tests. Dimensions were width=2.0 m, length=2.0 m and height=1.9 m. The inner walls of the cage were made of steel and the outer walls were made of copper.

B. Temperature sensor and signal conditioning

Due to the refraction index wavelength dependence, we have evaluated three different wavelengths for the sensor operation (660 nm, 850 nm and 1300 nm), as well as several different types of oils, with a slightly different refraction index. For our range of interest the best results we have obtained were with vegetable oils, operating in the infrared range [4].

The sensor was fabricated using a multimode patch-cord with ST connectors on both ends, which is commercially available. First, the patch-cord is divided in halves. A 30 mm portion of jacket and plastic buffers are mechanically removed from both ends. After that, a 20 mm glass tube with an external diameter of 1.1 mm is introduced through one of the ends, and both ends of the fiber are joined together with a fusion splicer (RXS-X74). Then the fiber without buffer of this portion is treated with an acid, to remove partially the glass cladding. The acid attack is stopped when the transmitted power falls 30% from its initial value. The glass tube is then located in the central part of the fiber and is filled with the oil. Finally, both ends of the glass tube are sealed with epoxy glue. The Figure 3 shows a detailed outline of the probe described above.

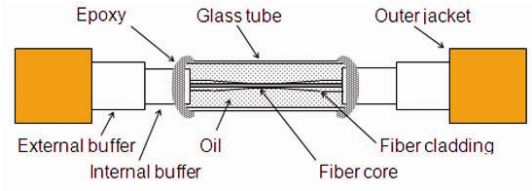

Fig. 3 Detailed outline of the constructed sensor (not in scale).

C. Positioning stage

This stage is constituted by a personal computer (PC), a microcontroller and a PC controlled automated positioning system. The PC is IBM compatible. It sends the data that correspond to a position selected by the user toward the minimum system. This PC is located inside the anechoic chamber and it is externally operated through an optical fiber communication system. The communication between the PC and the minimum system is carried out through the communications port COM1 [5].

The temperature sensors are displaced in an axis through the phantom by means of an automated positioning system. Two DC motors controlled by the minimum system by means of the feedback signal that provides an optical encoder impel this. The maximum lineal travel distance is of 35 cm, with a resolution of 2.5 mm. The physical construction of the positioning system is built on a square base of acrylic of 65 x 120 cm of external area, of 1 cm thick. Bars of Nylamid were also used for support. The used materials minimize the interaction with the electromagnetic fields that could be present. In the Fig. 4 an outline of the positioning stage is shown.

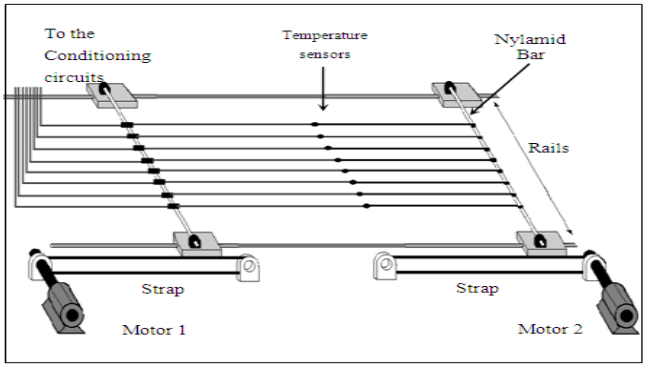

Fig. 4 Positioning stage. The square acrylic base (65 x 120 x 1 cm) contained the rails for the displacement of the sensors; the maximum lineal distance for the displacement was 35 cm.

D. Communication and control stage

The communication system is based on the use of two IBM compatible computers, one of them inside the anechoic chamber (remote) and the other one in the exterior (local). The communication among both computers was carried out through an optical fiber cable; the local PC operates the remote PC. The local PC controls all the equipment inside the chamber and captures all the acquired information.

An optical fiber based net card was used to communicate the two computers (3C905B-FX(SC), 3Com 100Base-FX). It possesses a speed of transmission of 100 Mbps. The protocol used to communicate both computers was the TCP/IP. The package used for the communication was the Remote Administrator v2.0, which allows control all the devices and programs of the remote computer from the local computer. The analog signals coming from the eight conditioning circuits were digitized by means of a 12 bits analog to digital card (Lab PC-1200 A/I, National Instruments) that is installed in the remote computer.

The communication system is based on the use of two IBM compatible computers, one of them inside the anechoic chamber (remote) and the other one in the exterior (local). The communication among both computers was carried out through an optical fiber cable; the local PC operates the remote PC. The local PC controls all the equipment inside the chamber and captures all the acquired information.

E. Visualization and control software

Software was developed in the LabWindows CVI programming language (National Instruments). By means of this software the user can control all the controllable devices that conforms the automated laboratory. Data like the radiation time and frequency, the distance between the radiator and the phantom, the quantity of temperature measurements in a plane of the phantom, the quantity of phantom mappings, sensor thermal response time, the elapsed time between each temperature mapping, among other, should be provided by the user.

Once the experiment begins, the laboratory operates automatically and allows the user to visualize the results obtained in each temperature mapping. In the Fig. 5 the main screen of the program is shown.

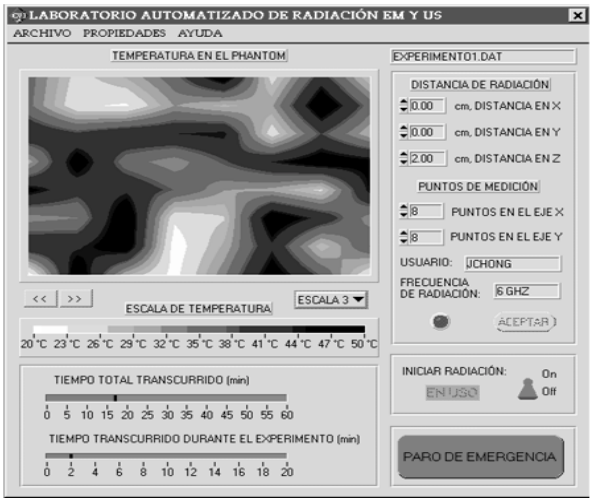

Fig. 5 Software main screen. The distribution of temperature in the phantom is shown in the window.

F. Visualization and control software

This system generated electromagnetic radiation. The radiation equipment consisted by a sweep oscillator and a power amplifier which works in the range of 1 to 3 GHz. The power level is from 1 to 50 W.

III. Results

Results are show according to each part of the system. The shielding effectiveness of the anechoic chamber is over -60 dB. Fig. 6 shows a block diagram of an emissions test system in accordance with ANSI C63.4.ANSI used to obtain the shielding effectiveness in the anechoic chamber. The test set-up is composed of a receive antenna, a first interconnecting cable, a preamplifier, a second interconnecting cable, and a radio noise meter.

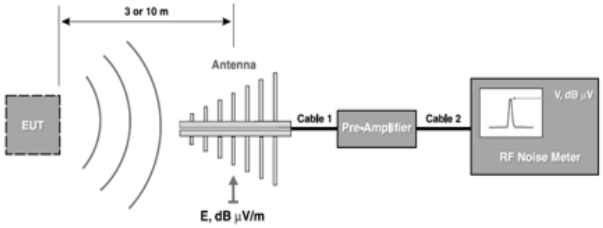

Fig. 6 Fig. 6. Diagram of an emissions test system in accordance with ANSI C63.4. The radiation in the exterior of the anechoic chamber is detected by the antenna, which sent the signal to a preamplifier. Finally the radio receptor indicated the radiation present during the exposition.

The calibration of the sensor was done using a thermostatic bath and a thermocouple thermometer with an accuracy

of 0.1°C (TES-1310). Several calibration curves in different days were taken for the sensor, as shown in Fig. 7. With these curves we evaluated the repeatability and the stability of the sensor. We also evaluated the thermal time constant of the sensor, resulting in a value of 1.9 s.

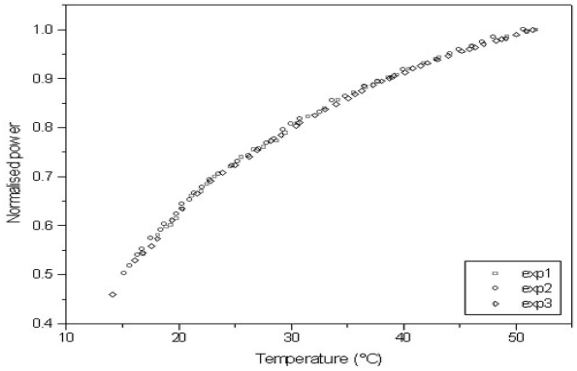

Fig. 7 Calibration curves for three experiments. The transmitted power increased with the temperature. When the oil index equals the refraction index of the cladding, the transmitted power reached a maximum value, and the curve showed a saturation effect.

As we see, the transmitted power increases with the temperature. While the temperature increases, the refraction index of the cladding decreases in a linear way. At low temperatures (below 5°C), the refraction index of the oil is higher than the refraction index of the core, and no power is transmitted through the fiber, because waveguiding conditions are not satisfied. As the refraction index decreases the power transmitted increases, due to the increasing number of guided modes in the fiber. When the oil index equals the refraction index of the cladding, the transmitted power reaches a maximum value, and the curve shows a saturation effect.

In the positioning stage, the repeatability and precision of the displacements of the positioning system, the stage of power and the signal conditioning circuits were evaluated. The developed system is able to locate the temperature sensors with 2.5 mm of spatial resolution. The system has 3 Kg of load capacity, which is more than enough for the required application.

The control and visualization software was evaluated carrying out each one of the functions for those that it was designed. Errors were not presented in the execution of the commands that the software is able to carry out.

IV. CONCLUSIONS

The system of automated positioning presented repetitive and precise movements, inside the appropriate limits for the application. The materials used for their construction did not present interferences in the electromagnetic field. In the evaluation of the capabilities of the control and visualization software, satisfactory results were obtained under operation conditions, although still left carry out validation tests according to the corresponding standards. The program introduced a user-friendly graphic interface, according to the expert's evaluation, that which facilitates the operation of this system like integral part of the hyperthermia laboratory.

REFERENCES

1. National Cancer Institute, "Hyperthermia in Cancer Treatment: Questions and Answers". Reviewed: 08/12/04, http://www.cancer.gov/
2. Dewey WC. Arrhenius relationships from the molecule and cell to the clinic. International Journal of Hyperthermia 1994;10:457–483.
3. H.W. Ott. (1988) "Noise reduction techniques in electronic systems". Ed. Wiley. pp. 166-169. USA.
4. Pennisi, C.P.A. Leija, L. Fonseca, W.H. Vera, A. (2002) Fiber optic temperature sensor for use in experimental microwave hyperthermia.
5. J. Chong, L. Leija, R. Posada, W. Fonseca, A. Vera, (2000) "Design and construction of an automated laboratory for electromagnetic and ultrasonic radiation in the study of hypertermia in biological systems". Proceedings of the 2000 Annual Fall Meeting of the Biomedical Engineering Society. Seattle, WA. Oct 11-15, 2000.

Electrically Mediated Gene Delivery to the Skin

R. Heller[1, 2], B. Ferraro[2], A. Donate[1, 2], and M.J. Jaroszeski[3]

[1] Old Dominion University, Frank Reidy Research Center for Bioelectrics, Norfolk, VA, United States
[2] University of South Florida, Department of Molecular Medicine, Tampa, FL, United States
[3] University of South Florida, Department of Chemical Engineering, Tampa, FL, United States

Abstract— **The easy accessibility of skin makes it an excellent target for gene transfer protocols. To fully take advantage of skin as a target for gene transfer, it is important to establish an efficient and reproducible delivery system. Electroporation as a tool for delivery of plasmid DNA is a strong candidate to meet these delivery criteria. Electroporation of the skin is a simple, direct, in vivo method to deliver genes for therapy. Efficient delivery to the skin can be utilized for both prophylactic and therapeutic approaches. In previous work, we evaluated delivery conditions to the skin utilizing a plasmid encoding luciferase. These studies were performed in various animal models. Most recently, the work has been performed in a guinea pig model to evaluate the potential of this approach in an animal model with skin thickness and structure similar to human. Results clearly showed that effective delivery was related to both the electrode and the parameters chosen. For delivery of DNA vaccines, a multielectrode array was utilized to deliver a plasmid encoding hepatitis b surface antigen resulted in high antibody levels. Use of this array reduced muscle twitches associated with administration of pulses. This approach was also assessed for delivery of angiogenic growth factors to the skin in areas of ischemia. For this work a 4-plate electrode was utilized with parameters for therapeutic delivery of angiogenic growth factors such as vascular endothelial growth factor (VEGF). Delivery resulted in accelerated wound healing when compared to no treatment or injection of plasmid without electroporation. These results further demonstrate that electroporation can be used to augment the efficiency of direct injection of plasmid DNA to skin and may have utility in several therapeutic applications.**

Keywords— **Skin; Electroporation; Gene Transfer; Vaccines; Wound Healing.**

I. Introduction

A critical aspect of gene transfer is effective delivery of the transgene to the appropriate target. Both biological (viral) and non-viral approaches have been evaluated. A drawback of non-viral is ineffective expression of the transferred gene. This is typically related to the inefficient delivery of the plasmid DNA [1-2]. Electrically mediated delivery (electroporation) of plasmid DNA is quickly being accepted as a viable approach to achieve effective delivery [3-5]. The versatility inherent in this delivery system is an important reason for this growth. Careful selection of tissue target and delivery parameters including electrode and electrical conditions allows an investigator to obtain the type of transgene expression necessary for a particular therapeutic application.

The skin is an excellent target for gene transfer protocols, particularly because of the easy accessibility. Cutaneous diseases can be treated directly. In addition, the skin is a suitable target for delivering expressed proteins systemically. As with any gene transfer approach it is essential to develop a reliable delivery system. Electroporation has been demonstrated to be an effective means of delivering plasmid DNA to the skin [6-18]. Several studies have shown that electroporation efficiently delivers plasmid DNA to the skin resulting in increased local and serum expression levels compared to injection alone [6-13, 17, 18]. Skin electroporation delivery was successfully performed in rodent, porcine and non-human primate model systems [7]. Electroporation as a tool for the delivery of plasmid DNA is a strong candidate to meet these delivery criteria.

II. Materials and Methods

A. Plasmids

Luciferase plasmid (gWizLuc) was obtained from Aldevron, LLC. For *in vivo* electroporation, gWizLuc suspended to 2 µg/µl in sterile injectible saline was injected intradermally. Plasmid encoding Hepatitis B surface antigen was obtained from Aldevron. The human $VEGF_{165}$ plasmid was cloned by sub-cloning the hEF1-HTLV-hVEGF165 sequence from pBLAST49-hVEGF Invivogen) into the promoterless backbone of pVAX1. For *in vivo* use, all plasmids were commercially prepared (Aldevron). Endotoxin levels were <0.1 EU/µg plasmid.

O. Dössel and W.C. Schlegel (Eds.): WC 2009, IFMBE Proceedings 25/XIII, pp. 136–139, 2009.
www.springerlink.com

B. Luciferase reporter assay

Luciferase activity was quantified as previously described [17]. Activity is expressed in total ng luciferase per tissue sample. Values represent mean and standard error.

C. Animals

Female Hartley guinea pigs (250-300 g) or 200-250 gram male Sprague Dawley rats were anesthetized in an induction chamber charged with 3% isoflurane in O_2 then fitted with a standard rodent mask and kept under general anesthesia during treatment.

D. Random skin flap model

To create a rostral-based single pedicle RSF on the left lateral flank, rats were shaved and an 8-cm by 3-cm template was traced with a surgical marker. Full thickness incisions were made along the traced template lines. The skin and subcutaneous tissue were then elevated and sutured back to its bed using simple interrupted and running stitches with 4-0 non-absorbable sutures.

III. Results

A. Intradermal delivery

Electroporation mediated delivery to the skin was previously optimized in both mouse and rat skin utilizing a specially constructed electrode containing 4 plates (4PE) arranged in a 6X6 mm square [17-18]. To reduce the sensation/pain associated with the administration of electric pulses through these electrodes another electrode configuration was developed and tested. This multielectrode array (MEA) contained 16 stainless steel electrodes configured in 4 rows of 4 electrodes with 2 mm separating each row. Intradermal delivery of gWizLUC was used to evaluate the effectiveness of this new design. Several electroporation parameters were tested and the levels of expression compared to delivery with the 4PE. The experiments were done in Sprague Dawley rats.

Results show that both electrode configurations can effectively deliver a plasmid encoding for luciferase (Table 1). While it was necessary to increase the field strength to achieve comparable expression patterns with the MEA, muscle stimulation during pulse administration was greatly reduced or eliminated when the conformable applicator was used compared to the pronounced muscle contactions seen with the 4PE and caliper electrodes. This suggests that the concept that this electrode design would reduce or eliminate potential discomfort is valid.

Table 1 Intradermal delivery of gWizLUC
48 hours after delivery the area of skin that was treated was removed, homogenized and the amount of luciferase present was quantified.

	Total pg/ Sample	SD	N
Injection only	24.3	7.8	8
MEA 100 V/cm 150 ms	369.8	111.7	8
MEA 300 V/cm 150 ms	12,630.4	6338.3	8
MEA 100 V/cm 300 ms	640.6	471.6	8
4PE 100 V/cm 150ms	6350.4	2130.2	8
4PE 200 V/cm 20 ms	13,900.3	3370.5	8

To better simulate delivery to skin of similar thickness to human skin, a second series of experiments to test the MEA were performed utilizing guinea pigs. Results are reported in Table 2. Expression in guinea pig skin was higher than that observed in rat skin. An applied field strength of 300 V/cm at a pulse width of 150 ms resulted in the highest level of expression.

Table 2 Intradermal delivery of gWizLUC to guinea pig skin
48 hours after delivery the area of skin that was treated was removed, homogenized and the amount of luciferase present was quantified.

	Total pg/ Sample	SD	N
Injection only	19.2	10.6	8
MEA 100 V/cm 150 ms	34.7	34.1	8
MEA 200 V/cm 20 ms	55.2	87.4	8
MEA 200 V/cm 150 ms	353.2	918.2	8
MEA 250 V/cm 150ms	6333.8	8627.3	8
MEA 300 V/cm 150 ms	33504.5	41060.1	8

B. Delivery of DNA vaccines

Results described above using luciferase plasmid demonstrated the utility of using the MEA for intradermal delivery of plasmid DNA. To further evaluate the utility of this electrode array, a plasmid encoding hepatitis B surface antigen was delivered. Pulses parameters that demonstrated "reasonable" and reproducible expression with the MEA (300 V/cm, 150 ms) were used to determine if an antibody response to could be induced to hepatitis B Surface antigen. Results are shown in Figure 1. There was a definite increase in antibody titers when the plasmid was delivered with electroporation compared to just injecting the plasmid.

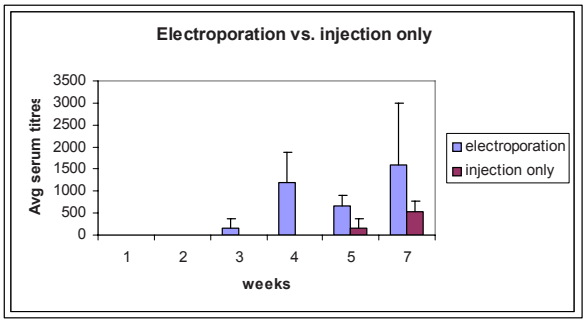

Fig. 1. Antibody titers after delivery of HepBSAg. Plasmid encoding for hepatitis B surface antigen was delivered to guinea pig skin utilizing electroporation delivery. Delivery was done on Day 0 (Prime) and then Day 14 (boost). N=3 for each group.

C. Wound healing

To further evaluate the utility of electroporation mediated plasmid delivery to the skin, delivery of a plasmid encoding vascular endothelial growth factor (pVEGF) was delivered to a random flap on the flank of a Spraque Dawley rat. Treatment was administered at 4 treatment sites along the midline of the flap at approximately 2 cm apart [19]. The treatment was administered 2 days postoperatively to allow for peak VEGF expression during the beginning of the proliferative phase of wound healing. Effective delivery of pVEGF would result in induction of angiogenesis thereby increasing perfusion to the affected area and decreasing the effects of ischemia and preventing necrosis. All animals were observed for 14 days.

Flaps were evaluated at multiple time points between 4 and 14 days. Non-surviving areas of the flap were defined as dark necrotic skin or scabbed necrotic lesions. The surviving portion of the flap was determined by subtracting the non-surviving area from the total area of the distal end of the flap. Delivery of pVEGF with electroporation increased distal flap healing at 7 days postoperatively (89.4 ± 4.3, $p < 0.05$) compared to injection of pVEGE without electroporation (56.6 ± 10.6), injection of the backbone plasmid with electroporation (59.3 ± 9.8) and no treatment (60.2 ± 9.6). The surviving area increased approximately 5 to 10% in all groups at day 14 postoperatively, but healing was still greater and more consistent in the pVEGF with electroporation group (95.2 ± 2.2) compared to pVEGF injection only (65.6 ± 9.3), backbone plasmid with electroporation (70.6 ± 7.4) and no treatment (73.5 ± 4.1) ($p < 0.01$).

IV. Conclussions

Electroporation is a powerful tool for the non-viral delivery of plasmid DNA. Efficient and effective delivery has been demonstrated in a variety of tissues and for multiple therapeutic applications [3, 20]. The first clinical trials utilizing this delivery approach for gene therapy have been initiated. The results from the first trial have been reported and have demonstrated the effectiveness of this approach [21]. Electroporation was used to deliver a plasmid encoding IL-12 to melanoma tumors. In addition to increased levels of IL-12, significant tumor regression was observed including complete regression of all lesions included treated and untreated in 2 patients [21].

We report here the use of this approach for delivering plasmid DNA to the skin. Two possible applications were explored. Enhancement of DNA vaccines and increased wound healing was demonstrated. These results support the continued evaluation of this delivery approach for both therapeutic and prophylactic applications.

Acknowledgment

Supported in part by research grants from the National Institutes of Health R21 DK055588 and R01 EB005441; from National Aeronautics and Space Association (NNJ05HE62G), from Florida Center of Excellence for Biomolecular Identification and targeted Therapeutics and by the Center for Molecular Delivery at the University of South Florida. Genetronics, Inc donated the pulse generator used in this work.

References

1. Gao, X., Kim, K.S. and Liu, D. (2007). Nonviral gene delivery: what we know and what is next. AAPS J. 23;9(1):E92-104.
2. Preuss, M.A., Curiel, D.T. Gene therapy: science fiction or reality? South Med J 100(1):101-104, 2007.
3. Heller, L.C. and Heller, R. (2006). In vivo electroporation for gene therapy. Human Gene Therapy, 17(9):890-897.
4. Favard, C., Dean, D.S. and Rols, M.P. (2007). Elecrtrotransfer as a non viral method of gene delivery. Curr Gene Ther 7(1):67-77.
5. Heller, L.C., Ugen, K.E. and Heller, R. (2005). Electroporation for targeted gene transfer. Expert Opinion in Drug Delivery, 2(2):255-268.
6. Titomirov AV, Sukharev S, Kistanova E. (1991). In vivo electroporation and stable transformation of skin cells of newborn mice by plasmid DNA. Biochim Biophys Acta, 1088: 131-4.
7. Glasspool-Malone J, Somiari S, Drabick JJ, Malone RW. (2000). Efficient nonviral cutaneous transfection. Mol Ther , 2: 140-6.

8. Drabick JJ, Glasspool-Malone J, King A, Malone RW (2001). Cutaneous transfection and immune responses to intradermal nucleic acid vaccination are significantly enhanced by in vivo electropermeabilization. Mol Ther, 3: 249-255.
9. Chesnoy S, Huang L. (2002). : Enhanced cutaneous gene delivery following intradermal injection of naked DNA in a high ionic strength solution. Mol Ther, 5: 57-62.
10. Maruyama H, Ataka K, Higuchi N, Sakamoto F, Gejyo F, Miyazaki J. (2001). Skin-targeted gene transfer using in vivo electroporation. Gene Ther, 8: 1808-12.
11. Dujardin N, Van Der SP, Preat V. (2001). Topical gene transfer into rat skin using electroporation. Pharm Res, 18: 61-66.
12. Zhang L, Nolan E, Kreitschitz S, Rabussay DP. (2002). Enhanced delivery of naked DNA to the skin by non-invasive in vivo electroporation. Biochimica et Biophysica Acta-General Subjects, 1572: 1-9.
13. Heller R, Schultz J, Lucas ML, Jaroszeski MJ, Heller LC, Gilbert RA *et al*. (2001). Intradermal delivery of interleukin-12 plasmid DNA by in vivo electroporation. DNA Cell Biol, 20: 381.
14. Medi BM, Hoselton S, Marepalli RB, Singh J. (2005). Skin targeted DNA vaccine delivery using electroporation in rabbits. I: efficacy. Int J Pharm, 294: 53-63.
15. Pavselj N, Preat V. (2005). DNA electrotransfer into the skin using a combination of one high- and one low-voltage pulse. J Control Release, 106: 407-415.
16. Babiuk S, Baca-Estrada ME, Foldvari M, Baizer L, Stout R, Storms M *et al. (2003).* Needle-free topical electroporation improves gene expression from plasmids administered in porcine skin. Mol Ther, 8: 992-998.
17. Heller LC, Jaroszeski MJ, Coppola D, Mccray AN, Hickey J, Heller R: Optimization of cutaneous electrically mediated plasmid DNA delivery using novel electrode. Gene Ther 2007, 14: 275-280.
18. Heller, L.C., Jaroszeski, M.J., Coppola, D. and Heller, R. Comparison of electrically mediated and liposome-complexed plasmid DNA delivery to the skin. Genetic Vaccines and Therapy 2008, 6:16
19. Ferraro, B., Cruz, Y.L., Coppola, D. and Heller, R. (2009). Intradermal Delivery of Plasmid $VEGF_{165}$ by Electroporation Promotes Wound Healing. Mol. Ther. Published online 24 February.
20. Bodles-Brakhop, A.M., Heller, R. and Draghia-Akli, R. (2009). Electroporation for the Delivery of DNA-based Vaccines and Immunotherapeutics: Current Clinical Developments. Mol. Ther. Published online 17 February.
21. Daud, A.I., DeConti, R.C. Andrews, S., Urbas, P., Riker, A.L., Sondak, V.K., Munster, P.N., Sullivan, D.M., Ugen, K.E., Messina, J.L., and Heller, R. First human trial of *in vivo* electroporation mediated gene transfer: safety profile and tumor regression after IL-12 plasmid delivery to metastatic melanoma patients. *Journal Clinical Oncology*, 26(36): 5896–5903, 2008.

Author: Richard Heller, Ph.D.
Institute: Old Dominion University, Frank Reidy Research Center for Bioelectrics
Street: 830 Southampton Avenue, Suite 5100
City: Norfolk, Virginia
Country: United States
Email: rheller@odu.edu

Independent Treatment Time Verification for 3D Conformational Radiotherapy with Cobalt-60 Beam Data from IAEA-TECDOC-1540

O.M. Makam Kom[1,2,3] and N. Licht[1,2]

[1] Saarland University Hospital/radiotherapy and Radiooncology, Homburg, Germany
[2] University of Douala/Centre for Atomic Molecular Physics and Quantum Optics (CEPAMOQ), Douala, Cameroon
[3] Yaounde General Hospital/Service of radiotherapy, Yaounde, Cameroon

***Abstract*— An Excel spreadsheet MU tool used at Saarland University Hospital for 6 MV and higher photon energies is presented in this study. This tool has been modified and successfully adapted for time verification of Cobalt-60 beam using input data from the IAEA-TECDOC-1540. The design and configuration of this tool is very simple and no special programming skills are needed for its implementation. With the quite good achieved accuracy level, this Excel based-program may be an alternative for commercial software and thus a very cost effective tool for radiotherapy centers in developing world where the 1.25 MV Cobalt-60 photon beam is the most used energy.**

Keywords— **Cobalt-60, TECDOC-1540, treatment time verification, 3D radiotherapy.**

I. Introduction

The main problems faces in medical physics in the developing world are the lack of technology equipment and well qualified medical physicists. Further more, the setting of medical physics training programs at the higher education and the provision of capital intensive medical equipment are of less importance and considered as an unaffordable luxury in comparison of basic needs for food, housing, basic health care and primary education.

Recognizing the fact that radiation therapy departments in the developing world make significant use of Cobalt-60 gamma ray beams, the main objective of the present work is to present a simple and nearly cost-free tool for the verification of the treatment time in 3D conformational radiotherapy.

II. Materiels and methods

A. Accuracy in the patient delivered dose

In radiation therapy, the dose delivered to the patient should be kept as close as possible to the prescribed dose. Generally, a 5% deviation is recommended. In order to fulfill this requirement, quality assurance procedures for the different stages involved in the whole process of radiation are available. One of the most important phases is the computerized treatment planification which in most cases leads to the derivation of the number of monitor units (MU or time for Cobalt units) necessary to deliver the prescribed dose. As computer technology evolves and becomes more compact, so did the treatment planning system (TPS) that should be controlled to assure the treatment quality. An independent check of MU (or time) is recommended as part of the QA of the TPS. This check can be performed either using hand calculations or one of many software packages, both homemade and commercial.

B. Independent time calculation tool

The time verification tool presented in this study has been adapted from the MU tool used at the Saarland University Hospital (SUH). It is a homemade Excel spreadsheet program (Mucheck) using lookup table of beam measurements [1, 2].

To check MU derived from ADAC Pinnacle³ (PHILIPS) using 6 MV, 15 MV and 23 MV photon energies at SUH, the following equation was implemented in an Excel spreadsheet:

$$MU = \frac{D_{presc}}{OAR \cdot OF \cdot TTF \cdot PDD \cdot \left(\frac{D}{MU}\right) \cdot \left(\frac{100+Z}{SPD}\right)^2}$$

D_{presc} is the prescribed dose; *PDD* is the percent depth dose of the calculation point for a given depth *Z* and field size; *OAR* is the off-axis ratio that accounts for changes in intensity as a function of depth and the off-axis distance in the wedge angle direction when the reference point is placed off the central axis ; *TTF* is the total transmission factor that corrects the machine output for beam modifiers such as trays and compensators; *(D/MU)* is the dose per monitor unit at the point of calibration determined in cGy/MU for each photon energy; *SPD* is the source to point distance; $[(100+Z)/SPD]^2$ is the inverse square correction factor that

O. Dössel and W.C. Schlegel (Eds.): WC 2009, IFMBE Proceedings 25/XIII, pp. 140–142, 2009.
www.springerlink.com

provides the output factor correction when non standard treatment distances are used and *OF* is the output factor for the collimator setting.

The different parameters of this equation were inserted in the Excel spreadsheet from lookup table of measured data. External functions from Excel were used to ease the data reading, their amount been so huge that a simple hand reading could not only lead to errors but was also time consuming.

In fact, the packet "XlXtrFunDistribution" contains very helpful functions for this purpose. The most useful for Mucheck was the "LookupClosetValue" function provided that for each treatment unit, all outputs factors (OF), percent depth dose and dose profile values been classified in separate spreadsheets per photon energy and per physical wedge or open beam setups. But the LookupClosestValue2D function does not interpolate between measured data. It rather returns the element in a XY-array which is at the intersection of the column which contains the closest X-Value and the row which contains the closest Y-Value. However, the intern accuracy of Mucheck could be significantly modified because the gap between measured data was very narrow.

After the implementation, a statistical study based on 404 beams from 110 individual treatment plans was performed to determine the accuracy of Mucheck. For each beam, the MU were calculated with Mucheck and compared to those computed with Pinnacle[3]. A relatively high accuracy level was achieved (94 % of beam deviations within 5%) in all treatment sites except for tangential breast fields. This was mostly due to the missing tissue effect and beam oblique incidence. A missing tissue factor [2] was derived to correct these discrepancies in such a way that the accuracies were comparable in all sites. As such, Mucheck is been used for the routine verification of MU at SUH.

The used of Mucheck for Cobalt units is straightforward provided that the beam input data of both the TPS and Mucheck been replaced with those of Cobalt-60 and the dose rate in the above-mentioned equation been given in cGy/min. But the main problem we faced was the lack of these input data. Nowadays, almost all cancer centers in developed countries used photon beams produced by linear accelerators, Cobalt units are rarely found in these centers

C. Input beam data

The TPS and Mucheck input data where taken from the recently published IAEA Technical Document (TECDOC-1540) [3] on specification and acceptance testing of TPSs. This report provides a protocol that can be follows by the manufacturers and users during the acceptance testing of new TPSs. It has been published together with a CD-ROM of input data for beam modeling and a test data package for 6 MV, 10 MV and 18 MV photon beams and gamma rays of Cobalt-60.

The input data for Cobalt-60 were measured at SSD 80 cm and 70 cm and include the following:

- *Depth dose data*
  Open beam central axis depth dose data for square field sizes from 5.3 to 36 (cm x cm) and for depths from 0 up to 30 cm.

- *Profiles*
  Open beam depth profiles data for square Fields at depths d_{max}, 5, 10, 20 and 30 cm.

- *Wedged field data*
  Depth dose and profile data from 45° wedged fields for square field sizes of 5.3, 8, 10, 12 and 15 x 20 (cm x cm) rectangular field at depths d_{max}, 5, 10, 20 and 30 cm.

- *Output factors*
  Output factors versus square and rectangular open and wedges fields. The reference conditions for the determination of these factors were: field size of 10 x 10 cm^2, a depth of 10 cm, and SSD of 70 cm.

- *Tray factor, block transmission*
  Tray and block transmission factors and machine specifications of the system where the data were measured.

III. Results and Discussion

The input data for Cobalt-60 were entered in the physics module of the SUH's TPS (ADAC Pinnacle[3] from PHILIPS) for the modeling of the 1.25 MV photon beam. After beam modeling, 35 plans of patients treated at the SUH were selected from the clinic data base. For each of these plans, a new dose trial was recomputed using the Cobalt beam. Then, the treatment time for all fields of the trial was recalculated using Mucheck and compared to the value derived from the TPS. Fig. 1 presents the frequency distribution of the time difference ($T_{Mucheck}$ - $T_{Pinnacle}$) between Mucheck and Pinnacle[3] for the 167 fields obtained from the 35 selected plans. These differences were expressed in seconds.

We have chosen to present the results in terms of time difference because percent deviations were not significantly relevant of the real accuracy. In opposition to the 6 MV and greater photon energies (where Mucheck had been proved to work very well) which perform higher dose depositions in great depths; the Cobalt-60 beam achieves depositions

only in smaller depths. Consequently a large number of fields (with smaller treatment time) must be used to obtain an acceptable dose distribution. As such, the percent deviation of a beam may be high (≥ 5 %) while the time difference remains below 3 seconds.

The average difference and the standard deviation of the data presented in Fig. 1 were -0.79 and 1.04 respectively. 98 % of the time differences were below 3 seconds which is a quite good accuracy level.

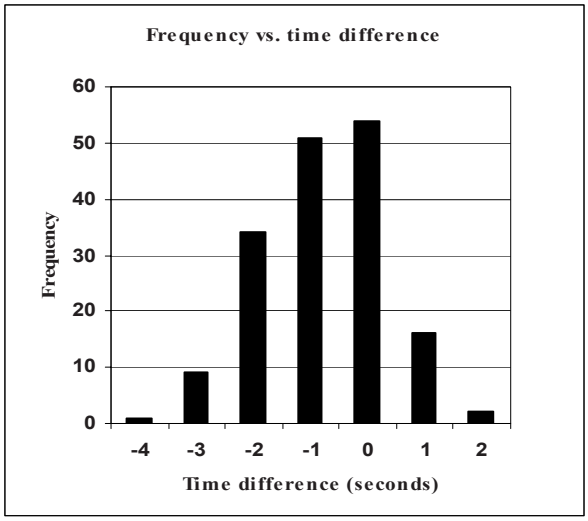

Fig. 1: Frequency distribution of time difference (in seconds) between Mucheck and Pinnacle[3] calculation.

It appears from Fig.1 that most time differences are less than or equal to zero. This can be explained by the fact that input data (percent depth dose and profile) are measured in a flat water phantom with full scatter conditions. Therefore, Mucheck underestimates the time comparatively to the TPS where the same input data are used but tissue heterogeneity and irregular body contour are taking into account by the dose engine.

IV. Conclusion

An Excel spreadsheet MU tool (Mucheck) used for 6 MV and higher energies has been presented above. This tool has been modified using input data from the IAEA-TECDOC-1540 and successfully adapted for time verification of Cobalt-60 beam. The design and configuration of this tool is very simple and no special programming skills are needed for its implementation. With the quite good achieved accuracy level, Mucheck may be an alternative for commercial software and thus a very cost effective tool for radiotherapy centers in developing world where Cobalt-60 beam is the most used energy.

Moreover the IAEA-TECDOC-1540 may be seen as a cost effective tool for developing world cancer centers and also for developed world centers because it provides a simple and straightforward protocol (with input data for beam modeling and a test data package) for the acceptance testing of new TPSs. This technical document can also be used for training purpose and intercomparison between different users.

In future works, we plan to reconfigure Mucheck with input data of the Cobalt unit at the Radiotherapy Service of the Yaounde General Hospital in Cameroon in order to implement it for routine check of the treatment time.

References

1. Makam Kom O M, Licht N et al. (2008) Evaluation of independent calculation of monitor unit for 3D conformational radiotherapy. Poster (CDROM), Annual Congres of the German Association for Medical Physics (DGMP). Oldenburg
2. Makam Kom O M, Licht N et al. (2008) Evaluation of a correction factor for MU validation in tangential breast fields. Poster (CDROM), Annual Congres of the German Association for Medical Physics (DGMP). Oldenburg
3. International Atomic Energy Agency (2007) Specifications and Acceptance Testing of Radiotherapy Treatment Planning Systems. IAEA-TECDOC-1540, IAEA. Vienna

Corresponding Author: Licht Norbert
Institute: Saarland University Hospital
Street: Kirrberger Straße
City: D-66421 Homburg (Saar)
Country: Germany
Email: norbert.licht@uks.eu

Medical Physics Education and Training in South East Asia

A.Krisanachinda[1], N.V.Hoa[2], J.C.L.Lee[3], K.H.Ng[4], A.P. Peralta[5], D.Soejoko[6], T.J.Wong[3]

[1]Faculty of Medicine, Chulalongkorn University, Bangkok, Thailand
[2]Cho Ray Hospital, HCM City, Vietnam
[3]National Cancer Centre, Singapore
[4]University of Malaya, Kuala Lumpur, Malaysia
[5]The Bureau of Health Devices and Technology, Department of Health, Manila, Philippines
[6] Physics Department, Faculty of Mathematics and Sciences, University of Indonesia Jakarta, Indonesia

Abstract - **The Association of South- East Asian Nations (ASEAN) established in 1967 comprises 10 countries located in South East Asia. Eight countries with Medical Physicists are Brunei, Indonesia, Malaysia, Myanmar, Philippines, Singapore, Thailand, and Vietnam where Cambodia and Laos have no medical physicists. The South East Asian Federation of Organizations in Medical Physics (SEAFOMP) was setup in 2000 with 5 ASEAN members and 2 members joined in 2002 and 2005. Due to the limited number of medical physicists, Myanmar, Laos and Cambodia have not been members of SEAFOMP.**

The medical physics education and training as Master of Science program in Medical Physics was started at Thailand in 1972, followed by Philippines in 1981, Malaysia in 1994, and Indonesia in 1998. Vietnam established M.Sc. in Bio-Medical Engineering in 2003. Currently, thirteen universities in South-East Asia provide medical physics education and training at different levels. The survey of the status of medical physics in South East Asia was performed at 6 countries for the level and the period of education and training, the clinical training, the total number of medical physicists, the Certification and the Accreditation.

Keywords – **SEAFOMP, Education, Training, Medical Physics, Survey.**

I. Introduction

The shortage of medical physicists has been a major problem in South East Asian Countries since 1970s. The need for medical physicists is recognized when the technology of treatment and diagnosis of the cancer and other diseases are increasing in complexity with the raising expectations of good health care as well as the implementation of radiation protection and safety standards. However, the number of medical physicists has not kept up with demand and the shortage is worsening. Therefore, the South East Asian Federation of Organizations for Medical Physics (SEAFOMP) [1] was founded during the World Congress of Medical Physics in Chicago, USA in 2000. The objectives are to promote (i) cooperation and communication between medical physics organizations in the region, (ii) medical physics and related activities in the region, (iii) the advancement in status and standard of practice of the medical physics profession, (iv) to organize and/or sponsor international and regional conferences, meetings or courses, (v) to collaborate or affiliate with other scientific organizations.

SEAFOMP has organized 7 Congresses since 2001 till 2009 at Kuala Lumpur Malaysia (2001), Bangkok Thailand (2003), Kuala Lumpur Malaysia (2004), Jakarta Indonesia (2006), Manila Philippines (2007), Ho Chi Minh City Vietnam (2008) and Chiang Mai Thailand (2009). As the International Atomic Energy Agency initiated the Regional Cooperative Agreements (RCA) RAS 6038 title "Strengthening of Medical Physics in Asia and Pacific through Education and Training" the meetings were held more often at this region. The status of medical physics in the region had been updated and informed. [2] The IAEA competency training for Radiation Oncology Medical Physicist (ROMP) was started in Thailand in 2007 and Philippines in 2008. The countries planned for ROMP training are Indonesia and Vietnam.

II. Education and Training in ASEAN Members

The survey was performed to determine the education and training with the level and the year of establishment at 6 countries. The details of information were received from 7 medical physicists in ASEAN. All of them represent SEAFOMP executive committee; some represent Asian Federation of Organizations for Medical Physics (AFOMP) executive committee and the International Organization in Medical Physics (IOMP) committee. The survey covered the following fields

2.1 List of University with Medical Physics Program or equivalent
2.2 Degree obtained
2.3 Year of establishment

III. Clinical Training for Medical Physicist

The program is aimed at both education and practical experience leading to the certification as a qualified medical physicist in some countries. The training material as well as the assessment was arranged by IAEA for the pilot countries such as Thailand, Philippines and Indonesia. The survey shows the detail of the training centers and the period of the program. The resident presentation on their research work is arranged at the AOCMP, SEACOMP or the national annual meeting of the Society. The entrance admission is exclusive required as an M.Sc. in Medical Physics, the mid-course workshop and the competency assessments are recommended by the IAEA. [3]

O. Dössel and W.C. Schlegel (Eds.): WC 2009, IFMBE Proceedings 25/XIII, pp. 143–145, 2009.
www.springerlink.com

IV. RESULTS

The result of the survey is shown in Table 1 and 2

Table 1. The Medical Physics education and training at 6 SEAFOMP members.

ASEAN Members	MP Education University/ Level/ Year of Establishment		No. of MP in country
INDONESIA	University of Indonesia (2002)	M.Sc.	40
MALAYSIA	University Science Malaysia (1994) University of Malaya (1998)	M.Sc. M.MedPhys	100
PHILIPPINES	University of Santo Tomas (1981) (2004)	M.S. (Applied Physics) M.Medical Physics	62
SINGAPORE	None at Postgraduate Level		20
THAILAND	Ramathibodi Hospital, Mahidol University.(1972) Siriraj Hospital Mahidol University (1990) Chiang Mai University .(2001) Chulalongkorn University .(2003) Khon Kaen University.(2006)	M.Sc Med.Phys M.Sc Radiol Sc. M.Sc Med Phys M.Sc Med Imaging M.Sc. Med Phys	110
VIETNAM	University of Natural Sciences at HCMC. (1985)	M.Sc Physics – Physics applied in Medicine	71

Table 2. Structured clinical training program for radiation oncology at SEAFOMP members.

ASEAN Members	Centers	Year of Establish ment
PHILIPPINES	1. Cardinal Santos Medical Center, San Juan City 2. Makati Medical Center, Makati City 3. Perpetual Help Medical Center, Paranaque City 4. St. Luke's Medical Center, Quezon City 5. University of Santo Tomas Hospital, Manila 6. The Medical City, Pasig City	2008
THAILAND	1. Ramathibodi Hospital, 2. Siriraj Hospital 3. Chulalongkorn University 4. Chiang Mai University	2007

V. CONCLUSION

Within ASEAN having a total of 403 medical physicists, there are eleven education programs in Medical Physics and relevant. Five Master of Science program in Medical Physics, (Indonesia- 1, Malaysia -1 , Thailand -3), two in Applied Physics (Philippines – 1, Vietnam -1), two Master in Medical Physics (Malaysia – 1, Philippines – 1), two Master of Science in Medical Imaging and Radiological Sciences (Thailand – 2). The period of education program varies from one to two years. The clinical training in Vietnam is equivalent to On –the –Job-Training for medical physicists. There are ten centers for IAEA competency training for Radiation Oncology Medical Physicist (Philippines – 6, Thailand – 4). The centers have been carefully selected according to the appropriate number of Clinical Supervisors, the facilities and the support from the department. The training material is supplied by IAEA. The period of training ranges from two to three years. The mid course workshop, the final assessment are planned. Certification will be offered to those who successfully complete the training and the assessment.

The situation of education, training and accreditation in medical physics in this region is variable. Indonesia plans for the IAEA radiation oncology medical physics clinical training in the couple years. Malaysia is the only SEAFOMP member established the accreditation for M.MedPhys by the Institute of Physics and Engineering in Medicine (IPEM), UK. In the Philippines, the degree is recognized by the Commission on Higher Education. Singapore is the only developed country with the established clinical training of medical physicists. The accreditation of medical physics education in Thailand is performed by the Ministry of Education.

SEAFOMP plays an important role in the cooperation among the advanced technology in this field. ASEAN College of Medical Physics was planned for the continued professional

development to the young medical physicist to be aware of the basic concepts up to the advanced technology available in this region. The survey should be repeated to map the trends in medical physics employment and to provide the data for long – term planning for the training development for medical physicists in the South- East Asian region.

Acknowledgement

The authors wish to acknowledge Dr.John Drew, Dr.Lisa Duggan, Dr.Brian Thomas and Dr.Prinath Dias for the supports on the IAEA clinical training for radiation oncology medical physicist in 2007.

References

1. Ng KH, Wong JHD. The South East Asian Federation of Organizations for Medical Physics (SEAFOMP): Its history and role in the ASEAN countries. Biomed Imaging Interv J 2008;4(2):e21

2. Kron T, Cheung KY, Dai J, Soejoko D, Inamura K, Song JY, Bold L, Srivastava R, Rodriguez L, Wong TJ, Krisanachinda A, Nguyen XC, Ng KH. Medical Physics Aspects of Cancer Care in the Asia Pacific Region. Biomed Imaging Interv J 2008; 4(3) : e33 doi: 10.2349/biij 4.3.e33

3. IAEA. Guide for the clinical training of radiation oncology medical physicists: Developed through the RCA project RAS 6038 :2009;1-216

Author: Anchali Krisanachinda
Institute: Department of Radiology Faculty of Medicine
Chulalongkorn University
Street: Rama IV Road
City: Bangkok
Country: Thailand
Email: kanchali@yahoo.com

The Assessment of Heart Rate Variability (HRV) and Task Load Index (TLI) as Physiological Markers for Physical Stress

A. Nassef [1], M. Mahfouf[1], D.A. Linkens[1], E. Elsamahy[1,] A. Roberts[2], P. Nickel[2], G.R.J. Hockey[2], and G. Panoutsos[1]

[1] Automatic Control and Systems Engineering Department, The University of Sheffield, Sheffield, UK
[2] Department of Psychology, The University of Sheffield, Sheffield, UK

Abstract—**This paper presents a new research study relating to the sensitivity of a number of psycho-physiological markers to physical workload. The workload profile was of a cyclic-loading type and the markers included the Heart Rate Variability (HRV) and the Task Load Index (TLI) as ECG and EEG representatives, respectively. These markers were smoothed to extract their trends and to study their respective correlations with the workload. The average values relating to the 'rest'-'load'-'rest' sequence showed that these markers correlate with the workload with a decrease of HRV and increase of TLI values. The effect of the amount of workload on these markers showed that HRV decreases as the workload increases and vice versa, while TLI showed that it increases as the workload increases and vice versa.**

Keywords— **Heart Rate Variability, Electroencephalogram, Signal Processing, Curve Smoothing.**

I. Introduction

Several research studies which were conducted recently and in the past have reinforced the sensitivity of the ECG markers, in terms of the HRV [1-4], as well as the EEG markers, in terms of their power activities [5-7], to mental stress. However, such markers have only been exploited in mental-task modelling [8]. The aim of this work is to investigate the sensitivity of the same psycho-physiological markers to another type of stress, i.e. the physical stress.

Hence, this paper is organized as follows: Section 2 presents a clue about the subjects' information and reviews the experimental set-up and data acquisition. However, Section 3 outlines the data analysis and Section 4 provides the mathematical calculations of the proposed stress markers. Finally, Section 5 draws the conclusions in relation to this overall study, including future research directions.

II. Experimental Setup

Subjects Data

The participants were represented by eleven (11) healthy subjects, all PhD students at the University of Sheffield. The averages ± standard deviation (SD), of the demographic data of the well-trained subjects, having approximately the same fitness levels, are shown in Table 1.

Table 1 Average and standard deviation of participants' information

	Age (years)	Weight (kg)	Height (m)
Average ± SD	26.72 ± 1.74	71 ± 11.05	1.74 ± 0.04

Hardware Setup

The experimental set up included the following equipment:

- The Cateye Ergociser EC-3700 high performance fitness bicycle for simulating physical stress;
- Two Personal computers for data capture and analyses;
- The Biosemi®/AciView data acquisition hardware for measuring the physiological EEG and ECG signals.

Data Acquisition

Each subject underwent two different sessions, taking into account the change in the physiological state of each person during the day. Consequently, the second session was arranged to be at the same time of day as in the first session.

Prior to the experiment, each volunteer was instructed:

1. Not to eat 2 hours before the session;
2. Not to expose himself/herself to any physical stress 2 hours before the experiment;
3. To wear comfortable and sufficiently large clothes.

At the experimental session, the subject was asked to sit on the bike and then all electrodes were attached. The Biosemi® system was used for collecting the EEG signals via a 32-channel head-cap while the ECG signal was acquired via 3 electrodes representing Nehb's triangle. The sampling rate was 2048 Hz. The subject was asked to pedal

O. Dössel and W.C. Schlegel (Eds.): WC 2009, IFMBE Proceedings 25/XIII, pp. 146–149, 2009.
www.springerlink.com

with a constant cadence at a speed of approximately 60 rpm when he was informed to start pedalling. The workload was in the form of seven (7) cyclic-loading steps (stepwise increment/decrement) and lasted for 21 min preceded and followed by 5-min rest periods. Each workload step lasts for 3 min to achieve the hear-rate (HR) entrainment.

III. Data analysis

The EEG and ECG signals were analysed via the "Brain Vision Analyzer©" software for 9 out of the 11 subjects due to data corruption of 2 subjects.

EEG Signals Data Analysis

The EEG electrodes were referenced to the mastoids and the signals were then filtered using high and low pass filters having cut-off frequencies of 1.6 and 50 Hz, respectively. The adequate channels such as Fz, Pz, AFz, CPz and POz were selected and the whole signals were partitioned into 2-s segments. The ocular correction to remove artifacts due to eye movements [9] was applied. Finally, the power spectra using Fast Fourier Transform (FFT) of the signals and extracting a specific range for quantifying the α (alpha) and the θ (theta) activities were performed.

ECG Signals Data Analysis

The ECG data were extracted from the Nehb's triangle (LL, LA, and RA signals) as shown in Fig. 1, using the following formula:

$$ECG = LL - LA \tag{1}$$

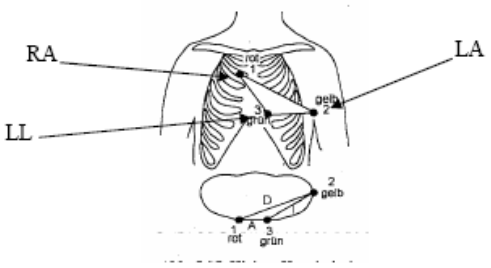

Fig. 1 The ECG electrodes sites on the body (Nehb's triangle)

The ECG signal was then filtered using a low-pass filter with cut-off frequency of 5 Hz. The R-peak in the signal was triggered by level indicator (1 mV) and time-stamped by a marker. Time-stamps were exported to separate files and the instantaneous heart rate (HR) and the 0.1 Hz component of the HRV were calculated using the LabVIEW© (National Instruments, USA) as [4].

IV. Markers to physical stress

Heart Rate Variability (HRV) Indicators

The HRV can be represented by two types of indicators, HRV1 and HRV2. On the one hand, HRV1 defines the heart-rate-variability factor which represents the 0.1 Hz component of the HR signal. Therefore, HRV1 is calculated by averaging the power spectrum of the HR signal collected within a period of 128 s in the frequency range from 0.07 Hz to 0.14 Hz [4]. On the other hand, HRV2 is considered as the ratio between the standard deviation over the mean value of the HR signal within the same 128-s period.

Task Load Index (TLI) Indicators

The Task load index (TLI) is the so called engagement-index and is defined by two formulas, TLI1 and TLI2. However, these indices were calculated as follows:

$$TLI_1 = \frac{P_{\theta,Fz}}{P_{\alpha,Pz}} \tag{2}$$

$$TLI_2 = \frac{P_{\theta,AF_z}}{P_{\alpha,CP_zPO_z}} \tag{3}$$

where P_θ and P_α denote the theta- and alpha-band power, respectively. $P_{\theta,Fz}$ and $P_{\theta,AFz}$ are the theta activities of Fz and AFz electrodes respectively. The θ (theta) activity was calculated by averaging the power spectrum of the θ frequency range (4-7.5 Hz). Similarly, $P_{\alpha,Pz}$ and $P_{\alpha,CPzPOz}$ are the α (alpha) activities of Pz and the pool of CPz and POz electrodes, respectively. The α activity was calculated by averaging the power spectrum of the α frequency range (8-12.5) [6, 7].

The resulting signals are shown in Fig. 2. The first 128 s data values of the HRV indicators were ignored because of their unreliability due to the moving-average calculations.

The signals' trends were used instead of the raw data to represent the HRV and TLI indicators. Therefore, a curve smoothing algorithm (see equation (4)) developed by Moon [10] was applied to the raw HRV and TLI data with 50 and 500 iterations, respectively.

$$y_n = \sum_{j=1}^{7} \lambda_j x_{n+j} - 4 \tag{4}$$

where x is the original signal, y is the smoothed signal, $\lambda_1 = \lambda_7 = 1/380$; $\lambda_2 = \lambda_6 = 16/380$; $\lambda_3 = \lambda_5 = 77/380$; $\lambda_4 = 192/380$, and n is the current sample index.

The resulting smoothed signals from 'Session 1' relating to subject 'P01' are shown in Fig. 3.

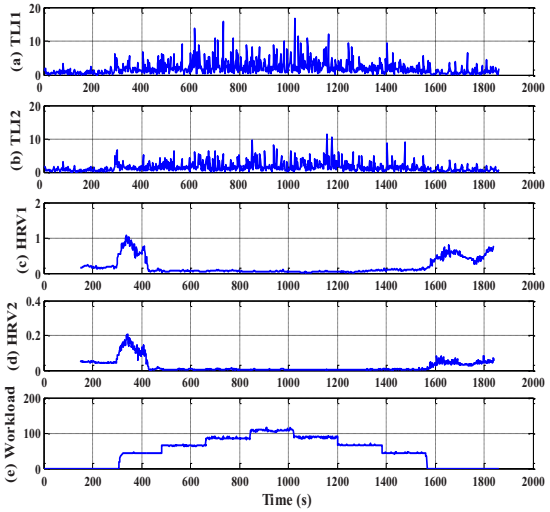

Fig. 2 The raw data of the psycho-physiological markers to a physical cyclic-loading.

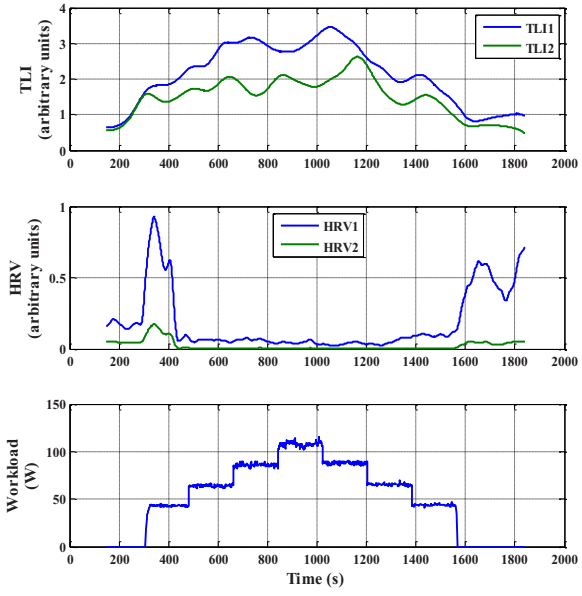

Fig. 3 The smoothed TLI1 & TLI2 (top Figure) and HRV1 & HRV2 (middle Figure) due to cyclic-loading physical workload (bottom Figure).

Fig. 3 shows that the TLI markers correlate and proportional to the workload, while the HRV markers are positively correlate and inversely proportional to the workload. Moreover, the HRV indicators have relatively high differentiation values at the On-set and the Off-set of the load.

The average values of the proposed 4 indicators were calculated for the 3 consecutive periods of the experiment ('rest', 'load', and 'rest'). Fig. 4 shows the plots of these values of all markers for 9 subjects (left column) and the total average of each marker (right column) of 'Sessions 1'.

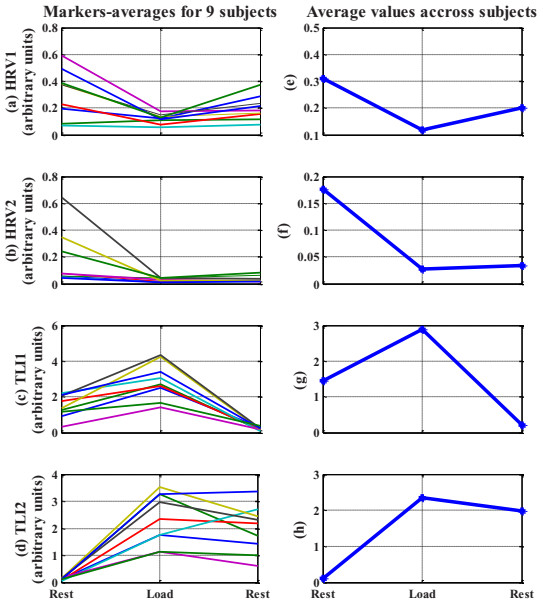

Fig. 4 The mean values of the physiological variables of the 9 subjects' data during the consecutive 'rest', 'load', and 'rest' periods for 'Session 1' data (left column); the averages across subjects.

From Fig. 4, it can be noticed that, as far as the average is concerned, HRV1 and TLI1 have a higher correlation with the physical workload over their corresponding HRV2 and TLI2 values, respectively. Furthermore, the HRV indicators have higher values during the 'rest' period just before the workload than the 'rest' period just after the workload. The average value for TLI1 during the 'rest' period just before the workload is higher than its corresponding value during the 'rest' period just after the load is released. However, the reverse can be said of TLI2.

Influence of Workload Amount on the Psycho-physiological Markers

The study was extended to investigate the influence of the amount of physical workload on the proposed indicators during the 'load' period only. The results reinforced the previous findings that HRV1 and TLI1 are highly correlated with the workload than HRV2 and TLI2, respectively as illustrated in Fig. 5

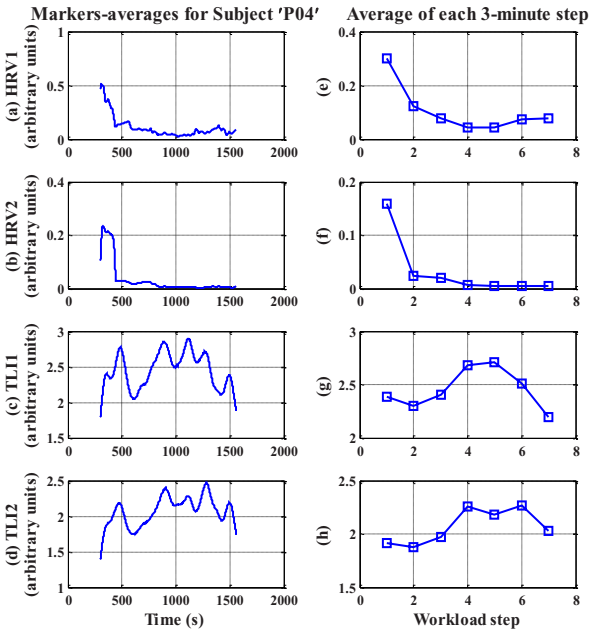

Fig. 5 The smoothed psycho-physiological variables of 'Session 2' data relating to the 'load' period for Subject 'P04' (left column); the corresponding 3-minute periods' averages (right column); each workload step corresponds to 3 minutes.

V. CONCLUSIONS

This paper addressed the results of a research study which relates to the sensitivity of EEG and ECG psycho-physiological markers to physical workload. The workload profile was a cyclic-loading and the markers were HRV (HRV1 and HRV2) and TLI (TLI1 and TLI2). The HRV1 and the TLI1 provided high correlation values to the workload. In conclusion, HRV1 and TLI1 can indeed be used as markers for physical workload to be exploited for future successful investigations. These markers can also be used in collaboration with the mental stress markers to discriminate between different stress types.

ACKNOWLEDGEMENT

All authors wish to acknowledge financial support from the UK-EPSRC under Grant GR/S66985/01. They also wish to thank Dr. J. Zhang for his help in collecting data. A. Nassef wishes to thank the Faculty of Engineering, Tanta University (Egypt) for its financial support.

REFERENCES

1. Bernardi, L., Wdowczyk-Szulc, J., Valenti, C., et al., (2000) "Effects of controlled breathing, mental activity and mental stress with or without verbalization on heart rate variability," Journal of the American College of Cardiology **35**, pp. 1462-1469.
2. Hjortskov, N., Risse´, D., Blangsted, A. K., et al., (2004) "The effect of mental stress on heart rate variability and blood pressure during computer work," Eur J Appl Physiol **92**, pp. 84–89.
3. Miyake, S., (1997) "Factors influencing mental workload indexes," J UOEH **19**, pp. 313-325.
4. Nickel, P. and Nachreiner, F., (2003) "Sensitivity and diagnosticity of the 0.1-Hz component of heart rate variability as an indicator of mental workload," Humman Factors **45**, pp. 575-590.
5. Gevins, A., Smith, M. E., McEvoy, L., et al., (1997) "High-resolution EEG Mapping of Cortical," Cereb. Cortex **7**, pp. 374–385.
6. Nickel, P., Hockey, G. R. J., Roberts, A. C., et al., presented at the International Ergonomics Association Conference, 2006.
7. Nickel, P., Roberts, A. C. and Hockey, R. J., "Assessment of high risk operator functional state markers in dynamic systems – preliminary results and implications," in *Developments in Human Factors in Transportation, Design, and Evaluation,* edited by D. d. Waard, K. A. Brookhuis and A. Toffetti (Shaker Publishing BV, Maartenslaan, 2006).
8. Nassef, A., Ting, C. H., Mahfouf, M., et al., (2008) A New Framework for Real-Time Adaptive Fuzzy Monitoring and Control For Humans Under Psychophysiological Stress, BIOSIGNALS 2008, International Conference on Bio-inspired Systems and Signal Processing, Funchal, Madeira - Portugal, 2008 of Conference, pp. 320-325.
9. Gratton, G., Coles, M. G. H. and Donchin, E., (1983) "A New Method for Off-Line Removal of Ocular Artifact," Electroencephalogr. Clin. Neurophysiol. **55**, pp. 468-484.
10. Moon, B. S., (1998) "A curve smoothing method by using fuzzy sets," Fuzzy Sets and Systems **96**, pp. 353-358.

Corresponding author:

Author: M. Mahfouf
Institute: Automatic Control & Systems Engineering Department, University of Sheffield.
Street: Mappin Street,
City: Sheffield,
Country: United Kingdom.
Email: m.mahfouf@sheffield.ac.uk

Method for treatment planning of tissue ablation by irreversible electroporation

A. Zupanic[1], D. Miklavcic[1]

[1] University of Ljubljana/Faculty of Electrical Engineering, Laboratory of Biocybernetics, Ljubljana, Slovenia

Abstract— **Irreversible electroporation has in recent years emerged as a promising new tissue ablation method. Successful tissue ablation by irreversible electroporation requires that the entire target tissue volume is subjected to a sufficiently high electric field, while the electric field in the surrounding healthy tissue is as low as possible to prevent damage. Both can be achieved by appropriate positioning of the electrodes and appropriate choice of electric parameters. We used a 3D finite element numerical models and a genetic optimization algorithm to determine the optimum electrode positioning and optimum amplitude of electric pulses for ablation of a realistic subcutaneous tumor model that was acquired from medical images. The calculated optimum treatment parameters predicted adequate electric field distribution in the whole tumor volume and minimal damage to the adjacent organ at risk. Our treatment planning method could be a useful tool in the clinical electroporation-based tissue ablation, e.g. treatment of cancer.**

Keywords— **Irreversible electroporation, Treatment planning, Optimization, Genetic algorithm, Finite element method.**

I. Introduction

Electroporation, a phenomenon in which high-voltage electric pulses applied to biological cells cause an increase in the exposed cell membrane permeabilization, has in recent years become increasingly popular in various biomedical and medical applications. In cancer treatment two different modes of electroporation are used. Electrochemotherapy uses reversible electroporation, which transiently permeabilizes the affected cell membranes and thus enables more efficient uptake of cytotoxic drugs, such as bleomycin or cisplatin, that eventually kill the cancer cells [1,2]. On the contrary, tissue ablation by irreversible electroporation does not require use of additional drugs, as it uses a higher number electric pulses of higher voltages that kill the affected cells directly [3,4]. These pulses permanently permeabilize the cell membrane or to the extent that it cannot recover. What distinguishes irreversible electroporation from other cancer ablation techniques is its non-thermal nature and a very sharp delineation between treated and untreated tissue [5].

Both electroporation-based treatments are local and depend on the effects of a physical modality; it is the local electric field distribution determines the extent of affected tissue. As such, both treatments have a lot in common with yet another cancer treatment – radiation therapy, which owes much of its success to highly sophisticated treatment planning procedures that are based on numerical calculations of Compton scattering in 3D anatomical models constructed from patient medical images [6]. Treatment planning enables oncologists to target the tumor volume and cause the least possible damage to surrounding healthy tissue. The same, in principle, can also be achieved in electroporation-based cancer treatment. Treatment planning can provide oncologists with electrode positions and amplitudes of electric pulses that result in adequate electric field distribution in and around the tumor, thus killing all cancer cells and minimizing damage to healthy tissue [7].

In this paper we present a method for treatment planning of tissue ablation of irreversible electroporation and demonstrate its use on a hypothetical case of a subcutaneous tumor. The model that we developed took into account the latest measurements of the irreversible electroporation thresholds and changes in tissue electric properties during application of electric pulses. The optimization criteria used in the treatment planning procedure were based on the electric field distribution in and around the targeted tissue.

II. Methods

A. Tissue properties and model geometry

Our model of a subcutaneous tumor consisted of three tissues, the target tumor tissue, the geometry of which was taken from Sel et al. [8], adjacent organ at risk - a sphere with diameter of 2 cm, and surrounding healthy tissue (Fig. 1). All tissues were considered isotropic and homogeneous, the assigned conductivity values being 0.4 S/m for the tumor and 0.2 S/m for the healthy tissue and organ at risk. The conductivity values were chosen in accordance with previous measurements of tumor and tissue conductivity and models of subcutaneous tumor and skin electropermeabilization [9]. The electric field distribution was calculated for an array of three needle electrode pairs (same distances between all three pairs) that has been used before in electrochemotherapy [10].

O. Dössel and W.C. Schlegel (Eds.): WC 2009, IFMBE Proceedings 25/XIII, pp. 150–153, 2009.
www.springerlink.com

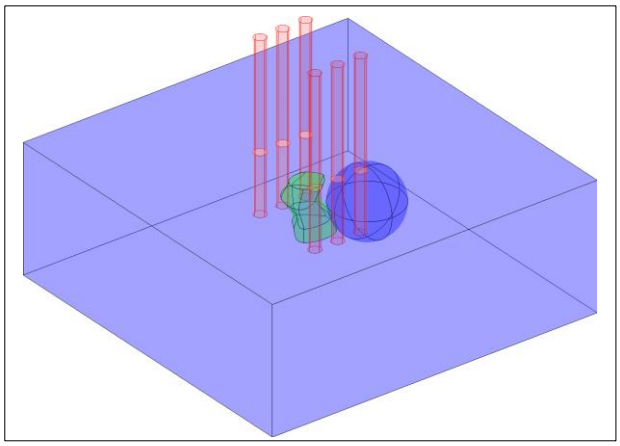

Fig. 1 Model geometry. Healthy tissue, tumor, organ at risk (sphere), needle electrodes. Electrodes are inserted into healthy tissue around the tumor and appropriate electric potentials are assigned to each electrode so that the entire tumor volume and the least possible volume of the organ at risk is irreversibly electroporated.

B. Numerical modeling

All numerical calculations were performed with a commercial finite element software package COMSOL Multiphysics 3.5 (COMSOL AB, Sweden) and run on a desktop PC (Windows XP, 3.0 GHz Pentium 4, 4 GB RAM). Electric field distribution in the tissue, caused by an electric pulse, was determined by solving the Laplace equation for static electric currents:

$$-\nabla\cdot(\sigma\cdot\nabla\varphi)=0 \tag{1}$$

where σ and φ stand for electric conductivity of the tissue and electric potential, respectively. The boundary conditions used in our calculations were a constant potential on the surface of the electrodes and electric insulation on all outer boundaries of the model. Results were controlled for numerical errors by increasing the size of our model and mesh density, until a further increase had little effect on the result. Irreversible electroporation threshold E_{irrev} of 800 V/cm for all tissues was taken from literature [5]. Changes in bulk conductivity during electroporation were taken into account by using a sequential model of electroporation previously developed and is described in detail in [11] and [12].

C. Optimization algorithm

The genetic algorithm [13] was written in MATLAB 2007a (Mathworks, USA) and was run together with the numerical calculation using the link between MATLAB and COMSOL. Optimization was run for the following six parameters: distance between both rows of electrodes (Fig. 1), distance between electrodes in a row, depth of electrode insertion (all electrodes inserted equally deep) x and y coordinates of the electrode array central point and the voltage between rows of electrodes. The initial population of chromosomes was generated randomly, taking into account the following model constraints: range of distances between electrodes, range of depth of electrode insertion into tissue and range of voltages between the electrodes. These constraints were chosen so that the calculation domain size, COMSOL meshing capabilities and oncology experts' demands for a safety margin [14], when treating solid tumors, were all respected. Chromosomes for reproduction were selected proportionally to their fitness, according to the fitness function:

$$F=100\cdot V_T-10\cdot V_O-V_H, \tag{2}$$

where F stands for fitness, while V_T, V_O and V_H stand for tumor, organ at risk and healthy tissue volumes subjected to the local electric field above E_{irrev}, respectively. The weights in the fitness function were set with respect to the importance of individual parameters for efficient irreversible electroporation. Namely, tumor ablation represented by V_T is crucial for efficient irreversible electroporation; therefore its weight is larger (100) than the weight damage to organ at risk - V_O (10), which was in turn larger than the weight of damage to other healthy tissue - V_H.

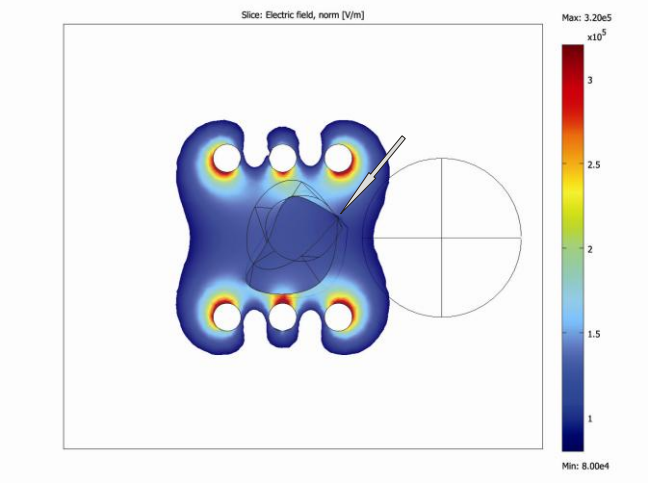

Fig. 2 Local electric field distribution of the final treatment plan is shown in the XY plane through the center of the tumor. White arrow marks part of the tumor, where electric field is barely over irreversible electroporation threshold (800 V/cm). False color legend ranges from 800 V/cm to the maximum electric field strength of 3300 V/cm achieved around the electrodes.

The selected chromosomes reproduced by cross-over or mutation. The genetic algorithm was terminated after 100 generations, when the fitness of the highest ranking solution usually reached a plateau. The algorithm always converged to an optimum solution. Average computation time of the algorithm was four hours.

III. Results and Discussion

The aim of our study was to provide a treatment plan for tumor ablation by irreversible electroporation, i.e. the electrode positioning around the tumor and applied electric pulse amplitude. Our approach of using numerical modeling together with the genetic algorithm optimization resulted in complete coverage of the tumor with a sufficiently high ($E > E_{irrev}$) electric field, while damage to the adjacent organ at risk was minimized.

The final treatment plan is presented in Figs. 2 and 3. We can see that the electric field distribution around the tumor is rather homogeneous (Fig. 2); the field is very high only very close to the electrodes and just above the E_{irrev} inside the tumor. Electric field is quite high in the part of the organ at risk closest to the tumor – all in all E_{irrev} is exceeded in 2.4 % of the organ at risk.

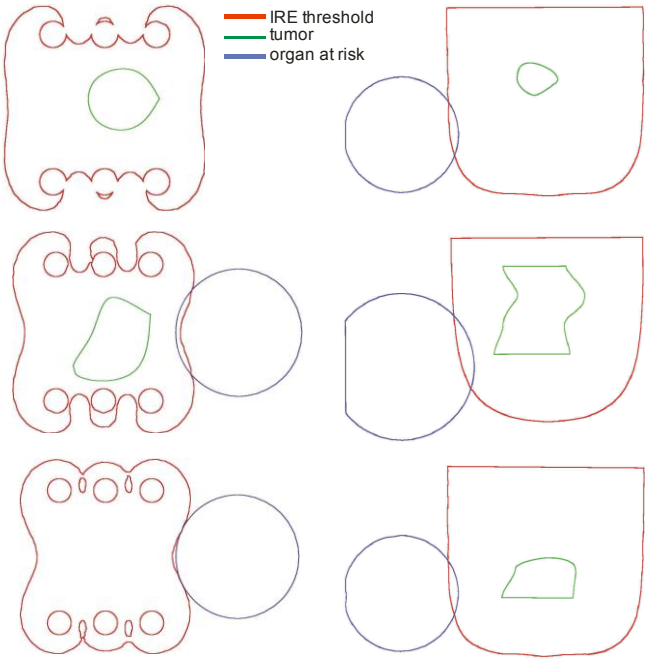

Fig. 3 Target tissue, organ at risk and achieved irreversible electroporation are presented as contours in the XY plane (left) at three different depths (top: 8 mm; middle: 23 mm; bottom: 38 mm) and in the XZ plane (right) at three different cross-sections (middle: tumor center; top and bottom: 1.2 mm from tumor center).

At a first glance it seems that the electric field exceeds E_{irrev} in a large volume outside the target tissue and that the treatment planning algorithm should give better results. The obvious change to improve the result would be to put the electrodes more to the left, so that less of the organ at risk gets affected. Unfortunately, this does not work (data not shown). Moving the electrodes further left causes the electric field on the edge of the tumor (Fig. 2) to fall below E_{irrev} – as a result the potential on the electrodes has to be increased so that the whole tumor volume is covered, but this in turn increases the affected volume of the organ at risk.

Other weight values that kept a similar ratio gave similar results.

Usefulness of numerical modeling in predicting electroporation outcomes has already been demonstrated [15,16]. We examined whether combining existing electroporation models with an optimization algorithm could provide a reliable treatment planning method for irreversible electroporation. We chose the genetic algorithm as an optimization method, since different linear and non-linear constraints, such as technical limitations of high-voltage electric pulse generator (maximum output voltage and current) can be easily taken into account. Genetic algorithm also allows optimization of a large number of continuous, discrete and categorical parameters, e.g. type of electrodes, and can give as result many solutions of similar quality that can nevertheless be topologically very different. This gives the treating physician more alternatives for the positioning of electrodes, which can be very useful. The major drawback of genetic algorithm is a relatively long computation time. However, since it can be considerably shortened by using a more powerful computer or by making the optimization parameters discrete instead of continuous, we do not consider this to be a significant issue and believe that the approach is well suited to the problem being addressed.

Even though our algorithm gives good results, several challenges remain to be addressed before it can be used for treatment planning in irreversible electroporation. In this study we did not take into account the possibility of several consecutive pulses being used, of changing the electric field orientation or of moving the electrodes during treatment of a larger tumor; all of these option have to be considered in the future [17]. Another necessary development missing at this time would be an algorithm that converts medical images of the treatment area into 3D structures ready to be imported into numerical modeling software.

IV. Conclusions

We demonstrated that numerical modeling and optimization procedure can be efficiently combined for treatment planning of tissue ablation by irreversible electroporation on an example of a tumor by providing the optimum electrode positions and amplitude of electric pulses. Our algorithm is a step forward to effective treatment planning, not only in irreversible electroporation, but also in other electroporation-based clinical treatments.

Acknowledgment

This research was supported by the Slovenian Research Agency.

References

1. Mir LM, Glass LF, Sersa G et al. (1998) Effective treatment of cutaneous and subcutaneous malignant tumours by electrochemotherapy. Brit J Cancer 77: 2336-2342
2. Sersa G, Cemazar M, Miklavcic D et al. (2006) Electrochemotherapy of tumours. Radiol & Oncol 40: 163-174
3. Rubinsky B, Onik G, Mikus P (2007) Irreversible electroporation: A new ablation modality – Clinical implications. Technol Cancer Res Treat 6: 37-48
4. Onik G, Mikus P, Rubinsky B (2007) Irreversible electroporation: Implications for prostate ablation. Technol Cancer Res Treat 6: 295-300
5. Davalos RV, Mir LM, Rubinsky B (2005) Tissue ablation with irreversible electroporation. Ann Biomed Eng 33: 223-231 DOI 10.1007/s10439-005-8981-8
6. Bortfeld T (2006) IMRT: a review and preview. Phys Med Biol 51: R363-R379 DOI 10.1088/0031-9155/51/13/R21
7. Corovic S, Zupanic A, Miklavcic D (2008) Numerical modeling and optimization of electric field distribution in subcutaneous tumor treated with electrochemotherapy using needle electrodes. IEEE Trans Plasma Sci 36: 1665-1672 DOI 10.1109/TPS.2008.2000996
8. Sel D, Lebar AM, Miklavcic D (2007) Feasibility of employing model-based optimization of pulse amplitude and electrode distance for effective tumor electropermeabilization. IEEE Trans Biomed Eng 54**:** 773-781 DOI 10.1109/TBME.2006.889196
9. Pavselj N, Bregar Z, Cukjati D (2005) The course of tissue permeabilization studied on a mathematical model of a subcutaneous tumor in small animals. IEEE Trans Biomed Eng 52: 1373-1381 DOI 10.1109/TBME.2005.851524
10. Marty M, Sersa G, Garbay JR et al. (2006) Electrochemotherapy - An easy, highly effective and safe treatment of cutaneous and subcutaneous metastases: Results of ESOPE (European Standard Operating Procedures of Electrochemotherapy) study. Eur J Cancer Suppl 4: 3-13 DOI 10.1016/j.ejcsup.2006.08.002
11. Sel D, Cukjati D, Batiuskaite D et al. (2005) Sequential finite element model of tissue electropermeabilization. IEEE Trans Biomed Eng 52**:** 816-827 DOI 10.1109/TBME.2005.845212
12. Pavselj N, Preat V, Miklavcic D (2007) A numerical model of skin electropermeabilization based on *in vivo* experiments. Ann Biomed Eng 35: 2138-2144 DOI 10.1007/s10439-007-9378-7
13. Holland JH (1992) Adaptation in Natural and Artificial Systems: An Introductory Analysis with Applications to Biology, Control, and Artificial Intelligence. MIT Press, Cambridge.
14. Gehl J, Geertsen PF (2006) Palliation of haemorrhaging and ulcerated cutaneous tumours using electrochemotherapy. Eur J Cancer Suppl 4: 35-37 DOI 10.1016/j.ejcsup.2006.07.007
15. Corovic S, Pavlin M, Miklavcic D (2007) Analytical and numerical quantification and comparison of the local electric field in the tissue for different electrode configurations. Biomed Eng Online 6: 1-14 DOI 10.1186/1475-925X-6-37
16. Zupanic A, Corovic S, Miklavcic D (2008) Optimization of electrode position and electric pulse amplitude in electrochemotherapy. Radiol Oncol 42: 93-101 DOI 10.2478/v10019-008-0005-5
17. Sersa G, Čemazar M, Šemrov D et al. (1996) Changing electrode orientation improves the efficacy of electrochemotherapy of solid tumors in mice. Bioelectrochem Bioenerg 39: 61-66

Author: Anze Zupanic
Institute: University of Ljubljana, Faculty of Electrical Engineering
Street: Trzaska 25
City: Ljubljana
Country: Slovenia
Email: anze.zupanic@fe.uni-lj.si

Effects of automation to the surgeons

N. Geißler[1], G. Strauss[1, 2], P Jannin[3], W. Korb[1]

[1] Universität Leipzig / Faculty of Medicine, Innovation Center Computer Assisted Surgery (ICCAS), Leipzig, Germany
[2] University Hospital Leipzig, Department of Otorhinolaryngology/PlasticSurgery, Germany
[3] Visages U746, INSERM INRIA, Faculté de Médecine, Université de Rennes 1, Rennes, France

Abstract— **In this paper, part of the invited session - Automation in medicine, the different effects of automation to the surgeon are discussed, including positive and negative consequences. One approach to analyze effects of automation is explained, and exemplarily shown on a study of the mode error at the computer assisted surgery (CAS) system navigated control.**

Keywords— **Automation Consequences, Navigated Control, Mode Error, Evaluation.**

I. Introduction

Automation can be defined as a device or system that accomplishes (partially or in full) a function that was previously, or conceivably could be, carried out (partially or in full) by a human operator [1]. Automation is any sensing, detection, information-processing, decision-making, or control action that could be performed by humans but is actually performed by machine [2]. In a modern operating room (OR) are many examples of automation to observe. It is important to investigate the effects of automation to the human-machine interaction (HMI). In this context the results of a study by Matern et al. [3] of German surgeons are interesting: 70% of the surgeons declared that they can't fully control their systems and 52% of the surgeons were wishing an improvement of the usability of technical medical systems. These results show the importance of the analysis of the HMI in medicine. Based on this situation basic concepts of automation and framework requirements in the context of medicine are explained. The approach is explained on the example of the computer assisted surgery (CAS) system navigated control.

II. Automation in Surgery

Positive and Negative Automation Consequences: The goal of automation is to increase flexibility, efficiency, accuracy and safety. These goals can only be reached if automation is running free of errors. If the automation is erroneous the human has again to take control of the process. Because of relying on the automation, he might not be prepared for controlling the machine manually. Hence the human may react inadequately in such situations ("Ironies of automation", cf. [4]).

To avoid such situations, it is important to use "human-centered automation concepts" for the design of human-machine-systems. A central assumption for "human-centered automation" is the following, cf. [5]:

The user has to have the ability to recognize his responsibility and functions during the complete process of applying a man-machine-system. In surgery this means, the surgeon always bears overall responsibility for patient safety. Surgeons always must be in command of the surgical process.

Human Performance Consequences Various authors have defined evaluative criteria for such a human-centered automation design. These criteria are called "human performance consequences" (Tab 1).

Table 1 Criteria for Human Performance Consequences

Criteria	Description
Trust into automation	The belief of a person, that the machine will support him in an uncertain situation (cf. [6]).
Commission Error	Obey an automatically generated wrong advice without verification and although further contradictory statements are available [7].
Omission Error:	A lacking response on a system error, because the automation does not show this system error either [7].
Complacency	The lack of human control of a (automation) device; i.e. the operator is performing control more seldom than the automation of the system would require [1; 8].
Loss of (manual) skills	With the introduction of new systems, the users may loose the ability to finish a task in the traditional way in case of a system's failure. Further with automation systems some manual skills may not be taught to the novice surgeons [1].
Maintaining situation awareness	Situation awareness is the subjective representation of the work environment, i.e. the perception of the elements in the environment within a volume of time and space, the comprehension of their meaning and the projection of their status into the near future [1; 9].
Cognitive Workload	Evidence shows that automation can lead to decreasing or increasing mental workload [10].
Mode error	When a user misclassifies the mode resulting in actions that are appropriate for the analysis of the mode but inappropriate for the true mode [11].

O. Dössel and W.C. Schlegel (Eds.): WC 2009, IFMBE Proceedings 25/XIII, pp. 154–157, 2009.
www.springerlink.com

All these criteria may also influence the surgeon's performance if he/she is using surgical automation systems. For the evaluation of these effects of automation, a framework is used, which was developed by Jannin and Korb [12], based on the standards of the Health Care Technology Assessment (HCTA).

In this paper that framework is applied for the assessment of the *effects of automation.* The first step in the framework is careful study planning with the following tasks:

1. *Systems description:* Definition of the system and the system status in the engineering life cycle (design, sample, prototype, certified system, etc.)
2. *Surgical context and intented use*: This includes a description of the surgical procedure followed by the surgeon when using the system.
3. *Assessment level:* HCTA defines different assessment levels, to categorize the intented assessment objective:
   - Technical feasibility,
   - Reliability of the system,
   - Efficacy, i.e. the benefit of using a technology for a particular problem under ideal conditions,
   - Effectiveness, i.e. the benefit of using a technology under general conditions,
   - Efficiency,
   - Social, legal and ethical impacts.
4. *Criterion and measures:* For the described system in a specific surgical context, a study objective needs to be defined. This means to select one of the criteria of Tab. 1 and an appropriate measure (please refer to the indicated references in Tab. 1 for each criterion). This decision allows also defining the hypothesis.
5. *Study conditions:* After the study objective and the hypothesis are defined, the conditions that can further influence a study are considered: scenarios, operators, locations, environment and patient data sets.
6. *Assessment methods:* A detailed description of the methods, including metrics, statistical analysis and calculations of the results need to be done, before conducting the study.

After study planning, the framework recommends conditions how to perform the study and how to report the study [12].

To demonstrate the approach of the framework, in the following section the method of study planning is applied for an investigation of the navigated control system (NC).

III. MODE ERROR IN NAVIGATED CONTROL (NC)

Systems description and indented use: NC [13] is a surgical navigation system which has two different modes. Different modes are a common architecture in modern machines [14] they represent different states or functions in a certain system [15]. In the "free mode" the surgeon can use the navigation and has no limitations for using his surgical tool in the *situs*. In the "navigated controlled" mode the system automatically switches off the surgical instrument in pre-defined areas of risk. These areas of risk are defined preoperatively by segmentation of the "region of interest". If the tip of the tracked instrument is within this region, the instrument performs the milling, outside this region the instrument is switched off, even if activated by the surgeon with the foot pedal.

These NC-systems are currently in the development status "performing clinical patient trials" [16; 17].

Surgical Context and intended use: Currently these systems are available for endoscopic rhino surgery, otosurgery (mastoidectomy), dental implant drilling and spine surgery. For the use of NC some preparations are needed. First a workspace planning is necessary, which includes a fixation of markers to the patient for the later registration. This is followed by a CT-scan of the patient including the markers. The preoperative segmentation, so that the areas of risk will be save, is done in this CT-scan. The workspace model is imported in NC, than the scanned markers on the patient and the instrument are registered to track the patient and the instrument intraoperatively. Finally NC is used for milling and to remove tissue e.g. bone.

Assessment Level: The authors were interested in the effects of automation and the consequences to the reliability of the system (Level 2)

Criterion and measures: It may be dangerous if the user doesn't know in which mode he is in [15], because an identical user input is interpreted differently by the system in different modes [11]. If the user anticipates that he is in a certain mode and acts correct for the anticipated mode but incorrect for the real actual mode it is called a *mode error* [11].

Through a frequent mode change or an unplanned event (i.e. other medical complications or other deflections) it can come to a limitation of the knowledge about the current mode. So that the surgeon doesn't know in which mode he is in. Reasons for a mode switch can be for example the personal preferences of the surgeon or a changed situation

in the *situs*. In the context of navigated control a mode error is defined if the user thinks he is in the "navigated controlled" mode and operates with less care and full strength even close to risk structures like the facial nerve or blood vessels. This procedure would be acceptable in the "navigated controlled" mode, but not in the actual "free mode", so that the input of the surgeon through the pedal is not stopped in the area of risk so that he can hurt a risk structure.

It is a potential risk to use different modes but in certain medical systems like NC there is no alternative. So it is essential to have an adequate advisory system for the modes to minimize the risk of mode errors.

For the measurement of the *mode error in NC* a within-group design was chosen to compare different advisory systems:

a) a system where the mode switch was signaled only through a single sound and a change in the standard display of the system.

b) a system which additionally gives a continuous aduditory signal during the free mode, and

c) a system which augments the actual mode into the surgical microscope.

It is assumed that the test persons will improve to correct anticipation of the errors, if the mode is displayed through additional advisory systems (i.e. auditory or visual).

Study conditions: The *mode error* is studied in a scenario in a surgical demonstrator OR. The advantage of demonstrator scenarios includes that they are quite realistic and controllable [12]. Another advantage is that critical situations and errors can be simulated, and probabilities for errors be measured [18] which couldn't be done in clinical studies.

An interdisciplinary generic phantom [19] (similar to the phantom in [20]) was developed in cooperation with Phacon and clinical partners (Fig. 1).

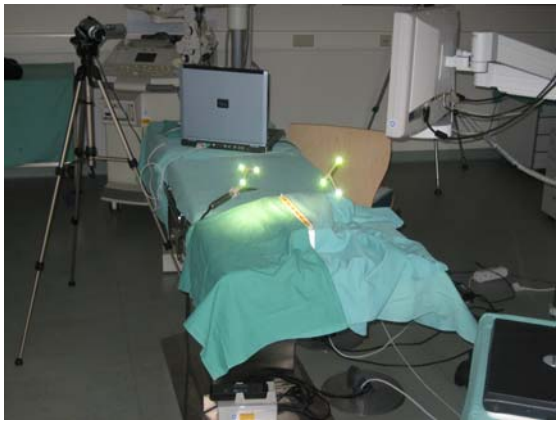

Fig. 1 Validation of the generic phantom in the demonstrator OR

It represents generic milling tasks near to risk structures / organs, which are applied in different surgical specialties (e.g. ENT, neurosurgery, orthopaedic and maxillofacial surgery) [19].

The validation through clinical experts (ENT and neurosurgery) showed that, as a mean, a milling volume of 500 mm^3 is the best amount for a task over 1 minute [19]. The prestudy showed also that the phantom is comparable to the clinical practise concerning i.e. the abrasion resistance, the haptics, the milling, the learnability of the task and overall the task and the study design itself [19].

The scenario for the evaluation of mode errors is based on this phantom. The primary task includes not only the correct milling of this phantom without injuries but also a change of mode. This means that the test person has to switch with a foot pedal from "free mode" to "navigated-controlled" mode and back. The green fields are milled in "navigated-controlled" mode, the red in "free mode". This is in accordance with the software, which displays the current mode with a red and green button, respectively.

However, it is important to perform the study planning carefully. One main issue in study planning is the selection of test persons with careful consideration of the needed expertise and size of the study groups (overall and for each group). To gain medical experts in reliable numbers for studies is quite difficult without cooperation with clinical partners. The estimation of the needed numbers is based on the correct considerations especially of the anticipated effect size, the statistical methods, the number of compared groups, the design and the number of trials for each person or group (particularly for skills criteria, multiple sessions for each person may be required). In the assessment of CAS, often expert opinions are used as reference.

Assessment methods: For the above-mentioned hypothesis it is reasonable to measure different independent variables and to combine the results of the different variables in the analysis. Additively to questionnaires of the self estimation of the achievement, the trust in the system and the subjective workload (NASA-TLX), behavioral measures (log files, workflow analysis) and the results of the quality of primary task (this is the task, which is explained to the study-participant) will be measured. We will combine several measures, because the strength and weakness of each method should be optimally compared.

IV. CONCLUSIONS

To analyze the consequences of automation for surgeons it is helpful to combine experimental and clinical studies, because both approaches have their strengths. In some cases it is not ethical to conduct clinical studies with patients,

particularly if automation systems are going to be manipulated. In general it is helpful to use both, objective and subjective measures in clinical and experimental studies to reach a higher validity of the studies.

It is also important to work in interdisciplinary teams, especially with medical scientists, engineers and psychologists, to combine the competences. Another important aspect is the use of data from CIRS-systems (critical incident reporting system). Such data gives insight into current incidents which show a trend for upcoming human factors problems.

Finally it is necessary that the focus of the research is on both positive advances as well as risks of automation in surgery. The evaluation is important of the possible improvements and risks.

For the system NC we can summarize, besides other aspects that the availability of two modes is an advantage because the free mode allows changing the workspace intraoperatively. There is also the disadvantage that the two different modes (navigated control vs. free mode) can lead to mode errors; this means the surgeon forgets to switch on the navigated control mode without noticing this fact. So our scientific goal is to test the current advisory system of NC and compare it with alternatives.

The framework [12] proved as a suitable guideline to plan the assessment of effects of automation. The study conditions were validated in a preliminary study [19]. The next step will be the analysis of mode errors by using different advisory systems in our main study.

Acknowledgment

We would like to thank Prof. Manzey, Dr. Jennifer Elin Bahner and Stefan Röttger from the TU Berlin for the scientific input. We would also like to thank Anke Hoffmeier, Andreas Seifert, Michael Stephan and Andrej Machno from the ASSESS Team in ICCAS and our clinical partners from the ENT and neurosurgery of the UKL Leipzig for their support. We would like to thank the Bundesministerium für Bildung und Forschung, which has made our research possible by supporting the project with the program "Unternehmen Region".

References

1. Parasuraman R, Sheridan TB, Wickens CD (2000) A model for types and levels of human interaction with automation IEEE Trans Syst Man Cybern A Syst Hum 30:286-97.
2. Moray N, Inagaki T, Itoh M (2000). Adaptive automation, trust, and self-confidence in fault management of time-critical tasks. Journal of Experimental Psychology: Applied, Vol. 6, No. 1, S. 44-58.
3. Matern U, Koneczny S, Scherrer M, Gerlings T(2006) Arbeitsbedingungen und Sicherheit am Arbeitsplatz OP, Deutsches Ärzteblatt Jg. 103, Heft 47
4. Bainbridge, L. (1983). Ironies of automation, Automatica, 19, 775-779.
5. Manzey D (2008). Systemgestaltung und Automatisierung. In: P Badke-Schaub, G Hofinger, K Lauche (Eds.): Psychologie sicheren Handelns in Risikobranchen. 307-326.
6. Lee JD, See KA (2004) Trust in Automation: Designing for Appropriate Reliance. HUMAN FACTORS 46: 1, 50-80.
7. Skitka LJ, Mosier KL, Burdick M (1999) Does automation bias decision making? Int. J. Human-Computer Studies, 51, 991-1006.
8. Manzey D, Bahner JE (2005). Vertrauen in Automation als Aspekt der Verlässlichkeit von Mensch-Maschine-Systemen. In: K Karrer, B Gauss, C Steffens (Eds.), Beiträge zur Mensch-Maschine-Systemtechnik aus Forschung und Praxis, Düsseldorf: Symposion. 93-109.
9. Endsley MR, Garland DJ (2000) Situation Awareness Analysis and Measurement: Analysis and Measurement. Lawrence Erlbaum Associates
10. Hart SG, Staveland LE (1988) Development of NASA-TLX (Task Load Index): Results of experimental and theoretical research. http://ntrs.nasa.gov/archive/nasa/casi.ntrs.nasa.gov/20000004342_1999205624.pdf (last access: 13.02.2009)
11. Norman DA (1981) Categorization of action slips, Psychol Rev Vol. 88, 1-15.
12. Jannin P, Korb W (2008) Assessment of Image-Guided Interventions. In: Peters TM and Cleary K (Eds): Image-Guided Intervention Principles and Applications. Springer, Berlin-Heidelberg. pp.531-549
13. Lüth T, Bier J, Bier A, Hein A (2001): Verfahren und Gerätesystem zum Materialabtrag oder zur Materialbearbeitung, Patent DE 101 17 403 C2.
14. Monk A (1986) Mode-Errors: A user centered analysis and some preventive measures using keying-kontingent sound. International Journal of Man-Machine Studies 24, 313-327.
15. Andre A, Degani A (1997) Do you know what Mode you`re in? An analysis of Mode error in everyday things. In: M Mouloua, JM Koonce (Eds.), Human-automation interaction: Research and practice (19-28). Mahwah, N.J.:Lawence Erlbaum.
16. Strauß G, Koulechov K, Lueth T et al. (2006) Evaluation of a navigation system for ENT under surgical efficiency criteria. Laryngoscope 116(2006), 564-572.
17. Strauß G, Koulechov K, Lüth T et al. (2005) Navigated Control: Ein neues Konzept fur die Computer-Assistierte-HNO-Chirurgie. Laryngorhinootologie 84, 567-576.
18. Hoelscher UM, Mueller KA, Stier A, Nachreiner F (2008).: Analyzing Medical Device Error Proneness through Differentiation of Error Components the "Steinfurt Method", www.heps2008.org/abstract/data/PDF/Hoelscher.pdf (last access: 13.02.2009)
19. Geißler N, Wedekind M, Strauß G, Korb W (2009)Analyse seltener Fehler bei der Mensch-Maschine-Interaktion im Operationssaal. i-com: Zeitschrift für interaktive und kooperative Medien. Vol 8 (No. 1), in press.
20. Möckel H, Grunert R, Korb W et al. (2007) ElePhant: Ein anatomisch-elektronisches Simulationssystem für die Evaluation Computerassistierter Eingriffe und die chirurgische Ausbildung, Biomedizinische Technik 52 No. 6, 375-382.

Author: Dr. Norman Geißler
Institute: ICCAS
Street: Semmelweisstraße 14
City: 04103 Leipzig
Country: Germany
Email: norman.geissler@iccas.de

Analysis of Mechanisms Involved in Gene Electrotransfer – Theoretical and an in Vitro Study

M. Pavlin, M. Kandušer, and D. Miklavčič

University of Ljubljana, Faculty of Electrical Engineering, Tržaška 25, Ljubljana, Slovenia

Abstract— **Gene electrotransfer is an established method for gene delivery which uses high-voltage pulses to increase permeability of a cell membrane and thus enables transfer of genes. It was shown that critical steps of electrotransfection are cell electropermeabilization, contact of plasmid DNA with the cell membrane, translocation, entering the nucleus and gene expression. However, mechanisms of the processes are still not fully understood. In this paper we theoretically and experimentally analyze electrophoretic mobility and efficiency of gene electrotransfer by using combinations of high-voltage (HV) and low-voltage pulses (LV) in vitro on CHO cells. We used i.e. optimal plasmid concentrations for in vitro conditions as well as lower sub-optimal concentrations in order to mimic in vivo conditions. We observed that short HV pulses of 1 kV/cm alone were sufficient to deliver DNA into cells for optimal plasmid concentrations, while adding LV (75 V/cm) pulse did not increase transfection efficiency. However, for sub-optimal plasmid concentrations combining HV and LV pulses increased the transfection rate significantly. Our results suggest that low-voltage pulses increase transfection in conditions where plasmid concentration is low, typically in vivo where mobility of DNA is limited due to the extra cellular matrix. LV pulses provide additional electrophoretic force, which drags DNA toward the cell membrane and/or provides additional force for insertion in the cell membrane, and consequently increase transfection efficiency, while for sufficiently high concentrations of the plasmid (usually used in vitro) electrophoretic LV pulses do not have an important role. Our theoretical analysis shows that 100 ms LV pulse results in 10 times longer traveled distance of a DNA molecule (≈ 10 µm), compared to 4 × 200 µs HV pulses. We assume that in order to obtain efficient transfection several tens of molecules have to be brought in contact with the cell membrane.**

Keywords—**gene therapy, gene electrotransfer, electrophoresis, high-voltage low-voltage pulses, mobility.**

I. Introduction

Gene electro transfer of cells was first achieved already 25 years ago [1]. It was shown that high-voltage pulses (electroporation) enable delivery of DNA into the cell and successful expression of the gene. The method combines addition of plasmid DNA and local application of electric pulses which increase permeability of the membrane for DNA molecules. Gene electro transfer is already an established method for gene transfer in vitro, currently is being extensively studied on animal models in vivo and also first clinical trials are in progress. EGT is a nonviral gene therapy, which in comparison to viral gene therapy, represents a safer method and is not hampered in terms of immunogenicy and pathogenicity. Recent studies show that gene electro transfer is a promising method for cancer gene therapy, DNA vaccination, autoimmune and inflammatory diseases and several other illnesses [2].

Up to now several mechanisms were proposed for electric-field mediated gene transfer. First hypothesis suggested that the electric pulses create pores in the cell membrane, and this membrane pores consequently enable free diffusion of the DNA molecules through the membrane [1] due to the concentration gradient similarly as diffusion of small molecules. However, further studies showed that delivery of DNA molecule across the cell membrane is much more complex process which can not be explained only by simple diffusion through membrane pores [2-7]. By direct visualization of DNA complexes on the cell membrane it was demonstrated that one of the crucial steps is the interaction of DNA molecules with the cell membrane [5]. Currently, we can define several steps that are crucial for electrotransfection: cell membrane electropermeabilization, contact of the plasmid with the cell membrane, translocation across the membrane followed by mobility through cytoplasm, entering the nucleus and gene expression.

Further studies showed importance of electrophoretic movement of DNA during the pulses. In a single in vitro study they showed that using combination of high-voltage pulses (HV) and low-voltage (LV) pulses enhance DNA electrotransfer [6]. The authors suggested that HV electric pulses destabilize the cell membrane and enable insertion DNA into the cell membrane whereas LV pulses produces electrophoretic force which drags negatively charged DNA molecule into the cell and is crucial for providing contact and/or insertion in the cell membrane. This was later confirmed in vivo [7]. Only few studies theoretically analysed electrophoretic mobility of DNA in vitro and provided some theoretical analysis of DNA mobility during electric pulses in agarose gels [8].

In our present study we investigated both theoretically and experimentally the effect of HV and LV pulses on

O. Dössel and W.C. Schlegel (Eds.): WC 2009, IFMBE Proceedings 25/XIII, pp. 158–161, 2009.
www.springerlink.com

plasmid mobility and efficiency of gene electrotransfer in vitro. In order to compare gene electrotransfer in in vivo and in vitro conditions we used different plasmid concentrations from optimal typically used in vitro to sub-optimal, which are usually present in in vivo conditions. We furthermore theoretically analyzed the distance traveled by DNA molecules due to electrophoretic force and estimated how many molecules are available for contact with the membrane for our specific conditions.

II. Theory

A. Permeabilization of the cell membrane

Several studies have shown that one of the key parameters for successful gene electrotransfer is the induced transmembrane voltage, even though the exact mechanisms of cell electroporation and related gene electrotransfer are not fully understood. If the induced transmembrane voltage is above a certain critical value increased permeability of the membrane is observed [1]. It was shown that the observed threshold value of the field strength for gene electrotransfer is the same as the one needed to induce permeabilization [3]. Therefore electric field induced destabilization of the cell membrane is a critical step of gene electrotransfer.

From Schwan equation

$$U_m = 1.5\,ER\cos\theta\,, \tag{1}$$

one can obtain that the total area exposed to above-threshold transmembrane voltage – the permeabilized area:

$$S_c = S_0(1 - E_c / E), \tag{2}$$

where E_c is the threshold applied electric field and S_0 is total surface of the cell membrane.

B. Electrophoretic mobility

Electrophoresis is another mechanism which was shown to be important for the delivery of DNA molecules into cells by electric pulses. The electrophoretic driving force acts on the negatively charged DNA molecules and drags it toward the cathodic side of the membrane. It depends on the local electric field (E_{loc}) and on the effective charge of a given molecule (e_{eff}):

$$F = e_{eff} E_{loc}\,, \tag{3}$$

where the effective charge depends on the ionic strength of the solution and length of the plasmid. The velocity v of the molecular movement is proportional to electrophoretic mobility μ

$$v = \mu E_{loc}\,, \quad \mu = e_{eff} / f\,, \tag{4}$$

which depends on the friction drag f and effective charge. The distance L traveled due to electrophoresis can be calculated from total duration of the electric pulses t_E:

$$L = v\, t_E\,. \tag{5}$$

III. Materials & methods

A. Cells

Chinese hamster ovary CHO cells (European Collection of Cell Cultures) were grown as a monolayer culture in a nutrient mixture F12 HAM (Gibco) supplemented with 2 mM glutamine, 10% fetal bovine serum (Sigma-Aldrich Chemie GmbH, Deisenhofen, Germany) and antibiotics at 37°C in a humidified 5% CO_2 atmosphere in the incubator.

B. Electrotransfection protocol

To generate electric pulses high-voltage generator Cliniporator™ was used which enabled use of either only high-voltage (HV) pulses, only low-voltage (LV) pulses or combination of both pulses (HV+LV). A pair of parallel wire electrodes was used with the distance d between the electrodes being 2 mm. In pulsing protocols we used four HV pulses of 200 µs duration with amplitude E_{HV} = 1.0 kV/cm (U = 200 V) and one LV pulse with E_{LV} = 0.075 kV/cm (U = 15 V).

C. Experiments

Plasmid DNA pEGFP-N1 purified with Endofree Plasmid mega kit (Qiagen) coding for GFP (green fluorescent protein) was used to analyze efficiency of gene electrotransfer. The experiments were performed on plated cells seeded in 24 multiwell plates. Initial concentration of plated cells was 5×10^4 cells per well. On the day of experiment the growth media was removed and replaced with the mixture of plasmid DNA and isoosmolar pulsing buffer (pH 7.4, 10 mM Na_2HPO_4/NaH_2PO_4, 1 mM $MgCl_2$ and 250 mM sucrose). Final concentration of plasmid was 2 µg/ml, 5 µg/ml and 10 µg/ml (optimal plasmid concentration). The optimal concentration was determined experimentally as the concentration above which the increase in concentration of the plasmid did not further increase the transfection efficiency.

We incubated cells in the pulsing buffer for 2-3 minutes at room temperature (22° C). Then different combinations of high-voltage and low-voltage pulses were delivered. Treated cells were incubated for 5 minutes at 37° C to allow

cell membrane resealing and then grown for 24h in cell culture medium at 37° C in a humidified 5% CO2 atmosphere in the incubator to allow GFP expression.

Efficiency of transfection was determined by fluorescent microscopy (Zeiss 200, Axiovert, ZR Germany). The images were recorded using imaging system (MetaMorph imaging system, Visitron, ZR Germany) and at least five phase contrast and five fluorescence images were acquired per each parameter. The cells were counted manually and the relative transfection efficiency was determined by the ratio between the number of fluorescent cells and the number of cells counted under the phase contrast. Cell survival was obtained as the ratio between the number of viable cells in the treated sample and the number of viable cells in the control sample. At least three independent experiments were performed for each parameter and results are presented as a mean values ± standard deviation.

IV. Results

A. Experimental results

In order to determine the effect of HV and LV pulses on the transfection efficiency and to compare our in vitro results with in vivo studies we used different plasmid concentrations from sub-optimal 2 μg/ml to optimal 10 μg/ml.

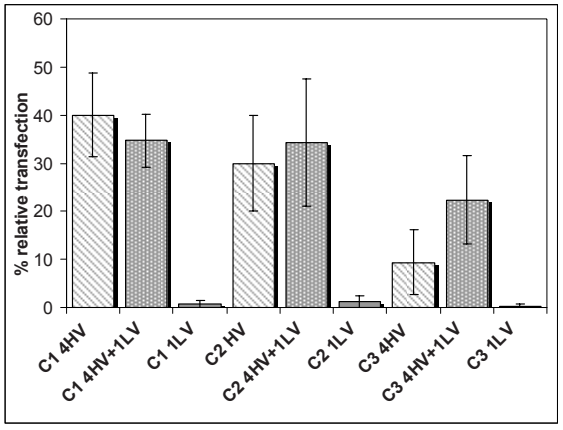

Fig. 1 Relative transfection efficiency with different plasmid concentrations (C1=10 μg/ml, C2 = 5 and C3 = 2 μg/ml. Combinations of 4HV pulses, 200 μs duration pulse amplitudes E_{HV} = 1.0 kV/cm (200 V), repetition frequency 1 Hz and 1LV pulse E_{LV} = 0.075 kV/cm (15 V), 100 ms duration were used. Results are presented as a mean and vertical bars represent standard deviation.

As it can be seen in Fig. 1 for sub-optimal plasmid concentration C3 we obtained a significant increase in transfection efficiency if combination of HV and LV pulses was used compared to the application of HV pulses only. For optimal plasmid concentration (10 μg/ml) there was however no statistical difference between applying only HV pulses or combination of HV and LV pulses. Cell survival was around 80% for HV or HV+LV pulses for all plasmid concentrations (data not shown).

In order to present this effect more clearly we additionally calculated the difference in the relative transfection (Tr) between 4HV+1LV and only 4HV pulses for each experiment *i*: $\Delta_i\% = Tr_{HV+LV} - Tr_{HV}$ and calculated the average difference Δ% and standard deviation of the differences as shown in Table 1 for different plasmid concentrations. It can be seen that there is an average increase of 13% for sub-optimal plasmid concentration (C3).

Table 1 The difference in the relative transfection (Tr) between 4HV+1LV and only 4HV pulses for each experiment i: $\Delta i\% = Tr_{HV+LV} - Tr_{HV}$ at sub-optimal plasmid concentration. From this the average difference Δ and standard deviation of the differences was obtained.

$\Delta\% = Tr_{HV+LV} - Tr_{HV}$	C1=10 μg/ml	C2=5 μg/ml	C3=1 μg/ml
average Δ% ± std	-5.2 ± 10.2	4.4 ± 7.4	12.9 ± 4.8

B. Estimation of the traveled distance during electrophoresis and number of DNA molecule in contact with the membrane

First we calculate velocities during high-voltage and low-voltage pulses:

$$\begin{aligned} v_{LV} &= \mu\ E_{LV} = 1.4\times10^4\ \tfrac{\mu m^2}{Vs}\cdot 75\tfrac{V}{cm} \approx 0.1\,\text{mm/s}\ , \\ v_{HV} &= \mu\ E_{LV} = 1.4\times10^4\ \tfrac{\mu m^2}{Vs}\cdot 1000\tfrac{V}{cm} \approx 1.4\,\text{mm/s}\ , \end{aligned} \tag{6}$$

where we used approximation that mobility is approx. the same μ = 1.4×10^4 μm^2/Vs [8]. The traveled distance during HV and LV pulses can be obtained from Eqs. 4 and 5:

$$\begin{aligned} L_{LV} &= v_{LV}t_{LV} \approx 0.1\,\text{mm/s}\times 0.1\,\text{s} \approx 10\,\mu\text{m}, \\ L_{HV} &= v_{HV}t_{HV} \approx 1.4\,\text{mm/s}\times 0.0008\,\text{s} \approx 1.1\,\mu\text{m}\,. \end{aligned} \tag{7}$$

We can see that our 100 ms LV pulse contributes to 10 times longer traveled distance than 4×200 μ*s* HV pulses.

From a given concentration of plasmid DNA in a suspension C [μg/ml] we can calculate concentration in terms of number of DNA molecules in a given volume c_N. For a 4.7 kbp DNA molecule and C1=10 μg/ml we obtain that c_1 = 2×10^9 μl^{-1}. If we assume that electrophoretic force drags DNA molecules which are in a distance less that *L* from a cathodic site of a cell we can estimate number of DNA molecules *N* in this volume *V*. For our plated CHO cells we obtained following average geometrical data: height of a cell *h* = 4 μm and radius of the permeabilized cap r_p = 5 μm and therefore the corresponding volume is: $V = L\times 2r_p\times h$

(see Fig. 2). From this we can estimate the number of molecules available for contact with membrane at optimal plasmid concentration C1 = 10 μg/ml: $N_{HV} \approx c_1 \times L_{HV} \times 2r_p \times h \approx 88$ and similarly $N_{LV} \approx 800$. For the suboptimal concentration C3 = 1 μg/ml we obtain $N_{HV} \approx 9$ molecules and $N_{LV} \approx 80$ molecules.

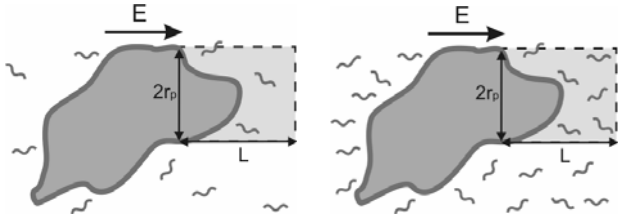

Fig. 2 Schematic representation of the number of molecules available for contact with the cell membrane at (left) sub-optimal concentration of plasmid and (right) optimal concentration, where L is the typical distance traveled during the pulse and r_p is radius of the permeabilized cap. Bright shaded region represents volume V from which DNA molecules are brought in contact with the cell membrane by electrophoretic force.

V. Discussion & conclusions

In the presented study we theoretically and experimentally analyze electrophoretic mobility and efficiency of gene electrotransfer by using combinations of high-voltage (HV) and low-voltage pulses (LV) in vitro. We obtained that short HV pulses alone were sufficient to deliver DNA into cells for optimal plasmid concentration (10 μg/ml) and that combination of HV and LV pulse did not increase transfection efficiency. However, for sub-optimal plasmid concentration (1 μg/ml) combining HV and LV pulses increased the transfection rate significantly. Our results suggest that LV pulses increase transfection in conditions where plasmid concentration is low, which typically represents in vivo conditions where mobility of DNA is limited by the extracellular matrix. LV pulses provide additional electrophoretic force which drags DNA toward the cell membrane and consequently increases the number of molecules in contact with the cell membrane and/or provides additional force for insertion in the cell membrane. On the other hand, for sufficiently high concentrations of the plasmid usually used, in vitro electrophoretic LV pulses do not increase transfection rate.

In order to estimate what is a typical displacement of a DNA molecule during electric pulses (L) we used plasmid mobility extrapolated from in vitro study on gels [8]. Our theoretical analysis showed that a single 100 ms LV pulse of 75 V/cm resulted in 10 times longer traveled distance of a DNA molecule ($L_{LV} \approx 10$ μm) compared to 4×200 μs HV pulses of 1 kV/cm where $L_{HV} \approx 1.1$ μm and consequently the number of molecules in contact is much lower during HV pulses. From our results we can estimate that for efficient transfection several tens of molecules have to be available (in contact) - around 10, while for smaller number <10 the transfection is very small (see Fig. 1 for c3 and HV pulses). Our theoretical calculation of L_{HV} and L_{LV} demonstrate why higher transfection can be obtained by using longer pulses in vivo, and why it is also possible to obtain efficient transfection with short pulses of sufficiently high electric field for optimal plasmid concentration.

Acknowledgments

This research was supported by the Slovenian Research Agency under the grants J2-9770 and P2-0249. Authors thank also Dr. Alenka Grošelj (Institute of Oncology, Ljubljana, Slovenia) for kindly providing plasmid DNA, Dr. Michel F. Bureau (CNRS, France) for his valuable suggestions and Dr. Tomaž Jarm (University of Ljubljana, Slovenia) for his help with statistical analysis of data.

References

1. Neumann E, Schaefer-Ridder M, Wang Y et al. (1982) Gene transfer into mause lyoma cells by electroporation in high electric fields. EMBO J 1: 841-845.
2. Prud'homme GJ, Glinka Y, Khan AS et al. (2006) Electroporation-enhanced nonviral gene transfer for the prevention or treatment of immunological, endocrine and neoplastic diseases. Curr Gene Ther. 6: 243-273
3. Wolf H, Rols MP, Boldt E et al. (1994) Control by pulse parameters of electric field-mediated gene-transfer in mammalian cells. Biophys J 66: 524-531
4. Kanduser M, Miklavcic D, Pavlin M (2009) Mechanisms involved in gene electrotransfer using high- and low-voltage pulses — an in vitro study. Bioelectrochem 74: 265-271
5. Golzio M, Teissié J, Rols MP (2002) Direct visualization at the single cell level of electrically mediated gene delivery. PNAS 99: 1292-1297
6. Sukharev SI, Klenchin VA, Serov SM et al. (1992) Electroporation and electrphoretic DNA transfer into cells. The effect of DNA interaction with electropores. Biophys J 63: 1320-1327
7. Satkauskas S, Andre F, Bureau MF et al. (2005) Electrophoretic component of electric pulses determines the efficacy of in vivo DNA elec-tro transfer. Hum Gene Ther 16:1194-1201
8. Henshaw JW, Zaharoff DA, Mossop BJ et al. (2006) A single molecule detection method for understanding mechanisms of electric field-mediated interstitial transport of genes. Bioelectrochem 69: 248-253

Address of the corresponding author:

Author: Mojca Pavlin
Institute: University of Ljubljana, Faculty of Electrical Engineering
Street: Tržaška 25
City: Ljubljana
Country: Slovenia
Email: mojca.pavlin@fe.uni-lj.si

Reviewing and Editing of Scientific Papers

F. Nüsslin

Klinikum rechts der Isar/Klinik für Radioonkologie, Technische Universität München, Germany

Abstract— **Writing, reviewing and editing are the essential steps in publishing a scientific paper. The format and most important rules for writing are briefly summarized. The reviewer's role is to assess the scientific essence and relevance of the paper and by his experience and expertise to support the author in the revision of the manuscript. The editor by his decision on the acceptance of a manuscript for publication has to ensure that the paper meets the requirements of the journal, such as the thematic spectrum and the level of excellence to attract the reader. Author, reviewer and editor act according to standards evolutionary developed in the scientific community. Any failures and deficiencies occurring when processing the manuscript bear risks of delay in publication, wasting efforts and time of the involved people and at least of harming the scientific level and the economic basis of the journal. In conclusion, disseminating research results presents challenges to good publishing practice.**

Keywords— **Scientific writing, reviewing, editing, scientific manuscript.**

I. Introduction

There is a saying of Charles Darwin that "a naturalist´s life is a happy one if he had only to observe and never to write" [1] which emphasizes the split role of a scientist, to do good research and to communicate the results of that research. In fact, an excellent scientist is not always equivalently good both in doing and writing science. It is certainly not the principal goal of scientific research to publish [2], but without publishing even the most spectacular research results will hardly have any impact on science and the public. Journals are to be considered the key players in disseminating the scientist's work to the science community. Besides the aspect of innovation, reproducibility is the prime criterion of good research. Therefore, a second but not less important role of a scientific journal is to provide all details of the method the author applied to allow other scientists working in the author's field to follow all details of the study and for the purpose of cross-checking with the reader's own work, and even to retrace step by step the procedures that led to the published data. The reader of a scientific paper should be able not only to understand the research results, but also to reproduce them. An evolution of science norms for scientific publishing has emanated and is demanded by all scientific journals. Typically, these norms form the basis of the information for and specific instructions to authors found in each issue of a journal. A good reference is the "Uniform Requirements for Manuscripts" created by the International Committee of Medical Journal Editors (ICMJE) [3] where generally agreed guidelines for scientific publishing have been established. Other more practical translations of those requirements may also be consulted, for instance [2]. Summarizing the manifold previous publications on this topic, this paper aims to review the characteristics of the publishing process including the standards which should be applied by the author, the reviewer and the editor.

This article focuses on reviewership (section III) and editorship (section IV). However, due to the close interdependence between author, reviewer and editor, some brief remarks on authorship (section II) may not be ignored. But the fourth player in the publishing process, the publisher, is not addressed here.

II. The writing process

A. Types of scientific publications

Different requirements are applied to the various types of scientific publications. However, common to all scientific contributions, written and oral, is the fundamental demand for a clear, understandable, logically structured presentation of original data or findings, new observations, innovative ideas and an overview of a research field. It is primarily the decision of the author to select the appropriate form of publication. However, in some cases the choice between the most frequent types of a scientific paper, a short technical note, or a scientific letter may be finally decided during the reviewing process. To update the community in a large field of science, a review article might be the appropriate form. Another frequently used form of scientific communication is a congress contribution (oral or poster presentation, extended abstract, conference report). A book chapter is typically comparable to a review article.

O. Dössel and W.C. Schlegel (Eds.): WC 2009, IFMBE Proceedings 25/XIII, pp. 162–165, 2009.
www.springerlink.com

B. Preparation of manuscript (IMRAD)

Scientific writing needs a proper format requiring some basic rules of manuscript preparation. Additionally, the writer has to carefully follow the specific instructions normally printed in each issue of any journal.

Corner stones of good research are starting from a clear hypothesis, selecting the most appropriate method for verification or rejection of the hypothesis, and drawing the right conclusions. Actually, reporting the findings of an investigation is mirroring the consecutive processes of good research, requiring precision and clarity in the definition of the problem / hypothesis, describing the methods and results, discussing the meaning and consequences of the study and displaying consistent conclusions. Accordingly, the author should not deviate from the uniform requirements [3] for structuring a manuscript:

- Introduction: to briefly make the reader familiar with the basics of the research subject, to emphasize the innovative aspect of the work and finally to clearly present the hypothesis / problem which is best put in a single phrase or question.
- Materials & Methods: to describe all the individual steps leading to the described results. The reader should at least understand the way the author came to the presented results, and the expert reader should be able to replicate the study.
- Results: to provide all data found in the study and to present it in a clear format (tables, graphs etc.).
- Discussion: to critically compare the results with those from other scientists in the field and to outline the value and consequences of the study.
- Conclusion: to draw the right conclusions within the limits and constraints of the study and to outline the perspective of follow-up work.
- Acknowledgment: to acknowledge the contribution of significant parts of the work by collaborating scientists.
- References: to list all publications used in the study.

This highly structured format called IMRAD (Introduction, Methods, Results, And Discussion) has been propagated by ICMJE [3] and is widely accepted by most scientific journals today.

III. The reviewing process

It is common practice in all leading journals to subject manuscripts to a peer review process. This means usually that the manuscript is evaluated by at least two independent reviewers who are peers in the author's field and not members of the editorial staff. A thoughtful, unbiased and critical assessment of a manuscript is a prerequisite for good practice in scientific publishing. Author, editor, publisher and the entire science community benefit from and depend on the reviewer's skills, scientific expertise and professional judgment. The reviewer's work is most often less acknowledged than he would deserve. However, - and this is particularly the case when reviewing good papers -, the reviewer is repaid for his investment of time end effort by having access to priority information on new developments, keeping up in the field, and, through a feed back loop, steadily acquiring skills in research assessment which may be useful for writing and evaluating any type of scientific communication, reports and grant applications.

The reviewer's report needs the same clearness as that demanded from the writer. The reviewer should emphasize both the strength of the paper and the limitations / weaknesses of the manuscript in a well balanced way. It is discouraging for the author to find critical remarks only. Many journals provide the reviewer with an additional checklist for evaluation. The reviewer should particularly address the following criteria:

Originality, sound hypothesis, clarity of presentation (including number and content of tables and figures), adequacy of methods and materials, correctness of results (e.g. statistics), adequacy of discussion and conclusion, references (number, relevance).

Additionally the reviewer is asked to provide comments to the editor which are not seen by the author.

Ethical requirements include the responsibility of the reviewer to maintain confidentiality; the reviewer's report should not be accessible outside the editorial staff. The reviewer must not acquire any benefit from his privilege position of having advanced knowledge of the author's work. He is obliged to disclose to the editor-in -chief any conflict of interest when evaluating the manuscript.

IV. The editing process

Editing is the process of adapting the format, language and style of the manuscript to the requested publishing standards as given in the instructions to the author. Normally, editing is part of the entire reviewing process and includes checking spelling, terminology and language used. Some publishers have employed editorial assistants who correct errors and recommend proper style and language. Editing may be a cumbersome process, particularly for non–native English speaking authors, but it is essential.

V. Responsibilities of the Author, Reviewer and Editor-in-Chief

A. Author

An author is a scientist who contributed significantly to the entire investigation reported in the manuscript. This means both that no one should be left out from the author list who earned authorship by contributing an essential part of the study, and also that no one should be listed as an author (e.g. honorary authorship) who was engaged only peripherally in the study. Those scientists who contributed indirectly or only to a lesser extent, may be mentioned in an acknowledgement. According to the uniform requirements of ICJME [3] three criteria are essential to distinguish between an author and other scientists: (i) substantial contribution to the conception, design and performing of experiments, data acquisition and analysis, (ii) drafting at least larger parts of the paper, and (iii) processing the manuscript up to the final approval. There are a few journals that have begun to demand specification of the contributions of each person in the author list.

It is the liberty of the author to select the journal where the manuscript will be submitted. This decision is guided primarily by the prestige, access and impact of the specific journal.

When preparing a manuscript (section II) the author should put a major effort into the preparation of the manuscript rather than speculating on a second run when in a revised version all requested modifications are performed. The latter behaviour is an abuse of the editor's and reviewer's time.

B. Reviewer

The reviewer is committed both to the editor-in-chief and to the author. The editor-in-chief expects from the reviewer a critical, science based and fair evaluation of the manuscript within a reasonable time. If the invited reviewer is unable to deliver a report under these constraints, it is in the interest of the editor and the author to avoid delay in the publication process by immediate declining the opportunity. The reviewer's obligation to the author is primarily to help, either to get the manuscript accepted or to make specific recommendations for revision. If the reviewer recommends rejection, the reasons for rejection should be clearly explained. In particular, when rejecting a manuscript the efforts of the author should be acknowledged and no emotional terms should appear in the report.

C. Editor

The editor-in-chief is ultimately responsible for the whole content and the scientific profile of the journal. Therefore, the editor has the freedom to accept or reject a manuscript. The editor accompanies the manuscript from the first step of submission up to the final decision of acceptance or rejection. When the manuscript is submitted the editorial staff decides whether to initiate the peer review process. Occasionally it may happen that a paper is rejected without review,, for instance if it falls outside the mission of the journal. In the majority of cases the manuscript is carefully evaluated by reviewers who evaluate and the author who revises the manuscript as guided by the reviewers. Finally, based on the recommendation of the reviewers the editor decides to accept or reject the manuscript. The threshold of acceptance is of course different with different journals and is partly influenced by the ranking of the journal by the science community. The editor has to carefully consider the ethical rules in scientific publishing. A particular problem is plagiarism. Any form of scientific fraud presents challenges to take appropriate measures by the editor and the publisher [4]. Development of the Internet has abetted plagiarism, although computer programs have been developed to help detect plagiarism.

The Worlds Association of Medical Editor's (WAME) [5] has created 12 rules describing the responsibilities of an editor. These rules provide guidance to help the editor overcome the challenges of the position..

VI. Conclusion

Since publishing is an integral part of research it needs a well structured format according to established and internationally accepted standards. The uniform requirements for manuscripts submitted to biomedical journals defined by ICJME [3] turned are such a standard and they facilitate the proper management of scientific manuscripts.

References

1. Trelease S.F. (1958) How to write scientific and technical papers. Williams & Wilkins Co., Baltimore
2. Day R.A., Gastel B. (2006) How to write and publish a scientific paper. Greenwood Press, London
3. International Committee of Medical Journal Editors (2008) Uniform requirements for manuscripts submitted to biomedical journals: writing and editing for biomedical publication. ICMJE at http://www.ICMJE.org

4. Hendee W.R (2007) A concern about plagiarism J.Med.Phys. 32:143-144
5. World Association of Medical Editors (WAME) (2009), http://www.wame.org

Acknowledgment

The author would like to thank W.Hendee and P.Vaupel for their careful revising of the manuscript.

Author: Fridtjof Nüsslin
Institute: Klinikum rechts der Isar der Technischen Universität München
Street: Ismaningerstr. 22
City: D-81675 München
Country: Germany
Email: nuesslin@lrz.tum.de

Object-oriented Model Library of the Cardiovascular System Including Physiological Control Loops

A. Brunberg[1], J. Maschuw[1], R. Autschbach[2] and D. Abel[1]

[1] Institute of Automatic Control, RWTH Aachen University, Aachen, Germany
[2] Department for Cardiac and Thorax Surgery, University Hospital Aachen, Aachen, Germany

Abstract— **"HumanLib" is an object-oriented component library for modeling and simulation of the human cardiovascular system including physiological control loops. Possible fields of application comprise analysis of physiological processes, development and testing of assist devices (e.g. TAH, VAD) and education and training. A graphical user interface encapsulates the most important clinical parameters, thus providing an easy-to-use interface to the more complex model.**

Keywords— **Modeling, simulation, cardiovascular system, physiological control loops, graphical user interface**

I. Introduction

A properly functioning cardiovascular system is indispensable for the survival and for the well-being of a human being. Furthermore, understanding the fundamental physiological processes is not only necessary in clinical practice but also in the development of technological assist devices for disturbed physiological functions. However, the cardiovascular system is highly complex and individual parameters are influenced by various mechanisms and interactions. In particular, in a healthy body, a large number of physiological control loops guarantees the adjustment of different quantities to each other and the adaption to physiological stress, e.g. movement or environmental influences.

Arterial blood pressure, for example, is an important factor in providing sufficient organ perfusion at all times. Changes of the vascular tone, and thus, of vascular resistance to flow, in peripheral vessels influence arterial pressure directly. Additionally, heart rate, contraction strength of the heart muscle, and, among others, blood gases and various hormones affect blood pressure. The baroreflex is one example of a physiological control loop helping to stabilize arterial blood pressure in the presence of short-term disturbances.

Simulation of this highly complex system can lead to better understanding and to improvements in the developing process of adaptive assist devices. In [1, 2], a new approach to modeling of the cardiovascular system was presented: "HumanLib", an object-oriented component library programmed in Modelica / Dymola which reflects physiological structures in its internal structure. This mode of programming leads to intuitively understandable models, as physical interfaces instead of directed signals connect subcomponents. Similar approaches have been applied successfully in other fields of engineering, such as the simulation of power plants [3].

The development of technological assist devices requires a multidisciplinary co-operation involving both engineers and physicians. A clear and comprehensible representation of the simulation model and a user-friendly interface for carrying out simulations and for accessing simulation results can facilitate co-operation.

In the following sections, first the structure and the technical side of simulation with components of "HumanLib" will be presented. Subsequently, a graphical user interface (GUI) implemented in Matlab will be introduced. This GUI provides a good overview of the most important model and simulation parameters as well as plots of simulated variables.

II. Materials and methods

A. Library structure

"HumanLib" is a component library comprising various mathematical descriptions or modeling approaches [1, 4–13]. In contrast to previous models which have been programmed in a signal-oriented way, in "HumanLib", an object-oriented approach was taken. This leads to several advantages, such as non-directional communication, encapsulation of data or inheritance [1, 2].

The library is divided into two main parts which in turn consist of several packages each. The *Basic* part contains fundamental properties and components for all library components. The *Components* section includes models for several classes of components of the cardiovascular system and physiological control loops, as well as data records with parameters and initial values for these components necessary for simulation. An overview of "HumanLib" is given in Fig. 1: a part of the library structure can be seen on the left; on the right, an exemplary simulation model is shown.

O. Dössel and W.C. Schlegel (Eds.): WC 2009, IFMBE Proceedings 25/XIII, pp. 166–169, 2009.
www.springerlink.com

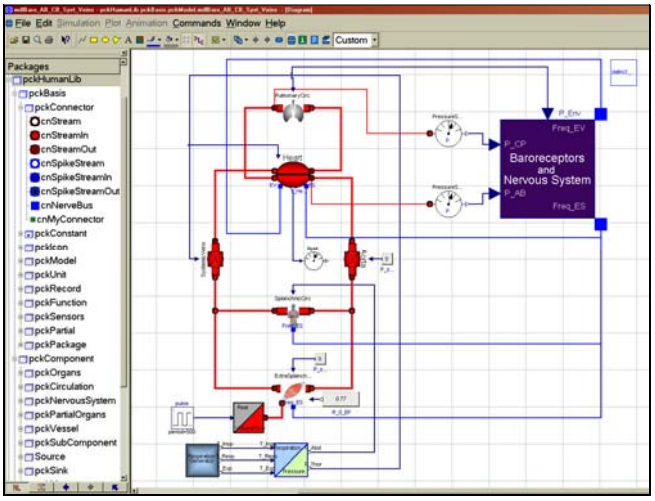

Fig. 1 Library structure and simulation model in Dymola.

Some of the packages will be introduced in more detail in the following.

pckConnector: This package contains the definition of interfaces between components; i.e. here, it is defined which quantities are transferred between different components and by what principle they are linked. Two classes of connectors have been established so far, one for vascular components and one for nerval signals. Additionally, single nerval signals can be bundled to form a nerve bus.

pckUnit: In contrast to most other fields of engineering, in a medical environment, often non-SI units are used, e.g. millimeters mercury, mmHg. As Modelica / Dymola operates with units, a number of new units had to be defined to be able to keep the simulation in accordance with commonly used units:

```
type Pressure_mmHg = Real (final
quantity = "Pressure", final unit="mmHg")
"1 mmHg = 1 Torr = 133,322 Pa";
```

pckPartial: One of the main advantages of object-oriented programming is use of the inheritance principle. Common characteristics of several components are abstracted and later inherited to all of these components by use of so-called partial models. This reduces redundancy and facilitates changes or expansion of the library.

pckOrgans: In this package, all components of the cardiovascular / respiratory system which are neither vessels nor part of the nervous system are summarized. At the current state, mainly the heart and a block representing respiratory mechanics fall into this category. Several models for the heart exist. All of them have identical connectors so that a heart model ideally suited for the simulation purpose at hand can be chosen. As a default setting, all components are automatically linked to a data record containing a matching set of parameters for the model. Parameters are normalized for the same body weight to facilitate interchanging components.

pckVessel: The most basic vascular model in this package consists of the (linear) electric analogon of the fluid dynamic description of the transmission of blood flow and pressure waves [13]. However, as most vascular components show a nonlinear behavior in reality, models for these relations were included as well [2]. Similar to *pckOrgans*, a default set of parameters is linked to most components.

pckCirculation: Often, a model consists of several larger vascular compartments, each encapsulating more than one vessel. For example, pulmonary circulation can be considered as a series connection of an arterial, a peripheral and a venous vessel. Similar approaches for splanchnic and extrasplanchnic circulation are contained in this package as well.

pckNervousSystem: This package consist of models for physiological control mechanisms, e.g. the baroreflex for blood pressure stabilization. Receptor dynamics, dynamic and static characteristics of afferent and efferent nerval pathways, and the reactions of the autonomous nervous system are included. Similar to, for example, the *pckOrgans*, several different models for the same effect are included in the library, and the user can choose the one with the right amount of detail for the problem at hand. Again, by default, a matching set of parameters is assigned to each component.

B. Graphical user interface

A graphical user interface (GUI) was developed in order to provide an easy-to-use interface for a simulation model implemented in Dymola with components of “HumanLib”. Opening up the highly complex model to a wider field of applications and users was the main objective in the process. This provides an opportunity to apply the models in medical training, for example.

The GUI reduces the number of output simulation values to the clinically most relevant ones. Additionally, only few simulation settings (e.g. duration of simulation, input values such as blood loss) can be changed via this interface to the model – integration algorithm or initial values for the simulation cannot be changed.

Fig. 2 shows a screenshot of the interface: in two plot windows, various clinically relevant blood pressures or flows, as well as e.g. total blood volume or heart rate, can be plotted against time. Moreover, pressure-volume (P-V) diagrams can be plotted for right and left ventricle.

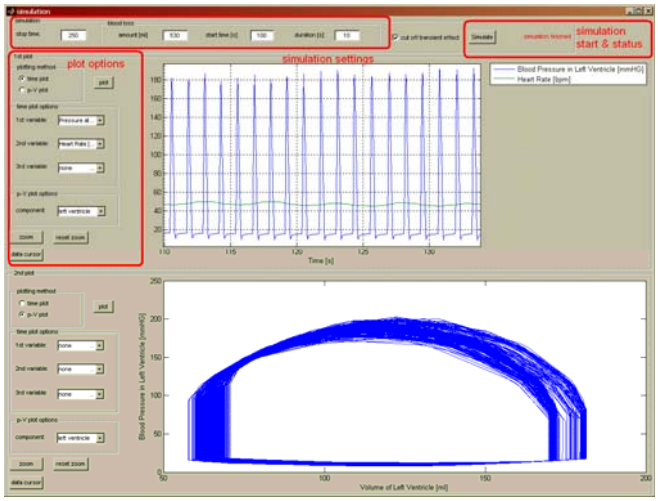

Fig. 2 GUI in Matlab with plots of left ventricular blood pressure and heart rate (top), and P-V diagram of left ventricle (bottom).

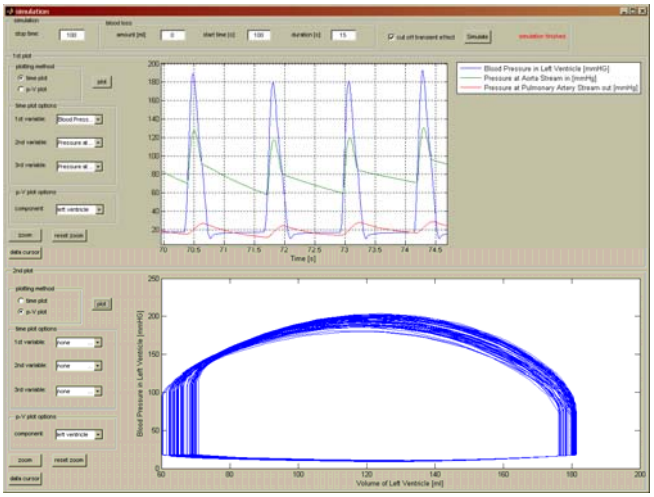

Fig. 3 A simulation using the GUI in Matlab: Blood pressure in left atrium and ventricle and in the aorta (top plot), pressure-volume curve of the left ventricle (bottom plot).

The GUI was implemented in Matlab using the GUI Design Environment (GUIDE) for several practical reasons:

- GUIDE allows fast and comfortable graphical implementation of the GUI.
- Modifications during the testing phase can be conducted easily.
- The Matlab function `dymosim.m` provides a ready-for-use method to simulate a Dymola model from Matlab with full functionality.

Firstly, the Dymola simulation model must be compiled to obtain the Dynamic Model Simulator (Dymosim). The result, `dymosim.exe`, is a stand-alone executable program file generated by Dymola to simulate the model [14]. In a command line function call from Matlab, initial values can be set or read from a file, the integration method can be chosen, and other simulation settings such as tolerance or the number of integration intervals can be set. Basically, use of this function yields the same functionality a simulation in Dymola would offer. Most of these commands are encapsulated in the GUI, only duration of simulation and amount, start und duration of hemorrhaging can be set by the user.

However, as `dymosim.exe` is a stand-alone program, graphical interfaces are not limited to Matlab. It is possible to switch to C-code, for example, after the initial testing phase is completed.

III. Results

Fig. 3 shows an exemplary simulation started from the GUI in Matlab. The model used is based mostly on work from Ursino et al. [4-6]: a fluid dynamic model of the vascular system is coupled to a pulsating heart. A schematic representation is shown in Fig. 4. The model includes three physiological control loops: arterial and cardiopulmonary baroreflexes, and the lung stretch reflex.

Comparison with textbook data [15] shows a good qualitative correspondence of the plotted variables, although a rather high pressure difference between ventricular and aortic pressure can be seen. This corresponds to a higher than normal flow resistance through the aortic valve; according to Hagen-Poiseuille's law that corresponds to stenosis of the aortic valve.

IV. Discussion

The results presented in the previous section show qualitatively good results. Quantitatively, further parameter adaption will have to be made. For that reason, and for analysis of the general behavior of various simulation models, in vivo validation is planned.

Initial tests with the GUI system showed good performance and comfortable operability. However, some adaptions will have to be made before the system can be applied in education, for example. This includes, among others, differ-

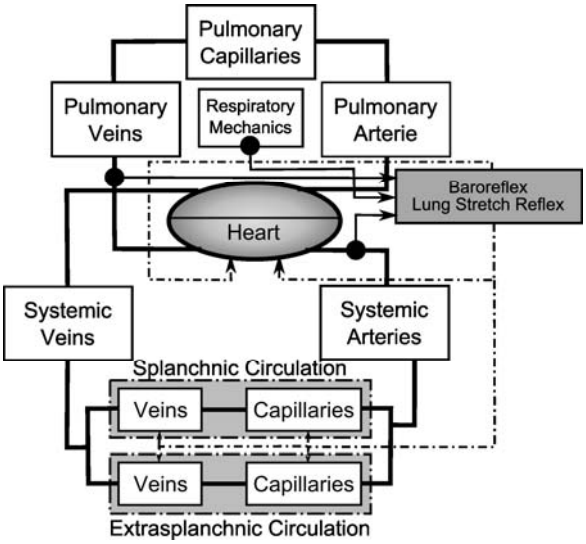

Fig. 4 Schematic representation of the simulation model.

ent simulation settings with different choices of input variables and initial condition, and a choice of variables to be plotted which matches the simulation setting. Finally, a stand-alone graphical interface instead of the Matlab-based one will be implemented.

"HumanLib" contains, as of yet, mostly components describing fluid dynamic processes in the heart and vasculature, as well as centrally controlled physiological control mechanisms. Additionally, autonomous control mechanisms, gas exchange and transport and connected regulatory mechanisms will have to be included into the library. Furthermore, so far mainly short-term processes were considered, even though long-term processes are highly relevant for example in blood pressure control (renin-angiotensin system etc.).

V. Conclusions

"HumanLib" provides a new way of modeling and simulating the human cardiovascular system: an object-oriented component library which lets the user choose from a number of component models and build a simulation model specifically suited for the current problem. To facilitate use of the model especially for people without a technical background (e.g. in educational purposes), a graphical user interface was developed. Basic values can be plotted, and the most important simulation settings can be changed.

"HumanLib" can not only be of good use in medical education and training, furthermore, it is a variable design and testing platform for the development of assist devices such as ventricular assist devices or the totally artificial heart.

References

1. Brunberg A, Autschbach R, Abel D (2008) Ein objektorientierter Ansatz zur Modellierung des menschlichen Herz-Kreislauf-Systems. at – Automatisierungstechnik 56: 476–482
2. Brunberg A, Abel D, Autschbach R (2008) An Object-oriented Model of the Cardiovascular System with a Focus on Physiological Control Loops. IFMBE Proceedings Vol. 22, 4th European Congress For Medical and Biomedical Engineering, Antwerp, Belgium 2008, DOI 10.1007/978-3-540-89208-3
3. Nötges T, Hölemann S, Bayer Botero N, Abel D (2007) Objektorientierte Modellierung, Simulation und Regelung dynamischer Systeme am Beispiel eines Oxyfuel-Kraftwerksprozesses. at – Automatisierungstechnik 55: 236–243
4. Ursino M (1998) Interaction between carotid baroregulation and the pulsating heart: a mathematical model. Am J Physiol 275: H1733–H1747
5. Magosso E, Biavati V, Ursino M (2001) Role of the Baroreflex in Cardiovascular Instability: A Modeling Study. Cardiovascular Engineering 1: 101–115
6. Ursino M, Magosso E (2003) Role of short-term cardiovascular regulation in heart period variability: a modeling study. Am J Physiol Heart Circ Physiol 284: H1479–H1493
7. Lu K, Clark JW, Ghorbel FH, Ware DL, Bidani A (2001). A human cardiopulmonary system model applied to the analysis of the Valsalva maneuver. Am J Physiol Heart Circ Physiol 281: H2661–H2679
8. Liu CH, Niranjan SC, Clark JW, San KY, Zwischenberger JB, Bidani A (1998) Airway mechanics, gas exchange, and blood flow in a nonlinear model of the normal human lung. J Appl Physiol 84: 1447–1469
9. Suga H, Sagawa K (1974) Instantaneous pressure-volume relationships and their ratio in the excised, supported canine left ventricle. Circ Res 35: 117–126
10. Gaasch WH, Cole JS, Quinones MA, Alexander JK (1975) Dynamic determinants of letf ventricular diastolic pressure-volume relations in man. Circulation 51 : 317–323
11. Piene H (1984) Impedance matching between ventricle and load. Ann Biomed Eng 12: 191–207
12. Hunter WC, Janicki JS, Weber KT, Nordergraaf A (1983) Systolic mechanical properties of the left ventricle. Effects of volume and contractile state. Circ Res 52: 319–327
13. Noordergraaf A, Verdrouw D, Boom HB (1963) The Use of an Analog Computer in a Circulation Model. Prog Cardiovasc Dis 5: 419–439
14. Dynasim AB (2004) Dymola User's Manual Version 5
15. Klinke R, Pape H, Silbernagl S (2003) Physiologie. Georg Thieme Verlag, Stuttgart

Corresponding author:

Author: Anja Brunberg
Institute: Institute of Automatic Control, RWTH Aachen University
Street: Steinbachstr. 54
City: 52074 Aachen
Country: Germany
Email: a.brunberg@irt.rwth-aachen.de

Artificial heart valves, flow acceleration and shear stresses

Ali A Sakhaeimanesh[1]

[1] Biomedical Engineering Group, Faculty of Engineering, University of Isfahan, Isfahan, Iran

Abstract---**In the reviewed literature, it was found that estimated turbulent shear stresses under pulsatile flow were higher than those found under steady flow conditions for the same valve. To find the possible cause of the flow acceleration on elevating turbulent shear stresses, mechanical energy (sum of kinetic and pressure energies) differences across the St. Vincent valve were calculated under both pulsatile and steady flow conditions at the same flow rate and compared. An Eulerian approach, which is preferred in fluid mechanics, was used to find temporal flow acceleration in the St. Vincent valve. Two sample windows of 10 ms were selected during the acceleration and deceleration phases of the St. Vincent valve where instantaneous flow rates were 15 or 26 l/min (at cardiac outputs of 4, 5.5 and 7 l/min). These two instantaneous flow rates were identical to the flow rates established in steady flow investigation. Using the energy equations, kinetic and pressure energy differences across the valve in the pulsatile flow and steady flow and the difference were calculated. It was found that the energy of the flow due to the flow acceleration was:**

$H_{acc-dec(viscous-dissipation)-at\,26l/\min} = H_{Pulsatile-acc-dec} - H_{steady}$

=3.655 *Watts*

Due to the fact that size and shape of the valve, blood analogue fluid, shape and size of valve chambers and Reynolds numbers were the same in both steady and pulsatile flow investigations (for the instantaneous flow rate identical to that of steady flow), the differences between mechanical energies of the pulsatile flow and of the steady flow, $H_{acc-dec(viscous-dissipation)}$, was associated with the temporal acceleration of the fluid flow, which existed in a pulsatile flow regime. In the other word, higher estimated stresses in the pulsatile flow degraded from these mechanical energies, $H_{acc-dec(viscous-dissipation)}$, into thermal as viscous dissipation.

Keywords---**pulsatile flow, turbulent shear stress, St. Vincent valve, flow acceleration, steady flow**

I. Introduction

Despite the fact that the Bernoulli equation is derived with the assumption of (1) steady flow; (2) fluid is incompressible; (3) no viscous dissipation and (4) the flow is laminar along a streamline, its application will be useful in flow through constrictions and across valve orifices. Gorlin and Gorlin [1] were the first to use this equation in the clinical literature to determine the effective orifice area. With the assumption of inviscid incompressible fluid under steady flow conditions, the Bernoulli equation is given by:

$$\Delta(P + \frac{\rho V^2}{2} + \rho g Z) = 0$$

This formula shows the conservation of Kinetic, potential and pressure energy passing through two cross sections of a control volume. Using the first law of thermodynamics, a mechanical energy balance for a control volume can be obtained as

$$\Delta(\frac{\overline{V}^2}{2}) + g\Delta Z + \frac{\Delta P}{\rho} + \Phi + W = 0$$

where Φ is rate of energy dissipation (or gained) in the control volume mostly in the form of viscous dissipation

And W is the rate of work down by (or on) the control volume.

In the reviewed literature, it was found that estimated turbulent shear stresses under pulsatile flow were higher than those found under steady flow conditions (except in the study of Hanle *et al*., [2]) for the same valve but to the author knowledge, the cause has not been assessed. In this study, also turbulent shear stresses under pulsatile flow were found to be higher than those found under steady flow. To find the possible cause of the flow acceleration or deceleration on elevating turbulent shear stresses, this study was carried out.

II. Method

To investigate the effects of acceleration on elevating turbulent shear stresses, St.Vincent valve was selected. The St. Vincent valve is reminiscent of the Björk-Shiley standard model but uses a Derlin flat disc. Diagram of mock circulation for pulsatile flow investigation is shown in figure 1. A model of the left ventricle and load was incorporated with the drive unit for testing St. Vincent valve in the aortic position under practical flow and loading conditions. The artificial heart and connecting tubes were arranged vertically and valves were mounted in their correct position in an especially molded flexible ventricle. Flow was driven by a servo-controlled piston pump (VSI pump) that compressed the ventricle to simulate the physiological

O. Dössel and W.C. Schlegel (Eds.): WC 2009, IFMBE Proceedings 25/XIII, pp. 170–173, 2009.
www.springerlink.com

flow. A programmed waveform generator was used to control the pump. Four unique waveforms, including physiological waveform were stored in the memory and these capacitated the waveform generator to produce calibrated waveforms in eight selectable frequencies.

For steady flow investigation, pulse duplicator was removed from mock circulation and a centrifugal pump was installed downstream of the valve. The flow rate through the steady flow system could be varied from 0 to 26.5 l/min with the aid of the gate valve. In this study, flow rates of 15 and 26 l/min were established. These produced mean velocities of 0.8 and 1.4 m/s across the valve chamber respectively. Velocity measurements were made across the valve at downstream of the valve.

A blood analogue fluid of water-saline solution with a bulk viscosity of 1.006×10^{-3} Pa S was contained inside the ventricle chamber and was separated from the piston pump by the polymeric flexible ventricle. In the inlet of the flexible ventricle chamber (mitral position) a Björk-Shiley tilting disc valve was installed.

To reduce optical noise, the aortic-valve flow section was placed in an index matching enclosure filled with water for LDA measurements. An electromagnetic square-wave flowmeter, which was calibrated before measurement, was installed 2D downstream of the valve so that the instantaneous flow rates could be determined. The pressure pulses were measured by three disposable and physiological blood pressure transducers in the left ventricle, downstream of the aortic valve and in the compliance chamber. Pressure taps were located in the wall of the ventricular chamber (close to inlet of the aortic valve), in the wall of compliance chamber and at 2D downstream of the aortic valve. Flow measurements were done at cardiac outputs of 4, 5.5 and 7 l/min. All experiments were conducted at a heart rate of 1.2 Hz (72 beats/min).

A Dantec (Skovlunde, Denmark) two-component LDA system was used to determine the flow field at various locations downstream of the valve. The system comprises a two-color, four-beam optical arrangement utilizing the green (wave length = 514.5 nm) and blue (wave length = 488 nm) lines of a 5 W Argon-Ion laser.

For steady flow measurements, data acquisition was used in continuous mode with number of samples of 3000 and stop mode on validated 3000 samples while the dead time mode was off to ensure that data acquisition terminated on the number of validated samples to be collected. In the pulsatile flow measurements, data was collected in continuous mode over 100 to 200 cycles, depending on the collected data rate to ensure that at least 1000 samples would be collected during every 5 ms of the forward flow phase. After collecting data over complete cycles, data from each cycle is divided into 168 sample windows, each 5 ms duration. Then data belong to nth sample window of each cycle was complied into nth bin and averaged to yield fluctuating and mean components.

The axial and radial mean velocities, $\overline{U}$ and $\overline{V}$, the r.m.s of axial and radial fluctuation components, turbulent intensity and the cross, $\overline{uv}$, were calculated.

More details of steady and pulsatile mock circulatory systems and LDA technique are given elsewhere [3 & 4].

Sample windows of 10 ms were selected during the acceleration and deceleration phases of the St. Vincent valve where instantaneous flow rates were 26 and 15 l/min respectively (at cardiac output of 4 and 5.5 and 7 l/min). These instantaneous flow rates were identical to the flow rate established in steady flow investigation. From the flow and pressure signals (e.g. at cardiac output of 7 l/min during acceleration phase) which were recorded during these sampling windows and in the neighboring sample windows, it was found that flow velocity and pressure were 1.38 m/s (corresponding to an instantaneous flow rate of 26 l/min) and 223.9 mm Hg respectively. In the steady flow investigation, pressure drops across the St. Vincent valves were found to be 5 and 9 mm Hg under flow rates of 15 and 26 l/min respectively. Mean axial velocities were 0.796 and 1.38 m/s under flow rates of 15 and 26 l/min respectively.

Using the energy equations, the relationship between kinetic and pressure energy differences across the valve in the pulsatile flow and steady flow and the difference between calculated energies can be described as:

$$\left[(P_1Q_1-P_2Q_2)+\rho g(Z_1Q_1-Z_2Q_2)+\frac{\rho(V_1^2Q_1-V_2^2Q_2)}{2}\right]_{pulsatile\,acc-dec}=H_{Pulsatile\,acc-dec}$$

$$\left[(P_1-P_2)Q+\rho g(Z_1-Z_2)Q+\left(\frac{\rho V_1^2-\rho V_2^2}{2}\right)Q\right]_{steady}=H_{steady}$$

$$H_{acc-dec(viscous-dissipation)}=H_{Pulsatile\,acc-dec}-H_{steady}$$

The last formula indicates that difference between calculated mechanical energy differences across the valve in the pulsatile and steady flow is equal to energy associated with the flow acceleration or deceleration, $H_{acc-dec(viscous-dissipation)}$.

Mechanical energies of flow were measured at up and downstream of the valve. Flow was assumed to be incompressible and convective flow acceleration was neglected. Gravitational effects, $\rho g(Z_1Q_1 - Z_2Q_2)$ and $\rho g(Z_1 - Z_2)Q$, were neglected in all measurements due to the fact that height difference between points of flow measurements, $(Z_1 - Z_2)$, was less

than 5 cm. By assumption that at a velocity of 0.8 m/s or higher (at instantaneous flow rate of 15 l/min or higher), it takes a maximum of 10 ms time for a fluid particle to pass across the valve, then the change in flow velocity can be obtained from the flow signals recorded in neighboring sample windows of the cardiac cycle. Therefore, velocity, V_2 were measured directly by electromagnetic flowmeter and V_1 was estimated from flow signal recorded in a 10 ms earlier sample window of the cardiac cycle. In the above formulas Q indicates flow rate, m^3 /s, P is pressure, N/m^2, and V is velocity, m/s. As flow velocity is constant in steady flow, the value of $\frac{\rho V_1^2 - \rho V_2^2}{2}$ in the steady term of the formula becomes zero and the formula changes to: $[(P_1 - P_2)Q]_{steady} = H_{steady}$ In the pulsatile flow where flow accelerates, velocity varies with time and $\frac{\rho(V_1^2 Q_1 - V_2^2 Q_2)}{2}$ will not be equal to zero.

III. Results and Discussion

A comparison between shear stresses (mean and maximum) and the r.m.s of the axial velocities (mean and maximum) in the steady flow and pulsatile flow experiments at 0.5D (D, diameter. mm) downstream of the St. Vincent valve are presented in table 1. Data presented for the instantaneous flow rate of 15 and 26 l/min belongs to sample window of 5 ms of the cardiac cycle during acceleration or deceleration phases of the St. Vincent valve (at cardiac outputs of 4, 5.5 and 7 l/min).

By substituting pressure and velocity values in the energy equations, the energy of the flow was calculated at cardiac output of 7 l/min during acceleration phase where instantaneous flow rate was 26 l/min as:

$$H_{Pulsatile-acc} = (223.9 \times 1.94 - 256.98 \times 1.38) \times 3.14 \times 10^{-4} \times 133.3 + \frac{1000 \times (1.94^3 - 1.38^3) \times 3.14 \times 10^{-4}}{2} = 4.175 Watts$$

$$H_{steady} = 9 \times 1.38 \times 3.14 \times 10^{-4} \times 133.3 = 0.52 Watts$$

$$H_{acceleration(viscous-dissipation)-at\,26l/\min} = H_{Pulsatile-acc} - H_{steady} = 3.655\ Watts$$

The results of flow acceleration and deceleration energies are presented in table 2 for all measured velocity and pressure values during acceleration and deceleration phases at cardiac outputs of 4, 5.5 and 7 l/min.

As can be seen in table 1 and 2, there is a direct relationship between flow acceleration or deceleration with energy dissipations and estimated turbulent shear stresses.

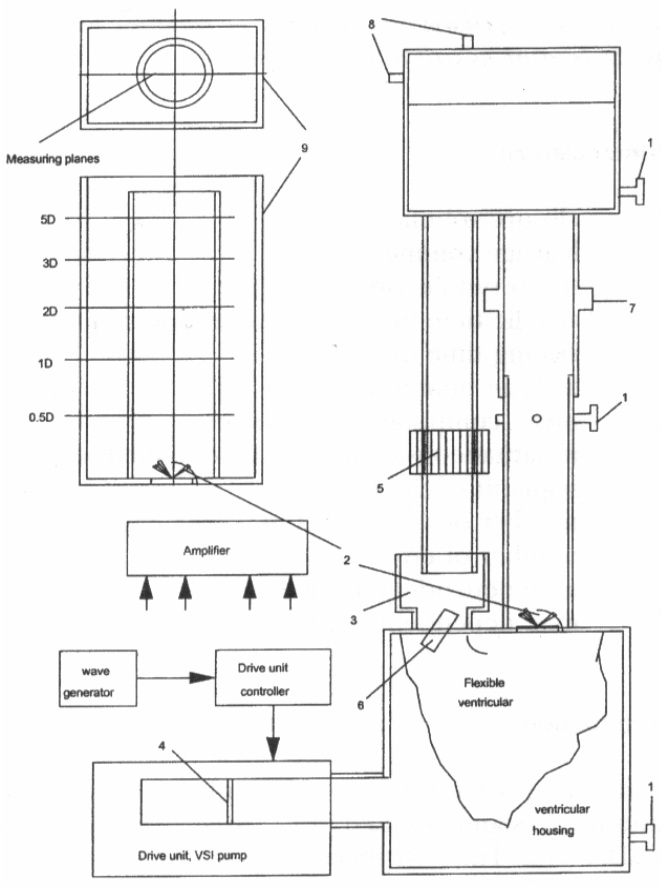

Fig. 1: Diagram of the pulse duplicator used in this study (not in scale), (1) ventricular, aortic and compliance pressure taps; (2) aortic valves; (3) mitral chamber; (4) pump piston; (5) adjustable resistance; (6) mitral valve; (7) electromagnetic flow meter probe; (8) air releaser and air pump; (9) index matching box.

As all parameters affecting Reynolds number are the same, it can be emphasized that higher magnitude of flow acceleration or deceleration results in higher energy dissipation which is attributed with shear stress estimation.

Due to the fact that size and shape of the valve, blood analogue fluid, shape and size of valve chambers and Reynolds numbers were the same in both steady and pulsatile flow investigations (for the instantaneous flow rate identical to that of steady flow), the differences between mechanical energies of the pulsatile flow and of the steady flow, $H_{acc-dec(viscous-dissipation)}$, is associated with the

temporal acceleration of the fluid flow, which exists in a pulsatile flow regime. In the other word, higher estimated shear stresses in the pulsatile flow degraded from these mechanical energies, $H_{acc-dec(viscous-dissipation)}$, into thermal as viscous dissipation.

Table 1: Comparison between shear stresses and r.m.s of axial velocities obtained 0.5Downstream at of the St. Vincent valve in steady and pulsatile flow experiments with the same flow rates.

Steady flow			pulsatile flow			
At 0.5D downstream of the St. Vincent valve			During acceleration phase, between 50-55 ms at cardiac output of 4 l/min	During deceleration phase, between 125-130 ms at cardiac output of 5.5 l/min.	During acceleration phase, between 55-60 ms at cardiac output of 7 l/min.	During deceleration phase, between 185-190 ms at cardiac output of 7 l/min.
Flow rates (Q), l/min	15	26	15	26	26	26
Max. shear stresses, N/m2	31	57	38	60	69.46	63.09
Mean shear stresses, N/m2	7.8	16.9	9.8	19.6	29.24	17.23
Max. r.m.s of axial velocities, m/s	0.47	0.63	0.53	0.710	0.80	0.738

Table 2: Mechanical energies of steady and pulsatile flow and the differences which are associated with flow acceleration or deceleration.

	$H_{Pulsatile-acc-dec}$, *Watts*	H_{steady}, *Watts*	$H_{acc-dec(viscous-dissipation)}$, *Watts*
At cardiac output of 7 l/min during acceleration phase where instantaneous flow rate was 26 l/min	4.17	0.52	3.655
At cardiac output of 7 l/min during deceleration phase where instantaneous flow rate was 26 l/min	2.077	0.52	1.557
At cardiac output of 5.5 l/min during acceleration phase where instantaneous flow rate was 26 l/min	3.590	0.52	3.070
At cardiac output of 5.5 l/min during deceleration phase where instantaneous flow rate was 26 l/min	1.01	0.52	0.4918
At cardiac output of 4 l/min during acceleration phase where instantaneous flow rate was 15 l/min	2.75	0.166	2.585
At cardiac output of 4 l/min during deceleration phase where instantaneous flow rate was 15 l/min	0.461	0.166	0.2950

Reference

1. Gorlin R. and Gorlin S. G. (1951) Hydraulic formula for the calculation of the area of stenotic mitral valve, other cardiac valves and central circulatory shunts. Am. Heart J., 41, 1.
2. Hanle, D.D., Harrison, E.C., Yoganathan, A.P., Allen, D.T. and Corcoran, W.H. (1989) In vitro flow dynamics of four prosthetic valves, a comparative analysis. Journal of Biomechanics, 22, 597 – 607.
3. Morsi Yos S. and Sakhaeimanesh Ali A. (2000) Flow characteristics past jellyfish and St. Vincent valves in the aortic position under physiological pulsatile flow conditions. Artificial Organs, 24(7), 564-574.
4. Sakhaeimanesh Ali A. (2008) Effect of oscillation on elevating sheer stresses. Journal of Medical Engineering and Technology, 32(6), 434-439.

Author: Ali. A. Sakhaeimanesh
Institute: Biomedical Engineering Group, Faculty of Engineering, University of Isfahan
City: Isfahan
Country: Iran
Email: sakhaei@eng.ui.ac.ir

Optimization of Clinical Radiofrequency Hyperthermia by Use of MR-Thermography in a Hybrid System

P. Wust[1], M. Weihrauch[1], M. Weiser[2], J. Gellermann[1], S. Eisenhardt[1], T. Chobrok[1], and V. Budach[1]

[1] Charité Universitätsmedizin Berlin, Clinic for Radiation Oncology, 13353 Berlin, Germany
[2] Konrad Zuse Institut, Department of Numerical Analysis and Modeling, 14195 Berlin, Germany

Abstract— **The method to acquire MR-temperature datasets by the proton-resonance-shift method is outlined and verified in phantoms and patients. An online adaptation process has been developed to achieve agreement between planning calculations and MR-temperature measurements. This is used as a basis to optimize the pattern by a control loop. This procedure is successful after the second iteration step in phantoms. In patients an increase of SAR (specific absorption rate) in the tumor relative to the surroundings has been demonstrated for the MR-temperature increase as optimization variable. The optimization results are even improved under clinical conditions, if perfusion and thermal conduction are considered during the optimization procedure. The mathematical background is presented.**

Keywords— **MR-thermography, online-control, optimization, radiofrequency hyperthermia.**

I. Introduction

Relevant improvements of power deposition patterns (specific absorption rate in W/kg) and temperature distributions during regional hyperthermia are only possible by an appropriate feedback on-line control. Non-invasive MR-thermography for on-line control has been successfully utilized and verified in homogeneous and heterogeneous (anthropomorphic) phantoms (Weihrauch et al 2007, Med.Phys.). The fundamental reason for this necessity is the inaccuracy of treatment planning. Slight uncertainties in the planning process accumulate and prevent the congruence of the theoretical (planned) and measured (actual) patterns. We identified as main error sources phase and amplitude errors (partially caused by antenna coupling) and (more important) distortion of the radiating antenna functions.

This study attempts to establish an MR-controlled feedback control in clinical heat treatments.

II. Methods

The pattern achieved in phantoms or patients can be derived from phase differences acquired by GRE sequences with proper TR and TE. A proper drift correction is indispensable (Gellermann et al 2005a). Non-invasive MR monitoring works in phantoms (Gellermann et al 2005b) as well as in pelvic and lower extremities tumors (Gellermann et al 2005c, 2006a).

In phantoms severe deviations have been found between the MR temperature distributions and planning calculations for a specific setup derived from a CT model. At first a significant improvement of the agreement is achieved after adaptation of antenna functions using a Gauss-Newton method. The re-calculated base functions are used to optimize the pattern. In the next step an improved pattern and a satisfactory agreement between a second MR measurement and the optimized pattern is achieved. This procedure (adaptation and optimization) can be repeated and leads to further improvement. However, the first iteration yields the highest advancement (Gellermann et al 2006b, Weihrauch et al 2007).

Employing this method we attempted to refine the MR temperature distributions in 20 heat treatments of 9 patients. The procedure is based on the simple assumption that MR temperature increase can be equated with SAR, meanwhile perfusion and thermal diffusion are neglected.

III. Results

An online control was possible in 8/20 heat treatments of 4 patients. In each of these 8 treatments a satisfactory agreement between the calculated pattern (applying the adapted antenna functions) and the following MR-acquisition could be achieved. After switching to an optimized setup in each of these 8 sessions a quantitative increase of MR temperatures per time in the tumor (relative to muscle tissue) could be demonstrated. In all sessions the improvement of the MR temperature distribution was also evident from the qualitative inspection.

In 14 optimized settings (phases, amplitudes) during the 8 sessions a mean SAR in the tumor of 0.3 °C/min per 1000 W was achieved. This value (of 0.3 °C/min) is accepted as indication of an effective regional hyperthermia. The mean elevation of SAR above the non-optimized pattern was the significant amount of 0.1 °C/min per 1000 W.

O. Dössel and W.C. Schlegel (Eds.): WC 2009, IFMBE Proceedings 25/XIII, pp. 174–175, 2009.
www.springerlink.com

In the other 12/20 heat treatments (in 5 patients) the on-line control failed by various reasons, in particular because of deficiencies of the MR-data (noise), patient movements and differences between the pre-treatment model of the patient and his actual position. The analysis shows that the success rate can be considerably increased under routine conditions.

We used as objective function the mean temperature increase in the tumor (target) relative to the normal tissue (muscle). This criterion simply aims to enlarge the SAR in the tumor region. However, patterns derived from these SAR-based objective functions are known (Wust et al 1996) to generate hot spots, and this kind of side effect was in fact clinically observed in some treatments. Therefore, a more sophisticated optimization algorithm is needed, which considers perfusion and thermal diffusion of every tissue.

IV. Conclusions

The tools for MR-controlled regional hyperthermia have been developed. A strategy is available to achieve agreement between planning calculations and MR-temperature distributions. Better temperature patterns can be achieved in most heat treatments by switching to an optimized phase setup. However, consideration of diffusion and perfusion will probably yield even better results. Advanced algorithms for this purpose are under development.

Acknowledgments

This work is supported by the Deutsche Forschungsgemeinschaft (DFG), Projects Wu 235/1-2.

References

1. Gellermann, J., W. Wlodarczyk, A. Feussner, H. Fähling, J. Nadobny, B. Hildebrandt, R. Felix, P. Wust: Methods and potentials of magnetic resonance imaging for monitoring radiofrequency hyperthermia in a hybrid system. Int. J. Hyperthermia 2005a; 21,6: 497-513
2. Gellermann J, Wlodarczyk W, Ganter H et al. (2005b) A Practical Approach to Thermograph in a Hyperthermia/ Magnetic Resonance Hybrid System: Validation in a Heterogeneous Phantom. Int J Radiat Oncol Biol Phys 2005b; 61: 267–277
3. Gellermann J, Wlodarczyk W, Hildebrandt B et al. Non-invasive magnetic resonance thermography of recurrent rectal carcinoma in a 1.5 Tesla hybrid system. Cancer Res 2005c; 65: 5872-80
4. Gellermann J, Hildebrandt B, Issels RD et al. Non-invasive MR-thermography of soft tissue sarcomas during regional hyperthermia: Correlation with response and direct thermometry. Cancer 2006a; 107: 1373-1382
5. Gellermann J, Weihrauch M, Cho CH et al. Comparison of MR-thermogaphy and planning calculations in phantoms. Med Phys 2006b; 33: 3912-3920
6. Weihrauch M, Wust P, Weiser M et al. Adaptation of antenna profiles for control of MR guided hyperthermia (HT) in a hybrid MR-HT system. Med Phys 2007; 34: 4717-4725
7. Wust, P., M. Seebass, J. Nadobny, P. Deuflhard, G. Mönich, R. Felix: Simulation studies promote technological development of radiofrequency phased array hyperthermia. Int. J. Hyperthermia 12,4 (1996) 477 – 494

Corresponding author:

Prof. Dr. Peter Wust
Charité Universitätsmedizin Berlin – Campus Virchow Klinikum
Department of Radiation Oncology
Augustenburger Platz 1
13353 Berlin
Germany
Email: peter.wust@charite.de

Xenon Biosensors for Multi-Purpose Molecular Imaging

Leif Schröder[1,2], Tyler Meldrum[1,3], Monica Smith[1,3], Franz Schilling[1,4], Philipp Denger[5], Sina Zapf[4], David Wemmer[1,3] and Alexander Pines[1,3]

[1] Lawrence Berkeley National Lab, Materials Sciences and Physical Biosciences Divisions, Berkeley, USA
[2] Leibniz-Institut für Molekulare Pharmakologie, Berlin, Germany
[3] University of California at Berkeley, Department of Chemistry and qb3 Institute for Quantitative Biosciences, Berkeley, USA
[4] Julius-Maximilians-Universität Würzburg, Experimentelle Physik V, Würzburg, Germany
[5] Deutsches Krebsforschungszentrum, Abteilung Medizinische Physik in der Radiologie, Heidelberg, Germany

Abstract—

Hyperpolarized xenon is an exquisite NMR probe for sensing molecular environments of the noble gas in solution. By trapping it in molecular cages like cryptophane-A, ^{129}Xe can report information about molecular-specific binding events or resolve multiple signals simultaneously from different micro-environments in a lipid emulsion—a macroscopically-homogeneous phase that mimics properties of biological relevance. The Hyper-CEST detection scheme can be used in this context to pair significant signal enhancement with high specificity of xenon NMR resonances. Hyper-CEST can reduce the measurement time by a factor of up to 16 million and is currently able to detect biosensor concentrations as low as 1.4 nM. When combined with highly frequency-selective pulses, it also allows for demonstration of multiplexing potential using a single cage type as contrast agent for different environments in NMR imaging. This molecular imaging approach enables a switchable contrast that includes also temperature-sensitive imaging with molecular sensors that can be functionalized with various targeting molecules to bind, e.g., specifically to receptors of cancer cells.

Keywords— **Biosensors, Hyper-CEST, xenon, hyperpolarization, molecular imaging.**

I. Introduction

Recently, several groups have focused attention on xenon-based NMR biosensors, a new type of targeted MRI contrast agents using cryptophane as a host molecule for xenon. Because xenon can be hyperpolarized and its NMR resonance frequency is extraordinarily sensitive to its chemical environment, it easily reports a significantly different chemical shift while associated with the biosensor than while dissociated. Furthermore, xenon atoms trapped in different biosensors exhibit different chemical shifts [1, 2], a property that Berthault et al. capitalized upon in demonstrating the potential for multiplexing—detecting two chemically distinguishable biosensor targets simultaneously, albeit in physically separated solvents—and extended this multiplexing to an imaging modality [3].

Although the application of hyperpolarization provides huge signal amplification and is therefore the appropriate method to overcome typical NMR sensitivity limitations, the signal obtained directly from the Xe encapsulated in the biosensor cage is rather small compared to the signal from hyperpolarized Xe dissolved in the surrounding medium [4]. This paper demonstrates the potential of xenon biosensors for MR imaging when detected with a new approach based on chemical exchange saturation transfer (CEST).

II. Methodology

A. Xenon Biosensors

Xenon biosensors exploit the fact that the resonance frequency of hyperpolarized ^{129}Xe in solution is strongly shifted when it associates with a molecular cage such as cryptophane [5, 6]. Such cages can be functionalized with a targeting unit (antibody or ligand) to form xenon biosensors [2] in order to track a specific analyte upon biochemical binding. Biotinylated cage constructs are common examples for detecting avidin, and protein-linked cages have the potential to bind to specific cell membrane receptors. An example for the modular structure of such sensors is given in Fig. 1. Also, the resonance frequency for encapsulated Xe depends on the ambient temperature. Shielding of the local field experienced by the noble gas inside the cage increases with higher temperatures, thus shifting the resonance to lower chemical shifts [7]. This effect can be used for temperature monitoring.

B. Hyper-CEST Detection

CEST experiments with hyperpolarized nuclei (Hyper-CEST) have been demonstrated to significantly enhance the sensitivity for detection of a dilute spin species via the intense signal of an abundant spin reservoir that is in chemical exchange with the nuclei of interest [8]. Hyper-CEST is

O. Dössel and W.C. Schlegel (Eds.): WC 2009, IFMBE Proceedings 25/XIII, pp. 176–179, 2009.
www.springerlink.com

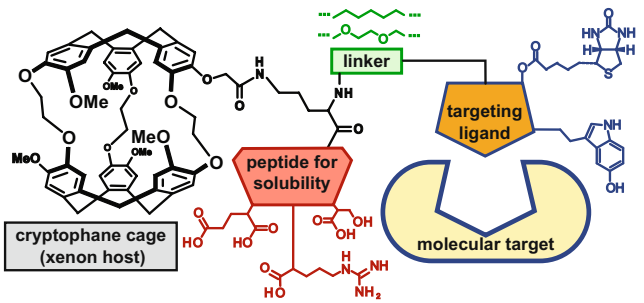

Fig. 1: Modular structure of xenon biosensors. The molecular cage (cryptophane-A in this case) to trap the hyperpolarized xenon and give it a unique resonance frequency is connected to a targeting ligand (e.g., biotin or serotonin) that enables binding to a specific biochemical target.

based on selective saturation of the Xe biosensor signal at ca. 65 ppm and subsequent 2-dimensional mapping of the bulk Xe resonance at 193 ppm. This scheme enables relative fast acquisition of molecular images that show the spatial distribution of the sensor. Since the sensitivity enhancement is based on the exchange dynamics of the encapsulated hyperpolerized nuclei [9], the image contrast also depends on the in situ temperature of the micro-environment of the sensors. Eventually, selective saturation of this magnetization allows an efficient depletion of the intense Xe signal from outside the cage. A two-dimensional phase-encoding MR imaging technique (standard CSI) can then be used to map the spatial distribution of the Xe that was affected by the saturation.

C. Xe-MRI and NMR of Perfusion Phantoms

Imaging experiments were performed on a 2-compartment phantom that contains immobilized avidin-agarose beads. Fig. 2 shows a transverse and sagittal ^{1}H NMR image of the setup. Compartment 2 also contains a biotinylzed Xe biosensor [7] that binds to the beads via its interaction with avidin. A flow system provides perfusion of the phantom with water that was previously bubbled with hyperpolarized Xe. The temperature of the water perfusing the imaging phantom can be adjusted with a controlled heating cable mounted onto the tubing that delivers water to the bead-containing cell. A delay of 0.5-2 s is used for continuous wave saturation prior to each step of the phase encoding.

A ^{129}Xe nuclear spin polarization of ca. 5% was produced by flowing a gas mixture of 89% He, 10% N_2, and 1% xenon (natural abundance of ^{129}Xe: 26%) through a hyperpolarizer (XenoSpin^{TM}, Amersham Health, Durham, NC) where spin exchange with optically pumped rubidium vapor takes place [10]. Data were recorded on a NMR spectrometer (Unity Inova, Varian Inc., Palo Alto, CA) at 7.05 T with a 10 mm ^{1}H/^{129}Xe NMR probe.

D. Xe Biosensors in Solutions of Lipid Bilayers

To demonstrate the multiplexing potential, we used only one type of biosensor as a host for xenon in dilute lipid emulsion, a macroscopically-homogeneous system with two chemically distinct micro-environments. Lipid vesicles of diameter ca. 100 μm are similar in size and composition to cells, making this an important intermediate step toward understanding the in vivo properties of xenon biosensors. For these experiments the hyperpolarized gas mixture was bubbled directly into the sample solution as described previously [4].

III. Results

A. Biosensor Imaging

Fig. 3 shows ^{129}Xe NMR images obtained from a transverse 10 mm slice in the above mentioned perfusion phantom. An illustration of the signal from Xe nuclei in solution displays both compartments as in Fig. 3a when the saturation pulse is applied off-resonant. Changing the saturation frequency to that of the biosensor resonance at ca. 65 ppm yields a selective image of volume 1 without the sensor (Fig. 3b). Hence, the difference image in Fig. 3c directly maps the compartment where the functionalized molecule is present. The concentration of biosensor in compartment 2 is 5 μmM and would require an acquisition time of ca. 45 days when using conventional, direct detection of the sensor signal [11]. Hyper-CEST detection allows to reduce the measurement time by 99.97% to ca. 20 minutes.

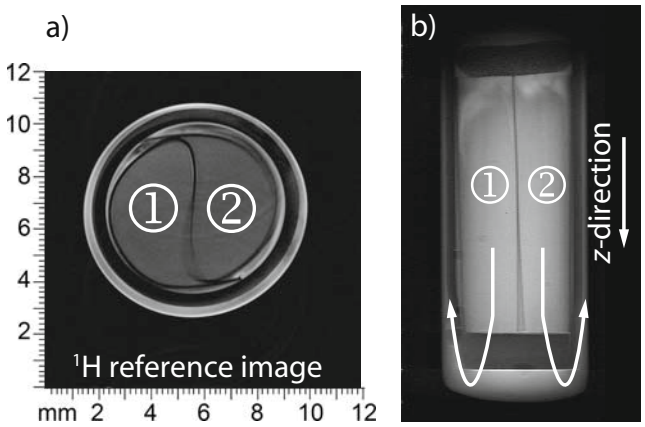

Fig. 2: Transverse (a) and sagittal (b) MR images of the perfusion phantom carrying avidin-labeled agarose beads. Compartment 2 also contains the biosensor with biotin as targeting unit. The arrows indicate the flow path of the xenon-bubbled water through the cell.

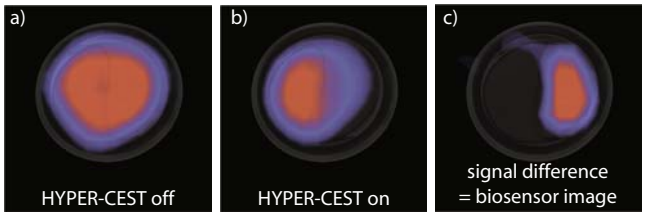

Fig. 3: Demonstration of a biotin-labeled xenon biosensor as contrast agent for detection of the protein avidin. The Hyper-CEST detection scheme allows for selective signal depletion in the compartment where the sensor is bound to the target (b) whereas off-resonant saturation shows no effect (a). The difference image shows the spatial distribution of the selective contrast agent (c).

B. Ultra-Sensitive NMR Spectroscopy

Since the efficiency of the Hyper-CEST effect depends on the exchange dynamics of the temporarily trapped xenon, this effect can be used for ultra-sensitive biosensor detection at elevated temperatures. In a typical setup, the resonance of dissolved, uncaged xenon at 193 ppm can be detected with a signal-to-noise ratio of S/N $\approx$ 185 after 8 acquisitions at 295 K, whereas the diluted encapsulated xenon signal (ca. 33 μM cage concentration) at 65 ppm gives only a S/N $\approx$ 11. Hence, direct detection of nanomolar sensor concentrations would be extremely time consuming. Heating the sample to 313 K and using a saturation pulse of 25.8 μT for 20 sec allows the detection of 10 nM cage concentration, which corresponds to a concentration of encapsulated ^{129}Xe of only 1.4 nM [12] with a Hyper-CEST induced reduction in measurement time from ca. 55 years to ca. 100 sec. This NMR method is even more sensitive than conventional benchtop uv-visible absorbance detection of the cryptophane-A cage ($\varepsilon_{282} = 8000\,\mathrm{M}^{-1}\,\mathrm{cm}^{-1}$, [9])

C. Biosensor-based Thermometry

Xe biosensors can be used for absolute temperature measurements and for monitoring relative temperature changes. An example for the latter case is given by the change in Hyper-CEST contrast upon heating of the perfusion medium. The saturation parameters are chosen to induce low signal transfer onto the solution peak at the initial temperature (Fig. 4a). Upon heating the water flowing through the setup, the CEST effect becomes more efficient and induces a signal contrast in the compartment with the biosensor (Fig. 4b).

For absolute temperature measurements, the temperature dependence of the resonance for a recently developed biosensor precursor [12] was determined to be ca. 0.3 ppm/K (Fig. 5). In contrast, the chemical shift of the free Xe in solution shifts only by 0.04 ppm/Hz. The frequency difference between both peaks can be measured in CSI data sets and allows an absolute temperature determination with an accuracy of ca. 0.1 K when the cage construct is present at a concentrations of 176 μM.

D. Multiplexing

^{129}Xe NMR spectra of cryptophanes in lipid emulsions show two separate resonances for encapsulated Xe: the well-known signal from the cage construct in aqueous solution and a second signal from cryptophanes in lipid environment which appears ca. 10 ppm downfield for the original resonance (Fig. 6a). Using very selective saturation pulses (ca. 12 Hz bandwidth), each signal can be addressed separately to induce a CEST effect for the solution peak. The same saturation scheme can also be used for MR imaging to turn contrast on and off at will (Fig. 6b) for the different microenvironments.

IV. Conclusion

Applying the Hyper-CEST detection scheme to MR imaging with xenon biosensors illustrates how these molecules can be used as very sensitive functionalized contrast agents. They enable discrimination of multiple targets in

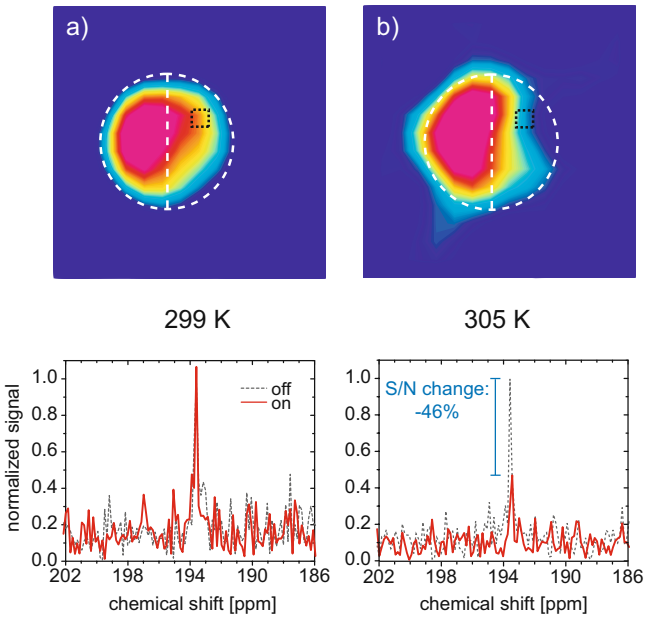

Fig. 4: Temperature-induced contrast change upon increasing the efficiency of the CEST effect. At 299 K, the saturation pulse has almost no impact on the solution peak, as shown by a representative spectrum from a voxel in the ^{129}Xe MRI (a). Heating the water in the perfusion setup by 6 K causes a signal depletion in the compartment with the biosensor (b).

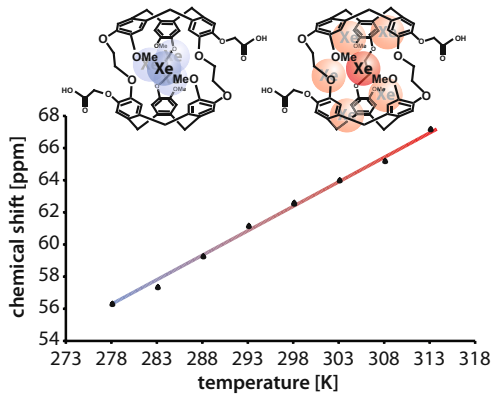

Fig. 5: Temperature-induced variation of the chemical shift of Xe trapped in cryptophane-A with two carboxyl groups. At higher temperatures, the noble gas is involved in more interactions with the outer part of the cavity, resulting in increased shielding of the nucleus and increased chemical shifts.

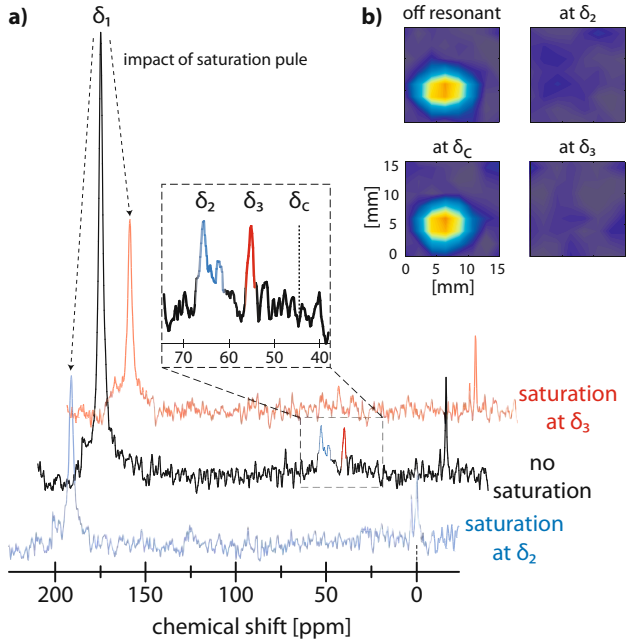

Fig. 6: Demonstrating multiplexing capability with Hyper-CEST. (a) ^{129}Xe spectra for cryptophane in lipid emulsion. δ_2 and δ_3 indicate Xe@cage in lipid and Xe@cage in aqueous environment, respectively. When the saturation pulse is applied at a control frequency corresponding to δ_c, no response is observed. Applying the pulse to either of the peaks, the intensity of the solution peak (δ_1) is significantly reduced. (b) Incorporating the same saturation scheme into imaging illustrates that the contrast can be turned on and of at will with selective saturation pulses

a macroscopically-homogeneous system. Furthermore, the achieved sensitivity and selectivity of the Hyper-CEST detection minimizes the need for atypically high concentrations of or direct chemical modifications to the biosensor to enhance the chemical shift range of xenon.

When studying temperature sensitivity, Xe in Cryptophane-A shows a linear dependence on the temperature that is much more accurate than the standard MR thermometry method using the proton resonance frequency (PRF) shift in ^{1}H MRI [13]. Overall, Xe biosensors hold promising potential for novel multi-purpose contrast agents in molecular MR imaging.

Acknowledgements

L.S. gratefully acknowledges the IOMP executive committee for awarding the 2009 IUPAP Young Scientist Award in Medical Physics to this project. Research and experiments were supported by the Director, Office of Science, Office of Basic Energy Sciences, Materials Sciences and Engineering Division, of the U.S. Department of Energy under Contract No. DE-AC02-05CH11231. Further funding was provided by the Deutsche Forschungsgemeinschaft (grants SCHR 995/1-1 and SCHR 995/2-1 for L.S.), the Studienstiftung des Deutschen Volkes (F.S.) and the Deutsche Akademischer Austausch Dienst (S.Z.)

References

1. Brotin T et al *Eur. J. Org. Chem.* 2003:973.
2. Spence M M et al. *Proc. Natl. Acad. Sci. USA.* 2001;98:10654.
3. Berthault P et al. *J. Am. Chem. Soc.* 2008;130:16456.
4. Han S-I et al. *Anal. Chem.* 2005;77(13):4008.
5. Bartik K et al. *J. Am. Chem. Soc.* 1998;120:784.
6. Huber G et al. *J. Am. Chem. Soc.* 2006;128:6239.
7. Lowery T J et al. *ChemBioChem.* 2006;7:65.
8. Schröder L. et al. *Science.* 2006;314:446.
9. Spence M M et al. *J. Am. Chem. Soc.* 2004;126:15287.
10. Goodson B M. *Concepts Magn. Res.* 1999;11(4):203.
11. Hilty C et al. *Angew. Chem. Int. Ed.* 2006;45:70.
12. Schröder L al. *Phys. Rev. Lett.* 2008;100:257603.
13. DePorter J et al. *J. Magn. Reson. B.* 1994;103:234.

Author: Leif Schröder
Institute: Leibniz-Institut für Molekulare Pharmakologie
Street: Robert-Rössle-Str. 10
City: 13125 Berlin
Country: Germany
Email: schroeder@waugh.cchem.berkeley.edu

Automation in Rehabilitation: How to Include the Human into the Loop

R. Riener[1], A. Duschau-Wicke[1,2], A. König[1], M. Bolliger[1], M. Wieser[1], and H. Vallery[1]

[1] Sensory-Motor Systems Lab, ETH Zurich and University Hospital Balgrist, Switzerland
[2] Hocoma AG, Volketswil, Switzerland

Abstract— **Within rehabilitation robotic applications, integrating the human into the loop can be considered not only from a biomechanical view but also with regard to psycho-physiological aspects. Biomechanical integration involves ensuring that the system to be used is ergonomically acceptable and "user-cooperative". Psycho-physiological integration involves recording and controlling the patient's physiological reactions so that the patient receives appropriate stimuli and is challenged in a moderate but engaging and motivating way without causing undue stress or harm. In this paper, we present examples of biomechanical and psycho-physiological integration of patients verified with the gait robot Lokomat and the dynamic tilt and stepping device Erigo.**

Keywords— **Rehabilitation robotics, patient cooperative, human centered, human in the loop, gait.**

I. Introduction

Several conventional rehabilitation devices work with patients in a "master-slave" relationship, thus, forcing the patients to follow a predetermined motion without consideration of voluntary efforts. The patient or therapist just presses a button or moves a joystick, and a primitive "if-then" algorithm executes a predefined unilateral (unidirectional) action on the human. This action can be the execution of a movement with the support of a machine, or the display of audiovisual information. During such unidirectional communication, biomechanical and psycho-physiological effects on the human are not taken into account for subsequent actions. Thus, the loop is not closed by the human in order to adjust the device to the biomechanical or physiological state of the patient, or his or her behaviour and intention. The possibilities of the human to intervene are reduced to "initiation" and "perturbation". In contrast, novel rehabilitation technologies offer a new approach by placing the human into the loop, where the human feeds back the biomechanical and physiological information to a processing unit. The interaction becomes bi-directional and the technical system takes into account the patient's properties, intentions and actions. Integrating the human into the loop can be considered from biomechanical, physiological and even psychological viewpoints (Fig. 1). Biomechanical integration involves ensuring that the system to be used is safe, ergonomically acceptable and "user-cooperative". Thus, with respect to rehabilitation robotics, the robot assists just as much as needed so that the patient can contribute to the movement with own voluntary effort. Psycho-physiological integration involves recording and controlling the patient's physiological reactions so that the patient receives appropriate stimuli and is challenged in a moderate but engaging and motivating way without causing undue stress or harm.

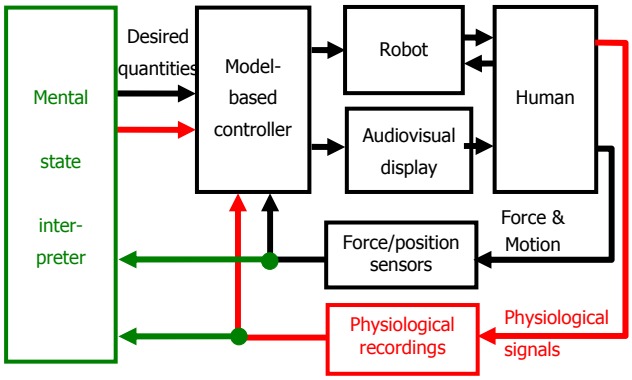

Fig. 1 The human is in the loop with respect to biomechanical (black), physiological (red) and psychological aspects (green).

II. Human Biomechanics in the Loop

A. User-cooperative control of movement

Classical control algorithms for rehabilitations robots such as the Lokomat (Fig. 2) track a predefined movement trajectory, thus, they disregard the activity of the human subject. The human may remain passive during this kind of training [1]. In contrast, new results indicate that training efficacy can be increased by challenging active participation of the human. This is the aim of the user-cooperative Path Control strategy [2], where the human is enabled to influence the movement of the robot and to perform individual motion patterns in a self-determined way – receiving just as much support as needed.

O. Dössel and W.C. Schlegel (Eds.): WC 2009, IFMBE Proceedings 25/XIII, pp. 180–183, 2009.
www.springerlink.com

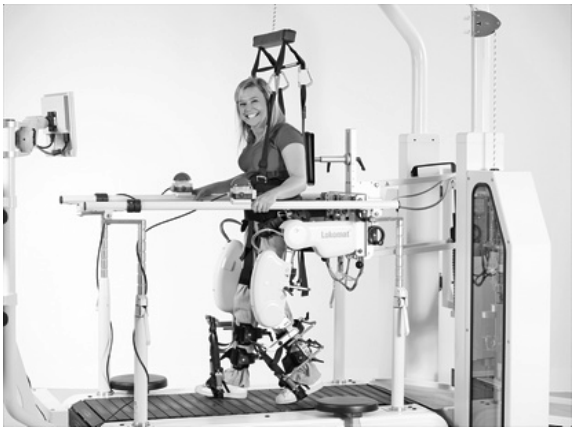

Fig. 2 Human subject training with the Lokomat robot (Hocoma AG, Volketswil, Switzerland

The Path Control strategy is based on an impedance controller that moves the leg along a predefined reference trajectory with an adjustable impedance force [3]. In the Path Controller the time-dependent walking trajectories are converted to walking paths with free timing. This is comparable to compliantly coupling the patient's feet to rails, thus, limiting the accessible domain of leg postures, which can be calculated as a function of hip and knee angle. Along these "virtual rails", which form a template for possible motions in space, the patients are free to move on their own.

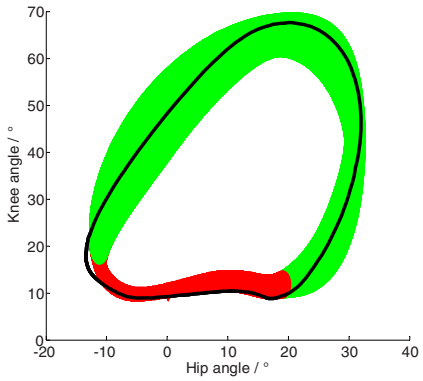

Fig. 3: Desired spatial path (solid line) and mean resulting trajectory +/- standard deviation (stance phase in red, swing phase in green) of 12 subjects with incomplete spinal cord injury.

B. *Evaluation of the Path Controller*

We tested the Path Control strategy on 12 subjects with incomplete spinal cord injury. The subjects were actively trying to match desired movements presented to them via a visual display. The angles of the hip and knee joint where recorded with the sensors of the Lokomat. The data was cut into single strides and normalized in time to 0–100% of the gait cycle. For each instant of the gait cycle, the mean and the standard deviation of the joint angles were calculated. The subjects produced walking trajectories that qualitatively match the spatial path of the desired walking pattern (Fig. 3). During stance phase (red shaded area in Fig. 3), subjects systematically showed more knee flexion than the desired pattern. Largest variance occurred during swing phase (green area, Fig. 3).

C. *Discussion on the feasibility of the Path Controller*

The results show that the subjects were able to freely influence their movements within the spatial constraints of the desired walking pattern. Although the controller leaves maximum freedom, it still ensures functional gait in critical situations. Particularly during stance, where subjects were not able to keep their knees extended, the controller assisted the subjects by keeping them around the desired walking pattern. Thus, the user-cooperative Path Controller provides a safe training environment and makes the human an active component in the biomechanical control loop of the gait rehabilitation robot Lokomat (Fig. 2).

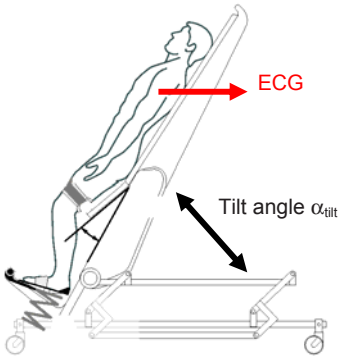

Fig. 4 Dynamic tilt table Erigo with the input tilt angle α_{tilt} and resulting ECG signals

III. Physiology in the Loop

A. *Controlling heart rate via body posture*

Body posture (inclination) has an influence on the cardiovascular system. Cardiovascular adaptation depends on the proper interplay of the hemodynamic circulation system and the reflex mechanisms that maintain blood pressure homeostasis [4, 5]. Thus, heart rate (HR) and heart rate variability (HRV) change with body posture. Controlling HR (and HRV) can be important to limit stress and arousal during motor treatment. The dynamic tilt table Erigo

(Hocoma, Switzerland) is used to investigate and control the relationship between body posture and heart rate. Subjects are tightly fixed to the Erigo by a belt system, and they can be tilted between an inclination angle α_{tilt} of 0° and 76° (Fig. 4). Using both an inverse human cardiovascular model and a proportional controller, the "model-based controller" determines the required angle α_{tilt} to track a desired heart rate (Fig. 5). The HR is extracted online from ECG, which is acquired by a PowerLab amplifier (ADInstruments, Germany) and an ECG recording system.

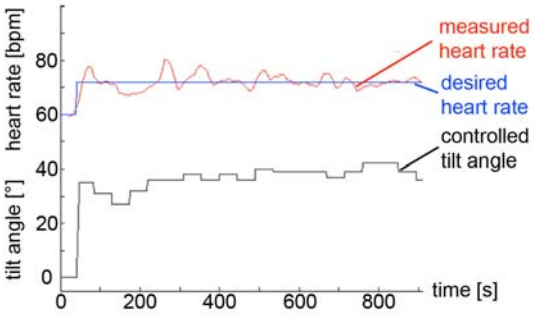

Fig. 5 Result of an HR control experiment with varying tilt angle α_{tilt}.

B. *Evaluation of the heart rate controller*

The HR controller was evaluated in an experimental study with a single healthy subject. The desired HR is a step function, with a step from 0 to 72 bpm after 30 s (Fig. 5). Following the inverted model within the controller, the tilt angle of the Erigo initially increases to 36°, and the HR responds with an overshoot. It can be seen that the measured HR responds to changes in the tilt angle with a short delay. The controller adjusts the tilt angle in such a way that the measured HR settles down to the desired HR of 72 bpm after a few minutes.

C. *Discussion on the feasibility of heart rate control*

In this single experiment, it was possible to control HR by means of the tilting angle α_{tilt}. In the meantime, further results were obtained showing that heart rate can be influenced within a rather large range not only by varying posture but also by varying stepping frequency. In the future, we will investigate also the effects on blood pressure and other physiological quantities. Controlling cardiovascular and other signals with mechanical inputs such as posture and movement may have a great potential for the treatment of patients during motor rehabilitation as well as for the monitoring of patients in the intensive care unit.

IV. Psychology in the Loop

A. *Controlling psychology via physiology*

In several therapeutic applications there is the desire to identify the actual psychological state in order to assess whether the patient is bored or engaged, or even stressed. Controlling the psychological state would be desirable, because it is known that high motivation and active participation can enhance the rehabilitation outcome [6]. In our approach we try to control the desired psychological state by controlling respective physiological quantities (Figs. 1, 8). The psychological state of a subject is reflected in numerous physiological signals affected by the autonomous nervous system. We selected heart rate (HR) and HR variability obtained by ECG recordings [7], skin conductance response (SCR) [8], skin temperature, breathing frequency and joint torques. Other physiological signals (EEG, EMG, spirometry, eye movements) were tested but omitted as recording turned out to be too cumbersome or too unreliable. All these signals are defined as human "output" signals during a Lokomat training intervention. Input signals are stimuli that were provided to the human during the training intervention. They include motor aspects (e.g. treadmill speed, body weight support) as well as audiovisual stimuli provided by an audiovisual display. The relationships between input and output signals are being established experimentally. Once these relationships are known, we intend to control the physiology and, thereby, control also particular psychological states that can be related to those physiological states.

B. *Evaluation of psychological control*

The first step towards control of psychological states is to understand the effects of physical and mental stress on the physiological signals. To stimulate the human and observe different physiological outputs, we provoked different physical and mental stress situations in seven healthy subjects. Mild physical stress was produced by presenting a particular gait scenario while walking inside the Lokomat (Fig. 2). Mental stress was produced by giving the subject a particular arithmetic task. Data was recorded at the four (randomized) conditions standing, walking, standing + arithmetic task, walking + arithmetic task. Results showed that the number of SCR events increased when subjects had to perform mental arithmetic tasks [8], whereas skin temperature decreased significantly during mental arithmetic tasks. HR increased with physical load, but it also increased with mental workload [9], Table I.

Table I Effects of mental and physical load on physiological parameters

	SCR events [-]	**HR [1/min]**	**Skin temp.**	**Breathing frequency [1/min]**
Standing (baseline)	2±1.3	74±12/1	→	12±3.9
Walking	8±7.0	89±17.4	↓↑	20±3.8
Standing & arithmetic task	25±7.5	100±24.4	↓	-
Walking & arithmetic task	25±10.8	91±19.4	↓	-

C. Discussion on the feasibility of controlling psychology

The isolated findings are congruent with the literature: Both heart rate and SCR events increase with physical or mental workload. The interesting observation is that physical activity in the Lokomat does not occlude the effects of mental workload. In a next step, we will examine the influence of different virtual environments and tasks presented by an audiovisual display. Finally, we will close the loop around the subject and interactively adapt the Lokomat and the virtual environment in such way that the psychophysiological state can be regulated to a desired level.

V. Discussion and Conclusion

Placing the human into the loop can be considered from various viewpoints and realized for different applications. It can allow controlling biomechanical, physiological as well as psychological aspects of the human, who represents the plant within the control system. In the biomechanical loop (chapter 2), the human even partially takes over the function of a controller. In several applications (chapters 2 and 4) the human-in-the-loop structure allows to optimize mechanical or mental engagement of the subject, thus, improving motivation. This has the potential to increase the training efficiency and therapeutic outcome. Other applications (chapter 3) guarantee that the patient is training in a save range by keeping relevant physiological values such as HR or blood pressure in an appropriate range.

References

1. Israel J, Campbell D, Kahn J, and Hornby G (2006). Metabolic costs and muscle activity patterns during robotic- and therapist-assisted treadmill walking […]. *Phys. Therapy*, 86(11):1466-1478.
2. Duschau-Wicke A, von Zitzewitz J, et al. (2007). Path control – a strategy for patient-cooperative training of gait timing. In *Proc. 7th Automed Workshop*, Munich, pp. 1-2.
3. Riener R, Lünenburger L, Jezernik S, et al. (2005). Patient-cooperative strategies for robot-aided treadmill training: first experimental results. *IEEE Trans. Neural Syst. Rehabil. Eng.*, 13(3):380-394.
4. Held, T. (2004) Computational models of cardiovascular response to orthostatic stress. Doctoral dissertation, Harvard - MIT Division of Health Science and Technology, USA
5. Hainsworth, R., Al-Shamma, Y. (1988) Cardiovascular responses to upright tilting. *Clinical Science*, 74:17 22.
6. Lotze M., Braun C., Birbaumer N., et al. (2003). Motor learning elicited by voluntary drive. *Brain*, 126(4):866-872
7. Malik M., (1996), Heart rate variability – Standards of measurement, physiological interpretation and clinical use, *European Heart Journal*, 17:354pp
8. Fowles D., Christie M.,Edelberg R., Grings W., Lykken D., Venables P., (2007), Public recommendations for rlectrodermal measurements, *Psychophysiology*, 18(3): 232-239
9. Neumann, S.A. and Waldstein, S.R. (2001) Similar patterns of cardiovascular response during emotional activation as a function of affective valence and arousal and gender. *Journal of Psychosomatic Research*, 50: 245-253.

Research in Medical Physics: What, Why, and How

J.M. Boone

University of California Davis, Department of Radiology, Sacramento, CA, USA

Abstract—**Research in medical physics has led to a huge number of innovations over the past 30 years. Medical physics is of course a broad scientific field, but in general can be categorized as either diagnostic imaging physics or the physics of radiation oncology. In this paper, these two areas will be discussed separately.**

I. Research in radiation oncology

What:

Medical physicist researchers working in radiation oncology sought to improve the conformality of the radiation beam to the shape of the targeted lesion through a number of creative ways. The development of the multi-leaf collimator allowed computer control of the shape of the x-ray field at any given beam angle about the patient. This computer control in concert with a higher number of beams could then be used to achieve higher dose levels in the targeted lesion, with lowered doses to the surrounding normal tissue. Shortly after the development of the multi-leaf collimator, modulating the intensity of the x-ray beam as a function of position also became possible due to the efforts of many researchers in the field. So-called image modulated radiation therapy (IMRT) is now used to routinely in radiation oncology centers throughout the world. Additional ways to achieve better conformality include the incorporation of a rotating x-ray source with the narrow beam of radiation. The use of a rotating x-ray source with a suitably adapted multi-leaf collimator can lead to even higher degrees of dose conformality to the tumor. Other researchers have developed robotically controlled x-ray sources, which are not limited to rotational trajectories but rather can place an x-ray beamlet in a large number of positions.

Why:

The gradual transformation from a few number of x-ray ports to a full rotational image modulated radiation therapy treatment has led to a complete paradigm shift in radiation oncology. Instead of relying almost exclusively on the ability of normal tissue to repair itself, the increased ability to focus the x-ray dose distribution to the site of the tumor, while avoiding high doses to the surrounding normal tissues, has led to higher dose levels to the tumor while simultaneously improving normal tissue tolerance. Thus, the "therapeutic ratio" of radiation oncology has improved dramatically. This goal has been the driving force, that is, the purpose or "why" that this research was performed. In the end, dramatically improved patient care has resulted.

How:

The methods (or "how") of how the technological developments which led to IMRT followed a number of paths, depending upon the individual researchers. In general, however, the development of physical systems for depositing radiation in tissue was and is studied in a computer simulation environment first. Computer simulation allows the researcher to test "what if" scenarios in a timely and cost-effective manner. Computer simulation, however, requires a great deal of preparation and skill to assure the right answers, and it is necessary to verify the output of so-called Monte Carlo calculations against physically measured data as well. Once a physical system is built for deploying radiation treatment, the dose distribution is typically measured at a large number of spatial locations using thermal luminescent dosimeters, MOSFET dosimeters, or other similar technologies. Interestingly, these technological developments which are commonly used for patient care in radiation oncology today were not subjected to large scale clinical trials which is the norm in drug development. Rather, technologies which are capable of delivering better conformality are considered better technologies, based upon the assumption that more optimal treatment plans lead to more optimal patient outcomes.

II. Research in medical imaging

What

Since the 1980's, there have been dramatic developments in imaging systems used for clinical diagnosis. The development of mammography for breast cancer screening has progressed steadily over the past three decades, where now high-resolution digital mammography is the standard. The use of magnetic resonance for imaging in patients was first postulated in the 1970s, implemented in the 1980s, and is currently used worldwide for patient diagnostic studies. Magnetic resonance imaging is capable of imaging oxygen levels, and this ability has led to functional MRI studies

O. Dössel and W.C. Schlegel (Eds.): WC 2009, IFMBE Proceedings 25/XIII, pp. 184–185, 2009.
www.springerlink.com

which can be used to study the workings of the human brain. Computed tomography was introduced in 1972 as a fledgling imaging system which required four minutes to acquire two slices. Research in CT hardware has led to image acquisition speeds of less than 0.1 seconds, making cardiac imaging a reality. These are just three examples of what has been studied in the field of medical imaging physics over the past quarter century.

Why

The purpose of the research in medical imaging ostensibly is to improve the information provided by the imaging physician, which in turn leads to a better diagnosis and improved healthcare to patients. For example, with the introduction of breast cancer screening during the 1980s in the United States and in Europe, dramatic reductions in breast cancer mortality have been realized over the past 30 years. While improved surgical practice and chemotherapy have contributed in part to this reduction in mortality, breast cancer screening has surely been responsible for a very large component of this success. MRI is exquisitely sensitive to various tissues, and is used extensively in neuroradiology applications. Its ability to measure flow has also allowed magnetic resonance angiography to be used for the assessment of vascular disease. CT has become so widely used (70 million studies annually in the US) that there are now serious concerns in regards to over utilization, both in terms of radiation risk and medical costs.

How

The path for the development of these imaging modalities involved strong interactions between academic medical physicist and corporate collaborators. While academic medical physicists sometimes present new ideas for improving imaging, medical physicists and other scientists working for industry are in some cases better able to develop new imaging hardware. In general, the evaluation of new imaging systems and modalities involves a collaboration between scientists working for industrial vendors and imaging physicians, and medical physicists usually play an important role in this collaboration as well.

III. Summary

Advancements in medical imaging and radiation oncology over the past three decades have been highly dependent upon medical physicist researchers. The driving force (the "why) behind these research programs has in most cases been motivated by the desire to improve patient care. The methods ("How") used for developing new technologies can differ significantly from the typical hypothesis driven methods used more commonly in biological science. The engineering model for technology development is the one most commonly used in medical physics - this model assumes that physical metrics such as dose conformality in radiation therapy or spatial resolution in medical imaging (just two examples) can be used to measure the improvement in technology, and clinical trials are not necessary for the implementation of new technologies. Of course the topic of the research ("what") is typically dictated by medical significance, the interests and training of the individual medical physicist, the infrastructure available to perform the research, and the time available for doing research. Research is best done not as the requirement of a job position, but rather should be driven by the passion of the individual scientist, combined with his or her ability to leverage the resources towards realizing the scientific endpoint.

Email:

AFOMP's Draft Policy #2: "Recommended Clinical Radiation Oncology Medical Physicist Staffing Levels in AFOMP Countries"

W.H. Round[1], Y.K. Tay[2] and K.H. Ng[3]

[1] Engineering Dept, University of Waikato, Hamilton, New Zealand
[2] Radiation Oncology Centre, Gleneagles Hospital, Singapore
[3] Dept of Biomedical Imaging and Medical Physics Unit, University of Malaya, Malaysia

Abstract— **The AFOMP (Asia-Oceania Federation of Organizations for Medical Physics) Professional Development Committee (PDC) has been drafting of a set of policy statements which give recommendations and guidelines on issues such as the definitions on the roles and responsibility of medical physicists, their professional and quality standards, and the standard and structure of education and training of medical physicists. This policy statement, which is the second of a series of documents, outlines the official views of AFOMP on recommended clinical medical physicist staffing levels in radiation oncology departments. It aims to serve as a guideline or reference document for AFOMP organizations.**

The philosophy and rationale in defining suitable radiation oncology medical physicist staffing levels will be explained.

Proposed recommended staffing guidelines include:

- **Every radiation oncology department must employ at least one qualified clinical radiation oncology medical physicist as specified in AFOMP Policy Number 1.**
- **The number of qualified medical physicists in a department must generally exceed the number of unqualified clinical radiation oncology medical physicist being trained within the department.**
- **Time must be provided for continuing professional development, teaching and training.**
- **Senior physicists must be provided with sufficient time to train and mentor trainee/junior/registrar/resident physicists.**

Currently activity is focused on developing EFT-based guideline for departments.

Keywords— **Radiation oncology, medical physicists, staffing.**

I. INTRODUCTION

The Asia-Oceania Federation of Organizations for Medical Physics (AFOMP) was founded during the World Congress on Medical Physics and Biomedical Engineering in Chicago in July 2000 [1].

The current membership includes sixteen national organizations which together represent about 3000 medical physicists.

AFOMP was officially inaugurated and admitted by IOMP as one of its Regional Chapters in 2000. The formation of AFOMP aims to provide a solid platform for closer collaboration and mutual support amongst the medical physics organizations in the Asia and Oceania regions for the primary purpose of promoting the advancement of medical physics and related scientific activities and the development of the standard of practice and professional status of the medical physicists. To help achieving these goals and objectives, AFOMP has established three committees, namely Professional Development Committee (PDC), Education & Training Committee (ETC) and Scientific Committee (SC) to work on a number of important tasks. Among them are drafting of a set of policy statements which give recommendations and guidelines on issues such as the definitions on the roles and responsibility of medical physicists, their professional and quality standards, and the standard and structure of education and training of medical physicists. This policy statement, which is the second of a series of documents being prepared by the joint efforts of the PDC, outlines the official views of AFOMP on recommended clinical medical physicist staffing levels in radiation oncology departments. It aims to serve as a guideline or reference document for AFOMP member organizations.

II. DEFINING SUITABLE RADIATION ONCOLOGY MEDICAL PHYSICIST STAFFING LEVELS

It is difficult to define how many qualified clinical medical physicists are required in radiation oncology departments in all countries represented by the AFOMP. This is because staffing requirements are difficult to specify because work practices vary from country-to-country, within a country from hospital-to-hospital, and within a department from procedure-to-procedure. In some places, due to the current shortage of qualified clinical radiation oncology physicists, tasks carried out by physicists

O. Dössel and W.C. Schlegel (Eds.): WC 2009, IFMBE Proceedings 25/XIII, pp. 186–189, 2009.
www.springerlink.com

elsewhere are carried out by radiation technologists, technicians, commercial providers, service engineers, radiation safety officers, administrators, etc under the supervision of a qualified physicist rather than by a physicist. This is not ideal, and the supply of qualified clinical radiation oncology physicists must be improved.

The level of service and technical expertise will vary from department-to-department depending on:

- Funding availability
- Expertise availability
- Equipment availability
- The clinical procedures and types of treatment offered
- Training and teaching requirements
- Research opportunities
- Legal requirements and responsibilities

A broad figure of one physicist per 400 treatment patients suggested by the IAEA [2] is sufficient to provide a very basic service for routine treatments, especially when highly technical and sophisticated equipment is used. This is inadequate for many modern situations. Recommendations have been made by medical physics organizations in other countries [3-5]. Some of these are quite detailed and permit the qualified clinical radiation oncology physicist requirements to be estimated for any particular department according to the equipment levels, patient numbers, complexity of treatments offered, etc.

The duties of a radiation oncology physicist are quite diverse and require a high level of education, training and expertise for the physicist to operate safely and effectively. It is important that as well as sufficient staff being employed to provide an adequate and safe medical physics service, time is also provided for continuing professional development. To ensure that medical physicist staffing needs are met in the future, senior physicists must be provided with sufficient time to train and mentor trainee/junior/registrar/resident physicists. Time for continuing professional development, and teaching and training time must be factored into the physicists' workload requirements of a radiation oncology department.

It must be stressed that every radiation oncology department must employ at least one qualified clinical radiation oncology medical physicist as specified in AFOMP Policy Number 1 'Definition of a Medical Physicist'[6]. The number of qualified medical physicists in a department must generally exceed the number of unqualified clinical radiation oncology medical physicist being trained within the department.

III. Recommended staffing guideline

The guidelines in Table 1 can be used to ascertain the number of physicists required by a department. Generally a range of equivalent full time (EFT) physicist numbers is given. The lower values would be adequate in situations where the tasks are mostly carried out by non-physics and trainee physicist staff under the supervision of a qualified physicist. The higher values are more pertinent to where the tasks are mostly carried out by a qualified physicist. The higher values should be used in a modern, properly staffed and well-equipped radiation oncology department.

IV. Discussion

The levels suggested by Table 1 are quite debatable as work practices will vary from country-to-country, hospital-to-hospital and procedure-to-procedure. Further work on the suitability of the staffing levels suggested by Table 1 is required and this will be the subject of some further discussion by the AFOMP CPD.

However, notwithstanding such debate, it is strongly recommended that

- Every radiation oncology department must employ at least one qualified clinical radiation oncology medical physicist as specified in AFOMP Policy Number 1.
- The number of qualified medical physicists in a department must generally exceed the number of unqualified clinical radiation oncology medical physicist being trained within the department.
- Time must be provided for continuing professional development, teaching and training.
- Senior physicists must be provided with sufficient time to train and mentor trainee/junior/registrar/resident physicists.

These four strong recommendations are considered to be fundamental if there is to be any basis for provision of a competent medical physics service in a radiation oncology department where there is to be safe practice, where staff are able to keep up to date with modern practice and where there is assured to be a workforce capable of meeting future needs.

Table 1 EFT-based staffing levels

	EFT physicist
EQUIPMENT RELATED	
Multiple-energy photon/electron linac	1.0 – 1.5
Single energy linac	0.5 – 1.0
Multileaf collimator, portal imaging, IGRT and other accessories	0.0 – 0.5
Co60 unit	0.25 – 0.5
Patient imaging systems	0.1 – 0.5
2-D planning system	0.2 – 0.5
3-D scanning system	0.5 – 1.0
Afterloading brachytherapy system	0.1 – 0.4
Dosimetry equipment QA per system	0.05 – 0.2
PATIENT RELATED	
Planning per 1000 courses per annum	0.2 – 1.0
Complex treatment plans per 100 cases (e.g. conformal, IMRT)	0.2 – 0.8
Basic brachytherapy per 100 cases per annum	0.2 – 0.5
Direct patient monitoring and related measurements per 100 cases per annum (e.g. TLD , diode, MOSFET)	0.05 – 0.2
Special therapies per 100 cases per annum (e.g. stereotactic, intraoperative, TBI, HBI, TSET,LTI, hyperthermia, I-131, Sr-90, neutron generation)	0.1 – 0.5
MISCELLANEOUS	
Departmental Radiation Safety Officer	0.05 – 0.2
Teaching/examination (for non-physics staff, students etc)	0.0 – 0.2
Commissioning	Extra as required
PHYSICS STAFF RELATED	
Management/administration per staff supervised	0.05 – 0.1
Staff development per staff (e.g. conferences, courses, workshops)	0.02 – 0.05
Leave relief per staff	0.1
Training and mentoring trainee/physicist registrar per trainee/registrar	0.1
Research, development, clinical projects per staff involved	Extra as required

ACKNOWLEDGEMENT

The authors acknowledge the input from the other members of the AFOMP CPD Committee in formulating the Policy: Yoshihisa Akiyama, Kin Yin Cheung, Yimin Hu, Kiyonari Inamura, Hee Joung Kim, Anchali Krisanachinda, Joyce Leung, A S Pradhan, Rompin Shih, Yak Koon Tay, Toh Jui Wong and Byong Yong Yi

REFERENCES

1. AFOMP History (2009) at http://www.afomp.org/
2. International Atomic Energy Agency (2008) Setting up a Radiotherapy Programme: Clinical, Medical Physics, Radiation Protection and Safety Aspects. (ISBN 92-0-101807-X)
3. The European Federation of Organisations for Medical Physics (1997) Criteria for the Staffing Levels in a

Medical Physics Department, Policy Statement at http:www.efomp.org/policy/stafflev.pdf
4. Institute of Physics and Engineering in Medicine (2002) Guidelines for the Provision of a Physics Service to Radiotherapy at http://www.ipem.org.uk/ipem_public/article.asp?id=359&did=49&aid=2208&st=&oaid=-1
5. Oliver L, Fitchew R, Drew, J (2001) Requirements for Radiation Oncology Physics in Australia and New Zealand. Aust Phys Eng Sci Med 20:1–18
6. AFOMP PDC Committee (2007) Policy #1: Definition of a Medical Physicist at http://afomp.org/zboard/zboard.php?id=afomp_develop

Corresponding author:

Author: Prof K-H Ng
Institute: Department of Biomedical Imaging (Radiology), University of Malaya
Street: Federal Highway
City: Kuala Lumpur
Country: Malaysia 50603
Email: dwlng@tm.net.my

Technology of Cancer Particle Radiation Therapy Based on Ultrafast Intense Laser Generated Proton- and Ion Beams

T. Tajima[1,2]

[1] Munich-Centre for Advanced Photonics, D-85748 Garching, Germany
[2] Photo-Medical Research Center, JAEA, Kyoto, 619-0215, Japan

Abstract— **Based on a compact laser accelerator of ions, we can now envision a compact beam therapeutic machine of cancer treatment (and some other difficult diseases). Taking advantage of laser accelerator, we look for a cure of small and localized tumors combined with an early detection at the stage of small tumors. We design our accelerator system to fit with the existing electron/ photon therapy infrastructure. The gantry is designed to bend small angle ion beams combined with the flexible control of laser angle. The system is suitable for the tunably controlled laser irradiation on the target and the shoot-and-ascertain-the-dose approach. In order to increase the ion energy gain while dispensing the large dose per shot, we adopt the mass-limited target so that laser irradiation is more effectively coupled with the efficient energy transfer of small number of highly energetic ions. We suggest a couple of technology strategies for accomplishing this goal, the one pursued at Munich Center for Advanced Photonics and the other at Photo Medical Research Center. These are complementary and yet based on the same vision.**

Keywords— **Enter up to five keywords and separate them by commas.**

I. Introduction

The proton (and carbon) beam radiooncology allows reduced dose on healthy tissues upon the irradiation of the patient than the alternatives. The challenge for the technology provider for the beam therapy is to provide this with an affordable cost to the patient. The introduction of the laser ion acceleration promises such a possibility. The acceleration gradient of this acceleration method [1] is many orders of magnitude greater than the conventional rf accelerator technology. However, it takes the realization of this possibility as well as important accompanying development to deliver the beam to the patient in a satisfactory fashion.

The current paper outlines the research strategy that charts out what we consider is a route for this realization. We outline the physics bases for compact ion acceleration toward necessary energies for therapy (80MeV for shallow tumors, and 200MeV for deeper ones). We describe the characteristics of our concept of laser ion accelerators that distinguish themselves, such as the smaller dose in a small spatial and temporal extent, the flexible irradiation handling, the possibility of shoot-verify-shoot-verify-… cycle (dosimetry-guided targeting through auto-radioactivation as well as image-guided targeting), the concept of mass-limited laser target that allows more efficacious laser acceleration, etc.

II. Accelerator system

The recent progress in laser ion acceleration is remarkable. Since the beginning of the experimental reports on laser ion acceleration [2-4] the energy increase of accelerated ions has been rather modest in spite of its huge potential. I attribute this to the choice of relatively large mass targets, either by the mass density or thickness or both. However, some endeavors of mass-limited experiments have been envisaged and tried [5] and theoretical background advocated[6.7]. In particular of late experiments with ultrathin foil with ultra high contrast (UHC) laser pulse have been conducted to a great success [8,9] at MAP. Meanwhile, an alternative strategy of mass-limited targets via clusters has been explored, to a serendipitous discovery of acceleration of high energy ions from even a modest energy laser[10]. In [8] a modest energy ultrafast UHC laser drove protons to highest energies in this class of laser irradiation. In [9] a high energy (150J) longer-pulsed UHC laser accelerated carbon ions to unprecedented several hundred MeV. In [10] a modest energy ultrafast laser was self-channeled in the cluster medium to produce several hundred MeV ions. None of these is yet sufficient by themselves for even energy per se for radio therapy requirements, but they do represent a quantum leap of energy gain sometimes by an order of magnitude. More importantly to my opinion, these experiments hold an element that may be extrapolated toward the required energies and some other prerogatives for therapeutic applications. In fact, the recent theoretical understanding behind these experiments indicates a route that scales toward therapeutic applications [11]. Buoyed by this progress, let me describe some systems developmental concept below.

The mass-limited optimal condition is represented by the condition

O. Dössel and W.C. Schlegel (Eds.): WC 2009, IFMBE Proceedings 25/XIII, pp. 190–192, 2009.
www.springerlink.com

$$a_0 \sim \sigma = \frac{n_0}{n_c}\frac{d}{\lambda}$$

where a_0 and d are the normalized vector potential of laser and the thickness of the target. This condition is well satisfied in the experiment [5],[8] and to an extent in [9], while it is possible that such is realized in [10]. When such a condition is fulfilled, it was shown that the typical ion energy gain may be given as

$$\varepsilon_{\max,i} = (2\alpha+1)QE_{\max}$$

where $E_{\max}$ is the electron energy given by such an estimate as $mc^2(\gamma\text{-}1)$ with $\gamma = \sqrt{(1+a_0^2)}$, Q is the charge state of ions, and α reflects how coherent the electron dynamics is and is an exponent given in [11]. This equation gives us a strategy how to extrapolate the ion energy. First, there may be ways to boost the electron energy beyond the estimate above. For example, if and when electrons are driven by laser and move together with the laser pulse over a sufficiently long distance, the energy gain may be a function of an exponent to a_0 greater than unity (such as a_0^2). A radiation driven ion acceleration is an example for this [6,12,13]. Secondly, we may introduce an arrangement in which the laser group velocity at the impingement on the target is so small compared with the speed of light that even heavy ions may get accelerated by the cloud of electrons that are driven by the laser pulse. This is a concept of adiabatic pickup and acceleration of ions [5, 14]. In fact in the experiment [10] the cluster may provide an environment to slow down photons so that electrons and ions move gradually from 0 to larger values. In [10] the electron density averaged over all clusters is about the critical density, which in fact translates into the photon group velocity of zero.

Summarizing, one strategy in mass-limited target is to take a foil as thin as it is allowed before it burns through for the laser. In the ultrathin target case, when a_0 is around 70, protons gain energy of 250 MeV. If the exponent to a_0 is as large as 2 [7], at $a_0 = 8$, we are already reaching sufficient energies. The other strategy is to have an averaged electron density near critical so that photon group velocity stays close to zero in the beginning phase of laser-target interaction, as created in the clustered target. From the current limited energy of laser (150 mJ) with 50 fs pulse length in [10], it is speculated in a clustered target that the energy gain is proportional to the pulse length (with the laser intensity kept). If this is in fact the case, with mere an order of 1-2 J with the pulse length of a half ps, one would get the necessary energy gain. The first strategy was pioneered by the MAP Group, while the second by the PMRC Group. These are distinct and complementary strategies, and yet are based on the same vision how to get ions to be highly energetic with a limited amount of laser power.

III. Therapeutic system

In order to realize a therapeutic machine, we need far more than a compact accelerator. What we need are:

1) The beam transport and beam irradiator as well as the radiation shield have to be compact enough to make the over all system size to become compactified. In our concept the compactified gantry should fit within the conventional electron / photon radio therapy infrastructure.
2) We make the best case out of the characteristics of laser accelerators. That is, its small transverse emittance and flexible directioinal and parameter variations combined with limited amount of dose, we seek a niche of treatments of small and early tumors. The future imaging advances are surely toward the detection of small and early tumors, so that this is consistent with the future detection trend.
3) Coupled with the above characteristics, it is both advantage and a necessity to bring in the capability of real time feedback and dose control on the patient, while we carry out the spotscanning treatment of the tumor by the laser ion therapy system. The autoradioactivation by laser produced ion beam in the patient (at and near the tumor) may be a key to ascertaining the actual dose and to reduce unwanted dose on the healthy tissues. At the same time this brings in an opportunity to introduce a radically more accurate therapy technique to dosimetry-guided targeting and image-guided targeting.
4) Small and efficient laser system. Particularly if the scaling of the clustered target proves to be the case, such a laser with modest power with longer than the ultrafast time scales may be an ideal system for the future highly efficient LD pumped compact laser system (using such as the Yb based laser medium).

With these combined, we should be able to fit the overall system compact and perhaps within the existing infrastructure of X-ray therapy facilities. In particular the gantry can contain necessary functions of beam transport, selection, and irradiation along with shielding but yet it may be loaded in a compact frame comparable to the X-ray/electron machine.

IV. Future directions

If we intend to transfer the technology of laser acceleration to the clinical applications of therapy, it is necessary to establish the science of laser acceleration of ions, but also to develop a therapeutic system that conforms to all the neces-

sary therapy machine requirements, including all important safety and accuracy and reliability criteria. This requires collaboration of not only laser physicists, but also medical physicists, biologists, radiooncologists (clinicians), and systems engineers. It is also necessary to envision a developmental strategy to spread loads over shoulders to reduce the risk of introducing highly innovative (and in fact revolutionary) therapeutic machinery. In this light I note that the two organizations MAP and PMRC simultaneously came to a similar vision of laser driven compact beam therapy systems with somewhat separate target strategies with a common vision of the systems development. It is natural and perhaps imperative to have these highly respected two organizations to forge a strategic research alliance to assess and reduce the risk of the development by broadening the operational variations and parameter options, as well as sharing experiences, without compromising some of the essential intellectual properties of particular / partners companies. It is also noted that the speed by which discovery happens is quickening and to ensure rapid dissemination of the best strategy of research is essential to minimize risks and maximizing rewards.

Acknowledgment

This work is supported in part by the DFG Cluster of Excellence MAP (Munich-Centre for Advanced Photonics). It is also supported in part by the Special Coordination Fund (SCF) for Promoting Science and Technology commissioned by the Ministry of Education, Culture, Sports, Science and Technology (MEXT) of Japan. We are deeply indebted to our colleagues Dieter Habs, Fridtjof Nuesslin, Michael Molls, Ferenc Krausz, Yoshiaki Kato, Paul Bolton, Shunichi Kawanishi, Sergei Bulanov, Masao Murakami, Y. Hishikawa, and Mitsuyuki Abe.

References

1. Tajima, T., J. Jpn. Soc. Ther. Radiol. Oncol. **9**, Suppl. 2, 83 (1997).
2. E. Clarke et al., Phys. Rev. Lett.**84**,670 (2000) .
3. A. Maksimchuk, et al, Phys. Rev. Lett.**84**, 4108 (2000).
4. R.A. Snavely, et al, Phys. Rev. Lett. **85**, 2945 (2000).
5. K. Matsukado, et al. , Phys. Rev. Lett. **91**, 215001(2003).
6. Esirkepov, T., Borghesi. M., Bulanov. S. V., Mourou, G., and Tajima, T., Phys. Rev. Lett.**92**,175003(2004).
7. O. Klimo, et al., Phys. Rev. ST Accel.Beams **11**, 031301(2008).
8. Steinke, S., Henig, A., Schnuerer, M., Sokollik, T., Nickles, P.V., Jung, D., Kiefer., D., Schreiber, J., Tajima, T., Yan, X.Q., Meyer-ter-Vehn, J., Hegelich, M., Sandner, W., Habs, D., submitted to Phys. Rev. Lett. (2009).
9. B.M. Hegelich, et al. Nature (2009).
10. Y. Fukuda et al., submitted to PRL.
11. X.Q. Yan, T. Tajima, M. Hegelich, D. Habs, submitted to New J. Phys.
12. X. Yan et al., Phys. Rev. Lett. **100**, 135003 (2008).
13. S.G. Rykovanov, J. Schreiber, J. Meyer-ter-Vehn, C. Bellei, A. Henig, H.C. Wu and M. Geissler, New J. Phys. **10**, 113005 (2008).
14. M. Murakami, Y. Hishikawa, S. Miyajima, Y. Okazaki, K.L. Sutherland, M. Abe, S.V. Bulanov, H. Daido, T.Zh. Esirkepov, J. Koga, M. Yamagiwa, and T. Tajima, in "First International Symposium on Laser-Driven Relativistic Plasmas Applied to Science, Industry and Medicine", Eds. S.V. Bulanov and H. Daido, AIP Conference Proceedings (AIP, NY, 2008) p. 275.

Author: Toshiki Tajima
Institute: Munich-Centre for Advanced Photonics
Street: Am Coulombwall 1
City: 85748 Garching
Country: Germany
Email: toshiki.tajima@physik.uni-muenchen.de

(invited for session 'Automation in medicine')
Mechanical Ventilation: Much Ado about Ventilation Modes

F. Dietz[1]

[1] Predevelopment Emergency Medicine, Weinmann Geräte für Medizin GmbH+Co. KG, Hamburg, Germany

Abstract—**Over 40 ventilation modes and over 65 names lead to disturbed users due to conflicting names or synonyms and missing structure in the nomenclature. This is astonishing since only two manipulated values are available and two goals of therapy exist: optimal gas exchange and protection of the lungs.**

The goal of this paper is to give users and manufacturers a structured nomenclature describing the phase control, feedback control and other control tactics and strategies with a minimum of characters, without redundancy, and a maximum of description information as possible, free of conflicts with existing mode names and their descriptions. The result shall not be a single solution for everybody, but it should help to translate between different names of modes.

The article uses decomposition of the ventilation problem into different control tasks and hierarchy levels. Separation of important and detailed information and definition of small sets of descriptive abbreviations help in finding a universal nomenclature for ventilation modes composed of those abbreviations.

The success of the approach is shown by translating several existing modes into the new nomenclature and by testing, which information is left to be given to get a full picture of the ventilation mode functionality.

Keywords— **Mechanical Ventilation, Ventilation Mode, Feedback Control, Nomenclature**

I. Introduction

Mechanical ventilation was developed to support medical staff to keep up the mechanical gas exchange of patients with respiratory diseases while protecting the lungs as much as possible. Automation in mechanical ventilation today is stretched out from pure surrogate for simple manual bag-valve-ventilation to very sophisticated closed loop ventilators that include the current patient status (or part of it) into their control law. The range of application reaches from first scene resuscitation over transport ventilators to anaesthesia ventilators and fully equipped intensive care ventilators [3].

To command the behavior of the ventilator the device is set by the selection of a certain ventilation mode. Such a mode roughly describes the amount of ventilation work that is taken over by the machine. There are pure mandatory ventilation modes to bear the whole work of ventilation, mixed modes to only support existing spontaneous breathing and mere breathing aids which help e.g. to keep a minimum airway pressure. The latter does not support the ventilation in any way, so the patient has to afford the ventilation work on its own.

Taking a closer look at a ventilation mode it can be realized that its definition describes the succession of inspiration and expiration during a single breath, the manipulated variable for inspiration, limits for security matters, support levels, and sometimes also the behavior over several consecutive breaths, to mention only a part of the most important issues in ventilation.

Currently there are over 40 different ventilation modes with over 65 different names including synonyms used in literature and technical documents (English language only!). Since there are only two different physical values available for control by a mechanical ventilator, i.e. gas flow or pressure, the huge amount of different names surprises in the first place. At a second look on the possible combinations of parameters to adjust ventilation it is getting clear to have that vast amount of modes on the market:

- Positive end-expiratory pressure (PEEP)
- Inspiratory pressure or tidal volume or inspiratory flow
- Pressure limit for volume controlled ventilation and volume limit for pressure controlled ventilation
- Course of flow or pressure during inspiration (ramps, constant flow, decreasing flow, sinusoidal flow, etc.)
- Respiration rate
- Inspiration-expiration-ratio or inspiration time
- Activity and level of inspiratory trigger and/or expiratory trigger (breath cycle)
- Synchrony of mandatory breaths with spontaneous breaths, maybe also the length of synchronization intervals (synchronization window)
- Support level for augmented breaths
- Exhalation support during start of expiration
- Inspiratory pause (no-flow interval at the end of inspiration)

These are only the most popular parameters to control the ventilation during a breath. Between breaths or over several breaths there are additional possibilities to control ventilation. Here just a small amount of parameters is listed:

O. Dössel and W.C. Schlegel (Eds.): WC 2009, IFMBE Proceedings 25/XIII, pp. 193–196, 2009.
www.springerlink.com

- Tidal or minute volume during pressure controlled ventilation to keep a minimum volume limit
- Expiratory pressure (PEEP) for open lung concept, a maneuver to recruit atelectasis for ventilation
- Sighs, i.e. additional deep inspirations every several minutes, also to recruit atelectasis
- Pressure support to adjust the support level to wean a patient from tube/tracheal cannula by observing tidal volume, respiration rate, and end-tidal carbon dioxide

Looking at all these manipulable parameters for ventilation it seems probable for many additional ventilation modes and names to turn up in the near future.

The advantage to adjust mechanical ventilation in a very detailed manner stands facing the situation of disturbed and/or poorly educated users many of whom can neither distinguish any more between the dozens of modes nor tell the differences between the modes of different ventilators.

Momentarily the ISO technical committee TC 121 SC3 is working on a standardized nomenclature for the description of ventilator functions as an addition to the standard IEC 60601-2-12:2001 [1]. Unfortunately the work is not yet published.

Chatburn published a thorough overview and proposal on a systematic description of ventilation modes and an additional terminology in 2007 [2], but did not try to introduce a universal nomenclature. Also some ambiguous approaches have been proposed on the so called dual control which is referenced again as auto-setpoint control and limits.

II. Aim Of This Work

The aim of this work is to introduce a proposal for an extensive, universal and uniform nomenclature for most of the ventilation mode properties. The resulting nomenclature is not intended to replace all existing names for ventilation modes but rather to establish a consensus for ventilation mode descriptions that shall help manufacturers and users to understand device functionality and distinguish between the different models and mode implementations.

The nomenclature shall provide maximal information about the mode's functionality while showing a syntax with minimal redundancy. The semantics shall be easy to understand, structured, and suppressing unused features. Also the nomenclature shall represent abbreviations that are already widely agreed on in today's practice of ventilation.

The nomenclature proposed shall be a further step in the discussion to achieve a structured approach for consensus. The author would like to invite anybody interested in ventilation to discuss the proposed nomenclature.

III. Universal Nomenclature

The method used to find a universal uniform nomenclature for most of the existing and possible future ventilation modes is divided into three parts:

1. Decomposition of the task and functionality of ventilation in different control tasks and in different hierarchy levels of control.
2. Structuring, defining, and naming the different control tasks on different hierarchy levels.
3. Composition of a nomenclature taking into account all or most of the tasks and names.

1. Decomposition: The problem of ventilation can be divided into the following control tasks and hierarchies:

- Starting inspiration to insufflate the lungs
- Ending inspiration (and starting expiration)
- Control pneumatic energy during inspiration and/or expiration, i.e. tactical control within a breath
- Watch and react to additional limits during pneumatic control, i.e. tactical limits within a breath
- Control laws over several breaths (strategic control) to react on changing or different patient conditions.
- Additional properties like conditional variables that are not listed in tactical or strategic control, device-dependent peculiarities due to different technical implementations or other issues like maneuvers etc.

2. Structuring: In the following paragraphs the definitions and names for the ventilation tasks are shown:

Breath Sequence: According to the hierarchical classification of Chatburn [2] the type of breath sequence should always be named to get a first grip on the ventilation mode. The breath sequence tells (within a breath) if an inspiration is started / ended by the machine or by the patient. Mandatory breaths are always ended by the machine, spontaneous breaths are always started and ended by the patient's breathing effort. As a first step there are three abbreviations widely used and agreed on:

1. CMV: continuous mandatory ventilation; indicating that all inspirations are mandatory, i.e. ended by the mechanical ventilator
2. IMV: intermittend mandatory ventilation; mandatory controlled inspirations with spontaneous breaths permitted in between
3. CSV: continuous spontaneous ventilation; indicating continuous spontaneously started and ended inspiration.

Synchrony: These names classify the first two properties of ventilation: A) inspiratory trigger, and B) expiratory trigger (breath cycle). Unfortunately, the possibility to syn-

chronize mandatory breaths to spontaneous breathing effort is not taken into account in contrast to the differentiation of mandatory and spontaneous breaths. To cover the full scope of breath sequence control it is suggested to use the prefix 'S' as used in SIMV.

Phase Control: Both breath sequence and synchrony can be summed up in a breath phase control according to Table 1. Only inspirations started by the machine and ended by the patient are not applicable, though such a control could be part of future implementations.

Table 1 Overview of breath phase control nomenclature

Start of Inspiration by	End of Inspiration by		
	Machine	Machine or Patient	Patient
Machine	CMV	IMV	-
Patient	SCMV	SIMV	CSV

Primary Breath-Control Variable: Similar to the proposal of Chatburn [1] it is crucial for the nomenclature of ventilation modes to name the variable the ventilation is controlled by during mandatory inspiration (as a feed-forward or feedback control). As stated in part I of this paper there are only two physically controllable variables for ventilation: Airway pressure or gas flow. Therefore we have *pressure control* (PC) as first primary breath-control. The second one is *volume control* (VC), since the relevant part of controlled gas flow is its integral: the tidal volume of one breath.

Secondary Breath-Control Variable: Instead of talking of dual-control when addressing the switch to another control variable during mandatory inspiration (e.g. switch from VC to PC due to pressure limited volume controlled ventilation) it could be more appropriate and more practical to introduce a secondary control variable (within a breath) that is activated when certain limits are reached. The nature of pneumatics determines one dependent variable during breath control on which limits can be imposed: During volume control (VC) only pressure limits can be valid, during pressure control (PC) only flow limits or – more practically – volume limits can be valid. Since the dependent variable during inspiration can be limited to a maximum and to a minimum there are four different control aims to take into account:

1. PL – *pressure limited*: Volume control that is switched to pressure control when reaching an upper pressure limit
2. PA – *pressure assured*: Volume control that is switched to pressure control when falling below a lower pressure limit (e.g. set PEEP). This happens for instance when the patient breaths spontaneously during a volume controlled mandatory breath
3. VL – *volume limited*: Pressure control that is switched to volume control when a certain tidal volume is reached or supposed to be exceeded
4. VA – *volume assured*: Pressure control that is switched to volume control when a minimum tidal volume is likely not to be achieved during inspiration

Mandatory Breath Control: In summary both primary and secondary breath-control variable can appear in certain combinations only:

Table 2 Overview of mandatory breath control nomenclature

Primary Breath-Control Variable	Limitation of Dependent Variable			
	No Limit	Only Upper Limit	Only Lower Limit	Both Limits
Pressure	PC	PCVL	PCVA	PCVLA
Volume	VC	VCPL	VCPA	VCPLA

When using both limits for a ventilation mode the naming of the breath control can be shortened, as can be seen in the last column of Table 2. The quoted names should be used as a prefix before the name of the breath phase control name, e.g. PC-CMV for pressure controlled CMV.

In order to consider additional spontaneous breaths it is mandatory to define a third breath-control variable:

Tertiary Breath-Control Variable: Inspirations initiated by spontaneous breathing effort that are to be ended by a patient's expiratory trigger usually are pressure supported (controlled). But nothing can prevent implementation of volume controlled assisted ventilation. Because of an uncertain end of the assisted breath one could only talk of flow control. Additionally, spontaneous breath support can be achieved by a kind of servo control as used in proportional pressure support: The assisting pressure is dependent on the flow and / or volume produced by the patient; another variant of this kind of control is the automatic compensation of endotracheal tube resistances. Hence, additionally to the eight names for mandatory breath control the following names for spontaneous breath control are suggested:

1. *PS – Pressure Support*: Pressure control during spontaneous breaths
2. *FS – Flow Support:* Flow control during spontaneous breaths
3. *PPS – Proportional Pressure Support:* An additional supporting pressure is controlled proportionally to flow and / or volume or to some other measured value (i.e. to neural potential as with NAVA)

The names for the tertiary breath-control variable shall be used as a post-fix after the name of the breath phase control as for instance in CSV-PS, formerly known as ASB.

A fourth breath-control variable shall be mentioned without a special consideration in the nomenclature: The positive end-expiratory pressure (PEEP) is (if applicable) always pressure controlled. Therefore no special name seems to be afforded in the nomenclature.

Strategic Control: Between breaths additional control laws can be established. For instance the respiration rate can be limited to an upper or lower limit, the tidal volume or the minute volume can be adjusted successively from breath to breath. Special strategies to consider changing patient conditions can reach a complexity that exceeds the range of this approach very quickly. For the more rudimentary control mechanisms between breaths some names are given here as an example for future discussion:

1. *FL – Frequency Limited:* The respiration rate is mandatory limited to prevent tachypnoe
2. *FA- Frequency Assured:* The respiration rate is assured by mandatory breaths to prevent bradypnoe or apnoe
3. *MVL – Minute Volume Limited:* The minute volume is limited
4. *MVA - Minute Volume Assured:* A certain minute volume is assured by additional support or additional mandatory ventilation
5. *VL – Tidal Volume Limited:* The tidal volume is limited over several breaths
6. *VA – Tidal Volume Assured:* Tidal volume is assured by adjusting the pressure level from breath to breath.

All strategic control names shall be positioned between round brackets as last part of the name.

IV. CONCLUSIONS

As result it can be stated that with the proposed nomenclature a huge amount of existing ventilation modes can be described in a clear forward and structured manner. Table 3 shows the translations for 16 modes with 13 synonyms.

Several things are still open for discussion: The possibility to consider a positive expiratory pressure (PEEP) in the nomenclature is momentarily not given (as done with IPPV and CPPV). But it could be useful to distinguish between devices able to provide a PEEP and those that are not. Manually initiated/ended breaths or sigh ventilation are not yet considered in the nomenclature. Also the completeness of the names for strategic control should be discussed.

Table 3 Ventilation modes described with the new nomenclature

Conventional Ventilation Mode	Description of the Ventilation Mode with New Nomenclature
CPAP	CSV
ASB, PSV, IPS, IFA	CSV-PS
VCV, IPPV	VC-CMV
PLV	VCPL-CMV
SIMV	VC-SIMV
PCV	PC-CMV
BiLevel, BIPAP, Bi-Vent	PC-SIMV-PS
BiLevel-VG	PC-SIMV-PS (VA)
APRV	PC-IMV
PPS, PPV, PAV	CSV-PPS
NAVA	CSV-PPS
ATC	-PPS (can be added to diff. modes)
A/C, IPPVassist, S-IPPV, VAC	VC-SCMV or PC-SCMV
PRVC, APV, Autoflow	PC-CMV (VA) or PC-SIMV (VA)
MMV	VC-SIMV-PS (FA,MVA) or VC-SIMV-PS (FA,VA)
VS	CSV-PS (VA,MVA)

It seems to be clear that the manufacturers have to give the full technical data about parameter set ranges and specific technical information about the implementation of pneumatics and additional features (e.g. trigger methods) to round the picture of the new nomenclature.

It would be very useful to additionally standardize several performance issues to objectively distinguish between different ventilators using the same modes.

REFERENCES

1. IEC 60601-2-12:2001; Medical electrical equipment -- Part 2-12: Particular requirements for the safety of lung ventilators -- Critical care ventilators
2. Chatburn R L (2007) Classification of Ventilator Modes: Update and Proposal for Implementation. Resp Care 52(3):301–323
3. Oczenski W et al (2008) Atmen - Atemhilfen. Thieme, Stuttgart

Author: Florian Dietz
Institute: Weinmann Geräte für Medizin GmbH+Co. KG
Street: Kronsaalsweg 40
City: 22525 Hamburg
Country: Germany
Email: F.Dietz@weinmann.de

Fundamentals and Medical Applications of Neutron and Light Spectroscopy of Confined Liquids

K.A. Chalyy[1], L.A. Bulavin[2], V.F. Chekhun[3], A.V. Chalyi[4], Ya.V. Tsekhmister[4], and L.M. Chernenko[5]

[1] Department of Medical Informatics, National Medical Academy, Kiev, Ukraine
[2] Department of Molecular Physics, Kiev National University, Kiev, Ukraine
[3] Institute of Experimental Pathology, Oncology and Radiology, NAS of Ukraine, Kiev, Ukraine
[4] Department of Medical and Biological Physics, National Medical University, Kiev, Ukraine
[5] Institute of Surface Chemistry, NAS of Ukraine, Kiev, Ukraine

Abstract— **Fundamental and applied aspects of critical behavior of liquids at restricted geometry are discussed. The number of defining features of universality for the finite-size systems is proposed. At simultaneous implementation of all indicated characteristics, the critical behavior of the confined systems of a different nature have to be isomorphous and it must belong to the matching universality class. Using the fundamental ideas of isomorphism and universality of the critical finite-size behavior under appropriate conditions, the following applications to medical and biological systems are studied: (a) the dependence of the light molecular scattering spectrum (namely, the widths of the central Rayleigh line and Mandelstam-Brillouin components, the Landau-Placzek relation) on the temperature variable and geometrical factor in water suspensions of plasmatic membranes as well as (c) the temperature and size dependence of the width of quasi-elastic peak in neutron scattering data and the diffusion coefficient are obtained theoretically and confirmed experimentally for the water suspensions of plasmatic membranes of tumor cells. These powerful physical methods of light and neutron spectroscopy give a possibility to create a new diagnostic test for the process of tumor formation which is nowadays in course of practical evaluation. The results of application of Quasi-Elastic Slow Neutron Scattering for study of selfdiffusion of water molecules in suspensions of plasmatic membranes of tumor cells are presented. It is shown, that influence of antitumor antibiotics on Guerin's carcinoma manifests in the notable increase of connectibility of albuminous molecules of tumor cells with the molecules of water.**

Keywords— **Isomorphism, finite-size liquids, light molecular scattering spectrum, quasi-elastic slow neutron scattering.**

I. Light critical opalescence spectrum

Peculiarities of the light critical opalescence spectrum in confined liquids, namely of the medical and biological nature are principle point of this publication. Main reasons for the study are as follows: (a) large responses of a system to external fields (say, electromagnetic radiation) are mostly connected with the critical state or the vicinity of bifurcation points [1]; (b) biological liquids are usually located in small volumes such as synaptic clefts, ion channels, vesicles, porous structures, etc.; (c) phase transitions and critical phenomena undergoing in liquids at restricted geometry have a very specific behavior [2]; (d) spectra of light scattering give the broad information about equilibrium and non-equilibrium properties of these objects [3]. Therefore, the above-mentioned problem seems to be of a great importance for a deeper understands the critical behavior of physical properties in finite-size biological liquids.

The dynamical scaling hypothesis for confined liquids was formulated in [4] to study the width Γ_c of the central Rayleigh line of the critical opalescence spectrum with fluctuation effects taking into account. Here, we are going to pay a special attention to such characteristics of the light critical opalescence spectrum in confined liquids as: 1) the width Γ_{MB} of Mandelstam-Brillouin components, 2) the frequency shift of the side (Mandelstam-Brillouin) components from the central (Rayleigh) line, 3) the Landau-Placzek relation $I_c/2I_{MB}$.

A leading contribution to the width Γ_{MB} of the Mandelstam-Brillouin components is given by the following formula [3]:

$$\Gamma_{MB} = \left[\left(\frac{4}{3}\eta(q)+\zeta(q)\right)+\frac{\kappa(q)}{C_V(q)}-\frac{\kappa(q)}{C_P(q)}\right]\frac{q^2}{\rho} \quad . \tag{1}$$

Here η and ζ are the shear and bulk viscosities, κ is the thermal conductivity, C_P and C_V are the specific heats at constant pressure and volume, ρ is the liquid density, $q=(2\pi/\lambda)\sqrt{2\varepsilon_0}(1-\cos\theta)^{1/2}$ is the change of the wave vector on scattering by an angle θ, λ is the light wave length, ε_0 is an average part of the dielectric permittivity.

In accordance with the equilibrium finite-size scaling hypothesis, the critical behavior of any quantity is determined by the singularity of the correlation length of a system under consideration. As any other physical quantity of confined

O. Dössel and W.C. Schlegel (Eds.): WC 2009, IFMBE Proceedings 25/XIII, pp. 197–199, 2009.
www.springerlink.com

systems, the correlation length ξ depends not only on the thermodynamic variables (temperature, chemical potential, etc.) but also on a characteristic linear size L of a system's spatial limitation.

For a plane-parallel liquid layer with its thickness $H \leq \xi$ (this geometry fits good to such biological object as a synaptic cleft) the correlation length ξ of density fluctuations in confined liquids was found in [5] as follows:

$$\xi = \xi_0 \left[\tau + \left(\frac{\pi \xi_0}{H} \right)^{1/\nu} (1+\tau) \right]^{-\nu} . \quad (2)$$

Here ξ_0 is the amplitude of the correlation length, $\tau = (T - T_c)/T_c$ is the temperature variable, $\nu \approx 0{,}63$ is the critical exponent.

Another geometry of a liquid volume of the cylindrical form with a linear size along its axis $L_z >> \xi$ and radius $R \leq \xi$ corresponds to porous structures or ion channels in biological membranes. In this case the correlation length of density fluctuation is given by the formula:

$$\xi = \xi_0 \left[\tau + \left(\frac{\mu_1 \xi_0}{R} \right)^{1/\nu} (1+\tau) \right]^{-\nu} \quad (3)$$

with μ_1=2,4048 being the first naught of the Bessel function $J_0(z)$.

Thus, the width Γ_{MB} of the Mandelstam-Brillouin components of the light critical opalescence spectrum satisfies the following formula for confined liquids in liquids (including liquids of biological nature):

a) for a cylindrical geometry (e.g. ion channels, pores, etc.)

$$\Gamma_{\mathrm{MB}} \propto \Gamma_{\mathrm{MB}}{}^{0} \left[\tau + \left(\frac{\mu_1 \xi_0}{R} \right)^{1/\nu} (1+\tau) \right]^{-3\nu} ; \quad (4)$$

b) for a plane-parallel geometry (synaptic clefts, biological membranes, etc.)

$$\Gamma_{\mathrm{MB}} \propto \Gamma_{\mathrm{MB}}{}^{0} \left[\tau + \left(\frac{\pi \xi_0}{H} \right)^{1/\nu} (1+\tau) \right]^{-3\nu} , \quad (5)$$

where $\Gamma_{\mathrm{MB}}{}^{0} \cong \varsigma_0 q^2 / \rho$, ς_0 is the amplitude of the singular part of the bulk viscosity.

It is seen that, on taking the actual factor of spatial limitation into account, the critical behavior of such characteristics of the light molecular scattering spectra as the width of the side (Mandelstam-Brillouin) components, their frequency shifts, the Landau-Placzek relation, together with the width of the central (Rayleigh), should be essentially changed in compare with its behavior in large liquid volumes.

Namely, with *decreasing (increasing)* the characteristic system's size L at bulk critical temperature:

1) the width Γ_{MB} of Mandelstam-Brillouin components is *strongly shortening (broadening)* according to the relation $\Gamma_{MB} \propto L^{3}$;

2) the frequency shift of the side (Mandelstam-Brillouin) components from the central (Rayleigh) line is *weakly increasing (decreasing)* in accordance with such a relation $\Delta \Omega_{\mathrm{MB}} \propto L^{-0{,}087}$;

3) the Landau-Placzek relation is *essentially decreasing (increasing)* as is seen from $I_c/2I_{\mathrm{MB}} \propto L^{1{,}79}$.

The following important consequences can be obtained using experimental data of light critical opalescence spectra from suspension of tumor cells: while the membrane thickness H is increasing in 1,5 times (i.e. 50%) during the process of proliferation, one should expect that 1) the width of the central (Rayleigh) line is shortening more than twice (2,25 times), 2) the frequency shift $\Delta \Omega_{\mathrm{MB}}$ of the side components is increasing in 3,6%, 3) the width of the side (Mandelstam-Brillouin) components is broadening more than in 3 times (3,375 times).

Here we use results for the width of the central (Rayleigh) line $\Gamma_c \propto H^{-2}$ due to the diffusion mechanism which is in fact governing for the size dependence of the quasi-elastic peak of the neutron scattering studied in the water suspensions of plasmatic membranes of tumor cells.

Thus, results of the proposed studies give a reliable background to introduce a new diagnostic method of the crucial process of tumor formation. This method is based upon the following results for the light critical opalescence spectra (in addition to studies of the quasi-elastic neutron scattering) in water suspension of plasmatic membranes of tumor cells: 1) the width of the central (Rayleigh) line $\Gamma_c \propto H^{-2}$, 2) the width of the side (Mandelstam-Brillouin) components $\Gamma_{MB} \propto H^{3}$ where H is the average thickness of proliferated membranes.

II. Selfdiffusion of water molecules in the suspensions of plasmatic membranes

Plasmatic membranes play an important part in forming of resistivity of tumular cells to action of antitumor medicinal substances (for example, doxorubicine). The definite features of transport properties [6] of plasmatic membranes in relation to doxorubicine are exist [7]. In [8] in the system of in vivo was observed the reduction of mobility of lipoacid tailings in composition of lipids of plasmatic membranes of Guerin's carcinoma associated with the forming

of resistivity to doxorubicine. It results in the rise of microviscosity of plasmatic membranes and reduction of passive diffusion of xenobiotics. The mobility of lipoacid tails and heads of phospholipids of plasmatic membranes correlates with the number of water molecules that are bound to them.

It should be mentioned that cell's membranes represents the typical finite-size biological object. In such complex systems, geometrical factor of spatial restriction could cause profound changes of static and dynamic properties [9] of liquid matter. The detailed analysis of selfdiffusion parameters of water molecules in suspensions of plasmatic membranes of tumular cells (subcultures of Guerin's carcinoma) which are sensible and resistant to the doxorubicine (before and after the course of chemotherapy) is highly expedient for the collecting of clear data in relation to the mechanism of this phenomenon.

The method of Quasi-Elastic Slow Neutron Scattering (QESNS) is the powerful instrument for conducting of such researches. Application of this method for research of water solutions and suspensions of biological objects of is based on that fact, that the cross-section of dispersion of neutrons on the atoms of hydrogen and hydrogen-containing molecules of albumins exceeds on an order the cross-section of dispersion of neutrons on the atoms of other chemical elements [1].

Investigation of the influence of antitumor antibiotics on the dynamic state of molecules of water in liquid suspensions of plasmatic membranes of cells of tumors was the purpose of this work. Biological tissues of Guerin's carcinoma that were taken from laboratory male rats had become an object for the research.

The plasmatic membranes of tumular cells were separated by the method of differential ultra-centrifuging in the gradient of sucrose with concentration 0,1 mg/ml on an albumin. Research of the samples by a QESNS method was conducted on a spectrometer. The atomic reactor of the Institute of Nuclear Researches of NAS of Ukraine was the source of the neutrons for this spectrometer. During the experiment was observed the power spectrum of neutrons which were scattered by the samples. The analysis of broadening of the peaks of such spectrums allows to determine the changes of water molecules selfdiffusion coefficient in explored water suspensions of plasmatic membranes of tumours cells.

From the QESNS spectrums for every angle of dispersion the width of quasi-elastic peak ΔE was determined and its intensity I_0. Basic information about diffusive motions of water molecules is contained in the experimental dependence of broadening of quasi-elastic peak ΔE on the square of the passed impulse q^2 (on the angle of dispersion) [4]. Analysis of these spectrums, namely, analysis of broadening of QESNS peak ΔE, allows to define the coefficients of selfdiffusion of water molecules and mean lifetime of hydrogen bonds in water suspensions of plasmatic membranes of tumular cells of sensible and resistant to doxorubicine.

The experimental findings of QESNS measurments in water suspensions of tumular cells plasmatic membranes of Guerin's carcinoma can be analyzed within the framework of existent models of diffusion. Quasi-elastic scattering of neutrons (dispersion, that takes place with the small change of energy and wavelength of neutron) gives insignificant, but noticeable, broadening of the spectrum's peak. The magnitude of peak's broadening ΔE indicates on the degree of development of diffusion in a liquid.

It is shown, that influence of antitumor antibiotics on Guerin's carcinoma shows the noticeable increase of connective power of albuminous molecules of tumor cells in relation to the water molecules. Existence of the correlation between the change of selfdiffusion coefficient of water molecules and sensitiveness of different groups of biological tissues to antitumor drugs enables to estimate the efficiency of its application.

References

1. Patashinskii A.Z., Pokrovskii V.L. (1979) The Fluctuation Theory of Phase Transitions. Oxford, Pergamon Press
2. Fisher M.E. (1971) Critical Phenomena. Proceedings of the International School of Physics "Enrico Fermi", ed. M.S. Green. -**51**. New York, Academic
3. Fabelinskii I.L. (1968) Molecular Scattering of Light. New York, Plenum Press
4. Bulavin L.A., Chalyy K.A. (2006) Neutron Studies of the Critical Properties of Mesoscale Liquids. Kiev, Naukova Dumka
5. Chalyi A.V., Tsehmister Ya.V., Chalyy K.A. (2001) Processes of ordering and self-organization in fluctuational models of the open systems, Kiev, Vipol
6. Bulavin L.A. (1977) Neutron researches of dynamics of liquids. – Kiev, Vyscha Shkola
7. Tritton T.R. (1991) Cell surface actions of adriamycin // Pharmacol.Ther. - Vol. 49, № 3. –p. 293-309
8. Chekhun V.F., Lebed O.I., Tryndyak V.P. et al (2002) Structural alterations of plasma membranes of Guerin's carcinoma cells upon the development of resistance to doxorubicine // Exp.Oncol. Vol. 24. –p. 279-283
9. Chalyy K.A. (2003) Model of Choline Receptor: Properties of Liquid System With Geometry of Long Bar // Physics of Alive, Vol. 11, p. 51-57

Author: Chalyy K.A.
Institute: National Medical Academy
Street: Dorogojitskaya, 9
City: Kiev
Country: Ukraine
Email: kirchal@univ.kiev.ua

Phase contrast imaging for medical diagnostics: towards clinical application with compact laser-based X-ray sources

P. Coan[1,4], P.C. Diemoz[1,4], A. Bravin[1,4], T. Schlossbauer[2,4], M. Reiser[2,4], D. Habs[3,4], T. Schneider[2,4] and C. Glaser[2,4]

[1] European Synchrotron Radiation Facility (ESRF)/Biomedical beamline (ID17), Grenoble, France
[2] Institute of Clinical Radiology, Klinikum Ludwig-Maximilians-Universität, Munich, Germany
[3] Department of Physics, Ludwig-Maximilians-Universität, Munich, Germany
[4] Munich-Centre for Advance Photonics, Munich, Germany

Abstract—**At Munich centre for Advance Photonics, one of the main aims of the project is the development and application of phase contrast imaging techniques for medical diagnostics to be performed with a new compact high brilliant and energetic X-ray source. High resolution phase contrast tomography of breast and cartilage tissues with characteristics of clinical interest have been performed producing outstanding results. Accurate visualization of fine structures and tissue degeneration in the imaged samples was obtained representing a real step forward in the direction of clinical applications of the high sensitive phase contrast X-ray imaging.**

Keywords— **Phase contrast imaging, Biomedical diagnostics applications, High resolution imaging**

I. Introduction

Among the different imaging techniques, conventional radiography has the highest spatial resolution and is the initial, most economical and most abundantly used imaging method in medical diagnostics.

In standard radiography the contrast results from variations in X-ray absorption arising from density differences and from variations in the thickness and composition of the specimen. The sensitivity of the technique is drastically decreased when the sample consists of low Z elements, for which the differences in the absorption coefficients are very small for hard X-rays [1].

Weakly absorbing objects are often encountered in the life sciences, because organic matter is made mainly of carbon, hydrogen, oxygen and nitrogen. The difference in the absorption coefficient, for these elements, is of the order of 0.1-0.3 cm^{-1} in the range of energies commonly used in radiology (10-60 keV).

For this reason, conventional imaging-based diagnostics of soft tissue degenerations and pathologies may often suffer from the lack of image contrast and sensitivity. The diagnosis is in some cases particularly difficult since the intrinsic limitations of the technique itself.

Over the last two decades, a completely different approach has been proposed and developed. It consists in the application to the medical physics of the so-called phase contrast techniques, already largely used in other fields of research in physics at lower energies.

The interest for phase sensitive techniques in medical applications resides in the fact that it is possible to observe contrast due to the phase modulation of the signal, even if the amplitude modulation is weak or absent, with a dose to the tissues similar or even reduced compared to conventional absorption radiography [2].

Phase contrast techniques have been successfully applied to mammographic studies [3-5] and orthopaedics for cartilage investigations [2, 6], leading to exciting results in terms of visualization of early lesions in soft tissues.

Intrinsic limitations in mammography and in practically all medical imaging technologies with respect articular cartilage calls for the discovery and development of new techniques that are sensitive to early stages of breast cancer and to stages preceding the point of irreversible damage of cartilage tissue.

- Breast cancer imaging

Breast cancer is one of the principal causes of death among women in developed countries [7]. Early detection of malignant tumors is closely related to a better survival rate. In mammography approximately 10-20% of palpable breast cancers are not visible on mammograms, mainly as a result of insufficient radiographic contrast between soft tissues of the mammary gland. In addition, only 5-10% of screening mammograms that are interpreted as abnormal turn out to harbor cancer [4].

- Articular cartilage imaging

Osteoarthritis (OA) is a degenerative disorder characterized by loss of articular cartilage, thickening of the underlying subchondral bone, and osteophyte (bone excrescence) formation. OA is a poorly understood disease for which, presently, no cure exists. The principal treatment objectives

O. Dössel and W.C. Schlegel (Eds.): WC 2009, IFMBE Proceedings 25/XIII, pp. 200–203, 2009.
www.springerlink.com

are to control pain adequately, to improve function, and to reduce disability. Tools conventionally used to monitor the progression of OA remain unsatisfactory. For OA assessment the principal hallmarks are still the clinical observations of pain, inflammation, joint mobility, gait, and radiography. Unfortunately, these diagnostic modalities can be sensitive only in cases of advanced stages of OA since they do not allow visualization or detection of very early degenerative alterations in joint tissue. Many other imaging techniques are used (i.e. computed tomography (CT), magnetic resonance imaging (MRI), ultrasound (UI), biomarker detection) but each of these presents its own intrinsic limitations.

In the light if these facts, breast cancer detection and cartilage imaging are two examples of medical fields in which a high resolution, non-invasive detection and monitoring technique is particularly desirable and needed. In-vitro studies performed in the last years on mammography and OA samples have clearly proven that X-ray phase contrast modalities could play an important role in filling the gap in the capability of early and precise visualization of breast and cartilage damages.

A. The Munich-centre for Advance Photonics (MAP)

In this scenario that the excellence cluster "Munich-Centre for Advanced Photonics" [8] got started in November 2006 at the Munich universities. The main aim of the project is to develop advanced laser sources, which can be applied in many fields. One usage is to build a compact machine capable of delivering brilliant high flux X-ray beams comparable to classical X-FELs, but producing higher X-ray energies, which are important for medical diagnostics.

The demonstration of the applicability and the potential of phase contrast imaging in selected medical diagnostic areas in which conventional X-ray absorption-based imaging tools are not considered sufficient yet is one of the final goals of the cluster.

The peculiarity of the MAP mission in the field of biomedical diagnostics leads in the very clinically oriented character of its research.

In mammography the aim is to perform phase contrast imaging of whole breast by focusing on dense breast samples, where conventional mammography has great difficulties in identifying tumors due to a lack of contrast. This will be already a significant improvement with respect to the published works: in the literature the analysis of small tissue samples (up to 10 cm of diamter) only has been reported. For radiologists this represents a very important limit; in fact, the observation of the breast architecture is one of the essential points in a diagnosis. Thanks to the large collaboration within MAP it will be possible to access full breast samples. A further aim is to detect tumors earlier and of smaller size.

Cartilage is the second focus of high resolution, high sensitive phase contrast imaging in the framework of the MAP project. The aim is to identify disruptions in the collageneous fibre architecture, which are an essential tool in diagnosing early stages of osteoarthritis. Automatic pattern recognition has to be developed to filter from the large amount of high resolution raw data the areas of abnormality.

The work presented in this paper has been carried out in the framework of the cluster MAP and its purpose is to prove that high-resolution phase contrast imaging in tomography modality (CT) can substantially improve the radiographic contrast of both breast and cartilage in vitro in comparison with conventional diagnostic radiography.

The development and optimization of biomedical applications of phase contrast imaging to be exploited by using the high brilliant X-rays produced by an ultra-compact machine is one of the goals of the MAP project and represents a challenge of high medical diagnostics interest.

II. Material and methods

In order to exploit the X-ray phase shifts occurring to an electromagnetic wave passing through a sample for imaging, different techniques have been developed over the last decades. They include the propagation-based imaging [9, 10], the analyzer-based imaging [11-13] and the interferometric techniques [14, 15]. Detailed descriptions of each of these techniques may be found in the indicated references, hereafter some set-up and experimental basics are reported.

A. Propagation-based imaging (PBI)

In the propagation-based method, quasi-coherent radiation illuminates the object that can give rise to a spatially varying phase shift. As the radiation propagates from the sample, parts of the wavefront, which have experienced different deflections, interfere giving rise to a characteristic pattern that is then recorded by a detector set at a convenient distance. Thanks to the Fresnel diffraction, the phase shifts are therefore transformed in detectable intensity variations [16].

Among the phase contrast techniques, this imaging modality is characterized by a very simple set-up. The absence of optical elements implies that such an imaging method is intrinsically free from the usual aberrations, with achievable

resolution depending largely, but not entirely, on the size of the source [17].

B. Analyzer-based imaging (ABI)

This phase contrast imaging technique is based on the use of an analyzer crystal placed between the sample and the imaging detector. As a highly collimated monochromatic beam traverses the sample, photons are deviated according to the gradient of the real part of the refractive index. The analyzer crystal acts as an angular filter, selectively accepting or rejecting such photons: only a narrow range of X-rays, those satisfying the Bragg law for the diffraction ($2d\sin\theta = \lambda$, where d is the crystal d-spacing, θ is the grazing angle of incidence to the crystal and λ the radiation wavelength), can reach the detector and then contribute to the image formation [18]. The filter function is given by the rocking curve (RC) (which actually corresponds to the convolution of the monochromator and analyzer reflectivity curves) of the crystal and typically features an acceptance window (given by the RC full-width at half maximum FWHM) of a few microradians or tens of microradians. As an example, the FWHM for the reflection 111 of the silicon spans the range 17.6–4.3μrad for the energy interval 15–60 keV.

C. Interferometric technique (grating-based interferometry-GIFM)

The X-ray interferometry is owed to Bonse and Hart [19] Different interferometric configurations have been developed and applied. More recently a new version of the interferometry technique has been proposed [15, 20]. It consists in a two-grating interferometer for hard X-rays that can be used for phase imaging and tomography. A silicon phase grating positioned just downstream of the object under study splits the distorted wavefront into essentially a positive and a negative first-order beam. At a given distance from this beam-splitter grating, where the two beams still mostly overlap, they form a pattern of interference fringes that is distorted according to the wavefront distortions. The fringes may be finer than the resolution of an area detector used to record the signal, but an absorption grating with suitable pitch, put in front of the detection plane, allows the detection of intensity variations that correspond to the derivative of the wavefront phase taken along the direction perpendicular to the grating lines. A combination of this technique with the phase-stepping method, in which several exposures are made which differ in the phase of the fringe pattern, allows to eliminate effects of non-uniform intensity due to inhomogeneous illumination and edge-enhancing inline phase contrast.

Fig. 1 Propagation-based phase contrast image in tomographic modality of a breast tissue of 15 cm of diameter. X-rays of 35 keV, a sample-to-detector distance of 11 meters and a detector with a pixel size of 46 microns were used.

In this work, the choice of the techniques to be used has depended on the characteristics of sample to image and in some cases all these three phase contrast imaging modalities have been used in order to find out which technique is the most suitable for a given application. The purpose is to identify the technique that is the most suitable for being implemented at the new X-ray source and the most adapted for a given medical application.

III. Results

High resolution phase contrast imaging both in projection and tomographic modality has been performed on whole and dense excised breast tissues and on cartilage/bone cylinders from human patellae.

In this work, different X-ray energies and detector spatial resolutions have been used in order to optimize the image contrast depending on these experimental parameters.

Fig. 1 shows a high resolution computed tomography image of an excised whole breast tissue (diameter of 15 cm) produced during a MAP experiment at the European Synchrotron Radiation Facility (France). X-rays of 35 keV and an imaging detector with a pixel size of 46 μm (FReLoN camera) were used. The images were obtained by applying the PBI technique with sample-to-detector distance of 11 meters. This is an example of the first results ever of phase contrast images on so big breast samples. Despite the large dimension of the sample, the different anatomical structures of the tissues are well depicted, edges and interfaces between different types of tissues are accurately shown. The darkest uniform areas are mainly adipose tissue. Final validation of results is being made by comparison with conven-

tional clinical techniques (histology, conventional mammography etc.).

Phase contrast projections and CT of cartilage samples were also produced and results show excellent depiction of the architecture of subchondral bone in PBI, ABI and GIFM modes. A zonal pattern within the cartilage matrix totally invisible in absorption-based imaging and similar to collagenous fibre orientation in scanning electron-microscopy (SEM) could be visualized.

IV. CONCLUSIONS

Results produced in this study clearly demonstrate that high resolution phase contrast CT imaging may allow acquisition of an accurate three dimensional (3D) image of the entire tissues. Obviously, this could improve detection of minor diseases in dense breasts and in cartilage or lesions hidden by superimposed structures. The volumetric breast imaging technique would also eliminate the painful compression of breasts, used in mammography.

With regard to cartilage imaging, high resolution phase contrast microtomography as one single imaging approach is able to reveal structural detail in both subchondral bone and cartilage suggesting a high potential of the technique for future diagnostic workup of OA.

In this scenario, the availability of tabletop, intense monochromatic sources may therefore fundamentally change the practice of X-ray imaging in clinical diagnostics.

Such a source could provide an X-ray beam with properties similar to those of synchrotron radiation. In particular, the radiation would possess an adequate degree of coherence that is important for performing phase contrast imaging.

It has been proven that polychromatic spectrum generated by conventional microfocus X-ray tube can still allow for the exploitation of some phase contrast modalities [21, 22]. The main limitation for clinical biomedical applications is given in this case by the X-ray intensity and therefore by the long exposure time needed.

The idea of the project is to first optimize the phase contrast X-ray imaging techniques by using synchrotron radiation as the gold standard radiation and then to transfer the technology into a clinical environment through the installation and exploitation of a compact X-ray source.

ACKNOWLEDGMENT

Authors would like to thank Dr. H. Requardt, Dr. C. Nemoz and T. Brochard for their precious support in the experimental work.

REFERENCES

1. Henke B, Gullikson E, Davis J (1993) X-Ray Interactions: photoabsorption, scattering, transmission and reflection at E= 50-30000 eV, Z= 1-92. Atomic Data Nuclear Data Tables 54:181-342
2. Mollenhauer J, Aurich ME, Zhong Z et al. (2002) Diffraction-enhanced X-ray imaging of articular cartilage. OsteoCart. 10:163-171
3. Arfelli F, Bonvicini V, Bravin A et al. (2000) Mammography with synchrotron radiation: phase-detection techniques. Radiology 215(1):286-93
4. Pisano ED, Johnston RE, Chapman D et al. (2000) Human breast cancer specimens: diffraction-enhanced imaging with histologic correlation--improved conspicuity of lesion detail compared with digital radiography. Radiology 214(3):895-901
5. Keyriläinen J, Fernández M, Karjalainen-Lindsberg ML et al. (2008) Towards high-contrast breast CT at low radiation dose. Radiology 249(1):321-327
6. Coan P, Mollenhauer J, Wagner A et al. (2008) Analyzer-based imaging technique in tomography of cartilage and metal implants: A study at the ESRF. Eur. J. Radiology 68S:S41-S48
7. Parkin DM, Bray FI, Devesa SS (2001) Cancer burden in the year 2000 the global picture. Eur. J. Cancer 37:S4-S66
8. MAP - http://www.munich-photonics.de/
9. Snigirev A, Snigireva I, Kohn V et al. (1995) On the possibility of x-ray phase contrast microimaging by coherent high-energy synchrotron radiation. Rev. Sci. Instrum. 66(12):5486-92
10. Cloetens P, Barrett R, Baruchel J et al. (1996) Phase objects in synchrotron radiation hard X-ray imaging. J. Phys D: App Phys 29:133-146
11. Bravin A (2003) Exploiting the X-ray refraction contrast with an analyser: the state of the art. J. Phys D: App Phys 36:A24-A29
12. Förster E, Goetz K, Zaumseil P (1980) Double crystal diffractometry for the characterization of targets for laser fusion experiments. Kristall Technik 15:937-945
13. Davis T, Gureyev T, Gao D et al. (1995) X-ray image contrast from a simple phase object. Phys. Rev. Lett. 74(16):3173-3176
14. Momose A, Takeda T, Itai Y et al. (1996) Phase-contrast X-ray computed tomography for observing biological soft tissues. Nat Med 2(4):473-5
15. David C, Nohammer B, Solak H et al. (2002) Differential X-ray phase contrast imaging using a shearing interferometer. Appl Phys Lett 81(17):3287-3289
16. Born M, Wolf E, Principles of optics: electromagnetic theory of propagation, interference and diffraction of light. 7th ed, ed. C.U. Press. 1999, Cambridge.
17. Pogany A, Gao D, Wilkins S (1997) Contrast and resolution in imaging with a microfocus x-ray source. Rev. Sci. Instrum. 68(7)
18. Podurets K, Somenkov V, Shilstein S (1989) Refraction-contrast radiography. Sov Phys - Tech Phys 34(6):654-657
19. Bonse U, Hart M (1965) Appl. Phys. Lett. 6:155-156
20. Weitkamp T, Diaz Z, Nöhammer B et al. (2004) Hard X-ray phase imaging and tomography with a grating interferometer. SPIE
21. Wilkins S, Gureyev T, Gao D et al. (1996) Phase-contrast imaging using polychromatic hard X-rays. Nature 384:335-338
22. Pfeiffer F, Weitkamp T, Bunk O et al. (2006) Phase retrieval and differential phase-contrast imaging with low-brilliance X-ray sources. Nature Physics 2:258-261

Author: Paola Coan
Institute: European Synchrotron Radiation Facility and MAP-Munich
Street: 6, rue J. Horowitz
City: Grenoble
Country: France
Email: coan@esrf..fr

ETHICS IN RESEARCH

William R. Hendee PhD
Distinguished Professor
Medical College of Wisconsin
P.O. Box 170970
Whitefish Bay, WI 53217
whendee@mcw.edu
414.351.6527 (H)
414.531.1756 (M)

Individuals conducting research in medical physics and biomedical engineering have certain rights and responsibilities that should always be respected. About two years ago the International Organization of Medical Physics (IOMP) created a Bill of Rights for Scientists and Engineers that contains 10 clauses addressing the rights of research physicists and engineers. The Bill of Rights emphasizes that a Scientist or Engineer must be free to theorize and experiment unimpeded by political pressures, religious dogma or fear of reprisal. The Bill of Rights has been adopted by the IOMP, the International Federation Medical and Biological Engineering (IFMBE), and the International Union for Physical and Engineering Sciences in Medicine (IUPESM). The Bill of Rights is consistent with the Statement on the Universality of Science of the International Council for Science (ICSU).

The final clause of the Bill of Rights states that at all times a Scientist or Engineer shall adhere to universal ethical and moral standards. The challenge is to define these standards in a manner that is applicable to scientists and engineers conducting research in a variety of environments. This challenge can best be addressed by acknowledging that scientists and engineers must possess certain attributes that assure that their work is of the highest integrity. Among these attributes are Honesty, Forthrightness, Diligence, Respect for Persons, Service to Others, Continuous Self-Improvement, and the Primacy of Patient Welfare when working in a clinical setting. Scientific and professional organizations have an obligation to aid scientists and engineers in their pursuit of these attributes.

Many issues are encompassed in the adherence of scientists and engineers to universal ethical and moral standards. They include Respect for Patient Privacy and Autonomy; Recognition and Acknowledgement of Conflicts of Interest; Responsible Conduct of Peer Review; Reporting Unethical Behavior of Others; Research Principles and Avoidance of Misconduct; Ethical Considerations of Research with Humans and Animals; Challenges of Vendor-Sponsored Research; Responsibilities of Authors and Reviewers of Scientific Publications; Special Sensitivities of Student-Mentor Relationships; and Employer-Employee Considerations.

O. Dössel and W.C. Schlegel (Eds.): WC 2009, IFMBE Proceedings 25/XIII, pp. 204–205, 2009.
www.springerlink.com

These issues are addressed to a greater or lesser degree in the Codes of Ethics of various scientific and professional organizations. However, there is no single document that encompasses all of the issues, and yet scientists and engineers are responsible for adhering to all of them.

WORKSHOP
THE CHALLENGE AND THE REWARD OF BEING AN ENTREPRENEUR IN MEDICAL PHYSICS AND BIOMEDICAL ENGINEERING

William R. Hendee PhD
Distinguished Professor
Medical College of Wisconsin
P.O. Box 170970
Whitefish Bay, WI 53217
whendee@mcw.edu
414.351.6527 (H)
414.531.1756 (M)

Most medical physicists and biomedical engineers think of research in terms of the following paradigm: Conducting research leads to the discovery of new information. When this new information is placed in the context of what is already known through scientific publications and presentations of others, it constitutes new knowledge. This new knowledge becomes the subject of one or more scientific publications. These publications enhance the prospects of the physicist or engineer for new and continued research funding. The funding supports additional research that leads to discovery of more information, leading to additional new knowledge and publications. Through this process, the cycle repeats itself over and over – at least if the investigator is able to sustain his or her funding.

This process serves the investigator well, but its value to society and to the sick and infirmed is marginal. It begs the question of why society is making an investment in support of biomedical research, and how this investment is benefitting anyone other than the investigator and other individuals working in the same area of research. It is this question that has given rise to efforts of the National Institutes of Health in the United States to develop funding programs that emphasize the utility of biomedical research to improve public health and to reduce pain and suffering of patients. Every investigator should ask the same question for the research he or she is doing – What is the value of my research to people and to society?

The creation of new knowledge can lead not just to publications and enhancement of one's resume and reputation, but also to innovations in current ways of providing care to patients that ultimately yield new technologies, procedures and products. These new services reflect the purposeful migration of research results from the laboratory bench to the bedside of patients – a process referred to as translational research and, when tested on patients and normal volunteers, clinical research. Emphasis on this process enhances and certainly does not impede the closed loop of using research results to generate scientific papers that support applications for continued research support. In addition, it can lead to a sense of fulfillment in the investigator because the results of

O. Dössel and W.C. Schlegel (Eds.): WC 2009, IFMBE Proceedings 25/XIII, pp. 206–207, 2009.
www.springerlink.com

research are seen to be helping people in need.

The way to benefit many patients through research is to move innovations not just to the bedside of a few patients in an institution, but to the bedsides of many patients through the commercialization of new technologies, procedures and products. This is the process of entrepreneurship, which can be facilitated or hindered by an investigator's institution or organization, depending on the prevailing attitude towards investigators assuming the role of entrepreneurs as well as researchers. An institution or organization that encourages entrepreneurship will provide resources to an investigator for protecting intellectual property, licensing intellectual property to commercial entities, and facilitating the launch of start-up companies around broad developments in medical innovations. Such an institution or organization will be viewed favorably by more energetic and innovative investigators who are looking for ways to help patients and society through the products of their research. This favoritism can ultimately make the institution or organization a very exciting place for scientific research and innovation.

The Art of Grantsmanship

H.J. Khoury

Nuclear Energy Department, Federal University of Pernambuco, Recife, Brazil

Abstract— This paper discusses the requirements needed to optimize the probability of success in a grant application. The objective of this discussion is to assist investigators to improve their chances when competing for financial resources.

Keywords—research, grants

I- INTRODUCTION

Funding is critical to materializing research and development (R&D) projects and to consolidating research groups. In general, the coordinators of R&D projects spend a lot of time drafting proposals aimed at getting funds from national and/or international agencies.

Often, despite of the fact that the proposal is based on good ideas, it is not approved. Why does this happen? Many factors influence the process of selection and approval of a project.

A successful grant application is an exercise of communicating a good idea to the institution which funds R&D projects.

A good idea is necessary but not sufficient. Grantsmanship is the art to obtain a grant to fund R&D projects. Clearly, a grantsmanship can not improve the quality of the research or improve bad ideas.

However, a good idea can be wasted by a poorly written project. The difference between success and failure to achieve funding generally depends on the clarity and focus of the ideas of the project.

This paper discusses the requirements needed to optimize the chances of success in a grant application. The comments and suggestions are based on my experience as a full professor at the Nuclear Energy Department of the Federal University of Pernambuco, where I coordinate several research projects supported by national and international funding agencies.

II- THE BASIC PRINCIPLES OF GRANTSMANSHIP

The main objective of grantsmanship is to ensure that the proposals to be submitted are focused, clear, accurate and well organized. It is important to remember that the results of the project to be developed will open or close new opportunities for funding. Good project management ensures the project success. But project success also depends on a motivated and skilled team involved with the project. It works like a mechanical gear, as shown in Figure 1

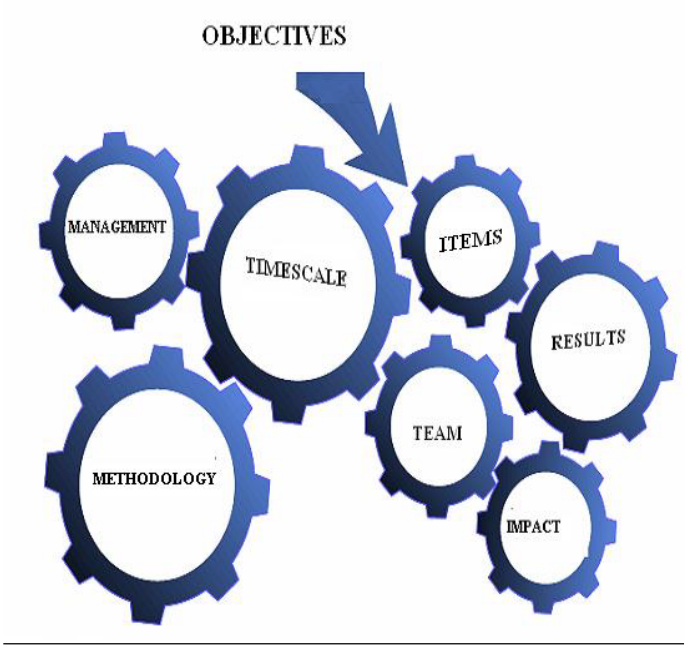

Figure 1- Representation of how the components of the project operate as a mechanical gear

O. Dössel and W.C. Schlegel (Eds.): WC 2009, IFMBE Proceedings 25/XIII, pp. 208–209, 2009.
www.springerlink.com

First Principle

The first important thought, before starting to write a project, is the careful reading of the Guidelines and the Application Forms to make sure that the proposal matches the mission of the agency. Institutions funding R&D projects do not exist to fund what you wish them to fund. They fund work that furthers their mission, which is evidenced in program announcements or requests for the grant application. Pay attention to the agency's objectives and established criteria. It is a waste of time to apply to the "wrong" agency. The system helps those who know the system. **So, the first principle of grantsmanship is: "be acquainted with the funding agency"**

Second Principle

Before starting to write the proposal, you should begin by clarifying your ideas. Ask yourself the following questions: Are the objectives and aims of the project coming into focus? Why are you elaborating the project? Is there enough innovation in the project? What is the impact of the project? Discussing your ideas with colleagues working in similar areas, will help you to clarify and focus your ideas and to identify possible gaps in the organization of the project.

Writing the text of the project takes time. Starting the process early gives time to review the text and polish your application. Define the problem, the methodology to be used, try to explain the relevance and innovation of the proposed research clearly. It is important to elaborate the proposal well focused, very clear, organized and accurate. Be sure you are up-to-date on techniques, literature and interpretations of ideas and theories. Be sure your topic is appropriate for financial support the proposal. Be specific about purpose, products and past work. **Therefore, the second principle of grantsmanship is: "focus your thinking and write an organized document"**

Third Principle

The third principle is "get inside the reviewer's head". Try to answer the question: what do reviewers primarily look for? Remember that the reviewers are performing reviews as a task over and above their daily activities. So, they will read the proposal very quickly. For this reason, the more clear and organized your text is, the more success you will have. Frequently, reviewers are not experts in your area of research, so you have to communicate with them using only a minimum amount of technical jargon . Reviewers pay attention to bureaucratic details. They expect you to follow the instructions precisely and to provide an easy-to-read format. You also need to convince them of your excellent and relevant training, and that you already have substantive preliminary data and pilot studies which prove your capability to develop the research.

After the merits of the proposal have been decided, the budget is analyzed and a score is given. Often, review committee members are under an obligation to reduce the budget. Therefore, make sure that the budget is well documented, realistic, appropriate and justified. Do not inflate, overbudget, or underbudget. Check carefully whether the agency supports certain items (e.g. travel, purchase of books, etc.). Do not request items that are not allowed. Give sufficient details for each item to make it difficult and unreasonable for the reviewers to arbitrarily suggest major cuts in the expenses. For equipment, document convincingly why a piece is essential, and why the specified model is required. Inform them if you are receiving other grants.

These are the main principles to increase the chances of success. Remember that your proposal will compete with several other proposals, which can be better prepared. The fact that the reviewers criticize or reject your proposal should not discourage you. Try to understand the criticisms made by the reviewers and correct the identified flaws. For example, some common errors are:

- The proposal includes a lifetime's work and is unrealistically ambitious.
- There are no clearly defined priorities and the timetable is unrealistic,
- The literature and background reviews are like an undergraduate's review.
- The application is fragmented and disjointed.

III CONCLUSION

O course, nobody likes to receive a negative for the proposal. But it can be an opportunity for improvement and growth. If you consider the criticism received and seek to correct the failures, revising your proposal for a resubmission, you will certainly achieve success. As said before, grantsmanship is an art that combines a good idea with an effective communication.

Author: Helen Jamil Khoury
Institute: Universidade Federal de Pernambuco
Street: Av. Prof Luiz Freire, 1000
City: Recife
Country: Brazil
Email: hjkhoury@gmail..com

Influence of anisotropic tissue electrical conductivity on electric field and temperature distribution during electroporation-based therapy

I. Lacković[1], R. Magjarević[1] and D. Miklavčič[2]

[1] University of Zagreb, Faculty of Electrical Engineering and Computing, Zagreb, Croatia
[2] University of Ljubljana, Faculty of Electrical Engineering, Ljubljana, Slovenia

Abstract— **Electroporation is a biophysical phenomenon caused by externally applied high-intensity electric field to cells that results in the increase of membrane conductivity and permeability. Among many applications it is used for *in vivo* drug delivery to tumors (electrochemotherapy) and for non-viral delivery of foreign genes into various tissues (gene electrotransfer). Since high-intensity electric field is applied and strong current passes through tissue, it can produce heating (Joule effect) which can cause tissue thermal damage. In our study we evaluated electric field and temperature distribution during typical electrochemotherapy pulsing protocol and gene electrotransfer specific protocol in tissue with anisotropic electrical conductivity (e.g. skeletal muscle). We developed a coupled electrical-thermal model and used finite-element method to solve it for a pair of needle electrodes 0.7 mm in diameter, 8 mm apart. The results show markedly different electric field and temperature distribution if electrode axis (defined by the line connecting two needle electrodes) is positioned along muscle fibres (i.e. longitudinally, in parallel) when compared to the position when electrode axis is across muscle fibers (i.e. transversally, perpendicularly). If electrodes are applied in the direction where electrode axis is along muscle fibers, tissue heating is higher than in the case when electrodes are applied across muscle fibers. For the two examined pulse protocols and skeletal muscle as a target tissue, temperature increase due to electric pulses was within physiological range (< 43 ºC) except near the needle tip. Increase of pulse amplitude, duration or number of pulses might induce thermal damage which is more likely to occur in gene electrotransfer protocol specially if electrode axis is oriented along muscle fibers.**

Keywords— **electroporation, anisotropic conductivity, Joule heating, finite-element method, gene therapy**

I. Introduction

Electroporation is a biophysical phenomenon occurring when cells are exposed to a high-intensity electric field that induces structural defects to the plasma membrane, allowing the transport of molecules across the membrane to which it is normally impermeable. Application of electroporatio *in vivo* allows for potentiation of drug delivery to tumors (electrochemotherapy) and transfer of DNA into skin, liver cells or skeletal muscle (non-viral gene delivery). Electroporation-based gene delivery to skelatal muscle as a target tissue has been of great interest not only for treating muscular dystrophy, but to using muscle for systemic delivery of therapeutic proteins [1, 2].

Exact mechanisms involved in electrotransfer of DNA across cell membrane are not yet fully understood. It is clear that electroporation is effective only when plasmid DNA is injected into the muscle prior to, not after, electroporation. Use of much longer pulses (20-50 ms) for electrotransfection than for electrochemotherapy (100 µs), has shown beneficial results, that were attributed to the contribution of electrophoretic transport [3-5].

Since large electric field and current flow are involved, Joule heating might pose a problem which could cause tissue thermal damage and unsuccessful outcome of electrotransfection. In our previous works [6-8], we modeled different pulsing protocols and electrode geometries, for electrically and thermally isotropic tissue (liver). Modeling studies by others also assumed isotropic tissue [9-11]. The aim of this study was however to evaluate the influence of anisotropic tissue electrical conductivity (characteristic for skeletal muscles) on electric field and temperature distribution. We analyzed pulse trains of both short (100 µs) high voltage and long (50 ms) low voltage electric pulses.

II. Methods

A. Coupled electric thermal model

The electric potential φ during electric pulses (assuming that the electric current density in tissue is divergence-free) can be described as:

$$\nabla \cdot (\sigma \nabla \varphi) = 0 \tag{1}$$

where σ is the electric conductivity tensor:

$$\sigma = \begin{bmatrix} \sigma_x & 0 & 0 \\ 0 & \sigma_y & 0 \\ 0 & 0 & \sigma_z \end{bmatrix} \tag{2}$$

O. Dössel and W.C. Schlegel (Eds.): WC 2009, IFMBE Proceedings 25/XIII, pp. 210–213, 2009.
www.springerlink.com

Heat transfer in tissue is assumed to be governed by the bioheat equation in which the Joule heating term $\mathbf{JE} = \sigma|\mathbf{E}|^2$ is added as a distributed heat source:

$$\rho c \frac{\partial T}{\partial t} = \nabla \cdot (k \nabla T) - \rho_b \omega_b c_b (T - T_b) + Q_m + \mathbf{JE} \quad (3)$$

Here T is the temperature, t is the time, ρ, c and k are the density, the heat capacity and the thermal conductivity of tissue respectively, ω_b is the blood perfusion, ρ_b and c_b are the density and the heat capacity of blood, T_b is the temperature of the arterial blood respectively, Q_m is the metabolic heat, $\mathbf{E} = -\nabla\varphi$ is the electric field and $\mathbf{J} = \sigma\mathbf{E}$ is the current density. Temperature dependence of tissue electrical conductivity is also incorporated in the model as:

$$\sigma = \sigma_0 [1 + \alpha (T - T_0)] \quad (4)$$

where α is the temperature coefficient, and σ_0 is nominal tissue conductivity tensor at temperature T_0. Tissue properties except electric conductivity were taken from the literature [12]. For all simulations longitudinal skeletal muscle conductivity was 0.52 S/m, and transversal 0.076 S/m [13].

B. Geometry

Geometry of our model comprised of a pair of needle electrodes inserted in a tissue block, as shown in Fig. 1. Due to symmetry only one forth of the entire geometry was used.

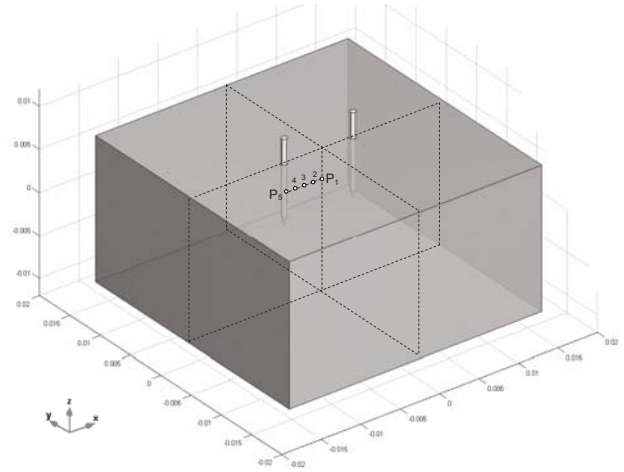

Fig. 1 Geometrical model of tissue and electrodes. The length (*x*), the width (*y*) and the thickness (*z*) of tissue block: 32 mm × 32 mm × 16 mm. Needle diameter: 0.7 mm; interelectrode distance: 8 mm; insertion depth of electrodes: 7 mm. Dashed lines represent symmetry planes. Circles represent 5 selected locations (P_1, P_2 to P_5) at the depth of 3.5 mm. P_1 is located in the middle between two electrodes, P_5 is at the contact between electrode and tissue, and other points are equally spaced between them.

III. Results

Fig. 2 shows calculated electric field distribution in muscle tissue during high voltage pulse for perpendicular and parallel orientation. Influence of anisotropic conductivity can be observed. Electric field is suppressed in the direction of lower conductivity and stretched in the direction of higher conductivity.

Fig. 3 shows temperature distributions for a train of short high voltage pulses (8 pulses, 100 µs duration, 1 Hz repetition frequency, 800 V amplitude).

Fig. 4 shows temperature distributions for gene electrotransfer protocol using long lower voltage pulses (8 pulses, 50 ms duration, 1 Hz repetition frequency, 80 V amplitude).

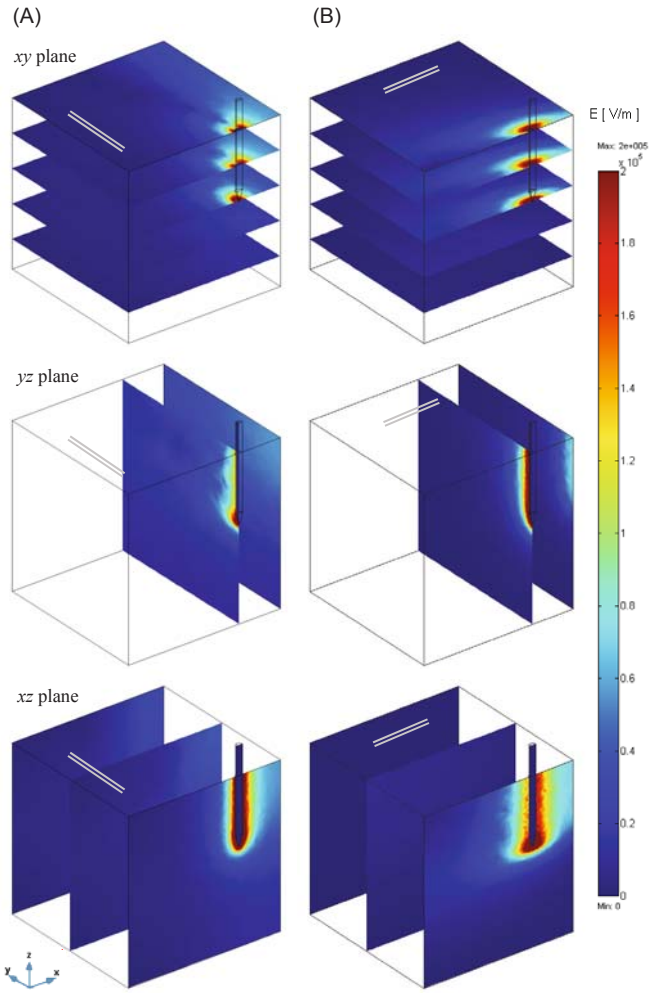

Fig. 2 Electric field distribution during pulse delivery (cross-sections in *xy*, *yz* i *xz* plane). Grey lines (||) indicate direction of muscle fibres. (A) Electrode axis perpendicular to the axis with higher tissue electrical conductivity $\sigma_{0x}=\sigma_{0z}$ = 0.076 S/m, σ_{0y} = 0.52 S/m. (B) Electrode axis parallel to the axis with higher tissue electrical conductivity σ_{0x} = 0.52 S/m, $\sigma_{0y}=\sigma_{0z}$ = 0.076 S/m. Pulse amplitude 800 V for both cases.

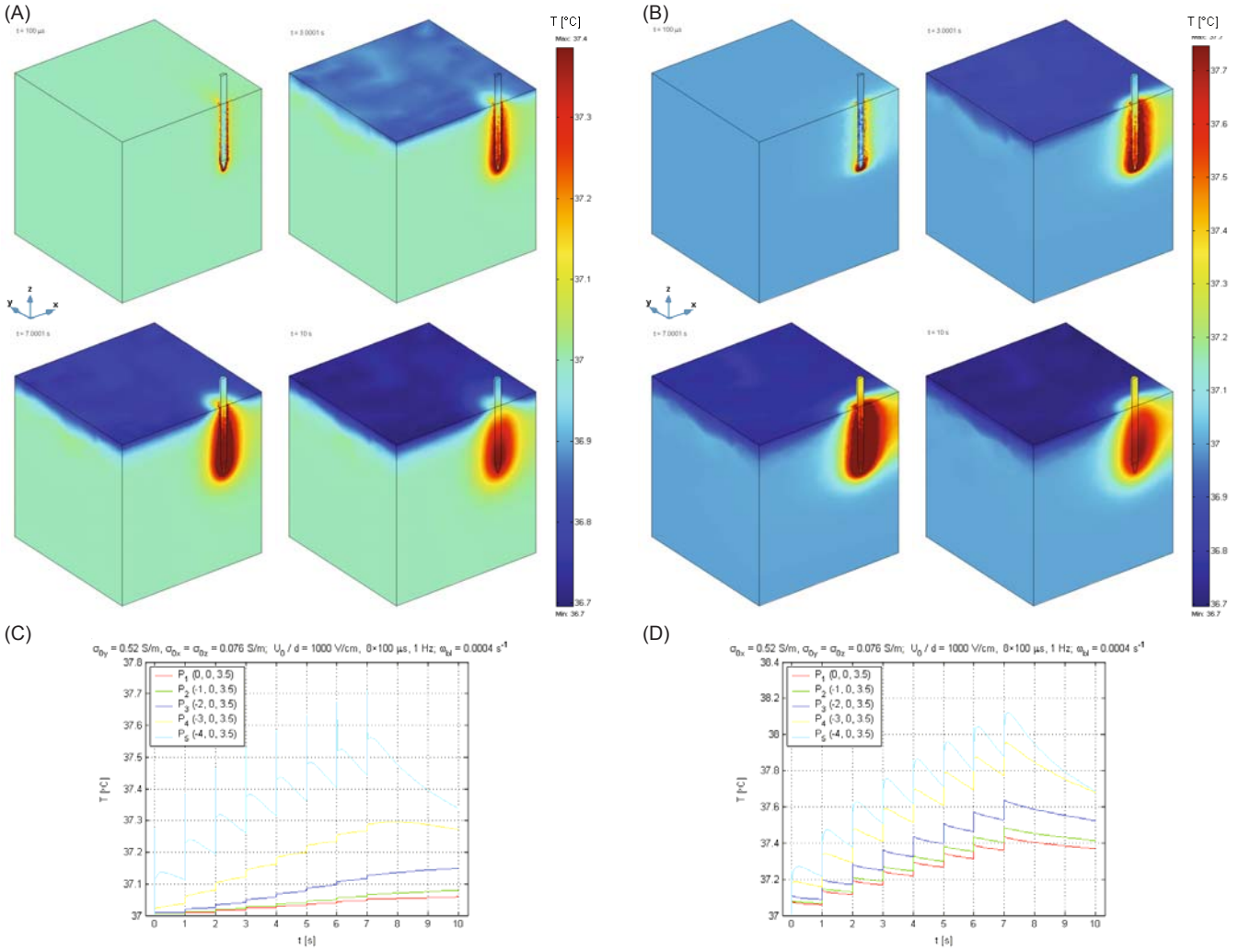

Fig. 3 Temperature distribution during HV pulse train (8×100 µs, 1 Hz, 800 V) after 1st, 4th, 8th pulse and at the end of simulation (t=10 s). (A) Electrode axis perpendicular to the axis with higher tissue electrical conductivity $\sigma_{0x}=\sigma_{0z}$ = 0.076 S/m, σ_{0y} = 0.52 S/m. (B) Electrode axis parallel to the axis with higher tissue electrical conductivity. σ_{0x} = 0.52 S/m, $\sigma_{0y}=\sigma_{0z}$ = 0.076 S/m. (C) Time course of temperature in selected locations corresponding to case (A) i.e. parallel orientation. (D) Time course of temperature corresponding to case (B) i.e. perpendicular orientation.

IV. Conclusions

For both protocols and skeletal muscle as target tissue, temperature increase due to electric pulses is within physiological range (< 43 ºC) except near the needle electrode tip. Increase of pulse amplitude, duration or number of pulses might induce thermal damage which is more likely to occur for gene electrotransfer protocol and if electrode axis is oriented along muscle fibers.

Acknowledgment

This work was funded within the program of bilateral scientific cooperation between the Republic of Croatia and the Republic of Slovenia.

References

1. Mir LM, Bureau MF, Gehl J et al. (1999) High-efficiency gene transfer into skeletal muscle mediated by electric pulses. Proc Natl Acad Sci USA 96:4262–4267.
2. Yin D, Tang JG (2001) Gene therapy for streptozotocin-induced diabetic mice by electroporational transfer of naked human insulin precursor DNA into skeletal muscle in vivo. FEBS Lett 495:16–20
3. Šatkauskas S, Bureau MF, Puc M et al. (2002) Mechanisms of in vivo DNA electrotransfer: respective contributions of cell electropermeabilization and DNA electrophoresis. Mol Ther 5:133-140
4. Rols MP (2008) Mechanism by which electroporation mediates DNA migration and entry into cells and targeted tissues. Methods Mol Biol 423:19-33.
5. Kanduser M, Miklavcic D, Pavlin, M (2009) Mechanisms involved in gene electrotransfer using high- and low-voltage pulses — An in vitro study, Bioelectrochem 74:265-271

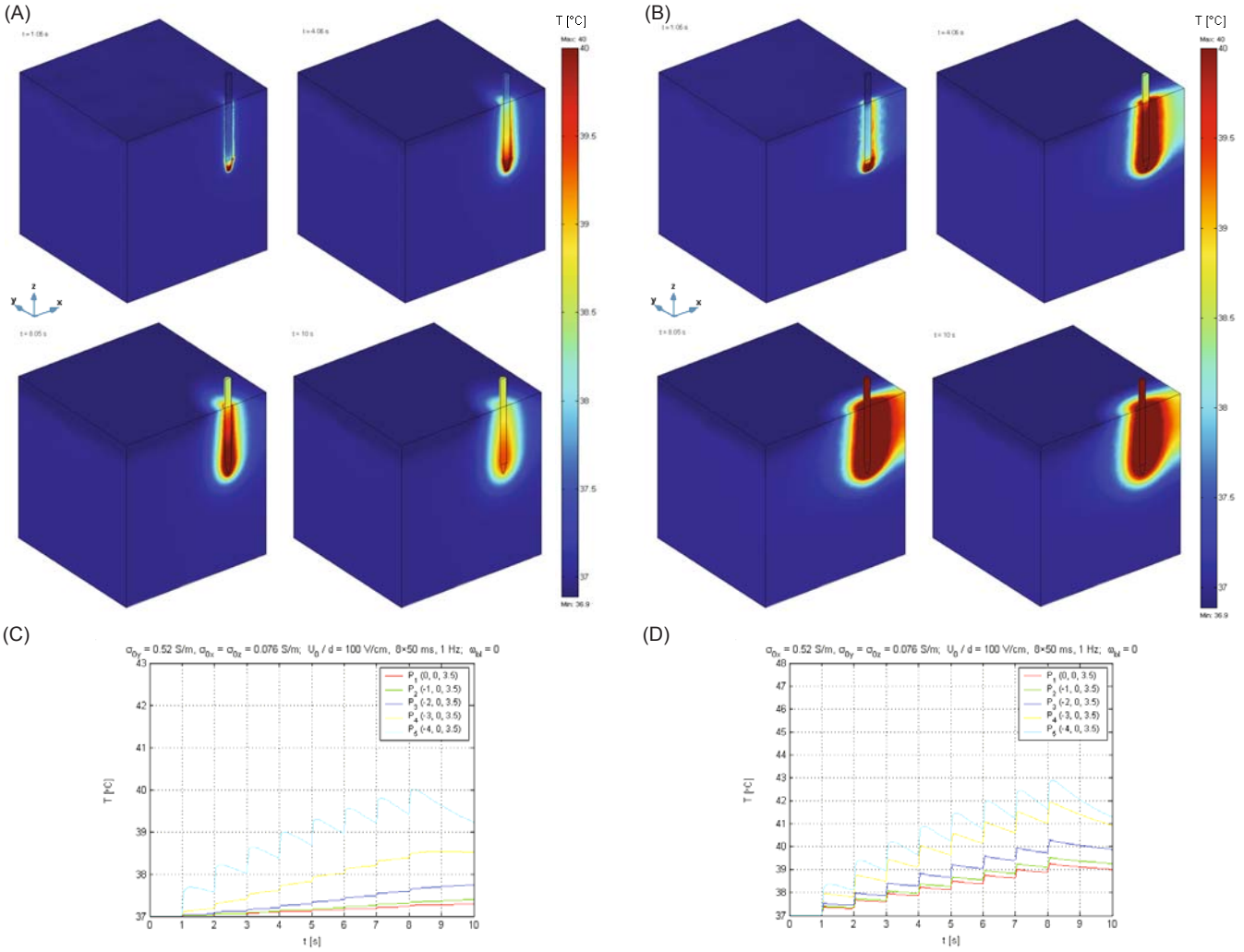

Fig. 4 Temperature distribution during LV pulse train (8×50 ms, 1 Hz, 80V) after 1st, 4th, 8th pulse and at the end of simulation (t=10 s). (A) Electrode axis perpendicular to the axis with higher tissue electrical conductivity $\sigma_{0x}=\sigma_{0z}$ = 0.076 S/m, σ_{0y} = 0.52 S/m. (B) Electrode axis parallel to the axis with higher tissue electrical conductivity. σ_{0x} = 0.52 S/m, $\sigma_{0y}=\sigma_{0z}$ = 0.076 S/m. (C) Time course of temperature in selected locations corresponding to case (A) i.e. parallel orientation. (D) Time course of temperature corresponding to case (B) i.e. perpendicular orientation.

6. Lackovic I, Magjarevic R, Miklavcic D (2005) Analysis of tissue heating during electroporation based therapy: A 3D FEM model for plate electrodes, IFMBE Proc. vol. 8, 6th Asian-Pacific Conf. on Med. & Biol. Eng., Tsukuba, Japan, 2005
7. Lackovic I, Magjarevic R, Miklavcic D (2007) Analysis of tissue heating during electroporation based therapy: A 3D FEM model for a pair of needle electrodes, IFMBE Proc. vol. 16, 11th Medit. Conf. on Med. & Biol. Eng. & Comput., Ljubljana, Slovenia, pp. 631-634
8. Lackovic I, Magjarevic R, Miklavcic D (2008) A Multiphysics Model for Studying the Influence of Pulse Repetition Frequency on Tissue Heating During Electrochemotherapy, IFMBE Proc. vol. 22, 4th Eur. Conf. of the IFMBE, Antwerp, Belgium, pp. 2609-2613
9. Davalos RV, Rubinsky B, Mir LM (2003) Theoretical analysis of the thermal effects during in vivo tissue electroporation. Bioelectrochem 61:99–107
10. Pliquett U (2003) Joule heating during solid tissue electroporation. Med Biol Eng Comput 41:215–219
11. Davalos RV, Rubinsky B (2008) Temperature considerations during irreversible electroporation, Int J Heat and Mass Transfer 51:5617-5622
12. Duck FA (1990) Physical properties of tissue: A comprehensive reference book. Academic Press, London
13. Foster K, Schwan HP (1989) Dielectric properties of tissues and biological materials: A critical review. Crit Rev Biomed Eng 17:25-104

Author: Igor Lacković
Institute: University of Zagreb Faculty of Electrical Engineering and Computing
Street: Unska 3
City: Zagreb
Country: Croatia
Email: igor.lackovic@fer.hr

Mapping the Brazilian Medical Device Innovation System: A Wide Field for Biomedical Engineering Development

E.J.V. Oliveira[1,2], V.L.S.N. Button[2], and V.C.M. Oliveira[3]

[1] DCIIS/SCTIE/MS, Brazilian Ministry of Health, Brasília, Brazil
[2] DEB /FEEC/UNICAMP, State University of Campinas, Campinas, Brazil
[3] GQUIP/GGTPS/ANVISA, Brazilian National Health Surveillance Agency, Brasília, Brazil

Abstract— **The article analyzes the interchange net and the partnerships between the main players of the Brazilian National Innovation System of Medical Devices. It is presented a panorama of the medical device sector around the world an in Brazil, a definition of National Innovation System and its importance in the social-economic development of a country. In this way, the R&D and Innovation activities demanded by the Innovation System configures a wide work field for Biomedical Engineers .**

Keywords— **Medical Devices, Biomedical Engineering, Innovation Systems, Health Industrial Complex, Industrial and Sectorial Policies.**

I. Introduction

The health configurates a complex set of productive activities of goods and services that leverage key segments of the modern society. Beyond its social dimension linked to citizenship, health has its own economic dimension, articulating public and private entities in a wide network of health care - through the Brazilian Unified Health System (SUS) and the Brazilian Health Insurance System – besides an industrial park that provides a wide chain of products designated to health care activities, including medical devices. It is a unique source of opportunity to promote national development in the context of the health policies and the National Productive Development Policy (PDP).

The Industrial Health Complex (CIS), incorporates industrial sectors that are interrelated with the national network of health services constituting a highly dynamic set of economic activities related to a pattern of development that may involve economic growth and equity. It is important to emphasize that, in Brazil, the main health care provider is the public system which is consumes direct and indirect for approximately 70% of all medical devices commercialized in the country – US$ 4 billion market.

The current political conjecture of the country aims to establish a long-term horizon in which the domestic industry falls in a technologically innovative context, establishing solid criteria for changing the production platform, innovation of products and industrial processes. In this context we can highlight the Innovation Law, the PDP mentioned above, and the Program: More Health instituted by the Brazilian Ministry of Health, which establish the CIS as one of the priorities in order to promote economic and social development of the country.

The World Health Organization - WHO data also show that in 2006 the world market for medical devices was approximately US$ 260 billion. Studies conducted by the European Union show an annual growth rate of 16% for the market. Five countries concentrate about 80% of the entire world market for medical devices, U.S., Japan, Germany, the Netherlands and France. The United States is the world's largest market, accounting 43-48% of the market, European market 30-34%. Latin America accounts for 3-5% of the market and Brazil 1.2% of world market [1].

The Brazilian medical device industry has emerged in the 50's and reached its apex in the 70's. In the last three decades changes in national and international scene have brought new challenges to the sector. The market opening in the 90's exhausted the formal model of imports replacement and promoted the appearance of a new competitive environment for the sector. The market regulation initiated by the MS in 1993 and its developments catalyzed by the National Health Agency - ANVISA brought to light new concepts and requirements of minimum quality requirements for the industry.

It is important to emphasize that on one hand the new regulatory and economic approach made more difficult the sector expansion, in the other induced a significant improvement in the quality of the technologies produced in the country. This can be observed by examining the data from three Brazilian Survey of Industrial Innovation (PINTEC) conducted by Brazilian Institute of Geography and Statistics (IBGE), where the medical device sector appears to be one of the ten most innovative sectors in the country. In this period, new regulatory concepts were strongly placed on the market: Good Manufacturing Practices (GMP) and Compulsory Certification of medical equipment under the National Institute of Metrology, Standardization and Industrial Quality (INMETRO).

O. Dössel and W.C. Schlegel (Eds.): WC 2009, IFMBE Proceedings 25/XIII, pp. 214–217, 2009.
www.springerlink.com

Another fact to be noted is the constant technological evolution of materials and components used in the manufacture of medical devices this is one of the factors that inputs short market life cycle for those products (18 to 24 months). This dynamic in the technological evolution of the sector combined with technological gap found in the country and hence the huge dependence on imports, puts the SUS in a position of vulnerability that can be extremely harmful to the welfare of the population. The programs of medical care (using diagnostic devices, medical equipment, orthoses, prostheses and other technology) among others can not be subject to the fluctuations of international financial market and hostage of competitive strategies detached to the national interest.

To minimize this impact, actions and strategies have been proposed in order to place the Medical device sector a priority within the Brazilian health policies and the Productive Development Policy (PDP), which is reflected in the funding strategies of the Brazilian foment institutions. In this context, the Department of Industrial Complex and Innovation in Health within the Secretariat of Science, Technology and Strategic Inputs (DCIIS/SCTIE/MS) started to act as an important catalyst for the industrial policy.

II. The Brazilian Medical Devices Innovation System

A National Innovation System (SNI) can be defined as a network of public and private institutions that integrate their actions towards the promotion the scientific and technological development of a country. Among the actors of a innovation system can be detached in the government: the foment institutions, regulatory agencies, and the scientific and technological institutions (ICT) (ex. Universities, Technology institutes, technical schools); in the private sector: firms and class associations. Within the SNI the knowledge and innovation activities are considered crucial, and the productive sector its spine. However, it is not possible to innovate in a isolate process, due to innovation is an interactive process and, in this way, depends on the interaction between different actors and institutions. In the SNI relays the fact that the knowledge diffusion is the key for innovation generation.

The great merit of the actual SNI definitions is not limit the innovative activity or technological development as exclusively factors to the R&D (Research and Development) activities made by the productive sector, but as a dynamic relation that involves heterogenic actors, endowed with distinguished competences, motivations and organizational patterns. Another preponderant factor is that the technology is not only developed but also spread out and incorporated in the society, showing that the technological evolution exceeds the technical process, in the matter where it adds other elements in the system as the changes in the political-institutional conjuncture and in the way as agents interact between themselves. This approach describe a scenario were the innovation process does not occur due to a single agent, but as a result of an interactive and dynamic collective learning process.

In figure 1 it is show the structure of the Brazilian Medical Devices Innovation System (SNIPM), were the where the diverse bonds between the actors are described as follows.

In the star 1 we have the Health Industrial Complex (CIS) concept elaborated by Gadelha (2003) [2] in which the productive activities are inserted in a peculiar political-institutional context, involving the provision of health services as the economic space for which the all production flows. In Gadelha's proposition the CIS is composed by the health services providers (ex. Hospitals, clinics, diagnostic and treatment services.) and by the industrial sectors (ex. Biotech and Chemical Based Industry and the Medical Device Industry). The original configuration of the CIS (doted black line) did not show the providers of technological services (ex. Medical equipment maintenance, installations and structure support)

One important observation regarding the innovation process in the CIS is the relevance of the R&D activities in the health sector as described by Hicks and & Katz (1996) [3]: the attributions of the hospitals as part of the research system. These authors investigated the British hospitals and their relationships with other institutes and universities.

By analyzing the collaboration between different authors from different institutions, they found out that those hospitals make R&D groups with strong bounds, in opposition to the groups composed by the industry, universities and government. It was identified that the British health sector was responsible for 25% of all British scientific production in the 80's.

In the star 2, we have the Medical devices Industry, which have a strong relationship with the health service providers in the early beginning of the device commercialization process (arrow a), after that the health service start to develop a new relationship with the technological service providers (arrow b), who execute activities related with the preventive and corrective maintenance of medical equipments and installations and, in some cases, managing the technological evaluation process.

This sector is characterized by a strong interdisciplinary content. Furthermore, it is heavily dependent on developments made in other areas of knowledge and in other industrial sectors. The weight of spill-over is huge, thoroughly described in study cases for the main medical innovations. The examples are diverse and very interesting [4]. According to Albuquerque e Cassiolato (2000) [5] the set of relations

with other industrial sectors can not be underestimated: it is not coincidental that so many medical device innovations come from companies that are already established in other sectors (GE, Siemens, HP etc.). Most of the medical innovations are excellent examples of "economies of scope" and are related to diversification of the activities of large companies.

The star number 3 shows that after the vending process, the technological services sector starts to offer and demand services and goods from the manufactures and also offers services and goods to the healthcare providers (arrow b).

We should highlight that none of the innovations in the medical devices sector is an automatic consequence of developments made by other industrial sectors (star 4 – arrow c). The developments of innovations in the medical device field are process predominantly considered to be incremental. In those processes, the involvement of health care professional is crucial, either to identify the need of new technology, or to define its indication and purpose, establish its security requirements and effectively, participate in the construction of prototypes and to suggest improvements during the development of a technology. In other words, the innovation process does not occur only in the industrial labs, it also happens within the health system [5].

In star 5 we have the "S" System which was created in the 40's and is composed by 11 entities. This system receives a budget from the federal government in order to support activities such as technical training and qualification of the industry work force, these activities regards training on empreneurship management, support to technological projects, specialized training and actions towards the density of productive chains (arrow d).

In 6, is presented the two main financial agents for the industrial sector: The Brazilian Innovation Agency (FINEP) and the Brazilian Development Bank (BNDES). The main goal of those institutions is to provide long-term financing aimed at enhancing Brazil's development, and, therefore, improving the competitiveness of the Brazilian economy and the standard of living of the Brazilian population (arrow e).

In 7 it is shown the Technological and scientific Institutions (ICT). The Arrow "f" indicates the offers and demands of R&D activities. At this point there is an important fragility between the ICT's relationship with the productive sector, saved some exemptions. In general the R&D production within the ICT is not attaché to the demands of the medical device industry. In the "g" arrow, there are the offers and demands of qualified human recourses. However, it is not observed a strong relationship between the Professional profile demanded by the industry and those offered by the academia.

The role of the academia in the scientific sector and in the medical device sector is obvious. Furthermore, the role of basic research as trainer of specialized personnel for the innovative activities in the industry, as proposed Pavitt (1990) [7], is particularly visible in this sector. The number of scientific and technological flows of information that are originated in or are destined for these institutions is great. The universities are characterized as a real focus and a convergence center of knowledge flows. This crucial position is a manifestation of the proximity that technological progress of the sector has with science [5].

The Regulatory Agencies (ex.: Brazilian Health Agency - ANS, The National Health Surveillance Agency – ANVISA, The National Institute of Metrology, Standardization and Industrial Quality - INMETRO), the professional associations and medical schools act like a filter for innovations. The combined actions of these institutions shows the singular role played by selective non-market environments in health. Nelson & Winter (1982) [6] had pointed the importance of medical profession in the selection of new treatments (arrow L).

In Brazil, the most structured relationship between the ICT's and the productive sector appears in the arrow "h" and a related with the regulatory demand from ANVISA and INMETRO (star 8 – arrow h). The regulatory agencies coordinate the modus operandi of the compulsory certification system for medical equipment. For this point, the relationship between the ICT and the firms is more "commercial related" since, in this case, the ICT's are the main providers of technical analysis for the certification process and this services constitutes an additional budget for the institutions.

At the star 9 we have the traditional agencies for ICT's promotion and foment: the National Council for Scientific and Technological Development (CNPq), the FINEP, the Coordination of Improvement of Higher Education Personnel (CAPES), the States Foundations for R&D support (FAP's), the BNDES with its Technology Fund (FUNTEC). These institutions are responsible to financing the R&D, training and personnel qualification and technological development actions (arrow j).

In 10 there is the Brazilian Ministry of Health in the foment process to the actions of science and technology through the Secretariat of Science, Technology and Strategic Products (SCTIE) that develops different activities for generation, dissemination and application of new knowledge, seeking to answer needs of SUS and bring the scientific innovations and technological developments to the health actions related with prevention and control of the Brazilian population health problems.

Finally, there is the more recent entity of the system (star 11): the Brazilian Agency for Industrial Development (ABDI). This agency was established in 2005 by the Federal Government with the responsibility to articulate the various actors of the Brazilian State. It is responsible for actions to

promote the economic and industrial development with the productive sector and civil society (arrow k).

III. Conclusions

In the presented scenario, it is suggested that in SNIPM, the initial efforts in science, technology and innovation should be guided by the Brazilian Public Health System (SUS) in the light of its demands for goods and economic services and the social and regional needs of the country. The definition of strategic themes should compose the sectorial policies in order establish a structured and articulated linkages between the various actors and institutions of the SNIPM.

It is also verified that the actual conjecture of the SNIPM demands specialized technological services specially those provided by the Biomedical Engineering. The diverse foment and financial policies created by the Brazilian Government places the Biomedical Engineering as a strategic activity that will strengthen and modernize the sector of medical products, aiming to extend its innovative capacity of the firms and change of its competitive level from the technological demands of the SUS and initiatives of articulation of public and private actions to promote the development of the country technology base.

References

1. OLIVEIRA, E. J. V. (2007) Termo de Referência do Programa Nacional para Qualificação, Produção e Inovação no Complexo Industrial da Saúde - Equipamentos e Materiais de Uso em Saúde, Pesquisa para Saúde 2007, Ministério da Saúde;
2. GADELHA, C. (2003) "O complexo industrial da saúde e a necessidade de um enfoque dinâmico na economia da saúde." Ciência & Saúde Coletiva, 8(2): 521-535;
3. HICKS, D. e KATZ, J. (1996) "Hospitals: the Hidden Research System". Science and Public Policy, 23 (5): 297-304, October;
4. GELIJNS, A. e ROSENBERG, N. (1995)"The Changing Nature of Medical Technology Development". In ROSENBERG, N., GELIJNS, A. e DAWKINS, H.;
5. ALBUQUERQUE, E. M., CASSIOLATO, J. E. (2002) As Especificidades do Sistema de Inovação do Setor Saúde. Revista de Economia Política, vol. 22, nº 4 (88), outubro-dezembro;
6. NELSON, R. e WINTER, S. (1982) An Evolutionary Theory of Economic Change. Cambridge, Mass; London: The Belknap Press of Harvard University Press;
7. PAVITT, K. (1991) "What Makes Basic Research Economically Useful?" Research Policy, 20 (2): 109-119.Smith J, Jones M Jr, Houghton L et al. (1999) Future of health insurance. N Engl J Med 965:325–329.

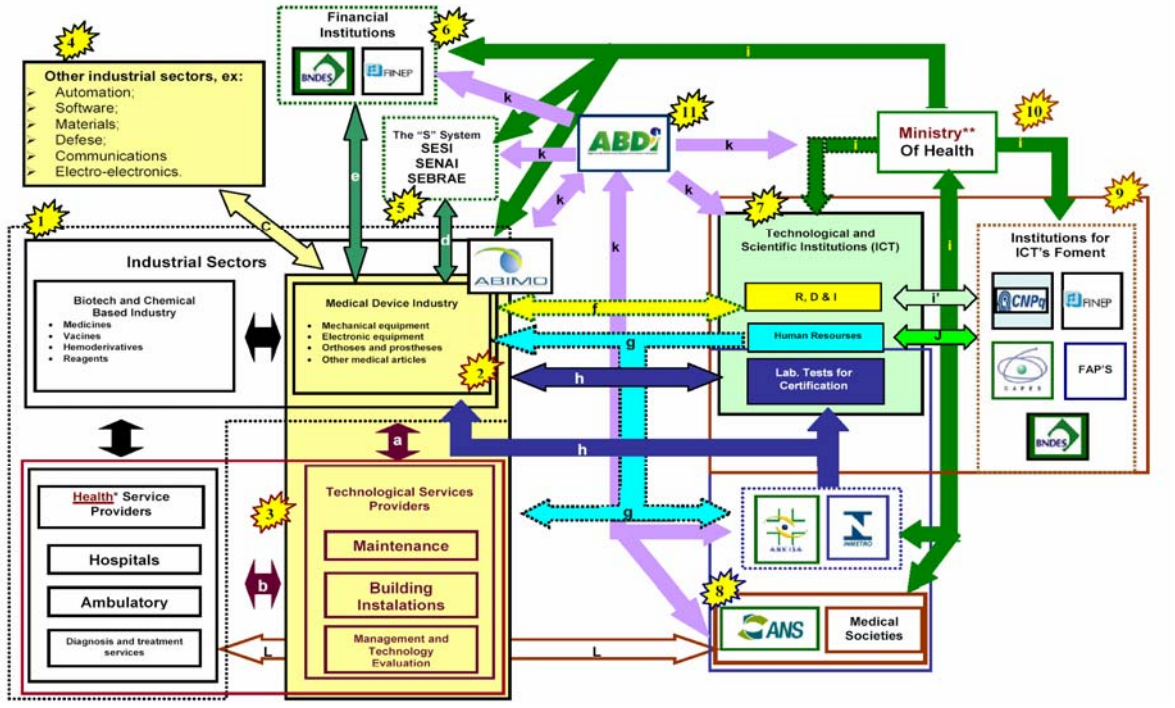

Fig. 1 Actual conjecture of the Brazilian National Innovation System of Medical Devices.

Cell Tracking and Single Cell Imaging by MRI

Brian Rutt

Department of Radiology
Stanford University, Stanford, California, USA

Abstract – **Cellular MRI technology utilizing superparmagnetic iron oxide nanoparticles has progressed quickly over the past decade. Current research is increasingly using clinical MR field strengths, and has demonstrated extremely high detection sensitivity, all the way down to single cell detection in vivo, at both 1.5T and 3T. Our recent work has focused on the optimization of these methods at 3T, and the demonstration of the benefits of 3T over 1.5T for single cell applications such as metastatic cancer cell detection.**

Keywords – **magnetic resonance imaging, cell tracking, iron oxide nanoparticles, single cell imaging, cancer.**

I. Introduction

The field of cellular imaging is a newly emerging discipline of imaging research that has been broadly defined as the application of imaging techniques for the non-invasive and repetitive imaging of targeted cells and cellular processes in living organisms. Cellular MR imaging combines the ability to obtain high resolution MR data with the use of magnetic contrast agents for labeling specific cells, thereby enhancing their detectability. MRI has a number of characteristics that make it ideal for cell tracking. MRI can produce images with high spatial resolution and exquisite soft tissue contrast. Current micro-MRI techniques can achieve *in vivo* resolution on the order of tens of micrometers. MRI is noninvasive, nondestructive and 3D. Unlike histological analyses, which provide only a "snapshot" of the overall process, cellular MR imaging can provide a more dynamic view of cellular events. In comparison, MR imaging delivers faster results, requires fewer animals, is free from sectioning related artifacts and may provide a more complete picture of the overall biological process under investigation.

Superparamagnetic iron oxide (SPIO) nanoparticles represent a class of contrast agents used for cellular MR imaging that exhibit extremely high relaxivity. SPIO contrast agents consist of a magnetite core(s) surrounded by a matrix material such as dextran. The presence of this magnetic label causes a distortion in the magnetic field and leads to abnormal signal hypo-intensities in T2 or T2* weighted images. Areas containing SPIO labeled cells therefore appear as regions of low signal intensity on MRI images; creating negative contrast. The large magnetic susceptibility of these particles affects an area much larger than the actual size of the particles. This effect is known as a 'blooming artifact', and leads to an exaggeration of the region occupied by iron oxide. The development of a broad repertoire of SPIO contrast agents, as well as techniques for incorporating these labels into cells, has stimulated a variety of applications of this cell-tracking MRI technique. SPIO has been used to label and track a wide variety of cell types including T-lymphoctyes, macrophages, cancer cells, and stem cells with minimal impact on cell function over a period of several weeks and over multiple cell divisions.

II. Cellular detection limits

Compared to other imaging modalities such as PET, SPECT and optical fluorescence imaging, MRI has traditionally been thought of as having a low sensitivity. In fact, the majority of studies utilizing MRI for the detection of SPIO labeled cells have only examined large groups of cells (10^6-10^7 cells). While MRI of large numbers of cells may be suitable for the spatial localization of a large cluster of transplanted cells, it does not allow an analysis of the migration patterns of small numbers of cells. The ability to detect small groups of cells or single cells would provide a more accurate picture of the fate of transplanted cells—a characteristic that is especially important in studies of cancer cell metastasis and transplantation. Pushing the limits of detection of SPIO labeled cells has therefore become an active area of research in the field of cellular imaging.

III. In vitro single cell imaging

The *in vitro* detection of single cells using MRI was first demonstrated by Dodd *et al.* for SPIO-labeled T cells in gelatin.[Dodd 1999] The authors met the requirements for

O. Dössel and W.C. Schlegel (Eds.): WC 2009, IFMBE Proceedings 25/XIII, pp. 218–220, 2009.
www.springerlink.com

single cell detection by scanning at high resolution (25 μm isotropic), and by using optimized RF coils, long scan times (2 hours) and high field (7T) to achieve adequate SNR. To perform single cell detection *in vivo*, images with high resolution and high SNR have to be achieved under less optimal imaging conditions (larger diameter RF coil, animal/organ motion, and lower signal due to decreased tissue T2 compared to gel). Because of these stringent imaging requirements, *in vivo* single cell MRI was considered improbable at the time.

IV. In vivo single cell imaging

With respect to *in vivo* detection of small numbers of SPIO-labelled cells, a number of groups have reported progress in this area. Hoehn *et al.* demonstrated an *in vivo* detection limit of 500 embryonic stem cells implanted in rat brain and imaged at 7 T.[Hoehn 2002] Kircher *et al.* showed that as few as three SPIO labeled cytotoxic lymphocytes/voxel could be detected at 8.5 T in tumors in live mice.[Kircher 2003] Our lab has focused on developing and improving cellular MRI tools in order to increase detection sensitivity. This was indeed achieved when we showed that individual SPIO-labeled cells could be detected *in vitro* [Foster-Gareau 2003] and, for the first time, *in vivo* [Heyn 2006a] in a mouse brain using a balanced steady-state free precession imaging sequence (FIESTA, GE, Healthcare, Milwaukee, WI) and a high-performance insertable gradient system operating within a clinical 1.5T scanner. These images were acquired with voxel size of ($100\times100\times200$ mm^3) and a scan time of 1.5 hours.

V. MR acquisition issues

Advances in cell labeling techniques and MR hardware and pulse sequence design may hold the keys to unlocking the full potential of MR for single cell detection and tracking *in vivo*. A number of techniques are now available which have drastically improved the amount of SPIO that can be incorporated into a cell (picogram quantities) with minimal impact on cell function. Traditionally, SPIO-labeled cells have been imaged using two types of pulse sequences: spoiled gradient echo (SPGR) or spin echo (SE). The SPGR sequence is extremely sensitive to the magnetic-field inhomogeneities created by SPIO. This sensitivity for magnetic field inhomogeneity comes at the cost of lower SNR efficiency which is a disadvantage for high resolution microimaging required for single cell detection *in vivo*. Spin echo (SE) pulse sequences, on the other hand, have a better SNR efficiency than SPGR but the refocusing of magnetization which is responsible for the improved SNR, reduces the sensitivity of SE sequences for detecting SPIO.

More recently, balanced steady state free precession (SSFP) sequences have gained favor as clinical pulse sequences because of their high SNR at short repetition times. In addition to higher SNR efficiency, balanced SSFP pulse sequences are extremely sensitive to resonance offsets created by B_0 field inhomogeneities. This aspect of balanced SSFP was originally problematic, resulting in periodic banding artifacts in images, but has since been minimized by a number of techniques (eg. improved shimming techniques, minimized TR, phase cycling). The sensitivity of balanced SSFP to resonant offsets, which was once a nuisance, now provides a new mechanism for detecting SPIO-labeled cells. The high SNR efficiency of balanced SSFP along with its sensitivity to resonance offset motivates our choice of this pulse sequence for the detection of SPIO-labeled cells *in vivo*.

Our early single-cell studies demonstrated that one factor that significantly improves single cell contrast is spatial resolution.[Heyn 2005] To acquire higher resolution images at 1.5T would require scan times that quickly become prohibitive for *in vivo* serial scanning of animal models (i.e. 100mm isotropic images with the same SNR as those presented in [Heyn 2006a, Heyn 2006b] would require ~ 6 hours). We have therefore investigated the use of the higher (but still clinical) magnetic field strength of 3T, to allow for smaller voxel size, yielding higher contrast and better detection of single iron-labeled cells, while maintaining reasonable scan time. We have examined various scanning parameters and strategies on our ability to detect single cells *in vivo*.

We began by studying the commonly seen banding artifact that is produced by off-resonance spins in balanced SSFP images. One solution to this problem is to decrease TR. However, we found that dramatic decreases in TR were difficult to achieve because of the much greater gradient demands, even on our high performance gradient system, and also that such TR decreases led to reduction in single cell contrast. Therefore, we implemented a multiple acquisition SSFP scheme [Bangerter 2004] to suppress banding artifact while permitting the use of moderate TR (10 ms range).

Once we had improved our 3T balanced SSFP images to be relatively free of adverse banding artifact, different scanning parameters were varied and comparisons were conducted in order to determine the optimal combination of scanning parameters for detecting single iron-labeled cells *ex vivo*. The first comparison investigated the effect of increased field strength and the associated gain in SNR on single cell detection. To do so, a mouse head was scanned with identical 1.5 and 3T scanners using the same exact

parameters and scan time. It was observed that the more-than-doubled SNR obtained with 3T imaging resulted in the detection of double the number of cells. Furthermore, even though the mean fractional signal loss (ΔS/S) of all the cells detected was not significantly different between the two scans, when considering the cells detected only in both scans, the average ΔS/S for was found to be significantly higher. These results suggest that the alteration of one variable, namely SNR, can lower the single cell detection threshold dramatically.

We also investigated the effect of receiver bandwidth and its associated effect on cell detection. Four bandwidth values were studied: ±23, 13, 8, and 5 kHz. The lowest bandwidth used (±5 kHz) gave the highest ΔS/S, yet it did not result in the detection of any more voids compared to the second lowest BW used (±8kHz). In addition, the lowest bandwidth produced images with other features which made the detection of signal voids more difficult. One of these features was increased artifact associated with motion/vibration. The other problem was the enhanced blooming effect with very low BW, which made it difficult to distinguish between two closely positioned voids. For these reasons, we have settled on bandwidths in the ±8-21 kHz range for our *in vivo* single cell imaging at 3T.

Finally, we investigated the effect of decreased voxel size. In this experiment, where the optimal BW of ±8 kHz and a matched SNR of ~100 were used, it was observed that the higher resolution images (100mm isotropic) resulted in a significantly higher ΔS/S compared to the lower resolution 100×100×200 mm^3). However, the number of detected cells was not greatly affected. From these comparisons, we have concluded that the optimal scanning protocol for single iron-labeled cell detection *ex vivo* utilizes a BW of ±8 kHz with a corresponding TE/TR of 7.3/14.7, an SNR of ~100, and a spatial resolution of 100×100×200 mm^3. For in vivo scanning, we have opted for a higher bandwidth, ±21 kHz, which we have found to be a better compromise between cell detection and motion sensitivity.

VI. Summary

Cellular MRI technology utilizing superparmagnetic iron oxide particles has progressed quickly over the past decade. Current research is increasingly using clinical MR field strengths, and has demonstrated extremely high detection sensitivity, all the way down to single cell detection in vivo, at both 1.5T and 3T. Our recent work has focused on the optimization of these methods at 3T, and the demonstration of the benefits of 3T over 1.5T for single cell applications such as metastatic cancer cell detection.

References

Dodd SJ, Williams M, Suhan JP, Williams DS, Koretsky AP, Ho C. Detection of single mammalian cells by high-resolution magnetic resonance imaging. Biophys J. 1999 Jan;76(1 Pt 1):103-9.

Hoehn M, Kustermann E, Blunk J, Wiedermann D, Trapp T, Wecker S, Focking M, Arnold H, Hescheler J, Fleischmann BK, Schwindt W, Buhrle C. Monitoring of implanted stem cell migration in vivo: a highly resolved in vivo magnetic resonance imaging investigation of experimental stroke in rat. Proc Natl Acad Sci U S A. 2002 Dec 10;99(25):16267-72.

Kircher MF, Allport JR, Graves EE, Love V, Josephson L, Lichtman AH, Weissleder R. In vivo high resolution three-dimensional imaging of antigen-specific cytotoxic T-lymphocyte trafficking to tumors. Cancer Res. 2003 Oct 15;63(20):6838-46.

Foster-Gareau P, Heyn C, Alejski A, Rutt BK. Imaging single mammalian cells with a 1.5 T clinical MRI scanner. Magn Reson Med. 2003 May;49(5):968-71.

Heyn C, Ronald JA, Mackenzie LT, MacDonald IC, Chambers AF, Rutt BK, Foster PJ. In vivo magnetic resonance imaging of single cells in mouse brain with optical validation. Magn Reson Med. 2006a Jan;55(1):23-9.

Heyn C, Bowen CV, Rutt BK, Foster PJ. Detection threshold of single SPIO-labeled cells with FIESTA. Magn Reson Med. 2005 Feb;53(2):312-20.

Heyn C, Ronald JA, Ramadan SS, Snir JA, Barry AM, MacKenzie LT, Mikulis DJ, Palmieri D, Bronder JL, Steeg PS, Yoneda T, MacDonald IC, Chambers AF, Rutt BK, Foster PJ. In vivo MRI of cancer cell fate at the single-cell level in a mouse model of breast cancer metastasis to the brain. Magn Reson Med. 2006b Nov;56(5):1001-10.

Bangerter NK, Hargreaves BA, Vasanawala SS, Pauly JM, Gold GE, Nishimura DG. Analysis of multiple-acquisition SSFP. Magn Reson Med. 2004 May;51(5):1038-47.

The Heat Is on in Cancer

R. Issels

Helmholtz Zentrum Munich, Institute for Molecular Immunology, Munich, Germany and Klinikum Grosshadern Med. Ctr, Univ. of Munich, Munich, Germany

The hallmarks of hyperthermia and its pleotropic effects are in favour of its combined use with chemotherapy and/or radiotherapy.. Preclinical research reveals that for heat killing and synergistic effects the thermal dose is most critical. Thermal enhancement of drug cytotoxicity is accompanied by cellular death and necrosis without increasing its oncogenic potential. The induction of genetically defined stress responses can deliver danger signals to activate the host's immune system. The positive results of randomized trials have definitely established hyperthermia in combination with chemotherapy and/or radiotherapy as a novel clinical modality for the treatment of cancer. Hyperthermia targets the action of standard therapy within the heated tumour region without affecting systemic toxicity. In specific clinical settings regional hyperthermia (RHT) has proved its value and deserve a greater focus and investigation in other malignancies. In Europe, more specialized centres should be created and maintained as network of excellence for hyperthermia in the field of oncology.

O. Dössel and W.C. Schlegel (Eds.): WC 2009, IFMBE Proceedings 25/XIII, p. 221, 2009.
www.springerlink.com

Nano-medicine in Cancer Therapy

Dag Rune Olsen

Institute for Cancer Research, Oslo University Hospital, University of Oslo
d.r.olsen@fys.uio.no

Abstract – **Nano-particles have been launched as a promising strategy for targeted cancer therapy. Quantum dots are nano-particles in the size range of 2-10 nm possessing unique features that may be of critical importance for targeting cancer cells. Currently the possibility of using quantum dots in sensitization of radiotherapy of cancer is being explored as quantum dots may yield electrons and radicals upon exposure to radiation. Recent data published by Juzeans et al. have demonstrated increased tumor cell kill by following ionizing radiation exposure in the presence of quantum dots. Localized release of cytotoxic agents encapsulated in sono-sensitive liposomes upon ultrasound exposure is another example of non-sized particles in targeted cancer therapy. The targeting ability and the selectivity of these emerging technologies are yet to be revealed and the clinical effectiveness to be established in future clinical trails.**

Keywords – **Nano-medicine, Quantum dots, cancer therapy.**

O. Dössel and W.C. Schlegel (Eds.): WC 2009, IFMBE Proceedings 25/XIII, p. 222, 2009.
www.springerlink.com

Advice for Writing a Successful Research Proposal

Paul Keall

Associate Professor and Director, Radiation Physics
Department of Radiation Oncology, Stanford University

In this presentation I will describe the tools and methods that I have learned from several mentors and also from experience to write successful grant applications. I will refer to examples of grants I have submitted. From the reviewer's perspective, almost all grants received by panels are very good and worthy of funding. Not being funded is not an indication that the grant proposal is bad. The challenge is to make the proposal as clear and compelling as possible to make the proposal the top or amongst the top of the competing applications, and therefore funded.

Unfortunately, I have not yet found any tricks or shortcuts to make writing successful research proposals easy. There are however five common elements: alignment of the program goals, the idea, clarity, the team and effort.

The proposal needs to be aligned with the goals of the funding body that will potentially support your research. When you start the proposal preparation process, carefully read the grant announcement. Review previously successful grant applications funded under the program. Does you research align with the announcement? Call the program official listed on the grant announcement. Talk about your idea. Does your idea broadly fit within the overall research theme? If not, do not be discouraged from applying and also seek funding opportunities more closely aligned with your research.

The idea, and the presentation of the idea, are key. Is the idea compelling? Is it novel? It the formulation of the idea built on the your and others previous work? Will the research be significant and change practice? Is it feasible? Is there appropriate discussion of the potential obstacles and how these will be overcome?

Clarity cannot be understated. Your proposal will likely be reviewed by experts and non-experts, and therefore the significance of the work needs to be portrayed to both audiences. The research plan, particularly what will be done needs to be clearly explained. Do all parts of the proposal make the case for, and strengthen the grant? Have a non-expert review the grant for clarity, and ask them to explain back to you what the grant is about.

The team for the grant needs to have the appropriate skills to ensure that the proposal could be completed if funded, and can often be multidisciplinary. It is important to have experts than can help with guidance and particularly to help overcome any obstacles. The team should be consulted on the grant aims and have the opportunity to give input the grant during the formulation.

Writing a successful proposal requires enormous effort. You need to understand and put in perspective the previous work- your own and others- on which the idea is based. You need to create important hypotheses and describe clear experiments of how the hypotheses will be tested. You need to be prepared to write, and rewrite the application, and review and revise many times prior to submission.

In summary, it is easy to write a grant proposal. However, it is an arduous, consuming, painstaking, soul searching and ultimately exhilarating process to write a successful grant application.

O. Dössel and W.C. Schlegel (Eds.): WC 2009, IFMBE Proceedings 25/XIII, p. 223, 2009.
www.springerlink.com

Author Index